ISBN: 0-8247-0575-0

This book is printed on acid-free paper.

Headquarters
Marcel Dekker, Inc.
270 Madison Avenue, New York, NY 10016
tel: 212-696-9000; fax: 212-685-4540

Eastern Hemisphere Distribution
Marcel Dekker AG
Hutgasse 4, Postfach 812, CH-4001 Basel, Switzerland
tel: 41-61-261-8482; fax: 41-61-261-8896

World Wide Web
http://www.dekker.com

The publisher offers discounts on this book when ordered in bulk quantities. For more information, write to Special Sales/Professional Marketing at the headquarters address above.

Neither this book nor any part may be reproduced or transmitted in any form or by any means, electronic or mechanical, including photocopying, microfilming, and recording, or by any information storage and retrieval system without permission in writing from the publisher.

Current printing (last digit):
10 9 8 7 6 5 4 3 2 1

PRINTED IN THE UNITED STATES OF AMERICA

Preface

Thin-walled structures in the form of plates and shells are encountered in many branches of technology, such as civil, mechanical, aeronautical, marine, and chemical engineering. Such a widespread use of plate and shell structures arises from their intrinsic properties. When suitably designed, even very thin plates, and especially shells, can support large loads. Thus, they are utilized in structures such as aerospace vehicles in which light weight is essential.

In preparing this book, we had three main objectives: first, to offer a comprehensive and methodical presentation of the fundamentals of thin plate and shell theories, based on a strong foundation of mathematics and mechanics with emphasis on engineering aspects. Second, we wanted to acquaint readers with the most useful and contemporary analytical and numerical methods for solving linear and nonlinear plate and shell problems. Our third goal was to apply the theories and methods developed in the book to the analysis and design of thin plate-shell structures in engineering. This book is intended as a text for graduate and postgraduate students in civil, architectural, mechanical, chemical, aeronautical, aerospace, and ocean engineering, and engineering mechanics. It can also serve as a reference book for practicing engineers, designers, and stress analysts who are involved in the analysis and design of thin-walled structures.

As a textbook, it contains enough materal for a two-semester senior or graduate course on the theory and applications of thin plates and shells. Also, a special effort has been made to have the chapters as independent from one another as possible, so that a course can be taught in one semester by selecting appropriate chapters, or through equivalent self-study.

The textbook is divided into two parts. Part I (Chapters 1–9) presents plate bending theory and its application and Part II (Chapters 10–20) covers the theory, analysis, and principles of shell structures.

Contents

Preface

PART I. THIN PLATES

1 Introduction
  1.1 General
  1.2 History of Plate Theory Development
  1.3 General Behavior of Plates
  1.4 Survey of Elasticity Theory
  References

2 The Fundamentals of the Small-Deflection Plate Bending Theory
  2.1 Introduction
  2.2 Strain–Curvature Relations (Kinematic Equations)
  2.3 Stresses, Stress Resultants, and Stress Couples
  2.4 The Governing Equation for Deflections of Plates in Cartesian Coordinates
  2.5 Boundary Conditions
  2.6 Variational Formulation of Plate Bending Problems
  Problems
  References

3 Rectangular Plates
  3.1 Introduction
  3.2 The Elementary Cases of Plate Bending
  3.3 Navier's Method (Double Series Solution)

3.4 Rectangular Plates Subjected to a Concentrated Lateral Force *P*
3.5 Levy's Solution (Single Series Solution)
3.6 Continuous Plates
3.7 Plates on an Elastic Foundation
3.8 Plates with Variable Stiffness
3.9 Rectangular Plates Under Combined Lateral and Direct Loads
3.10 Bending of Plates with Small Initial Curvature
Problems
References

4 Circular Plates
4.1 Introduction
4.2 Basic Relations in Polar Coordinates
4.3 Axisymmetric Bending of Circular Plates
4.4 The Use of Superposition for the Axisymmetric Analysis of Circular Plates
4.5 Circular Plates on Elastic Foundation
4.6 Asymmetric Bending of Circular Plates
4.7 Circular Plates Loaded by an Eccentric Lateral Concentrated Forc
4.8 Circular Plates of Variable Thickness
Problems
References

5 Bending of Plates of Various Shapes
5.1 Introduction
5.2 Elliptical Plates
5.3 Sector-Shaped Plates
5.4 Triangular Plates
5.5 Skew Plates
Problems
References

6 Plate Bending by Approximate and Numerical Methods
6.1 Introduction
6.2 The Finite Difference Method (FDM)
6.3 The Boundary Collocation Method (BCM)
6.4 The Boundary Element Method (BEM)
6.5 The Galerkin Method
6.6 The Ritz Method
6.7 The Finite Element Method (FEM)
Problems
References

7 Advanced Topics
7.1 Thermal Stresses in Plates
7.2 Orthotropic and Stiffened Plates
7.3 The Effect of Transverse Shear Deformation on the Bending of Elastic Plates

- 7.4 Large-Deflection Theory of Thin Plates
- 7.5 Multilayered Plates
- 7.6 Sandwich Plates
- Problems
- References

8 Buckling of Plates
- 8.1 Introduction
- 8.2 General Postulations of the Theory of Stability of Plates
- 8.3 The Equilibrium Method
- 8.4 The Energy Method
- 8.5 Buckling Analysis of Orthotropic and Stiffened Plates
- 8.6 Postbuckling Behavior of Plates
- 8.7 Buckling of Sandwich Plates
- Problems
- References

9 Vibration of Plates
- 9.1 Introduction
- 9.2 Free Flexural Vibrations of Rectangular Plates
- 9.3 Approximate Methods in Vibration Analysis
- 9.4 Free Flexural Vibrations of Circular Plates
- 9.5 Forced Flexural Vibrations of Plates
- Problems
- References

PART II. THIN SHELLS

10 Introduction to the General Linear Shell Theory
- 10.1 Shells in Engineering Structures
- 10.2 General Definitions and Fundamentals of Shells
- 10.3 Brief Outline of the Linear Shell Theories
- 10.4 Loading-Carrying Mechanism of Shells
- References

11 Geometry of the Middle Surface
- 11.1 Coordinate System of the Surface
- 11.2 Principal Directions and Lines of Curvature
- 11.3 The First and Second Quadratic Forms of Surfaces
- 11.4 Principal Curvatures
- 11.5 Unit Vectors
- 11.6 Equations of Codazzi and Gauss. Gaussian Curvature.
- 11.7 Classification of Shell Surfaces
- 11.8 Specialization of Shell Geometry
- Problems
- References

12 The General Linear Theory of Shells
- 12.1 Basic Assumptions
- 12.2 Kinematics of Shells
- 12.3 Statics of Shells
- 12.4 Strain Energy of Shells
- 12.5 Boundary Conditions
- 12.6 Discussion of the Governing Equations of the General Linear Shell Theory
- 12.7 Types of State of Stress for Thin Shells
- Problems
- References

13 The Membrane Theory of Shells
- 13.1 Preliminary Remarks
- 13.2 The Fundamental Equations of the Membrane Theory of Thin Shells
- 13.3 Applicability of the Membrane Theory
- 13.4 The Membrane Theory of Shells of Revolution
- 13.5 Symmetrically Loaded Shells of Revolution
- 13.6 Membrane Analysis of Cylindrical and Conical Shells
- 13.7 The Membrane Theory of Shells of an Arbitrary Shape in Cartesian Coordinates
- Problems
- References

14 Application of the Membrane Theory to the Analysis of Shell Structures
- 14.1 Membrane Analysis of Roof Shell Structures
- 14.2 Membrane Analysis of Liquid Storage Facilities
- 14.3 Axisymmetric Pressure Vessels
- Problems
- References

15 Moment Theory of Circular Cylindrical Shells
- 15.1 Introduction
- 15.2 Circular Cylindrical Shells Under General Loads
- 15.3 Axisymmetrically Loaded Circular Cylindrical Shells
- 15.4 Circular Cylindrical Shell of Variable Thickness Under Axisymmetric Loading
- Problems
- References

16 The Moment Theory of Shells of Revolution
- 16.1 Introduction
- 16.2 Governing Equations
- 16.3 Shells of Revolution Under Axisymmetrical Loads
- 16.4 Approximate Method for Solution of the Governing Equations (16.30)

16.5 Axisymmetric Spherical Shells, Analysis of the State of Stress at the Spherical-to-Cylindrical Junction
16.6 Axisymmetrically Loaded Conical Shells
16.7 Axisymmetric Deformation of Toroidal Shells
Problems
References

17 Approximate Theories of Shell Analysis and Their Applications
17.1 Introduction
17.2 The Semi-Membrane Theory of Cylindrical Shells
17.3 The Donnel–Mushtari–Vlasov Theory of Thin Shells
17.4 Theory of Shallow Shells
17.5 The Theory of Edge Effect
Problems
References

18 Advanced Topics
18.1 Thermal Stresses in Thin Shells
18.2 The Geometrically Nonlinear Shell Theory
18.3 Orthotropic and Stiffened Shells
18.4 Multilayered Shells
18.5 Sandwich Shells
18.6 The Finite Element Representations of Shells
18.7 Approximate and Numerical Methods for Solution of Nonlinear Equations
Problems
References

19 Buckling of Shells
19.1 Introduction
19.2 Basic Concepts of Thin Shells Stability
19.3 Linear Buckling Analysis of Circular Cylindrical Shells
19.4 Postbuckling Analysis of Circular Cylindrical Shells
19.5 Buckling of Orthotropic and Stiffened Cylindrical Shells
19.6 Stability of Cylindrical Sandwich Shells
19.7 Stability of Shallow Shells Under External Normal Pressure
19.8 Buckling of Conical Shells
19.9 Buckling of Spherical Shells
19.10 Design Stability Analysis
Problems
References

20 Vibrations of Shells
20.1 Introduction
20.2 Free Vibrations of Cylindrical Shells
20.3 Free Vibrations of Conical Shells
20.4 Free Vibrations of Shallow Shells
20.5 Free Vibrations of Stiffened Shells

20.6 Forced Vibrations of Shells
Problems
References

Appendix A. Some Reference Data
A.1 Typical Properties of Selected Engineering Materials at Room Temperatures (U.S. Customary Units)
A.2 Typical Properties of Selected Engineering Materials at Room Temperatures (International System (SI) Units)
A.3 Units and Conversion Factors
A.4 Some Useful Data
A.5 Typical Values of Allowable Loads
A.6 Failure Criteria

Appendix B. Fourier Series Expansion
B.1 Dirichlet's Conditions
B.2 The Series Sum
B.3 Coefficients of the Fourier Series
B.4 Modification of Relations for the Coefficients of Fourier's Series
B.5 The Order of the Fourier Series Coefficients
B.6 Double Fourier Series
B.7 Sharpening of Convergence of the Fourier Series
References

Appendix C. Verification of Relations of the Theory of Surfaces
C.1 Geometry of Space Curves
C.2 Geometry of a Surface
C.3 Derivatives of Unit Coordinate Vectors
C.4 Verification of Codazzi and Gauss Equations

Appendix D. Derivation of the Strain–Displacement Relations
D.1 Variation of the Displacements Across the Shell Thickness
D.2 Strain Components of the Shell

Appendix E. Verification of Equilibrium Equations

Part I

Thin Plates

1

Introduction

1.1 GENERAL

Thin plates are initially flat structural members bounded by two parallel planes, called *faces*, and a cylindrical surface, called an *edge* or *boundary*. The generators of the cylindrical surface are perpendicular to the plane faces. The distance between the plane faces is called the *thickness* (h) of the plate. It will be assumed that the plate thickness is small compared with other characteristic dimensions of the faces (length, width, diameter, etc.). Geometrically, plates are bounded either by straight or curved boundaries (Fig. 1.1). The static or dynamic loads carried by plates are predominantly perpendicular to the plate faces.

The load-carrying action of a plate is similar, to a certain extent, to that of beams or cables; thus, plates can be approximated by a gridwork of an infinite number of beams or by a network of an infinite number of cables, depending on the flexural rigidity of the structures. This two-dimensional structural action of plates results in lighter structures, and therefore offers numerous economic advantages. The plate, being originally flat, develops shear forces, bending and twisting moments to resist transverse loads. Because the loads are generally carried in both directions and because the twisting rigidity in isotropic plates is quite significant, a plate is considerably stiffer than a beam of comparable span and thickness. So, thin plates combine light weight and a form efficiency with high load-carrying capacity, economy, and technological effectiveness.

Because of the distinct advantages discussed above, thin plates are extensively used in all fields of engineering. Plates are used in architectural structures, bridges, hydraulic structures, pavements, containers, airplanes, missiles, ships, instruments, machine parts, etc. (Fig. 1.2).

We consider a plate, for which it is common to divide the thickness h into equal halves by a plane parallel to its faces. This plane is called the *middle plane* (or simply,

the *midplane*) of the plate (Fig. 1.3). Being subjected to transverse loads, an initially flat plate deforms and the midplane passes into some curvilinear surface, which is referred to as the *middle surface*. With the exception of Secs 3.8 and 4.8, we will consider only plates of constant thickness. For such plates, the shape of a plate is adequately defined by describing the geometry of its middle plane. Depending on the shape of this midplane, we will distinguish between rectangular, circular, elliptic, etc., plates.

A plate resists transverse loads by means of bending, exclusively. The flexural properties of a plate depend greatly upon its thickness in comparison with other dimensions. Plates may be classified into three groups according to the ratio a/h, where a is a typical dimension of a plate in a plane and h is a plate thickness. These groups are

1. The first group is presented by *thick plates* having ratios $a/h \leq 8 \ldots 10$. The analysis of such bodies includes all the components of stresses, strains, and displacements as for solid bodies using the general equations of three-dimensional elasticity.

2. The second group refers to plates with ratios $a/h \geq 80 \ldots 100$. These plates are referred to as *membranes* and they are devoid of flexural rigidity. Membranes carry the lateral loads by axial tensile forces N (and shear forces) acting in the plate middle surface as shown in Fig. 1.7. These forces are called *membrane forces*; they produce projection on a vertical axis and thus balance a lateral load applied to the plate-membrane.

3. The most extensive group represents an intermediate type of plate, so-called *thin plate* with $8 \ldots 10 \leq a/h \leq 80 \ldots 100$. Depending on the value of the ratio w/h, the ratio of the maximum deflection of the plate to its thickness, the part of flexural and membrane forces here may be different. Therefore, this group, in turn, may also be subdivided into two different classes.

a. *Stiff plates*. A plate can be classified as a stiff plate if $w/h \leq 0.2$. Stiff plates are flexurally rigid thin plates. They carry loads two dimensionally, mostly by internal bending and twisting moments and by transverse shear forces. The middle plane deformations and the membrane forces are negligible. In engineering practice, the term plate is understood to mean a stiff plate, unless otherwise specified. The concept of stiff plates introduces serious simplifications that are discussed later. A funda-

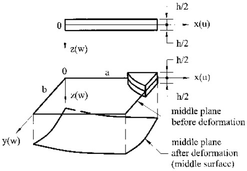

Fig. 1.3

rectangular plates in compression, while Dinnik [34], Nadai [35], Meissner [36], etc., completed the buckling problem for circular compressed plates. An effect of the direct shear forces on the buckling of a rectangular simply supported plate was first studied by Southwell and Skan [37]. The buckling behavior of a rectangular plate under nonuniform direct compressive forces was studied by Timoshenko and Gere [38] and Bubnov [14]. The postbuckling behavior of plates of various shapes was analyzed by Karman *et al*. [39], Levy [40], Marguerre [41], etc. A comprehensive analysis of linear and nonlinear buckling problems for thin plates of various shapes under various types of loads, as well as a considerable presentation of available results for critical forces and buckling modes, which can be used in engineering design, were presented by Timoshenko and Gere [38], Gerard and Becker [42], Volmir [43], Cox [44], etc.

A differential equation of motion of thin plates may be obtained by applying either the D'Alambert principle or work formulation based on the conservation of energy. The first exact solution of the free vibration problem for rectangular plates, whose two opposite sides are simply supported, was achieved by Voight [45]. Ritz [46] used the problem of free vibration of a rectangular plate with free edges to demonstrate his famous method for extending the Rayleigh principle for obtaining upper bounds on vibration frequencies. Poisson [7] analyzed the free vibration equation for circular plates. The monographs by Timoshenko and Young [47], Den Hartog [48], Thompson [49], etc., contain a comprehensive analysis and design considerations of free and forced vibrations of plates of various shapes. A reference book by Leissa [50] presents a considerable set of available results for the frequencies and mode shapes of free vibrations of plates could be provided for the design and for a researcher in the field of plate vibrations.

The recent trend in the development of plate theories is characterized by a heavy reliance on modern high-speed computers and the development of the most complete computer-oriented numerical methods, as well as by introduction of more rigorous theories with regard to various physical effects, types of loading, etc.

The above summary is a very brief survey of the historical background of the plate bending theory and its application. The interested reader is referred to special monographs [51,52] where this historical development of plates is presented in detail.

1.3 GENERAL BEHAVIOR OF PLATES

Consider a load-free plate, shown in Fig.1.3, in which the xy plane coincides with the plate's midplane and the z coordinate is perpendicular to it and is directed downwards. The fundamental assumptions of the linear, elastic, small-deflection theory of bending for thin plates may be stated as follows:

1. The material of the plate is elastic, homogeneous, and isotropic.
2. The plate is initially flat.
3. The deflection (the normal component of the displacement vector) of the midplane is small compared with the thickness of the plate. The slope of the deflected surface is therefore very small and the square of the slope is a negligible quantity in comparison with unity.
4. The straight lines, initially normal to the middle plane before bending, remain straight and normal to the middle surface during the deformation,

and the length of such elements is not altered. This means that the vertical shear strains γ_{xz} and γ_{yz} are negligible and the normal strain ε_z may also be omitted. This assumption is referred to as the "*hypothesis of straight normals*."

5. The stress normal to the middle plane, σ_z, is small compared with the other stress components and may be neglected in the stress–strain relations.
6. Since the displacements of a plate are small, it is assumed that the middle surface remains unstrained after bending.

Many of these assumptions, known as *Kirchhoff's hypotheses*, are analogous to those associated with the simple bending theory of beams. These assumptions result in the reduction of a three-dimensional plate problem to a two-dimensional one. Consequently, the governing plate equation can be derived in a concise and straightforward manner. The plate bending theory based on the above assumptions is referred to as the *classical* or *Kirchhoff's plate theory*. Unless otherwise stated, the validity of the Kirchhoff plate theory is assumed throughout this book.

1.4 SURVEY OF ELASTICITY THEORY

The classical theories of plates and shells are an important application of the theory of elasticity, which deals with relationships of forces, displacements, stresses, and strains in an elastic body. When a solid body is subjected to external forces, it deforms, producing internal strains and stresses. The deformation depends on the geometrical configuration of the body, on applied loading, and on the mechanical properties of its material. In the theory of elasticity we restrict our attention to *linear elastic materials*; i.e., the relationships between stress and strain are linear, and the deformations and stresses disappear when the external forces are removed. The classical theory of elasticity assumes the material is *homogeneous* and *isotropic*, i.e., its mechanical properties are the same in all directions and at all points.

The present section contains only a brief survey of the elasticity theory that will be useful for the development of the plate theory. All equations and relations will be given without derivation. The reader who desires to review details is urged to refer to any book on elasticity theory – for example [53–55].

1.4.1 Stress at a point: stress tensor

Consider an elastic body of any general shape subjected to external loads which are in equilibrium. Then, consider a material point anywhere in the interior of the body. If we assign a Cartesian coordinate frame with axes x, y, and z, as shown in Fig. 1.5, it is convenient to assign an infinitesimal element in the form of parallelepiped $(\mathrm{d}x, \mathrm{d}y, \mathrm{d}z)$, with faces parallel to the coordinate planes. Stresses acting on the faces of this element describe the intensity of the internal forces at a point on a particular face. These stresses can be broken down into a normal component (*normal stress*) and tangent component (*shear stress*) to the particular face. As a result, the three stress components, denoted by $\sigma_{xx}, \tau_{xy}, \tau_{xz}, \ldots,$ will act on each face of the element. The subscript notation for the stress components is interpreted as follows: the first subscript indicates the direction of an outer normal to the face on which the stress component acts; the second subscript relates to the direction of the stress itself.

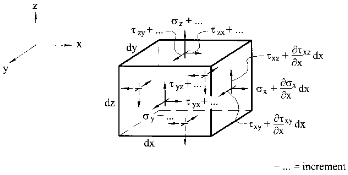
z
x
y
$\sigma_z + \ldots$
$\tau_{zy} + \ldots$
$\tau_{zx} + \ldots$
dy
$\tau_{xz} + \frac{\partial \tau_{xz}}{\partial x} dx$
$\tau_{yz} + \ldots$
$\sigma_x + \frac{\partial \sigma_x}{\partial x} dx$
dz
$\tau_{yx} + \ldots$
$\sigma_y - \ldots$
$\tau_{xy} + \frac{\partial \tau_{xy}}{\partial x} dx$
dx
$- \ldots$ = increment

Fig. 1.5

Repeated subscripts will be omitted in the future, i.e., the normal stresses will have only one subscript indicating the stress direction. The following sign convention will be adapted for the stress components: the positive sign for the normal stress will correspond to a tensile stress, while the negative sign will correspond to a compressive stress. The sign agreement for the shear stresses follows from the relationship between the direction of an outer normal drawn to a particular face and the direction of the shear stress component on the same face. If both the outer normal and the shear stress are either in positive or negative directions relative to the coordinate axes, then the shear stress is positive. If the outer normal points in a positive direction while the stress is in a negative direction (or vice versa), the shear stress is negative. On this basis, all the stress components shown in Fig. 1.5 are positive. On any one face these three stress components comprise a vector, called a *surface traction*. The above-mentioned set of the stress components acting on the faces of the element forms the *stress tensor*, T_{S}, i.e.,

$$T_{\mathrm{S}} = \begin{pmatrix} \sigma_x \tau_{xy} \tau_{xz} \\ \tau_{yx} \sigma_y \tau_{yz} \\ \tau_{zx} \tau_{zy} \sigma_z \end{pmatrix}, \tag{1.1}$$

which is symmetric with respect to the principal diagonal because of the *reciprocity law of shear stresses*, i.e.,

$$\tau_{xy} = \tau_{yx};\ \tau_{xz} = \tau_{zx};\ \tau_{yz} = \tau_{zy}. \tag{1.2}$$

Thus, only the six stress components out of nine in the stress tensor (1.1) are independent. The stress tensor, T_{S}, completely characterizes the three-dimensional state of stress at a point of interest.

For elastic stress analysis of plates, the two-dimensional state of stress is of special importance. In this case, $\sigma_z = \tau_{yz} = \tau_{xz} = 0$; thus, the two-dimensional stress tensor has a form

$$T_{\mathrm{S}} = \begin{pmatrix} \sigma_x \tau_{xy} \\ \tau_{yx} \sigma_y \end{pmatrix}, \text{ where } \tau_{xy} = \tau_{yx} \tag{1.3}$$

1.4.2 Strains and displacements

Assume that the elastic body shown in Fig. 1.6 is supported in such a way that rigid body displacements (translations and rotations) are prevented. Thus, this body deforms under the action of external forces and each of its points has small elastic displacements. For example, a point M had the coordinates x, y, and z in initial undeformed state. After deformation, this point moved into position $M'$and its coordinates became the following $x' = x + u$, $y' = y + v$, $z' = z' + w$, where u, v, and w are projections of the displacement vector of point M, vector $\mathbf{MM}'$, on the coordinate axes x, y and z. In the general case, u, v, and w are functions of x, y, and z.

Again, consider an infinitesimal element in the form of parallelepiped enclosing point of interest M. Assuming that a deformation of this parallelepiped is small, we can represent it in the form of the six simplest deformations shown in Fig. 1.7. The first three deformations shown in Fig. 1.7a, b, and c define the elongation (or contraction) of edges of the parallelepiped in the direction of the coordinate axes and can be defined as

$$\varepsilon_x = \frac{\delta(\mathrm{d}x)}{\mathrm{d}x},\ \varepsilon_y = \frac{\delta(\mathrm{d}y)}{\mathrm{d}y},\ \varepsilon_z = \frac{\delta(\mathrm{d}z)}{\mathrm{d}z}, \tag{1.4}$$

and they are called the *normal* or *linear strains*. In Eqs (1.4), the increments $\delta \mathrm{d}x$ can be expressed by the second term in the Taylor series, i.e., $\delta \mathrm{d}x = (\partial u/\partial x)\mathrm{d}x$, etc.; thus, we can write

$$\varepsilon_x = \frac{\partial u}{\partial x},\ \varepsilon_y = \frac{\partial v}{\partial y},\ \varepsilon_z = \frac{\partial w}{\partial z}. \tag{1.5a}$$

The three other deformations shown in Fig. 1.7d, e, and f are referred to as *shear strains* because they define a distortion of an initially right angle between the edges of the parallelepiped. They are denoted by γ_{xy}, γ_{xz}, and γ_{yz}. The subscripts indicate the coordinate planes in which the shear strains occur. Let us determine, for example, the shear strain in the xy coordinate plane. Consider the projection of the parallelepiped, shown in Fig. 1.7d, on this coordinate plane. Figure 1.8 shows this projec-

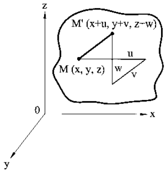

Fig. 1.6

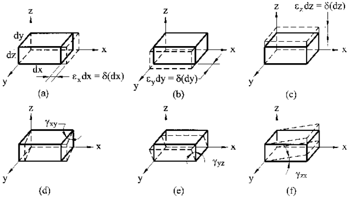
z
dy
dz
x
dx
y
$\varepsilon_x dx = \delta(dx)$
(a)
z
x
y
$\varepsilon_y dy = \delta(dy)$
(b)
z
$\varepsilon_z dz = \delta(dz)$
x
y
(c)
z
γ_{xy}
x
y
(d)
z
x
γ_{yz}
y
(e)
z
x
y
γ_{zx}
(f)

Fig. 1.7

tion in the form of the rectangle before deformation ($ABCD$) and after deformation ($A'B'C'D'$). The angle BAD in Fig. 1.8 deforms to the angle $B'A'D'$, the deformation being the angle $\gamma' + \gamma''$; thus, the shear strain is

$$\gamma_{xy} = \gamma' + \gamma'' \tag{a}$$

or it can be determined in terms of the in-plane displacements, u and v, as follows:

$$\gamma_{xy} = \frac{\frac{\partial v}{\partial x}\mathrm{d}x}{\mathrm{d}x + \frac{\partial u}{\partial x}\mathrm{d}x} + \frac{\frac{\partial u}{\partial y}\mathrm{d}y}{\mathrm{d}y + \frac{\partial v}{\partial y}\mathrm{d}y} = \frac{\frac{\partial v}{\partial x}}{1 + \frac{\partial u}{\partial x}} + \frac{\frac{\partial u}{\partial y}}{1 + \frac{\partial v}{\partial y}}.$$

Since we have confined ourselves to the case of very small deformations, we may omit the quantities $\partial u/\partial x$ and $\partial v/\partial y$ in the denominator of the last expression, as being negligibly small compared with unity. Finally, we obtain

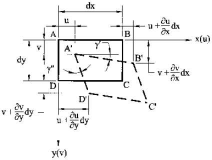
dx
u
$u + \frac{\partial u}{\partial x}dx$
A
B
x(u)
v
A'
γ'
dy
B'
$v + \frac{\partial v}{\partial x}dx$
γ''
D
C
D'
C'
$v + \frac{\partial v}{\partial y}dy$
$u + \frac{\partial u}{\partial y}dy$
y(v)

Fig. 1.8

$$w^z = w(x, y),\ \ u^z = -z\frac{\partial w}{\partial x},\ \ v^z = -z\frac{\partial w}{\partial y}. \tag{2.3}$$

As it follows from the above, the displacements u^z and v^z of an arbitrary horizontal layer vary linearly over a plate thickness while the deflection does not vary over the thickness.

Figure 2.1 shows a section of the plate by a plane parallel to Oxz, $y = \text{const.}$, before and after deformation. Consider a segment AB in the positive z direction. We focus on an arbitrary point B which initially lies at a distance z from the undeformed middle plane (from the point A). During the deformation, point A displaces a distance w parallel to the original z direction to point A_1. Since the transverse shear deformations are neglected, the deformed position of point B must lie on the normal to the deformed middle plane erected at point A_1(assumption (4)). Its final position is denoted by B_1. Due to the assumptions (4) and (5), the distance z between the above-mentioned points during deformation remains unchanged and is also equal to z.

We can also represent the displacement components u^z and v^z, Eqs (2.2), in the form

$$u^z = -z\vartheta_x,\ \ v^z = -z\vartheta_y, \tag{2.4}$$

where

$$\vartheta_x = \frac{\partial w}{\partial x},\ \ \vartheta_y = \frac{\partial w}{\partial y} \tag{2.5}$$

are the angles of rotation of the normal (normal I–I in Fig. 2.1) to the middle surface in the Oxz and Oyz plane, respectively. Owing to the assumption (4) of Sec. 1.3, ϑ_x and ϑ_y are also slopes of the tangents to the traces of the middle surface in the above-mentioned planes.

Substitution of Eqs (2.3) into the first two Eqs (1.5a) and into the first Eq. (1.5b), yields

$$\varepsilon_x^z = -z\frac{\partial^2 w}{\partial x^2},\ \ \varepsilon_y^z = -z\frac{\partial^2 w}{\partial y^2},\ \ \gamma_{xy}^z = -2z\frac{\partial^2 w}{\partial x \partial y}, \tag{2.6}$$

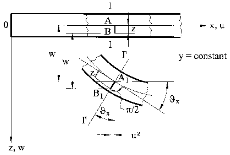

Fig. 2.1

where the superscript z refers to the in-plane strain components at a point of the plate located at a distance z from the middle surface. Since the middle surface deformations are neglected due to the assumption (6), from here on, this superscript will be omitted for all the strain and stress components at points across the plate thickness.

The second derivatives of the deflection on the right-hand side of Eqs. (2.6) have a certain geometrical meaning. Let a section MNP represent some plane curve in which the middle surface of the deflected plate is intersected by a plane $y = const$. (Fig. 2.2).

Due to the assumption 3 (Sec. 1.3), this curve is shallow and the square of the slope angle may be regarded as negligible compared with unity, i.e., $(\partial w/\partial x)^2 \ll 1$. Then, the second derivative of the deflection, $\partial^2 w/\partial x^2$ will define approximately the curvature of the section along the x axis, χ_x. Similarly, $\partial^2 w/\partial y^2$ defines the curvature of the middle surface χ_y along the y axis. The curvatures χ_x and χ_y characterize the phenomenon of bending of the middle surface in planes parallel to the Oxz and Oyz coordinate planes, respectively. They are referred to as *bending curvature* and are defined by

$$\chi_x = \frac{1}{\rho_x} = -\frac{\partial^2 w}{\partial x^2},\ \chi_y = \frac{1}{\rho_y} = -\frac{\partial^2 w}{\partial y^2} \tag{2.7a}$$

We consider a bending curvature positive if it is convex downward, i.e., in the positive direction of the z axis. The negative sign is taken in Eqs. (2.7a) since, for example, for the deflection convex downward curve MNP (Fig. 2.2), the second derivative, $\partial^2 w/\partial x^2$ is negative.

The curvature $\partial^2 w/\partial x^2$ can be also defined as the rate of change of the angle $\vartheta_x = \partial w/\partial x$ with respect to distance x along this curve. However, the above angle can vary in the y direction also. It is seen from comparison of the curves MNP and $M_1N_1P_1$ (Fig. 2.2), separated by a distance dy. If the slope for the curve MNP is $\partial w/\partial x$ then for the curve $M_1N_1P_1$ this angle becomes equal to $\left[\frac{\partial w}{\partial x} - \frac{\partial}{\partial y}\left(\frac{\partial w}{\partial x}\right)dy\right]$ or $\left(\frac{\partial w}{\partial x} - \frac{\partial^2 w}{\partial x \partial y}dy\right)$. The rate of change of the angle $\partial w/\partial x$ per unit length will be $(-\partial^2 w/\partial x \partial y)$. The negative sign is taken here because it is assumed

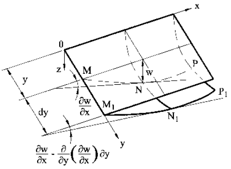

Fig. 2.2

that when y increases, the slope angle of the tangent to the curve decreases (by analogy with the sign convention for the bending curvatures χ_x and χ_y). Similarly, can be convinced that in the perpendicular section (for the variable x), the rate of change of the angle $\partial w/\partial y$ is characterized by the same mixed derivative $(-\partial^2 w/\partial x \partial y)$. By analogy with the torsion theory of rods, the derivative $\partial^2 w/\partial x \partial y$ defines the warping of the middle surface at a point with coordinates x and y is called the *twisting curvature with respect to the* x *and* y *axes and is denotes by* χ_{xy}. Thus,

$$\chi_{xy} = \chi_{yx} = \frac{1}{\rho_{xy}} = -\frac{\partial^2 w}{\partial x \partial y} \tag{2.7b}$$

Taking into account Eqs (2.7) we can rewrite Eqs (2.6) as follows

$$\varepsilon_x = z\chi_x; \;\; \varepsilon_y = z\chi_y; \;\; \gamma_{xy} = 2z\chi_{xy}. \tag{2.8}$$

2.3 STRESSES, STRESS RESULTANTS, AND STRESS COUPLES

In the case of a three-dimensional state of stress, stress and strain are related by the Eqs (1.8) of the generalized Hooke's law. As was mentioned earlier, Kirchhoff's assumptions of Sec. 1.3 brought us to Eqs (2.1). From a mathematical standpoint, this means that the three new equations (2.1) are added to the system of governing equations of the theory of elasticity. So, the latter becomes overdetermined and, therefore, it is necessary to also drop three equations. As a result, the three relations out of six of Hookes' law (see Eqs (1.8)) for strains (2.1) are discarded. Moreover, the normal stress component $\sigma_z = 0$. Solving Eqs (1.8) for stress components σ_x, σ_y, and τ_{xy}, yields

$$\sigma_x = \frac{E}{1-\nu^2}(\varepsilon_x + \nu\varepsilon_y); \;\; \sigma_y = \frac{E}{1-\nu^2}(\varepsilon_y + \nu\varepsilon_x); \;\; \tau_{xy} = G\gamma_{xy}. \tag{2.9}$$

The stress components are shown in Fig. 2.3a. The subscript notation and sign convention for the stresses were given in Sec. 1.4.

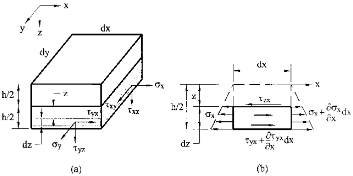

Fig. 2.3

Introducing the plate curvatures, Eqs (2.7) and using Eqs (2.8), the above equations appear as follows:

$$\begin{aligned}
\sigma_x &= \frac{Ez}{1-\nu^2}(\chi_x + \nu\chi_y) = -\frac{Ez}{1-\nu^2}\left(\frac{\partial^2 w}{\partial x^2} + \nu\frac{\partial^2 w}{\partial y^2}\right);\\
\sigma_y &= \frac{Ez}{1-\nu^2}(\chi_y + \nu\chi_x) = -\frac{Ez}{1-\nu^2}\left(\frac{\partial^2 w}{\partial y^2} + \nu\frac{\partial^2 w}{\partial x^2}\right);\\
\tau_{xy} &= \frac{Ez}{1+\nu}\chi_{xy} = -\frac{Ez}{1+\nu}\frac{\partial^2 w}{\partial x \partial y}.
\end{aligned} \tag{2.10}$$

It is seen from Eqs. (2.10) that Kirchhoff's assumptions have led to a completely defined law of variation of the stresses through the thickness of the plate. Therefore, as in the theory of beams, it is convenient to introduce, instead of the stress components at a point problem, the total statically equivalent forces and moments applied to the middle surface, which are known as the *stress resultants* and *stress couples*. The stress resultants and stress couples are referred to as the *shear forces*, Q_x and Q_y, as well as the *bending* and *twisting moments* M_x, M_y, and M_{xy}, respectively. Thus, Kirchhoff's assumptions have reduced the three-dimensional plate straining problem to the two-dimensional problem of straining the middle surface of the plate. Referring to Fig. 2.3, we can express the bending and twisting moments, as well as the shear forces, in terms of the stress components, i.e.,

$$\begin{Bmatrix} M_x \\ M_y \\ M_{xy} \end{Bmatrix} = \int_{-h/2}^{h/2} \begin{Bmatrix} \sigma_x \\ \sigma_y \\ \tau_{xy} \end{Bmatrix} z\mathrm{d}z \tag{2.11}$$

and

$$\begin{Bmatrix} Q_x \\ Q_y \end{Bmatrix} = \int_{-h/2}^{h/2} \begin{Bmatrix} \tau_{xz} \\ \tau_{yz} \end{Bmatrix} \mathrm{d}z. \tag{2.12}$$

Because of the reciprocity law of shear stresses ($\tau_{xy} = \tau_{yx}$), the twisting moments on perpendicular faces of an infinitesimal plate element are identical, i.e., $M_{yx} = M_{xy}$.

The sign convention for the shear forces and the twisting moments is the same as that for the shear stresses (see Sec. 1.4). A positive bending moment is one which results in positive (tensile) stresses in the bottom half of the plate. Accordingly, all the moments and the shear forces acting on the element in Fig. 2.4 are positive.

Note that the relations (2.11) and (2.12) determine the intensities of moments and shear forces, i.e., moments and forces per unit length of the plate midplane. Therefore, they have dimensional units as [*force* $\cdot$ *length*/*length*] or simply [*force*] for moments and [*force*/*length*] for shear forces, respectively.

It is important to mention that while the theory of thin plates omits the effect of the strain components $\gamma_{xz} = \tau_{xz}/G$ and $\gamma_{yz} = \tau_{yz}/G$ on bending, the vertical shear forces Q_x and Q_y are not negligible. In fact, they are necessary for equilibrium of the plate element.

tions of equilibrium for a plate element under a general state of stress (1.10) (assuming that the body forces are zero) serve well for this purpose, however. If the faces of the plate are free of any tangent external loads, then τ_{xz} and τ_{yz} are zero for $z = \pm h/2$. From the first two Eqs (1.10) and Eqs (2.9) and (2.10), the shear stresses τ_{xz} (Fig. 2.3(b)) and τ_{yz} are

$$\begin{aligned} \tau_{xz} &= -\int\limits_{-h/2}^{h/2} \left(\frac{\partial \sigma_x}{\partial x} + \frac{\partial \tau_{xy}}{\partial y} \right) \mathrm{d}z = \frac{E\left(z^2 - h^2/4\right)}{2\left(1 - \nu^2\right)} \frac{\partial}{\partial x} \nabla^2 w, \\ \tau_{yz} &= -\int\limits_{-h/2}^{h/2} \left(\frac{\partial \sigma_y}{\partial y} + \frac{\partial \tau_{yx}}{\partial x} \right) \mathrm{d}z = \frac{E\left(z^2 - h^2/4\right)}{2\left(1 - \nu^2\right)} \frac{\partial}{\partial y} \nabla^2 w, \end{aligned} \tag{2.16}$$

where $\nabla^2(\ )$ is the *Laplace operator*, given by

$$\nabla^2 w = \frac{\partial^2 w}{\partial x^2} + \frac{\partial^2 w}{\partial y^2}. \tag{2.17}$$

It is observed from Eqs (2.15) and (2.16) that the stress components σ_x, σ_y, and τ_{xy} (in-plane stresses) vary linearly over the plate thickness, whereas the shear stresses τ_{xz} and τ_{yz} vary according to a parabolic law, as shown in Fig. 2.5.

The component σ_z is determined by using the third of Eqs (1.10), upon substitution of τ_{xz} and τ_{yz} from Eqs (2.16) and integration. As a result, we obtain

$$\sigma_z = -\frac{E}{2(1 - \nu^2)} \left(\frac{h^3}{12} - \frac{h^2 z}{4} + \frac{z^3}{3} \right) \nabla^2 \nabla^2 w. \tag{2.18}$$

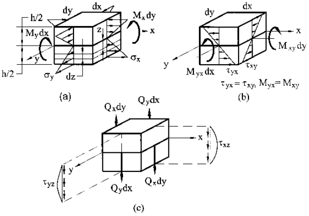

Fig. 2.5

2.4 GOVERNING EQUATION FOR DEFLECTION OF PLATES IN CARTESIAN COORDINATES

The components of stress (and, thus, the stress resultants and stress couples) generally vary from point to point in a loaded plate. These variations are governed by the static conditions of equilibrium.

Consider equilibrium of an element $\mathrm{d}x \times \mathrm{d}y$ of the plate subject to a vertical distributed load of intensity $p(x, y)$ applied to an upper surface of the plate, as shown in Fig. 2.4. Since the stress resultants and stress couples are assumed to be applied to the middle plane of this element, a distributed load $p(x, y)$ is transferred to the midplane. Note that as the element is very small, the force and moment components may be considered to be distributed uniformly over the midplane of the plate element: in Fig. 2.4 they are shown, for the sake of simplicity, by a single vector. As shown in Fig. 2.4, in passing from the section x to the section $x + \mathrm{d}x$ an intensity of stress resultants changes by a value of partial differential, for example, by $\partial M_x = \frac{\partial M_x}{\partial x}\mathrm{d}x$. The same is true for the sections y and $y + \mathrm{d}y$. For the system of forces and moments shown in Fig. 2.4 , the following three independent conditions of equilibrium may be set up:

(a) The force summation in the z axis gives

$$\frac{\partial Q_x}{\partial x}\mathrm{d}x\mathrm{d}y + \frac{\partial Q_y}{\partial y}\mathrm{d}x\mathrm{d}y + p\mathrm{d}x\mathrm{d}y = 0,$$

from which

$$\frac{\partial Q_x}{\partial x} + \frac{\partial Q_y}{\partial y} + p = 0. \tag{2.19}$$

(b) The moment summation about the x axis leads to

$$\frac{\partial M_{xy}}{\partial x}\mathrm{d}x\mathrm{d}y + \frac{\partial M_y}{\partial y}\mathrm{d}x\mathrm{d}y - Q_y\mathrm{d}x\mathrm{d}y = 0$$

or

$$\frac{\partial M_{xy}}{\partial x} + \frac{\partial M_y}{\partial y} - Q_y = 0. \tag{2.20}$$

Note that products of infinitesimal terms, such as the moment of the load p and the moment due to the change in Q_y have been omitted in Eq. (2.20) as terms with a higher order of smallness.

(c) The moment summation about the y axis results in

$$\frac{\partial M_{yx}}{\partial y} + \frac{\partial M_x}{\partial x} - Q_x = 0. \tag{2.21}$$

It follows from the expressions (2.20) and (2.21), that the shear forces Q_x and Q_y can be expressed in terms of the moments, as follows:

$$Q_x = \frac{\partial M_x}{\partial x} + \frac{\partial M_{xy}}{\partial y} \tag{2.22a}$$

$$\sigma_z = -\frac{3p}{4}\left[\frac{2}{3} - \frac{2z}{h} + \frac{1}{3}\left(\frac{2z}{h}\right)^3\right]. \tag{2.28}$$

The maximum shear stress, as in the case of a beam of rectangular cross section, occurs at $z = 0$ (see Fig. 2.5), and is represented by the formula

$$\max.\tau_{xz} = \frac{3}{2}\frac{Q_x}{h}, \quad \max.\tau_{yz} = \frac{3}{2}\frac{Q_y}{h}.$$

It is significant that the sum of the bending moments defined by Eqs (2.13) is invariant; i.e.,

$$M_x + M_y = -D(1+\nu)\left(\frac{\partial^2 w}{\partial x^2} + \frac{\partial^2 w}{\partial y^2}\right) = -D(1+\nu)\nabla^2 w$$

or

$$\frac{M_x + M_y}{1+\nu} = -D\nabla^2 w \tag{2.29}$$

Letting M denote the moment function or the so-called moment sum,

$$M = \frac{M_x + M_y}{1+\nu} = -D\nabla^2 w, \tag{2.30}$$

the expressions for the shear forces can be written as

$$Q_x = \frac{\partial M}{\partial x}, \quad Q_y = \frac{\partial M}{\partial y} \tag{2.31}$$

and we can represent Eq. (2.24) in the form

$$\begin{aligned} \frac{\partial^2 M}{\partial x^2} + \frac{\partial^2 M}{\partial y^2} &= -p, \\ \frac{\partial^2 w}{\partial x^2} + \frac{\partial^2 w}{\partial y^2} &= -\frac{M}{D}. \end{aligned} \tag{2.32}$$

Thus, the plate bending equation $\nabla^4 w = p/D$ is reduced to two second-order partial differential equations which are sometimes preferred, depending upon the method of solution to be employed.

Summarizing the arguments set forth in this section, we come to the conclusion that the deformation of a plate under the action of the transverse load $p(x, y)$ applied to its upper plane is determined by the differential equation (2.24). This deformation results from:

(a) bending produced by bending moments M_x and M_y, as well as by the shear forces Q_x and Q_y;
(b) torsion produced by the twisting moments $M_{xy} = M_{yz}$.

Both of these phenomena are generally inseparable in a plate. Indeed, let us replace the plate by a flooring composed of separate rods, each of which will bend under the action of the load acting on it irrespective of the neighboring rods. Let them now be tied together in a solid slab (plate). If we load only one rod, then, deflecting, it will carry along the adjacent rods, applying to their faces those shear forces which we have designated here by Q_x and Q_y. These forces will cause rotation of the cross section, i.e., twisting of the rod. This approximation of a plate with a grillage of rods (or beams) is known as the “grillage, or gridwork analogy” [3].

2.5 BOUNDARY CONDITIONS

As pointed out earlier, the boundary conditions are the known conditions on the surfaces of the plate which must be prescribed in advance in order to obtain the solution of Eq. (2.24) corresponding to a particular problem. Such conditions include the load $p(x, y)$ on the upper and lower faces of the plate; however, the load has been taken into account in the formulation of the general problem of bending of plates and it enters in the right-hand side of Eq. (2.24). It remains to clarify the conditions on the cylindrical surface, i.e., at the edges of the plate, depending on the fastening or supporting conditions. For a plate, the solution of Eq. (2.24) requires that two boundary conditions be satisfied at each edge. These may be a given deflection and slope, or force and moment, or some combination of these.

For the sake of simplicity, let us begin with the case of rectangular plate whose edges are parallel to the axes Ox and Oy. Figure 2.6 shows the rectangular plate one edge of which ($y = 0$) is built-in, the edge $x = a$ is simply supported, the edge $x = 0$ is supported by a beam, and the edge $y = b$ is free.

We consider below all the above-mentioned boundary conditions:

(1) *Clamped, or built-in, or fixed edge* $y = 0$

At the clamped edge $y = 0$ the deflection and slope are zero, i.e.,

$$w = 0|_{y=0} \quad \text{and} \quad \vartheta_y \equiv \frac{\partial w}{\partial y} = 0\bigg|_{y=0}. \tag{2.33}$$

(2) *Simply supported edge* $x = a$

At these edges the deflection and bending moment M_x are both zero, i.e.,

$$w = 0|_{x=a}, \quad M_x = -D\left(\frac{\partial^2 w}{\partial x^2} + \nu\frac{\partial^2 w}{\partial y^2}\right) = 0\bigg|_{x=a}. \tag{2.34}$$

The first of these equations implies that along the edge $x = a$ all the derivatives of w with respect to y are zero, i.e., if $x = a$ and $w = 0$, then $\frac{\partial w}{\partial y} = \frac{\partial^2 w}{\partial y^2} = 0$.

It follows that conditions expressed by Eqs (2.34) may appear in the following equivalent form:

$$w = 0|_{x=a}, \quad \frac{\partial^2 w}{\partial x^2} = 0\bigg|_{x=a}. \tag{2.35}$$

(3) *Free edge* $y = b$

Suppose that the edge $y = b$ is perfectly free. Since no stresses act over this edge, then it is reasonable to equate all the stress resultants and stress couples occurring at points of this edge to zero, i.e.,

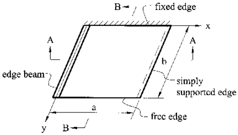

Plane View

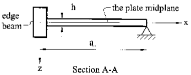

Section A-A

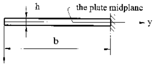

Section B-B

Fig. 2.6

$$M_y = 0\big|_{y=b},\ \ Q_y = 0\big|_{y=b},\ \ M_{yx} = 0\big|_{y=b} \tag{2.36}$$

and this gives three boundary conditions. These conditions were formulated by Poisson.

It has been mentioned earlier that three boundary conditions are too many to be accommodated in the governing differential equation (2.24). Kirchhoff suggested the following way to overcome this difficulty. He showed that conditions imposed on the twisting moment and shear force are not independent for the presented small-deflection plate bending theory and may be reduced to one condition only. It should be noted that Lord Kelvin (Thomson) gave a physical explanation of this reduction [4].

Figure 2.7a shows two adjacent elements, each of length dx belonging to the edge $y = b$. It is seen that, a twisting moment $M_{yx}\mathrm{d}x$ acts on the left-hand element, while the right-hand element is subjected to $\left[M_{yx} + \left(\partial M_{yx}/\partial x\right)\mathrm{d}x\right]\mathrm{d}x$. These moments are resultant couples produced by a system of horizontal shear stresses τ_{yx}. Replace them by couples of vertical forces M_{yx} and $M_{yx} + \frac{\partial M_{yx}}{\partial x}\mathrm{d}x$ with the

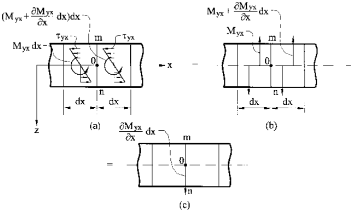

Fig. 2.7

moment arm dx having the same moment (Fig. 2.7b), i.e., as if rotating the above-mentioned couples of horizontal forces through 90°.

Such statically equivalent replacement of couples of horizontal forces by couples of vertical forces is well tolerable in the context of Kirchhoff's plate bending theory. Indeed, small elements to which they are applied can be considered as absolutely rigid bodies (owing to assumption (4)). It is known that the above-mentioned replacement is quite legal for such a body because it does not disturb the equilibrium conditions, and any moment may be considered as a free vector.

Forces M_{yx} and $M_{yx} + \frac{\partial M_{yx}}{\partial x}\mathrm{d}x$ act along the line mn (Fig. 2.7b) in opposite directions. Having done this for all elements of the edge $y = b$ we see that at the boundaries of two neighboring elements a single unbalanced force $(\partial M_{yx}/\partial x)\mathrm{d}x$ is applied at points of the middle plane (Fig. 2.7c).

Thus, we have established that the twisting moment M_{yx} is statically equivalent to a distributed shear force of an intensity $\partial M_{yx}/\partial x$ along the edge $y = b$, for a smooth boundary. Proceeding from this, Kirchhoff proposed that the three boundary conditions at the free edge be combined into two by equating to zero the bending moment M_y and the so-called *effective shear force* per unit length V_y. The latter is equal to the sum of the shear force Q_y plus an unbalanced force $\partial M_{yx}/\partial x$, which reflects the influence of the twisting moment M_{yx} (for the edge $y = b$). Now we arrive at the following two conditions at the free edge:

$$M_y = 0\big|_{y=b}, \quad V_y = 0\big|_{y=b} \tag{2.37}$$

where

$$V_y = Q_y + \frac{\partial M_{xy}}{\partial x}. \tag{2.38}$$

The effective shear force V_y can be expressed in terms of the deflection w using Eqs (2.13) and (2.27). As a result, we obtain

$$V_y = -D \frac{\partial}{\partial y}\left[\frac{\partial^2 w}{\partial y^2} + (2-\nu)\frac{\partial^2 w}{\partial x^2}\right]. \tag{2.39a}$$

In a similar manner, we can obtain the effective shear force at the edge parallel to the x axis, i.e.,

$$V_x = -D \frac{\partial}{\partial x}\left[\frac{\partial^2 w}{\partial x^2} + (2-\nu)\frac{\partial^2 w}{\partial y^2}\right] \tag{2.39b}$$

Finally, the boundary conditions (2.37) may be rewritten in terms of the deflection as follows

$$\left.\frac{\partial^2 w}{\partial y^2} + \nu \frac{\partial^2 w}{\partial x^2} = 0\right|_{y=b} \text{ and } \left.-\frac{\partial}{\partial y}\left[\frac{\partial^2 w}{\partial y^2} + (2-\nu)\frac{\partial^2 w}{\partial x^2}\right] = 0\right|_{y=b}. \tag{2.40}$$

Similarly, the boundary conditions for the free edge parallel to the x axis can be formulated. This form of the boundary conditions for a free edge is conventional.

It should be noted that transforming the twisting moments – as it was mentioned above – we obtain not only continuously distributed edge forces V_x and V_y but, in addition, also nonvanishing, finite concentrated forces at corner points (on each side of a corner) of a rectangular plate. These are numerically equal to the value of the corresponding twisting moment (Fig. 2.8). The direction and the total magnitude of the corner forces can be established by analyzing boundary conditions of a plate and the deflection surface produced by a given loading.

The concept of the corner forces is not limited to the intersection of two free boundaries, where they obviously must vanish. In general, any right angle corner where at least one of the intersecting boundaries can develop M_{xy} and M_{yx} will have a corner force. Consider, as an example, the case of symmetrically loaded, simply supported rectangular plate, as shown in Fig. 2.9.

At the corners, $x = a$ and $y = b$, the above-discussed action of the twisting moments (because $M_{xy} = M_{yx}$) results in

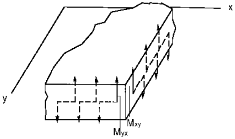

Fig. 2.8

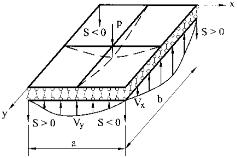

Fig. 2.9

$$S = 2M_{xy} = -2D(1-\nu)\frac{\partial^2 w}{\partial x \partial y}\bigg|_{x=a,y=b}. \tag{2.41}$$

Thus, the distributed twisting moments are statically equivalent to the distributed edge forces $\partial M_{yx}/\partial x$ and $\partial M_{xy}/\partial y$ over the plate boundary, as well as to the concentrated corner forces, $S = 2M_{xy}$ for a given rectangular plate. Note that the directions of the concentrated corner forces, S, are shown in Fig. 2.9 for a symmetrical downward directed loading of the plate. At the origin of the coordinate system, taking into account the nature of torsion of an adjacent element, we obtain for the moment M_{xy} and, consequently, for the force S, the minus sign. If we rotate the twisting moment $M_{xy} < 0$ through 90°, then we obtain at this corner point $(x = 0,\ y = 0)$ a downward force $S = 2M_{xy}$. At other corner points the signs of M_{xy} will alternate, but the above-mentioned corner forces will be directed downward everywhere for a symmetrical loading of a plate.

The concentrated corner force for plates having various boundary conditions may be determined similarly. In general, any right angle corner where at least one of the intersecting boundaries can develop M_{xy} or M_{yx} will have a corner force. For instance, when two adjacent plate edges are *fixed* or *free*, we have $S = 0$, since along these edges no twisting moments exist. If one edge of a plate is fixed and another one (perpendicular to the fixed edge) is simply supported, then $S = M_{xy}$. The case of non-right angle intersections will be examined later.

It is quite valid to utilize the above replacement of the shear force Q_y and twisting moment M_{xy} by the effective shear force V_y in the context of the approximate Kirchhoff's theory of plate bending, as it was mentioned earlier. But with respect to a real plate, equating of the effective shear force to zero does not mean that both the shear force and twisting moment are necessarily equal to zero. Hence, according to Kirchhoff's theory, we obtain such a solution when along a free edge, e.g., $y = \text{const}$, some system of shear stresses τ_{yz} (corresponding to Q_y) and τ_{yx} (corresponding to M_{yx}) is applied (of course, such a system of stresses and corresponding to them the stress resultants and stress couples appear on this free edge). This system is mutually balanced on the edge $y = \text{const}$ and it causes an additional stress field. The latter, however, due to Saint-Venant's principle, decays rapidly as we move away from this edge into the interior of the plate. The above-mentioned additional stress field cannot be determined by using the governing differential equation (2.24). Corrections can be obtained using the plate bending equations with regard to the shear strains γ_{xz} and γ_{yz} and will be discussed in Sec. 7.3. These corrections, as a rule, are negligible for solid isotropic plates.

(4) *Edge $x = 0$ supported by a beam*

The boundary conditions of the type (2.33), (2.35), and (2.37) are called *homogeneous* boundary conditions. *Nonhomogeneous* boundary conditions are commonly used in many important engineering structures – for example, when a plate is supported by an edge beam.

Assume that the cross section of the edge beam is symmetrical with respect to the middle surface of the plate and the edge beam has flexural and torsional rigidities. Since the edge beam and the plate are built monotonically (Fig. 2.10), they must have the same displacements and slopes.

$$w_{\mathrm{b}} = w\big|_{x=0} \quad \text{and} \quad \vartheta_{\mathrm{b}} = \vartheta\big|_{x=0} \quad \text{or} \quad \left(\frac{\partial \mathrm{w}}{\partial \mathrm{x}}\right)_{\mathrm{b}} = \frac{\partial w}{\partial x}\bigg|_{x=0}, \tag{2.42}$$

where the subscript b refers to the edge beam, and quantities relating to the plate have no subscripts.

Consider an element dy of the edge beam as a free body, as shown in Fig. 2.10. Equilibrium conditions of this element result in the following equations:

$$\sum F_z = 0{:} - Q_{\mathrm{b}} - V_x \mathrm{d}y + Q_{\mathrm{b}} + \frac{\mathrm{d}Q_{\mathrm{b}}}{\mathrm{d}y}\mathrm{d}y = 0$$

$$\sum M_y = 0{:} + T + M_x \mathrm{d}y - \left(T + \frac{\mathrm{d}T}{\mathrm{d}y}\mathrm{d}y\right) = 0 \quad \text{or}$$

$$V_x = \frac{\mathrm{d}Q_{\mathrm{b}}}{\mathrm{d}y}(0, y), \quad M_x = \frac{\mathrm{d}T}{\mathrm{d}y}(0, y) \tag{a}$$

where T is the twisting moment in the beam.

As it follows from the beam theory [5]

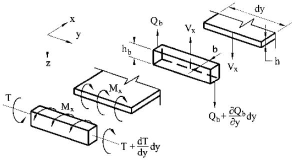

Fig. 2.10

$$\frac{\mathrm{d}Q_{\mathrm{b}}}{\mathrm{d}y}(0, y) = -(EI)_{\mathrm{b}} \frac{\partial^4 w_{\mathrm{b}}}{\partial y^4}(0, y) \quad \text{and} \tag{b}$$

$$T(0, y) = -(GJ)_{\mathrm{b}} \frac{d\vartheta_{\mathrm{b}}}{dy}(0, y) = -(GJ)_{\mathrm{b}} \frac{\partial^2 w_{\mathrm{b}}}{\partial x \partial y}(0, y), \tag{c}$$

where $(EI)_{\mathrm{b}}$ and $(GJ)_{\mathrm{b}}$ are the flexural rigidity and the torsional stiffness of the beam cross section, respectively.

Substituting (b) and (c) into Eq. (a) and taking into account the compatibility conditions (2.42), gives the boundary conditions for the plate edge $x = 0$ supported by the beam:

$$V_x = -(EI)_{\mathrm{b}} \frac{\partial^4 w_{\mathrm{b}}}{\partial y^4}\bigg|_{x=0}; \quad M_x = -(GJ)_{\mathrm{b}} \frac{\partial^3 w_{\mathrm{b}}}{\partial x \partial y^2}\bigg|_{x=0} \tag{2.43a}$$

Using the expressions for M_x and V_x, Eqs. (2.13), (2.39b), and Eqs (2.42), we can rewrite the boundary conditions (2.43a) in terms of w, as follows:

$$D\left[\frac{\partial^3 w}{\partial x^3} + (2 - \nu)\frac{\partial^3 w}{\partial x \partial y^2}\right] = (EI)_{\mathrm{b}} \frac{\partial^4 w}{\partial y^4}\bigg|_{x=0}; \quad D\left[\frac{\partial^2 w}{\partial x^2} + \nu \frac{\partial^2 w}{\partial y^2}\right] = (GJ)_{\mathrm{b}} \frac{\partial^3 w}{\partial x \partial y^2}\bigg|_{x=0}. \tag{2.43b}$$

Similar expressions can be written for edges $y = 0,\ b$.

Let us study the boundary conditions on skew edges. Consider a vertical section of the plate whose normal n makes an angle α with the x axis (Fig. 2.11a). Take the origin of the Cartesian coordinate system n (outward normal to the edge) and t (tangent to the edge) at some point of the edge. In a general case, the normal bending M_n and twisting M_{nt} moments, as well the transverse shear force Q_n will act at this section. Figure 2.11b shows the state of stress of a layer of the plate with the coordinate $z > 0$. The above moments at any point of the skew edge are

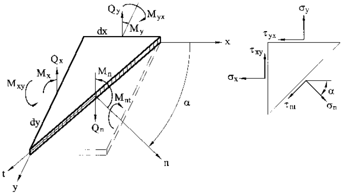

(a) (b)

Fig. 2.11

$$M_n = \int_{-h/2}^{h/2} \sigma_n z\mathrm{d}z, \quad M_{nt} = \int_{-h/2}^{h/2} \tau_{nt} z\mathrm{d}z. \tag{2.44}$$

The relationship between the stress components shown in Fig. 2.11b is given by [6,7]

$$\sigma_n = \sigma_x \cos^2\alpha + \sigma_y \sin^2\alpha + 2\tau_{xy}\cos\alpha\sin\alpha;$$
$$\tau_{nt} = \tau_{xy}\cos 2\alpha - (\sigma_x - \sigma_y)\sin\alpha\cos\alpha.$$

Substituting the above into Eqs (2.44), integrating over the plate thickness and taking into account Eqs (2.11), one obtains the following relationships

$$\begin{aligned} M_n &= M_x\cos^2\alpha + M_y\sin^2\alpha + M_{xy}\sin 2\alpha; \\ M_{nt} &= M_{xy}\cos 2\alpha - (M_x - M_y)\sin\alpha\cos\alpha. \end{aligned} \tag{2.45}$$

The shear force Q_n acting at a section of the edge having a normal n can be evaluated from condition of equilibrium of the plate element shown in Fig. 2.11a, as follows:

$$\begin{aligned} &Q_n\mathrm{d}s - Q_x\mathrm{d}y - Q_y\mathrm{d}x = 0, \text{ from which} \\ &\qquad Q_n = Q_x\cos\alpha + Q_y\sin\alpha. \end{aligned} \tag{2.46}$$

The effective shear force at a point of the skew edge can be determined similarly to (2.38), i.e.,

$$V_n = Q_n + \frac{\partial M_{nt}}{\partial t}, \tag{2.47}$$

where $\partial/\partial t$ denotes a differentiation with respect to the tangent of the skew edge.

The boundary conditions discussed above for rectilinear edge can be generalized to some curvilinear edge. Let n and t be the outward normal making the angle α with the x axis and tangent to the curvilinear edge at a point of interest (Fig. 2.12). Then the prescribed boundary conditions (2.33), (2.35), and (2.37), taking into account (2.47), can be rewritten at an arbitrary point of the above curvilinear edge, as follows:

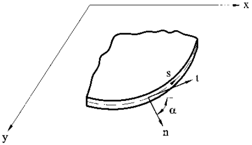

Fig. 2.12

(1) *Built-in curvilinear edge*

$$w = 0,\ \frac{\partial w}{\partial n} = 0. \tag{2.48a}$$

(2) *Simply supported edge*

$$w = 0,\ \ M_n = 0. \tag{2.48b}$$

(3) *Free curvilinear edge*

$$M_n = 0,\ V_n = Q_n + \frac{\partial M_{nt}}{\partial s} = 0. \tag{2.48c}$$

(4) *Curvilinear edge is elastically fixed*

$$w + \beta_1 V_n = 0, \frac{\partial w}{\partial n} + \beta_2 M_n = 0, \tag{2.48d}$$

where M_n and V_n are the normal bending moment and the normal effective shear force, respectively, defined by expressions (2.45) and (2.47). They can also be expressed in terms of the deflection w using Eqs (2.45)–(2.47) and Eqs (2.13) and (2.27). In Eqs (2.48) β_1 and β_2 are some coefficients that characterize a support compliance.

If adjacent edges of a plate have slopes of the normals α_1 and α_2 (Fig. 2.13), then the concentrated force S at a common corner point will be equal to

$$S = (M_{nt})_{\alpha_1} - (M_{nt})_{\alpha_2}. \tag{2.49}$$

When $\alpha_1 = 0$ *and* $\alpha_2 = \pi/2$ we will obtain the expression (2.41).

It is observed from the above that the boundary conditions are of the two basic kinds: *geometric* or *kinematic boundary conditions* describe edge constraint pertaining to deflection or slope; *static* or *natural boundary conditions* impose some restrictions on the internal forces and moments at the edges of the plate. Accordingly, in Eq. (2.48a) both conditions are kinematic; in Eq. (2.48c) they are both static; and in Eq. (2.48b) the boundary conditions are mixed.

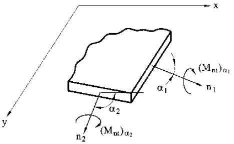

Fig. 2.13

2.6 VARIATIONAL FORMULATION OF PLATE BENDING PROBLEMS

It is known from the theory of elasticity that governing equations for stresses, strains, and displacements can be represented in the differential form. However, this is not a unique possible formulation of the problem for finding the stress–strain field of an elastic body. The problem of determining stresses, strains, and displacements can be reduced to some definite integral of one or another type of these functions called *functionals*. Then, the functions themselves (stresses, strains, and displacements) reflecting a real state of a body can be found from conditions of *extremum* for this functional. The mathematical techniques of such an approach is studied in the division of mathematics called the *calculus of variation*. Therefore, some postulates and statements that formulate properties of these functionals in the theory of elasticity are referred to as *variational principles*. The latter represent some basic theorems expressed in the form of integral equalities connecting stresses, strains, and displacements throughout the volume of a body and based on the properties of the work done by external and internal forces. A variety of powerful and efficient approximate methods for analysis of various linear and nonlinear problems of solid mechanics are based on the variational principles. Some of these methods will be described further in Chapter 6.

2.6.1 Strain energy of plates

A *functional* is a scalar quantity depending on some function or several functions, as from independent variables. The functional can be treated as a function of an infinite number of independent variables. The subject matter of the calculus of variation is searching of unknown functions $f_i(x, y, z)$ that give a maximum (minimum) or stationary value of a functional. For example,

$$\Pi = \iiint_V F\big[f_1(x, y, z), f_2(x, y, z), \ldots, f_n(x, y, z); f_1'(x, y, z), \ldots,$$
$$f_n'(x, y, z); x, y, z\big] \mathrm{d}V.$$

The above-mentioned functions for which the functional is maximum (minimum) or stationary are referred to as *extremals* of the given functional [8–11].

Let us consider a functional expressing the total potential energy of a deformed elastic body and the loads acting on it. The total potential energy, Π, consists of the strain energy of deformation (the potential of internal forces), U, and the potential energy of external forces (the potential of external forces), Ω, i.e.,

$$\Pi = U + \Omega. \tag{2.50}$$

By convention, let us assume that the potential energy at the initial, undeformed state, Π_0, is zero. Hence, the total energy Π presents a variation of the energy of internal and external forces in the transition from initial to deformed states. The potential energy of a body is measured by the work done by external and internal forces when this body returns from its final to an initial position (where it was mentioned above, $\Pi_0 = 0$).

Our study is mainly limited to linearly elastic bodies that dissipate no energy and have only one equilibrium configuration. We also require that loads keep the

brium. Hence, in this case, the total potential energy of a given system has a minimum. From the uniqueness theorem [6,7], the problem of the theory of elasticity, based on assumptions of small displacements and deformations defines only one equilibrium configuration, and this configuration of equilibrium is stable. Thus, if the small-deflection theory of an elastic body is being studied, then *the potential energy is a minimum in an equilibrium state*. So, the principle of minimum potential energy, proposed by Lagrange, can be formulated, as follows:

> Among all admissible configurations of an elastic body, the actual configuration (that satisfies static equilibrium conditions) makes the total potential energy, Π, stationary with respect to all small admissible virtual displacements. For stable equilibrium, Π is a minimum.

Notice that the above principle applies to a conservative system only.

It can be shown that the governing differential equation (2.24) and the boundary conditions (2.48) can be deduced from Lagrange's variational principle (2.64) [3,8–12]. However, the key importance of the variational principles discussed above is that they can be used to obtain approximate solutions of complicated problems of solid mechanics, in particular, plate-shell bending problems. These are obtained while avoiding mathematical difficulties associated with integration of differential equations in partial derivatives. The corresponding methods, called *variational methods* and based on the above-mentioned principles, are discussed further in Chapter 6. More complete information on the variational principles and their application in mechanics is available in the literature [8–12].

PROBLEMS

2.1 Verify the result given by Eq. (2.18).

2.2 Derive the governing differential equation for deflections of a plate subjected to a distributed moment load $m_x(x, y)$ and $m_y(x, y)$ applied to the middle surface.

2.3 Show that at the corner of a polygonal simply supported plate, $M_{xy} = 0$ unless the corner is 90°.

2.4 If a lateral deflection w is a known function of x and y, what are the maximum slope $\partial w/\partial n$ and the direction of axis n with respect to the x axis in terms of $\partial w/\partial x$ and $\partial w/\partial y$?

2.5 Show that the sum of bending curvatures in any two mutually perpendicular directions, n and t, at any point of the middle surface, is a constant, i.e.,

$$\chi_x + \chi_y = \chi_n + \chi_t = \text{const.}$$

2.6 Verify the expression given by Eq. (2.61).

2.7 Derive the expressions for the boundary quantities M_n, M_{nt}, and V_n in terms of the deflection w at a regular (smooth) point of the curvilinear contour of the plate using: (a) the local coordinates n and t where the coordinate n coincides with the direction of the outward normal and **t** – with the tangent direction to the boundary; (b) the intrinsic coordinates n and s, where s, is the arc length over the boundary.
Hint: use the following relations for part (b)

$$\frac{\partial \mathbf{n}}{\partial s} = \frac{1}{\rho}\mathbf{t}, \quad \frac{\partial \mathbf{t}}{\partial s} = -\frac{1}{\rho}\mathbf{n}$$

where **n** and **t** are the unit vectors of the intrinsic coordinate system directed along the outward normal and tangent to the boundary, respectively.

3

Rectangular Plates

3.1 INTRODUCTION

We begin the application of the developed plate bending theory with thin rectangular plates. These plates represent an excellent model for development and as a check of various methods for solving the governing differential equation (2.24).

In this chapter we consider some mathematically ''exact'' solutions in the form of double and single trigonometric series applied to rectangular plates with various types of supports and transverse loads, plates on an elastic foundation, continuous plates, etc.

3.2 THE ELEMENTARY CASES OF PLATE BENDING

Let us consider some elementary examples of plate bending of great importance for understanding how a plate resists the applied loads in bending. In addition, these elementary examples enable one to obtain closed-form solutions of the governing differential equation (2.24).

3.2.1 Cylindrical bending of a plate

Consider an infinitely long plate in the y axis direction. Assume that the plate is subjected to a transverse load which is a function of the variable x only, i.e., $p = p(x)$ (Fig. 3.1a). In this case all the strips of a unit width parallel to the x axis and isolated from the plate will bend identically. The plate as a whole is found to be bent over the cylindrical surface $w = w(x)$. Setting all the derivatives with respect to y equal zero in Eq. (2.24), we obtain the following equation for the deflection:

$$\frac{\mathrm{d}^4 w}{\mathrm{d}x^4} = \frac{p(x)}{D}. \tag{3.1}$$

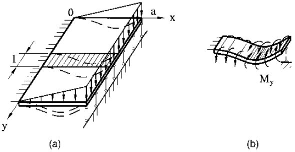

(a) (b)

Fig. 3.1

We have applied here the ordinary derivative notation since w depends now only on the variable x. Equation (3.1) describes a *cylindrical bending of thin plates*. It is seen that this equation coincides with the corresponding equation of bending of a beam if we replace the flexural rigidity of the beam, EI, by the flexural rigidity of a plate, D. Since $D > EI$, the strip of the unit width within the plate (it is cross-hatched in Fig. 3.1a) is always stiffer than an isolated beam having the same span and thickness.

An integration of Eq. (3.1) should present no problems. Let, for example, $p = p_0 \frac{x}{a}$, then the general solution of Eq. (3.1) is of the following form:

$$w = w_{\mathrm{h}} + w_{\mathrm{p}} = C_1 + C_2 x + C_3 x^2 + C_4 x^3 + \frac{p_0 x^5}{120aD}, \tag{3.2}$$

where w_{h} is a solution of homogeneous equation (3.1) and w_p is a particular solution depending on the right-hand side of Eq. (3.1), i.e., on a given type of the applied loading.

The boundary conditions for the plate-strip can be written as follows (Fig. 3.1a)

$$w = 0|_{x=0}, \frac{\mathrm{d}w}{\mathrm{d}x} = 0\bigg|_{x=0} \quad \text{and} \quad w = 0|_{x=a}, M_x = -D\frac{\mathrm{d}^2 w}{\mathrm{d}x^2} = 0\bigg|_{x=a}. \tag{3.3}$$

The constants of integration C_i $(i = 1, 2, 3, 4)$ can be evaluated from the boundary conditions (3.3). Substituting for w from (3.2) into (3.3), we obtain the following:

$$C_1 = C_2 = 0, C_3 = \frac{7p_0 a^2}{240D}, \quad C_4 = \frac{9p_0 a}{240D}.$$

Substituting the above into Eq. (3.2), yields Eq. (3.4), as shown below:

$$w = \frac{p_0 a^4}{240D}\left(7\frac{x^2}{a^2} - 9\frac{x^3}{a^3} + 2\frac{x^5}{a^5}\right) \tag{3.4}$$

This is the equation for the deflection of the plate in cylindrical bending.

The bending moments M_x and M_y may be obtained from Eqs (2.13) making all the derivatives of w with respect to y equal zero, i.e.,

$$M_x = -D\frac{d^2w}{dx^2}, \quad M_y = -\nu D\frac{d^2w}{dx^2} = \nu M_x, \quad M_{xy} = 0. \tag{3.5}$$

Substituting Eq. (3.4) into Eq. (3.5), we obtain

$$M_x = -\frac{p_0 a^2}{120}\left(7 - 27\frac{x}{a} + 20\frac{x^3}{a^3}\right). \tag{3.6}$$

The moment $M_y = \nu M_x$ is proportional to M_x.

A cylindrical bending of a plate with a finite size in the y direction is possible only if the moment M_y will be applied to edges that are parallel to the x axis, as shown for the strip isolated from an infinite plate of Fig. 3.1b. In the absence of these moments, the surface of deflections will deviate from the cylindrical one over part of the length along the y axis.

3.2.2 Pure bending of plates

Consider a rectangular plate with a free boundary and assume that this plate is subjected to distributed bending moments over its edges $M_x = m_1 = \text{const}$ and $M_y = m_2 = \text{const}$ (Fig. 3.2). In this particular case, the governing differential equation (2.24) becomes

$$\frac{\partial^4 w}{\partial x^4} + 2\frac{\partial^4 w}{\partial x^2 \partial y^2} + \frac{\partial^4 w}{\partial y^4} = 0. \tag{3.7}$$

This equation will be satisfied if we make

$$w = 0.5\left(C_1 x^2 + C_2 y^2\right). \tag{3.8}$$

The constants of integration C_1 and C_2 may be evaluated from the following boundary conditions:

$$M_x = m_1 \quad \text{and} \quad M_y = m_2. \tag{3.9}$$

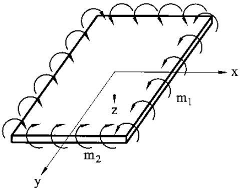

Fig. 3.2

Using Eqs (2.13), (3.8), and (3.9), we obtain

$$C_1 = \frac{\nu m_2 - m_1}{D(1-\nu^2)}, \quad C_2 = \frac{\nu m_1 - m_2}{D(1-\nu^2)}.$$

Substituting the above into Eq. (3.8) yields the deflection surface, as shown below:

$$w = \frac{1}{2D(1-\nu^2)}\left[(\nu m_2 - m_1)x^2 + (\nu m_1 - m_2)y^2\right] \tag{3.10}$$

Hence, in all sections of the plate parallel to the x and y axes, only the constant bending moments $M_x = m_1$ and $M_y = m_2$ will act. Other stress resultants and stress couples are zero, i.e.,

$$M_{xy} = Q_x = Q_y = 0.$$

This case of bending of plates may be referred to as a *pure bending*.

Let us consider some *particular cases of pure bending of plates*.

(a) Let $m_1 = m_2 = m$.
Then,

$$w = -\frac{m}{2D(1+\nu)}(x^2 + y^2). \tag{3.11}$$

This is an equation of the *elliptic paraboloid of revolution*. The curved plate in this case represents a part of a sphere because the radii of curvature are the same at all the planes and all the points of the plate.

(b) Let $m_1 = m, m_2 = 0$ (Fig. 3.3).
Then,

$$w = \frac{m}{2D(1-\nu^2)}\left(-x^2 + \nu y^2\right). \tag{3.12}$$

A surface described by this equation has a saddle shape and is called the *hyperbolic paraboloid of revolution* (Fig. 3.3). Horizontals of this surface are hyperbolas, asymptotes of which are given by the straight lines $\frac{x}{y} = \pm\sqrt{\nu}$. As is seen, due to the Poisson effect the plate bends not only in the plane of the applied bending moment $M_x = m_1 = m$ but it also has an opposite bending in the perpendicular plane.

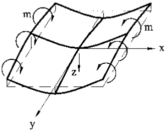

Fig. 3.3

(c) Let $m_1 = m, m_2 = -m$ (Fig. 3.4a).
Then

$$w = \frac{m}{2D(1-\nu)}(-x^2 + y^2). \tag{3.13}$$

This is an equation of an *hyperbolic paraboloid* with asymptotes inclined at 45° to the x and y axes.

Let us determine the moments M_n and M_{nt} from Eqs (2.45) in skew sections that are parallel to the asymptotes. Letting $\alpha = 45^\circ$, we obtain

$$M_n = 0, \quad M_{nt} = -m.$$

Thus, a part of the plate isolated from the whole plate and equally inclined to the x and y axes will be loaded along its boundary by uniform twisting moments of intensity m. Hence, this part of the plate is subjected to *pure twisting* (Fig. 3.4b). Let us replace the twisting moments by the effective shear forces V_α, rotating these moments through 90° (see Sec. 2.4). Along the whole sides of the isolated part we obtain $V_\alpha = 0$, but at the corner points the concentrated forces $S = 2m$ are applied. Thus, for the model of Kirchhoff's plate, an application of self-balanced concentrated forces at corners of a rectangular plate produces a deformation of pure torsion because over the whole surface of the plate $M_{nt} = m = \text{const}$.

Remark

Since the plate described above in pure bending has no supports, its deflections have been determined with an accuracy of the displacements of an absolutely rigid body.

3.3 NAVIER'S METHOD (DOUBLE SERIES SOLUTION)

In 1820, Navier presented a paper to the French Academy of Sciences on the solution of bending of simply supported plates by double trigonometric series [1].

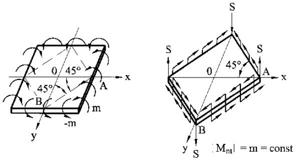

(a) (b)

Fig. 3.4

Consider a rectangular plate of sides a and b, simply supported on all edges and subjected to a uniform load $p(x, y)$. The origin of the coordinates is placed at the upper left corner as shown in Fig. 3.5.

The boundary conditions for a simply supported plate are the following (see Eqs (2.35):

$$w = 0|_{x=0,a}; \frac{\partial^2 w}{\partial x^2} = 0\Bigg|_{x=0,a} \quad \text{and} \quad w = 0|_{y=0,b}; \frac{\partial^2 w}{\partial y^2} = 0\Bigg|_{y=0,b}. \tag{3.14}$$

In this case, the solution of the governing differential equation (2.24), i.e., the expressions of the deflection surface, $w(x, y)$, and the distributed surface load, $p(x, y)$, have to be sought in the form of an infinite Fourier series (see Appendix B), as follows:

$$w(x, y) = \sum_{m=1}^{\infty} \sum_{n-1}^{\infty} w_{mn} \sin \frac{m\pi x}{a} \sin \frac{n\pi y}{b}, \tag{3.15a}$$

$$p(x, y) = \sum_{m=1}^{\infty} \sum_{n=1}^{\infty} p_{mn} \sin \frac{m\pi x}{a} \sin \frac{n\pi y}{b}, \tag{3.15b}$$

where w_{mn} and p_{mn} represent coefficients to be determined. It can be easily verified that the expression for deflections (3.15a) automatically satisfies the prescribed boundary conditions (3.14).

Let us consider a general load configuration. To determine the Fourier coefficients p_{mn}, each side of Eq. (3.15b) is multiplied by $\sin \frac{l\pi x}{a} \sin \frac{k\pi y}{b}$ and integrated twice between the limits $0,a$ and $0,b$, as follows (see Appendix B):

$$\int_0^a \int_0^b p(x, y) \sin \frac{l\pi x}{a} \sin \frac{k\pi y}{b} \, dx dy = \sum_{m=1}^{\infty} \sum_{n=1}^{\infty} p_{mn} \int_0^a \int_0^b \sin \frac{m\pi x}{a} \sin \frac{n\pi y}{b} \sin \frac{l\pi x}{a} \sin \frac{k\pi y}{b} \, dx dy. \tag{a}$$

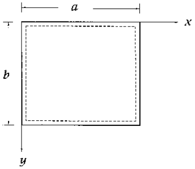

Fig. 3.5

$$
\begin{aligned}
M_x &= \frac{1}{\pi^2}\sum_{m=1}^{\infty}\sum_{n=1}^{\infty} p_{mn}\frac{[(m/a)^2+\nu(n/b)^2]}{[(m/a)^2+(n/b)^2]^2}\sin\frac{m\pi x}{a}\sin\frac{n\pi y}{b},\\
M_y &= \frac{1}{\pi^2}\sum_{m=1}^{\infty}\sum_{n=1}^{\infty} p_{mn}\frac{[(n/b)^2+\nu(m/a)^2]}{[(m/a)^2+(n/b)^2]^2}\sin\frac{m\pi x}{a}\sin\frac{n\pi y}{b},\\
M_{xy} &= -\frac{1_{\nu}}{\pi^2}\sum_{m=1}^{\infty}\sum_{n=1}^{\infty} p_{mn}\frac{mn}{ab[(m/a)^2+(n/b)^2]^2}\cos\frac{m\pi x}{a}\cos\frac{n\pi y}{b}.
\end{aligned}
\tag{3.20}
$$

The infinite series solution for the deflection (3.19) generally converges quickly; thus, satisfactory accuracy can be obtained by considering only a few terms. Since the stress resultants and couples are obtained from the second and third derivatives of the deflection $w(x, y)$, the convergence of the infinite series expressions of the internal forces and moments is less rapid, especially in the vicinity of the plate edges. This slow convergence is also accompanied by some loss of accuracy in the process of calculation. The accuracy of solutions and the convergence of series expressions of stress resultants and couples can be improved by considering more terms in the expansions and by using a special technique for an improvement of the convergence of Fourier's series (see Appendix B and Ref. [2]).

Example 3.1

A rectangular plate of sides a and b is simply supported on all edges and subjected to a uniform pressure $p(x, y) = p_0$, as shown in Fig 3.5. Determine the maximum deflection, moments, and stresses.

Solution

The coefficients p_{mn} of the double Fourier expansion of the load are obtained from Eq. (3.17). Substituting $p(x, y) = p_0 = \text{const}$ and integrating, yields the following

$$
p_{mn} = \frac{4p_0}{\pi^2 mn}(1-\cos m\pi)(1-\cos n\pi) \text{ or } p_{mn} = \frac{16p_0}{\pi^2 mn}(m, n = 1, 3, 5, \ldots). \tag{a}
$$

It is observed that because $p_{mn} = 0$ for even values of m and n, these integers assume only for odd values.

Substituting for p_{mn} from (a) into Eqs (3.19) and (3.20), we can obtain the expressions for deflections and moments. We obtain the following:

$$
w = \frac{16p_0}{D\pi^6}\sum_{m=1,3,\ldots}^{\infty}\sum_{n=1,3,\ldots}^{\infty}\frac{\sin\frac{m\pi x}{a}\sin\frac{n\pi y}{b}}{mn\left[(m/a)^2+(n/b)^2\right]^2}, \tag{3.21a}
$$

$$
M_x = \frac{16p_0}{\pi^4}\sum_{m=1,3,\ldots}^{\infty}\sum_{n=1,3,\ldots}^{\infty}\frac{(m/a)^2+\nu(n/b)^2}{mn\left[(m/a)^2+(n/b)^2\right]^2}\sin\frac{m\pi x}{a}\sin\frac{n\pi y}{b}, \tag{3.21b}
$$

$$
M_y = \frac{16p_0}{\pi^4}\sum_{m=1,3,\ldots}^{\infty}\sum_{n=1,3,\ldots}^{\infty}\frac{\nu(m/a)^2+(n/b)^2}{mn\left[(m/a)^2+(n/b)^2\right]^2}\sin\frac{m\pi x}{a}\sin\frac{n\pi y}{b}, \tag{3.21c}
$$

$$
M_{xy} = -\frac{16(1-\nu)}{\pi^4 ab}\sum_{m}^{\infty}\sum_{n}^{\infty}\frac{1}{[(m/a)^2+(n/b)^2]^2}\cos\frac{m\pi x}{a}\cos\frac{m\pi y}{b}. \tag{3.21d}
$$

As explained in Sec. 2.4, all the corner concentrated forces, S, for the simply supported rectangular plate that is subjected to a downward directed uniform load p_0, act downward also, i.e., in the positive z direction. Each such a force is given by Eq. (2.41), i.e.,

$$S = 2|M_{xy}| = 2\left[\frac{16(1-\nu)}{\pi^4 ab}\frac{a^3b^3}{(a^2+b^2)^2}\right].$$

Thus, a total force due to the corner forces acts in the positive z direction and is given by the following:

$$R_{\mathrm{S}} = 4S = 128\frac{p_0(1-\nu)}{\pi^4}\frac{a^3b^3}{(a^2+b^2)^2}. \tag{l}$$

Now, adding Eqs (j) and (l), we get

$$R_{\mathrm{p}} + R_{\mathrm{V}} + R_{\mathrm{S}} = 0.$$

The effective shear force distributions and concentrated corner forces are shown in Fig. 2.9. Thus, we have demonstrated the contribution of the corner forces to the overall equilibrium of the rectangular simply supported plate.

It is interesting to note that the boundary transverse shear forces, Q_x and Q_y, balance the external distributed load p_0. Indeed, let us compute the resultant R_{Q} of the shear forces on the boundary of the plate, as follows:

$$R_{\mathrm{Q}} = -\int_0^b \left[|Q_x(0,y)| + |Q_x(a,y)|\right]\mathrm{d}y - \int_0^a \left[|Q_y(x,0)| + |Q_y(x,b)|\right]\mathrm{d}x.$$

Substituting for Q_x and Q_y from the first two equations (f) into the above, we obtain

$$R_{\mathrm{Q}} = -\frac{64p_0}{\pi^4}ab, \tag{m}$$

where the negative sign indicates that R_{Q} points in the negative z direction, i.e., in the upward direction. Adding Eqs (g) and (m) results in

$$R_{\mathrm{p}} + R_{\mathrm{Q}} = 0.$$

However, following the logic of Kirchhoff's plate theory, the transverse shear force alone cannot be treated as the edge supporting reaction. Only the effective shear force may represent such a reaction. This result will also be discussed in detail later, in Sec. 7.3.

Example 3.2

A rectangular wall panel is taken to be simply supported on all edges and subjected to a patch load of intensity $p_0 = \text{const.}$ as shown in Fig. 3.6. Determine the deflected surface.

Solution

The constants of the Fourier expansion of the load are

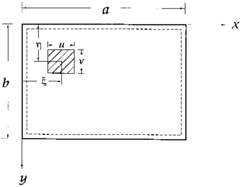

Fig. 3.6

$$p_{mn} = \frac{4p_0}{uv} \int\limits_{\xi-u/2}^{\xi+u/2} \int\limits_{\eta-v/2}^{\eta+v/2} \sin\frac{m\pi x}{a}\sin\frac{n\pi y}{b}\,\mathrm{d}x\mathrm{d}y$$
$$= \frac{16p_0}{\pi^2 mn}\sin\frac{m\pi\xi}{a}\sin\frac{n\pi\eta}{b}\sin\frac{m\pi u}{2a}\sin\frac{n\pi v}{2b}. \tag{3.22}$$

Inserting the above into Eqs (3.19), yields the double series expression of the following deflected surface

$$w(x, y) = \frac{16p_0}{\pi^6 D}\sum_{m=1}^{\infty}\sum_{n=1}^{\infty}\frac{\sin\frac{m\pi\xi}{a}\sin\frac{n\pi\eta}{b}\sin\frac{m\pi u}{2a}\sin\frac{n\pi v}{2b}\sin\frac{m\pi x}{a}\sin\frac{n\pi y}{b}}{mn\left[(m/a)^2+(n/b)^2\right]^2}. \tag{3.23}$$

The convergence of this solution is relatively fast if the dimensions u and v are not too small. The deflection can be obtained with sufficient accuracy by taking the first four terms of the series.

3.4 RECTANGULAR PLATES SUBJECTED TO A CONCENTRATED LATERAL FORCE *P*

Let us consider a rectangular plate simply supported on all edges of sides a and b and subjected to concentrated lateral force P applied at $x = \xi$ and $y = \eta$, as shown in Fig. 3.7.

Assume first that this force is uniformly distributed over the contact area of sides u and v (Fig. 3.6) i.e., its load intensity is defined as

$$p_0 = \frac{P}{uv}.$$

Substituting the above into Eq. (3.22), one obtains

$$p_{mn} = \frac{16P}{\pi^2 mnuv}\sin\frac{m\pi\xi}{a}\sin\frac{n\pi\eta}{b}\sin\frac{m\pi u}{2a}\sin\frac{n\pi v}{2b}. \tag{3.24}$$

Retaining the first nine terms of this series ($m = 1$, $n = 1, 3, 5$; $m = 3$, $n = 1, 3, 5$; $m = 5$, $n = 1, 3, 5$) we obtain

$$w_{\max} = \frac{4Pa^2}{\pi^4 D}\left[\frac{1}{4} + \frac{2}{100} + \frac{1}{324} + \frac{2}{625} + \frac{2}{1156} + \frac{1}{2500}\right] = 0.01142\frac{Pa^2}{D}.$$

The "exact" value is $w_{\max} = 0.01159\dfrac{Pa^2}{D}$ and the error is thus 1.5% [3].

This very simple Navier's solution, Eq. (3.28), converges sufficiently rapidly for calculating the deflections. However, it is unsuitable for calculating the bending moments and stresses because the series for the second derivatives $\partial^2 w/\partial x^2$ and $\partial^2 w/\partial y^2$ obtained by differentiating the series (3.28) converge extremely slowly. These series for bending moment, and consequently for stresses as well as for the shear forces, diverge directly at a point of application of a concentrated force, called a *singular point*. Thus, to calculate stress components in the vicinity of a concentrated force, it is necessary to use a more efficient technique, especially since the maximum stresses occur in the immediate vicinity of the singular point. Therefore, the problem of determining a correct stress distribution near such types of singular points is of practical interest.

We now consider one approach for determining the bending moment distribution near the above-mentioned singular point. Let us write the solution (3.27) in the form

$$w = \frac{4Pb^3}{\pi^4 a}\sum_{m=1}^{\infty} S_m \sin\frac{m\pi\xi}{a}\sin\frac{m\pi x}{a}, \tag{3.29a}$$

where

$$S_m = \frac{1}{2}\sum_{n=1}^{\infty}\frac{\cos\dfrac{n\pi}{b}(y-\eta) - \cos\dfrac{n\pi}{b}(y+\eta)}{\left(m^2b^2/a^2 + n^2\right)^2}. \tag{3.29b}$$

The series (3.29b) can be summed using the formula [4]:

$$\begin{aligned}\sum_{n=1}^{\infty}\frac{\cos nz}{(\alpha^2+n^2)^2} = {} & -\frac{1}{2\alpha^4} + \frac{\pi}{4\alpha^3}\frac{\cosh\alpha(\pi-z)}{\sin\pi\alpha} - \frac{\pi(\pi-z)}{4\alpha^2} - \frac{\sinh\alpha(\pi-z)}{\sinh\pi\alpha} \\ & + \frac{\pi^2}{4\alpha^2}\frac{\cosh\alpha(\pi-z)\cosh\pi\alpha}{\sin h^2\pi\alpha}.\end{aligned} \tag{a}$$

Using the above formula, we can represent the deflection surface (3.28) as

$$\begin{aligned} w(x,y) = {} & \frac{Pa^2}{\pi^3 D}\sum_{m=1}^{\infty}\left(1 + \beta_m\coth\beta_m - \frac{\beta_m y_1}{b}\coth\frac{\beta_m y_1}{b} - \frac{\beta_m\eta}{b}\coth\frac{\beta_m\eta}{b}\right) \\ & \times\frac{\sinh\dfrac{\beta_m\eta}{b}\sin h\dfrac{\beta_m y_1}{b}\sin\dfrac{m\pi\xi}{a}\sin\dfrac{m\pi x}{a}}{m^3\sinh\beta_m},\end{aligned} \tag{3.30}$$

where $\beta_m = \frac{m\pi b}{a,}$ $y_1 = b - y$, and $y \geq \eta$. If $y < \eta$, then the values y_1 and η must be replaced by y and $\eta_1 = b - \eta$, respectively.

Let us use an infinitely long (in the y-direction) plate loaded by a concentrated force P applied at $x = \xi$ and $y = 0$, as shown in Fig. 3.8, to illustrate the above-

Let us present the equations for the bending and twisting moments for points that are in the immediate vicinity from the point of application of force P but necessarily lying on the x axis. In this case, the values $(x-\xi)$ and y are very small and the following approximate equalities hold:

$$\cos\frac{\pi(x-\xi)}{a}\approx 1-\frac{\pi^2(x-\xi)^2}{2a^2};\quad \cosh\frac{\pi y}{a}\approx 1+\frac{\pi^2 y^2}{2a^2}. \tag{3.35}$$

Applying the expression (3.34) and the above approximate equalities to Eqs (3.33), we obtain the following equations for the bending moments:

$$\left.\begin{matrix} M_x \\ M_y \end{matrix}\right\} = \frac{P}{4\pi}\left\{(1+\nu)\ln\frac{2a\sin\frac{\pi\xi}{a}}{\pi r}\pm\frac{(1-\nu)y^2}{r^2}\right\};\quad r^2=(x-\xi)^2+y^2. \tag{3.36}$$

As seen from Eqs (3.36), the bending moments and, consequently, shear forces are unbounded at $r=0$, i.e., at a point where a concentrated force is applied. This is an evident reason of divergence of the Fourier series at the singular points. An occurrence of infinite stress resultants and stress couples can be physically explained. First, in reality there is no concentrated force. A load is always distributed over some finite area. It can be easily shown that a finite value of a concentrated force cannot balance the intensities of the shear forces and bending moments in the vicinity of a point of application of P. Indeed, let us cut from the square plate subjected to a center force P, a differential element of sides Δx and Δy surrounding this singular point (Fig. 3.9). Then, from a static equilibrium condition – namely, the force summation into the z direction is zero – we obtain

$$P-2Q_x\Delta x-2Q_y\Delta y=0,$$

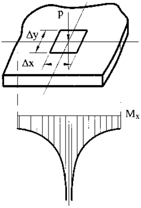

Fig. 3.9

Table 3.1

b/a	1.0	1.2	1.4	1.6	1.8	2.0	∞
γ_1	−0.565	−0.350	−0.211	−0.125	−0.073	−0.042	0
γ_2	0.135	0.115	0.085	0.057	0.037	0.023	0

where γ_1 and γ_2 are some coefficients depending on the plate dimensions. They are presented below in Table 3.1 [3].

Let us turn back to the expression (3.27) and write it in the following form

$$w = G(x, y; \xi, \eta) = \frac{4}{\pi^4 abD} \sum_{m=1}^{\infty} \sum_{n=1}^{\infty} \frac{\sin \frac{m\pi\xi}{a} \sin \frac{n\pi\eta}{b} \sin \frac{m\pi x}{a} \sin \frac{n\pi y}{b}}{\left[(m/a)^2 + (n/b)^2\right]^2}. \tag{3.39}$$

This is the equation of the deflected surface of the plate produced by a unit concentrated force $P = 1$ and it is denoted by $G(x, y; \xi, \eta)$. It is seen that $G(x, y; \xi, \eta)$ depends on two sets of coordinates: (a) the point of observation, (x, y) and (b) the point of application of the applied unit force, (ξ, η). This function is defined as *Green's function* and represents a deflection at the point of observation, (x, y), due to a unit force at the point of application, (ξ, η) or vice versa, because this function is symmetrical with respect to these coordinate sets, i.e., $G(x, y; \xi, \eta) = G(\xi, \eta; x, y)$. The latter immediately follows from the well-known reciprocity theorem. Sometimes, $G(x, y; \xi, \eta)$ is referred to as an *influence function*. Once Green's function is established for a plate, one can determine readily the deflection at any point of observation due to prescribed surface loading $p(\xi, \eta)$. Then, by superposition, we have the following:

$$w(x, y) = \int\int_S p(\xi, \eta) G(x, y; \xi, \eta) d\xi d\eta.$$

The Green's function approach is widely used in mechanics [6,7].

3.5 LEVY'S SOLUTION (SINGLE SERIES SOLUTION)

In the preceding sections it was shown that the calculation of bending moments and shear forces using Navier's solution is not very satisfactory because of slow convergence of the series.

In 1900 Levy developed a method for solving rectangular plate bending problems with simply supported two opposite edges and with arbitrary conditions of supports on the two remaining opposite edges using single Fourier series [8]. This method is more practical because it is easier to perform numerical calculations for single series that for double series and it is also applicable to plates with various boundary conditions.

Levy suggested the solution of Eq. (2.24) be expressed in terms of complementary, $w_{h,}$ and particular, w_p, parts, each of which consists of a single Fourier series where unknown functions are determined from the prescribed boundary conditions. Thus, the solution is expressed as follows:

$$
\begin{aligned}
M_{x\mathrm{h}} &= D\sum_{m=1}^{\infty}\left(\frac{m^2\pi^2}{a^2}f_m - \nu\frac{\mathrm{d}^2 f_m}{\mathrm{d}y^2}\right)\sin\frac{m\pi x}{a},\\
M_{y\mathrm{h}} &= D\sum_{m=1}^{\infty}\left(\nu\frac{m^2\pi^2}{a^2}f_m - \frac{\mathrm{d}^2 f_m}{\mathrm{d}y^2}\right)\sin\frac{m\pi x}{a},\\
M_{xy\mathrm{h}} &= -D(1-\nu)\sum_{m=1}^{\infty}\frac{m\pi}{a}\frac{\mathrm{d}f_m}{\mathrm{d}y}\cos\frac{m\pi x}{a},\\
V_{x\mathrm{h}} &= D\sum_{m=1}^{\infty}\left[\left(\frac{m\pi}{a}\right)^3 f_m - \frac{m\pi}{a}(2-\nu)\frac{\mathrm{d}^2 f_m}{\mathrm{d}y^2}\right]\cos\frac{m\pi x}{a},\\
V_{y\mathrm{h}} &= D\sum_{m=1}^{\infty}\left[-\frac{\mathrm{d}^3 f_m}{\mathrm{d}y^3} + (2-\nu)\left(\frac{m\pi}{a}\right)^2\frac{\mathrm{d}f_m}{\mathrm{d}y}\right]\sin\frac{m\pi x}{a}.
\end{aligned}
\tag{3.55}
$$

These homogeneous stress resultants and stress couple components must be complemented with particular ones.

Example 3.3

The rectangular simply supported plate on all edges and having dimensions a and b (Fig. 3.10) is subjected to a uniform load p_0. Determine the deflections and bending moments.

Solution

Since the boundary conditions are identical for all the edges of the plate and the load is constant, then we make the x axis coincident with the axis of symmetry of the plate. It will be shown later that this location of the x axis simplifies considerably the computational procedure.

For $p(x, y) = p_0$, Eq. (3.53) upon integration, becomes

$$
p_m = \frac{2p_0}{a}\int_0^a \sin\frac{m\pi x}{a}\mathrm{d}x = \frac{4p_0}{m\pi} \quad (m = 1, 3, 5, \ldots). \tag{a}
$$

Substituting the above into Eq. (3.54), one obtains

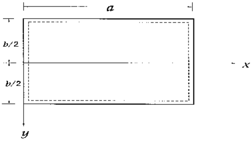

Fig. 3.10

$$M_x = M_y = 0.0479 p_0 a^2.$$

If $b/a \gg 1$ (the plate-strip), then $M_x = p_0 a^2/8$, $M_y = \nu M_x$. The series for the effective shear forces V_x and V_y are also convergent.

Example 3.4

For the simply supported plate subjected to hydrostatic loading ($p(x) = p_0 \frac{x}{a}$), as shown in Fig. 3.11, determine the deflection and bending moment equations.

Solution

Determine the coefficients p_m from Eq. (3.53). We have

$$\begin{aligned} p_m &= \frac{2}{a}\int_0^a p(x, y) \sin\frac{m\pi x}{a}\,\mathrm{d}x = \frac{2p_0}{a}\int_0^a \frac{x}{a}\sin\frac{m\pi x}{a}\,\mathrm{d}x \\ &= \frac{2p_0}{m\pi}(-1)^{m+1}, \quad m = 1, 2, 3 \ldots . \end{aligned} \tag{a}$$

The given loading is a constant along the y axis. Hence, the function g_m will be also a constant. Substituting the expression (a) into the right-hand side of Eq. (3.54), we obtain

$$g_m = \frac{2p_0 a^4}{m^5 \pi^5 D}(-1)^{m+1}. \tag{b}$$

Inserting (b) into Eq. (3.51), we obtain the particular solution of the following form:

$$w_{\mathrm{p}}(x, y) = \frac{2p_0 a^4}{\pi^5 D}\sum_{m=1,2,\ldots}^{\infty}\frac{(-1)^{m+1}}{m^5}\sin\frac{m\pi x}{a}. \tag{c}$$

Using Eqs (3.50) and (c), and letting $A_m = D_m = 0$ (because of the symmetry of the loading and boundary conditions about the x axis), we obtain the equation of the plate deflection in the following form:

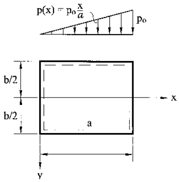

Fig. 3.11

Example 3.5

Derive expressions for the deflected surface and the bending moments in a floor plate-strip subjected to a uniformly distributed load q_0 along line $y = 0$, as shown in Fig. 3.12a. Assume the edges $x = 0$ and $x = a$ are simply supported.

Solution

If a plate is strongly lengthened in one direction – for example, in the y direction – then such a plate in some problems can be considered as an infinite one in this direction. Levy's solution can be applied advantageously with some modifications to obtain the expressions for the deflections and bending moments.

The solution of the governing differential equation (2.24) is sought in the form of Eq. (3.48). At the same time, since for $y \to \infty$ deflections cannot approach infinity, then the terms containing $e^{m\pi y/a}$ should be equated to zero because these terms and their derivatives do not vanish at $y \to \infty$. Hence, w_h can be represented as follows:

$$w_h = \sum_{m=1}^{\infty} \left(B'_m + \frac{m\pi y}{a} D'_m \right) e^{-m\pi y/a} \sin \frac{m\pi x}{a}. \tag{a}$$

The above satisfies Eq. (2.24) and the boundary conditions on the edges $x = 0$ and $x = a$.

Let us consider the lower part of the plate where $y \geq 0$. The constants B'_m and D'_m can be evaluated from the conditions of symmetry of the plate and loading at $y = 0$. First, due to the symmetry of the deflected middle surface of the plate with respect to the x axis, the derivative $\partial w/\partial y$ is zero at $y = 0$; this condition is satisfied if $B'_m = D'_m$. Therefore, Eq. (a) becomes (for the lower part of the plate)

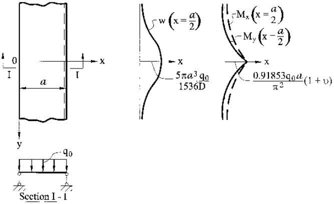
0
I
I
x
a
y
q_0
Section I - I
$w\left(x = \frac{a}{2}\right)$
x
$\frac{5\pi a^3 q_0}{1536D}$
$M_x\left(x = \frac{a}{2}\right)$
$M_y\left(x - \frac{a}{2}\right)$
x
$\frac{0.91853 q_0 a}{\pi^2}(1 + \upsilon)$

(a) (b)

Fig. 3.12

$$w_{\max} = \frac{q_0 a^3}{\pi^4 D} \sum_{m=1,3,\ldots}^{\infty} \frac{(-1)^{\frac{m-1}{2}}}{m^4} = \frac{5 q_0 \pi a^3}{1536 D},$$

$$M_{x,\max} = M_{y,\max} = \frac{q_0 a(1+\nu)}{\pi^2} \sum_{m=1,3,..}^{\infty} \frac{(-1)^{\frac{m-1}{2}}}{m^2} = \frac{0.91853 q_0 a(1+\nu)}{\pi^2}.$$

For $y = a$ the factor $\mathrm{e}^{\pi y/a} = \mathrm{e}^{-\pi} \approx 0.045$ and it is possible to consider that the bending moments and deflections vanish practically at a distance $y \approx a$. The deflection and bending moment diagrams are shown in Fig. 3.12b.

Example 3.6

A simply supported rectangular plate shown in Fig. 3.13 is loaded by an edge moment $m_x = f(x)$ along edge $x = 0$. Determine the equation for deflections of the plate middle surface.

Solution

We expand the given moment function $f(x)$ into the following Fourier series**:**

$$m_x = f(x) = \sum_{n=1}^{\infty} F_n \sin \frac{n\pi y}{b}, \tag{a}$$

where F_n are the constants of the Fourier expansion. Since a lateral load $p(x, y)$ is zero, the solution must satisfy the homogeneous differential equation (3.43). The solution of this homogeneous equation may be taken in the form

$$\begin{aligned} w = \sum_{n=1}^{\infty} \frac{1}{\beta_n^2} (C_{1n} \cosh \beta_n x + C_{2n} \beta_n x \sinh \beta_n x \\ + C_{3n} \sinh \beta_n x + C_{4n} \beta_n x \cosh \beta_n x) \sin \beta_n y, \end{aligned} \tag{b}$$

where $\beta_n = n\pi/b$. The constants of integration C_{in} $(i = 1, 2, 3, 4)$ can be evaluated from the prescribed boundary conditions on edges of the plate: namely,

$$w = 0|_{x=0,a}, \quad M_x = m_x\big|_{x=0}, \quad M_x = 0\big|_{x=a}, \tag{c}$$

$$w = 0|_{y=0,b}, \quad M_y = 0\big|_{y=0,b}; \tag{d}$$

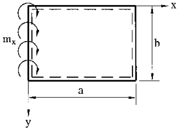

Fig. 3.13

w in the form of Eq. (b) satisfies Eq. (3.43) and the boundary conditions (d) exactly. Using the relations (2.12) and Eq. (a), the boundary conditions (c) can be rewritten, as follows

$$w = 0|_{x=0,a}; \quad \left[-D\left(\frac{\partial^2 w}{\partial x^2} + \nu \frac{\partial^2 w}{\partial y^2}\right)\right]\Big|_{x=0} = F_n \sin \beta_n y \text{ and } \left(\frac{\partial^2 w}{\partial x^2} + \nu \frac{\partial^2 w}{\partial y^2}\right)\Big|_{x=a} = 0. \tag{e}$$

Substitution of Eqs (b) into (e) and solving the obtained equations for C_{in}, one obtains

$$C_{1n} = 0,\ C_{2n} = -\frac{F_n}{2D},\ C_{3n} = \frac{F_n}{2D}\left(1 - \coth^2 \beta_n a\right)\beta_n a,\ C_{4n} = \frac{F_n}{2D}\coth \beta_n a. \tag{f}$$

Inserting the above into Eq. (f) yields the following:

$$w = \sum_{n=1}^{\infty} \frac{F_n}{2D\beta_n^2 \sinh \beta_n a}\left[\beta_n x \cosh \beta_n (a - x) - \beta_n a \frac{\sinh \beta_n x}{\sinh \beta_n a}\right] \sin \beta_n y. \tag{3.62}$$

As it follows from the above, in order to obtain a particular solution for plates subjected to various types of load distribution $p(x, y) = p_0 \cdot f(x)$ it is necessary to determine the coefficients p_m (see Eq. (3.53)). Table 3.2 furnishes the values of p_m for various types of load distributions.

3.6 CONTINUOUS PLATES

When a uniform plate extends over a support and has more than one span along its length or width, it is termed *continuous*. Such plates are of considerable practical interest.

Continuous plates are externally statically indeterminate members (note that a plate itself is also internally statically indeterminate). So, the well-known methods developed in structural mechanics can be used for the analysis of continuous plates. In this section, we consider the *force method* which is commonly used for the analysis of statically indeterminate systems. According to this method, the continuous plate is subdivided into individual, simple-span panels between intermediate supports by removing all redundant restraints. It can be established, for example, by introducing some fictitious hinges above the intermediate supports. In this way, the redundant moments acting along the intermediate supports are eliminated. Similar fictitious hinges can be used at the ends if those are fixed. The simple-span panel obtained in such a way is referred to as a *primary plate*. In order to restore the rejected restraints, the unknown redundant moments are applied to the primary plate. These moments can be determined from the solution of simultaneous algebraic equations expressing the compatibility of the slopes between the adjoining panels produced by both external loads and unknown redundant moments.

In our further discussion we assume that the supports are unyielding. For the sake of simplicity, we confine ourselves to a rectangular plate continuous in one direction only and having the same flexural rigidity. Obviously, the general procedure of the force method discussed below can be applied to plates continuous in both directions.

Consider the three-span simply supported continuous plate. The plate is subjected to a uniform load of intensities p_1, p_2, and p_3 as shown in Fig. 3.14a. Figure 3.14b illustrates the primary plate obtained by introducing the fictitious hinges above the intermediate supports; $\mu_1(y)$ and $\mu_2(y)$ are the redundant, unknown distributed moments replacing the removed restraints at the intermediate supports. These unknown bending moments may be represented by the following Fourier series:

$$\mu_1(y) = \sum_{m=1,3,\ldots}^{\infty} \mu_{1m} \sin \lambda_m y, \quad \mu_2(y) = \sum_{m=1,3,\ldots}^{\infty} \mu_{2m} \sin \lambda_m y, \quad \lambda_m = \frac{m\pi}{b}. \tag{3.63}$$

Since the deflection is symmetric with respect to the line $y = b/2$, the numbers m in the expansions (3.63) must be odd only. It is seen from Fig. 3.14b that the

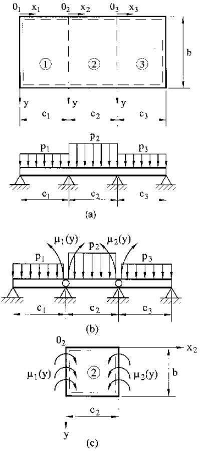
0₁
x₁
0₂
x₂
0₃
x₃
①
②
③
b
y
y
y
c₁
c₂
c₃
p₂
p₁
p₃
c₁
c₂
c₃
(a)
μ₁(y)
p₂
μ₂(y)
p₁
p₃
c₁
c₂
c₃
(b)
0₂
x₂
μ₁(y)
②
μ₂(y)
b
c₂
y
(c)

Fig. 3.14

primary plate consists of individual simple-span panels subjected to a given loading and the distributed edge moments $\mu_1(y)$ and $\mu_2(y)$, as shown in Fig. 3.14c.

The deflected surface of each simply supported individual panel may be obtained by application of Levy's method. The general solution for individual panels simply supported on all edges is given by Eqs (3.50) and (3.56a) if y is replaced by x_i, x by y, and a by b. We have the following:

$$\begin{aligned} w_i = \sum_{m=1,3,\ldots}^{\infty} \Big(& A_m^{(i)} \sinh \lambda_m x_i + B_m^{(i)} \cosh \lambda_m x_i + C_m^{(i)} \lambda_m x_i \sinh \lambda_m x_i \\ & + D_m^{(i)} \lambda_m x_i \cosh \lambda_m x_i + \frac{4 p_i b^4}{m^5 \pi^5 D} \Big) \sin \lambda_m y, \quad i = 1, 2, 3. \end{aligned} \tag{3.64}$$

The boundary conditions of each panel as well as the compatibility of deformations between any two panels across a common boundary (slopes continuity at the intermediate supports) are used to determine the constants in the solution (3.64) and the coefficients in the Fourier series (3.63). The boundary conditions for the plates 1, 2, and 3 are represented as follows:

$$w_1 = 0|_{x_1=0,c_1}, \ \frac{\partial^2 w_1}{\partial x_1^2} = 0 \Big|_{x_1=0}, \quad -D \frac{\partial^2 w_1}{\partial x_1^2} = \sum_{m=1,3,\ldots}^{\infty} \mu_{1m} \sin \lambda_m y \Big|_{x_1=c_1}, \tag{a}$$

$$\begin{aligned} & w_2 = 0|_{x_2=0,c_2}, -D \frac{\partial^2 w_2}{\partial x_2^2} = \sum_{m=1,3,\ldots}^{\infty} \mu_{1m} \sin \lambda_m y \Big|_{x_2=0}, \\ & -D \frac{\partial^2 w_2}{\partial x_2^2} = \sum_{m=1,3,\ldots}^{\infty} \mu_{2m} \sin \lambda_m y \Big|_{x_2=c_2} \end{aligned} \tag{b}$$

$$w_3 = 0|_{x_3=0,c_3}, \frac{\partial^2 w_3}{\partial x_3^2} = 0 \Big|_{x_3=c_3}, \quad -D \frac{\partial^2 w_3}{\partial x_3^2} = \sum_{m=1,3,\ldots}^{\infty} \mu_{2m} \sin \lambda_m y \Big|_{x_3=0}. \tag{c}$$

The compatibility conditions are expressed as follows

$$\left(\frac{\partial w_1}{\partial x_1} \right)_{x_1=c_1} = \left(\frac{\partial w_2}{\partial x_2} \right)_{x_2=0}, \quad \left(\frac{\partial w_2}{\partial x_2} \right)_{x_2=c_2} = \left(\frac{\partial w_3}{\partial x_3} \right)_{x_3=0}. \tag{d}$$

Let us consider the middle panel 2 (Fig. 3.14c). Application of the edge conditions (b) to Eq. (3.64) for $i = 2$ leads to the following values of the constants

$$\begin{aligned} A_m^{(2)} &= \frac{1}{D \sinh \lambda_m c_2} \left[\frac{4 p_2 b^4}{m^5 \pi^5} (\cosh \lambda_m c_2 - 1)(1 + 0.5 \lambda_m \operatorname{csch} \lambda_m c_2) \right. \\ & \quad \left. + \frac{c_2}{2 \lambda_m} (\mu_{1m} \operatorname{csch} \lambda_m c_2 - \mu_{2m} \coth \lambda_m c_2) \right], \\ B_m^{(2)} &= -\frac{4 p_2 b^4}{m^5 \pi^5 D}, C_m^{(2)} = \frac{2 p_2 b^4}{m^5 \pi^5 D} - \frac{\mu_{1m}}{2 D \lambda_m^2}, \\ D_m^{(2)} &= \frac{1}{2 D \sinh \lambda_m c_2} \left[\frac{4 p_2 b^4}{m^5 \pi^5} (1 - \cosh \lambda_m c_2) - \frac{1}{\lambda_m^2} (\mu_{2m} - \mu_{1m} \cosh \lambda_m c_2) \right]. \end{aligned} \tag{e}$$

The coefficients $A_m^{(1)}$, $B_m^{(1)}$, $C_m^{(1)}$, and $D_m^{(1)}$ are also given by Eqs (e) if p_2 is replaced by p_1, c_2 by c_1, μ_{2m} by μ_{1m} and letting $\mu_{1m} = 0$. Similarly, the coefficients $A_m^{(3)}$, $B_m^{(3)}$, $C_m^{(3)}$, and $D_m^{(3)}$ can be obtained by replacing c_2 by c_3, p_2 by p_3, μ_{1m} by μ_{2m} and letting $\mu_{2m} = 0$. Introducing Eqs (3.64) for $i = 1$ and $i = 2$ into the compatibility conditions (d), we obtain the following two additional equations:

$$\begin{aligned}
&A_m^{(1)} \cosh \lambda_m c_1 + B_m^{(1)} \sinh \lambda_m c_1 + C_m^{(1)}(\sinh \lambda_m c_1 + \lambda_m c_1 \cosh \lambda_m c_1) \\
&\quad + D_m^{(1)}(\cosh \lambda_m c_1 + \lambda_m c_1 \sinh \lambda_m c_1) = A_m^{(2)} + D_m^{(2)}, \\
&A_m^{(2)} \cosh \lambda_m c_2 + B_m^{(2)} \sinh \lambda_m c_2 + C_m^{(2)}(\sinh \lambda_m c_2 + \lambda_m c_2 \cosh \lambda_m c_2) \\
&\quad + D_m^{(2)}(\cosh \lambda_m c_2 + \lambda_m c_2 \sinh \lambda_m c_2) = A_m^{(3)} + D_m^{(3)}.
\end{aligned} \tag{f}$$

Having coefficients $A_m^{(i)}, B_m^{(i)}, C_m^{(i)}$, and $D_m^{(i)}$ $(i = 1, 2, 3)$ available, from Eqs (f) we obtain the moment coefficients μ_{1m} and μ_{2m}. Equations (3.64) then give the deflection of the continuous plate from which the moments and stresses can also be computed.

The foregoing approach may be extended to include the case of a long rectangular plate with many supports (see Timoshenko and Woinowski-Krieger [3]). However, as the number of panels increases, it becomes more tedious to find a solution by the classical methods. A more practical approach for solving such plates is to use the numerical methods introduced in Chapter 6.

Example 3.7

Determine the deflections and bending moments in the three-span, simply supported continuous plate loaded as shown in Fig. 3.15.

Solution

Letting $p_1 = p_0$, $p_2 = p_3 = 0$, and $c_1 = c_2 = c_3 = b = 2a$, we can obtain coefficients of integration $A_m^{(i)}$, $B_m^{(i)}$, $C_m^{(i)}$, and $D_m^{(i)}$ $(i = 1, 2, 3)$ and moment coefficients μ_{1m} and μ_{2m} from Eqs (e) and (f), respectively. Equations (3.64) then give the deflection of the continuous plate from which the bending moments are computed using Eqs (3.55).

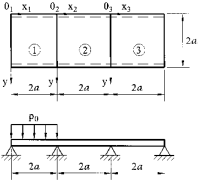

Fig. 3.15

The deflection w and bending moments M_x and M_y diagrams along the central section $y = a$ of the three-span plate are shown in Fig. 3.16 for $\nu = 0.3$.The maximum values of the deflection and bending moment are

$$w_{\max} = 0.64(1-\nu^2)\frac{p_0 a^4}{Eh^3} \text{ and } M_{x\max} = 0.177pa^2.$$

3.7 PLATES ON AN ELASTIC FOUNDATION

Many problems of considerable practical importance can be related to the solution of plates resting on an elastic foundation. Reinforced concrete pavements of highways and airport runways, foundation slabs of buildings, etc., are well-known direct application. However, an indirect application of this type of plate bending problem is of equal importance. For example, the shallow shell bending problems may be reduced to the solution of the problem for a plate on an elastic foundation; i.e., an analogy exists between the governing differential equation of a shallow shell and that of a plate on elastic foundation.

The key difficulty of this type of problem is in the correct mathematical description of a real elastic foundation. There exist a lot of various hypotheses – models of elastic foundations. The simplest of them has been suggested by Winkler [11]. It is based on the assumption that the foundation's reaction $q(x, y)$ can be described by the following relationship:

$$q(x, y) = kw, \tag{3.65}$$

where k is a constant termed the *foundation modulus,* which has the dimensions of force per unit surface area of the plate per unit deflection, e.g. $(\mathrm{lb/in^2})(1/\mathrm{in})$ in US units or $(\mathrm{N/m^2})(1/\mathrm{m})$ in SI units. Values of k for various soils are given in numerous references such as [9,12]. In Eq. (3.65) $q(x, y)$ is the resisting pressure of the foundation and w is the deflection of the plate.

When the plate is supported by a continuous elastic foundation, the external load acting in the lateral direction consists of the surface load $p(x, y)$ and of the

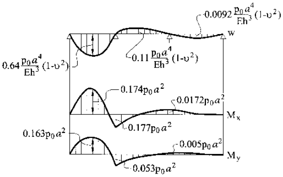
$0.0092\frac{p_0 a^4}{Eh^3}(1-\upsilon^2)$
w
$0.64\frac{p_0 a^4}{Eh^3}(1-\upsilon^2)$
$0.11\frac{p_0 a^4}{Eh^3}(1-\upsilon^2)$
$0.174p_0a^2$
$0.0172p_0a^2$
M_x
$0.177p_0a^2$
$0.163p_0a^2$
$0.005p_0a^2$
M_y
$0.053p_0a^2$

Fig. 3.16

reaction of the elastic foundation $q(x, y)$. Thus, the differential equation of the plate (2.24) becomes the following:

$$\frac{\partial^4 w}{\partial x^4} + 2\frac{\partial^4 w}{\partial x^2 \partial y^2} + \frac{\partial^4 w}{\partial y^4} = \frac{1}{D}[p(x, y) - q(x, y)]. \tag{3.66}$$

In this differential equation, the reactive force, $q(x, y)$, exerted by the elastic foundation is also unknown, because it depends on the deflection, $w(x, y)$, of the plate. Substituting Eq. (3.65) into (3.66), *the governing differential equation of the plate on an elastic foundation*, given by the Winkler model, can be written as

$$D\nabla^2\nabla^2 w + kw = p. \tag{3.67}$$

This equation can be solved for rectangular plates by the classical methods discussed earlier.

3.7.1 Application of Navier's solution

Let us consider a simply supported rectangular plate of sides $a \times b$ on an elastic foundation (Fig. 3.17). The deflection $w(x, y)$ and a given loading $p(x, y)$ can be expressed in the form of a double trigonometric series in the form of the expressions (3.15), as follows. Substituting the above expressions into the governing differential equation of the problem (3.67), we obtain the unknown amplitudes of the deflections, w_{mn}, for a specific set of m and n values, as follows:

$$w_{mn} = \frac{p_{mn}}{D\pi^4\left(m^2/a^2 + n^2/b^2\right)^2 + k}, \tag{3.68}$$

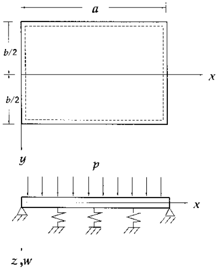

Fig. 3.17

$$w_p = \sum_{m=1}^{\infty} g_m(y) \sin \frac{m\pi x}{a}, \tag{3.76}$$

and the applied load as

$$p = \sum_{m=1}^{\infty} p_m(y) \sin \frac{m\pi x}{a}, \tag{3.77}$$

and then we substitute these equations into Eq. (3.66), we obtain

$$\frac{\mathrm{d}^4 g_m}{\mathrm{d}y^4} - 2\left(\frac{m\pi}{a}\right)^2 \frac{\mathrm{d}^2 g_m}{\mathrm{d}y^2} + \left(\frac{m^4\pi^4}{a^4} + \frac{k}{D}\right) g_m = \frac{p_m(y)}{D}. \tag{3.78}$$

Solving Eq. (3.78) for g_m, we can find the particular solution w_p. Therefore, Eq. (3.76) together with Eqs (3.73) and (3.74) describes the deflected surface of the plate.

Example 3.8

Find the equation for the deflection of a rectangular plate, resting on a Winkler foundation of modulus k and subjected to a uniform loading of intensity p_0. Assume that edges $x = 0$ and $x = a$ are simply supported while edges $y = \pm b/2$ are fixed.

Solution

For a uniform loading p, the right-hand side of Eq. (3.66) is constant. Thus, the particular solution is also a constant and may be taken in the following form:

$$g_m = B, \tag{a}$$

and the expression for p_m is given by (see Table 3.2)

$$p_m = \frac{4p_0}{m\pi}. \tag{b}$$

Substitution of (a) and (b) into Eq. (3.78) results in the following particular solution:

$$g_m = \frac{4p_0}{Dm\pi} \frac{1}{\left(\frac{m^4\pi^4}{a^4} + \frac{k}{D}\right)}. \tag{c}$$

Due to the symmetry of the deflection around the x axis, we can take $B_m = C_m = 0$ in Eq. (3.74) and the general solution for deflection becomes

$$w = \sum_{m=1}^{\infty} (A_m \sinh \alpha_m y \sin \beta_m y + D_m \cosh \alpha_m y \cos \beta_m y + g_m) \sin \frac{m\pi x}{a}, \tag{3.79}$$

where A_m and $B_m$are constants of integration. They have to be evaluated from the boundary conditions on the edges $y = \pm b/2$; namely,

$$w = 0|_{y=\pm b/2}, \frac{\partial w}{\partial y} = 0\bigg|_{y=\pm b/2}: \tag{d}$$

Substituting the expressions (3.79) into these boundary conditions, gives

$$A_m = \frac{g_m}{\gamma_1\left(\cosh\alpha_m \frac{b}{2}\cos\beta_m \frac{b}{2}\right)}; \quad D_m = -A_m \tanh\alpha_m \frac{b}{2}\tanh\beta_m \frac{b}{2} - \frac{g_m}{\cosh\alpha_m \frac{b}{2}\cos\beta_m \frac{b}{2}} \tag{e}$$

where

$$\begin{aligned}
&\gamma_1 = \frac{\gamma_2+\gamma_3}{\gamma_4-\gamma_5} - \tanh\alpha_m \frac{b}{2}\tanh\beta_m \frac{b}{2};\\
&\gamma_2 = \alpha_m \cosh\alpha_m \frac{b}{2}\sin\beta_m \frac{b}{2},\ \gamma_3 = \beta_m \sinh\alpha_m \frac{b}{2}\cos\beta_m \frac{b}{2};\\
&\gamma_4 = \alpha_m \sinh\alpha_m \frac{b}{2}\cos\beta_m \frac{b}{2},\ \gamma_5 = \beta_m \cosh\alpha_m \frac{b}{2}\sin\beta_m \frac{b}{2}.
\end{aligned} \tag{f}$$

Substituting the above into expression (3.79), we can obtain the deflection equation for the plate under consideration.

The Winkler model introduced above is the simplest model of an elastic foundation. It was based on the assumption that the subgrade of a foundation at some point of its surface is proportional to the pressure between the plate and the subgrade at the same point. This is correct in the case of a floating plate, but in the case of a coherent subgrade such a hypothesis approximates crudely the actual behavior of the subgrade. A better approximation can be obtained using the model of a semi-infinite elastic space, as shown in Fig. 3.18; the deflection of a semi-infinite space surface due to the distributed loads can be determined with the use of Boussinesq's solution [13]. So, the deflection at a point (x_i, y_i) of the semi-infinite space surface caused by an elementary distributed load $q\mathrm{d}x\mathrm{d}y$ applied at point (x, y) using the Boussinesq solution can be represented in the following form:

$$\mathrm{d}w_i = K[(x-x_i), (y-y_i)]q\mathrm{d}x\mathrm{d}y,$$

where $K[\,]$ is an influence function (or Green's function). It represents a deflection at point (x_i, y_i) of a semi-infinite space caused by a unit force $P = 1$ applied at point (x, y). This function $K[\ldots]$ can be derived from Boussinesq's solution. Then, an

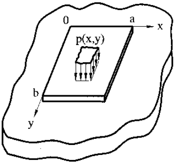

Fig. 3.18

arbitrary reaction load $q(x, y)$ occurring over a plate base causes the following deflection at point (x_i, y_i):

$$w(x_i, y_i) = \int_0^a \int_0^b K[(x - x_i), (y - y_i)] q(x, y) \mathrm{d}x \mathrm{d}y. \tag{3.80}$$

The above-mentioned function $K[\ldots]$ is given by the following [13]:

$$K[\ldots] = \frac{1 - \nu^2}{\pi E} \frac{1}{r}, \tag{3.81}$$

where r is the distance between the point of load application (x, y) and point of observation (x_i, y_i), $r^2 = (x - x_i)^2 + (y - y_i)^2$. With regard to expression (3.81) and replacing a unit force by $q \mathrm{d}x \mathrm{d}y$, Eq. (3.80) may be rewritten as

$$w(x_i, y_i) = \frac{1 - \nu^2}{\pi E} \int_0^a \int_0^b \frac{q(x, y) \mathrm{d}x \mathrm{d}y}{\sqrt{(x - x_i)^2 + (y - y_i)^2}}. \tag{3.82}$$

For this model, the relationship between the deflection of the foundation w and the foundation reaction q is much more complicated than for the Winkler model. Thus, the problem of bending of a plate resting on a semi-infinite space becomes more difficult. In the majority of cases, such plate bending problems can be solved numerically only.

3.8 PLATES WITH VARIABLE STIFFNESS

Let us consider bending of a rectangular plate having a variable thickness, $h = h(x, y)$. We assume that the above thickness varies gradually and there is no abrupt variation in thickness so that the expressions for the bending and twisting moments derived earlier for plates of constant thickness, Eqs (2.13), apply with sufficient accuracy to this case also. Substituting the above equations for the bending and twisting moments into the equation of static equilibrium (2.23) and taking into account that $D = D(x, y)$. One obtains the following:

$$\begin{aligned} D\nabla^2\nabla^2 w &+ 2\frac{\partial D}{\partial x}\frac{\partial}{\partial x}(\nabla^2 w) + 2\frac{\partial D}{\partial y}\frac{\partial}{\partial y}(\nabla^2 w) + \nabla^2 D(\nabla^2 w) \\ &- (1 - \nu)\left(\frac{\partial^2 D}{\partial x^2}\frac{\partial^2 w}{\partial y^2} - 2\frac{\partial^2 D}{\partial x \partial y}\frac{\partial^2 w}{\partial x \partial y} + \frac{\partial^2 D}{\partial y^2}\frac{\partial^2 w}{\partial x^2}\right) = p. \end{aligned} \tag{3.83}$$

This is the governing fourth-order partial differential equation with variable coefficients in w describing the bending of thin plates with variable thickness. A closed-form solution of this equation is possible in very special cases only. Practically, plates of variable thickness can be treated by approximate and numerical methods introduced in Chapter 6. Among them, the variational (the Ritz method) and finite element methods are widely used in practice. Analysis of plates with variable thickness can be efficiently carried out by the small parameter method [3]. Let us illustrate an application of this method to rectangular plates of variable stiffness.

$$
\begin{aligned}
w_0 &= \sum_{n=1}^{\infty} w_{0n} \sin\frac{n\pi x}{a};\\
w_1 &= \sum_{n=1}^{\infty} w_{1n} \sin\frac{n\pi x}{a};\\
w_2 &= \sum_{n=1}^{\infty} w_{2n} \sin\frac{n\pi x}{a}\\
&\text{etc} \ldots\ldots\ldots\ldots\ldots
\end{aligned}
\tag{3.88}
$$

where the coefficients w_{mn} $(m = 0, 1, 2, \ldots)$ are functions of the y only. Expand the given loading in the series also, as follows:

$$
p(x, y) = \sum_{n=1}^{\infty} p_n(y) \sin\frac{n\pi x}{a}. \tag{3.89}
$$

Substituting the first expression (3.88) and Eq. (3.89) into the first equation (3.87) and satisfying the boundary conditions prescribed on the plate edges $y = 0$ and $y = b$, we can determine w_{0n}. Then, substitution of the first and second expressions (3.88) into the second equation (3.87) gives w_{1n}. Similarly, each of the functions w_m can be found by substitution of $w_0, w_1, \ldots, w_{m-1}$ into the corresponding differential equation of the system (3.87) involving w_m into the left-hand side. Finally, the deflection surface of the plate is obtained by substituting for $w_0, w_1, w_2, \ldots, w_m$ from Eqs (3.88) into Eq. (3.86). The interested reader can find an application of this and other methods to plates of variable thickness in Ref. [14].

Example 3.9

A rectangular plate of variable thickness in the y direction is simply supported on edges $x = 0$ and $x = a$ and is fixed on edges $y = 0$ and $y = b$. The plate thickness varies according to the law $h = h_0(1 + \lambda y)$. The plate is subjected to a load $p = p_0 \sin\frac{n\pi x}{a} \sin\frac{m\pi y}{b}$. Find the deflections and bending moments in the plate.

Solution

This problem was solved numerically by using the above-presented general procedure of the small-parameter method. The boundary conditions are found to be as follows:

$$
w = \frac{\partial^2 w}{\partial x^2} = 0\bigg|_{x=0,a}; \; w = \frac{\partial w}{\partial y} = 0\bigg|_{y=0,b}.
$$

For the plate under consideration, $\Phi(y) \equiv y$. The values of the deflection and bending moment M_y at a plate section $x = a/2$ are given in Table 3.3. These results were obtained by using the three terms in the expansion (3.86) for a plate with the following geometric and mechanical parameters: $a = b = 1\,\text{m}$; $h_0 = 0.0625\,\text{m}$; $\lambda = 0.5$; and $\nu = 0.3$.

Table 3.3

y(m)	$\dfrac{w}{p_0/E}$	$M_y\left(\dfrac{1}{p_0}\right)$
0	0	−0.03510
0.2	15.851	0.00561
0.4	30.156	0.02321
0.6	26.04	0.02065
0.8	10.3432	−0.006025
1.0	0	−0.05646

3.9 RECTANGULAR PLATES UNDER COMBINED LATERAL AND DIRECT LOADS

To this point, it was assumed that a plate is bent by lateral load only and deflections are so small that the plate middle surface was assumed to be unstrained. Thus, the latter was considered as a neutral surface. Occasionally, however, direct forces (acting in the plane of the middle surface of the plate) are applied directly at the boundaries or they arise due to temperature changes (Chapter 7). The latter forces and the corresponding stresses are also referred to as the *membrane* or *in-plane forces* and the *membrane* or *in-plane stresses*, respectively.

Attention will now be directed to situations in which lateral and direct forces act on the plate simultaneously. We will distinguish two possible cases:

1. Stresses in the middle surface are small and, therefore, their influence on the plate bending is negligible. So, the total stress may be obtained by adding stresses caused by stretching and by bending of the plate middle surface.
2. Direct stresses are not small and their effect on the plate bending should be taken into account. These stresses may have a considerable effect on the bending of the plate and must be considered in deriving the corresponding differential equation of the deflection surface. The midsurface is strained subsequent to combined loading and assumption 6 of the Kirchhoff theory (see Sec. 1.3) is no longer valid. However, w is still regarded as small so that remaining assumptions of Sec. 1.3 hold, and yet large enough so that the products of the direct forces or their derivatives and the derivatives of w are of the same order of magnitude as the derivatives of the shear forces, Q_x and Q_y. Thus, as before, the internal forces and moments are given by Eqs (2.13) and (2.27).

We consider below the second case in detail. Let a plate element of sides dx and dy be subjected to direct forces N_x, N_y, and $N_{xy} = N_{yx}$ which are functions of x and y. The top and front views of such an element are shown in Fig. 3.19a and b, respectively. The lateral load of intensity $p(x, y)$ is applied to the element and the moments, due to this load, acting on the element are shown in Fig. 2.4. We will derive the differential equation of the plate straining due to the combined effect of direct and lateral loads.

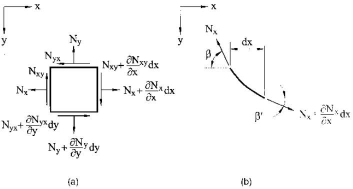
x
y
N_y
N_{yx}
N_{xy}
$N_{xy}+\frac{\partial N_{xy}}{\partial x}dx$
N_x
$N_x+\frac{\partial N_x}{\partial x}dx$
$N_{yx}+\frac{\partial N_{yx}}{\partial y}dy$
$N_y+\frac{\partial N_y}{\partial y}dy$
(a)
x
y
N_x
dx
β
β′
$N_x+\frac{\partial N_x}{\partial x}dx$
(b)

Fig. 3.19

Consider the equilibrium of the element shown in Fig. 3.19, which is subjected to the in-plane forces N_x, N_y, and N_{xy}, as well as to the lateral load $p(x, y)$. First, we apply the condition $\sum F_x = 0$. Referring to Fig. 3.19a, from the equilibrium of $N_x \mathrm{d}y$ forces into the x-direction, we obtain the following:

$$\left(N_x + \frac{\partial N_x}{\partial x}\mathrm{d}x\right)\mathrm{d}y\cos\beta' - N_x \mathrm{d}y\cos\beta, \tag{a}$$

where $\beta' = \beta + \mathrm{d}\beta = \beta + \frac{\partial\beta}{\partial x}\mathrm{d}x$. Noting that deflections are assumed to be very small and, hence, for β small $\cos\beta \approx 1$, and that likewise, $\cos\beta' \approx 1$, Eq. (a) reduces to $\frac{\partial N_x}{\partial x}\mathrm{d}x\mathrm{d}y$. The sum of the x components of $N_{xy}\mathrm{d}x$ is treated in a similar way. Thus, the force summation in the x direction leads to

$$\frac{\partial N_x}{\partial x} + \frac{\partial N_{xy}}{\partial y} = 0. \tag{3.90a}$$

Furthermore, the condition $\sum F_y = 0$ results in the following:

$$\frac{\partial N_{xy}}{\partial x} + \frac{\partial N_y}{\partial y} = 0. \tag{3.90b}$$

Equations (3.90) are independent from the equilibrium equations of Sec. 2.3 and may be studied separately.

Considering the projection of all the forces (direct and lateral) on the z axis, the plate deflection must be taken into account. Due to the bending of the plate in the xz plane, the z component of the normal force N_x is equal to (Fig. 3.19b)

$$-N_x \mathrm{d}y\sin\beta + \left(N_x + \frac{\partial N_x}{\partial x}\mathrm{d}x\right)\mathrm{d}y\sin\beta' \tag{b}$$

Inasmuch as β and β' are small, $\sin\beta \approx \beta \approx \partial w/\partial x$ and $\sin\beta' \approx \beta'$, where $\beta' = \beta + \mathrm{d}\beta$. The latter can be represented as

$$\beta' \approx \beta + \frac{\partial\beta}{\partial x}\mathrm{d}x = \frac{\partial w}{\partial x} + \frac{\partial^2 w}{\partial x^2}\mathrm{d}x;$$

substituting the above into Eq. (b) gives

$$-N_x \mathrm{d}y \frac{\partial w}{\partial x} + \left(N_x + \frac{\partial N_x}{\partial x} \mathrm{d}x \right) \left(\frac{\partial w}{\partial x} + \frac{\partial^2 w}{\partial x^2} dx \right) \mathrm{d}y.$$

Neglecting higher-order terms in this equation yields

$$N_x \frac{\partial^2 w}{\partial x^2} \mathrm{d}x\mathrm{d}y + \frac{\partial N_x}{\partial x} \frac{\partial w}{\partial x} \mathrm{d}x\mathrm{d}y.$$

The z components of the in-plane shear forces N_{xy} on the x edges of the element are determined as follows. The slopes of the deflection surface in the y direction on the x edges are equal to $\partial w/\partial y$ and $\partial w/\partial y + (\partial^2 w/\partial x \partial y)\mathrm{d}x$, respectively. The z directed component of N_{xy} is then

$$N_{xy} \frac{\partial^2 w}{\partial y \partial x} \mathrm{d}x\mathrm{d}y + \frac{\partial N_{xy}}{\partial x} \frac{\partial w}{\partial y} \mathrm{d}x\mathrm{d}y.$$

An expression identical to the above is found for the z projection of the in-plane shear forces N_{yx} acting on the y edges:

$$N_{yx} \frac{\partial^2 w}{\partial x \partial y} \mathrm{d}x\mathrm{d}y + \frac{\partial N_{yx}}{\partial y} \frac{\partial w}{\partial x} \mathrm{d}x\mathrm{d}y.$$

Finally, for the forces in Figs 3.19 and 2.4, from $\sum F_z = 0$, we have the following:

$$\frac{\partial Q_x}{\partial x} + \frac{\partial Q_y}{\partial y} + p + N_x \frac{\partial^2 w}{\partial x^2} + N_y \frac{\partial^2 w}{\partial y^2} + 2N_{xy} \frac{\partial^2 w}{\partial x \partial y}$$
$$+ \left(\frac{\partial N_x}{\partial x} + \frac{\partial N_{yx}}{\partial y} \right) \frac{\partial w}{\partial x} + \left(\frac{\partial N_{xy}}{\partial x} + \frac{\partial N_y}{\partial y} \right) \frac{\partial w}{\partial y} = 0.$$

As is seen from Eqs (3.90), the terms within the parentheses in the above expression vanish and we finally obtain the above equation in the following form:

$$\frac{\partial Q_x}{\partial x} + \frac{\partial Q_y}{\partial y} + p + N_x \frac{\partial^2 w}{\partial x^2} + N_y \frac{\partial^2 w}{\partial y^2} + 2N_{xy} \frac{\partial^2 w}{\partial x \partial y} = 0. \tag{3.91}$$

As the direct forces do not result in any moment along the edges of the element, Eqs (2.20) and (2.21), and, hence Eqs (2.27) are unchanged. Introduction of Eqs. (2.27) into Eq. (3.91), yields

$$\frac{\partial^4 w}{\partial x^4} + 2\frac{\partial^4 w}{\partial x^2 \partial y^2} + \frac{\partial^4 w}{\partial y^4} = \frac{1}{D} \left(p + N_x \frac{\partial^2 w}{\partial x^2} + N_y \frac{\partial^2 w}{\partial y^2} + 2N_{xy} \frac{\partial^2 w}{\partial x \partial y} \right). \tag{3.92}$$

Expressions (3.91) and (3.92) are *governing differential equations for a thin plate subjected to combined lateral and direct loads*. It is observed that Eq. (2.24) is now replaced by Eq. (3.92) to determine the deflection surface of the plate if the direct loads N_x, N_y, and N_{xy} are not small. Either Navier's or Levy's methods may be applied to obtain a solution.

Example 3.10

A rectangular plate with simply supported edges is subjected to the action of a combined uniform lateral load p and uniform tension N as shown in Fig. 3.20. Derive the equation of the deflection surface.

Solution

The lateral load p can be represented by the double trigonometric series (Eq. (a) of Example 3.1)

$$p = \frac{16p_0}{\pi^2} \sum_{m=1,3,5,\ldots}^{\infty} \sum_{n=1,3,5,\ldots}^{\infty} \frac{1}{mn} \sin\frac{m\pi x}{a} \sin\frac{n\pi y}{b}. \tag{a}$$

Inserting the above into Eq. (3.92), we obtain the following (letting $N_x = N$):

$$\frac{\partial^4 w}{\partial x^4} + 2\frac{\partial^4 w}{\partial x^2 \partial y^2} + \frac{\partial^4 w}{\partial y^4} - \frac{N}{D}\frac{\partial^2 w}{\partial x^2} = \frac{16p_0}{\pi^2} \sum_{m=1,3,5,\ldots}^{\infty} \sum_{n=1,3,5,\ldots}^{\infty} \frac{1}{mn} \sin\frac{m\pi x}{a} \sin\frac{n\pi y}{b}. \tag{b}$$

The boundary conditions of a simply supported plate will be satisfied if we take the deflection w in the form of series

$$w = \sum_m \sum_n w_{mn} \sin\frac{m\pi x}{a} \sin\frac{n\pi y}{b}. \tag{c}$$

Substituting this series into Eq. (b), we find the following values for coefficients w_{mn}:

$$w_{mn} = \frac{16p_0}{D\pi^6 mn\left[\left(m^2/a^2 + n^2/b^2\right)^2 + \dfrac{Nm^2}{\pi^2 Da^2}\right]}; \quad m, n = 1, 3, 5, \ldots. \tag{d}$$

Hence, the deflection surface of the plate is given by

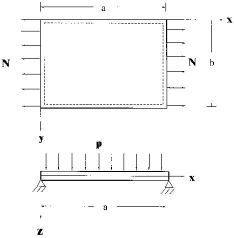

Fig. 3.20

Example 3.11

Consider a simply supported plate with sides a and b. Assume that the initial deflection is defined by the following equation:

$$w_0 = \alpha_{11} \sin \frac{\pi x}{a} \sin \frac{\pi y}{b}. \tag{a}$$

The plate edges $x = 0$ and $x = a$ are subjected to an in-plane uniform compressive force $N_x = -N$, as shown in Fig. 3.21. Find the deflected surface of the plate.

Solution

The differential equation (3.94) together with Eq. (a) will take the following form for the problem under consideration:

$$\frac{\partial^4 w_1}{\partial x^4} + 2\frac{\partial^4 w_1}{\partial x^2 \partial y^2} + \frac{\partial^4 w_1}{\partial y^4} = \frac{N}{D}\left(\frac{\alpha_{11}\pi^2}{a^2} \sin \frac{\pi x}{a} \sin \frac{\pi y}{b} - \frac{\partial^2 w_1}{\partial x^2}\right). \tag{b}$$

Let us represent a solution of the above equation in the form

$$w_1 = A \sin \frac{\pi x}{a} \sin \frac{\pi y}{b}, \tag{c}$$

where A is unknown parameter. This solution satisfies exactly the simply supported boundary conditions. Inserting Eq. (c) into Eq. (b) yields

$$A = \frac{\alpha_{11} N}{\frac{\pi^2 D}{a^2}\left(1 + \frac{a^2}{b^2}\right)^2 - N}. \tag{d}$$

Substituting for A from Eq. (d) into Eq. (c), one obtains the deflection w_1, caused by the compressive forces N. Adding this deflection to the initial deflection (a), gives the following total deflection of the plate:

$$w = w_0 + w_1 = \frac{\alpha_{11}}{1 - \beta} \sin \frac{\pi x}{a} \sin \frac{\pi y}{b}, \tag{e}$$

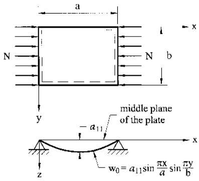

Fig. 3.21

4

Circular Plates

4.1 INTRODUCTION

Circular plates are common in many structures such as nozzle covers, end closures in pressure vessels, pump diaphragms, turbine disks, and bulkheads in submarines and airplanes, etc. When circular plates are analyzed, it is convenient to express the governing differential equation (2.24) in polar coordinates. This can be readily accomplished by a coordinate transformation. An alternative approach based on the procedure presented in Chapter 3 for rectangular plates to derive the basic relationships for the lateral deflections of circular plates may be used also.

4.2 BASIC RELATIONS IN POLAR COORDINATES

As mentioned earlier, we use the polar coordinates r and φ in solving the bending problems for circular plates. If the coordinate transformation technique is used, the following geometrical relations between the Cartesian and polar coordinates are applicable (see Fig. 4.1a):

$$x = r\cos\varphi,\ \ y = r\sin\varphi \text{ and } r^2 = x^2 + y^2, \varphi = \tan^{-1}\frac{y}{x}. \tag{4.1}$$

Referring to the above

$$\begin{aligned} &\frac{\partial r}{\partial x} = \frac{x}{r} = \cos\varphi, \quad \frac{\partial r}{\partial y} = \frac{y}{r} = \sin\varphi, \\ &\frac{\partial\varphi}{\partial x} = -\frac{y}{r^2} = -\frac{\sin\varphi}{r}, \quad \frac{\partial\varphi}{\partial y} = \frac{x}{r^2} = \frac{\cos\varphi}{r}. \end{aligned} \tag{4.2}$$

Inasmuch as the deflection is a function of r and φ, the chain rule together with the relations (4.2) lead to the following

$$\frac{\partial w}{\partial x} = \frac{\partial w}{\partial r}\frac{\partial r}{\partial x} + \frac{\partial w}{\partial \varphi}\frac{\partial \varphi}{\partial x} = \frac{\partial w}{\partial r}\cos\varphi - \frac{1}{r}\frac{\partial w}{\partial \varphi}\sin\varphi. \tag{4.3}$$

To evaluate the expression $\partial^2 w/\partial x^2$, we can repeat the operation (4.3) twice. As a result, we obtain

$$\begin{aligned}\frac{\partial^2 w}{\partial x^2} &= \cos\varphi\frac{\partial}{\partial r}\left(\frac{\partial w}{\partial x}\right) - \frac{1}{r}\sin\varphi\frac{\partial}{\partial \varphi}\left(\frac{\partial w}{\partial x}\right) \\ &= \frac{\partial^2 w}{\partial r^2}\cos^2\varphi - \frac{\partial^2 w}{\partial \varphi \partial r}\frac{\sin 2\varphi}{r} + \frac{\partial w}{\partial r}\frac{\sin^2\varphi}{r} + \frac{\partial w}{\partial \varphi}\frac{\sin 2\varphi}{r^2} + \frac{\partial^2 w}{\partial \varphi^2}\frac{\sin^2\varphi}{r^2}.\end{aligned} \tag{4.4a}$$

Similarly,

$$\frac{\partial^2 w}{\partial y^2} = \frac{\partial^2 w}{\partial r^2}\sin^2\varphi + \frac{\partial^2 w}{\partial r \partial \varphi}\frac{\sin 2\varphi}{r} + \frac{\partial w}{\partial r}\frac{\cos^2\varphi}{r} - \frac{\partial w}{\partial \varphi}\frac{\sin 2\varphi}{r^2} + \frac{\partial^2 w}{\partial \varphi^2}\frac{\cos^2\varphi}{r^2}, \tag{4.4b}$$

$$\frac{\partial^2 w}{\partial x \partial y} = \frac{\partial^2 w}{\partial r^2}\frac{\sin 2\varphi}{2} + \frac{\partial^2 w}{\partial r \partial \varphi}\frac{\cos 2\varphi}{r} - \frac{\partial w}{\partial \varphi}\frac{\cos 2\varphi}{r^2} - \frac{\partial w}{\partial r}\frac{\sin 2\varphi}{2r} - \frac{\partial^2 w}{\partial \varphi^2}\frac{\sin 2\varphi}{2r^2}. \tag{4.4c}$$

Adding term by term the relations (4.4a) and (4.4b), yields

$$\nabla_r^2 w \equiv \frac{\partial^2 w}{\partial x^2} + \frac{\partial^2 w}{\partial y^2} = \frac{\partial^2 w}{\partial r^2} + \frac{1}{r}\frac{\partial w}{\partial r} + \frac{1}{r^2}\frac{\partial^2 w}{\partial \varphi^2}. \tag{4.5}$$

After repeating twice the operation ∇_r^2, the governing differential equation for the plate deflection (2.26) in polar coordinates becomes

$$\nabla_r^4 w \equiv \left(\frac{\partial^2}{\partial r^2} + \frac{1}{r}\frac{\partial}{\partial r} + \frac{1}{r^2}\frac{\partial^2}{\partial \varphi^2}\right)\left(\frac{\partial^2 w}{\partial r^2} + \frac{1}{r}\frac{\partial w}{\partial r} + \frac{1}{r^2}\frac{\partial^2 w}{\partial \varphi^2}\right) = \frac{p}{D}, \tag{4.6a}$$

or in the expended form

$$\frac{\partial^4 w}{\partial r^4} + \frac{2}{r}\frac{\partial^3 w}{\partial r^3} - \frac{1}{r^2}\frac{\partial^2 w}{\partial r^2} + \frac{1}{r^3}\frac{\partial w}{\partial r} + \frac{2}{r^2}\frac{\partial^4 w}{\partial r^2 \partial \varphi^2} - \frac{2}{r^3}\frac{\partial^3 w}{\partial \varphi^2 \partial r} + \frac{4}{r^4}\frac{\partial^2 w}{\partial \varphi^2} + \frac{1}{r^4}\frac{\partial^4 w}{\partial \varphi^4} = \frac{p}{D}. \tag{4.6b}$$

Let us set up the relationships between moments and curvatures. Consider now the state of moment and shear force on an infinitesimal element of thickness h, described in polar coordinates, as shown in Fig. 4.1b. Note that, to simplify the derivations, the x axis is taken in the direction of the radius r, at $\varphi = 0$ (Fig. 4.1b). Then, the radial M_r, tangential M_t, twisting M_{rt} moments, and the vertical shear forces Q_r, Q_t will have the same values as the moments M_x, M_y, and M_{xy}, and shears Q_x, Q_y at the same point in the plate. Thus, transforming the expressions for moments (2.13) and shear forces (2.27) into polar coordinates, we can write the following:

equation (4.17) is given by the expressions (4.18)–(4.20). For the solid plate, which contains no concentrated loads at $r = 0$, it is easy to see that the terms involving the logarithms in Eq. (4.19) yield an infinite displacement and bending moment, and the shear force for all values of C_1 and C_2, except zero; therefore, $C_1 = C_2 = 0$. Thus, for a solid circular plate subjected to an axisymmetric distributed load with arbitrary boundary conditions, the deflection surface is given by

$$w = C_3 r^2 + C_4 + w_{\mathrm{p}}. \tag{4.23}$$

The constants of integration C_3 and C_4 in this equation are determined from boundary conditions specified at boundary $r = a$. Let us consider some particular cases of plates and loadings that are commonly encountered in practice.

(a) Plate with simply supported edge under a uniform load p_0 (Fig. 4.2a).

The boundary conditions are

$$w = 0|_{r=a},\ M_r = 0\big|_{r=a}. \tag{a}$$

Substituting for w_{p} from Eq. (4.21) into Eq. (4.23), we obtain the equation for the deflected surface:

$$w = C_3 r^2 + C_4 + \frac{p_0 r^4}{64D}, \tag{4.24}$$

and the expression for M_r may be obtained from Eq. (4.22) by making $C_1 = C_2 = 0$:

$$M_r = -D\left[2C_3(1+\nu) + \frac{p_0 r^2}{16D}(3+\nu)\right]. \tag{4.25}$$

Introducing Eqs (4.24) and (4.25) into the boundary conditions (a), one obtains the system of two algebraic equations in C_3 and C_4. Solving the above system, yields

$$C_3 = -\frac{p_0 a^2}{32D}\frac{(3+\nu)}{(1+\nu)},\ C_4 = \frac{p_0 a^4(5+\nu)}{64D(1+\nu)}. \tag{b}$$

Substituting the above into Eq. (4.24) gives the plate deflection in the form

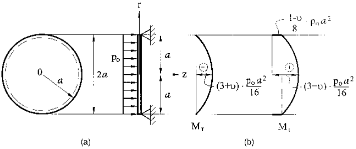

Fig. 4.2

$$w = \frac{p_0(a^2 - r^2)}{64D}\left(\frac{5+\nu}{1+\nu}a^2 - r^2\right). \tag{4.26}$$

The maximum deflection, which occurs at $r = 0$, is thus

$$w_{\max} = \frac{p_0 a^4}{64D}\left(\frac{5+\nu}{1+\nu}\right). \tag{c}$$

Given the deflection curve w, the moment equation can readily be obtained from Eqs (4.22) by substituting for C_3 and C_4 from (b) and making $C_1 = C_2 = 0$. Thus, we obtain

$$M_r = \frac{p_0}{16}(3+\nu)\left(a^2 - r^2\right),\ M_t = \frac{p_0}{16}\left[(3+\nu)a^2 - (1+3\nu)r^2\right]. \tag{4.27}$$

The bending moment diagrams are shown in Fig. 4.2b. The maximum moments also occur at the plate center, i.e., at $r = 0$. Thus, we have

$$\max M_r = \max M_t = \frac{p_0 a^2}{16}(3+\nu). \tag{4.28}$$

(b) Plate with clamped edge under a uniform load p_0 (Fig. 4.3a)

The boundary conditions are

$$w = 0|_{r=a}, \quad \frac{\mathrm{d}w}{\mathrm{d}r} = 0\bigg|_{r=a}. \tag{d}$$

Introducing the deflection surface in the form of Eq. (4.24) into the conditions (d), we obtain

$$C_3 = -\frac{p_0 a^2}{32D},\ C_4 = \frac{p_0 a^4}{64D}. \tag{e}$$

Similarly to the procedure for the previous case, the deflection is then

$$w = \frac{p_0}{64D}\left(a^2 - r^2\right)^2. \tag{4.29}$$

The maximum deflection occurs at the center of the plate:

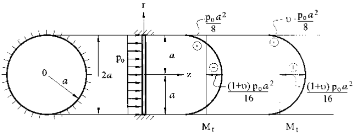
r
0
a
2a
p_0
a
a
z
$\frac{p_0 a^2}{8}$
+
−
$\frac{(1+\nu)\,p_0 a^2}{16}$
M_r
$\nu \cdot \frac{p_0 a^2}{8}$
+
+
$\frac{(1+\nu)\,p_0 a^2}{16}$
M_t

(a) (b)

Fig. 4.3

$$w_{\max} = \frac{p_0 a^4}{64D}. \tag{f}$$

Expressions for the bending moments are calculated by means of Eqs (4.22). Substituting for C_3 and C_4 from Eqs (e) into Eqs (4.22) and letting $C_1 = C_2 = 0$, we obtain

$$M_r = \frac{p_0}{16}\left[(1+\nu)a^2 - (3+\nu)r^2\right]; \quad M_t = \frac{p_0}{16}\left[(1+\nu)a^2 - (1+3\nu)r^2\right]. \tag{4.30}$$

The bending moment distributions are shown in Fig. 4.3b. The maximum bending moment M_r occurs at the edge of the plate (at $r = a$), where

$$\max M_r = -\frac{p_0 a^2}{8}. \tag{4.31a}$$

The maximum bending moment M_t takes place at the plate center (at $r = 0$), where

$$\max M_t = \frac{p_0 a^2 (1+\nu)}{16}. \tag{4.31b}$$

If $\nu = 0.3$, comparing Eqs (c) and (f), we see that the maximum deflection for the simply supported plate is about four times as great as that for the plate with a clamped edge. For the same value of ν, the maximum bending moment for a simply supported plate is about 1.7 times as great as that for the plate with clamped edge.

(c) Circular plate under a concentrated force at its center

When a concentrated or a point load acts at the plate center, one can set $p_0 = 0$ and, thus, $w_{\mathrm{p}} = 0$ in Eq. (4.18). Referring to Eq. (4.19), we can conclude that C_1 must be taken as zero in order that the deflection should be finite at $r = 0$. The term involving C_2 must now be retained because of the very high shear stresses present in the vicinity of the center (see Sec. 3.4). The deflection surface of the plate is then represented, as follows:

$$w = C_2 r^2 \ln r + C_3 r^2 + C_4. \tag{4.32}$$

The constants C_2, C_3, and C_4 are evaluated from the boundary conditions and from conditions at the point of application of the concentrated force. As an example, consider *the plate with clamped edge loaded by a concentrated force* P applied at plate center O, as shown in Fig. 4.4a. The boundary conditions (d), when introduced into Eq. (4.32) lead to

$$\begin{aligned} &C_2 a^2 \ln a + C_3 a^2 + C_4 = 0, \\ &C_2 a(2\ln a + 1) + 2C_3 = 0. \end{aligned} \tag{g}$$

The additional condition can be set up from the following consideration. Let us isolate a small cylinder of radius r in the vicinity of the application of P (Fig. 4.5).

From equilibrium of this cylinder, we obtain

$$\sum F_z = 0: \quad Q_r(2\pi r) + P = 0 \quad \text{or} \quad Q_r = -\frac{P}{2\pi r}.$$

Substituting for Q_r from Eq. (4.22) into the above and letting $p_0 = 0$, we obtain

As seen, the bending moments for both plates approach infinity at the point of application of concentrated force ($r \to 0$) (see Fig. 4.4b). The appearance here of a singularity in the bending moments has the same nature as that discussed earlier for rectangular plates loaded by a concentrated force. A detailed explanation of this phenomenon is provided in Sec. 3.4.

(d) Simply supported circular plate subjected to a symmetric lateral load which linearly increases from the center of the edge (Fig. 4.6)

Substituting $p = p_0 \frac{r}{a}$ into Eq. (4.20) for the particular solution gives

$$w_{\mathrm{p}} = \int \frac{1}{r} \int r \int \frac{1}{r} \int \frac{1}{D} r \left(p_0 \frac{r}{a} \right) \mathrm{d}r \mathrm{d}r \mathrm{d}r \mathrm{d}r = \frac{p_0 r^5}{225aD}. \tag{4.36}$$

Substituting the above into Eq. (4.23), yields the general solution of the form

$$w = C_3 r^2 + C_4 + \frac{p_0 r^5}{225aD}. \tag{a}$$

Substituting (a) into the boundary conditions (4.11) leads to the following values of the constants of integration:

$$C_3 = -\frac{p_0 a^2}{90D}\left(\frac{4+\nu}{1+\nu}\right), \quad C_4 = \frac{p_0 a^4}{45D}\left[\frac{4+\nu}{2(1+\nu)} - \frac{1}{5}\right]. \tag{b}$$

Equation (a) with known coefficients C_3 and C_4 determines the deflected plate surface

$$w = \frac{p_0 a^2}{45D}\left\{ \frac{r^2}{2}\left(\frac{4+\nu}{1+\nu}\right) + a^2\left[\frac{4+\nu}{2(1+\nu)} - \frac{1}{5}\right] + \frac{r^5}{5a^3} \right\}. \tag{c}$$

Example 4.1

A cylindrical tank and flat thin plate bottom are subjected to internal pressure p, as shown in Fig. 4.7a. Determine a required thickness of the bottom, h, and calculate its maximum deflection. Use $R = 0.25\,\mathrm{m}$, $p = 2.5\,\mathrm{MPa}$, $E = 200\,\mathrm{GPa}$, and $\nu = 0.3$, respectively. The allowable stress σ_{all} is 150 MPa.

Solution

The cylindrical tank bottom represents a circular solid plate. It is necessary to establish a type of boundary conditions on the plate edge, which depends on a rigidity of the cylinder, and the presence of the gasket at the connection. If the

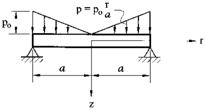

Fig. 4.6

cylinder itself is sufficiently rigid, the plate of radius is R (Fig. 4.7b) is thin and, in addition, the bottom is inserted without a soft gasket, then we can assume the circular plate edge to be clamped over the contour of the bolts arrangement and the plate. If the cylinder walls are compliant and the soft gaskets are at the connection, one can take the plate edge to be simply supported (Fig. 4.7c). In practice, a real type of plate support is an intermediate one between the above-mentioned extreme cases, i.e., they (the supports) represent an elastic restraint support. In order to gain a clear impression of real stresses and deformations occurring in the bottom, it makes sense to consider both extreme cases. The deflection surfaces and bending moments for these cases are given by Eqs (4.29), (4.30), and (4.26), (4.27). The bending moment, M_r and M_t, diagrams are shown in Figs 4.3 and 4.4 for both extreme cases. Referring to these diagrams, we can conclude that the maximum bending moment for a simply supported circular plate occurs at the center, while for the plate with clamped edge the maximum bending moment is at the plate edge. The value of the maximum bending moment for a simply supported plate is nearly 1.7 times larger than for a plate with a clamped edge (for $\nu = 0.3$). However, taking into account that the plate edge is rather clamped than simply supported, one can expect that the value of the maximum bending moment at the plate center does not exceed $p_0R^2/8$, i.e., the value of the bending moment at the clamped edge. Therefore, the circular plate with a clamped edge can be taken as the design variant of the tank head. The maximum normal stress occurs at the clamped edge (i.e., for $r = R$ and $z = \pm h/2$). From Eq. (4.8), $\sigma_{\max}$ is given by

$$\sigma_{r,\max} = \frac{M_{r,\max}}{h^2/6} = \frac{6pR^2}{8h^2}, \quad \sigma_{t,\max} = \frac{M_{t,\max}}{h^2/6} = \nu\frac{6pR^2}{8h^2}.$$

The third principal stress $\sigma_3 = \sigma_z = 0$, according to the general assumptions adopted in the plate bending theory. Since the material of the plate is assumed to be a ductile, the maximum shear (Tresca) criterion of yielding (see Appendix A.6.2) can be applied: namely,

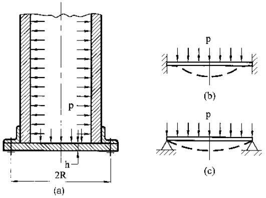

Fig. 4.7

$$\sigma_e = \sigma_1 - \sigma_3 = \frac{6pR^2}{8h^2} \le \sigma_{\text{all}}.$$

Solving this for the plate thickness, h, yields

$$h = \sqrt{\frac{6pR^2}{8\sigma_{\text{all}}}} = \sqrt{\frac{6(2.5 \times 10^6)(0.25)^2}{8(150 \times 10^6)}} \approx 28\,\text{mm};$$

$$D = \frac{Eh^3}{12(1-\nu^2)} = 40.2 \times 10^4\,\text{N} \cdot \text{m}$$

Note that if the simply supported plate was chosen as a design variant, then the plate thickness was found to be $h \approx 36\,\text{mm}$.

The maximum deflection for the selected design variant of the tank head is given by Eq. (f) (case (b) in Sec. 4.3.1), as follows:

$$w_{\max} = \frac{pR^4}{64D}.$$

Substituting the given numerical data into the above equation gives

$$w_{\max} = 0.38\,\text{mm}.$$

Example 4.2

Find the expression for the deflection of the clamped solid plate shown in Fig. 4.8a due to line load p distributed along a circle with radius $r = b$.

Solution

To solve this problem, one first divides the plate problem into two parts (Fig. 4.8b): an inner solution for a solid plate 1 extending over the region $0 \le r \le b$, and an outer solution for an annular plate 2 over the region $b \le r \le a$. In each case, the governing equation are (for $p = 0$)

$$\nabla_r^4 w_1 = 0; \ \nabla_r^4 w_2 = 0.$$

For the inner plate 1 the solution w_1 is of the form (see Eq. (4.23))

$$w_1 = C_3^{(1)} r^2 + C_4^{(1)}, \tag{a}$$

and for plate 2 the corresponding solution is

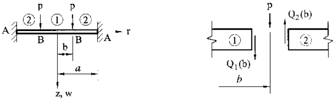

(a) (b)

Fig. 4.8

$$w_2 = C_1^{(2)} \ln r + C_2^{(2)} r^2 \ln r + C_3^{(2)} r^2 + C_4^{(2)}. \tag{b}$$

The six constants in Eqs (a) and (b) are determined from the boundary conditions at $r = a$, i.e.,

$$w_2 = 0\big|_{r=a} \quad \frac{\mathrm{d}w_2}{\mathrm{d}r} = 0\bigg|_{r=a} \tag{c}$$

and from the continuity conditions at the junction of the two plate segments. The latter have the form

$$w_1\big|_{r=b} = w_2\big|_{r=b}; \ \frac{\mathrm{d}w_1}{\mathrm{d}r}\bigg|_{r=b} = \frac{\mathrm{d}w_2}{\mathrm{d}r}\bigg|_{r=b}; \quad M_r^{(1)}\Big|_{r=b} = M_r^{(2)}\Big|_{r=b}; \quad p = Q_r^{(1)}\Big|_{r=b} - Q_r^{(2)}\Big|_{r=b}. \tag{d}$$

Since the inner plate is in pure bending (see Eq. (a)), then $Q_r^{(1)} = 0$ and the last condition (d) is of the form

$$p = -Q_r^{(2)}\Big|_{r=b}. \tag{e}$$

The last condition (e) is illustrated in Fig. 4.8b. Introducing expressions (a) and (b) into conditions (c), (d), and (e) together with Eqs (4.14), we can find the six constants of integration. The final solution is, as follows:

– *for the inner plate* $1, \ 0 \le r \le b$

$$w = \frac{pb}{8a^2 D}\left[\left(a^2 - b^2\right)\left(a^2 + r^2\right) - 2a^2\left(b^2 + r^2\right)\ln\frac{a}{b}\right]; \tag{4.37a}$$

– *for the outer annular plate* $2, \ b \le r \le a$

$$w = \frac{pb}{8a^2 D}\left[\left(a^2 + b^2\right)\left(a^2 - r^2\right) + 2a^2\left(b^2 + r^2\right)\ln\frac{r}{a}\right]. \tag{4.37b}$$

4.3.2 Annular circular plates

In this section, we discuss the bending of circular plates with concentric circular holes, the so-called *annular plates* (Fig. 4.9).

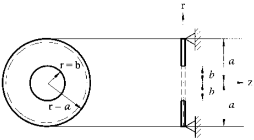

Fig. 4.9

The outer and inner radii of a plate are denoted by a and b, respectively. For annular plates the homogeneous solution is given by Eq. (4.19). The solution of an axially symmetric bending of circular plates with central holes may follow a procedure similar to the one discussed in the foregoing section, but one must consider the boundary conditions at the outer ($r = a$) as well as the inner ($r = b$) boundaries. Two typical cases of loading are illustrated below.

(a) Simply supported annular plate loaded by edge moments (Fig. 4.10)

For this case of loading, $w_{\mathrm{p}} = 0$ and the general solution is given by

$$w = C_1 \ln r + C_2 r^2 \ln r + C_3 r^2 + C_4. \tag{4.38}$$

The boundary conditions are

$$M_r = m_1\big|_{r=b}; \quad Q_r = 0\big|_{r=b}; \quad M_r = m_2\big|_{r=a}; \quad w = 0|_{r=a}. \tag{a}$$

Introducing Eq. (4.38) into the boundary conditions (a), with the use of Eqs (4.14), yields the following expressions for the constants of integration:

$$\begin{aligned} C_1 &= \frac{(m_1 - m_2)a^2 b^2}{D(1-\nu)\left(a^2 - b^2\right)}, \quad C_2 = 0,\ C_3 = \frac{m_1 b^2 - m_2 a^2}{2D(1+\nu)\left(a^2 - b^2\right)}, \\ C_4 &= -\frac{(m_1 - m_2)a^2 b^2}{D(1-\nu)\left(a^2 - b^2\right)} \ln a - \frac{\left(m_1 b^2 - m_2 a^2\right)}{2D(1+\nu)\left(a^2 - b^2\right)} a^2. \end{aligned} \tag{b}$$

Substituting the above into Eq. (4.38) yields the expression for deflections:

$$w = \frac{(m_1 - m_2)a^2 b^2}{D(1-\nu)\left(a^2 - b^2\right)} \ln \frac{r}{a} + \frac{m_1 b^2 - m_2 a^2}{2D(1+\nu)\left(a^2 - b^2\right)} \left(r^2 - a^2\right). \tag{4.39}$$

Substituting the above expression into Eqs (4.14) gives the expressions for bending moments:

$$M_r = -\frac{m_1 b^2 - m_2 a^2}{a^2 - b^2} + \frac{a^2 b^2 (m_1 - m_2)}{r^2\left(a^2 - b^2\right)}; \ M_t = -\frac{m_1 b^2 - m_2 a^2}{a^2 - b^2} - \frac{a^2 b^2 (m_1 - m_2)}{r^2\left(a^2 - b^2\right)}. \tag{4.40}$$

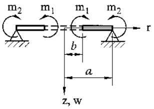

Fig. 4.10

(b) Simply supported plate under a line load uniformly distributed along the inner edge (Fig. 4.11)

Again, $w_\mathrm{p} = 0$, and the general solution is given by Eqs (4.38). The boundary conditions are

$$w = 0|_{r=a}; \quad M_r = 0\Big|_{r=a}; \quad M_r = 0\Big|_{r=b}; \quad Q_r = -p\Big|_{r=b}. \tag{4.41}$$

Substituting expressions (4.14) and (4.38) into boundary conditions (4.41), we find

$$C_1 = p\frac{b}{4D}\frac{2(1+\nu)\ln\frac{b}{a}}{(1-\nu)(a^2-b^2)}a^2b^2, \quad C_2 = p\frac{b}{4D},$$

$$C_3 = p\frac{b}{4D}\left(\frac{b^2\ln\frac{b}{a}}{a^2-b^2} - \ln a - \frac{3+\nu}{2(1+\nu)}\right),$$

$$C_4 = -p\frac{b}{4D}\left\{\frac{a^2b^2\ln\frac{b}{a}}{a^2-b^2}\left[\frac{2(1+\nu)}{1-\nu}+\right] - \frac{(3+\nu)a^2}{2(1+\nu)}\right\}.$$

Substitution of the above into Eq. (4.38) gives the following expression for the deflection:

$$\begin{aligned} w = p\frac{a^2b}{4D}\Bigg\{&\left(1-\frac{r^2}{a^2}\right)\left[\frac{3+\vartheta}{2(1+\vartheta)} - \frac{b^2}{a^2-b^2}\ln\frac{b}{a}\right] \\ &+\frac{r^2}{a^2}\ln\frac{r}{a} + \frac{2b^2}{a^2-b^2}\frac{1+\vartheta}{1-\vartheta}\ln\frac{b}{a}\ln\frac{r}{a}\Bigg\}. \end{aligned} \tag{4.42}$$

It is observed that if $b \to 0$, $b^2 \ln (b/a)$ vanishes, and Eq. (4.42), letting $p = P/2\pi b$, reduces to the first equation (4.35) for a solid circular plate under a concentrated force applied at its center.

4.4 THE USE OF SUPERPOSITION FOR THE AXISYMMETRIC ANALYSIS OF CIRCULAR PLATES

The procedure discussed in Sec. 4.3 for determining the deflections and bending moments of symmetrically loaded circular plates is applicable to other cases of loading and boundary conditions. For complicated configurations of loads and boundary conditions, the method of superposition may be used to good advantage

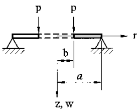

Fig. 4.11

to simplify the analysis. Superposition is a valid method of solution if the response of a structure is directly proportional to the load that produces it and deflections are small. Then, if a static loading is broken into simpler components, the final response is independent of whether component loads are applied simultaneously or added in arbitrary sequence. Let us illustrate an application of the method of superposition in the following examples.

Example 4.3

Find the center deflection, w_0, in the solid clamped plate loaded as shown in Fig. 4.12a.

Solution

Consider a solid plate with clamped edge loaded by a line load p around a circle of radius c, as shown in Fig. 4.12b. The center deflection, w_0, is given by expression (4.37a). Setting $b = c$ and $r = 0$, we obtain the center deflection, w_0, as follows:

$$w_0 = \frac{pc}{8D}\left(a^2 - c^2 + 2c^2 \ln \frac{c}{a}\right). \tag{a}$$

Having the deflection for a load uniformly distributed along a concentric circle, we can determine the deflection for the given loading using the method of superposition. In fact, consider an infinitesimal line load $p_0 \mathrm{d}c$ around a circle of radius c on a plate, as shown in Fig. 4.12c. Then, the center deflection for the given loading is obtained from Eq. (a), replacing p by $p_0 \mathrm{d}c$ and integrating from 0 to b. We have

$$\begin{aligned} w_c &= \frac{p_0}{8D}\int_0^b \left(a^2 c - c^3 + 2c^3 \ln c - 2c^3 \ln a\right)\mathrm{d}c \\ &= \frac{p_0}{8D}\left[a^2\frac{c^2}{2} - \frac{c^4}{4} + 2 \ln a \cdot \frac{c^4}{4} + 2\left(\frac{c^4}{4}\ln c - \frac{c^4}{16}\right)\right]\Bigg|_0^b . \end{aligned}$$

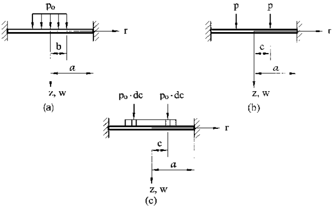

Fig. 4.12

Finally, we obtain

$$w_c = \frac{p_0 b^2}{16D}\left(a^2 - \frac{3}{4}b^2 + b^2 \ln\frac{b}{a}\right). \tag{4.43}$$

Example 4.4

The plate shown in Fig. 4.13a is stepped so that the central disk has twice the flexural rigidity of the outer annulus. Find the maximum deflection and bending moment M_r at $r = 0.5a$, caused by concentrated force P. Use $\nu = 0.3$.

Solution

The plate can be separated into two components (Fig. 4.13b): an inner part of the plate of radius $a/2$ and outer part in the form of an annular plate ($a/2 \le r \le a$). Continuity between the inner and outer plates is maintained by applying an unknown moment, M_r, as shown in Fig. 4.13b.

First, consider the solution for the inner plate. The slope at $r = a/2$ is

$$\frac{\mathrm{d}w_{\mathrm{i}}}{\mathrm{d}r} = \frac{\mathrm{d}w_{\mathrm{i}}}{\mathrm{d}r}(P) + \frac{\mathrm{d}w_{\mathrm{i}}}{\mathrm{d}r}(M_r), \tag{a}$$

where $\frac{\mathrm{d}w_{\mathrm{i}}}{\mathrm{d}r}(P)$ and $\frac{\mathrm{d}w_{\mathrm{i}}}{\mathrm{d}r}(M_r)$ are the slopes of the inner plate at $r = a/2$ produced by an external concentrated force P and bending moment M_r, respectively. The above slopes can be obtained by differentiating the expressions for the deflections given by the first equation (4.35) and Eq. (4.39) and then setting $r = a/2$ in the equation for $\frac{\mathrm{d}w_{\mathrm{i}}}{\mathrm{d}r}(P)$ and $r = a/2, m_1 = 0,\ b = 0,$ and $m_2 = M_r$ in the equation for $\frac{\mathrm{d}w_{\mathrm{i}}}{\mathrm{d}r}(M_r)$. Thus, we obtain the following:

$$\frac{\mathrm{d}w_{\mathrm{i}}}{\mathrm{d}r}(P) = -0.0612\frac{P(0.5a)}{2D} = -0.0153\frac{Pa}{D};$$

$$\frac{\mathrm{d}w_{\mathrm{i}}}{\mathrm{d}r}(M_r) = C_1\frac{0.5a}{2} + C_2\frac{1}{0.5a} = \frac{0.5a}{2}\left(-\frac{2(0.25a^2)M_r}{1.3(0.25a^2)2D}\right) = -0.1923\frac{M_r a}{D}. \tag{b}$$

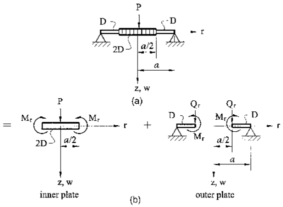

Fig. 4.13

Thus, at the plate center, at $r = 0$, the maximum deflection is given as

$$w_{\max} = 0.0505\frac{P(0.25a^2)}{2D} + \frac{M_r a^2}{4D(1+\nu)} - \frac{M_r b^2}{D(a^2-b^2)} \left[\frac{2}{1+\nu}\frac{b^2-a^2}{4} + \frac{a^2}{1-\nu}\ln\frac{b}{a}\right] + 0.1934 Q_r \frac{a^3}{D}.$$

Substituting here Q_r from Eq. (d) for M_r from Eq. (j), we compute the center deflection:

$$w_{\max} = 0.03224\frac{Pa^2}{D}$$

4.5 CIRCULAR PLATES ON ELASTIC FOUNDATION

We consider in this section circular plates loaded symmetrically with respect to their center and resting on a Winkler-type foundation, which was discussed earlier in chapter 3. The foundation reaction, $q(r)$, can be described by

$$q(r) = k \cdot w(r), \tag{4.44}$$

where $k(k = \text{const})$ is the modulus of the foundation.

Introducing the reaction of the foundation from Eq. (4.44) into Eq. (4.15b), we obtain the governing differential equation of bending of circular plates resting on a Winkler-type foundation:

$$\left(\frac{d^2}{dr^2} + \frac{1}{r}\frac{d}{dr}\right)\left(\frac{d^2 w}{dr^2} + \frac{1}{r}\frac{dw}{dr}\right) = \frac{1}{D}(p - kw), \tag{4.45}$$

where p is a given surface load. Denoting

$$l = \sqrt[4]{\frac{D}{k}}, \tag{4.46}$$

and introducing the dimensionless coordinate $\zeta = r/l$, one can write Eq. (4.45) in the form

$$\left(\frac{d^2}{d\zeta^2} + \frac{1}{\zeta}\frac{d}{d\zeta}\right)^2 w + w = \frac{pl^4}{D}. \tag{4.47}$$

Introducing the following notation

$$\nabla_\zeta^2 = \frac{d^2}{d\zeta^2} + \frac{1}{\zeta}\frac{d}{d\zeta}, \tag{4.48}$$

we can rewrite Eq. (4.47) as follows:

$$\nabla_\zeta^4 w + w = \frac{pl^4}{D}. \tag{4.49}$$

For $p = 0$, the homogeneous equation (4.49) is reduced to a system of the following two second-order differential equations:

The constants of integration, $A_n, \ldots, D_n$, can be determined from boundary conditions of the plate. The boundary conditions on curvilinear edges of the circular plates are given by the expressions (4.10)–(4.12). The stress resultants and stress couples within the plate and on its edge are given by Eqs (4.7) and (4.9). Some details of an asymmetrical circular plate analysis are explained by considering the following illustrative problems.

Example 4.7

The edge of a solid circular plate of radius a is fixed over its boundary and the applied load is expressed as

$$p = p_0\left(1 + \frac{x}{a}\right) = p_0\left(1 + \frac{r}{a}\cos\varphi\right). \tag{a}$$

Find an expression for the deflections (Fig. 4.14).

Solution

Comparing Eq. (a) with Eq. (4.62), we can see that only two terms of the series are present in the example: an axisymmetric component p_0 and component $p_n(r)\cos n\varphi$ for $n = 1$ i.e., $p_1(r) = p_0 \frac{r}{a}\cos\varphi$. The axisymmetric part of the solution, caused by load p_0,w_0, has been obtained in Sec. 4.3 and is expressed by formulas (4.29) and (4.30).

Find the asymmetrical part of the solution, w_1, that corresponds to the load component $p_1(r)$. The above part of the solution can also be represented in the form of Eq. (4.18). The homogeneous solution is given by the second equation (4.61), i.e.,

$$w_{\mathrm{h}}^{(1)} = f_1(r)\cos\varphi = \left(A_1 r + B_1 r^{-1} + C_1 r^3 + D_1 r \ln\frac{r}{a}\right)\cos\varphi, \tag{b}$$

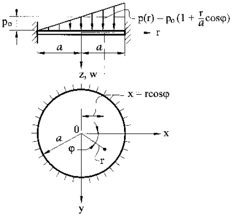

Fig. 4.14

The bending moments can be obtained by substitution for w from (g) into Eqs (4.7).

Stress analysis of circular plates having various boundary conditions and subjected to asymmetrical loading can be successfully carried out by numerical and approximate methods introduced in Chapter 6. Among other methods, the *reciprocity theorem* [4] may enable a simple approach for computation of the center displacements in circular plates with symmetrical boundary conditions under asymmetrical loading.

Consider a circular plate that carries two loads P_C and P_D applied at points C and D, respectively. Maxwell's reciprocal theorem is formulated, as follows [6]:

$$P_C \Delta_{CD} = P_D \Delta_{DC}, \tag{4.64}$$

where Δ_{CD} is the displacement component at point C in the direction of load P_C and due to load P_D; Δ_{DC} is the displacement component at point D in the direction of load P_D and due to load P_C. Equation (4.64) states that work done by the load P_C in moving through displacement produced by the load P_D is equal to work done by the load P_D in moving through displacement produced by the load P_C. The words ''load'' and ''displacement'' can be given by their general meanings, i.e., concentrated forces and deflections, couples and their rotations; at last, distributed load and the corresponding deflections are included.

Let point C be the center of a circular plate and point D be some point located at a distance r from that center. Denote $\Delta_{CD} = w_C$ and $\Delta_{DC} = w(r)$. Evidently $w(r)$ is a deflection at point D due to the unit force applied at the plate center. In the cases of fixed and simply supported plates, $w(r)$ is given by expressions obtained in Eqs (4.33) and (4.35), respectively. Then, let $P_C = 1$ and $P_D = p(r, \varphi)$. Substituting the above into Eq. (4.64), one obtains

$$w_C = \int_0^{2\pi}\int_0^{a} p(r,\varphi) w(r) r \mathrm{d}r \mathrm{d}\varphi \tag{4.65}$$

where a is the radius of a circular plate.

To illustrate the application of Eq. (4.65), reconsider Example 4.7. Upon substituting $p(r,\varphi) = p_0\left(1 + \frac{r}{a}\cos\varphi\right)$ and Eq. (4.33) into Eq. (4.65), setting $P = 1$ and integrating, we obtain

$$w_C = \frac{p_0}{16\pi D}\int_0^{2\pi}\int_0^{a}\left(1 + \frac{r}{a}\cos\varphi\right)\left(2r^2 \ln\frac{r}{a} + a^2 - r^2\right) r \mathrm{d}r \mathrm{d}\varphi = \frac{p_0 a^4}{64D}. \tag{4.66}$$

The above coincides exactly with the value given by Eq. (i) in Example 4.7.

4.7 CIRCULAR PLATES LOADED BY AN ECCENTRIC LATERAL CONCENTRATED FORCE

The solution for circular plates under an arbitrary concentrated load can be considered one of the fundamental problems in the theory of plates, because this solution can be used as the Green's function (see Sec. 3.4) for determining deflections of the plate caused by an arbitrary asymmetric loading.

Consider a bending problem for a clamped circular plate of radius R loaded by a concentrated force P applied at a distance b from the center of the plate. Represent the given concentrated force in the following form of series:

$$\frac{P}{\pi b}\left(\frac{1}{2}+\sum_{n=1}^{\infty}\cos n\varphi\right).$$

This series is quite analogous to the series applied earlier for the case of a rectangular plate loaded by a concentrated force. Then, the deflected surface of the plate, $w(r, \varphi)$, can be sought also in the form of the trigonometric series corresponding to the given loading. The next procedure for obtaining a solution of Eq. (4.6) will be quite similar to that discussed in Sec. 4.6. An approach for obtaining the solution of the problem leads to a rapidly convergent series for deflections. However the series in the solutions for the bending moments and shear forces do not convergent rapidly, and, directly at the point of application of the concentrated force these series are divergent (see Sec. 3.4). Therefore, a solution of this problem in the closed form is of a special interest. Such a solution was first obtained by Michell [5]. We present Michell's solution below.

At first, let us remind ourselves of one well-known definition of a circle given in analytical geometry. Let point M^0 be any point on the circumference, points O_1 and O_2 some fixed points on the xy coordinate plane and r_1^0 and r_2^0 some distances from point M^0 to points O_1 and O_2 as shown in Fig. 4.15a.

Then, any circle can be defined as a locus of points for which the ratio r_1^0/r_2^0 is a constant. In fact, as follows from Fig. 4.15a,

$$r_1^0=\sqrt{R^2+(\lambda R)^2-2R\cdot(\lambda R)\cos\varphi};\quad r_2^0=\sqrt{R^2+(R/\lambda)^2-2R\cdot(R/\lambda)\cos\varphi}, \tag{4.67}$$

where λ is some parameter. It can be shown that

$$\frac{r_1^0}{r_2^0}=\lambda=\text{const}. \tag{4.68}$$

Let the concentrated force P be applied at point O_1 at a distance λR from the center, as shown in Fig. 4.15b. Locate an arbitrary point M of the plate by coordinates r_1 and r_2, which are the distances from the above point to some fixed points O_1 and O_2.

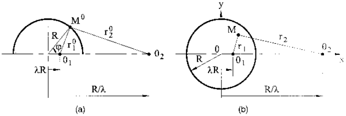

Fig. 4.15

$$w = \frac{P}{8\pi D} r_1^2 \ln \frac{r_1}{\lambda r_2} + C_3 \left(r_2^2 - \frac{r_1^2}{\lambda^2} \right). \tag{4.76}$$

The constant C_3 is determined from the condition that on the boundary $\partial w / \partial n = 0$. Since $w = 0$, then to satisfy this boundary condition it is sufficient that $\partial w / \partial r_1 = 0$ on the boundary, i.e., for $r_1 = \lambda r_2$. As it follows from the above, $C_3 = \frac{P}{8\pi D} \frac{\lambda^2}{2}$. Finally, we obtain

$$w = \frac{P}{8\pi D} \left[r_1^2 \ln \frac{r_1}{\lambda r_2} + \frac{1}{2} (\lambda^2 r_2^2 - r_1^2) \right]. \tag{4.77}$$

At the point of application of the concentrated force, i.e., for $r_1 = 0$ and $r_2 = R\left(\frac{1}{\lambda} - \lambda\right)$ (see Fig. 4.15b), the deflection is

$$w = \frac{PR^2}{16\pi D} (1 - \lambda^2). \tag{4.78}$$

The closed-form equation for the deflections enables one to determine the bending moments in the closed form also. For this purpose, we first find the derivatives of w and the bending moments in the Cartesian coordinate system using Eqs (4.70). The bending moments at points of the diameter passing through the point of application of the force ($y = 0$) are found to be

$$\begin{aligned} M_x = M_r &= \frac{P}{8\pi D} \left[2(1+\nu) \ln \frac{r_1}{\lambda r_2} + 2 + \lambda^2 (1+\nu) + \frac{r_1^2}{r_2^2} (1-\nu) \right], \\ M_y = M_t &= \frac{P}{8\pi D} \left[2(1+\nu) \ln \frac{r_1}{\lambda r_2} + 2\nu + \lambda^2 (1+\nu) - \frac{r_1^2}{r_2^2} (1-\nu) \right]. \end{aligned} \tag{4.79}$$

where $r_1 = x - \lambda R,\ r_2 = R/\lambda - x$.

In the particular case of a clamped circular plate loaded by a concentrated force P applied at its center, $\lambda \to 0$ and Eqs (4.78) and (4.79) will coincide with those obtained in Sec. 4.3 for an axisymmetrically loaded circular plate (see Eqs (4.33) and (4.34)).

4.8 CIRCULAR PLATES OF VARIABLE THICKNESS

We limit ourselves to axisymmetric bending, since this is the type most widely encountered in engineering – for example, in many machine parts, such as turbine blades, bellows, springs, etc. Following Szillard [6], we derive the governing equation of these plates.

Due to the symmetry, Q_t and M_{rt} vanish and only internal forces and moments show in Fig. 4.16a act on the plate element, as follows

$$(Q_r + \mathrm{d}Q_r)(r + \mathrm{d}r)\mathrm{d}\varphi - Q_r r \mathrm{d}\varphi + p \mathrm{d}s \mathrm{d}r = 0, \tag{4.80}$$

$$\left(M_r + \frac{\mathrm{d}M_r}{\mathrm{d}r} \mathrm{d}r \right)(r + \mathrm{d}r)\mathrm{d}\varphi - M_r r \mathrm{d}\varphi - Q_r r \mathrm{d}\varphi \mathrm{d}r - M_t \mathrm{d}r \mathrm{d}\varphi = 0. \tag{4.81}$$

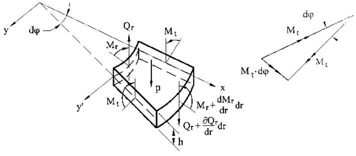
y
dφ
Q_r
M_t
M_r
p
x
y'
M_t
$M_r + \frac{dM_r}{dr} dr$
$Q_r + \frac{\partial Q_r}{dr} dr$
h
dφ
M_t
$M_t \cdot d\varphi$
M_t

(a) (b)

Fig. 4.16

The last term on the left-hand side of Eq. (4.81) is due to the resultant moment shown in Fig. 4.16b. Replacing $\mathrm{d}s = r\mathrm{d}\varphi$, canceling the common factor $\mathrm{d}r\mathrm{d}\varphi$ and neglecting small quantities of higher order, Eqs (4.80) and (4.81) become

$$-\frac{1}{r}\frac{\mathrm{d}}{\mathrm{d}r}(rQ_r) = p, \tag{4.82}$$

$$Q_r = \frac{\mathrm{d}M_r}{\mathrm{d}r} + \frac{1}{r}(M_r - M_t). \tag{4.83}$$

Substituting for M_r and $M_t$from Eqs (4.14) into Eq. (4.83) and making $D = D(r)$, we obtain

$$\frac{\mathrm{d}^3 w}{\mathrm{d}r^3} + \frac{\mathrm{d}^2 w}{\mathrm{d}r^2}\left(\frac{1}{D}\frac{\mathrm{d}D}{\mathrm{d}r} + \frac{1}{r}\right) + \frac{\mathrm{d}w}{\mathrm{d}r}\left(\frac{\nu}{rD}\frac{\mathrm{d}D}{\mathrm{d}r} - \frac{1}{r^2}\right) + \frac{Q_r}{D} = 0. \tag{4.84}$$

If we substitute for Q_r from the third equation (4.14) into Eq. (4.82), we obtain

$$\frac{1}{r}\frac{\mathrm{d}}{\mathrm{d}r}\left\{rD\frac{\mathrm{d}}{\mathrm{d}r}\left[\frac{1}{r}\frac{\mathrm{d}}{\mathrm{d}r}\left(r\frac{\mathrm{d}w}{\mathrm{d}r}\right)\right]\right\} = p(r). \tag{4.85}$$

Either of the two equations, (4.84) or (4.85), can be used as the governing differential equations of axisymmetrically loaded circular plates of variable thickness.

In order to lower the order of differential equation (4.84), let us introduce a new variable

$$\vartheta = -\frac{\mathrm{d}w}{\mathrm{d}r}, \tag{4.86}$$

where ϑ is the angle of rotation of the normal to the plate middle surface. The negative sign for ϑ is because, as seen from Fig. 4.17, this angle is counted off in the direction which is opposite to the rotation from the r axis to the z axis. The expressions for bending moments, Eqs (4.14), can be also written in terms of ϑ, as follows:

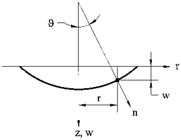

Fig. 4.17

$$M_r = D\left(\frac{\mathrm{d}\vartheta}{\mathrm{d}r} + \nu\frac{\vartheta}{r}\right); \; M_t = D\left(\frac{\vartheta}{r} + \nu\frac{\mathrm{d}\vartheta}{\mathrm{d}r}\right). \tag{4.87}$$

Finally, introducing ϑ in the form of Eq. (4.86) into Eq. (4.84) yields the following:

$$\frac{\mathrm{d}^2\vartheta}{\mathrm{d}r^2} + \left[\frac{1}{r} + \frac{1}{D}\frac{\mathrm{d}D}{\mathrm{d}r}\right]\frac{\mathrm{d}\vartheta}{\mathrm{d}r} + \left[\frac{\nu}{D}\frac{\mathrm{d}D}{\mathrm{d}r} - \frac{1}{r}\right]\frac{\vartheta}{r} = \frac{Q_r}{D}. \tag{4.88}$$

If $D = \text{const}$, Eq. (4.88) reduces to

$$\frac{\mathrm{d}^2\vartheta}{\mathrm{d}r^2} + \frac{1}{r}\frac{\mathrm{d}\vartheta}{\mathrm{d}r} - \frac{1}{r^2}\vartheta = \frac{Q_r}{D}. \tag{4.89}$$

Equation (4.88) can also be considered as the governing differential equation of bending of an axisymmetrically loaded circular plate having a variable stiffness. It is assumed that the right-hand side of this equation is a known function of r. Q_r can be obtained from the free-body equilibrium. In a general case, when h is an arbitrary function of r, Eq. (4.88) can be solved numerically only using the approximate methods introduced in Chapter 6. The small-parameter method, introduced in Chapter 3 for treating rectangular plates with a variable thickness, can also be applied to the solution of Eq. (4.88).

However, there is an important particular case when a closed-form solution of Eq. (4.88) is available. This is a case when the plate thickness varies according to the following law:

$$h = Cr^{\alpha}. \tag{4.90}$$

Depending on the exponent α, the shape of the plate may be different (Fig. 4.18). The problem of an axisymmetric bending of the circular plate having a form that corresponds to $\alpha < 0$ is encountered, in particular, in the analysis of turbine disks loaded by an axial load.

Let r_1 be the inner radius and h_1 the plate thickness on the inner edge of an annular circular plate. Taking into account Eq. (4.90), we can represent the plate thickness as

$$h = h_1\left(\frac{r}{r_1}\right)^{\alpha}. \tag{4.91}$$

The flexural rigidity of the arbitrary point of the plate for this case is

$$Q_r = -p_0 \frac{r^2 - r_1^2}{2r}.$$

Substituting the above into the right-hand side of Eq. (4.93), we can seek a particular solution in the following form $\vartheta_{\mathrm{p}} = Br^{\gamma}$. After a simple transformation, we obtain

$$\vartheta_{\mathrm{p}} = -\frac{p_0 r_1^{3\alpha}}{2D_0}\left[\frac{r^{3(1-\alpha)}}{8 - 9\alpha + 3\alpha\nu} + \frac{r^{(1-3\alpha)} r_1^2}{3\alpha(1-\nu)}\right]. \tag{4.97}$$

If a concentrated load P is distributed over the inner edge, we can find, by analogy, that

$$Q_r = -\frac{P}{2\pi r} \quad \text{and} \quad \vartheta_{\mathrm{p}} = \frac{\mathrm{Pr}_1^{3\alpha} r^{(1-3\alpha)}}{6\pi D_0 \alpha (1-\nu)}. \tag{4.98}$$

The general solution of Eq. (4.93) for a plate subjected to uniform pressure p_0 and concentrated force P distributed over the inner edge of the plate can be represented in the form

$$\begin{aligned}\vartheta &= C_1 r^{\left[-\frac{3}{2}\alpha + \sqrt{\frac{9\alpha^2}{4} + (1-3\nu\alpha)}\right]} + C_2 r^{\left[-\frac{3}{2}\alpha - \sqrt{\frac{9\alpha^2}{4} + (1-3\alpha\nu))}\right]}. \\ &\quad - \frac{p_0 r_1^{3\alpha}}{2D_0}\left[\frac{r^{3(1-\alpha)}}{8 - 9\alpha + 3\alpha\nu} + \frac{r^{(1-3\alpha)} r_1^2}{3\alpha(1-\nu)}\right] + \frac{\mathrm{Pr}_1^{3\alpha} r^{(1-3\alpha)}}{6\pi D_0 \alpha(1-\nu)}.\end{aligned} \tag{4.99}$$

The bending moments can be determined from Eqs (4.87). The deflection w is determined by integrating the expression (4.86). We have

$$w = -\int \vartheta \mathrm{d}r + C_3. \tag{4.100}$$

The constants of integration, C_1, C_2, and C_3, are to be determined from boundary conditions. The above conditions are of the following form:

if the plate edge is fixed, then $\vartheta = 0$;
if the plated edge is simply supported, then $M_r = D\left(\frac{\mathrm{d}\vartheta}{\mathrm{d}r} + \nu \frac{\vartheta}{r}\right) = 0$;

The third boundary condition is formulated, as follows: the deflection on the restrained edge is zero. One can also take a definite integral instead of indefinite Eq. (4.100), i.e.,

$$w = -\int_{r_0}^{r} \vartheta \mathrm{d}\bar{r}, \tag{4.101}$$

where r_0 is the radius on the plate support and r is the radius at a point of interest.

Example 4.9

Find the expressions for stresses and deflections in the circular plate with linearly varying thickness. The plate is simply supported on its edges and loaded by line forces P, as shown in Fig. 4.19a. Given $r_2 = \beta r_1,\ \nu = 1/3$.

Substituting the above into the expression (a) gives the following

$$\vartheta = \frac{P}{4\pi D_0} r_1 \left[\frac{5(1-\beta)}{1-\beta^3} + \frac{5(\beta^3-\beta)}{8(1-\beta^3)} \frac{r_1^3}{r^3} + \frac{r_1^2}{r^2} \right]. \tag{d}$$

Knowing ϑ we can determine the bending moments M_r and M_t from Eqs (4.87). We have

$$\begin{aligned} M_r &= D_0 \frac{r^3}{r_1^3} \left(\frac{\mathrm{d}\vartheta}{\mathrm{d}r} + \nu \frac{\vartheta}{r} \right) = \frac{5P}{12\pi} \left[\frac{r_1(\beta^2-1)\beta}{r(\beta^3-1)} - 1 + \frac{\beta-1}{\beta^3-1} \frac{r^2}{r_1^2} \right], \\ M_t &= D_0 \frac{r^3}{r_1^3} \left(\frac{\vartheta}{r} + \nu \frac{\mathrm{d}\vartheta}{\mathrm{d}r} \right) = \frac{P}{4\pi} \left[\frac{5(\beta-1)}{\beta^3-1} \frac{r^2}{r_1^2} + \frac{1}{3} \right]. \end{aligned} \tag{e}$$

The moment diagrams for $\beta = 3$ are shown in Fig. 4.19b. The maximum stress at $r = r_1$ is

$$\sigma_{t,\max} = \frac{6M_t}{h_1^2} = 1.08 \frac{P}{\pi h_1^2},$$

and at $r = r_2$

$$\sigma_{t,\max} = \frac{6M_t}{(3h_1)^2} = 0.63 \frac{P}{\pi h_1^2}.$$

The maximum deflection for $\beta = 3$ is found from Eq. (4.101) by substituting for ϑ from Eq. (d) into the above and making $r_0 = r_2 = \beta r_1$:

$$w_{\max} = -\int_{3r_1}^{r_1} \vartheta \mathrm{d}r = 0.295 \frac{\mathrm{P}r_1^2}{\pi D_0}.$$

Numerical results, given in Fig. 4.19, were taken from Ref. [7].

PROBLEMS

4.1 A circular plate of radius a is bent according to the following equation (the origin of the coordinate system is at the plate center):

$$w = C(a^2 - r^2)$$

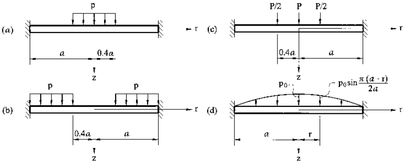

Fig. P4.1

How is the plate supported and what is the nature of the loading?

4.2 The equation of the deflected middle surface of the circular plate of radius a is given by the following equation:

$$w = C\left[(5+\nu)a^4 - 2(3+\nu)a^2r^2 + (1+\nu)r^4\right]$$

How is the plate supported and what is the nature of the loading?

4.3 It is known that at a concentrated load on a beam, the bending moment is finite at the point of application of the force. However, at a concentrated load on a plate, the bending moment is infinite at a point of application of the force according to Kirchhoff's plate bending theory. Explain physically, why there is this difference.

4.4 At each of the circular plates with the clamped edge and loaded, as shown in Fig. P.4.1, determine the deflection and bending moments equations. Find $w_{\max}$, $M_{r,\max}$, and $M_{t,\max}$.

4.5 At each of the circular plates with simply supported edge and loaded, as shown in Fig. P.4.2, determine the equations for deflections and bending moments. Find $w_{\max}$, $M_{r,\max}$, and $M_{t,\max}$.

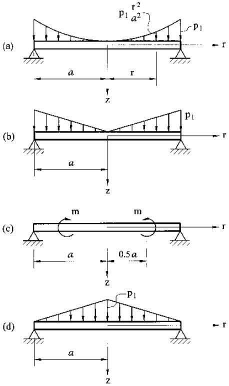

Fig. P4.2

4.6 Let a circular plate be subjected to an axially symmetric transverse load of intensity p. Show that $p = \frac{Q_r}{r} + \frac{\mathrm{d}Q_r}{\mathrm{d}r}$.

4.7 Show that the following relations are valid for the axisymmetrically loaded circular plate:

$$\frac{\mathrm{d}}{\mathrm{d}r}(\chi_r + \chi_t) = -\frac{Q_r}{D} \text{ and } \frac{\mathrm{d}}{\mathrm{d}r}(M_r + M_t) = -(1+\nu)Q_r.$$

4.8 At each of the annular circular plates and loaded, as shown in Fig. P.4.3, determine the equations for the deflections and bending moments. Find $w_{\max}$, $M_{r,\max}$, and $M_{t,\max}$.

4.9 Calculate the stresses and deflections in a diaphragm intended for measuring the rate of liquid (see Fig. P.4.3b). The resistance created by the diaphragm in flowing the liquid

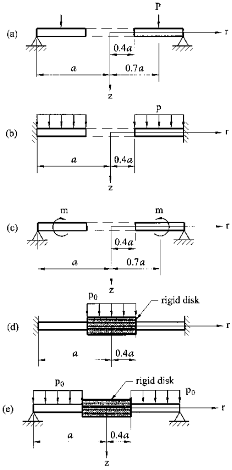
(a)
P
r
0.4a
a
0.7a
z
(b)
p
r
a
0.4a
z
(c)
m
m
r
0.4a
a
0.7a
z
p0
rigid disk
(d)
r
a
0.4a
p0
rigid disk
p0
(e)
r
a
0.4a
z

Fig. P4.3

causes a pressure drop of intensity p. Given: $a = 0.2\,\text{m}$, $p = 0.4\,\text{MPa}$, $\nu = 0.3$, $E = 220$ GPa, and $h = 0.02\,\text{m}$.

4.10 Calculate the stresses and deflections in the cap of a hatch. The cap is modeled by a circular plate simply supported on its outer edge and having a rigid cylinder welded to the plate's central part, as shown in Fig. P.4.3.e. Use: $a = 0.85\,\text{m}$, $p = 2\,\text{MPa}$, $E = 200\,\text{GPa}$, $\nu = 0.3$, and $h = 0.08\,\text{m}$.

4.11 Find the deflections and bending moments in the circular stepped plate shown in Fig. P.4.4. Assume $a = 2\,\text{m}$, $h = 0.2\,\text{m}$, $h_1 = 0.12\,\text{m}$, $p_0 = 1.5\,\text{MPa}$, $E = 200\,\text{GPa}$, and $\nu = 0.3$.

4.12 Redo Problem 4.11 for the case of the plate with fixed outer edge.

4.13 Find the expressions for deflections and bending moments in a circular plate subjected to load $p = \frac{p_0 r}{a}\cos\varphi$ (the origin is taken at the plate center) if the plate edge is fixed and a is the plate radius.

4.14 A circular simply supported plate is subjected to a transverse load $p = p_0\left(1 + \frac{r}{a}\cos\varphi\right)$ (the origin of the coordinate system is taken at the plate center) and a is the plate radius. Draw the deflection and bending moment diagrams along the diameter for $\varphi = \pi/4$. Use $a = 2.0\,\text{m}$, $h = 0.15\,\text{m}$, $p_0 = 5\,\text{MPa}$, $E = 200\,\text{GPa}$, and $\nu = 0.3$.

4.15 Derive expressions for the stress couples M_r, M_t, and M_{rt} in terms of the deflection, using the procedure presented in Sec. 2.3 for rectangular plates.

4.16 A concrete circular slab, simply supported on its edge, is subjected to the loading shown in Fig. P.4.5. Using the reciprocity theorem, determine the center deflection

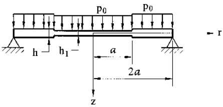

Fig. P4.4

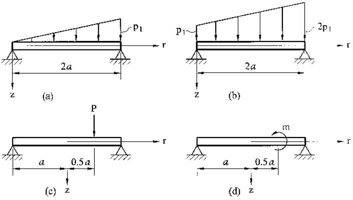

Fig. P4.5

of the plate due to a concentrated center force. A useful formula for a concentrated center force P and $\nu = 0$ is $w = \frac{1}{16\pi D}\left[2r^2 \ln\frac{r}{a} + 3(a^2 - r^2)\right]$.

4.17 For the circular plate, shown in Fig. P.4.5c, verify Eq. (4.64) using the Michell solution given by Eq. (4.77) and the solution (P.4.1) for the deflection due to a centrally applied concentrated force.

4.18 Derive the governing differential equation for a circular plate analogous to Eq. (2.44) for rectangular plates, using the procedure presented in Sec. 2.4.

REFERENCES

1. Korenev, B.G., *Besselevykh Funktsiiakh* Nekotorye Zadachi Teorii Uprugosti I Teploprovodnosti Reshaemye v, *Gos Izd Fiz-Mat Literatyru*, Moscow, 1960 (in Russian).
2. Watson, G.N., *Theory of Bessel Functions*, 2nd ed., Cambridge University Press, Cambridge, 1944.
3. Abramowitz, M. and Stegun, I.A., *Handbook of Mathematical Functions*, Bureau of Standards, Series No. 55, US Government Printing Office, Washington, DC, 1965.
4. Cook, R.D. and Young, W.C., *Advanced Mechanics of Materials*, Macmillan Publishing Company and Colliear Macmillan Publishers, New York and London, 1985.
5. Michell, J.H., *Proc. London Math. Soc.*, vol. 34, p. 223, 1902.
6. Szillard, R., *Theory and Analysis of Plates*, Prentice-Hall, Englewood Cliffs, New Jersey, 1974.
7. Boyarshinov, S.V., The Fundamentals of Structural Mechanics of Machines, Mashinostroenie, Moscow, 1973 (in Russian).

5

Bending of Plates of Various Shapes

5.1 INTRODUCTION

Structural members, common in engineering practice, consist of plates with shapes other than rectangular or circular. The analytical approaches to the solutions of such plate bending problems, discussed in Chapters 3 and 4, are usually too complicated to be considered for practical use. The more general forms are discussed in this chapter. We consider possible solutions, which can be obtained analytically with relative ease for some geometrical forms of plates different from rectangular and circular.

5.2 ELLIPTICAL PLATES

Elliptical plates with a clamped boundary, subjected to uniformly distributed loads, enable one to obtain an analytical solution. Let us consider the elliptical plate shown in Fig. 5.1. Take the origin of the coordinate system at the center of the plate. The equation of the contour of the plate (equation of the ellipse) is given by

$$\frac{x^2}{a^2}+\frac{y^2}{b^2}=1. \tag{a}$$

The boundary conditions for the clamped edge of the plate are

$$w=0, \frac{\partial w}{\partial n}=0. \tag{b}$$

It can be easily shown that these conditions are satisfied if the deflected surface is

$$w=w_0\left(\frac{x^2}{a^2}+\frac{y^2}{b^2}-1\right)^2, \tag{5.1}$$

The bending moments M_x at the end point of the semi-major axis and at the plate center are given by

$$M_x\big|_{x=\pm a, y=0} = -\frac{8w_0 D}{a^2}, \quad M_x\Big|_{x=0, y=0} = 4w_0 D\left(\frac{1}{a^2} + \frac{\nu}{b^2}\right). \tag{5.5}$$

Comparing these values of the bending moments, we can conclude that the end point of the semi-minor axis of the ellipse is the most stressed point.

In the particular case, for $a = b = R$, the relation (5.3) gives a value of the maximum deflection for a circular plate with clamped boundary:

$$w_0 = \frac{p_0 R^4}{64D}.$$

For an elliptical plate with a simply supported boundary, subjected to a uniformly distributed load, the deflected surface is a more intricate problem. Omitting the solution of this problem, we give only values of the maximum deflection

$$w_0 = \alpha \frac{p_0 b^4}{D}$$

and the bending moments at the center of the plate

$$M_x = \beta p_0 b^3, \quad M_y = \beta_1 p_0 b^2.$$

The values of the coefficients α, β, and β_1 are given in the Table 5.1 [1] for $\nu = 0.3$.

5.3 SECTOR-SHAPED PLATES

The general solution for circular plates (Sec. 4.2) can be used with some modifications for a plate in the form of a sector plate. We consider a uniformly loaded sector plate subtending the angle α and bounded by the lines $r = r_0$ and $r = r_1$. The plate is assumed to be simply supported along the straight edges, as shown in Fig. 5.2.

By expanding the lateral load $p = p_0 = \text{const}$ into a trigonometric series containing the sine terms only, we obtain the following expression for the load:

$$p = \frac{4p_0}{\pi} \sum_{m=1,3,5,\ldots}^{\infty} \frac{1}{m} \sin \frac{m\pi\varphi}{\alpha}. \tag{5.6}$$

The general solution of the problem is sought in the form

$$w = w_\mathrm{h} + w_\mathrm{p},$$

where the particular solution for the deflections, w_p, which satisfies the conditions of simple supports along the edges $\varphi = 0, \alpha$, is given by [2]

Table 5.1

a/b	1.0	1.2	1.5	2.0	3.0	4.0	5.0	∞
α	0.70	0.96	1.26	1.58	1.88	2.02	2.10	2.28
β	0.206	0.219	0.222	0.210	0.188	0.184	0.17	0.15
β_1	0.206	0.261	0.321	0.379	0.433	0.465	0.48	0.5

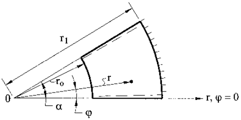

Fig. 5.2

$$w_{\mathrm{p}} = \frac{4p_0 r_0^4}{\pi}\rho^4 \sum_{m=1,3,5,\ldots}^{\infty} \frac{\sin\dfrac{m\pi\varphi}{\alpha}}{m\left(16 - m^2\pi^2/\alpha^2\right)\left(4 - m^2\pi^2/\alpha^2\right)}. \tag{5.7}$$

where $\rho = r/r_0$

The complementary solution, w_{h}, can be taken as

$$w_{\mathrm{h}} = F_0 + \sum_{m=1}^{\infty} F_m \sin\frac{m\pi\varphi}{\alpha}, \tag{5.8}$$

where

$$\begin{aligned} F_0 &= A_0 + B_0\rho^2 + C_0 \ln\rho + D_0\rho^2 \ln\rho, \\ F_m &= A_m\rho^{m\pi/\alpha} + B_m\rho^{-m\pi/\alpha} + C_m\rho^{2+m\pi/\alpha} + D_m\rho^{2-m\pi/\alpha}. \end{aligned} \tag{5.9}$$

The coefficients A_0, B_0, C_0, D_0, and A_m, B_m, C_m, D_m are determined from the boundary conditions at $r = r_0$ and $r = r_1$. Some analytical solutions for sector plates with various values of the angle $\alpha(\alpha = \pi/2$ and $\alpha = \pi)$ are given in Timoshenko and Woinowski-Krieger [1].

If the uniformly loaded and simply supported plate sector takes the form of a semicircle ($\alpha = \pi$), as shown in Fig. 5.3, then its solution assumes the form

$$w = \sum_{m=1,3,5,\ldots}^{\infty} \left(A_m r^m + C_m r^{m+2}\right)\sin m\varphi + \frac{4p_0 r^4}{\pi D} \sum_{m=1,3,5,\ldots}^{\infty} \frac{\sin m\varphi}{m\left(16 - m^2\right)\left(4 - m^2\right)}. \tag{5.10}$$

This solution satisfies the boundary conditions on the straight edge of the semicircular plate. The constants A_m and C_m are determined from the boundary conditions along the curvilinear edge of the semicircle. Determining the above constants and inserting them into Eq. (5.10), one finds

$$\begin{aligned} w = \frac{p_o r_0^4}{D} \sum_{m=1,3,5,\ldots}^{\infty} &\left\{ \frac{4\rho^4}{m\pi\left(16 - m^2\right)\left(4 - m^2\right)} \right. \\ &+ \frac{\rho^m(5 + m + \nu)}{m\pi\left(16 - m^2\right)(2 + m)[m + 0.5(1 + \nu)]} \\ &\left. - \frac{\rho^{m+2}(3 + m + \nu)}{m\pi(4 + m)(4 - m^2)[m + 0.5(1 + \nu)]} \right\} \sin m\varphi. \end{aligned} \tag{5.11}$$

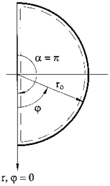

Fig. 5.3

5.4 TRIANGULAR PLATES

5.4.1 Isosceles right triangular plates

Consider a simply supported isosceles right triangular plate AOB, of length a under a concentrated force P acting at an arbitrary point $C(\xi, \eta)$, as shown in Fig. 5.4. To solve the given plate bending problem, the method of images, introduced by Nadai [2], may be used. According to this method, the given triangular plate is considered as one-half of a simply supported square plate, as indicated in Fig. 5.4 by dashed lines.

This square plate is subjected to the concentrated forces P (given force acting downward) and $-P$ (fictitious concentrated force acting upward) at points $C(\xi, \eta)$ and $C'(a-\xi, a-\eta)$, respectively. Point C' is the mirror or image point of C with respect to diagonal AB. The bending couple due to $+P$ and $-P$ results in a zero bending moment and deflection along diagonal AB of the square plate, i.e., the prescribed simply supported boundary conditions for the given triangular plate

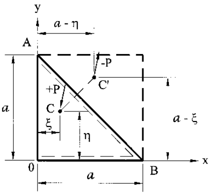

Fig. 5.4

will be satisfied. The deflection owing to the force P can be obtained from Eq. (3.27) by replacing b with a. Finally, we have

$$w_{+P} = \frac{4Pa^2}{\pi^4 D} \sum_{m=1}^{\infty} \sum_{n=1}^{\infty} \frac{\sin \dfrac{m\pi\xi}{a} \sin \dfrac{n\pi\eta}{b}}{\left(m^2 + n^2\right)^2} \sin \frac{m\pi x}{a} \sin \frac{n\pi y}{a}. \tag{5.12}$$

Upon substitution of $-P$ for P, $(a - \eta)$ for ξ, and $(a - \xi)$ for η in Eq. (5.12), we obtain the deflection due to the force $-P$ at C':

$$w_{-P} = -\frac{4Pa^2}{\pi^4 D} \sum_{m=1}^{\infty} \sum_{n=1}^{\infty} \frac{(-1)^{m+n} \sin \dfrac{m\pi\eta}{a} \sin \dfrac{m\pi\xi}{a}}{\left(m^2 + n^2\right)^2} \sin \frac{m\pi x}{a} \sin \frac{n\pi y}{a}. \tag{5.13}$$

The deflected surface of the triangular plate is obtained from

$$w = w_{+P} + w_{-P}, \tag{5.14}$$

where w_{+P} and w_{-P} are given by Eqs (5.12) and (5.13). Using the function w as Green's function, we can obtain the solution of an isosceles triangular, simply supported plate subjected to any type of loading $p(x, y)$. For example, the deflected surface of a triangular plate under a uniformly distributed load of intensity $p_0 = P/\mathrm{d}\xi\mathrm{d}\eta$ may be found from Eq. (5.14), after integration over the area of the plate, as follows:

$$\begin{aligned} w = \frac{16 p_0 a^4}{\pi^6 d} \Bigg[& \sum_{m=1,3\ldots}^{\infty} \sum_{n=2,4\ldots}^{\infty} \frac{n \sin \dfrac{m\pi x}{a} \sin \dfrac{n\pi y}{a}}{m\left(n^2 - m^2\right)\left(m^2 + n^2\right)^2} \\ & + \sum_{m=2,4\ldots}^{\infty} \sum_{n=1,3\ldots}^{\infty} \frac{m \sin \dfrac{m\pi x}{a} \sin \dfrac{n\pi y}{a}}{n\left(m^2 - n^2\right)\left(m^2 + n^2\right)^2} \Bigg]. \end{aligned} \tag{5.15}$$

This series converges very rapidly. With the expressions for the deflection of the plate determined, one can obtain the bending moments and stresses in the plate from Eqs (2.13) and (2.15), respectively.

5.4.2 Equilateral triangular plate

Consider a simply supported equilateral plate ABC shown in Fig. 5.5. The deflected surface of the equilateral triangular plate may be represented in the form

$$w = kF(x, y), \tag{5.16}$$

where k is a constant and $F(x, y)$ is some function that satisfies the prescribed simply supported boundary conditions for the plate. In particular, $F(x, y)$ can be represented as the product of the left-hand sides of equations of the three sides of the triangle. In this case,

$$\begin{aligned} F(x, y) &= \left(x + \frac{a}{3}\right)\left(\frac{x}{\sqrt{3}} + y - \frac{2a}{3\sqrt{3}}\right)\left(\frac{x}{\sqrt{3}} - y - \frac{2a}{3\sqrt{3}}\right) \\ &= \frac{x^3 - 3y^2 x}{3} - \frac{a(x^2 + y^2)}{3} + \frac{4a^3}{81}. \end{aligned} \tag{5.17}$$

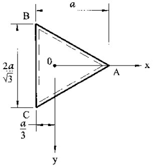

Fig. 5.5

It is evident that $F(x, y)$ is zero at the boundary. In the particular case of a uniformly loaded equilateral triangular plate, the deflection surface can be taken as [1]

$$w = \frac{p_0}{64aD}\left[x^3 - 3y^2x - a\left(x^2 + y^2\right) + \frac{4}{27}a^3\right]\left(\frac{4}{9}a^2 - x^2 - y^2\right), \tag{5.18}$$

where p_0 is the load intensity. It can be shown that this expression for w satisfies the governing differential equation (2.24) and the boundary conditions for a simply supported edge. Therefore, Eq. (5.18) is the solution. By employing Eqs (2.13), the bending moments may then be obtained. It can be shown that the center moments are

$$M_x = M_y = (1 + \nu)\frac{p_0a^2}{54}. \tag{5.19}$$

The largest moments occur on the planes bisecting the angles of the triangle. For example, at points along the x axis (Fig. 5.5), for $\nu = 0.3$, we obtain the following expressions:

$$M_{x,\max} = 0.0248p_0a^2 \ (x = -0.062a, y = 0);$$

$$M_{y,\max} = 0.0259p_0a^2 \ (x = 0.129a, y = 0).$$

The maximum stress is given by $\sigma_{y,\max} = 0.155p_0a^2/h^2$.

5.5 SKEW PLATES

Skew plates are widely used in modern structures. Swept wings of airplanes and parallelogram slabs in buildings and bridges are examples of the application of skew plates in engineering. Following Szillard [3], let us derive the governing differential equation of bending of skew plates by introducing an oblique coordinate system, ξ, η, as shown in Fig. 5.6. The coordinates of the rectangular (x, y) and oblique (ξ, η) systems are related by

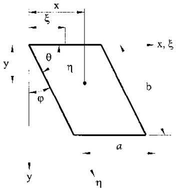

Fig. 5.6

$$\xi = x - y \tan \varphi \text{ and } \eta = \frac{1}{\cos \varphi} y. \tag{5.20}$$

Substitution of the expressions (5.20) into Eq. (2.17), transforms the Laplacian operator from the rectangular to oblique coordinate system, ∇_{o}^2, as follows:

$$\nabla_{\mathrm{o}}^2 = \frac{1}{\cos^2 \varphi} \left(\frac{\partial^2}{\partial \xi^2} - 2 \sin \varphi \frac{\partial^2}{\partial \xi \partial \eta} + \frac{\partial^2}{\partial \eta^2} \right) \tag{5.21}$$

Therefore, the governing differential equation of plate bending, expressed in terms of the oblique coordinates, is of the form

$$\frac{D}{\cos^4 \varphi} \left\{ \frac{\partial^4 w}{\partial \xi^4} + 2\left(1 + 2 \sin^2 \varphi\right) \frac{\partial^4 w}{\partial \xi^2 \partial \eta^2} - 4 \sin \varphi \left(\frac{\partial^4 w}{\partial \xi^3 \partial \eta} + \frac{\partial^4 w}{\partial \xi \partial \eta^3} \right) + \frac{\partial^4 w}{\partial \eta^4} \right\} = p(\xi, \eta). \tag{5.22}$$

or, more concisely,

$$D \nabla_{\mathrm{o}}^2 \nabla_{\mathrm{o}}^2 w(\xi, \eta) = p(\xi, \eta). \tag{5.23}$$

The analytical solution of Eq. (5.22) or (5.23) is complicated by the absence of orthogonal relationships and by the presence of singularities occurring at the obtuse corners. It can be solved only for a few particular cases. Thus, the analysis of the skew plates mentioned above can be carried out, primarily, by numerical methods discussed in Chapter 6. Some numerical solution procedures and the corresponding examples are discussed in Szillard [3].

PROBLEMS

5.1 Derive the equation for the bending moments, M_x and M_y, for a clamped elliptical plate under a uniformly distributed surface load p_0.

5.2 Derive the equations for the shear forces, Q_x and Q_y, for a clamped elliptical plate under a uniformly distributed surface load p_0.

5.3 With reference to Problem 5.2, show that a clamped elliptical plate under a uniformly distributed load p_0 is in a state of equilibrium, i.e., show that $P + R = 0$, where P is the resultant of distributed load p_0 and R is the resultant of the reactive forces on the plate boundary, $R = \oint \left(V_x \mathrm{d}y - V_y \mathrm{d}x \right)$.

5.4 Determine the required thickness of a fixed elliptical plate with $a = 25$ in. and $b = 18$ in. The plate is loaded by a uniform pressure of 120 psi. Take $\nu = 0.3$ and the allowable stress of 16 ksi.

5.5 Verify Eq. (5.11).

5.7 A simply supported wing panel in the form of an isosceles right triangle is subjected to a uniform distributed load p_0 (Fig. 5.4). By retaining only the first term of the series solution at point $C(x = a/4, y = a/4)$, determine (a) the deflection and (b) the bending moments.

5.8 Consider a simply supported equilateral triangular plate under a uniformly distributed load p_0. With reference to Eqs (2.32), show that

$$\nabla^2 M = -p_0;\ M = \frac{p_0}{4a}\left(x + \frac{a}{3}\right)\left(x - \frac{2}{3}a + y\sqrt{3}\right)\left(x - \frac{2}{3}a - y\sqrt{3}\right).$$

.

5.9 Verify Eq. (5.22).

5.10 Consider a clamped plate in the form of a parallelogram (Fig. 5.6) subjected to a uniform surface load p_0. Taking a solution of Eq. (5.22) in the form

$$w(\xi, \eta) = \frac{A}{4}\left(1 - \cos\frac{2\pi\xi}{a}\right)\left(1 - \cos\frac{2\pi\eta}{b}\right)$$

determine at point $\xi = a/2$ and $\eta = b/2$: (a) the deflection, (b) the bending moments. Use $\varphi = 15^\circ$.

5.11 Determine the expressions for M_x, M_y, and M_{xy} for skew plates by using the geometrical relationship (5.20) between the Cartesian and oblique coordinates.

REFERENCES

1. Timoshenko, S.P. and Woinowsky-Krieger, S., *Theory of Plates and Shells*, 2nd edn, McGraw-Hill, New York, 1959.
2. Nadai, A., *Die Elastichen Platten*, Springer-Verlag, Berlin, 1925.
3. Szillard, R., *Theory and Analysis of Plates*, Prentice-Hall, Englewood Cliffs, New Jersey, 1974.

6

Plate Bending by Approximate and Numerical Methods

6.1 INTRODUCTION

An exact solution in analytical form (i.e., exact solution formula) of plate bending problems using classical methods, discussed in Chapters 3, 4, and 5, is limited to relatively simple plate geometry, load configuration, and boundary supports. If these conditions are more complicated, the classical analysis methods become increasingly tedious or even impossible. In such cases, approximate methods are the only approaches that can be employed for the solution of practically important plate bending problems. Nevertheless, the classical solutions remain very valuable because they enable one to gain insight into the variation of stresses and strains with basic shape and property changes, and they provide an understanding of the physical plate behavior under an applied loading. In addition, they can be used as a basis for incisively evaluating the results of approximate solutions through quantitative comparisons and order-of-magnitude bounds.

In this chapter we consider some approximate methods that are widely used for plate and shell bending analysis. By convention, these approximate methods may be divided into two groups.

6.1.1 Indirect methods

These methods enable us to obtain numerical values of unknown functions by, primarily, direct discretization of the governing differential equation of the corresponding boundary value problem. Also they can be defined as methods for solving problems on computers. Note that computers have changed, almost revolutionized, numerical methods. These changes of the field as a whole, as well as many individual methods, are continuing. Here, we introduce such well-known methods as the finite difference method, the method of boundary collocations, the boundary element method, and the Galerkin method.

6.1.2 Direct methods

These methods use the variational principles introduced in Sec. 2.6 for determining numerical fields of unknown functions (deflections, internal forces, and moments), avoiding the differential equations of the plate or shell theory. The Ritz method is considered first and then the most efficient and well-accepted method at the present time – the finite element method – is also be presented. It should be noted that the above-mentioned division is very conventional because some approximate methods combine some distinguishing features of both groups of methods. For instance, the variational difference method is based on variational principles but unknown functions of deflection are represented in a numerical form at nodal points of the mesh drawn on the area of a plate midplane. In this chapter, all the above-mentioned methods are discussed only with application to plate bending problems. Their application to shell problems is considered in Part II.

6.2 THE FINITE DIFFERENCE METHOD (FDM)

6.2.1 General concepts

This is a method of the solution of boundary value problems for differential equations. The essence of the FDM lies in the following:

1. The middle plane of the plate is covered by a rectangular, triangular, or other reference network (Fig. 6.1), depending on the geometry of the plate. This network is called a *finite difference mesh* and points of intersection of this mesh are referred to as *mesh* or *nodal points*.
2. The governing differential equation inside the plate domain is replaced by the corresponding finite difference equations at the mesh points using the special *finite difference operators*.
3. Boundary conditions are also formulated with the use of the above-mentioned finite difference operators at mesh points located on the plate boundary.

As a result of such replacement, we obtain a closed set of linear algebraic equations written for every nodal point within the plate. Solving this system of equations, one obtains a numerical field of the nodal displacements.

6.2.2 Approximation of derivatives by finite differences

The key point of the FDM is the finite difference approximation of derivatives. Consider a development of the above approximations for the derivatives of a one-dimensional, continuous function $f(x)$. It is known that the derivative of a function $f(x)$ at point x_i is defined, as follows (Fig. 6.2a):

$$\left(\frac{\mathrm{d}f}{\mathrm{d}x}\right)_i = \lim_{\Delta\to 0}\frac{f_{i+1}-f_i}{\Delta} \quad \text{or} \quad \left(\frac{\mathrm{d}f}{\mathrm{d}x}\right)_i = \lim_{\Delta\to 0}\frac{f_i-f_{i-1}}{\Delta},$$

where $f_i = f(x_i)$, etc.; Δ is a finite increment of the variable x. Dropping the symbol of limit in the above equalities, we obtain

$$\left(\frac{\mathrm{d}f}{\mathrm{d}x}\right)_i \approx \frac{f_{i+1} - f_i}{\Delta}, \tag{6.1a}$$

$$\left(\frac{df}{dx}\right)_i \approx \frac{f_i - f_{i-1}}{\Delta}. \tag{6.1b}$$

Expressions (6.1a) and (6.1b) are called the first forward and backward approximations of the first derivative of $f(x)$ at point x_i, respectively. In practice, the expression for a central difference approximation of $(\mathrm{d}f/\mathrm{d}x)_i$ is often used, as follows:

$$\left(\frac{\mathrm{d}f}{\mathrm{d}x}\right)_i \approx \frac{f_{i+1} - f_{i-1}}{2\Delta}. \tag{6.2}$$

Expressions (6.1) and (6.2) are also referred to as the *finite difference operators of the first derivative*. It is clear that expressions (6.1) and (6.2) are more accurate as the value of Δ is smaller. From now on, for simplicity, we use the sign of equality in the above expressions instead of the sign of approximate equality.

Applying expressions (6.1) and (6.2) as operators we can derive the corresponding differential approximations of the second, third, and fourth derivatives of the function $f(x)$. We present below only the central difference approximations of the above derivatives, as follows:

$$\left(\frac{\mathrm{d}^2f}{\mathrm{d}x^2}\right)_i = \frac{f_{i-1} - 2f_i + f_{i+1}}{\Delta^2}, \tag{6.3}$$

$$\left(\frac{\mathrm{d}^3f}{\mathrm{d}x^3}\right)_i = \frac{f_{i+2} - 2f_{i+1} + 2f_{i-1} - f_{i-2}}{2\Delta^3}, \tag{6.4}$$

$$\left(\frac{\mathrm{d}^4f}{\mathrm{d}x^4}\right)_i = \frac{f_{i+2} - 4f_{i+1} + 6f_i - 4f_{i-1} + f_{i-2}}{\Delta^4}. \tag{6.5}$$

The coefficient patterns for the central finite difference operators of a one-dimensional function $f(x)$ are given in Fig. 6.2b.

By using the quadratic interpolation, one can obtain the expressions of the above derivatives for a nonuniformly spaced finite difference mesh shown in Fig. 6.3.

For example,

$$\begin{aligned} \left(\frac{\mathrm{d}f}{\mathrm{d}x}\right)_i &= \frac{-\alpha^2 f_{i-1} - \left(1 - \alpha^2\right) f_i + f_{i+1}}{\alpha(1+\alpha)\Delta}, \\ \left(\frac{\mathrm{d}^2f}{\mathrm{d}x^2}\right)_i &= \frac{2\left[\alpha f_{i-1} - (1+\alpha) f_i + f_{i+1}\right]}{\alpha(1+\alpha)\Delta^2}. \end{aligned} \tag{6.6}$$

We now discuss the case of a continuous function $F(x, y)$ of two variables. For this purpose, assume that a plate middle plane is approximated by a mesh with the mesh widths of Δ_x and Δ_y in the x and y directions, respectively. Let us restrict our derivation and application to equally spaced square meshes by introducing $\Delta x = \Delta y = \Delta$. It is evident that $\partial^i F/\mathrm{d}x^i$ and $\partial^j F/\partial y^j$ $(i, j = 1, 2, 3, 4)$ are

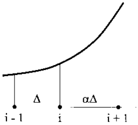

Fig. 6.3

approximated by the finite difference operators of the type (6.3)–(6.5). For example, for a central point k, we obtain

$$\left(\frac{\partial^2 F}{\partial x^2}\right)_k = \frac{F_a - 2F_k + F_c}{\Delta^2}; \quad \left(\frac{\partial^2 F}{\partial y^2}\right)_k = \frac{F_d - 2F_k + F_b}{\Delta^2}. \tag{6.7}$$

Adding the equalities (6.7), we obtain the finite difference approximation of the Laplace operator, as follows:

$$(\nabla^2 F)_k = \left(\frac{\partial^2 F}{\partial x^2} + \frac{\partial^2 F}{\partial y^2}\right) = \frac{F_a + F_b + F_c + F_d - 4F_k}{\Delta^2}. \tag{6.8}$$

The finite difference approximation of the biharmonic operator can be obtained by applying the Laplace operator (6.8) twice. We have the following:

$$(\nabla^2\nabla^2 F)_k = \frac{20F_k - 8(F_a + F_b + F_c + F_d) + 2\big(F_e + F_f + F_g + F_h\big) + (F_l + F_m + F_n + F_i)}{\Delta^4}. \tag{6.9}$$

The expression for the approximation of the second mixed derivative can be obtained following the pattern shown next:

$$\left(\frac{\partial^2 F}{\partial x \partial y}\right)_k = \frac{\partial}{\partial x}\left(\frac{\partial F}{\partial y}\right)_k = \frac{-(\partial F/\partial y)_a + (\partial F/\partial y)_c}{2\Delta} = \frac{F_h - F_e + F_f - F_g}{4\Delta^2}. \tag{6.10}$$

Applying this operator twice, one obtains the approximation of the fourth derivative of the function $F(x, y)$, $(\partial^4 F/\partial x^2 \partial y^2)_k$.

For reference purposes, some useful finite difference operators for a square mesh are represented in the form of coefficient patterns in Fig. 6.4. Notice that the center point in each case is the node about which each operator is written (the above point is outlined by a rectangle). In the case of a rectangular mesh with $\Delta x = \lambda_x$ and $\Delta y = \lambda_y$, one needs to replace Δ with λ_x, or Δ with λ_y. For example,

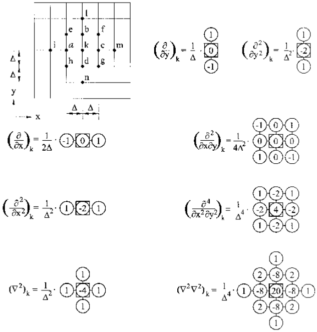
l
e
b
f
j
a
k
c
m
h
d
g
n
Δ
Δ
y
x
Δ
Δ
$\left(\frac{\partial}{\partial y}\right)_k = \frac{1}{\Delta}\cdot$
1
0
-1
$\left(\frac{\partial^2}{\partial y^2}\right)_k = \frac{1}{\Delta^2}\cdot$
1
-2
1
$\left(\frac{\partial}{\partial x}\right)_k = \frac{1}{2\Delta}\cdot$
-1 0 1
$\left(\frac{\partial^2}{\partial x \partial y}\right)_k = \frac{1}{4\Delta^2}\cdot$
-1 0 1
0 0 0
1 0 -1
$\left(\frac{\partial^2}{\partial x^2}\right)_k = \frac{1}{\Delta^2}\cdot$
1 -2 1
$\left(\frac{\partial^4}{\partial x^2 \partial y^2}\right)_k = \frac{1}{\Delta^4}\cdot$
1 -2 1
-2 4 -2
1 -2 1
$(\nabla^2)_k = \frac{1}{\Delta^2}\cdot$
1
1 -4 1
1
$(\nabla^2\nabla^2)_k = \frac{1}{\Delta^4}\cdot$
1
2 -8 2
1 -8 20 -8 1
2 -8 2
1

Fig. 6.4

$$\left(\frac{\partial F}{\partial x}\right)_k = \frac{F_a - F_c}{2\lambda_x}; \quad \left(\frac{\partial F}{\partial y}\right)_k = \frac{F_b - F_d}{2\lambda_y};$$
$$\left(\frac{\partial^2 F}{\partial x^2}\right)_k = \frac{F_a - 2F_k + F_c}{\lambda_x^2}; \left(\frac{\partial^2 F}{\partial y^2}\right)_k = \frac{F_b - 2F_k + F_d}{\lambda_y^2}; \text{etc.} \tag{6.11}$$

Up to this point, the finite difference operators have been derived using only Cartesian coordinates. The latter are well adapted to the solution of plate bending problems involving domains bounded by straight lines. For curvilinear plate domains, polar coordinates, can be conveniently applied. The finite difference operators in polar, or other coordinates, can be developed through the transformation of the corresponding equations relating the x and y coordinates to the set of coordinates of interest and using the coefficient patterns for finite difference operators given in Fig. 6.4.

6.2.3 Application of the finite difference method to plate bending problems

We can set up, with the use of a biharmonic operator (6.9), a finite difference expression of the governing differential equation (2.25) for every kth nodal point of the finite difference mesh within the plate at which $w_k \neq 0$:

$$\left(\nabla^2\nabla^2 w\right)_k = \frac{p_k}{D}, \quad k = 1, 2, \ldots N, \tag{6.12}$$

where p_k is an average load over an area $\Delta \times \Delta$ enclosing the nodal point k. If a concentrated force P is applied at a kth point, then $p_k = P/\Delta^2$. The finite difference operators for some moments and the effective shear forces are given in Fig. 6.5. They were obtained by replacing the partial derivatives in Eqs (2.13) and (2.39b) by the corresponding finite difference expressions.

Let us consider some finite difference expressions for typical boundary conditions for the plate edge $x = \text{const}$.

(a) Simply supported edge (Fig. 6.6a)

According to the boundary conditions for a simply supported edge, we have

$$w_k = 0 \text{ and } \left(\frac{\partial^2 w}{\partial x^2}\right)_k = 0, \tag{6.13a}$$

and applying the finite difference operator of the second derivative (see Fig. 6.4) yields

$$\frac{w_a - 2w_k + w_b}{\Delta^2} = 0,$$

from which, taking into account that $w_k = 0$, we can obtain

$$w_b = -w_a. \tag{6.13b}$$

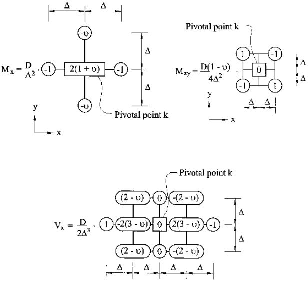

$M_x = \frac{D}{\Delta^2} \cdot$
-1
2(1 + υ)
-1
-υ
-υ
Δ
Pivotal point k
y
x
$M_{xy} = \frac{D(1-\upsilon)}{4\Delta^2} \cdot$
1
-1
0
-1
1
Pivotal point k
$V_x = \frac{D}{2\Delta^3} \cdot$
1
-2(3 - υ)
0
2(3 - υ)
-1
(2 - υ)
-(2 - υ)
Pivotal point k

Fig. 6.5

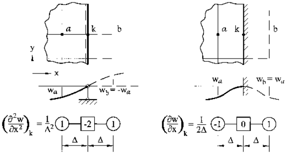
a
k
b
y
x
w_a
$w_b = -w_a$
$\left(\frac{\partial^2 w}{\partial x^2}\right)_k = \frac{1}{\Delta^2}$
1
-2
1
Δ
Δ
a
k
b
w_a
$w_b = w_a$
$\left(\frac{\partial w}{\partial x}\right)_k = \frac{1}{2\Delta}$
-1
0
1
Δ
Δ

(a) Simple Support

(b) Fixed

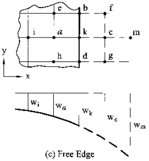
e
b
f
i
a
k
c
m
y
h
d
g
x
w_i
w_a
w_k
w_c
w_m

(c) Free Edge

Fig. 6.6

(b) Clamped edge (Fig. 6.6b)

Boundary conditions for the clamped edge of a plate can be written for the kth point as follows:

$$w_k = 0 \text{ and } \left(\frac{\partial w}{\partial x}\right)_k = 0. \tag{6.14a}$$

Applying the operator of the first derivative of w, the latter boundary condition becomes (see Fig. 6.4)

$$\frac{w_b - w_a}{2\Delta} = 0,$$

from which

$$w_b = w_a. \tag{6.14b}$$

(c) Free edge (Fig. 6.6c)

As shown in Sec. 2.4, the boundary conditions for a free edge, for instance, $x = \text{const}$, have the form

$$M_x = 0 \text{ and } V_x = 0. \tag{6.15a}$$

Applying the finite difference operators of forces and moments, given in Fig. 6.5, to the above boundary conditions, the latter are represented for a kth point on the plate edge as follows:

$$\begin{gathered}2(1+\nu)w_k - w_a - w_c - \nu(w_b + w_d) = 0,\\ 2(3-\nu)(w_c - w_a) + (2-\nu)\left(w_e + w_h - w_f - w_g\right) + w_i - w_m = 0.\end{gathered} \tag{6.15b}$$

There will be four fictitious nodes – f, c, g, and m – when the finite difference analog of the differential equation (6.12), Eq. (6.9) is applied to mesh point k on the free edge (Fig. 6.6c).

The expressions (6.13b), (6.14b), or (6.15b) are used either for eliminating the fictitious points mentioned above or for joining them to Eq. (6.9) as additional equations. As a result we obtain the closed system of linear algebraic equations with a square matrix. Solving this system of equations yields the numerical field of the plate deflections w_k $(k = 1, 2, \ldots, N)$.

Example 6.1

Find the approximate deflection values for a continuous rectangular plate, with loads and supports as shown in Fig. 6.7 [1].

Solution

The domain of the plate is divided into a number of small squares (28 squares, as shown in Fig. 6.7). We thus have $\Delta x = \Delta y = \Delta = 0.25a$. In labeling nodal points, the plate and loading symmetry about the x axis has been taken into account. At all the nodal points on the outer and inner $(x = a)$ boundaries the deflections are zero. At the fictitious nodes, located outside of the outer boundary, we have the following (with regard to the notation of the nodal points of Fig. 6.7):

$$\begin{aligned}&w_{1''} = w_1,\ w_{6''} = w_6,\ w_{5''} = w_5,\ w_{10''} = w_{10},\\ &w_{1'} = -w_1,\ w_{2'} = -w_2,\ w_{3'} = -w_3.\end{aligned} \tag{a}$$

Nodal loads on the right field of the plate (just to the right of the line $x = a$) are $p_4 = p_5 = p_9 = p_{10} = 0$, and on the left field of the plate (just to the left of the line $x = a$) they are $p_1 = p_2 = p_3 = p_6 = p_7 = p_8 = p = \text{const}$.

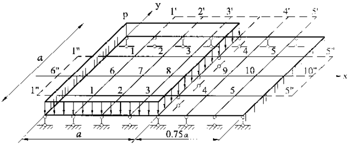

Fig. 6.7

Using the operator (6.9), we obtain a set of the algebraic equations (6.12) in the explicit form for the nodal points $1, 2, \ldots, 10$. Then, with the use of the relation for case (a), we can eliminate the deflections at the fictitious points $1''$, $5''$, $6''$, and $10''$ in the above system of equations. Solving the latter yields the following numerical values of the deflections at the nodal points of the mesh shown in Fig. 6.7:

$$w_1 = 0.00129\frac{pa^4}{D}, \quad w_2 = 0.002047\frac{pa^4}{D}, \quad w_3 = 0.001746\frac{pa^4}{D},$$

$$w_4 = -0.000246\frac{pa^4}{D}, \quad w_5 = -0.000133\frac{pa^4}{D}, \quad w_6 = 0.001746\frac{pa^4}{D}$$

$$w_7 = w_{\max} = 0.00278\frac{pa^4}{D}, \quad w_8 = 0.002019\frac{pa^4}{D}, \quad w_9 = -0.0003476\frac{pa^4}{D},$$

$$w_{10} = -0.0001875\frac{pa^4}{D}.$$

Having determined the numerical values of the deflections and applying the finite difference operators for moments (see Fig. 6.5), one can determine the bending and twisting moments, and then the corresponding stresses.

The FDM has become fairly popular in recent years. As mentioned earlier, according to this method the governing differential equation is replaced by a set of simultaneous algebraic equations: computers can be used to find the solution to these algebraic equations. The FDM has obvious advantages and disadvantages. Among its advantages, we can mention the following:

(a) it is straightforward in understanding and application;
(b) it is sufficiently universal, being applied to both linear and nonlinear problems; and
(c) it is well suited for computer application.

Disadvantages of this method are

(a) it requires (to a certain extent) mathematically trained operators;
(b) it requires more work to achieve complete automation of the procedure in program writing;
(c) the matrix of the approximating system of linear algebraic equations is asymmetric, causing some difficulties in numerical solution of this system; and
(d) an application of the FDM to domains of complicated geometry may run into serious difficulties.

This section contains only a brief description of the FDM and its application to plate bending problems. The interested reader is referred to other works [2,3].

6.3 THE BOUNDARY COLLOCATION METHOD (BCM)

The boundary collocation method (BCM) is among the simplest methods of solving partial differential equations, both from a conceptual, as well as a computational point of view. The solution is expressed as a sum of known solutions of the governing differential equation, and boundary conditions are satisfied at selected colloca-

However, the BCM has some disadvantages, among which are

(a) it is limited to linear problems;
(b) a complete set of solutions (the basic functions Φ_j) to the differential equations must be known; and
(c) the matrix [A] is full and sometimes ill-conditioned, and a known arbitrariness exists in the selection of the collocation points.

This section contains only a brief survey of the boundary collocation method. The interested reader is referred to other works [5,8,9].

Example 6.2

A 90° sectorial plate subjected to a uniform surface load of an intensity p_0 is simply supported along its straight edges. Determine the deflection, bending moments distribution along the x axis for (a) simply supported (Fig. 6.8a) and (b) clamped (Fig. 6.8b) conditions along its arc. Assume $\nu = 0.3$ (this example is taken from Ref. [9]).

Solution

The deflection $w(x, y)$ is approximated by the expression (6.17) and the trial functions are taken in polar coordinates according to Eqs (6.18), as follows:

$$w = \sum_{j=0}^{N} \left(a_j r^j + b_j r^{j+2}\right) \cos j\varphi + \frac{p_0 r^4}{64D}, \tag{a}$$

where the coefficients a_j and b_j are to be determined from the boundary conditions, and the upper limit of summation N is determined by the accuracy of solution desired from the BCM. The simply supported plate (Fig. 6.8a) is analyzed by using 14 boundary points and the plate simply supported along the straight edges and clamped along the arc (Fig. 6.8b) by using 12 boundary points. The results of the analysis are presented in Table 6.1, which shows these results, and in Fig. 6.9, where the moment distributions are shown.

In Table 6.1, the numerical results given by the BCM solutions are compared with exact solutions obtained in Ref. [7]. This comparison shows that the BCM solution agrees well with the exact solution both in the interior of the plate and at its boundary.

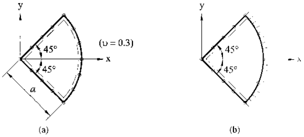

(a) (b)

Fig. 6.8

Several different boundary element approaches have already been proposed for the construction of the complementary solution. They are frequently referred to as *direct* and *indirect BEM formulations* [12,13]. In the indirect BEM formulation, the complementary function is represented by an integral in terms of some arbitrary functions, called *source functions*, over the boundary of a domain of the plate. These source functions may be visualized, for example, as fictitious force and moment distributions acting on the boundary of the given plate embedded in an infinite elastic plate (the term ‘‘fictitious’’ is used here because these loads are not resulting in transverse loads assigned for the plate). Finding these source functions, one can determine the deflections, bending and twisting moments anywhere within the plate or on its boundary.

In the direct formulation, the partial differential equation of the plate bending problem for the complementary function is transformed by the use of the reciprocal work identity to an integral equation in terms of boundary values of the deflections and the stress resultants. Both BEM formulations have certain advantages and disadvantages that are discussed in detail in Refs [12,13]. It has been established now that these two formulations have the same origin and theoretical basis. We discuss below both approaches, as applied to plate bending problems.

6.4.1 Indirect BEM for plates

The presentation of the indirect BEM below follows the approach of Ventsel [14]. Assume that a given plate, originally occupying a 2D domain Ω with a smooth boundary Γ, is to be extended infinitely. Then, apply to an infinite plate the above-mentioned fictitious loads in the form of transverse loads $q(\xi, \eta)$ and moments $m_n(\xi, \eta)$ distributed continuously over Γ, where (ξ, η) is some point on Γ (called the *source point*). The moments m_n act in the direction of the outward normal n to Γ at the source point (Fig. 6.10).

In order to determine the deflection surface of the infinite plate caused by the above-mentioned fictitious loads, find the so-called singular solutions of the biharmonic equation (2.24). In our case, these singular solutions correspond to the deflection of point (x, y) of the infinite plate (called the *observation point*) caused by a unit normal concentrated force, and by a unit concentrated moment; both are applied at

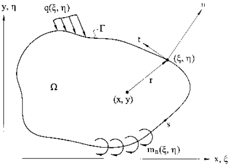

Fig. 6.10

Example 6.3

A square plate with a square central opening is subjected to a uniform surface load p. The external edges of the plate are simply supported and the internal edges are free, as shown in Fig. 6.11a. Determine the deflection at the points A, B, and C. Assume $\nu = 1/6$.

Solution

This problem has been analyzed by Tottenham [10]. He applied the direct and indirect BEM to the analysis of this plate. One-quarter of the plate was considered, with the nodes at the quarter points along each side, giving a total of 24 points – shown in Fig. 6.11b. Due to the symmetry, the boundary conditions were satisfied at 13 points – indicated also in Fig. 6.11b. The 26 algebraic equations for the 26 source functions specified at 13 points of the external and internal edges of the plate boundary have approximated the boundary integral equations of the indirect and direct BEM . The results obtained are compared with those using the finite element method (FEM) and variational finite difference method (VFDM) in Table 6.2. In both of the comparative cases (for BEM solutions) the mesh size was $a/16$ and the source functions are assumed to be constant over BEs along the boundary. In analyzing this problem, the corner points were ignored. As follows from Table 6.2, the numerical results obtained by BEM are very close to those obtained by FEM and VFDM (the discrepancy of the results does not exceed more than 2.5%).

Example 6.4

A quadrangular plate is subjected to a concentrated force P applied at the center of an inscribed circle, as shown in Fig. 6.12a. The radius of the inscribed circle $R = 2/3$ m. Poisson's ratio $\nu = 0.3$, the plate thickness $h = 2 \times 10^{-3}$ m, the modulus of elasticity $E = 2 \times 10^{5}$ Pa. Determine the deflection and bending moment distributions along section AB and along the boundary.

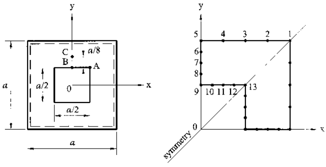

(a)

(b)

Fig. 6.11

Table 6.2

	Displacement ($\times pa^4/100D$)			
	Boundary element method			
Point	Indirect	Direct	Finite element method	Finite difference method
A	0.2188	0.2188	0.2185	0.2174
B	0.3107	0.3141	0.3156	0.3006
C	0.1558	0.1565	—	0.1541

Solution

This problem was analyzed by Ventsel [14]. He applied the indirect BEM to the analysis of the plate. The plate boundary was divided into 28 boundary elements (BEs), giving a total of 28 nodes. The boundary conditions were satisfied at these nodal points. Unknown edge forces, q, and the normal edge moments, m_n, were assumed to be constant over BEs. The two boundary integral equations (Eqs (6.29a) and (6.29b)) were approximated by 56 algebraic equations for the 56 nodal loads, $q^{(k)}$ and $m_n^{(k)}$ ($k = 1, 2, \ldots, 28$). Some results of the numerical analysis are shown in Fig. 6.12a, b in the form of the deflection and bending moment distributions along section AB and the boundary. The deflection and bending moments ordinates are given in Fig. 6.12 to within the following constant multipliers: p/D for the w and P for the function M.

In conclusion, it should be noted that the BEM is very powerful and efficient as applied to various linear plate bending problems. The method has the following advantages:

1. It can be easily adapted to any complicated geometry of the domain involved and to arbitrary boundary conditions, like the finite element method. However, unlike the FEM, an application of the BEM to boundary value problems enables us to reduce the dimensionality of the problem. The latter results in a smaller, than the FEM, system of equations and considerable reductions in the data required to run a problem.
2. The BEM is easily programmed for arbitrary plate configurations, loads, and boundary conditions.
3. The numerical accuracy of the BEM is generally greater than that of the FEM and other numerical methods. The numerical discretization of the method leads to a stable system of linear algebraic equations. The error of an approximate solution introduced by the BEM can be estimated a posteriori when the problem under consideration has been solved [14].
4. The method has been adapted well for the solution of the so-called singular problems, such as plates with crack-like defects, plates having holes, corners, etc.

However, this method has some disadvantages:

1. It can be successfully applied primarily to linear problems.
2. The method requires that a fundamental solution of a governing differential equation or Green's function be represented in the explicit analy-

be chosen in such a way that the operation of orthogonality would correspond to the application of the principle of virtual work to the given problem. Such an approach will result in a more rapid convergence of a solution.

Example 6.5

Find an analytical expression by Galerkin's method for the deflection of a uniformly loaded ($p = \text{const}$) rectangular plate with all edges clamped (Fig. 6.13).

Solution

The boundary conditions for the plate are given by

$$w = 0|_{\substack{x=\pm a\\ y=\pm b}}; \quad \frac{\partial w}{\partial x} = \frac{\partial w}{\partial y}\bigg|_{\substack{x=\pm a\\ y=\pm b}}. \tag{a}$$

Let us take the deflected plate surface in the following form

$$w = \alpha_1 f_1(x, y) + \alpha_2 f_2(x, y) + \alpha_3 f_3(x, y) + \ldots \tag{b}$$

where

$$f_1 = \left(x^2 - a^2\right)^2\left(y^2 - b^2\right)^2; \quad f_2 = \left(x^2 - a^2\right)^2\left(y^2 - b^2\right)^3; \text{ etc.}$$

The function (b) satisfies all the prescribed boundary conditions (a) exactly. To simplify the solution, let us consider only the first term in Eq. (b). Thus, Galerkin's equations (6.40) reduce to only one equation of the following type:

$$a_{11}\alpha_1 = b_1, \tag{c}$$

where

$$a_{11} = D\int\limits_{A}\int \nabla^2\nabla^2 f_1 \cdot f_1 \,\mathrm{d}x\mathrm{d}y; \quad b_1 = \int\limits_{A}\int p \cdot f_1 \,\mathrm{d}x\mathrm{d}y. \tag{d}$$

We have the following

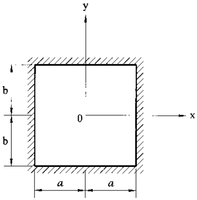

Fig. 6.13

Therefore, the extremum problem of the calculus of variations is transformed into the maximum–minimum problem of differential calculus, The latter problem, in turn, is solved by satisfying the following:

$$\frac{\partial \Pi}{\partial C_1} = 0, \quad \frac{\partial \Pi}{\partial C_2} = 0, \ldots, \quad \frac{\partial \Pi}{\partial C_i} = 0, \ldots . \tag{6.44}$$

Since U is a quadratic and Ω_p is a linear functional of w (see Eqs (2.54) and (2.57)), then Eqs (6.44) represent a system of linear nonhomogeneous algebraic equations for C_i. The solution of this system, being substituted into the expression (6.42), yields a final solution of the problem. It is evident that the accuracy of the Ritz method depends considerably on how well the assumed coordinate functions are capable of describing the actual deflection surface. These functions must satisfy the two conditions [6,24]:

1. For any i elements $f_1, f_2, \ldots, f_n$ should be linearly independent or, in other words, any element f_i cannot be expressed by a linear combination of others.
2. The sequence of elements (6.42) is a complete in the energy. This means that whatever element w and a number $\varepsilon > 0$ have been, one can find such a natural number N and such constants $C_1, C_2, \ldots, C_N$ that the following inequality could be satisfied:

$$\left\| w - \sum_{i=1}^{N} C_i f_i \right\| < \varepsilon.$$

where $\| \ \|$ is the norm in the energy space [6].

If the coordinate functions $f_i(x, y)$ satisfy the above-mentioned requirements (and the kinematic boundary conditions), then the infinite series (6.42) with the coefficients obtained from Eqs (6.44) represent an exact solution. In most cases, however, only several terms of the series (6.42) are retained. As a result, only an approximate solution of a problem is available, the accuracy of which depends to a greater degree on a selection of the coordinate functions $f_i(x, y)$ and on a number of terms N retained in the following expression:

$$w(x, y) = \sum_{i=1}^{N} C_i f_i(x, y). \tag{6.45}$$

Various methods for selecting suitable coordinate functions $f_i(x, y)$ for bending analysis of plates by the Ritz method are presented in Refs [24,25].

Example 6.6

Determine the deflection of a rectangular plate simply supported on two opposite edges $y = 0$ and $y = b$, clamped on edge $x = 0$, and free on the edge $x = a$, as shown in Fig. 6.14. The plate is subjected to a uniform load of intensity p_0.

Solution

The geometrical boundary conditions for the plate of Fig. 6.14 are

$$w = 0|_{y=0}; \quad w = 0|_{y=b}; \quad w = 0|_{x=0}; \quad \left. \frac{\partial w}{\partial x} = 0 \right|_{x=0}. \tag{a}$$

The expression for the deflection is

$$w=\frac{a^4p}{D}\cdot\frac{2(x/a)^2\sin\pi y/b}{\Psi}.$$

If we evaluate the deflection for $a/b=1$, $\nu=0.3$, $x=a$, and $y=b/2$, we obtain

$$w=0.1118\frac{pa^4}{D},$$

which deviates from the exact solution by approximately 1%.

Example 6.7

Determine the deflection of a semicircular plate ($h=\text{const}$) subjected to a concentrated force P, as shown in Fig. 6.15. It is fixed along the straight edge and is free along the arc edge.

Solution

The geometrical boundary conditions for this problem have the form

$$w=0|_{x=0},\quad \frac{\partial w}{\partial x}=0\bigg|_{x=0}. \tag{a}$$

These conditions will be satisfied if we take $w(x,y)$ in the form

$$w=x^2\left(C_0+C_{10}x+C_{01}y+C_{20}x^2+C_{11}xy+C_{02}y^2+\ldots\right). \tag{b}$$

After substitution of this expression into Eq. (2.60) and letting $p(x,y)=0$, an integration should be performed over the area of the semicircle. With this purpose, it is convenient to go to the polar coordinates, r and φ, replacing x with $r\cos\varphi$, y with $r\sin\varphi$ and the area element $\mathrm{d}x\mathrm{d}y$ with $r\mathrm{d}r\mathrm{d}\varphi$. The limits of integration will be: over the variable φ – from 0 to π and over the variable r – from 0 to R. Notice that the potential of the external forces will involve only a non-integral term, namely

$$\Omega_s=-P\cdot w_0,$$

where w_0 is the deflection at a point of the force application that is calculated from Eq. (b). Fairly awkward calculations do not present any key difficulties and allow us to determine the deflection surface $w(x,y)$ and then the bending moments. The

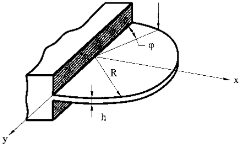

Fig. 6.15

accuracy of calculation of the bending moments depends mainly on the number of terms retained in the expansion (b).

If a plate has openings (Fig. 6.16), then the analysis can be performed similarly but the area of openings must be eliminated from the area of integration in calculating the total potential energy Π.

Let us discuss the advantages of the Ritz method.

(a) The basic advantage lies in the fact that the coordinate functions $f_i(x, y)$ must satisfy the kinematic (or geometrical) boundary conditions only. Therefore, the area of an application of the method to the plate bending problems is wider than of the classical analytical methods discussed in Chapter 3. Therefore, the Ritz method is very efficient for the analysis of plates having free edges, for plates with openings.

(b) The method can be also applied successfully to rectangular plates of variable thickness, because there is no difference between the expressions of Π for plates of constant and variable thicknesses.

(c) Another advantage of the method is that the matrix of the linear algebraic equations, following on from Eq. (6.44), is always symmetrical, resulting in stable and powerful logarithms for their numerical solution.

The basic disadvantages of the method are

(a) The Ritz method can be applicable only to simple configurations of plates (rectangular, circular, etc.), because of the complexity of selecting the coordinate functions for domains of complex geometry.

(b) The Ritz method approximation (6.44) results in the complete matrix of linear algebraic equations that produces some difficulties in its numerical implementation.

It should be noted that the Ritz method can serve as a basis for a such popular and powerful methods as the finite element method, which is discussed in the next section.

6.7 THE FINITE ELEMENT METHOD (FEM)

6.7.1 Introduction

The finite element method (FEM) is based on the concept that one can replace any continuum by an assemblage of simply shaped elements with well-defined force–

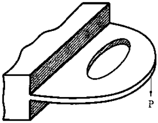

Fig. 6.16

displacement and material relationships. While one may not be able to derive a closed-form solution for the continuum, one can derive an approximate solution for the element assemblage that replaced it.

According to the FEM, a plate is discretized into a finite number of elements (usually, triangular or rectangular in shape), called *finite elements* and connected at their nodes and along interelement boundaries. Unknown functions (deflections, slopes, internal forces, and moments) are assigned in the form of undetermined parameters at those nodes. The equilibrium and compatibility conditions must be satisfied at each node and along the boundaries between finite elements. To determine the above-mentioned unknown functions at nodal points, one of the variational principles, introduced in Sec. 2.6, is applied. As a result, a system of algebraic equations is obtained. Its solution determines the state of stress and strain in a given plate.

There are a number of finite element methods. In this section we discuss only the commonly used finite element displacement approach wherein the governing set of algebraic equations is expressed in terms of unknown nodal displacements.

The FEM can be treated as some modification of the Ritz method. A difference between the classical Ritz approach and the FEM is in the technique of representation of displacements. In the Ritz method, the displacements are assigned in the entire domain occupied by the plate. A governing system of algebraic equations for this approach will have a completed, not banded structure. Since in the FEM the displacements are assigned element by element, the matrix of the system of algebraic equations is obtained as partially completed, and usually it has a banded structure. This is a profound advantage of the FEM compared with other numerical methods introduced in the preceding sections of this chapter.

The FEM has gained considerable attention and prominence after the publication of the classic paper by Turner *et al.* [26] that showed how one can use an assemblage of simple elements as a basis for computerized structural analysis. Courant [27], and later Argyris *et al.* [28] represent the initial attempts to provide the theoretical investigations of this method. Gallagher [29], Hughes [30], Zienkiewicz [31], and other investigators developed the general procedure of the FEM technique for plate and shell stress analysis.

For every finite plate (or shell) element there is a relationship between the generalized displacements at the nodal points and the corresponding forces and moments at the nodes. This relationship may be presented in the form of a matrix called a *stiffness matrix*. In this section, we discuss the stiffness matrices for rectangular and triangular plate elements. Then, we present the general procedure of the FEM for plate bending analysis. The derivations, given below, are based on the classical (Kirchhoff's) plate bending theory introduced in Chapter 2.

6.7.2 The rectangular plate element

Consider a flat rectangular plate which is subdivided into rectangular finite elements with dimensions c and d, as shown in Fig. 6.17. The properties belonging to such a finite element (abbreviated further as FE) is designated e. The geometrical position of a rectangular FE is determined by the four nodal (corner) points i, j, k, and l, and the straight line boundaries. At each node q ($q = i, j, k, l$) we consider the possible

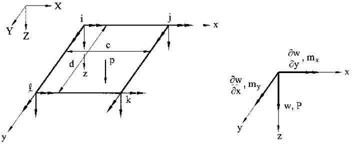

Fig. 6.17

nodal deflection w_q and rotations of the normal to the plate middle surface (slopes) about the x and y axes, i.e., $(\partial w/\partial y)_q$ and $(\partial w/\partial x)_q$, respectively.

The deflection w_q and two rotations $(\partial w/\partial y)_q$ and $(\partial w/\partial x)_q$ are referred to as a set of *nodal displacements*.

We assume that the FE is subjected to surface-distributed load $p(x, y)$ and external concentrated force P_q and moments m_{xq} and m_{yq}, applied at each nodal point q of the FE, as shown in Fig. 6.17. Do not confuse the external nodal moments m_{xq} and m_{yq} with the stress couples M_x and M_y introduced in Chapter 2. The nodal force and two moments are referred to as a set of *nodal forces*. The nodal displacements and nodal forces are assumed to be positive in the directions shown in Fig. 6.17. Two coordinate systems are introduced in Fig. 6.17: the coordinate set X, Y, Z is referred to as a global set for the entire structure while the set x, y, z is called the local set for the FE of interest.

We develop below a stiffness matrix for a given FE. Let us approximate the deflection field over the area of the rectangular FE shown in Fig. 6.17. The strain energy of the plate in bending involves the second derivatives of the deflections (see Eq. (2.60)). Hence, the degree of a polynomial that approximates this deflection field cannot be less than two. On the other hand, in order to characterize the shape of the FE by its nodal displacements with reference to Fig. 6.17, it is necessary to have 12 degrees of freedom (in the three degrees of freedom, w, $\partial w/\partial y$, $\partial w/\partial x$ at each of the four nodal points i, j, k, l of the above element). Consequently, we need to select a polynomial with 12 parameters. The polynomial selected is

$$\begin{aligned} w(x, y) = {} & \alpha_1 + \alpha_2 x + \alpha_3 y + \alpha_4 x^2 + \alpha_5 y^2 + \alpha_6 xy + \alpha_7 x^2 y + \alpha_8 xy^2 + \alpha_9 x^3 + \alpha_{10} y^3 \\ & + \alpha_{11} x^3 y + \alpha_{12} xy^3. \end{aligned} \tag{6.46}$$

Obviously, the above polynomial satisfies exactly the governing differential equation (2.24). However, this deflection function will not result in a fully compatible element. In the FEM formulation, it is required that the compatibility conditions (equality of the deflections and slopes) are satisfied at the nodal points. An accuracy of the FEM will be increased if the selected deflection function involves the compatibility of the deflections and slopes along a common boundary line of the adjacent FEs. It can be shown that the polynomial (6.46) provides the compatibility of deflections between elements and some slopes (normal) are continuous while other slopes (tangential) may not be continuous. In order to correct this problem, one needs to define four degrees of freedom at each node and, correspondingly, employ a deflection function with 16 terms [29,30]. Of course, the above polynomial leads to improved results, but the analysis becomes more involved than described below. At the same time, numerical and theoretical investigations showed that the use of the polynomial (6.46) provides a convergence of the solution by the FEM. So, the polynomial (6.46) is frequently used in engineering practice.

Let us represent the above polynomial approximating the deflection field over the FE designated by e in the matrix form as follows:

$$w_e = [N]\{\alpha\}, \tag{6.47}$$

where

$$[N] = \left[1, x, y, x^2, y^2, xy, x^2y, xy^2, x^3, y^3, x^3y, xy^3\right] \text{ and } \{\alpha\} = [\alpha_1, \alpha_2, \ldots, \alpha_{12}]^T. \tag{6.48}$$

Here and further, the subscript e refers to a finite element designated by this letter. We introduce the braces $\{\ldots\}$ to indicate a matrix of one column, the brackets $[\ldots]$ to represent a matrix (both, a square and row matrices); and the superscript T to represent the transpose of a matrix.

Introduce the element displacement matrix $\{\delta\}_e$ as follows:

$$\{\delta\}_e = \left[\delta_i, \delta_j, \delta_k, \delta_l\right]^T, \tag{6.49}$$

where

$$\left\{\delta_i\right\} = \left[w_i, (\partial w/\partial y)_i, (\partial w/\partial x)_i\right]^T; \quad \left\{\delta_j\right\} = \left[w_j, (\partial w/\partial y)_j, (\partial w/\partial x)_j\right]^T; \text{ etc.}$$

If we express the coefficients $\alpha_m (m = 1, 2, 3, \ldots, 12)$ via the nodal displacements w_q, $(\partial w/\partial y)_q$, and $(\partial w/\partial x)_q$ $(q = i, j, k, l)$ in the local coordinate system x, y, z, then we can write the following relationship:

$$\{\delta\}_e = [C]\{\alpha\}, \tag{6.50}$$

where $[C]$ is 12×12 matrix whose elements depend on the x and y coordinates of the nodal points of the finite element shown in Fig. 6.17.

From the foregoing, the solution for the unknown constants is

$$\{\alpha\} = [C]^{-1}\{\delta\}_e. \tag{6.51}$$

The inverse matrix $[C]^{-1}$ is given below for the rectangular FE of Fig. 6.17 in the explicit form in Table 6.3.

Upon substitution of $\{\alpha\}$ from Eq. (6.51) into Eq. (6.47) one obtains

$$w_e = [L]\{\delta\}_e, \tag{6.52}$$

where

$$[L] = [N][C]^{-1} \tag{6.53}$$

$$[B]_i = \left[-\frac{\partial^2 [L]_i}{\partial x^2}, -\frac{\partial^2 [L]_i}{\partial y^2}, -2\frac{\partial^2 [L]_i}{\partial x \partial y} \right]^T;$$

$$[B]_j = \left[-\frac{\partial^2 [L]_j}{\partial x^2}, -\frac{\partial^2 [L]_j}{\partial y^2}, -2\frac{\partial^2 [L]_j}{\partial x \partial y} \right]^T; \text{ etc.}$$

Now. let us introduce the stress resultants and stress couples relationships (see Eqs (2.13)) in the matrix form:

$$\{M\}_e = \begin{Bmatrix} M_x \\ M_y \\ M_{xy} \end{Bmatrix} = D \begin{bmatrix} 1 & \nu & 0 \\ \nu & 1 & 0 \\ 0 & 0 & (1-\nu)/2 \end{bmatrix} \begin{Bmatrix} \chi_x \\ \chi_y \\ 2\chi_{xy} \end{Bmatrix}, \tag{6.57a}$$

or symbolically as follows:

$$\{M\}_e = [D]\{\chi\}_e, \tag{6.57b}$$

where $[D]$ is the elasticity matrix. The stress–strain relationship, from Eqs (2.10), can be written in the matrix form as follows:

$$\{\sigma\}_e = z[D^*]\{\chi\}_e, \tag{6.58}$$

where the matrix $[D^*]$ is given by

$$[D^*] = \frac{12}{h^3}[D]. \tag{6.59}$$

To continue the development, it is necessary to define the set of discrete nodal forces corresponding to the prescribed nodal degrees, as shown in Fig. 6.17:

$$\{R\}_e = \left[R_i, R_j, R_k, R_l\right]^T, \tag{6.60a}$$

where

$$\left\{R_q\right\} = \left[P_q, m_{xq}, m_{yq}\right]^T; \quad q = i, j, k, l. \tag{6.60b}$$

We now employ the principle of minimum potential energy, introduced in Sec. 2.6.2, to derive the element stiffness matrix, $[k]_e$ and the element nodal force matrix $\{R\}_e$. Toward this end, we write the strain energy in the element as (see Eq. (2.61))

$$U_e = \frac{1}{2}\iint_{A_e} [\chi]_e^T \{M\}_e \mathrm{d}A_e. \tag{6.61}$$

Substituting for $[\chi]_e^T$ from Eq. (6.56) and for $\{M\}_e$ from Eq. (6.57b) into the above, we obtain

$$U_e = \frac{1}{2}\iint_{A_e} \{\delta\}_e^T [B]^T [D][B]\{\delta\}_e \mathrm{d}A_e = \{\delta\}_e^T \left\langle \frac{1}{2}\iint_{A_e} [B]^T [D][B] \mathrm{d}A_e \right\rangle \{\delta\}_e$$

or

$$U = \frac{1}{2}\{\delta\}_e^T[k]_e\{\delta\}_e, \tag{6.62}$$

where A_e is the rectangular area $c \times d$ of the FE of interest (see Fig. 6.17) and

$$[k]_e = \int\int_{A_e} [B]^T[D][B]\mathrm{d}A_e \tag{6.63}$$

is the (symmetric) *element stiffness matrix*.

The potential of external forces, Ω_e, acting upon the element is

$$\Omega_e = -\{\delta\}_e^T\{R\}_e - \int\int_{A_e} pw\mathrm{d}A_e, \tag{6.64}$$

where the first term on the right-hand side is the potential of the discrete nodal forces and the second term is the potential of the distributed load $p(x, y)$. If we substitute for w from Eq. (6.52) into the above equation, we obtain

$$\Omega_e = -\{\delta\}_e^T\{R\}_e - \int\int_{A_e} p[L]\{\delta\}_e\mathrm{d}A_e.$$

Since the potential of external forces is a scalar quantity, we may take the transpose without changing its value

$$\Omega_e = -\{\delta\}_e^T\left\langle\{R\}_e + \int\int_{A_e} p[L]^T\mathrm{d}A_e\right\rangle. \tag{6.65}$$

It is convenient to write the above equation in the form

$$\Omega_e = -\{\delta\}_e^T\{Q\}_e, \tag{6.66}$$

where

$$\{Q\}_e = \{R\}_e + \iint_{A_e} p[L]^T\mathrm{d}A_e \tag{6.67}$$

is the *element nodal force matrix*.

If $\Pi_e = U_e + \Omega_e$ is the total potential energy associated with the element, we have

$$\Pi_e = \frac{1}{2}\{\delta\}_e^T[k]_e\{\delta\}_e - \{\delta\}_e^T\{Q\}_e. \tag{6.68}$$

If we apply the principle of minimum potential energy to Eq. (6.68), we obtain

$$\frac{\partial\Pi_e}{\partial\{\delta\}_e} = 0 \quad \text{or} \quad \frac{\partial\Pi_e}{\partial\{\delta_q\}} = 0; \quad q = i, j, k, l. \tag{6.69}$$

This set of algebraic equations is then solved for the unknown displacements. The order of this system will be equal to the total number of unknown displacements of the discretized plate. The matrix $[K^*]$ can always be written in banded, symmetric form.

Once all displacements have been determined, we can utilize Eqs (6.56) and (6.57) to determine the bending and twisting moments. The general procedure for solving plate (or shell) bending problems by FEM is summarized as follows:

1. For every FE, having a number e and certain nodes numbering and displacements, the nodal force $\{Q\}_e$ and the element stiffness $[k]_e$ matrices are determined in the local coordinate system. A transition of the above matrices from the local to global coordinate system is carried out.
2. The governing system of equations (6.74) is set up where the global matrices $[K]$ and $\{Q\}$ are simply generated in elements as follows: $[K] = \sum_e [k]_e$ and $\{Q\} = \sum_e \{Q\}_e$.
3. The prescribed kinematic boundary conditions are inserted in the global stiffness matrix, as indicated earlier, and the set of equations (6.75) is formed for the entire plate.
4. The set of Eqs (6.75) is solved.
5. Output data are calculated. The element deflections, internal forces, and moments, as well as the stress components, are computed at all nodal points.

It should be noted that the procedure described can be efficient only by using powerful digital computers. At present, new powerful computer programs, based on FEM, have been developed for solving various linear and nonlinear plate (and shell) bending problems.

6.7.3 The triangular plate element

The triangular element can easily accommodate irregular boundaries and can be graduated in size to permit small elements in regions of stress concentration. Consequently, this element is widely used in the finite element technique. Let a flat plate be subdivided into a set of triangular finite elements referred to the local coordinate system xyz, where one of the coordinate axes (for instance, the y axis, as shown in Fig. 6.18) is directed along a particular side of the FE.

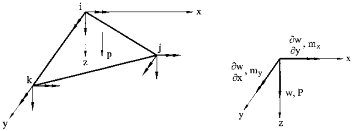
i
x
j
p
z
k
y
$\frac{\partial w}{\partial y}, m_x$
x
$\frac{\partial w}{\partial x}, m_y$
w, P
y
z

Fig. 6.18

The matrix of the nodal displacements for this FE includes the nodal deflections w_q and slopes $(\partial w/\partial y)_q, (\partial w/\partial x)_q$ where $q = i, j, k$. Thus, the triangular FE posseses nine degrees of freedom.

The problem of selecting a suitable polynomial to describe the displacement field over the triangular FE of interest is somewhat more difficult than for the rectangular element. The simplest expression for the deflection function $w(x, y)$ that satisfies all the general requirements, introduced in Sec. 6.7.2, is a cubic polynomial. However, a complete cubic polynomial contains 10 terms. Thus, one needs to fit this cubic polynomial to the nine-degree FE under consideration. Several different possibilities of the presentations of this polynomial were proposed to overcome this difficulty [29–31]. We consider only one of them. It was recommended to take the above cubic polynomial in the form

$$w(x, y) = \alpha_1 + \alpha_2 x + \alpha_3 y + \alpha_4 x^2 + \alpha_5 xy + \alpha_6 y^2 + \alpha_7 x^3 + \alpha_8 (x^2 y + y^2 x) + \alpha_9 y^3. \tag{6.76}$$

The triangular plate bending element, based on the polynomial (6.47), has several limitations. The continuity of slopes across element lines is not guaranteed. Further, its stiffness matrix may be singular for some orientations of sides of FE with respect to the local coordinate axes [30,31]. Thus, this type of element cannot always provide accurate results when used for the bending analysis of plates. However, because of its simplicity, this polynomial is used in engineering practice.

The nodal displacement matrix $\{\delta\}_e$ is of the form (see Fig. 6.18):

$$\{\delta\}_e = \left[\delta_i, \delta_j, \delta_k\right], \tag{6.77}$$

where

$$\left\{\delta_i\right\} = \left[w_i, (\partial w/\partial y)_i, (\partial w/\partial x)_i\right], \text{ etc.}$$

The matrix representing the deflection field is also given by Eq. (6. 47), but the matrices $[N]$ and $\{\alpha\}$ now have the following form:

$$[N] = \left[1, x, y, x^2, xy, y^2, x^3, x^2 y + y^2 x, y^3\right], \{\alpha\} = [\alpha_1, \alpha_2, \ldots, \alpha_9]^T. \tag{6.78}$$

Nodal displacements, upon introduction of Eq. (6.76) and the first derivatives of w with respect to x and y into Eq. (6.77), are next found. They are given by Eq. (6.50) in which the matrix $[C]$ is the 9×9 matrix that depends upon the nodal coordinates. Inversion of the above matrix provides the values of the unknown coefficients α_1, $\alpha_2, \ldots, \alpha_9$ and is given by Eq. (6.51). The displacement function is expressed by Eq. (6.52).

The nodal force matrix $\{R\}_e$ for the triangular FE represents a three-component vector of the form

$$\{R\}_e = \left[R_i, R_j, R_k\right]^T, \tag{6.79}$$

where $\{R\}_q (q = i, j, k)$ is given by Eq. (6.60b). The stiffness matrix, $[k]_e$, and the external nodal force matrix, $\left\{Q\right\}_e$, for the triangular plate element as well as the governing equation of the FEM for the entire plate can be obtained by employing the general procedure introduced in Sec. 6.7.2 for the rectangular plate element.

Let us discuss briefly some **advantages** of the FEM:

Table 6.4

Discretization	Number of nodes	A uniform distributed load			Concentrated force		
		α	β	γ	α_1	β_1	γ_1
2×2	9	34.44	4.427	-3.492	1.378	23.18	-6.505
4×4	25	39.45	4.694	-3.317	1.233	24.72	-6.184
8×8	81	40.40	4.728	-3.296	1.183	25.18	-6.032
16×16	289	40.58	4.781	-3.251	1.167	25.34	-6.085
[7]	—	40.62	4.789	-3.247	1.160	—	—

The results of calculations are given in Table 6.4 (taken from Ref. [32]), where these numerical results for varied numbers of the FEs are compared with those obtained from Ref. [7]. As seen from Table 6.4, a discrepancy of the corresponding numerical data is small even for a sufficiently large mesh of the plate discretization. A reduction of mesh dimensions (an increase in the number of the FEs) provides a monotonic convergence of the obtained results to an exact solution.

This section provides only a brief survey of the FEM and its application to plate bending problems. The literature associated with this method and its application is voluminous. The interested reader is referred to Refs [28–31].

PROBLEMS

6.1 Derive the finite difference expressions for the effective shear forces V_x and V_y. Referring to Fig. 6.5 check the correctness of the result for V_x.

6.2 Determine the finite difference expression corresponding to Eq. (2.25) at a pivotal point k for nonuniform spaced rectangular mesh widths Δx and Δy in the x and y axes directions, respectively.

6.3 Verify Eqs (6.15b).

6.4 Consider a clamped plate shown in Fig. P.6.1. The plate is acted upon by a uniformly distributed load of intensity p_0. Find the deflection w at the nodal points 1 through 5

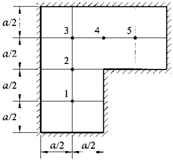

Fig. P6.1

and estimate the location of the point of maximum deflection and determine its magnitude. Use the method of finite differences.

6.5 With reference to Example 6.1 of Sec. 6.2, determine the bending moments M_x and M_y at nodal points of the mesh of the plate shown in Fig. 6.7 by utilizing the deflection field found at the nodal point in the above example.

6.6 Consider a square clamped plate with side a. The plate is subjected to a uniformly distributed load of intensity p_0. Analyze a convergence of numerical FDM solutions for the deflections w and the bending moments M_x and M_y at the plate center for varied plate mesh widths Δ. Take Δ equal to $a/2, a/4$, and $a/8$.

6.7 Derive Eq. (6.22) from the conditions of minimum of the error e_i, given by Eq. (6.21).

6.8 Consider a simply supported square plate $(0 \le x,\ y \le a)$ subjected to a uniformly distributed load p_0. Using the approximate representation of the deflection in the form of (a) in Example 6.2, write out the straightforward BCM governing collocation equations (6.19) for the collocation points on the plate boundary. Take the three points for each side of the plate boundary.

6.9 With reference to Fig. 6.10 write the expression for the singular solution $G_m(x, y; \xi, \eta)$ in the explicit form.

6.10 Write the boundary integral equations of the direct BEM formulation for a simply supported rectangular plate $(0 \le x \le a;\ 0 \le y \le b)$ subjected to a lateral surface load $p(x, y)$. Use the expressions (6.31) and (6.33).

6.11 Consider a square clamped plate with side a subjected to a uniformly distributed load p_0. Applying the indirect BEM approach, write the boundary integral equations in the explicit form. Use the expressions (6.25) and (6.27).

6.12 With reference to Example 6.5 of Sec. 6.5, find the maximum value of the bending moment M_x by retaining two and three terms in the expression (b) for the deflection surface. Compare the obtained value of $M_{\max}$ with the exact solution given in that example. Use the Galerkin method.

6.13 With reference to Fig. 6.13, solve the problem of Example 6.5 by taking the deflection surface of the plate in the following form

$$w = A\cos^2\frac{\pi x}{2a}\cos^2\frac{\pi y}{2b}$$

that satisfies all the boundary conditions of the plate. Applying the Galerkin method, find the maximum deflection and bending moments at the plate center and at a midpoint of the clamped edge.

6.14 Consider a rectangular plate under a uniformly distributed surface load p_0. The plate has edges $y = \pm b$ simply supported and the edges $x = \pm a$ clamped. Using the Galerkin method, determine the deflection and bending moments at the plate center and the bending moment M_x at the midpoint of the clamped edge $x = a$. Let $a = 1\,\mathrm{m}$, $b = 1.5\,\mathrm{m}$, $h = 12\,\mathrm{mm}$, $p_0 = 25\,\mathrm{MPa}$, $E = 200\,\mathrm{GPa}$, and $\nu = 0.3$. Assume a solution of the following form:

$$w = \frac{1}{2}C\left(1 - \cos\frac{2\pi x}{a}\right)\cos\frac{\pi y}{2b}.$$

Check that the above solution satisfies all the prescribed boundary conditions of the plate.

6.15 A rectangular plate with sides a and b $(0 \le x \le a, 0 \le y \le b)$ is subjected to a uniformly distributed load of intensity p_0. The plate edges $y = 0, b$ are simply supported, the edge $x = 0$ is clamped, while the edge $x = a$ is free. Determine the deflection w and stresses σ_x and σ_y at the plate center. Use the Ritz method and solution approximated by

$$w = C\left(\frac{x}{a}\right)^2\sin\frac{\pi y}{b}.$$

where α is the coefficient of thermal expansion. Over a moderate temperature change, α remains reasonably constant and represents an experimentally determined material property. In Eqs (7.1), ε_{xT}^z, ε_{yT}^z, and γ_{xyT}^z are the normal and shear thermal strain components, respectively, at a distance z from the plate middle surface. From Eqs (7.1) it follows that the temperature field has no effect on the shear strain components.

Also, from Eqs (7.1), taking the temperature effects into account, we must modify the general plate bending equations. For the sake of simplicity, we assume that the material properties of the plate are not affected by temperature changes: i.e., the modulus of elasticity, E, and Poisson's ratio, ν, are assumed to be constant. In general, a temperature increase or decrease produces changes in a plate's curvature and in the dimensions of the plate's middle surface.

7.1.2 Thermoelastic plate equations

We begin by modifying Hooke's law relations for Kirchhoff's plate theory. These relations are obtained by adding to strains resulting from external forces, the strains due to the thermal effects. The latter are given by Eqs (7.1). We have the following:

$$\varepsilon_x^z = \frac{1}{E}\left(\sigma_x^z - \nu\sigma_y^z\right) + \alpha T, \quad \varepsilon_y^z = \frac{1}{E}\left(\sigma_y^z - \nu\sigma_x^z\right) + \alpha T, \gamma_{xy}^z = \frac{1}{G}\tau_{xy}^z. \tag{7.2}$$

Solving these equations for the stress components, yields

$$\begin{aligned} \sigma_x^z &= \frac{E}{1-\nu^2}\left[\varepsilon_x^z + \nu\varepsilon_y^z - (1+\nu)\alpha T\right]; \\ \sigma_y^z &= \frac{E}{1-\nu^2}\left[\varepsilon_y^z + \nu\varepsilon_x^z - (1+\nu)\alpha T\right]; \ \tau_{xy}^z = G\gamma_{xy.}^z \end{aligned} \tag{7.3}$$

The assumptions of Kirchhoff's plate bending theory, introduced in Sec. 1.3, can be applied to the thermoelastic analysis of plates, with the exception of assumption 6. As mentioned earlier, a change in the temperature of a plate may result in a change in the dimensions of the middle surface, i.e., points of the middle surface can displace not only in the z but also in the x and y directions. Let u and v, as before, be the displacement components along the x and y axes on the middle surface, respectively. Thus, the total strain components for thermoelastic plates can be obtained by superimposing the strains due to stretching or contracting of the middle surface (Eqs 1.5a) and the strains associated with bending of the middle surface (Eqs 2.6), derived in Sec. 2.2. As result, the following expressions for the strains in terms of displacement components in the middle surface can be written:

$$\varepsilon_x^z = \frac{\partial u}{\partial x} - z\frac{\partial^2 w}{\partial x^2}; \quad \varepsilon_y^z = \frac{\partial v}{\partial y} - z\frac{\partial^2 w}{\partial y^2}; \quad \gamma_{xy}^z = \left(\frac{\partial u}{\partial y} + \frac{\partial v}{\partial x}\right) - 2z\frac{\partial^2 w}{\partial x \partial y}. \tag{7.4}$$

In the foregoing, the first terms on the right-hand sides of the above equations represent the strain components in the middle surface due to its stretching, and terms with w represent the strain components due to bending.

Owing to the deformation of the plate middle surface, the stresses distributed over the thickness of the plate result in the in-plane forces, N_x, N_y, N_{xy} and moments, M_x, M_y, M_{xy}, per unit length, as shown in Figs 3.19 and 2.4. The in-plane force components are represented by

and prescribed boundary conditions prevent free expansion or contraction of the middle surface of the plate. The equations governing the in-plane (membrane) resultants are given by Eqs (3.90). These equations are identically satisfied by introducing the stress function $\Phi(x, y)$, related to the force resultants, as follows:

$$N_x = \frac{\partial^2 \Phi}{\partial y^2}, \quad N_y = \frac{\partial^2 \Phi}{\partial x^2}, \quad N_{xy} = -\frac{\partial^2 \Phi}{\partial x \partial y}. \tag{7.11}$$

For a plate of a constant thickness and negligible weight, the equation of compatibility can be obtained by inserting Eqs (7.2) and (7.9) into Eq. (1.13) and making $M_x = M_y = M_{xy} = M_T = 0$. We obtain

$$\frac{\partial^2}{\partial y^2}\left(N_x - \nu N_y + N_T\right) + \frac{\partial^2}{\partial x^2}\left(N_y - \nu N_x + N_T\right) = 2(1+\nu)\frac{\partial^2 N_{xy}}{\partial x \partial y}. \tag{7.12}$$

Substitution of relations (7.11) into the above yields

$$\nabla^2\nabla^2\Phi = -\nabla^2 N_T \tag{7.13}$$

where N_T is given by Eq. (7.8). Equation (7.13) is the *governing differential equation for the two-dimensional thermoelastic problem of plane stress for thin plates*. Since we have assumed the validity of Kirchhoff's small-deflection theory, the governing equations of thermal bending, Equation (7.10), and thermal stretching or contracting, Eq. (7.13), are independent of each other. Equation (7.10) may be solved by the methods discussed in Chapters 3 and 6, while the methods discussed in the theory of elasticity for plane stress problems are available for solving Eq. (7.13) [1,2]. We discuss below some peculiarities associated with the solution of the thermoelastic plate bending problems. We modify the boundary conditions for thermoelastic plates. Let us consider the boundary conditions for rectangular plates again, as follows:

(a) *Simply supported edges* $x = 0$ and $x = a$

$$w = 0, \quad M_x = 0$$

From Eq. (7.7), the condition for the bending moment can be rewritten as

$$M_x = -D\left(\frac{\partial^2 w}{\partial x^2} + \nu\frac{\partial^2 w}{\partial y^2}\right) - \frac{M_T}{1-\nu} = 0\Bigg|_{x=0,x=a}. \tag{7.14}$$

Taking into account that for edges $x = 0, a$ the curvature $\partial^2 w/\partial y^2 = 0$, the above conditions can be simplified to the form

$$w = 0|_{x=0,a} \text{ and } D\frac{\partial^2 w}{\partial x^2} + \frac{M_T}{1-\nu} = 0\Bigg|_{x=0,a}. \tag{7.15}$$

(b) *Clamped edges* $x = 0$ and $x = a$

$$w = 0|_{x=0,a} \text{ and } \frac{\partial w}{\partial x} = 0|_{x=0,x=a}. \tag{7.16}$$

(c) *Free edges* $x = 0$ *and* $x = a$

The boundary conditions in this case are (see Chapter 2)

$$M_x = 0 \text{ and } V_x = 0. \tag{7.17}$$

The first condition (for the bending moment) is given by Eq. (7.14). The effective shear force is found to be (see Sec. 2.4) $V_x = Q_x + \partial M_{xy}/\partial y$. Using Eqs (2.22a) and (7.7), we can express V_x in the above equation in terms of the deflections w. Finally, the second equation (7.17) will take the following form:

$$\frac{\partial^3 w}{\partial x^3} + (2-\nu)\frac{\partial^3 w}{\partial x \partial y^2} + \frac{1}{D(1-\nu)}\frac{\partial M_T}{\partial x} = 0\bigg|_{x=0,a}. \tag{7.18}$$

Similarly, the boundary conditions can be represented for edges $y = 0$ and $y = b$. We observe from Eqs (7.15)–(7.18) that the boundary conditions for simply supported and free edges of thermoelasic plates are nonhomogeneous.

Small-deflection thermal bending problems of plates can be readily solved by the so-called *isothermal analogy* [1,2]. Let us introduce a fictitious lateral load as follows:

$$p_T = -\frac{1}{1-\nu}\nabla^2 M_{\mathrm{T}}. \tag{7.19}$$

Then, the thermoelastic plate bending problems can be reduced to the corresponding isothermal problems for a plate subjected to two types of surface lateral loads: an actual surface lateral load of intensity $p(x, y)$ and a fictitious load of intensity $p_T(x, y)$. It should be noted that the isothermal analogy might also require a modification of the boundary conditions. This means that in the mathematical formulation of the static boundary conditions, the thermal equivalent moment M_T must be included in accordance with Eqs (7.15) and (7.18) for bending problems.

Example 7.1

Consider a simply supported rectangular plate (see Fig. 3.5) that is subjected to a nonuniform temperature distribution. Determine the deflection surface of the plate.

Solution

The boundary conditions on the edges $x = 0, a$ of the plate are given by Eqs (7.15). Similar expressions can be written for edges $y = 0, b$ by replacing the variable x with y in the second equation (7.15). In general, M_T is a function of x, y, and T. From Eqs (7.15) and (7.7), the following expression applies to the boundary

$$D\nabla^2 w = -M_T \frac{1}{1-\nu}\bigg|_{\substack{x=0,a\\y=0,b}}. \tag{a}$$

Equation (7.10), setting $p = 0$, can be represented in an equivalent form, as follows:

$$\begin{gathered} D\nabla^2 w + M_T \frac{1}{1-\nu} = f(x, y); \\ \nabla^2 f = 0. \end{gathered} \tag{b}$$

Equation (a) and the first equation (b) results in

$$f = 0, \tag{c}$$

which is an appropriate solution of the second Eq. (b).

monly encountered cases of structurally orthotropic plates, shown in Fig. 7.1 [5], are listed below [4–6,7]:

(a) *Plate reinforced by equidistant stiffeners in one direction* (the x-direction) (Fig. 7.1a)

$$D_x = \frac{Eh^3}{12(1-\nu^2)} + \frac{E'b(H_1^3 - h^3)}{12t}, \quad D_y = H = \frac{Eh^3}{12(1-\nu^2)}. \tag{a}$$

(b) *Plate reinforced by a set of equidistant ribs* in one direction (Fig. 7.1b)

$$D_x = \frac{EI}{t}, D_y = \frac{Eh^3}{12\left(1 - \frac{b}{t} + \frac{bh^3}{tH_1^3}\right)}, \quad D_{xy} = 0, D_s \approx \frac{Ch^3}{12} + \frac{C}{2t}, \tag{b}$$

where I is the moment of inertia of a T-shaped section corresponding to one spacing of the rib location about its center axis (shown as shaded in Fig. 7.1c); C is the torsional rigidity of one rib about its centroidal axis. In Eqs (a), (b), and (c), E and

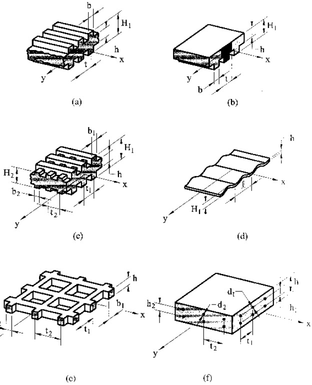
b
H1
h
x
y
t
(a)
H1
h
x
y
b
t
(b)
b1
H1
H2
h
x
b2
t1
t2
y
(c)
h
x
t
H1
y
(d)
h
b1
x
b2
t2
t1
y
(e)
d1
d2
h2
h
h1
x
t1
t2
y
(f)

Fig. 7.1

E' are the elastic moduli of the plating and stiffeners or ribs, respectively; ν is Poisson's ratio of plating.

(c) *Plate reinforced by equidistant* stiffeners in two directions (Fig.7.1c)

$$D_x = \frac{Eh^3}{12(1-\nu^2)} + \frac{E'b_1(H_1^3 - h^3)}{12t_1},$$
$$D_y = \frac{Eh^3}{12(1-\nu^2)} + \frac{E'b_2(H_2^3 - h^3)}{12t_2}, H \approx \frac{Eh^3}{12(1-\nu^2)}, \tag{c}$$

(d) *Corrugated plate with a sinusoidal corrugation* $z = H_1 \sin\frac{\pi y}{l}$ (Fig. 7.1d)

$$D_x = EI, \quad D_y = \frac{l}{s}\frac{Eh^3}{12(1-\nu^2)}, \quad D_{xy} = 0, H = \frac{s}{l}\frac{Eh^3}{12(1+\nu)} \tag{d}$$

where

$$I = 0.5H^2h\left[1 - \frac{0.81}{2.5(H/2l)^2}\right]$$

is the moment of inertia of one wave of the corrugation, and $s = l(1 + \pi^2H_1^2/4l^2)$ is an unfolded length of the one wave.

(e) *Open gridworks* (Fig. 7.1e)

$$D_x = \frac{b_1h^3}{12t_1}, \quad D_y = \frac{b_2h^3}{12t_2}, \quad D_{xy} \cong 0, \quad H = 2D_s = \frac{1}{2}\left(\frac{C_1}{t_1} + \frac{C_2}{t_2}\right), \tag{e}$$

where C_1 and C_2 are the torsional rigidities of the ribs that are parallel to the x and y axes.

(f) *Two-way reinforced concrete slab* (Fig. 7.1f)

$$D_x = \frac{E_c}{(1-\nu_c^2)}\left[\frac{h^3}{12} - I_{xs} + \frac{E_s}{E_c}I_{xs}\right], \quad D_y = \frac{E_c}{(1-\nu_c^2)}\left[\frac{h^3}{12} - I_{ys} + \frac{E_s}{E_c}I_{ys}\right],$$
$$D_s = \frac{1-\nu_c}{2}\sqrt{D_xD_y}, H = \sqrt{D_xD_y}, D_{xy} = \nu_c\sqrt{D_xD_y}, \tag{f}$$

where E_c, ν_c are the modulus of elasticity and Poisson's ratio for concrete, respectively; E_s is the modulus of elasticity for steel; and I_{xs}, I_{ys} are the moments of inertia of steel bars about the x and y axes, respectively.

Notice when $E_x = E_y = E$ and $\nu_x = \nu_y = \nu$, Eqs (7.23), (7.28), and (7.30) become

$$G = \frac{E}{2(1+\nu)}; \quad D_x = D_y = D = \frac{Eh^3}{12(1-\nu^2)}; \quad D_{xy} = \nu D = \nu\frac{Eh^3}{12(1-\nu^2)};$$
$$D_s = \frac{Eh^3}{24(1+\nu)}; \quad H = D_{xy} + 2D_s = D = \frac{Eh^3}{12(1-\nu^2)}.$$

and Eq. (7.31) reduces to that of an isotropic plate, Eq. (2.24), for this particular case.

7.2.4 Rectangular naturally and structurally orthotropic plates

The general procedure for the determination of the deflection, bending moments, and stress components in orthotropic plates is identical with that employed for isotropic plates. The analytical and numerical methods described earlier in Chapters 3 and 6 can be used for determining the deflections, stress resultants, and stress couples.

Example 7.2

A rectangular orthotropic plate with principal directions parallel to the sides is simply supported on all four edges (see Fig. 3.5) and bends under a normal load distributed according to some arbitrary law, i.e., $p = p(x, y)$. Determine the deflection surface for the plate.

Solution

The simply supported boundary conditions are given by Eqs (3.14). We now apply Navier's method discussed in Chapter 3 to treat this plate. Introduction of Eqs (3.15) into (7.31) yields the following:

$$\sum_{m=1}^{\infty}\sum_{n=1}^{\infty}\left\{w_{mn}\left(\frac{m^4\pi^4}{a^4}D_x + 2\frac{m^2n^2\pi^4}{a^2b^2}H + \frac{n^4\pi^4}{b^4}D_y\right) - p_{mn}\right\}\sin\frac{m\pi x}{a}\sin\frac{n\pi y}{b} = 0. \tag{a}$$

Since the above must be valid for all x and y, the terms in the braces must be zero. We obtain

$$w_{mn} = \frac{p_{mn}}{D_x\left(m^4\pi^4/a^4\right) + 2H\left(m^2n^2\pi^4/a^2b^2\right) + D_y\left(n^4\pi^4/b^4\right)}. \tag{b}$$

Substituting Eqs (b) and (3.17) into Eq. (3.15a), we obtain the expression for the following deflections:

$$w = \frac{4}{ab}\sum_{m=1}^{\infty}\sum_{n=1}^{\infty}\int_0^a\int_0^b \frac{p(x, y)\sin\frac{m\pi x}{a}\sin\frac{n\pi y}{b}\,\mathrm{d}x\mathrm{d}y}{D_x\left(m^4\pi^4/a^4\right) + 2H\left(m^2n^2\pi^4/a^2b^2\right) + D_y\left(n^4\pi^4/b^4\right)}. \tag{c}$$

In the particular case of a rectangular plate under a uniformly distributed load of intensity p_0, referring to Sec. 3.3, Eq. (c) is reduced to the following:

$$w = \frac{16p_0}{\pi^6}\sum_{m=1,3,\ldots}^{\infty}\sum_{n=1,3,\ldots}^{\infty}\frac{\sin\frac{m\pi x}{a}\sin\frac{n\pi y}{b}}{mn\left[D_x\left(m^4/a^4\right) + 2H\left(m^2n^2/a^2b^2\right) + D_y\left(n^4/b^4\right)\right]}. \tag{7.33}$$

For isotropic materials, letting $D_x = D_y = D_{xy} = D$, the above equation will coincide with Eq. (3.21a).

Example 7.3

An infinitely long (in the y direction) plate is reinforced by equidistant stiffeners in the direction of the x axis located symmetrically about the middle surface. This plate is modeled by an equivalent orthotropic plate with elastic properties given by Eqs (a) of Sec. 7.2.3. Assuming that the plate is simply supported on edges $x = 0, a$ and subjected to a uniform surface load p_0 (Fig. 7.2), determine the plate deflection surface.

The particular solution is given by Eq. (3.51). Substituting for w_p and p from Eqs (3.51) and (d) into Eq. (7.31), yields the following:

$$D_x\left(\frac{m\pi}{a}\right)^2 g_m - 2H\left(\frac{m\pi}{a}\right)^2\frac{d^2g_m}{dy^2} + D_y\frac{d^4g_m}{dy^4} = p_m.$$

The particular solution of this equation is presented next:

$$g_m = \frac{p_m}{D_x}\left(\frac{a}{m\pi}\right)^4 \quad \text{and}$$
$$w_p = \sum_{m=1,3,\ldots}^{\infty}\frac{p_m}{D_x}\left(\frac{a}{m\pi}\right)^4\sin\frac{m\pi x}{a} = \frac{4p_0}{\pi D_x}\left(\frac{a}{\pi}\right)^4\sum_{m=1,3,\ldots}^{\infty}\frac{1}{m^5}\sin\frac{m\pi x}{a} \tag{e}$$

The general solution w becomes

$$w = \sum_{m=1,3,\ldots}^{\infty}\left[C_{1m}e^{s_1y} + C_{2m}e^{s_2y} + C_{3m}e^{s_3y} + C_{4m}e^{s_4y} + \frac{4p_0}{\pi D_x}\left(\frac{a}{\pi}\right)^4\frac{1}{m^5}\right]\sin\frac{m\pi x}{a} \tag{7.34}$$

As y gets larger, the quantities e^{s_1y} and e^{s_3y} tend to approach infinity. Thus, we must set $C_{1m} = C_{3m} = 0$ and Eq. (7.34) reduces to the following:

$$w = \sum_{m=1,3,\ldots}^{\infty}\left[C_{2m}e^{s_2y} + C_{4m}e^{s_4y} + \frac{4p_0}{\pi D_x}\left(\frac{a}{\pi}\right)^4\frac{1}{m^5}\right]\sin\frac{m\pi x}{a} \tag{7.35}$$

7.2.5 Circular structurally orthotropic plates

Circular plates with frequently arranged annular ribs (Fig. 7.3a) or with rectangular corrugation (Fig. 7.3b) can be considered as examples of structurally orthotropic plates. These plates have a different stiffness in the radial and circumferential directions. In this case, as mentioned in Sec. 7.2.1, an inhomogeneouty of elastic properties of the plate in different directions is explained not by material properties, which are assumed to be isotropic and homogeneous, but the plate structure only. Strictly

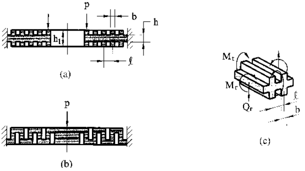

Fig. 7.3

speaking, the flexural rigidity of such plates varies along a radius by some periodical law: it has one value between ribs while another value along them. However, if the ribs are arranged sufficiently close to one other, then it can be assumed that the rigidity in the radial and circumferential directions has some average values, constant or smoothly varying along the radius, and the plates themselves are structurally orthotropic.

We derive the governing differential equation and general relationships for structurally orthotropic circular plates in the context of Kirchhoff's theory. As an example, consider an axisymmetric bending of a circular plate with annular ribs (Fig. 7.3a). We assume that the state of stress in the annular rib is uniaxial, i.e., $\sigma_z = \sigma_r = 0$. In deriving this governing equation, we follow the approach discussed in Sec. 4.8. Let $\vartheta = -\mathrm{d}w/\mathrm{d}r$ be the angle of rotation of the normal to the middle surface (Fig. 4.17). For axisymmetric deformation of the circular plate and uniaxial deformation of the rib, the following expressions for the strain and stress components can be set up:

For the plate

$$\begin{gathered}\varepsilon_r = \frac{\mathrm{d}\vartheta}{\mathrm{d}r}z; \quad \varepsilon_t = \frac{\vartheta}{r}z;\\ \sigma_r = \frac{Ez}{1-\nu^2}\left(\frac{\mathrm{d}\vartheta}{\mathrm{d}r} + \nu\frac{\vartheta}{r}\right); \quad \sigma_t = \frac{Ez}{1-\nu^2}\left(\frac{\vartheta}{r} + \frac{\mathrm{d}\vartheta}{\mathrm{d}r}\right).\end{gathered} \tag{7.36a}$$

For the rib

$$\varepsilon_t = \frac{\vartheta}{r}z; \quad \sigma_t = Ez\frac{\vartheta}{r}, \tag{7.36b}$$

where the subscripts r and t denote the radial and circumferential strain and stress components, respectively; z is a distance counted from the middle surface.

Integrating the stresses over the plate thickness and over the cross-sectional area of the rib, we can obtain the bending moments (per unit length) (see Fig. 7.3c) as follows:

$$\begin{gathered}M_r = \int_{-h/2}^{h/2} \sigma_r z \mathrm{d}z = D_r\left(\frac{\mathrm{d}\vartheta}{\mathrm{d}r} + \nu\frac{\vartheta}{r}\right);\\ M_t = \int_{-h/2}^{h/2} \sigma_t z \mathrm{d}z + \frac{1}{l}\int_A \sigma_t z \mathrm{d}A = D\left(\frac{\vartheta}{r} + \nu\frac{\mathrm{d}\vartheta}{\mathrm{d}r}\right) + \frac{EI_x}{l}\frac{\vartheta}{r};\end{gathered} \tag{7.37}$$

or

$$M_t = D_t\frac{\vartheta}{r} + \nu D_r\frac{\mathrm{d}\vartheta}{\mathrm{d}r}, \tag{7.38}$$

where l is the spacing of the ribs; $D = Eh^3/12(1-\nu^2)$ is the flexural rigidity of an unstiffened plate; $D_r = D$; $D_t = D(1 + EI_x/Dl)$ are transformed rigidities in the radial and circumferential directions, respectively; and $I_x = b\left(h_1^3 - h^3\right)/12$ is the moment of inertia of the area of the rib.

Substituting the expressions for the bending moments, Eqs (7.37) and (7.38), into the equation of equilibrium of a differential element of a circular axisymmetric

$$\vartheta = C_1 r^{\eta} + C_2 r^{-\eta} + \frac{pr^3}{2D_r\left(9 - \frac{D_t}{D_r}\right)}. \tag{7.45}$$

For the corrugated plate shown in Fig. 7.3b, the governing differential equation is of the same form as Eq. (7.39) but the flexural rigidities will be different – namely

$$D_r = \frac{Eh^3}{12\left(1-\nu^2\right)} \frac{l}{s}; \quad D_t = \frac{EI_x}{l\left(1-\nu^2\right)}, \tag{7.46}$$

where l is the spacing of the corrugation; s is an unfolded length of the middle line of one corrugation; h is a thickness which is assumed to be constant; and I_x is the moment of inertia of the cross section of one corrugation about the axis coinciding with the middle plane. The expressions for the bending moments and stresses in the corrugated plate have the form

$$\begin{gathered} M_r = D_r \frac{\mathrm{d}\vartheta}{\mathrm{d}r}; \quad M_t = D_t \frac{\vartheta}{r}; \\ \sigma_{r,\max} = \frac{6M_r}{h^2} + \nu \frac{M_t l}{I_x} z_{\max}; \quad \sigma_{t,\max} = \frac{M_t l}{I_x} z_{\max} + \nu \frac{6M_r}{h^2}, \end{gathered} \tag{7.47}$$

where $z_{\max}$ is the largest distance from the plate middle plane.

Analysis of circular plates with radial ribs can also be performed using the above-mentioned scheme of structural orthotropy (for a sufficiently larger number of stiffeners). However, this case is more complicated because the distances between such ribs vary along the plate radius and, therefore, the flexural rigidity is also variable. In addition, for a one-sided arrangement of ribs, stretching of the plate middle plane becomes significant and must be taken into account. Many references are available for orthotropic plate design. An interested reader is referred to other works [4–6,7].

7.3 THE EFFECT OF TRANSVERSE SHEAR DEFORMATION ON THE BENDING OF ELASTIC PLATES

7.3.1 Introduction

Kirchhoff's hypotheses, discussed in Sec. 1.3, permitted the creation of the classical (Kirchhoff's) bending theory of thin plates which for more than a century has been the basis for the calculation and design of structures in various areas of engineering and has yielded important theoretical and numerical results. However, just as for any other approximation theory, Kirchhoff's theory has some obvious drawbacks and deficiencies, two of which are:

1. A well-known disagreement exists between the order of Eq. (2.24) and the number of the boundary conditioners on the plate free edge. As a result, the boundary conditions of the classical theory take into account only two characteristics on the free edge of the plate rather than three characteristics corresponding to the reality (see Sec. 2.5). Of the two conditions of (2.37), only the first condition (imposed on the bending moment) has a clear physical interpretation. The reduction of the twisting moment

3. the middle plane remains unstrained subsequent to bending.

The only difference between these hypotheses and Kirchhoff's hypotheses discussed in Sec. 1.3 is that the former hypotheses do not require the straight line of the plate to be orthogonal to the bent midsurface of the plate, In this case, the straight line normal to the midsurface, called also the normal element, acquires three independent degrees of freedom corresponding to the deflection $w(x, y)$ and the angles of rotation ϑ_x and ϑ_y which are not related to the deflection w as it has taken place in Kirchhoff's theory (see Eqs (2.5)).

It has been shown in Sec. 2.2 that the displacement components over the plate thickness, according to the above-mentioned hypotheses, obey the following law (see Eqs (2.3)–(2.5)):

$$u = -z\vartheta_x(x, y), \quad v = -z\vartheta_y(x, y), \quad w = w(x, y). \tag{7.48}$$

By repeating the derivation of relations (2.13) discussed in Sec. 2.3, we obtain

$$\begin{aligned} M_x &= -D\left(\frac{\partial \vartheta_x}{\partial x} + \nu \frac{\partial \vartheta_y}{\partial y}\right); \quad M_y = -D\left(\frac{\partial \vartheta_y}{\partial y} + \nu \frac{\partial \vartheta_x}{\partial x}\right); \\ M_{xy} &= -\frac{1}{2}D(1-\nu)\left(\frac{\partial \vartheta_x}{\partial y} + \frac{\partial \vartheta_y}{\partial x}\right). \end{aligned} \tag{7.49}$$

Note that if the angles of rotation are related to the deflections by relations of the type of (2.5), the bending and twisting moment equations (7.49) will coincide with the relations (2.13) derived for the classical (Kirchhoff's) theory.

The stresses σ_x, σ_y, and τ_{xy} are related to the stress resultants M_x, M_y, and M_{xy} by relations (2.11) and the transverse shear forces, Q_x and Q_y are resultants of the transverse shear stresses, τ_{xz} and τ_{yz} (see Eqs (2.12)). As mentioned previously, the transverse shear forces cannot be obtained directly by integrating Eqs (2.12) in Kirchhoff's theory because of the hypotheses (2.1) adapted in this theory. However, the refined theory makes it possible to obtain Q_x and Q_y in terms of the deflection w and the angles of rotation ϑ_x and ϑ_y by integrating Eqs (2.12). Substituting for τ_{xz} and τ_{yz} from Eq. (1.8b) into Eqs (2.12) and using the second and third relations (1.5b) and (7.48), we obtain the following

$$Q_x = G\int_{-h/2}^{h/2}\left(\frac{\partial u}{\partial z} + \frac{\partial w}{\partial x}\right)\mathrm{d}z = Gh\left(-\vartheta_x + \frac{\partial w}{\partial x}\right). \tag{7.50}$$

Thus, within the framework of the theory, one can obtain the transverse shear forces as the stress resultants of the shear stress τ_{xz} and τ_{yz}. We have the following:

$$Q_x = C\eta_x; \quad Q_y = C\eta_y, \tag{7.51}$$

where

$$C = Gh; \quad \eta_x = -\vartheta_x + \frac{\partial w}{\partial x}; \quad \eta_y = -\vartheta_y + \frac{\partial w}{\partial y} \tag{7.52}$$

and C describes the shear stiffness of the plate in the planes xz and yz.

Considering the equilibrium of the plate element, as shown in Fig. 2.4, we obtain Eqs (2.19) and (2.22). Substituting for the stress resultants from the relations (7.49), (7.51) into Eqs (2.19) and (2.22), we arrive at the system of equations for

$$
\begin{aligned}
U = \int\!\!\int \Bigg[\frac{1}{2} \Bigg(& M_x \frac{\partial \vartheta_x}{\partial x} + M_y \frac{\partial \vartheta_y}{\partial y} + M_{xy} \left(\frac{\partial \vartheta_x}{\partial y} + \frac{\partial \vartheta_y}{\partial x} \right) \\
& + Q_x \eta_x + Q_y \eta_y \Bigg) - pw \Bigg] \mathrm{d}x \mathrm{d}y.
\end{aligned} \tag{7.76}
$$

7.3.3 Application of the refined theory

In order to illustrate an application of this theory, let us consider the classical commonly encountered problem: a simply supported rectangular plate with sides a and b ($0 \le x \le a$; $0 \le y \le b$) subjected to a uniformly distributed load of intensity p (see Fig. 3.5). This problem has been analyzed comprehensively by Kirchhoff's theory in Sec. 3.3. The deflected surface of the plate was given by Eq. (3.21a). We have ascertained that the edge supporting reactions (V_x and V_y) did not balance the given uniform load exerted on the plate (see Example 3.1). Note that the contour transverse shear forces, Q_x and Q_y, balance the external load, but according to Kirchhoff's theory they cannot be treated as the edge supporting reactions. Thus, as already discussed in the above example, there will be the concentrated reactions, S, at each corner to satisfy the equilibrium conditions for the plate as a solid.

Let us now consider the solution of this problem using the shear plate bending theory discussed above. To satisfy the boundary conditions (7.73), we seek the solution in the form of the series

$$
\phi = \sum_m \sum_n \phi_{mn} \sin \lambda_m x \sin \lambda_n y; \quad \psi = \sum_m \sum_n \psi_{mn} \cos \lambda_m x \cos \lambda_n y, \tag{7.77}
$$

where

$$
\lambda_m = \frac{m\pi}{a}, \quad \lambda_n = \frac{n\pi}{b}. \tag{7.78}
$$

By substituting the second series into Eq. (7.61), we obtain $\psi_{mn} = 0$, i.e., $\psi = 0$. Inserting the first series into Eqs (7.55) and expanding the surface load $p(x, y)$ into a similar series, we find ϕ_{mn} and then, using relation (7.57), we obtain the following expression for the plate deflections:

$$
w = \frac{1}{D} \sum_m \sum_n \frac{p_{mn} \left[1 + \frac{D}{C} \left(\lambda_m^2 + \lambda_n^2 \right) \right]}{\left(\lambda_m^2 + \lambda_n^2 \right)^2} \sin \lambda_m x \sin \lambda_n y. \tag{7.79}
$$

For a thin plate, the numerical difference between the solutions (3.21a) and (7.79) is small, but these solutions are sufficiently different. Unlike Kirchhoff's theory, in the shear theory the supporting reactions coincide with the contour transverse shear forces, Q_x and Q_y, given by Eqs (7.64); these forces balance the applied uniform load p exerted on the plate and exclude the existence of any corner forces. As mentioned earlier, the existence of these corner forces is also not confirmed by the solution of the three-dimensional theory of elasticity for this problem. Thus, Kirchhoff's plate bending theory leads to the edge supporting reactions that differ significantly from the reactions resulting from the refined plate theory discussed above.

elastic-sensitive elements of manometric devices. They can undergo significant deflections.

7.4.2 The rectangular flexible plates

In deriving the governing differential equations for large deflections in rectangular plates, the Cartesian coordinate system will be used. We consider all the three sets of equations: equilibrium of a plate element; compatibility conditions; and constitutive relations.

We begin our analysis with the *equilibrium equations*. Note that in the large-deflection force analysis of thin plates, in-plane forces N_x, N_y, and N_{xy} depend now not only on external forces applied at the middle plane but also on the stretching of the middle surface caused by its bending. A fundamental feature of the large-deflection plate bending problems is that the equations of static equilibrium must be set up for the *deformed (bent) configuration of plates*. However, in the case of a shallow bent surface of the plate, this point is of fundamental importance only for analyzing the force summation in the z direction. Thus, the assumptions adapted in the large-deflection theory, and discussed in Sec. 7.4.1, make it possible to employ the equilibrium equations (3.90) and (3.91) in the force analysis of a plate under transverse loading, resulting in relatively large elastic deflections.

We are coming now to the analysis of *deformations of the middle surface* of the plate caused by its bending. Let us attach the Cartesian fixed coordinate axes x and y to the middle plane of the plate. Consider three points $A(x, y, 0)$, $B(x + \mathrm{d}x, y, 0)$, and $C(x, y + \mathrm{d}y, 0)$ on the undeformed midplane of the plate (Fig. 7.4).

After deformation, the coordinates of these points will be

$$A_1(x+u, y+v, w),\ B_1\left(x+\mathrm{d}x+u+\frac{\partial u}{\partial x}\mathrm{d}x,\ y+v+\frac{\partial v}{\partial x}\mathrm{d}x,\ w+\frac{\partial w}{\partial x}\mathrm{d}x\right),$$

$$C_1\left(x+u+\frac{\partial u}{\partial y}\mathrm{d}y,\ y+v+\frac{\partial v}{\partial y}\mathrm{d}y,\ w+\frac{\partial w}{\partial y}\mathrm{d}y\right),$$

where u, v, and w are the displacement components of any point of the plate middle surface along the x, y, and z axes, respectively. Determine the distance between points A_1 and B_1:

$$A_1B_1 = \sqrt{\left(\mathrm{d}x+\frac{\partial u}{\partial x}\mathrm{d}x\right)^2+\left(\frac{\partial v}{\partial x}\mathrm{d}x\right)^2+\left(\frac{\partial w}{\partial x}\mathrm{d}x\right)^2}. \tag{a}$$

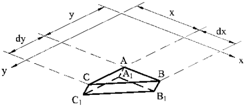

Fig. 7.4

The relative stretching of the line segment $AB = \mathrm{d}x$ on the plate middle surface in the direction of the x axis is

$$\varepsilon_x = \frac{A_1B_1 - AB}{AB} = \frac{\sqrt{\left(\mathrm{d}x + \frac{\partial u}{\partial x}\mathrm{d}x\right)^2 + \left(\frac{\partial v}{\partial x}\mathrm{d}x\right)^2 + \left(\frac{\partial w}{\partial x}\mathrm{d}x\right)^2} - \mathrm{d}x}{\mathrm{d}x}$$
$$= \sqrt{1 + 2\frac{\partial u}{\partial x} + \left(\frac{\partial u}{\partial x}\right)^2 + \left(\frac{\partial v}{\partial x}\right)^2 + \left(\frac{\partial w}{\partial x}\right)^2} - 1. \tag{b}$$

Due to the smallness of displacements u and v, one can neglect $(\partial u/\partial x)^2$ and $(\partial v/\partial x)^2$ under the radical sign (if w is comparable with the plate thickness, we can assume that $\partial u/\partial x$ and $\partial v/\partial y$ has the same order of smallness as the values $(\partial w/\partial x)^2$ and $(\partial w/\partial y)^2$, respectively). Thus, we can rewrite ε_x as follows:

$$\varepsilon_x = \sqrt{1 + 2\frac{\partial u}{\partial x} + \left(\frac{\partial w}{\partial x}\right)^2} - 1, \tag{c}$$

and after approximately taking the root, we obtain

$$\varepsilon_x = \frac{\partial u}{\partial x} + \frac{1}{2}\left(\frac{\partial w}{\partial x}\right)^2. \tag{7.80a}$$

Similarly,

$$\varepsilon_y = \frac{\partial v}{\partial y} + \frac{1}{2}\left(\frac{\partial w}{\partial y}\right)^2. \tag{7.80b}$$

Now we can proceed to determining a shear strain at point A (Fig. 7.4). Let us introduce the following designations:

S_1 is the distance A_1B_1; S_2 is the distance A_1C_1; S is the distance B_1C_1.

From the triangle $A_1B_1C_1$ we obtain

$$S^2 = S_1^2 + S_2^2 - 2S_1S_2\cos\beta, \tag{d}$$

where β represents the angle between line segments A_1B_1 and A_1C_1. Solving the above equation for $\cos\beta$, yields

$$\cos\beta = -\frac{S^2 - S_1^2 - S_2^2}{2S_1S_2}. \tag{e}$$

The distance S_1 may be found from Eq. (a), as follows:

$$S_1^2 = \left[\left(1 + \frac{\partial u}{\partial x}\right)^2 + \left(\frac{\partial v}{\partial x}\right)^2 + \left(\frac{\partial w}{\partial x}\right)^2\right]\mathrm{d}x^2 = (1 + \varepsilon_x)^2\mathrm{d}x^2.$$

Similarly, we can determine the following

$$S_2^2 = \left[\left(\frac{\partial u}{\partial x}\right)^2 + \left(1 + \frac{\partial v}{\partial x}\right)^2 + \left(\frac{\partial w}{\partial y}\right)^2\right]\mathrm{d}y^2 = (1 + \varepsilon_y)^2\mathrm{d}y^2;$$
$$S^2 = \left[\left(1 + \frac{\partial u}{\partial x}\right)\mathrm{d}x - \frac{\partial u}{\partial y}\mathrm{d}y\right]^2 + \left[\frac{\partial v}{\partial x}\mathrm{d}x - \left(1 + \frac{\partial v}{\partial y}\right)\mathrm{d}y\right]^2 + \left[\frac{\partial w}{\partial x}\mathrm{d}x - \frac{\partial w}{\partial y}\mathrm{d}y\right]^2.$$

$$\frac{1}{h}\left(A_y\frac{\partial^4\Phi}{\partial x^4}+2A_{xy}\frac{\partial^4\Phi}{\partial x^2\partial y^2}+A_x\frac{\partial^4\Phi}{\partial y^4}\right)=\left(\frac{\partial^2 w}{\partial x\partial y}\right)^2-\frac{\partial^2 w}{\partial x^2}\frac{\partial^2 w}{\partial y^2},$$

$$D_x\frac{\partial^4 w}{\partial x^4}+2H\frac{\partial^4 w}{\partial x^2\partial y^2}+D_y\frac{\partial^4 w}{\partial y^4}=p+\left(\frac{\partial^2\Phi}{\partial y^2}\frac{\partial^2 w}{\partial x^2}-2\frac{\partial^2\Phi}{\partial x\partial y}\frac{\partial^2 w}{\partial x\partial y}+\frac{\partial^2\Phi}{\partial x^2}\frac{\partial^2 w}{\partial y^2}\right), \tag{7.88}$$

where D_x, D_y, and H are given by Eqs (7.28) and (7.30). $A_x = 1/Ex$, $A_y = 1/Ey$, $A_{xy} = 1/2G - \partial y/Ey = 1/2G - \partial x/Ex$.

Example 7.4

Consider a rectangular plate subjected to a uniformly distributed load of intensity p (Fig. 7.5a). The plate is supported along all the edges by diaphragms that are absolutely rigid in their own plane and flexible out of their plane. This corresponds to the following boundary conditions:

$$w=0,\ \frac{\partial^2 w}{\partial x^2}=0,\quad N_x=0,\ v=0\Big|_{x=0,a}. \tag{a}$$

Similarly, the boundary conditions can be formulated on edges $y = 0$ and $y = b$. Carry out a qualitative bending analysis of the plate.

Solution

The solution of Eqs (7.87) will be sought in the following form:

$$w=\sum_{m,n}f_{mn}\sin\frac{m\pi x}{a}\sin\frac{n\pi y}{b};\quad \Phi=\sum_{i,j}\zeta_{ij}\sin\frac{i\pi x}{a}\sin\frac{j\pi y}{b}, \tag{7.89}$$

where f_{mn} and ζ_{ij} are unknown constants. It can be easily verified that the functions w and Φ in the form of (7.89) satisfy the prescribed boundary conditions (a).

We use the Galerkin method (see Sec. 6.5) to determine constants f_{mn} and ζ_{ij}. Substitute the expansions (7.89) into Eqs (7.87) and multiply the first equation by $\sin(i\pi x/a)\ \sin(j\pi y/b)$ and the second one by $\sin(m\pi x/a)\sin(n\pi y/b)$. Integrating each of the expressions obtained over the plate area and equating the results to

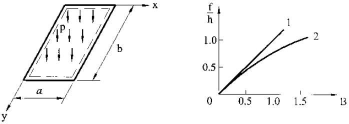

(a) (b)

Fig. 7.5

zero, we obtain the system of nonlinear algebraic equations for the constants f_{mn} and ζ_{ij}.

The numerical procedure is illustrated for the case when only one term is retained in the expansion (7.89), i.e.,

$$w = f \sin\frac{\pi x}{a}\sin\frac{\pi y}{b}; \quad \Phi = \zeta \sin\frac{\pi x}{a}\sin\frac{\pi y}{b}.$$

Upon substitution of the above into Eqs (7.87), one obtains

$$E_1^{(1)} = \zeta\frac{1}{Eh}\left(\frac{\pi^2}{a^2}+\frac{\pi^2}{b^2}\right)^2 \sin\frac{\pi x}{a}\sin\frac{\pi y}{b}$$

$$- f\frac{\pi^4}{a^2b^2}\left(\cos^2\frac{\pi x}{a}\cos^2\frac{\pi y}{b} - \sin^2\frac{\pi x}{a}\sin^2\frac{\pi y}{b}\right);$$

$$E_2^{(1)} = fD\left(\frac{\pi^2}{a^2}+\frac{\pi^2}{b^2}\right)^2 \sin\frac{\pi x}{a}\sin\frac{\pi y}{b}$$

$$- 2f\zeta\left(\frac{\pi^4}{a^2b^2}\right)\left(\sin^2\frac{\pi x}{a}\sin^2\frac{\pi y}{b} - \cos^2\frac{\pi x}{a}\cos^2\frac{\pi y}{b}\right) - p,$$

where $E_1^{(1)}$ and $E_2^{(1)}$ are the first term approximation of the residual error functions of the first and second equations (7.87), respectively. Applying the Galerkin method (see Sec. 6.5), multiply $E_1^{(1)}$ and $E_2^{(1)}$ by $\sin(\pi x/a)\sin(\pi y/b)$ and integrate over the plate area. We have

$$\begin{aligned}
&\zeta\left(\frac{\pi^2}{a^2}+\frac{\pi^2}{b^2}\right)^2 + f^2\frac{16\pi^2 Eh}{3a^2b^2} = 0;\\
&fD\left(\frac{\pi^2}{a^2}+\frac{\pi^2}{b^2}\right)^2 - f\zeta\frac{32\pi^2}{3a^2b^2} = \frac{16}{\pi^2}p.
\end{aligned} \tag{7.90}$$

This system of two equations can be reduced to one equation for the deflection amplitude f_{11}. For example, if $a/b = 1$, we have

$$\frac{f}{h} + \frac{128(1-\nu^2)}{3\pi^4}\frac{f^3}{h^3} = B, \tag{7.91}$$

where

$$B = \frac{4pa^4}{\pi^6 Dh}.$$

Equation (7.91) enables one to carry out a qualitative large-deflection bending analysis of the square plate. In order to obtain a more accurate result, it is necessary to retain in the expressions (7.89) a larger number of terms. Figure 7.5b illustrates the relationship of f/h versus B corresponding to the bending of square stiff (curve 1) and flexible (curve 2) plates for $\nu = 0.3$. A difference of 10% is already reached for the stiff plate for $f/h \approx 0.5$ in this case. The above example is taken from Ref. [21].

7.4.3 Axisymmetric bending of circular flexible plates and membranes

We use the polar coordinate system for the axisymmetric bending analysis of the flexible circular plates and membranes (see Fig. 4.1). Let u be a radial displacement of points in the middle surface, and ε_r and ε_t are the strain components in the radial and tangential (i.e., perpendicular to the radial) directions, respectively. In the analysis of flexible circular plates and membranes subjected to axisymmetric load p we follow the outline of Ref. [19].

Using the line of reasoning as in Sec. 7.4.2, we can conclude that ε_r is expressed by the relation similar to Eq. (7.80a) by replacing the partial derivatives in x with the ordinary derivatives in r. We have

$$\varepsilon_r = \frac{\mathrm{d}u}{\mathrm{d}r} + \frac{1}{2}\left(\frac{\mathrm{d}w}{\mathrm{d}r}\right)^2. \tag{7.92a}$$

Since for axisymmetric deformation of circular plates, $v = 0$ and $\partial^k(\ldots)/\partial\varphi^k = 0$ $(k = 1, 2, \ldots)$, the in-plane circumferential (or tangential) strain, ε_t, can occur as a result of the radial displacements only. So, if points on an infinitesimal arc length $\mathrm{d}s = r\mathrm{d}\varphi$ displace along the plate radius r by an amount u, then, after deformation, the arc length becomes $(r+u)\mathrm{d}\varphi$ and the corresponding circumferential strain component is

$$\begin{aligned} \varepsilon_t &= \frac{(r+u)\mathrm{d}\varphi - r\mathrm{d}\varphi}{r\mathrm{d}\varphi} \quad \text{or} \\ \varepsilon_t &= \frac{u}{r}. \end{aligned} \tag{7.92b}$$

The shear deformation is zero in axisymmetric bending. Substituting $u = \varepsilon_t r$ into Eq. (7.92a) results in the following compatibility of deformations equation:

$$\frac{\mathrm{d}}{\mathrm{d}r}(r\varepsilon_t) - \varepsilon_r = -\frac{1}{2}\left(\frac{\mathrm{d}w}{\mathrm{d}r}\right)^2. \tag{7.93}$$

The middle surface curvatures in the radial, χ_r, and tangential, χ_t, directions, can be obtained from Eqs (2.7) using the relations (4.4) and the conditions of axial symmetry discussed above. Thus, we have

$$\chi_r = -\frac{\mathrm{d}^2 w}{\mathrm{d}r^2}, \quad \chi_t = -\frac{1}{r}\frac{\mathrm{d}w}{\mathrm{d}r}. \tag{7.94a}$$

The twist of the middle surface, $\chi_{rt} = 0$.

Let ϑ be the angle of rotation of the normal to the plate middle surface (see Fig. 4.17), introduced by Eq. (4.86). Then, Eqs (7.94a) can be rewritten in terms of the above angle ϑ, as follows:

$$\chi_r = \frac{\mathrm{d}\vartheta}{\mathrm{d}r}, \chi_t = \frac{\vartheta}{r}. \tag{7.94b}$$

Consider now the state of moments and shear forces on an infinitesimal element of the plate, described in polar coordinates and shown in Fig. 7.6a. The x and y axes are taken in the radial and tangential directions, respectively, in the middle surface, as shown in Fig. 7.6a.

To describe equilibrium of the circular plate in the z direction, it is necessary, as we have seen in Sec. 3.9, to consider the plate in the deflected state. For the forces in Fig. 7.6b, acting on the interior part of the circular plate of radius r, from $\sum F_z = 0$, we have

$$Q(2\pi r) + N_r(2\pi r)\vartheta =, R, \tag{7.96}$$

where

$$R = \int_0^r p(2\pi r)\mathrm{d}r \tag{7.97}$$

is the resultant of the external distributed load.

Introduce the load function Ψ, as follows:

$$\Psi = \frac{1}{r}\frac{R}{2\pi} = \frac{1}{r}\int_0^r pr\mathrm{d}r. \tag{7.98}$$

Then, the shear force, Q, can be found from Eq. (7.96), as follows:

$$Q = \Psi - N_r\vartheta, \tag{7.99}$$

and the load intensity is given by

$$p = \frac{1}{r}\frac{\mathrm{d}}{\mathrm{d}r}(r\Psi). \tag{7.100}$$

The in-plane force–strain relations can be obtained by transforming Eqs (7.84) from Cartesian to polar coordinates. Solving the above equations for the in-plane forces, we obtain

$$N_r = \frac{Eh}{1-\nu^2}(\varepsilon_r + \nu\varepsilon_t), \; N_t = \frac{Eh}{1-\nu^2}(\varepsilon_t + \nu\varepsilon_r). \tag{7.101}$$

The bending moment–curvature relations are given by Eqs (4.14).

The equation of equilibrium (7.95a) will be satisfied if one introduces the stress function Φ by the following relations:

$$N_r = \frac{1}{r}\frac{\mathrm{d}\Phi}{\mathrm{d}r}, \quad N_t = \frac{\mathrm{d}^2\Phi}{\mathrm{d}r^2}. \tag{7.102}$$

Comparing Eqs (7.95b) and (7.99), one finds

$$\frac{\mathrm{d}M_r}{\mathrm{d}r} + \frac{M_r}{r} - \frac{M_t}{r} = -\Psi + N_r\vartheta. \tag{7.103}$$

Substituting for M_r from the first equation of Eq. (4.14) into Eq. (7.103) and using Eqs (7.102) and (4.86), we obtain, after some mathematics,

$$D\frac{\mathrm{d}}{\mathrm{d}r}\left[\frac{1}{r}\frac{\mathrm{d}}{\mathrm{d}r}\left(r\frac{\mathrm{d}w}{\mathrm{d}r}\right)\right] = \Psi + \frac{1}{r}\frac{\mathrm{d}\Phi}{\mathrm{d}r}\frac{\mathrm{d}w}{\mathrm{d}r} \tag{7.104}$$

or in the following form

$$D\frac{\mathrm{d}}{\mathrm{d}r}\left(\nabla^2 w\right) = \Psi + \frac{1}{r}\frac{\mathrm{d}\Phi}{\mathrm{d}r}\frac{\mathrm{d}w}{\mathrm{d}r}, \tag{7.105}$$

If a circular plate is fixed along edge $r = a$, then the boundary conditions are of the form

$$w = 0|_{r=a}, \frac{\mathrm{d}w}{\mathrm{d}r} = 0|_{r=a}. \tag{7.113b}$$

For solid plates having no concentric circular hole, the above boundary conditions must be complemented by the condition of no slope at the plate center, i.e.,

$$\vartheta = -\frac{\mathrm{d}w}{\mathrm{d}r} = 0|_{r=a}. \tag{7.114}$$

Let us describe the boundary conditions for the stress function Φ.

In the case when the edge points of the plate cannot displace in the radial direction, the following condition must be satisfied:

$$u = 0|_{r=a}. \tag{7.115}$$

Using the relations (7.92b) and (7.107), one obtains

$$\frac{u}{r} = Eh\left(\frac{\mathrm{d}^2\Phi}{\mathrm{d}r^2} - \frac{\nu}{r}\frac{\mathrm{d}\Phi}{\mathrm{d}r}\right),$$

and the boundary conditions (7.115) can be written in the form

$$\left(\frac{\mathrm{d}^2\Phi}{\mathrm{d}r^2} - \frac{\nu}{r}\frac{\mathrm{d}\Phi}{\mathrm{d}r}\right) = 0\Big|_{r=a}. \tag{7.116}$$

If the edge points of the plate are free to displace in the radial direction, then the corresponding boundary condition is of the form

$$N_r = \frac{1}{r}\frac{\mathrm{d}\Phi}{\mathrm{d}r} = 0\Big|_{r=a}. \tag{7.117}$$

The conditions (7.116) and (7.117) must be supplemented by the condition of boundedness of the derivative of the stress function, $\mathrm{d}\Phi/\mathrm{d}r$, for the entire plate: in particular, at $r = 0$. The value of N_r, and hence, σ_r, should be also bounded. Then, as seen from the expression (7.102), the following condition must be satisfied:

$$\frac{\mathrm{d}\Phi}{\mathrm{d}r} = 0\Big|_{r=0}. \tag{7.118}$$

Example 7.5

Consider a flexible circular plate of radius a with clamped edge under a uniform load p_0, as shown in Fig. 4.3a. Find the bending moments and normal stresses.

Solution

Let us approximate the deflected surface of the flexible circular plate with clamped edge by the expression

$$w = f\left(1 - \frac{r^2}{a^2}\right)^2, \tag{a}$$

$$2.762\zeta^3 + 5.862\zeta = p^*. \tag{q}$$

The in-plane normal stresses are

$$\begin{aligned} \sigma_{r0} &= \frac{Ef^2}{6a^2}\left(\frac{5-3\nu}{1-\nu} - 6\rho^2 + 4\rho^4 - \rho^6\right), \\ \sigma_{t0} &= \frac{Ef^2}{6a^2}\left(\frac{5-3\nu}{1-\nu} - 18\rho^2 + 20\rho^4 - 7\rho^6\right). \end{aligned} \tag{r}$$

At the plate center these stresses are

$$\sigma_{r0}^* = \sigma_{t0}^* = \frac{5-3\nu}{6(1-\nu)}\zeta^2,$$

and near the plate edge the in-plane normal stresses are given by

$$\sigma_{r0}^* = \frac{1}{3(1-\nu)}\zeta^2, \quad \sigma_{t0}^* = \frac{\nu}{3(1-\nu)}\zeta^2.$$

The bending normal stresses are determined by the previous equations (m) and (n).

7.5 MULTILAYERED PLATES

Plates composed of two or more thin bonded layers of isotropic or anisotropic materials are called *multilayered plates*. Such plates offer certain advantages over homogeneous plates. When suitably designed, they combine a moderate weight with a sufficient strength. Such multilayered plates are used extensively for flight structures, in plywood laminates, and ‘‘sandwich’’ structural assemblies; each layer may possess a different thickness orientation of the principal axes, and anisotropic properties. In formulating the governing differential equations within the frame of the classical plate bending theory, we assume that the individual layers are isotropic and that sliding between them is prevented. So, the strain–displacement relations for the kth layer (Fig. 7.7) can be written as follows:

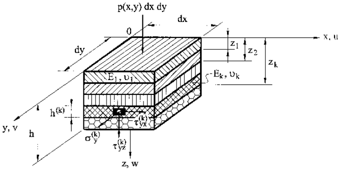

Fig. 7.7

$$\varepsilon_x^{(k)} = -z_k \frac{\partial^2 w}{\partial x^2}, \quad \varepsilon_y^{(k)} = -z_k \frac{\partial^2 w}{\partial y^2}, \gamma_{xy}^{(k)} = -2z_k \frac{\partial^2 w}{\partial x \partial y} \tag{7.119}$$

From Hooke's law, Eqs (2.9), we obtain

$$\begin{aligned} &\sigma_x^{(k)} = \frac{E_k}{1-\nu_k^2}\left(\varepsilon_x^{(k)} + \nu_k \varepsilon_y^{(k)}\right); \quad \sigma_y^{(k)} = \frac{E_k}{1-\nu_k^{(k)}}\left(\varepsilon_y^{(k)} + \nu_k \varepsilon_x^{(k)}\right); \\ &\tau_{xy}^{(k)} = \frac{E_k}{2(1+\nu_k)}\gamma_{xy}^{(k)}. \end{aligned} \tag{7.120}$$

Substituting the strains defined by Eqs (7.119) into the above, integrating over each layer and summing the results, we obtain the following bending and twisting moments:

$$\begin{Bmatrix} M_x \\ M_y \\ M_{xy} \end{Bmatrix} = \sum_k \int_{z_{k-1}}^{z_k} \begin{Bmatrix} \sigma_x \\ \sigma_y \\ \tau_{xy} \end{Bmatrix}^{(k)} z \mathrm{d}z. \tag{7.121}$$

The stress components defined in the kth layer can be calculated from

$$\begin{aligned} &\sigma_x^{(k)} = -z_k \frac{E_k}{1-\nu_k^2}\left(\frac{\partial^2 w}{\partial x^2} + \nu_k \frac{\partial^2 w}{\partial y^2}\right); \quad \sigma_y^{(k)} = -z_k \frac{E_k}{1-\nu_k^2}\left(\frac{\partial^2 w}{\partial y^2} + \nu_k \frac{\partial^2 w}{\partial x^2}\right); \\ &\tau_{xy}^{(k)} = -z_k \frac{E_k}{1+\nu_k}\frac{\partial^2 w}{\partial x \partial y}. \end{aligned} \tag{7.122}$$

The governing differential equation for multilayered plates can be derived similarly, as described in Sec. 2.4. This equation will be similar to that for homogeneous plates, but replacing the rigidity D by the so-called *transformed rigidity*, D_{t}, of the multilayered plates, as follows [22,23]:

$$D_{\mathrm{t}} \nabla^2 \nabla^2 w(x, y) = p(x, y), \tag{7.123}$$

where D_{t} is given by Pister and Dong in the form [22]

$$D_{\mathrm{t}} = \frac{AC - B^2}{A}, \tag{7.124}$$

and the constants A, B, and C are given by

$$\begin{aligned} &A = \sum_k \frac{E_k}{1-\nu_k^2}(z_k - z_{k-1}); \; B = \sum_k \frac{E_k}{1-\nu_k^2}\left(\frac{z_k^2 - z_{k-1}^2}{2}\right); \\ &C = \sum_k \frac{E_k}{1-\nu_k^2}\left(\frac{z_k^3 - z_{k-1}^3}{3}\right). \end{aligned} \tag{7.125}$$

The deflected surface of the multilayered plates can be determined by the same analytical and numerical methods as those discussed for homogeneous plates in Chapters 3, 4, and 6.

If multilayered plates are composed from $2n+1$ symmetrical isotropic layers, about the midplane then the transformed flexural rigidity D_{t} and Poisson's ratio ν_{t} can be determined from [21]

$$\begin{aligned} D_{\mathrm{t}} &= \frac{2}{3}\left[\sum_{k=1}^{n} \frac{E_k}{1-\nu_k^2}\left(h_k^3 - h_{k+1}^3\right) + \frac{E_{n+1}h_{n+1}^3}{1-\nu_{n+1}^2}\right]; \\ \nu_{\mathrm{t}} &= \frac{2}{3D_t}\left[\sum_{k=1}^{n} \frac{E_k \nu_k}{1-\nu_k^2}\left(h_k^3 - h_{k+1}^3\right) + \frac{E_{n+1}\nu_{n+1}h_{n+1}^3}{1-\nu_{n+1}^2}\right]. \end{aligned} \tag{7.126}$$

Lekhnitskii [3] and Ambartsumyan [23] gave similar expressions for multilayered orthotropic plates.

7.6 SANDWICH PLATES

Sandwich plates are frequently used in aerospace structures, shipbuilding, building structures, etc. There are many varieties of sandwich construction, but the basic notion is to separate two thin flat sheets (skins or faces) of strong material (metal or fiber composite) by a core material that is lightweight and comparatively weak. The latter is a hardened foam or has a honeycomb or corrugated construction.

Figure 7.8 shows a rectangular sandwich plate of dimensions $a \times b$. The middle plane of the plate lies in the xy plane. The faces are each of thickness t and the core is of thickness c. The small-deflection theory of the sandwich plates was first developed by Libove and Batdorf [24]. The difference between the sandwich and classical plate bending theories is the low transverse shear stiffness of the core, which can no longer be neglected and must be included in all sandwich calculations.

Following Libove and Batdorf [24], we present below the small-deflection plate bending theory. It is based on the following assumptions:

(a) The faces are made from different orthotropic materials and they are assumed to be thin in comparison with the thickness of the core, i.e., $t \ll c$. Thus, the flexural rigidity of the faces can be neglected.
(b) The faces carry all the bending and twisting moments. The core makes no contribution to the bending stiffness of the sandwich plate.
(c) The core may also be orthotropic. The material of the core is assumed to be absolutely rigid in the direction perpendicular to the middle surface of

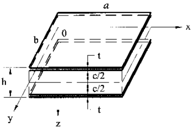

Fig. 7.8

the plate and quite compliant in the tangential direction. Therefore, only the transverse shear stresses τ_{xz} and τ_{yz} arise in the core material. They are nearly uniform throughout the thickness of the core.

(d) The x and y axes are the principal axes of orthotropy.

(e) A general small-deflection theory for flat orthotropic plates, in which deflections due to shear are taken into account, is applied to the sandwich plate. It is assumed that the sandwich behaves essentially as a plate, provided certain physical constants serve to describe the sandwich plate flexural behavior and they may be regarded as the fundamental properties of the plate.

These constants are:
– *flexural and twisting stiffnesses*, D_x, D_y, and D_{xy}:

$$D_x = -\frac{M_x}{\partial^2 w/\partial x^2}, \quad D_y = -\frac{M_y}{\partial^2 w/\partial y^2}; \quad D_{xy} - \frac{M_{xy}}{\partial^2 w/\partial x \partial y}.$$

– *the two transverse stiffnesses*, D_{Qx} and D_{Qy}:

$$D_{Qx} = \frac{Q_x}{\gamma_{xz}}, \quad D_{Qy} = \frac{Q_y}{\gamma_{yz}}. \tag{7.127}$$

– *the two Poisson's ratios*, ν_x and ν_y:

$$\nu_x = \frac{\partial^2 w/\partial y^2}{\partial^2 w/\partial x^2}, \quad \nu_y = -\frac{\partial^2 w/\partial x^2}{\partial^2 w/\partial y^2}.$$

The four constants, D_x, D_y, ν_x, and ν_y are not independent of each other. If three of them are known, the fourth can be determined from the following relation:

$$\nu_x D_y = \nu_y D_x,$$

which can be derived from Betti's reciprocal theorem [4]. For simpler types of sandwich construction the physical constants can be evaluated theoretically from the geometry and physical properties of the material used. For more complicated types of construction, these constants can be evaluated experimentally only. In the general case of the orthotropic faces and core, the expressions for the rigidities introduced above are presented for some practically important cases in Refs [26,27].

Let w be the deflection of the middle surface of the sandwich plate; the stress resultants and stress couples are also associated with the plate middle surface. We apply the same sign convention for the bending moments, and shear and in-plane forces as for homogeneous plates in Chapter 2. The deflection of the sandwich plates is produced by bending in the faces and by shear in the core. Thus, the curvatures in the xz and yz directions are made up of the components that are due to the bending moments, M_x and M_y, and that are due to the variation of the shear forces, Q_x and Q_y. The differential equations for the bending curvatures $\partial^2 w/\partial x^2$ can be represented in the form

$$\frac{\partial^2 w}{\partial x^2} = -\frac{M_x}{D_x} + \nu_y \frac{M_y}{D_y} + \frac{1}{D_{Q_x}} \frac{\partial Q_x}{\partial x}; \quad \frac{\partial^2 w}{\partial y^2} = \nu_x \frac{M_x}{D_x} - \frac{M_y}{D_y} + \frac{1}{D_{Q_y}} \frac{\partial Q_y}{\partial y}. \tag{7.128a}$$

PROBLEMS

7.1 Calculate the maximum deflection and maximum moments in Example 7.1 of Sec. 7.1. Take $m = n = 1$, $T = T_0 z/h$, $b = 2a$, $\nu = 0.3$.

7.2 Redo Problem 7.1 for the temperature field given by $T = T_0(2z/h)$.

7.3 With reference to Eqs. (7.8), derive the additional potential energy for the thermal bending and thermal stretching into the total potential energy of the plate (Eq. (2.60)).

7.4 Consider a built-in edge, rectangular plate ($-a/2 \leq x \leq a/2$, $-b/2 \leq y \leq b/2$) under a transverse temperature field $T = T_0(z^2/h)$. Find the expression for the deflection surface of the plate. Use the Ritz method and results of the Problem 7.3. Assume that w is given by

$$w = \frac{1}{4} w_0 \left(1 + \cos\frac{2\pi x}{a}\right)\left(1 + \cos\frac{2\pi y}{b}\right).$$

7.5 A simply supported plate with sides $a = 35$ in. and $b = 45$ in. and having a thickness of 3 in. is heated from both top and bottom such that, at a certain time, three thermocouples read $T(+h/2) = 350^\circ$F, $T(0) = 100^\circ$F, and $T(-h/2) = 350^\circ$F. If the stress-free temperature is 80°F, calculate the maximum deflection of the plate. Retain only one term ($m = n = 1$) in the series solution. Assume that the plate is made of aluminum with the following mechanical parameters: $E_{\text{al}} = 10 \times 10^6$ psi, $\alpha_{\text{al}} = 10 \times 10^{-6}$ in./in.°F , and $\nu = 0.3$.

7.6 Verify Eq. (7.32).

7.7 A rectangular, simply supported plate with sides a and b ($b = 1.5a$) is reinforced by single equidistant stiffeners (Fig. 7.1a). Compute the maximum deflection, $w_{\max}$. The plate and stiffeners are made of steel with $E = 200$ GPa, $\nu = 0.3$. Take $a = 1280$ mm, $t = 180$ mm, $h = 40$ mm, and $H_1 = 80$ mm.

7.8 Determine the rigidities of a steel bridge deck that may be approximated as a steel plate reinforced by a set of equidistant ribs in one direction (Fig. 7.1b). Take $h = 12$ mm, $H_1 = 36$ mm, $t = 120$ mm, $E = 210$ GPa, $\nu = 0.3$, and the torsional rigidity of one rib is $C = JG = 0.246b^3(H_1 - h)G$.

7.9 A rectangular, simply supported building floor slab with sides a and b is made of reinforced concrete. It is subjected to a uniformly distributed load of intensity p_0. Determine the expressions for (a) the deflection surface and (b) the bending moments. Take $b = 2a$, $m = n = 1$, $t_1 = a/10$, $t_2 = a/8$, $h = a/15$, $d_2 = d_1 = h/10$, $E_c = 21.4$ GPa, $\nu_c = 0.15$, $E_s = 200$ GPa, $\nu_s = 0.28$.

7.10 Find the maximum stresses in a simply supported rectangular plate with sides a and b. The plate is subjected to a uniformly applied load of intensity p_0. It is constructed of a alumina/epoxy laminate with $E_x = 33{,}000$ ksi, $E_y = 3000$ ksi, $G = 1000$ ksi, $\nu_x = 0.28$, and $\nu_y = 0.3$. Let $a = 35$ in., $b = 20$ in., and $h = 0.20$ in. Compare the result with that of an equivalent isotropic plate of $E = 17400$ ksi and $\nu = 0.35$.

7.11 An infinitely long plate of Example 7.3 of Sec. 7.2 is reinforced by a set of equidistant ribs in the x direction (Fig. 7.1b). The plate is subjected to a uniformly distributed load of intensity p_0. Determine the deflections and bending moments in the plate if $a = 12$ ft., $t = 12$ in., $h = 0.2$ in., $H_1 = 2.5$ in., and $b = 1.5$ in. Assume that the plate and ribs are made of the same material with $E = 30{,}000$ ksi and $\nu = 0.3$. Retain only one term in the series solution.

7.12 Verify Eq. (7.39).

7.13 Determine the particular solution of Eq. (7.39) for an orthotropic circular plate subjected to a concentrated force P applied at its center.

7.14 A circular, simply supported plate of radius R is reinforced by equidistant annular ribs (Fig. 7.3a). The plate is subjected to a uniform load p_0. Determine the maximum allowable value of p_0 if $w_{\max} = 0.2$ in. Take $R = 10$ ft, $h = 1$ in., $t = 10$ in., $b = 4$ in., and $h_1 = 6\,\text{in}$. Assume that the plate and ribs are made of the same material with $E = 29{,}000\,\text{ksi}$ and $\nu = 0.29$.

7.15 Verify Eqs (7.55) and (7.56).

7.16 Verify the boundary conditions for the free edge given by Eqs (7.70).

7.17 Solve the problem of Example 3.1 within the framework of the refined (shear) plate bending theory. Determine the deflection surface w and the bending moments M_x and M_y. Check the overall equilibrium of the plate.

7.18 Verify Eq. (7.87).

7.19 Transform Eqs (7.86) to plane polar coordinates r and φ. Show that in this case

$$N_r = \frac{1}{r}\frac{\partial \Phi}{\partial r} + \frac{1}{r^2}\frac{\partial^2 \Phi}{\partial \varphi^2}, \quad N_t = \frac{\partial^2 \Phi}{\partial r^2}, \quad N_{rt} = -\frac{\partial}{\partial r}\left(\frac{1}{r}\frac{\partial \Phi}{\partial \varphi}\right), \quad \text{and} \tag{P7.1}$$

$$\nabla^2\nabla^2\Phi = -\frac{1}{2}EhL(w, w),$$

$$\nabla^2\nabla^2 w = \frac{1}{D}[p + L(w, \Phi)], \tag{P7.2}$$

where

$$\begin{aligned} L(w, \Phi) = {} & \frac{\partial^2 w}{\partial r^2}\left(\frac{1}{r}\frac{\partial \Phi}{\partial r} + \frac{1}{r^2}\frac{\partial^2 \Phi}{\partial \varphi^2}\right) + \left(\frac{1}{r}\frac{\partial w}{\partial r} + \frac{1}{r^2}\frac{\partial^2 w}{\partial \varphi^2}\right)\frac{\partial^2 \Phi}{\partial r^2} \\ & - 2\frac{\partial}{\partial r}\left(\frac{1}{r}\frac{\partial \Phi}{\partial \varphi}\right)\frac{\partial}{\partial r}\left(\frac{1}{r}\frac{\partial w}{\partial \varphi}\right) \end{aligned} \tag{P.7.3}$$

and $L(w, w)$ is obtained by replacing Φ with w in the above equation.

7.20 Consider a rectangular isotropic, sandwich plate shown in Fig. 7.8. Following Plantema [28], introduce w_b and w_s as follows

$$w = w_b + w_s, \quad \gamma_{xz} = \frac{\partial w_s}{\partial x}, \quad \gamma_{yz} = \frac{\partial w_s}{\partial y}, \tag{P.7.4}$$

where w_b and w_s are the deflections of the above plate due to bending and shear, respectively. Show that Eqs (7.127), (7.129), and (7.135) will be transformed in terms of the partial deflections to the following relations and equations

$$\begin{aligned} & M_x = -D_s\left(\frac{\partial^2 w_b}{\partial x^2} + \nu\frac{\partial^2 w_b}{\partial y^2}\right), \quad M_y = -D_s\left(\frac{\partial^2 w_b}{\partial y^2} + \nu\frac{\partial^2 w_b}{\partial x^2}\right), \\ & M_{xy} = -D_s(1 - \nu)\frac{\partial^2 w_b}{\partial x \partial y}, \\ & Q_x = D_Q\frac{\partial w_s}{\partial x}, \quad Q_y = D_Q\frac{\partial w_s}{\partial y}, \end{aligned} \tag{P7.5}$$

$$\nabla^2\nabla^2 w_b = \frac{1}{D_s}p(x, y). \tag{P7.6}$$

Verify also that the relationship between the partial deflections is of the form

$$w_s = -\frac{D_s}{D_Q}\nabla^2 w_b + C, \tag{P7.7}$$

where C is an arbitrary integration constant which is to be determined from boundary conditions prescribed for w_s on the plate edges (see [27] for more detail). For a verification of Eq. (P7.7), use Eqs (2.22) together with Eqs (P7.2).

Depending mainly on values of the applied in-plane loads, an initial, flat configuration of a plate equilibrium may be stable or unstable. The initial configuration of elastic equilibrium is *stable*, if when the plate is displaced from this equilibrium state by an infinitesimal disturbance, say a small lateral force, the deflected plate will tend to come back to its initial, flat configuration when the disturbance is removed. The initial configuration of equilibrium is said to be *unstable* if, when the plate is displaced from this equilibrium position by a small lateral load, it will tend to displace still further when the load is removed. The unstable plate will find other (new) equilibrium state(s), which may be in the vicinity of the initial state or may be far away from the initial equilibrium configuration. If the plate remains at the displaced position even after the small lateral load is removed, it is said to be in *neutral equilibrium*; thus, the plate in neutral equilibrium is neither stable nor unstable.

The transition of the plate from the stable state of equilibrium to the unstable one is referred to as *buckling* or *structural instability*. The smallest value of the load producing buckling is called the *critical* or *buckling load.*

The importance of buckling is the initiation of a deflection pattern, which if the loads are further increased above their critical values, rapidly leads to very large lateral deflections. Consequently, it leads to large bending stresses, and eventually to complete failure of the plate.

It is important to note that a plate leading from the stable to unstable configuration of equilibrium always passes through the neutral state of equilibrium, which thus can be considered as a bordering state between the stable and unstable configurations. In the mathematical formulation of elastic stability problems, neutral equilibrium is associated with the existence of bifurcation of the deformations. According to this formulation, the *critical load can be identified with the load corresponding to the bifurcation of the equilibrium states, or in other words, the critical load is the smallest load at which both the flat equilibrium configuration of the plate and slightly deflected configuration are possible*.

The goal of the buckling analysis of plates is to determine the critical buckling loads and the corresponding buckled configuration of equilibrium. We consider below the linear buckling analysis of plates based on the following assumptions:

(a) Prior to loading, a plate is ideally flat and all the applied external loads act strictly in the middle plane of the plate.
(b) States of stress is described by equations of the linear plane elasticity. Any changes in the plate dimensions are neglected prior to buckling.
(c) All the loads applied to the plate are dead loads; that is, they are not changed either in magnitude or in direction when the plate deforms.
(d) The plate bending is described by Kirchhoff's plate bending theory discussed in Chapter 2.

The linear buckling analysis of plates based on these assumptions makes it possible to determine accurately the critical loads, which are of practical importance in the stability analysis of thin plates. However, this analysis gives no way of describing the behavior of plates after buckling, which is also of considerable interest. The postbuckling analysis of plates is usually difficult because it is basically a nonlinear problem. Some postbuckling plate problems will be discussed in Sec. 8.5. Classical

The solution of Eq. (8.3), $w(x, y)$, obtained by some analytical or numerical methods, introduced in Chapters 3 and 6, involves arbitrary constant coefficients C_i $(i = 1, 2, \ldots, n)$ to be determined from the prescribed boundary conditions. Consequently, Eq. (8.3) is reduced to a system of homogeneous, linear algebraic equations in C_i. For an existence of a nontrivial solution of the system, its determinant must be equal to zero. This results in the so-called characteristic equation in λ. Solving this characteristic equation, we obtain some specific values $\lambda_1, \lambda_2, \ldots, \lambda_n$ (the *characteristic numbers* or *eigenvalues*) and the corresponding nonzero solutions, called *characteristic functions* or *eigenfunctions*. The smallest of the characteristic numbers or eigenvalues not equal to zero will be the *critical value*, λ_{cr}, and the corresponding eigenfunctions will be the *buckling modes*. Then, the critical load is calculated by multiplying λ_{cr} and the corresponding reference value of the load.

The energy method

The energy method is based on the general theorems and principles of the equilibrium of mechanical systems discussed in Sec. 2.6. As mentioned in Sec. 2.6, the potential energy of a system has an extremum at equilibrium. Based on this statement, we can reformulate the concepts of stability and instability presented earlier. The equilibrium will be *stable* if the potential energy in that state has a minimum value in comparison with values corresponding to any possible states close to the state of equilibrium, *unstable* if the potential energy is a maximum, and *neutral* if the potential energy in the equilibrium state is neither a maximum nor a minimum.

Let us apply this potential energy criterion to the buckling analysis of plates. Two states of the plate are considered: an initial state of equilibrium under the given in-plane edge loads, in which the middle surface remains flat; a neighboring state, in which the middle surface is slightly curved due to small virtual displacements applied to the plate. Let Π_0 and Π be the potential energies in the flat and neighboring states of equilibrium, respectively. The equilibrium will be stable if for all possible small deflections $\Pi_0 < \Pi$, unstable if $\Pi_0 > \Pi$, and neutral if $\Pi_0 = \Pi$.

The increment in the total potential energy of the plate loaded by the edge in-plane external loads, after the transition of this plate from an initial configuration of equilibrium to the above-mentioned neighboring configuration of equilibrium is given by the following relationship:

$$\Delta\Pi = \Pi - \Pi_0 = \Delta U_0 + U_{\mathrm{b}} + \Delta\Omega_{\Gamma}, \tag{8.4}$$

where ΔU_0 is the increment of the strain energy of the plate middle surface in buckling; U_{b} is the strain energy of bending and twisting of the plate; and $\Delta\Omega_{\Gamma}$ is the increment in the potential of the in-plane external edge forces applied to the plate. Bifurcation of an initial configuration of equilibrium (corresponding to the neutral equilibrium) occurs when

$$\Delta\Pi = 0. \tag{8.5a}$$

This is *the general energy criterion for the buckling analysis of plates* (*and shells also*). The critical loads may be determined from this criterion at an additional condition of the minimum of the load parameter λ.

It can be shown [1,2] that the governing differential equation (8.1) can be obtained from the condition (8.5a). The latter can also be employed for constructing an approximate solution of the plate buckling problems, in particular for determining the critical loads, by the Ritz method (see Sec. 6.6). In this case, the deflection surface of the plate, $w(x, y)$, in the neighboring state of equilibrium is sought in the form of Eq. (6.42). If all external forces acting on the plate vary in the proportion to a load parameter λ, then substituting Eq. (6.42) into the condition (8.5a) yields

$$\Delta\Pi = \Delta\Pi(\lambda, C_1, C_2, \ldots, C_n) = 0, \tag{8.5b}$$

where C_i $(i = 1, 2, \ldots, C_n)$ are undetermined coefficients. Numerical implementation of the conditions (8.5) requires the usual minimization process (Eq. (6.44)). The latter also leads to a system of linear algebraic, homogeneous equations. So, applying the procedure discussed earlier for determining a nontrivial solution in the equilibrium method, we can find all the characteristic numbers λ_i, and their smallest value corresponding to the critical eigenvalue, λ_{cr}.

Dynamic or kinematic method

This method is the most general and universal and is associated with the mathematical problem of the stability of motion. The method is based on examining transverse oscillations of a thin plate subjected to in-plane edge loads. The smallest value of the load that results in unbounded growth of the amplitude of these oscillations in time is considered as a critical value of the applied loads.

The equilibrium and energy methods are now discussed in more detail.

8.3 THE EQUILIBRIUM METHOD

8.3.1 Buckling of rectangular plates

According to the equilibrium method, the critical values of applied in-plane forces may be found from the solution of the governing differential equation (8.1) or its equivalent analog (8.3). As mentioned in Sec. 8.2, this equation is a homogeneous, linear partial differential equation with, generally speaking, variable coefficients. It is impossible to find its analytical solution in the general case. However, for some particular but practically important cases this equation makes it possible to obtain an exact solution. The following examples illustrate the equilibrium method for obtaining the exact solutions associated with determining the critical forces in rectangular plates.

Example 8.1

Determine the critical buckling load for a simply supported plate subjected to a uniformly distributed compressive edge load q_x acting in the x direction, as shown in Fig. 8.1.

Solution

For this particular case $N_x = -q_x$ and $N_y = N_{xy} = 0$. The differential equation (8.1) becomes

$$D\nabla^2\nabla^2 w + N_x \frac{\partial^2 w}{\partial x^2} = 0. \tag{8.6}$$

is the *buckling load parameter*. For a given value of m, the parameter K depends only on the ratio a/b, called the *aspect ratio* of the plate. As follows from Eqs (8.7) and (8.8), the smallest value of q_x, and consequently, the value of the critical force $q_{x,\mathrm{cr}}$, depends on the number of half-sine waves in the longitudinal direction, m. For a given aspect ratio the critical load is obtained by selecting m so that it makes Eq. (8.7b) a minimum. Since only K depends on m, we have the following:

$$\frac{\mathrm{d}K}{\mathrm{d}m} = 2\left(\frac{mb}{a} + \frac{a}{mb}\right)\left(\frac{b}{a} - \frac{a}{m^2 b}\right) = 0.$$

Since the first factor in parentheses of the above is nonzero, we obtain

$$m = \frac{a}{b}. \tag{8.9}$$

This provides the following minimum values of the critical load:

$$\min q_x = q_{x,\mathrm{cr}} = \frac{4\pi^2 D}{b^2}. \tag{8.10}$$

The corresponding value of the buckling load parameter is $K = 4$. The corresponding critical stress is found to be

$$\sigma_{x,\mathrm{cr}} = \frac{N_{x,\mathrm{cr}}}{h} = \frac{q_{x,\mathrm{cr}}}{h} = \frac{4\pi^2 D}{b^2 h} = \frac{\pi^2 E}{3\left(1 - \nu^2\right)}\left(\frac{h}{b}\right)^2. \tag{8.11}$$

Thus, the critical values of q_x and σ_x correspond to such plate dimensions when its width, b, fits in its length, a, by whole numbers. In this case a bent plate is subdivided into square cells of side dimensions b. In the general case, $q_{x,\mathrm{cr}}$ may be determined from Eqs (8.7) and (8.8).

The variation of the buckling load parameter K as a function of the aspect ratio a/b for $m = 1, 2, 3, 4$ is shown in Fig. 8.2. Referring to this figure, the magnitude of $q_{x,\mathrm{cr}}$ and the number of half-waves m (in the direction of the applied compressive forces) for any value of the aspect ratio can readily be found. For example, if $a/b = 1.5$, we can find that $K = 4.34$ and $m = 2$. The corresponding critical load for this particular case is

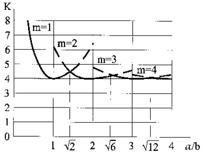

Fig. 8.2

$$q_{x,\mathrm{cr}} = 4.34\frac{\pi^2 D}{b^2}.$$

The plate will buckle under this load into two half-waves in the direction of the applied compressive loads and one-half in the perpendicular direction.

An analysis of the curves in Fig. 8.2 shows that for short and broad plates (for $a/b < 1$) a minimum value of the critical force is obtained for $m = 1$. For $a/b \ll 1$, that is for very short and broad plates, the ratio a/b can be neglected compared with the ratio b/a in Eq. (8.8). As a result, $\min.K \cong b^2/a^2$ and the value of the critical force for this particular case is

$$q_{x,\mathrm{cr}} = \frac{\pi^2 D}{a^2}.$$

Thus, in this case, the critical force does not depend on the plate width and depends only upon its length. The above expression represents the Euler critical load for a strip of unit width and of length a whose smallest value of flexural rigidity, EI, is replaced with the flexural rigidity of the plate, D.

Example 8.2

Determine the buckling critical load for a plate subjected to a uniformly distributed compressive edge load acting in the x direction. Assume that the edges $x = 0$ and $x = a$ are simply supported, the edge $y = 0$ is fixed, and the edge $y = b$ is free, as shown in Fig. 8.3.

Solution

It is convenient for this problem to employ Levy's method (see Sec. 3.5) for the solution. The boundary conditions at the edges $x = 0$ and $x = a$ will be automatically satisfied by setting

$$w(x, y) = \sum_{m=1}^{\infty} f_m(y) \sin\frac{m\pi x}{a}. \tag{a}$$

For this case, we also can set $N_x = -q_x$ and $N_y = N_{xy} = 0$. Substituting the above into Eq. (8.1) and imposing the condition that at least one of the terms multiplying $\sin(m\pi x/a)$ must vanish, we determine for $f_m(y)$ the following ordinary differential equation:

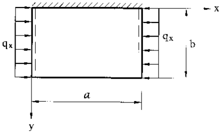

Fig. 8.3

sharp decrease in critical forces, etc. If the boundary conditions of a plate differ from simply supported ones, determining the critical forces even for simple cases of loadings represents a sufficiently complicated mathematical problem and can be obtained by numerical methods only [2–8].

For rectangular plates subjected to uniform compressive forces acting in the direction of one coordinate axis only (either the x or the y axis) with various boundary conditions, the critical stress, σ_{cr}, can be determined from the expression

$$\sigma_{\mathrm{cr}} = K\frac{\pi^2 D}{b^2 h}, \tag{8.19}$$

where the coefficients K are given in Fig. 8.4 versus the aspect ratios a/b [4].

Example 8.3

Determine the critical forces for the rectangular plate with simply supported edges and uniformly compressed in two directions, as shown in Fig. 8.5.

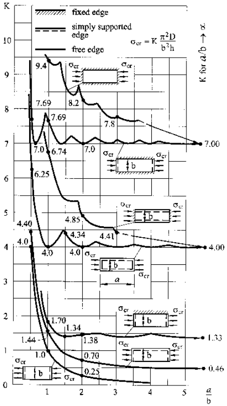

Fig. 8.4

It can be easily shown that the minimum value of q, q_{cr}, corresponds to $m = n = 1$. Thus,

$$q_{\mathrm{cr}} = \frac{\pi^2 D}{b^2}\left[1 + \left(\frac{b}{a}\right)^2\right]. \tag{8.23}$$

In particular, for the square plate ($a = b$), the above expression appears, as follows:

$$q_{\mathrm{cr}} = 2\frac{\pi^2 D}{b^2}.$$

Hence, if the square plate is compressed in two directions by the two equal system of forces, q, the critical value of these forces is two times less than that for the square plate compressed by the same force acting in one direction only (see Example 8.1).

2. Assume now that the compressive forces q_x and q_y applied to the plate of Fig. 8.5 will increase in the proportion to one parameter. For example, $q_x = \lambda$ and $q_y = \alpha\lambda$, where $\alpha > 0$ is some fixed known parameter. Then, from Eq. (8.22), we obtain

$$\lambda = \frac{\pi^2 D}{b^2}\frac{\left[\left(\frac{mb}{a}\right)^2 + n^2\right]}{\left(\frac{mb}{a}\right)^2 + \alpha n^2}. \tag{8.24}$$

For $a > b$, the minimum value of λ may be reached for $n = 1$ only. Thus,

$$\lambda_{\mathrm{cr}} = K\frac{\pi^2 D}{b^2}, \tag{8.25}$$

where

$$K = \frac{\left[(mb/a)^2 + 1\right]}{(mb/a)^2 + \alpha}. \tag{8.26}$$

For each ratio of a/b and each value of α it should be selected a number of the half-sine waves m from the condition of minimum of K as discussed in Example 8.1.

8.3.2 Buckling of circular plates

Circular plates in some measuring instruments are used as sensitive elements reacting to a change in the lateral pressure. In some cases – in temperature changes, in the process of their assembly – these elements are subjected to the action of radial compressive forces from a supporting structure. As a result, buckling of the circular plates can take place.

Let us consider a circular solid plate subjected to uniformly distributed in-plane compressive radial forces q_r, as shown in Fig. 8.6. We confine our buckling analysis to considering only axisymmetric configurations of equilibrium for the plate.

We can use the polar coordinates r and φ to transfer the governing differential equation of plate buckling (Eq. (8.1)), derived for a rectangular plate, to a circular plate. For the particular case of axisymmetric loading and equilibrium configurations, we have

$$N_x = N_y = N_r = -q_r, \quad N_{xy} = 0. \tag{8.27}$$

$$\Delta U_0 = W_{\mathrm{e}} + \frac{1}{2}\int_0^b\int_0^a \left[N_x\left(\frac{\partial w}{\partial x}\right)^2 + N_y\left(\frac{\partial w}{\partial y}\right)^2 + 2N_{xy}\frac{\partial w}{\partial x}\frac{\partial w}{\partial y}\right]\mathrm{d}x\mathrm{d}y. \tag{8.43}$$

It can be shown that the expression for ΔU_0 in the form of Eq. (8.43) is valid (replacing the limits of integration) for a plate of any geometry, not necessarily, rectangular.

The increment in the potential of the external, in-plane forces applied to the plate is equal to the negative value of the work done by these forces, i.e.,

$$\Delta\Omega_\Gamma = -W_{\mathrm{e}}. \tag{8.44}$$

The strain energy of the bending and twisting of a plate, U_b, is given by Eq. (2.53). Therefore, the increment in the total potential energy of the plate upon buckling, $\Delta\Pi$, can be obtained by substituting Eqs (2.53) and (8.43) with taking into account Eq. (8.44) on the right-hand side of Eq. (8.4).

$$\begin{aligned}\Delta\Pi = {} & \frac{1}{2}\iint_A D\left\{\left(\frac{\partial^2 w}{\partial x^2} + \frac{\partial^2 w}{\partial y^2}\right)^2 + 2(1-\nu)\left[\left(\frac{\partial^2 w}{\partial x\partial y}\right)^2 - \frac{\partial^2 w}{\partial x^2}\frac{\partial^2 w}{\partial y^2}\right]\right\}\mathrm{d}x\mathrm{d}y \\ & + \frac{1}{2}\iint_A \left[N_x\left(\frac{\partial w}{\partial x}\right)^2 + N_y\left(\frac{\partial w}{\partial y}\right)^2 + 2N_{xy}\frac{\partial w}{\partial x}\frac{\partial w}{\partial y}\right]\mathrm{d}x\mathrm{d}y\end{aligned} \tag{8.45}$$

As mentioned in Sec. 8.2, the energy criterion (8.5) may be employed be obtain the exact and approximate solutions of the plate buckling problems. In the latter case, this criterion may be combined with, for instance, the Ritz method together with the eigenvalue technique introduced in Sec. 8.2.

Note that in practice $\Delta\Pi = 0$ only if the form chosen for the deflection is exact. Any approximation form, when Eq. (8.45) is applied, will give a value of the critical force higher than the true value. Let us demonstrate the advantages of the energy criterion in illustrative examples.

Example 8.4

Using the Ritz method, determine the critical buckling load for the plate with three simply supported edges $x = 0, a$ and $y = 0$ and one free edge $y = b$, as shown in Fig. 8.7. The plate is loaded by linearly distributed compressive in-plane forces $q_x = q\left(1 + \eta\frac{y}{b}\right)$ along the simply supported edges $x = 0, a$, where $\eta > 0$ is some fixed parameter.

Solution

The deflection surface of the plate can be approximated, as follows:

$$w = \sin\frac{n\pi x}{a}\sum_{i=1}^{N} C_i y^i. \tag{a}$$

This approximate solution satisfies exactly the prescribed geometric boundary conditions, i.e.,

$$w = 0|_{x=0,a}, \quad w = 0|_{y=0}. \tag{b}$$

Retaining only one term ($i = 1$) in the series (a), we can find the following:

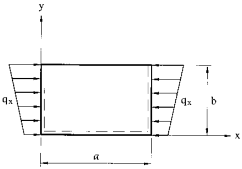

Fig. 8.7

$$\frac{\partial w}{\partial x} = C_1 y\left(\frac{n\pi}{a}\cos\frac{n\pi x}{a}\right), \frac{\partial^2 w}{\partial x^2} = -C_1 y\left(\frac{n\pi}{a}\right)^2 \sin\frac{n\pi x}{a},$$
$$\frac{\partial^2 w}{\partial x \partial y} = C_1\left(\frac{n\pi}{a}\cos\frac{n\pi x}{a}\right), \quad \frac{\partial^2 w}{\partial y^2} = 0.$$

For this type of loading, the solution of the plane stress problem is $N_x = -q_x$, $N_y = N_{xy} = 0$. Substituting the above into Eq. (8.45), and performing the operations of integration, we obtain

$$\Delta\Pi = C_1^2 \frac{ab}{4}\left\{D\left[\frac{b^2}{3}\left(\frac{n\pi}{a}\right)^4 + 2(1-\nu)\left(\frac{n\pi}{a}\right)^2\right] - q\left(\frac{n\pi}{a}\right)^2 b^2\left(\frac{1}{3}+\frac{\eta}{4}\right)\right\}.$$

The eigenvalues of the load q_x can be found from equation $\partial\Pi/\partial C_1 = 0$. We have

$$q_n = \frac{n^2\pi^2 D}{b^2}\left[\frac{b^2/a^2 + 6(1-\nu)/n^2\pi^2}{1+3\eta/4}\right].$$

For $n = 1$, the smallest eigenvalue is approximately equal to the critical value, i.e.,

$$q_{\mathrm{cr}} = \frac{b^2/a^2 + 6(1-\nu)/\pi^2}{1-3\eta/4} \cdot \frac{\pi^2 D}{b^2}. \tag{8.46}$$

Example 8.5

Determine the critical value of uniformly distributed in-plane shear forces q_{xy} for the simply supported rectangular plate shown in Fig. 8.8.

Solution

We assume that the deflection surface is adequately approximated as follows:

$$w = C_1 \sin\frac{\pi x}{a}\sin\frac{\pi y}{b} + C_2 \sin\frac{2\pi x}{a}\sin\frac{2\pi y}{b}, \tag{a}$$

where C_1 and C_2 are two unknown coefficients. It is obvious that w in the form of (a) satisfies exactly the prescribed geometrical boundary conditions ($w = 0$ on the boundary).

mutually perpendicular principal directions x and y; the shear modulus G; and Poisson's ratio ν_x. The second Poisson's ratio ν_y is related to ν_x by the expression (7.24). The constitutive equations, stress resultants–curvature equations, and the governing differential equation for the orthotropic plate in the framework of small-deflection plate bending theory have been derived in Sec. 7.2. Repeating the derivation of Eq. (3.92), we can represent the governing differential equation of the orthotropic plate buckling, as follows:

$$D_x \frac{\partial^4 w}{\partial x^4} + 2H \frac{\partial^4 w}{\partial x^2 \partial y^2} + D_y \frac{\partial^4 w}{\partial y^4} + N_x \frac{\partial^2 w}{\partial x^2} + N_y \frac{\partial^2 w}{\partial y^2} + 2N_{xy} \frac{\partial^2 w}{\partial x \partial y} = 0. \tag{8.48}$$

Let us analyze the stability of a rectangular, simply supported orthotropic plate subjected to in-plane compressive forces q_x, as shown in Fig. 8.1. The boundary conditions for simply supported edges of the orthotropic plate are

$$w = 0|_{\substack{x=0,a \\ y=0,b}}, \frac{\partial^2 w}{\partial x^2} + \nu_y \frac{\partial^2 w}{\partial y^2} = 0\bigg|_{x=0,a}, \frac{\partial^2 w}{\partial y^2} + \nu_x \frac{\partial^2 w}{\partial x^2} = 0\bigg|_{y=0,b}. \tag{a}$$

We take the deflection surface of the plate in the form

$$w = w_{11} \sin \frac{m\pi x}{a} \sin \frac{n\pi y}{b}. \tag{b}$$

The deflection surface in the form of (b) satisfies exactly the boundary conditions (a). Substituting (b) into Eq. (8.48) and letting $N_x = -q_x$, $N_y = N_{xy} = 0$, we obtain from the solution of this equation the following expression for the compressive forces q_x:

$$q_x = \frac{\pi^2 \sqrt{D_x D_y}}{b^2} \left[\sqrt{\frac{D_x}{D_y}} \left(\frac{mb}{a} \right)^2 + \frac{2H}{\sqrt{D_x D_y}} n^2 + \sqrt{\frac{D_y}{D_x}} \left(\frac{a}{mb} \right)^2 \right]. \tag{8.49}$$

It is evident that a minimum value of q_x is reached for $n = 1$. The critical value of the compressive force can be obtained by varying a number of half-waves m. For a plate that is lengthened along the x axis ($a \gg b$), we have the following:

$$q_{x,\mathrm{cr}} = \frac{2\pi^2 \sqrt{D_x D_y}}{b^2} \left(1 + \frac{H}{\sqrt{D_x D_y}} \right). \tag{8.50}$$

For a plate with a finite ratio of sides, it should be taken [4], that

$$m = 1 \text{ for } 0 < \frac{a}{b} < \sqrt[4]{4 \frac{D_x}{D_y}},$$

$$m = 2 \text{ for } \sqrt[4]{4 \frac{D_x}{D_y}} < \frac{a}{b} < \sqrt[4]{36 \frac{D_x}{D_y}},$$

$$m = 3 \text{ for } \sqrt[4]{36 \frac{D_x}{D_y}} < \frac{a}{b} < \sqrt[4]{144 \frac{D_x}{D_y}}, \text{ and so on.}$$

Making $D_x = D_y = H = D$, we obtain the expression (8.10) for $q_{x,\mathrm{cr}}$ in a rectangular, simply supported isotropic plate.

8.5.2 Stiffened plates

In the stability analysis of stiffened plates, two modes of buckling are usually considered. One possible mode is the local buckling of the plate between the stiffeners, provided that the plate is reinforced with strong stiffeners. In the second case, an overall buckling of the plate–stiffener combination occurs. The latter is called primary buckling in the pertinent literature.

A more economical design can be obtained if we permit simultaneous local and primary buckling at about the same stress level. Consequently, in the elastic stability analysis of stiffened plates, the structural interaction of plate and stiffeners should be taken into account.

Two approaches to the stability analysis of stiffened plates are possible. If a plate is reinforced with many equally spaced parallel stiffeners of the same size (or with a grid-stiffening arrangement), such an assembly can effectively be approximated by the orthotropic (structurally orthotropic) plate theory. This approach makes it possible to consider Eq. (8.48) for the buckling analysis of structurally orthotropic plates, and the rigidities on the left-hand side of this equation are determined according to the procedure introduced in Sec. 7.2.3. Evidently, this approach is applicable only in the case when the stiffeners are located close to one another: the value $1/n$ (n is the number of stiffeners or ribs taken over all the width of the plate) should be small compared with unity.

Another approach involves the buckling analysis of a plate which is reinforced with few stiffeners. For such a type of stiffened plates, the convenient orthotropic plate idealization cannot be used to obtain reliable values for the critical loads. Since the stiffeners are rigidly fastened to the plate, we should treat the plate and stiffeners as a structural unit; consequently, at mutual points, the stiffener deflects and twists in the same way as the plate. Since the numerical procedure of the first approach is quite similar to the one discussed in Sec. 8.5.1 and involves no new ideas and principles, the second approach will be introduced below only. The critical load may be determined by the equilibrium or energy methods. The following examples illustrate the application of both methods for the buckling analysis of the stiffened plate.

Example 8.6

This problem was analyzed by Timoshe [1]. Determine the critical load for a simply supported rectangular plate which is reinforced by a single longitudinal rib located along its centerline, as shown in Fig. 8.9. The plate is subjected to the in-plane compressive forces q_x uniformly distributed along the edges $x = 0, a$.

Solution

In our buckling analysis, we take into account only the bending stiffness of the rib in the plane perpendicular to the middle plane of the plate. We apply the differential equation (8.6) to one of the halves of the plate. Its integral is represented in the form

$$w(x, y) = F(y) \sin \frac{m\pi x}{a}. \tag{8.51}$$

the compressive forces q_x, then the equation for the elastic curve of the rib may be represented in the form

$$\left(EI_i\frac{\partial^4 w}{\partial x^4}+q_x\frac{\partial^2 w}{\partial x^2}+2D\frac{\partial^3 w}{\partial y^3}\right)_{y=0}=0,$$

or replacing $q_x = N_x = \sigma_x A_i$ for the rib, we obtain

$$\left(EI_i\frac{\partial^4 w}{\partial x^4}+\sigma_x A_i\frac{\partial^2 w}{\partial x^2}+2D\frac{\partial^3 w}{\partial y^3}\right)_{y=0}=0, \tag{8.58}$$

where I_i and A_i are the second moment of inertia and area of the rib cross section, respectively.

Let us introduce the following parameters:

$$\xi=\frac{a}{b},\quad \gamma=\frac{EI_i}{Db},\quad \delta=\frac{A_i}{bh}. \tag{8.59}$$

Introducing Eq. (8.53) into the conditions (8.55), (8.56), and (8.58), we obtain a system of linear algebraic homogeneous equations for $C_1,\ldots,C_4$. Equating the determinant of this system to zero, yields the following equation:

$$\left(\frac{1}{b\alpha}\tanh\frac{b\alpha}{2}-\frac{1}{b\beta}\tan\frac{b\beta}{2}\right)\left(\frac{\gamma m^2}{\alpha^2}-K\delta\right)\frac{m^2\pi^2}{\alpha^2}-4\frac{m}{\alpha}\sqrt{K}=0, \tag{8.60}$$

where

$$K=\frac{\sigma_{x,\mathrm{cr}}}{\sigma_{x,\mathrm{E}}} \tag{8.61}$$

and

$$\sigma_{x,\mathrm{cr}}=\frac{q_{x,\mathrm{cr}}}{h},\quad \sigma_{x,\mathrm{E}}=4\frac{\pi^2 D}{b^2 h} \tag{8.62}$$

where $\sigma_{x,E}$ is the critical stress for a rectangular, simply supported, unstiffened plate with the dimensions of Fig. 8.9 (see Eq. (8.11)). Equation (8.60) may be solved by the method of trial and errors. For $m = 1$ and $\xi > 2$, its solution, using the parameters introduced in Eqs (8.59), gives the following expression for $\sigma_{x,\mathrm{cr}}$:

$$\sigma_{x,\mathrm{cr}}=\frac{\pi^2 D}{b^2 h}\frac{\left(1+\xi^2\right)^2+2\gamma}{\xi^2(1+2\delta)}. \tag{8.63}$$

Now we analyze the stability problems for stiffened plates by the energy method.

Example 8.7

Determine the critical value of the in-plane compressive forces q_x acting on the plate reinforced by two equally spaced stiffeners, as shown in Fig. 8.10. The plate is simply supported on all edges. Let A_i and B_i ($B_i = EI_i$) be the area of the cross section and the bending stiffness of a stiffener, and c_i be spacing of the stiffeners.

$$q_{x,\mathrm{cr}} = \frac{\pi^4 D}{b^2} \frac{\left(1+\xi^2\right)+3\gamma}{\xi^2(1-3\delta)}, \tag{8.68}$$

where ξ, δ, and γ are given by formulas (8.59). The solution (8.68) is done in the first approximation, i.e., for $m = n = 1$. If a rectangular, simply supported plate is reinforced by i equally spaced stiffeners then the critical value of the compressive forces is the following:

$$q_{x,\mathrm{cr}} = \frac{\pi^2 D}{b^2} \frac{\left(1+\xi^2\right)^2 + 2\sum_i \gamma_i \sin^2(\pi c_i/b)}{\xi^2\left[1 + 2\sum_i \delta_i \sin^2(\pi c_i/b)\right]}. \tag{8.69}$$

8.6 POSTBUCKLING BEHAVIOR OF PLATES

8.6.1 Large deflections of plates in compression

Using the linearized buckling analysis introduced in Sec. 8.2, we have considered only the initial elastic buckling of flat plates and the critical forces and stresses have been found for some typical loadings and boundary conditions. The critical force is the force at which bifurcation of equilibrium states occurs and is of fundamental significance to the designer. So, the critical loads found in the previous sections represent merely the loads at which buckling begins. It should be noted that the postbuckling behavior of plates is markedly different from that of thin rods. While a small increase in the critical load for rods will produce a complete collapse, the load-carrying capacity of the plate is not exhausted and elastic plate can carry stresses higher than σ_{cr}. It can be explained, first of all, by the effect of large deflections in the postbuckling stage and, then, by the fact that the longitudinal edges of the plate are usually constrained to remain straight. Thus, the postbuckling mechanism of elastic plates is characterized not only by bending but also by the direct (or in-plane) stresses. It is important that the latter become comparable in magnitude with the former stresses.

The use of an additional strength due to the postbuckling effects is of great practical importance in the design of ship and aerospace structures. By considering the postbuckling behavior of plates, considerable weight savings can be achieved. In these structures, the edges of the plates are usually supported by stringers in such a way that they remain straight during buckling. After buckling, the central part of the plate bulges out, and an increasingly larger portion of the load is carried by the material close to the supported edges (stringers) of the plate.

The nonlinear, large-deflection plate bending theory, discussed in Sec. 7.4, can be used for the analysis of the postbuckling behavior of plates. Because of a nonlinearity of the governing differential equations of this analysis, the resulting mathematical difficulties are considerable and exact solutions can very seldom be obtained. The most generally used techniques for the treatment of postbuckling of plates are based on numerical methods [11,12].

For some simple cases an analytical solution can be obtained under some assumptions regarding the plate behavior, boundary conditions, etc. Consider a rectangular, simply supported plate, as shown in Fig. 8.1. The plate is subjected to

We consider below a rectangular plate that is pin-connected along its edges with rigid stiffeners. The plate is subjected to compressive forces in one direction, as shown in Fig. 8.11a.

Prior to buckling of the plate, the compressive stresses are uniformly distributed over its width, b, but after buckling the distribution of stresses along the loaded edges becomes progressively nonlinear: they increase more intensively in the vicinity of the plate edges and the stresses differ little from their critical values in the central part of the plate. A typical compressive stress distribution along the plate cross section is shown in Fig. 8.11b. The actual distribution of the compressive stresses depends on the boundary conditions and on the length-to-width ratio, a/b, provided that this ratio is less than 3.

When failure of the plate is impending, almost the total compressive load is carried by two strips, located along the unloaded edges.

Following the simplified approach proposed by von Karman *et al.* [13], we determine the ultimate load carried by the compressed plate. This approach is based on the following assumptions:

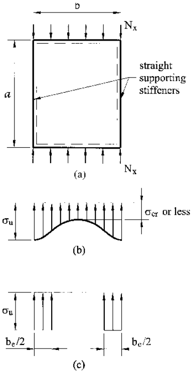

Fig. 8.11

(a) The initial (unloaded) plate is perfectly flat.
(b) The ultimate buckling load is carried exclusively by two strips of equal width, b_e, located along the unloaded edges.
(c) The maximum stress in the edge fiber of the plate, located in the middle surface, σ_u, is uniformly distributed over the two plate strips, b_e, as shown in Fig. 8.11c.
(d) The supporting stiffeners remain straight during the buckling and, jointly with the effective width portion of the plate, b_e, they act as columns.

Since the normal compressive stress is not uniform along the plate cross section, let us introduce the mean compressive stress, σ_m. From the above assumptions, it follows that the effective width, b_e, is

$$b_e = \frac{1}{\sigma_u}\int_0^b \sigma_m \mathrm{d}y. \tag{8.81}$$

Now we can determine the effective width of the bunched plate by using the reference value of the critical stress, σ_{cr}, in the following form:

$$\sigma_{cr} = \frac{N_{1cr}}{h} = K\frac{D}{h}\left(\frac{\pi}{b}\right)^2. \tag{8.82}$$

Due to the assumption (b), an expression similar to Eq. (8.82) can be written for the equivalent plate of width b_e:

$$\sigma_u = K\frac{D}{h}\left(\frac{\pi}{b_e}\right)^2. \tag{8.83}$$

Comparing Eqs (8.82) and (8.83) yields the following:

$$b_e = b\sqrt{\frac{\sigma_{cr}}{\sigma_u}}. \tag{8.84}$$

A more accurate postbuckling analysis estimates b_e as follows [16]:

$$b_e = b\cdot\sqrt[3]{\frac{\sigma_{cr}}{\sigma_u}}. \tag{8.85a}$$

Koiter [17] received the expressions for the effective width of flat plate in the form

$$b_e = b\left[1.2\left(\frac{\sigma_{cr}}{\sigma_u}\right)^{0.4} - 0.65\left(\frac{\sigma_{cr}}{\sigma_u}\right)^{0.8} + 0.45\left(\frac{\sigma_{cr}}{\sigma_u}\right)^{1.2}\right]. \tag{8.85b}$$

The ultimate load carried by the compressed plate is

$$P_u = \sigma_u b_e h. \tag{8.86}$$

To obtain estimates for the maximum edge stresses, σ_u, two cases are considered:

1. If the supporting stiffeners are relatively strong, the yield criterion can be conveniently used, in connection with the effective width concept, to determine σ_u the plate is able to carry. In this case, σ_u is simply equal to the yield stress σ_y, provided that the stiffeners and the adjacent plate

Example 8.8

A rectangular simply supported isotropic sandwich plate of Fig. 7.8 is subjected to an in-plane edge compressive load of intensity q_x, as shown in Fig. 8.1. Determine the critical value of this load if $a = 20$ in., $b = 10$ in., $t = 0.02$ in., $c = 0.2$ in., $E_f = 10 \times 10^6$ psi, $G_c = 12{,}000$ psi, $\nu = 0.3$.

Solution

The simply supported boundary conditions in terms of the deflections are given by Eqs (3.14). For the problem under consideration, $N_x = -q_x$ and $p_f = -q_x \partial^2 w / \partial x^2$. Therefore, Eq. (8.90) simplifies to the following form:

$$D_s \nabla^2 \nabla^2 w + q_x \left(1 - \frac{D_s}{D_Q} \nabla^2\right) \frac{\partial^2 w}{\partial x^2} = 0. \tag{a}$$

Equation (a) is a constant-coefficient equation. A solution of the form

$$w = C_1 \sin \frac{m\pi x}{a} \sin \frac{n\pi y}{b}; \quad m, n = 1, 2, 3, \ldots, \tag{b}$$

where C_1 is a constant, is seen to satisfy the boundary conditions (3.14). Introduction of that expression for w into Eq. (a) and rearrangement gives

$$q_x = \frac{\pi^2 D_s}{b^2} \frac{\left[(mb/a) + (n^2 a/mb)\right]^2}{1 + \psi\left[(mb/a)^2 + n^2\right]}, \tag{c}$$

where m and n are positive integers and

$$\psi = \frac{\pi^2 D_s}{b^2 D_Q}. \tag{d}$$

Equation (c) may now be written in the following alternative form:

$$q_x = K_s \frac{\pi^2 D_s}{b^2}, \tag{e}$$

where the nondimensional buckling coefficient K_s for sandwich plates is defined as

$$K_s = \frac{[mb/a + n^2 a/mb]^2}{1 + \psi\left[n^2 + (mb/a)^2\right]}. \tag{f}$$

For given values of the plate aspect ratio a/b and the shear stiffness parameter ψ, the value of the wave–length parameters m and n may be chosen by trial to give the smallest value of q_x, i.e., $q_{x,\mathrm{cr}}$.

It is seen that for $G_c \to \infty$, $\psi = 0$ and the buckling parameter $K_s \to K$ given by Eq. (8.8) (for $n = 1$). Thus, for this particular case when the transverse shear deformation is neglected, Eq. (c) reduces to the corresponding expression (8.7b) derived for buckling of homogeneous plates.

Using the numerical data of the problem, let us compute the rigidities. We have

$$D_s = \frac{E_s t(c+t)^2}{2(1-\nu^2)} = 5318 \text{ lb-in}, \quad D_Q = G_c \frac{(c+t)^2}{c} = 2904 \text{ lb/in},$$

$$\psi = \frac{\pi^2 D_s}{b^2 D_Q} = 1.831.$$

Introduction of these data into Eq. (f) reveals that the smallest value of the coefficient K_s corresponds to $n = 1$ and $m = 3$. For this value Eq. (g) gives $q_{x,\text{cr}} = 973.2$ lb/in.

If the core were omitted and the two face sheets bonded together to form a thin homogeneous plate 0.04 in. thick, the corresponding critical load would be only 23.4 lb.

PROBLEMS

8.1 Figure 8.2 shows the variation of the buckling load parameter K as a function of aspect ratio a/b for $m = 1, 2, 3, 4$. Based on this figure, determine the condition at which a transition from m to $m+1$ half-sine waves across the span of the plate, compressed in the x direction by a uniform edge loads.

8.2 Calculate the critical value of the uniform compressive edge loads q_x applied over two simply supported edges of length b if two opposite edges of the length a are fixed. Use $a = 2$ m, $b = 1$ m, $h = 0.1$ m, $E = 210$ GPa, and $\nu = 0.3$.

8.3 Calculate the critical value of the uniformly applied compressive edge loads for a rectangular plate of sides a and b with two simply supported opposite edges and two other opposite edges free. Assume that the load is applied over the free edges. Take $a = 10$ m, $b = 5$ m, $h = 0.15$ m, $E = 220$ GPa, and $\nu = 0.3$.

8.4 Let a rectangular, simply supported plate of sides a and b be loaded by uniformly distributed compressive q_x and tensile q_y forces. The q_x forces are applied parallel to the side a and q_y forces act in the direction parallel to the side b. Find the nontrivial solution of Eq. (8.20) for this type of loading and calculate the critical value of the parameter λ if $q_y = \lambda q_x$ and $a = b$. Compare this result with the case when the above plate is compressed in two directions (see Fig. 8.5).

8.5 Consider a circular plate uniformly compressed by in-plane radial forces q_r. Compare the critical values of q_r for two types of plate supports: (a) simply supported edge and (b) fixed edge. Use the radius of the plate $a = 40$ in., $h = 2.5$ in., $E = 25{,}000$ ksi, and $\nu = 0.3$.

8.6 Consider a rectangular plate of sides $2a$ and $2b$. The origin of the Cartesian coordinate system is taken at the plate center. The plate rests at its center upon columns and is compressed by uniformly distributed forces q_x applied parallel to the side $2a$. Assuming that the column support can be approximated by a point support, determine the critical value of q_x. Use the Ritz method and the approximate expression for the deflection in the form

$$w = C\left[\cos\frac{\pi x}{2a} + \cos\frac{\pi y}{2b}\right].$$

8.7 Let a rectangular plate of sides a and b $(a > b)$ with fixed edges be subjected to compressive linearly varying loads $q_x = q_0(1 - \eta y/b)(\eta < 1)$. The load is applied to short plate edges. The origin of the Cartesian coordinate system is attached at the left upper corner of the plate. Determine the critical value of the applied compressive load by the Ritz method. Assume that $a = 3$ m, $b = 1.5$ m, $h = 0.15$ m, $\eta = 0.5$, $E = 200$ GPa, and $\nu = 0.28$, and the approximate expression for deflections is

$$w = C\left(x^2 - a^2\right)^2\left(y^2 - b^2\right)^2.$$

8.8 Derive Eq. (8.48).

8.9 Consider an unstiffened, simply supported rectangular plate of sides a and b and a plate of the same geometry and boundary conditions but reinforced by a single longitudinal rib located along its centerline, as shown in Fig. 8.9. Compare the critical values of the compressive forces q_x uniformly distributed along the edges $x = 0, a$ for the above two plates. Assume that $a = b = 2\,\mathrm{m}$, $h = 0.15\,\mathrm{m}$, $E = 220\,\mathrm{GPa}$, and $\nu = 0.3$, and the rib has a cross section in the form of a channel section C75 × 6. In the buckling analysis, take into account the buckling stiffness of the rib in the plane that is perpendicular to the plate middle plane.

8.10 A simply supported square plate is reinforced by three equally spaced stiffeners of rectangular cross section of depth h_1 and of width t. The plate is subjected to in-plane uniform compressive forces q_x that act parallel to the stiffeners. Determine the critical value of the applied forces. Assume that the stiffeners and plate are made of the same material and stiffeners are symmetrical about the plate middle plane. Use $a = 5\,\mathrm{m}$, $h = 0.2\,\mathrm{m}$, $h_1 = 0.4\,\mathrm{m}$, $t = 0.1\,\mathrm{m}$, $E = 210\,\mathrm{GPa}$, and $\nu = 0.3$.

8.11 A long, simply supported rectangular plate ($a/b = 3$), subjected to uniform compressive forces q_x acting parallel to the long side a was reinforced by stiffeners symmetrically placed about the plate middle surface. Three variants of locations of the stiffeners had been discussed:

(a) First, the equally spaced transverse stiffeners (i.e., located in the perpendicular direction with respect to q_x) were suggested to locate at a distance equal to b;
(b) Secondly, the equally spaced transverse stiffeners were suggested to locate at a distance $b/2$;
(c) Thirdly, only one longitudinal stiffener located along the plate centerline (i.e., in the direction of the applied load) was suggested to apply.

Assuming buckling of the reinforced plate as a whole, determine the critical values of the applied forces q_x for all the above cases. If the geometrical and mechanical properties of the plate and stiffeners are known, draw conclusions about the efficient arrangement of stiffeners for the problem under consideration from the point of view of the buckling analysis.

8.12 Estimate the ultimate edge load of a rectangular plate, stiffened along both longitudinal edges and uniformly compressed in the x direction. Assume that the plate is simply supported along its edges and that the stiffeners and adjacent plate strips simultaneously approach the compressive yield strength. Let $a = 900\,\mathrm{mm}$, $b = 450\,\mathrm{mm}$, $h = 1\,\mathrm{mm}$, $E = 73\,\mathrm{GPa}$, $\nu = 0.3$, and $\sigma_y = 415\,\mathrm{MPa}$.

REFERENCES

1. Timoshenko, S.P. and Gere, J.M., *Theory of Elastic Stability*, McGraw-Hill, New York, 1961.
2. Cox, H.L., *The Buckling of Plates and Shells*, The Macmillan Company, New York, 1963.
3. Bulson, P.S., *The Stability of Plates*, American Elsevier Publishing Company, New York, 1969.
4. Volmir, A.S., *Stability of Elastic Systems*, Gos. Izd-vo Fiz.-Mat. Lit-ry, Moscow, 1963 (in Russian).
5. Carson, W.G. and Newton, R.E., Plate buckling analysis using a fully compatible finite elements, *AIAAJ*, vol. 7, No. 3, pp. 527–529, (1969).
6. Kapur, K.K. and Hartz, B.J., Stability of plates using the finite element method, J *Engng Mech Div, Proc ASCE*, vol. 92, pp. 177–195, 1966.

for exact solutions by solving the differential equations, then looking for approximate solutions.

The derivation of the governing differential equation of motion of plates is, in most cases, a simple extension of the static case by adding effective forces to the plate that result from accelerations of the mass of the plate. These are the *inertia forces*. For the most part, we take advantage of D'Alambert's principle to add the inertia forces as reversed effective forces. Other time-dependent forces may also be considered. The most common of these are *damping forces*.

We consider various kinds of motion of plates. There is a *free vibration,* which occurs in the absence of applied loads but may be initiated by applying initial conditions to the plate. The free vibration deals with natural characteristics of the plates, and these natural vibrations occur at discrete frequencies, depending only on the geometry and material of the plates. Then, there is a *forced vibration*, which results from an application of time-dependent loads. Forced vibrations come in two kinds: a harmonic response, when a periodic force is applied to the plate; and a transient response, when the applied force is not a periodic force.

In deriving the governing differential equation of motion, we use the general assumptions of Kirchhoff's plate bending theory introduced in Sec. 1.3. To adapt the elastic static equations derived for thin plates in Chapter 2, to model undamped structural dynamics, we need to consider only the dependent variables (the deflections, strains, and stresses) as functions of time. Let the applied loads be some functions of time, and explicitly include inertia forces in the surface lateral loads according to D'Alambert's principle. In this case, the forcing function appearing on the right-hand side of the governing differential equation (2.24) for the bending of thin plates becomes

$$p(x, y, t) - \rho h \frac{\partial^2 w}{\partial t^2}(x, y, t), \tag{9.1}$$

where both p and w are functions of time, as well as space; ρ is the mass density of the material, and h is the plate thickness. In the forced vibrations $p(x, y, t)$ causes the dynamic response.

Thus, the differential equation of forced, undamped motion of plates has the form

$$D\nabla^2\nabla^2 w(x, y, t) = p(x, y, t) - \rho h \frac{\partial^2 w}{\partial t^2}(x, y, t). \tag{9.2}$$

9.2 FREE FLEXURAL VIBRATIONS OF RECTANGULAR PLATES

Consider a rectangular plate with arbitrary supports. Let us assume that certain transverse surface loads distributed on the surface cause the particles, located in the middle surface, to attain the deflections and velocities directed perpendicularly to the initial (undeformed) middle surface. At a certain time, which is assumed to be the initial, the plate is suddenly released from all external loads. The unloaded plate, which has initial deflection and velocity, begins to vibrate. The particles located in the middle surface move in the direction perpendicular to the plate and, as a result, the plate becomes curved. Such vibrations are called *free* or *natural transverse vibrations*. The plate will execute *free* or *natural lateral vibrations*.

As stated previously, natural vibrations are functions of the material properties and the plate geometry only, and are inherent properties of the elastic plate, independent of any load. Thus, for natural or free vibrations, $p(x, y, t)$ is set equal to zero, and Eq. (9.2) becomes

$$D\nabla^2\nabla^2 w(x, y, t) + \rho h \frac{\partial^2 w}{\partial t^2}(x, y, t) = 0. \tag{9.3}$$

Deflection w must satisfy the boundary conditions at the plate edge (these conditions practically do not differ from those in the case of static equilibrium) and the following initial conditions:

$$\text{when } t = 0: \quad w = w_0(x, y), \quad \frac{\partial w}{\partial t} = v_0(x, y), \tag{9.4}$$

where w_0 and v_0 are the initial deflection and initial velocity for point (x, y).

Equation (9.3) is the governing, fourth-order homogeneous partial differential equation of the undamped, free, linear vibrations of plates. A complete solution of the problem of a freely vibrating plate is reduced to determining the deflections at any point for any moment of time. However, the most important part of the problem of free flexural vibrations of plates is to determine the *natural frequencies* and the *mode shapes of the vibration* (deflection surfaces in two dimensions) associated with each natural frequency. For such a problem (like in buckling), Eq. (9.3) is an eigenvalue problem. The natural frequencies are the *eigenvalues* and associated shape functions are the *eigenfunctions*. Values of these parameters are necessary for establishing the dynamic stresses caused by a variable load. A solution of Eq. (9.3) can be obtained by applying the classical analytical and approximate methods discussed in Chapters 3, 4, and 6 for static plate bending problems.

Let us describe a general *analytical method* (the Fourier method) for determining the natural frequencies of a freely vibrating plate. To solve Eq. (9.3) and obtain $w(x, y, t)$ in general, one can assume the following solution:

$$w(x, y, t) = (A\cos\omega t + B\sin\omega t)W(x, y), \tag{9.5}$$

which is a separable solution of the *shape function* $W(x, y)$ describing the modes of the vibration and some harmonic function of a time; ω is the natural frequency of the plate vibration which is related to vibration period T by the relationship $\omega = 2\pi/T$.

Introducing Eq. (9.5) into Eq. (9.3), we have

$$D\nabla^2\nabla^2 W(x, y) - \omega^2\rho h W = 0. \tag{9.6}$$

Let us represent a solution of this equation in the form of a Fourier series. Requiring the function W to satisfy the boundary conditions and to be the solution of Eq. (9.6), we obtain a system of homogeneous equations for the unknown constants. This system has solutions that differ from zero only in the case when its determinant $\Delta(\omega)$ is equal to zero; therefore we obtain the *frequency* or *characteristic equation,* which is

$$\Delta(\omega) = 0. \tag{9.7}$$

This equation will have an infinite number of solutions which constitute the frequency spectrum for a given plate. In general, the frequencies will depend on two parameters: m and n ($m = 1, 2, \ldots;\ n = 1, 2, \ldots$). The lowest frequency is called the *frequency of the fundamental mode* or the *fundamental natural frequency* and all other frequencies are called the *frequencies* of *higher harmonics*, or *overtones*. For each frequency ω_{mn}, there is a corresponding shape function $W_{mn}(x, y)$ that, on the basis of the homogeneous equations, is determined by a constant multiplier (which can be assumed as being equal to unity). For example, in the case of a rectangular, simply supported plate, the shape function may be taken as

$$W(x, y) = \sum_{m=1}^{\infty} \sum_{n=1}^{\infty} C_{mn} \sin \frac{m\pi x}{a} \sin \frac{n\pi y}{b}, \tag{9.8}$$

where a and b are the plate dimensions and C_{mn} is the vibration amplitude for each value of m and n. Substitution of Eq. (9.8) into Eq. (9.6) results in the homogeneous algebraic equation

$$\frac{m^4\pi^4}{a^4} + 2\frac{m^2\pi^2}{a^2}\frac{n^2\pi^2}{b^2} + \frac{n^4\pi^4}{b^4} - \frac{\omega^2 \rho h}{D} = 0. \tag{9.9}$$

Solving this equation for ω gives the natural frequencies

$$\omega_{mn} = \pi^2 \left(\frac{m^2}{a^2} + \frac{n^2}{b^2} \right) \sqrt{\frac{D}{\rho h}}. \tag{9.10}$$

The *fundamental natural frequency* can be obtained by letting $m = 1,\ n = 1$. Note that, again (as in the buckling analysis), the amplitude C_{mn} cannot be determined from the linear eigenvalue problem.

For a square plate of dimension a, Eq. (9.10) becomes

$$\omega_{mn} = \frac{\pi^2}{a^2} \sqrt{\frac{D}{\rho h}} (m^2 + n^2), \tag{9.11}$$

and the fundamental natural frequency is

$$\omega_{11} = \frac{2\pi^2}{a^2} \sqrt{\frac{D}{\rho h}}. \tag{9.12}$$

The fundamental mode of the flexural vibration is a single sine wave in the x and y directions. Figure 9.1a shows a plate view executing the vibrations of the fundamental tone with the natural frequency ω_{11}. The maximum deflection is at the plate center. The deflected surfaces that correspond to the natural frequencies ω_{21} and ω_{12} are depicted in Fig. 9.1b and c; in each case there are the two maximum deflections and one of the axes of symmetry is a nodal line.

9.3 APPROXIMATE METHODS IN VIBRATION ANALYSIS

9.3.1 Variational methods

An exact solution of the governing differential equation (9.3) in closed form is possible only for a limited number of cases regarding a plate's geometry and its boundary conditions. As mentioned previously, the natural fundamental frequencies are of the greatest importance in practice. Therefore, one has to determine these frequencies by the approximate methods discussed in Chapter 6.

the frequency (or the characteristic) equation (9.7), whose solutions, as mentioned previously, constitute the frequency spectrum for a given plate.

Example 9.1

Determine an approximate value of the natural frequencies for the clamped rectangular plate with dimensions $2a$ and $2b$, as shown in Fig. 9.2.

Solution

Assume that $W(x, y)$ is given by the following expression (the first approximation):

$$W(x, y) = C(x^2 - a^2)^2 (y^2 - b^2)^2. \tag{a}$$

This function satisfies the boundary conditions on the plate edges, i.e.,

$$W = \frac{\partial W}{\partial x} = 0\bigg|_{x=\pm a}, \; W = \frac{\partial W}{\partial y} = 0\bigg|_{y=\pm b}.$$

Substituting the expression (a) into Eq. (9.18) and evaluating the integrals, we obtain the fundamental natural frequencies in the form

$$\omega_{11} = 4\sqrt{2\left[\frac{1}{a^4} + \frac{1}{b^4} + \frac{2^8}{3^2 7^2}\frac{1}{a^2 b^2}\right]}\sqrt{\frac{D}{\rho h}}.$$

For a square plate ($a = b$), the frequency becomes

$$\omega_{11} = \frac{9.08}{a^2}\sqrt{\frac{D}{\rho h}}.$$

This result agrees (within 1.04%) with the value obtained from more accurate computation [1,2].

Approximate values of natural frequencies in rectangular plates with various combinations of boundary conditions, obtained by the Ritz method, are given in Ref. [2,3].

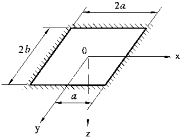

Fig. 9.2

9.3.2 The Galerkin method

The Galerkin method, introduced in Sec. 6.5, also may be used for determining the natural frequencies in vibrating plates. Assume again that a shape function for the plate is approximated by a series (9.20), which satisfies, term by term, all boundary conditions. Then, following the general procedure of the Galerkin method (see Sec. 6.5), the unknown coefficients C_i can be determined from the orthogonality conditions (6.37). For the vibration plate problems described by Eq. (9.6), the orthogonality conditions together with the expansion (9.20) result in the following equation:

$$\iint_A \left(D \sum_{i=1}^{n} C_i \nabla^2 \nabla^2 W_i - \rho h \omega^2 \sum_{i=1}^{n} C_i W_i \right) W_k \mathrm{d}x \mathrm{d}y = 0; \quad k = 1, 2, \ldots, n. \tag{9.22}$$

The numerical implementation of the above condition leads to the Galerkin system of linear algebraic homogeneous equations of the form

$$\begin{aligned} &a_{11} C_1 + a_{12} C_2 + \ldots\ldots\ldots\ldots\ldots = 0 \\ &\ldots\ldots\ldots\ldots\ldots\ldots\ldots\ldots\ldots\ldots\ldots \\ &a_{n1} C_1 + a_{n2} C_2 + \ldots\ldots\ldots\ldots\ldots = 0, \end{aligned} \tag{9.23}$$

where

$$a_{ik} = a_{ki} = \iint_A \left[D \nabla^2 \nabla^2 W_i - \rho h \omega^2 W_i \right] W_k \mathrm{d}x \mathrm{d}y. \tag{9.24}$$

This system of homogeneous equations has a nontrivial solution if its determinant made up of the coefficients a_{ik} is equal to zero. The latter results in the nth order characteristic equation (9.7) for determining the natural frequencies.

Let us represent the shape function $W(x, y)$ for a rectangular plate with dimensions a and b in the form

$$W(x, y) = \sum_i \sum_k C_{ik} W_{ik}(x, y), \tag{9.25}$$

where C_{ik} are unknown coefficients representing the amplitudes of the free vibration modes and $W_{ik}(x, y)$ is the product of the pertinent eigenfunctions of lateral beam vibrations,

$$W_{ik}(x, y) = F_i(x) F_k(y), \tag{9.26}$$

which satisfy the prescribed boundary conditions on the edges $x = 0$, $x = a$, and $y = 0$, $y = b$. In Eq. (9.26), $F_i(x)$ and $F_k(y)$ represent the ith and kth modes of freely vibrating beams with spans a and b, respectively.

Example 9.2

Determine the natural frequencies of the rectangular, simply supported plate of sides a and b with a uniformly distributed mass m and with four concentrated masses M, as shown in Fig. 9.3.

Part II

Thin Shells

10

Introduction to the General Shell Theory

10.1 SHELLS IN ENGINEERING STRUCTURES

Thin shells as structural elements occupy a leadership position in engineering and, in particular, in civil, mechanical, architectural, aeronautical, and marine engineering (Fig. 10.1). Examples of shell structures in civil and architectural engineering are large-span roofs, liquid-retaining structures and water tanks, containment shells of nuclear power plants, and concrete arch domes. In mechanical engineering, shell forms are used in piping systems, turbine disks, and pressure vessels technology. Aircrafts, missiles, rockets, ships, and submarines are examples of the use of shells in aeronautical and marine engineering. Another application of shell engineering is in the field of biomechanics: shells are found in various biological forms, such as the eye and the skull, and plant and animal shapes. This is only a small list of shell forms in engineering and nature.

The wide application of shell structures in engineering is conditioned by their following advantages:

1. *Efficiency of load-carrying behavior*.
2. *High degree of reserved strength and structural integrity*.
3. *High strength : weight ratio*. This criterion is commonly used to estimate a structural component efficiency: the larger this ratio, the more optimal is a structure. According to this criterion, shell structures are much superior to other structural systems having the same span and overall dimensions.
4. *Very high stiffness*.
5. *Containment of space*.

In addition to these mechanical advantages, shell structures enjoy the unique position of having extremely high aesthetic value in various architectural designs.

Contemporary engineers using scientifically justified methods of design tend to develop a structure that combines maximum strength, functional perfection, and economy during its lifetime. In addition, it is important that the best engineering solution ensues, other things being equal, at the expense of the selection of structural form and by not increasing the strength properties of the structure, e.g., by increasing its cross section. Note that the latter approach is easier. Shell structures support applied external forces efficiently by virtue of their geometrical form, i.e., spatial curvatures; as a result, shells are much stronger and stiffer than other structural forms.

10.2 GENERAL DEFINITIONS AND FUNDAMENTALS OF SHELLS

We now formulate some definitions and principles in shell theory. The term *shell* is applied to bodies bounded by two curved surfaces, where the distance between the surfaces is small in comparison with other body dimensions (Fig. 10.2).

The locus of points that lie at equal distances from these two curved surfaces defines the *middle surface* of the shell. The length of the segment, which is perpendicular to the curved surfaces, is called the *thickness* of the shell and is denoted by h. The geometry of a shell is entirely defined by specifying the form of the middle surface and thickness of the shell at each point. In this book we consider mainly shells of a constant thickness.

Shells have all the characteristics of plates, along with an additional one – curvature. The curvature could be chosen as the primary classifier of a shell because a shell's behavior under an applied loading is primarily governed by curvature (see Sec. 10.4). Depending on the curvature of the surface, shells are divided into cylindrical (noncircular and circular), conical, spherical, ellipsoidal, paraboloidal, toroidal, and hyperbolic paraboloidal shells. Owing to the curvature of the surface, shells are more complicated than flat plates because their bending cannot, in general, be separated from their stretching. On the other hand, a plate may be considered as a special limiting case of a shell that has no curvature; consequently, shells are sometimes referred to as curved plates. This is the basis for the adoption of methods from the theory of plates, discussed in Part I, into the theory of shells.

There are two different classes of shells: thick shells and thin shells. A shell is called *thin* if the maximum value of the ratio h/R (where R is the radius of curvature of the middle surface) can be neglected in comparison with unity. For an engineering accuracy, a shell may be regarded as thin if [1] the following condition is satisfied:

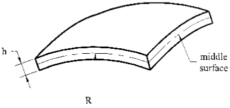

Fig. 10.2

11

Geometry of the Middle Surface

11.1 COORDINATE SYSTEM OF THE SURFACE

A surface Ω can be defined as a locus of points whose position vector, $\mathbf{r}$, directed from the origin 0 of the global coordinate system, $OXYZ$, is a function of two independent parameters α and β (see Fig. 11.1).

The parametric representation of the surface can be given, as follows:

$$\textit{in vector form} \text{ as } \mathbf{r} = \mathbf{r}(\alpha, \beta); \tag{11.1}$$

or

$$\textit{in scalar form} \text{ as } X = X(\alpha, \beta), \quad Y = Y(\alpha, \beta), \quad Z = Z(\alpha, \beta), \tag{11.2}$$

where $X(\alpha, \beta)$, $Y(\alpha, \beta)$, and $Z(\alpha, \beta)$ are some definite, continuous, and single-valued functions of two variable coordinates α and β. If we eliminate the parameters α and β from Eqs (11.2), then the equation of the surface becomes

$$F(X, Y, Z) = 0. \tag{11.3}$$

The parametric equation (11.1) may also be written in the form

$$\mathbf{r} = X(\alpha, \beta)\mathbf{i} + Y(\alpha, \beta)\mathbf{j} + Z(\alpha, \beta)\mathbf{k}, \tag{11.4}$$

in which $\mathbf{i}, \mathbf{j}$, and $\mathbf{k}$ are unit vectors along the X, Y, and Z axes, respectively.

We assume that there is a one-to-one correspondence between the pairs of numbers (α, β) belonging to Ω and points of the surface. Therefore these parameters, α and β, can be called *curvilinear coordinates of a given surface*. If one of the coordinates, e.g., α, is incremented $\alpha = \alpha_1$, $\alpha = \alpha_2, \ldots, \alpha = \alpha_n$, we define a series of parametric curves on the surface, along which only a parameter β varies. These curves are termed the *α-coordinate lines*. Similarly, if a parameter β takes on the values $\beta = \beta_1$, $\beta = \beta_2, \ldots, \beta = \beta_n$, we obtain the *$\beta$-coordinate lines*.

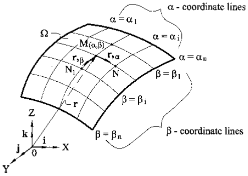

Fig. 11.1

If the α- and β-coordinate lines are mutually perpendicular at all points on a surface Ω (i.e., the angles between the tangents to these lines are equal to 90°), the *curvilinear coordinates* are said to be *orthogonal*. Orthogonal curvilinear coordinates are used extensively in this book.

The derivatives of the position vector **r** with respect to the curvilinear coordinates α and β are given by the following:

$$\frac{\partial \mathbf{r}}{\partial \alpha} = \mathbf{r},_{\alpha} \quad \text{and} \quad \frac{\partial \mathbf{r}}{\partial \beta} = \mathbf{r},_{\beta}, \tag{11.5}$$

where we have introduced the comma notation to denote partial derivatives with respect to α and β; $\mathbf{r},_{\alpha}$ and $\mathbf{r},_{\beta}$ are the tangent vectors at any point of the surface to the α- and β-coordinate lines, respectively (Fig. 11.1). Indeed, since α and β are scalar quantities, the directions of vectors $\mathbf{r},_{\alpha}$ and $\mathbf{r},_{\beta}$ coincide with directions of the vector $d\mathbf{r}$. This vector $d\mathbf{r}$ points to the chords joining points M and N for $\mathbf{r},_{\alpha}$, and M and N_1 for $\mathbf{r},_{\beta}$. In the limit, as $\Delta\alpha \to 0$ and $\Delta\beta \to 0$, these chords approach the tangents at a point M along the coordinate lines α and β, respectively. Since the latter are assumed to be orthogonal, then

$$\mathbf{r},_{\alpha} \cdot \mathbf{r},_{\beta} = 0. \tag{11.6}$$

11.2 PRINCIPAL DIRECTIONS AND LINES OF CURVATURE

Consider a small region of a smooth surface Ω near a typical point M. By "smooth" we mean that the surface is continuous, and contains no discontinuities of slope, i.e., creases or vertices. If we draw various curves along the surface Ω through point M, then the tangents to these curves are placed on one plane called the *tangent plane* to the surface at M (plane P in Fig. 11.2). A line that is perpendicular to the tangent plane and passes through point M is called the *normal* to the surface Ω at point M, and it is denoted by **n**. Since the surface is smooth (as defined above), the tangent plane and, hence, the normal are uniquely determined.

A *normal section* of the surface Ω at point M can be defined as the section by some plane containing a normal to the surface at that point. Such a section repre-

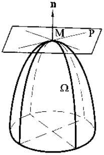

Fig. 11.2

sents a plane curve. Obviously, an infinite number of different normal sections may be drawn through point M of surface Ω (sections aa, bb, cc, etc., in Fig. 11.3)

Consider one of such normal sections as a plane curve, as shown in Fig. 11.4. The position of a point M on the curve is determined by a single arc length coordinate s, measured from a suitable datum point. Let M and M_1 be two neighboring points defining a short arc of length $\mathrm{d}s$. At M and M_1 the normals OM and OM_1 are drawn to the curve (there is only one normal at each point, since the curve is smooth) and they are inclined with respect to a suitable datum direction at angles ϕ and $\phi+\mathrm{d}\phi$, respectively. Assume that the two normals intersect at a point O (the *center of curvature of the arc*). The center of curvature is defined strictly in terms of a limiting process in which $\mathrm{d}s \to 0$. The length OM (i.e., the distance from the center of curvature to point M) is called the *radius of curvature,* ρ, of the given curve at point M.

It follows by simple trigonometry from the above description that

$$\rho = \frac{\mathrm{d}s}{\mathrm{d}\phi}. \tag{11.7a}$$

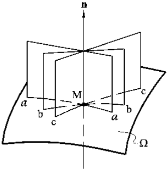

Fig. 11.3

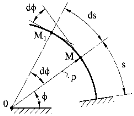

Fig. 11.4

In practice it is more convenient to use the *curvature* κ as a variable; this is defined as

$$\kappa = 1/\rho. \tag{11.7b}$$

It follows from the above that there are an infinite number of possible radii of curvature and curvatures at a point M of the surface because an infinite number of normal sections may be drawn through that point. However, there are two orthogonal normal sections at any point of a surface oriented such that one radius of curvature is the maximum of all possible, whereas the second radius of curvature is the minimum of all possible. These normal sections are called *principal normal sections* or *principal directions*. The curvatures of these sections and the corresponding radii are referred to as *principal curvatures* (denoted by κ_1 and κ_2) and *principal radii* (denoted by $R_1 = 1/\kappa_1$ and $R_2 = 1/\kappa_2$) at a point.

We also introduce *lines of the principal curvature* or simply *lines of curvature*. A *line of curvature* is a curve on the surface with the property that, at any point of the curve, it has a common tangent with the principal directions. From the above, it follows that the curvature takes on an extreme value at that point of the lines of curvature. Hence, at any point of a smooth surface there is at least one set of principal directions and two orthogonal lines of curvature.

The principal directions and lines of curvature may coincide or may not coincide, depending upon the surface geometry. Figure 11.5a shows the surface of revolution. It is described by rotating a plane curve (called a *meridian*) about the axis of rotation (the Z axis in Fig. 11.5).

The meridional plane L contains the axis of rotation. Each point of the meridian, when it rotates about the Z axis, describes a rotating *parallel circle* whose plane T is perpendicular to the Z axis. Normals to the surface of revolution, $\mathbf{n}$ and $\mathbf{n}_1$, drawn at neighboring points of the meridian, M and M_1, lie in plane L and they intersect in the same plane at point O_1. Thus, *meridians* at any point of the surface are one of the *lines of curvature* and, at the same time, one of the *principal normal sections*. The *radius of curvature of the meridian* equals MO_1 and it is the *first principal radius of curvature of the surface of revolution*, R_1. Normals to the surface, $\mathbf{n}$ and $\mathbf{n_2}$, drawn at neighboring points of the parallel circle, M and M_2, do not lie in plane T. They are located on some conical surface K and intersect at its vertex O_2 (Fig. 11.5b). The latter always lies on the Z axis, independently of the shape of a meridian curve. The *second principal normal section* of the surface of revolution is a curve, Γ, which lies in the plane that is tangent to the conical surface K at point M. It follows from the above that the second principal section

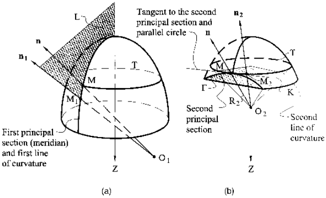
L
n
n_1
M
M_1
T
First principal section (meridian) and first line of curvature
Z
O_1
Tangent to the second principal section and parallel circle
n_2
n
T
M
M_2
K
Γ
R_2
O_2
Second principal section
Second line of curvature
Z
(a)
(b)

Fig. 11.5

and parallel circle have a common tangent at point M. Thus, the *parallel circles* of the surface of revolution represent the *second lines of curvature* but they are not the second principal normal sections or principal directions. The *generator* MO_2 of the conical surface K is the *second principal radius of curvature of the surface of revolution*, R_2. This radius is numerically equal to the distance along a normal to the meridian curve from a point of interest of this curve to the axis of rotation (the Z axis).

In Sec. 11.1 we made no special assumptions about the curvilinear coordinates of a shell middle surface. However, from now on we assume that the *coordinate lines* α and β *are the lines of curvature*. This system of the coordinate lines has particularly simple properties, so that the equations of the theory of shells acquire a relatively simple form in this system. To be able to use the corresponding formulas of the general theory of shells, knowledge of the lines of curvature is required, and the determination of these curves for a given surface is, in general, a fairly complicated problem. However, for many of types of shells used in practice, the geometry of the middle surface is of a simple nature (e.g., surfaces of revolution, cylindrical surfaces, etc.), so that the lines of curvature are already known.

11.3 THE FIRST AND SECOND QUADRATIC FORMS OF SURFACES

Let us study a surface Ω of an arbitrary geometry near typical point M, as shown in Fig. 11.6. Consider two points $M(\alpha, \beta)$ and $M_1(\alpha + \mathrm{d}\alpha, \beta + \mathrm{d}\beta)$ arbitrarily near to each other and both lying on the surface. Let their position vectors be $\mathbf{r}$ and $\mathbf{r} + \mathrm{d}\mathbf{r}$, respectively.

Determine the length of the arc $\mathrm{d}s$ joining the points M and M_1 on the surface. In the limit, $\mathrm{d}s$ approaches $|\mathrm{d}\mathbf{r}|$, where $|\mathrm{d}\mathbf{r}|$ is the modulus of the increment in the vector $\mathbf{r}$ going from point M to point M_1, as defined by

$$\mathrm{d}\mathbf{r} = \mathbf{r},_{\alpha}\,\mathrm{d}\alpha + \mathbf{r},_{\beta}\,\mathrm{d}\beta. \tag{11.8}$$

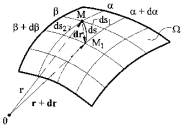

Fig. 11.6

The square of this differential of the arc length is

$$\mathrm{d}s^2 = |\mathrm{d}\mathbf{r}|^2 = \mathrm{d}\mathbf{r}\cdot\mathrm{d}\mathbf{r} = \mathbf{r},_\alpha\cdot\mathbf{r},_\alpha(\mathrm{d}\alpha)^2 + 2\mathbf{r},_\alpha\cdot\mathbf{r},_\beta\,\mathrm{d}\alpha\mathrm{d}\beta + \mathbf{r},_\beta\cdot\mathbf{r},_\beta(\mathrm{d}\beta)^2. \tag{11.9}$$

Denoting

$$a_{11} = (\mathbf{r},_\alpha\cdot\mathbf{r},_\alpha); \quad a_{12} = (\mathbf{r},_\alpha\cdot\mathbf{r},_\beta); \quad a_{22} = (\mathbf{r},_\beta\cdot\mathbf{r},_\beta), \tag{11.10}$$

we can rewrite Eq. (11.9), as follows:

$$\mathrm{d}s^2 = a_{11}(\mathrm{d}\alpha)^2 + 2a_{12}\mathrm{d}\alpha\mathrm{d}\beta + a_{22}(\mathrm{d}\beta)^2. \tag{11.11}$$

The expression on the right-hand side of this equation is called *the first quadratic form of the surface* defined by the vector $\mathbf{r}(\alpha, \beta)$ and a_{ik} $(i, k = 1, 2)$ are the *coefficients of that form*.

If the coordinate lines α and β form an orthogonal net, then $\mathbf{r},_\alpha\cdot\mathbf{r},_\beta = 0$ and, hence, $a_{12} = 0$. Denoting

$$A = (a_{11})^{1/2}; \quad B = (b_{11})^{1/2}, \tag{11.12}$$

we can rewrite the first quadratic form (Eq. (11.11)) for this particular case as

$$\mathrm{d}s^2 = A^2(\mathrm{d}\alpha)^2 + B^2(\mathrm{d}\beta)^2. \tag{11.13}$$

The quantities A and B are termed the *Lamé parameters*. To interpret the meaning of A and B geometrically, we rewrite Eq. (11.13), as follows:

$$\mathrm{d}s^2 = \mathrm{d}s_1^2 + \mathrm{d}s_2^2, \tag{11.14a}$$

where $\mathrm{d}s_1$ and $\mathrm{d}s_2$ are the lengths of linear arc elements corresponding to the increments in the curvilinear coordinates α and β, respectively (Fig.11.6), and

$$\mathrm{d}s_1 = A\mathrm{d}\alpha \quad \text{and} \quad \mathrm{d}s_2 = B\mathrm{d}\beta. \tag{11.14b}$$

We can see that the Lamé parameters are quantities which relate a change in arc length on the surface to the corresponding change in curvilinear coordinate or, in other words, they may be treated as some distortion coefficients transforming the change in curvilinear coordinates (dimensional or dimensionless) into the change in arc length of linear segments, $\mathrm{d}s_1$ and $\mathrm{d}s_2$.

The coefficients of the first quadratic form can also be computed in terms of the Cartesian coordinates by substituting Eq. (11.4) into the relations (11.10). We obtain

11.5 UNIT VECTORS

As mentioned previously, all vector quantities in the theory of shells, which are functions of points on the middle surface, will be given in terms of their projections on the directions of the tangents to some reference axes (the coordinate lines α and β, and normal to the surface at a point of interest). Since these reference axes change their directions when passing from one point of the surface to another one, it is necessary to investigate the differentiation of these vector quantities with respect to α and β.

A triad of the unit orthogonal vectors composed at a point on the middle surface of tangent vectors $\mathbf{e}_1$ and $\mathbf{e}_2$ to the coordinate lines α and β, and an inward normal vector $\mathbf{e}_3$ directed toward the center of curvature of the shell, represent a local vectorial basis to which the displacements, stress resultants, and stress couples are assigned. This basis defines a right-hand system, as shown in Fig. 11.7. Taking into account the expressions (11.5), (11.10), and (11.12), we can introduce the unit vectors as follows:

$$\mathbf{e}_1 = \frac{\mathbf{r},_\alpha}{|\mathbf{r},_\alpha|} = \frac{\mathbf{r},_\alpha}{A}, \quad \mathbf{e}_2 = \frac{\mathbf{r},_\beta}{|\mathbf{r},_\beta|} = \frac{\mathbf{r},_\beta}{B}, \quad \mathbf{e}_3 = \mathbf{e}_1 \times \mathbf{e}_2 = \frac{1}{AB}\left(\mathbf{r},_\alpha \times \mathbf{r},_\beta\right) \tag{11.24}$$

Any vector $\mathbf{T}$ may be represented in terms of the introduced orthogonal unit vectors, as follows:

$$\mathbf{T} = T_1\mathbf{e}_1 + T_2\mathbf{e}_2 + T_3\mathbf{e}_3,$$

where T_1, T_2, and T_3 are components of the vector in the coordinate basis (Eq. (11.24)). A partial derivative of the above vector $\mathbf{T}$ with respect to any coordinate may be represented as

$$\frac{\partial \mathbf{T}}{\partial \alpha} = \frac{\partial T_1}{\partial \alpha}\mathbf{e}_1 + \frac{\partial T_2}{\partial \alpha}\mathbf{e}_2 + \frac{\partial T_3}{\partial \alpha}\mathbf{e}_3 + T_1\frac{\partial \mathbf{e}_1}{\partial \alpha} + T_2\frac{\partial \mathbf{e}_2}{\partial \alpha} + T_3\frac{\partial \mathbf{e}_3}{\partial \alpha}. \tag{11.25}$$

The laws of differentiating the vectors, represented by Eq. (11.25), are reduced to the following form (a detailed derivation of these expressions is given in Appendix C.3):

$$\begin{aligned}
&\frac{\partial \mathbf{e}_1}{\partial \alpha} = -\frac{1}{B}\frac{\partial A}{\partial \beta}\mathbf{e}_2 + \frac{A}{R_1}\mathbf{e}_3, \quad \frac{\partial \mathbf{e}_1}{\partial \beta} = \frac{1}{A}\frac{\partial B}{\partial \alpha}\mathbf{e}_2,\\
&\frac{\partial \mathbf{e}_2}{\partial \alpha} = \frac{1}{B}\frac{\partial A}{\partial \beta}\mathbf{e}_1, \quad \frac{\partial \mathbf{e}_2}{\partial \beta} = -\frac{1}{A}\frac{\partial B}{\partial \alpha}\mathbf{e}_1 + \frac{B}{R_2}\mathbf{e}_3,\\
&\frac{\partial \mathbf{e}_3}{\partial \alpha} = -\frac{A}{R_1}\mathbf{e}_1, \quad \frac{\partial \mathbf{e}_3}{\partial \beta} = -\frac{B}{R_2}\mathbf{e}_2.
\end{aligned} \tag{11.26}$$

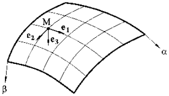

Fig. 11.7

11.6 EQUATIONS OF CODAZZI AND GAUSS. GAUSSIAN CURVATURE.

We present some important relations between the Lamé parameters A and B and the principal curvatures $k_1 = 1/R_1$ and $k_2 = 1/R_2$. These relations will be given below without proof (a detailed derivation is given in Appendix C.4), as follows:

$$\frac{\partial}{\partial\beta}\left(\frac{A}{R_1}\right) = \frac{1}{R_2}\frac{\partial A}{\partial\beta}; \quad \frac{\partial}{\partial\alpha}\left(\frac{B}{R_2}\right) = \frac{1}{R_1}\frac{\partial B}{\partial\alpha} \tag{11.27a}$$

and

$$\frac{\partial}{\partial\alpha}\left(\frac{1}{A}\frac{\partial B}{\partial\alpha}\right) + \frac{\partial}{\partial\beta}\left(\frac{1}{B}\frac{\partial A}{\partial\beta}\right) = -\frac{AB}{R_1R_2}. \tag{11.27b}$$

Equations (11.27a) are referred to as the *conditions of Codazzi*, whereas Eq. (11.27b) is known as the *condition of Gauss*.

Thus, the four functions A, B, R_1, and R_2 of the two parameters α and β are the Lamé parameters and principal radii of curvature of any surface only in the case when they are related to one another by the conditions of Codazzi and Gauss (11.27). From the above, it follows that the latter equations constitute necessary conditions for the existence of a surface.

Let us determine the product and semi-sum of the principal curvatures based on Eq. (11.19), as follows:

$$\Gamma = k_1k_2 = \frac{b_{11}b_{22} - b_{12}^2}{a_{11}a_{22} - a_{12}^2}, \tag{11.28}$$

$$K = \frac{k_1 + k_2}{2} = -\frac{2a_{12}b_{12} - a_{11}b_{22} - a_{22}b_{11}}{2\left(a_{11}a_{22} - a_{12}^2\right)}. \tag{11.29}$$

The first of these quantities is called the *Gaussian curvature* and the second is the *mean curvature* of a surface. The concept of Gaussian curvature is fundamental in the theory of surfaces. If the coordinate curves are lines of curvature, then the expression for Γ, Eq. (11.28), is reduced to the following equation (because $a_{12} = b_{12} = 0$) :

$$\Gamma = k_1k_2 = \frac{b_{11}b_{22}}{A^2B^2}, \tag{11.30}$$

where b_{11} and b_{22} are given by Eqs (11.17).

From the algebraic sign of the Gaussian curvature, the form of a surface in the neighborhood of a given point can be inferred. If $\Gamma > 0$, then, as follows from Eq. (11.28), the principal curvatures have the same sign. This means that both centers of principal curvature (O_1 and O_2 in Fig.11.8a) lie on the same side of the surface. The centers of curvature of all other normal sections will also lie on the segment $O_1\,O_2$. Point M of a surface whose centers of a curvature are located in such a way, called the *elliptic* point. On the contrary, for the centers of curvature O_1 and O_2 lie on opposite sides of the surface, as shown in Fig. 11.8b. The corresponding point of the surface is called *hyperbolic*. At last, if $\Gamma = 0$, then one of the two principal curvatures is zero, and the corresponding center of curvature (Fig.11.8c) is on an infinity. Point M of the surface in this case is called a *parabolic*.

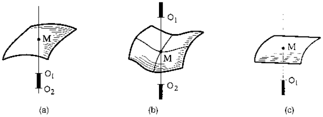

Fig. 11.8

For example, a sphere and an ellipsoid are examples of surfaces with positive Gaussian curvature. The so-called pseudo-sphere has a negative Γ that is a constant for all points. Cylindrical and conical surfaces have zero Gaussian curvatures.

The above sections contain only a brief survey of the geometry of surfaces. The interested reader is referred to Appendix C of the book and to Refs [1–3].

11.7 CLASSIFICATION OF SHELL SURFACES

We define here some of the surfaces that are commonly used for shell structures in engineering practice. There are several possible classifications of these surfaces. One such classification, associated with the Gaussian curvature, was discussed in Sec. 11.6. Following Ref. [4], we now discuss other categories of shell surfaces associated with their shape and geometric developability.

11.7.1 Classification based on geometric form

(a) Surfaces of revolution (Fig. 11.9)

As mentioned previously, surfaces of revolution are generated by rotating a plane curve, called the meridian, about an axis that is not necessarily intersecting the meridian. Circular cylinders, cones, spherical or elliptical domes, hyperboloids of revolution, and toroids (see Fig. 11.9) are some examples of surfaces of revolution. It can be seen that for the circular cylinder and cone (Fig. 11.9a and b), the meridian is a straight line, and hence, $k_1 = 0$, which gives $\Gamma = 0$. These are shells of zero Gaussian curvature. For ellipsoids and paraboloids of revolution and spheres (Fig. 11.9c, d, and e), both the principal curvatures are in the same direction and, thus, these surfaces have a positive Gaussian curvature ($\Gamma > 0$). They are synclastic surfaces. For the hyperboloid of revolution (Fig. 11.9f), the curvatures of the meridian and the second line of curvature are in opposite directions (i.e., the principal radii R_1 and R_2 lie on opposite sides of the surface for all points on the surface). For the toroid (Fig. 11.9g), the Gaussian curvature changes from positive to negative as we move along the surface.

(b) Surfaces of translation (Fig. 11.10)

A surface of translation is defined as the surface generated by keeping a plane curve parallel to its initial plane as we move it along another plane curve. The two planes containing the two curves are at right angles to each other. An elliptic paraboloid is

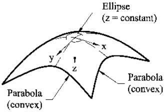

Fig. 11.10

shown in Fig. 11.10 as an example of such a type of surfaces. It is obtained by translation of a parabola on another parabola; both parabolas have their curvatures in the same direction. Therefore, this shell has a positive Gaussian curvature. For this surface sections $x =$ const and $y =$ const are parabolas, whereas a section $z =$ const represents an ellipse: hence its name, "elliptic paraboloid."

(c) Ruled surfaces (Fig. 11.11)

Ruled surfaces are obtained by the translation of straight lines over two end curves (Fig. 11.11). The straight lines are not necessarily at right angles to the planes containing the end curves. The frustum of a cone can thus be considered as a ruled surface, since it can be generated by translation of a straight line (the generator) over two curves at its ends. It is also, of course, a shell of revolution. The hyperboloid of revolution of one sheet, shown in Fig. 11.11a, represents another example of ruled surfaces. It can be generated also by the translation of a straight line over two circles at its ends. Figure 11.11b shows a surface generated by a translation of a straight line on a circular curve at one end and on a straight line at the other end. Such surfaces are referred to as conoids. Both surfaces shown in Fig. 11.11 have negative Gaussian curvatures.

11.7.2 Classification based on shell curvature

(a) Singly curved shells

These shells have a zero Gaussian curvature. Some shells of revolution (circular cylinders, cones), shells of translation, or ruled surfaces (circular or noncircular cylinders and cones) are examples of singly curved shells.

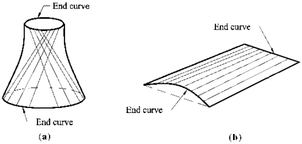

Fig. 11.11

(b) Doubly curved shells of positive Gaussian curvature

Some shells of revolution (circular domes, ellipsoids and paraboloids of revolution) and shells of translation and ruled surfaces (elliptic paraboloids, paraboloids of revolution) can be assigned to this category of surfaces.

(c) Doubly curved shells of negative Gaussian curvature

This category of surfaces consists of some shells of revolution (hyperboloids of revolution of one sheet) and shells of translation or ruled surfaces (paraboloids, conoids, hyperboloids of revolution of one sheet).

It is seen from this classification that the same type of shell may appear in more than one category.

11.7.3 Classification based on geometrical developability

(a) Developable surfaces

Developable surfaces are defined as surfaces that can be "developed" into a plane form without cutting and/or stretching their middle surface. All singly curved surfaces are examples of developable surfaces.

(b) Non-developable surfaces

A non-developable surface is a surface that has to be cut and/or stretched in order to be developed into a planar form. Surfaces with double curvature are usually non-developable.

The classification of shell surfaces into developable and non-developable has a certain mechanical meaning. From a physical point of view, shells with non-developable surfaces require more external energy to be deformed than do developable shells, i.e., to collapse into a plane form. Hence, one may conclude that non-developable shells are, in general, stronger and more stable than the corresponding developable shells having the same overall dimensions. On the other hand, developable shells have some advantages associated with their technological effectiveness.

11.8 SPECIALIZATION OF SHELL GEOMETRY

It is shown in the next chapter that the governing equations and relations of the general theory of thin shells are formulated in terms of the Lamé parameters A and B as well as of the principal curvatures $\kappa_1 = 1/R_1$ and $\kappa_2 = 1/R_2$. In the general case of shells having an arbitrary geometry of the middle surface, the coefficients of the first and second quadratic forms and the principal curvatures are some functions of the curvilinear coordinates. We determine the Lamé parameters for some shell geometries that are commonly encountered in engineering practice.

11.8.1 Shells of revolution

The shells of revolution were discussed in Secs 11.2 and 11.7. As for the curvilinear coordinate lines α and β, the meridians and parallels may be chosen: they are the lines of principal curvatures and form an orthogonal mesh on the shell middle surface. Figure 11.12a shows a surface of revolution where R_1 is the principal radius of the meridian, R_2 is the principal radius of the parallel circle (as shown in Sec.11.2, R_2

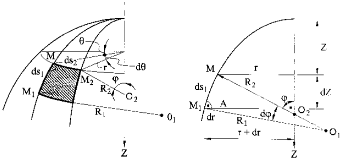

(a) (b)

Fig. 11.12

is the distance along a normal to the meridional curve drawn from a point of interest to the axis of revolution of the surface), and r is the radius of the parallel circle.

There are several possibilities for a choice of the curvilinear coordinates α and β.

(a) First, consider the *cylindrical coordinate system*, taking

$$\alpha = Z, \quad \beta = \theta, \tag{11.31}$$

where Z indicates the vertical position of a point M and θ denotes an angular position of the point along the parallel circle from some arbitrary origin. The latter angle may be referred to as the *circumferential angle*.

Consider a differential element isolated by two neighboring meridional sections and two parallel circles (the cross-hatched element in Fig. 11.12a). Let the arc lengths of sidesMM_1 and MM_2 be $\mathrm{d}s_1$ and $\mathrm{d}s_2$, respectively. From the triangle AMM_1 of Fig. 11.12b, we have

$$\cos\left(\frac{\pi}{2} - \varphi\right) = \frac{\mathrm{d}Z}{\mathrm{d}s_1}, \tag{11.32}$$

from which

$$\mathrm{d}s_1 = \frac{\mathrm{d}Z}{\sin\varphi} = \mathrm{d}Z\sqrt{1 + \cot^2\varphi}, \tag{11.33}$$

where φ is the angle formed by the extended normal to the surface at point M and the axis of rotation. This angle is referred to as the *meridional angle*.

For shells of revolution the radius of a parallel circle, r, is a function of Z, i.e., $r = r(Z)$. By inspection of Fig. 11.12b, we have the following:

$$\mathrm{d}s_1 = \sqrt{\mathrm{d}Z^2 + AM_1^2} = \sqrt{\mathrm{d}Z^2 + (\mathrm{d}r)^2} = \mathrm{d}Z\sqrt{1 + r_{,z}^2}. \tag{11.34}$$

On the other hand, as follows from Fig. 11.12a, we have

$$MM_2 = \mathrm{d}s_2 = r\mathrm{d}\theta. \tag{11.35}$$

Using the general expressions (11.14b), and taking into account that for the cylindrical coordinates given by the expression (11.31), $d\alpha = dZ$ and $d\beta = d\theta$, we can finally determine the Lamé parameters in the following form:

$$A = \sqrt{1 + \left(\frac{dr}{dZ}\right)^2}, \quad B = r. \tag{11.36}$$

(b) Next, consider the *spherical coordinate system*, taking

$$\alpha = \varphi, \quad \beta = \theta. \tag{11.37}$$

It can be easily shown that the spherical coordinates (Eqs (11.37)) also define uniquely a point M on the surface of revolution. By inspection of Fig. 11.12, the following obvious relations hold:

$$ds_1 = R_1 d\varphi = R_1 d\alpha \quad \text{and} \quad ds_2 = r d\theta = r d\beta. \tag{11.38}$$

Comparing the above with the expressions (11.14), we obtain the Lamé parameters in the form

$$A = R_1, \quad B = r, \tag{11.39}$$

or noting that $r = R_2 \sin\varphi$ (see Fig. 11.12b), we can rewrite the expressions (11.39) as follows:

$$A = R_1, \quad B = R_2 \sin\varphi. \tag{11.40}$$

The first two of the relations of the Codazzi–Gauss equations (Eqs (11.27a)) are identically satisfied in this case, whereas the third equation (Eq. (11.27b)) gives the following:

$$\frac{d(R_2 \sin\varphi)}{d\varphi} = R_1 \cos\varphi. \tag{11.41}$$

Determine *the principal curvatures and principal radii of curvatures for shells of revolution*. Let a shell of revolution be assigned in the global coordinate system by the following equations:

$$X = r(Z)\cos\theta, \quad Y = r(Z)\sin\theta, \quad Z = Z, \tag{11.42}$$

where r is the radius of the parallel circle at a section $Z = \text{const}$ and θ is the angle of rotation of the meridional plane. Substituting Eqs (11.42) into Eqs (11.15) and (C.12), we obtain, after some mathematics, the following:

$$\begin{aligned} &a_{11} = 1 + r_{,Z}^2, \quad a_{12} = 0, \quad a_{22} = r^2, \quad \omega = r\sqrt{1 + r_{,Z}^2}, \\ &b_{11} = -\frac{r_{,ZZ}}{\sqrt{1 + r_{,Z}^2}}, \quad b_{12} = 0, \quad b_{22} = \frac{r}{\sqrt{1 + r_{,Z}^2}} \end{aligned}. \tag{11.43}$$

Substituting the above into Eqs (11.22), yields the following expressions for the principal curvatures:

$$\kappa_1 = \frac{1}{R_1} = -\frac{r_{,ZZ}}{\left(1 + r_{,Z}^2\right)^{3/2}}, \quad \kappa_2 = \frac{1}{r\left(1 + r_{,Z}^2\right)^{1/2}}. \tag{11.44}$$

It can be seen from Eqs (11.44) that κ_2 is always positive, whereas κ_1 may be either positive or negative depending upon the sign of the value of $r,_{ZZ}$. If a convexity of the meridian curve is directed to the Z axis, as in Fig. 11.9f, then, $r,_{ZZ} > 0$, and κ_1 for such a shell is negative.

Hence, if the equation of the meridional curve, i.e., $r = r(Z)$, is known, one can determine the principal curvatures and principal radii of shells of revolution using Eqs (11.44).

We consider below some specific forms of shells of revolution that are commonly used in applications and present the principal curvatures and principal radii for them.

(a) Ellipsoid of revolution (Fig. 11.9c)

The equation of the meridian of an ellipsoid has the form

$$b^2r^2 + a^2Z^2 = a^2b^2, \tag{a}$$

where a and b are lengths of the major and minor semi-axes, respectively. So, Eq. (a) can be written as

$$\frac{r^2}{a^2} + \frac{Z^2}{b^2} = 1,$$

which gives us r as a function of Z, as follows:

$$r = \frac{a}{b}\sqrt{b^2 - Z^2}. \tag{b}$$

Upon determining $r,_Z$ and $r,_{ZZ}$, and substituting into Eqs (11.44), we can readily obtain the expressions for the principal radii of curvature, as follows:

$$R_1 = \frac{1}{\kappa_1} = a^2b^2\left(\frac{r^2}{a^4} + \frac{Z^2}{b^4}\right)^{3/2}, \quad R_2 = \frac{1}{\kappa_2} = \frac{1}{b^2}\left(b^4r^2 + Z^2a^4\right)^{1/2}. \tag{11.45}$$

We would prefer to have R_1 and R_2 as functions of φ (see Fig. 11.12a), and hence, we must eliminate Z and r from the above. To do this, we consider a triangle formed by the sides $\mathrm{d}s_1$ (along the meridian), $\mathrm{d}r$, and dZ (see Fig. 11.12b). We can write the following:

$$\tan\varphi = \frac{\mathrm{d}Z}{\mathrm{d}r}.$$

Using this equation and Eq. (b), we can express r and Z as functions of φ and the lengths of ellipse axes, a and b. We have the following:

$$r = \frac{a^2\sin\varphi}{\left(a^2\sin^2\varphi + b^2\cos^2\varphi\right)^{1/2}} \text{ and } Z = \pm\frac{b^2\cos\varphi}{\left(a^2\sin^2\varphi + b^2\cos^2\varphi\right)^{1/2}}. \tag{c}$$

Substituting for r and Z from Eqs (c) into the expressions for R_1 and R_2, Eqs (11.45), gives

$$R_1 = \frac{a^2b^2}{\left(a^2\sin^2\varphi + b^2\cos^2\varphi\right)^{3/2}}, \quad R_2 = \frac{a^2}{\left(a^2\sin^2\varphi + b^2\cos^2\varphi\right)^{1/2}}. \tag{11.46}$$

(b) Paraboloid of revolution (Fig. 11.9d)

The equation of the meridional curve is given by

$$r^2 - 2pZ = 0 \quad \text{or} \quad r^2 = \frac{a^2}{b}Z, \tag{d}$$

where p is a parameter of the parabola. Using the technique considered above for the ellipsoid of revolution, we present below the final expressions for the principal radii of curvature for the paraboloid, dropping the intermediate mathematics,

$$R_1 = \frac{a^2}{2b}\frac{1}{\left(\cos^2\varphi\right)^{3/2}}, \quad R_2 = \frac{a^2}{2b}\frac{1}{\cos\varphi}, \tag{11.47}$$

where b is the height of the paraboloid and a is one-half the length of the paraboloid base.

(c) Sphere (Fig. 11.9e)

Consider a spherical shell of radius a. It can be easily shown that the principal radius of the meridian is equal to the radius of the generating circle a. Indeed, the equation of the meridian is

$$Z^2 + r^2 = a^2.$$

With $r,_Z = -Z/r$ and $r,_{ZZ} = -(1/r)\left(1 + Z^2/r^2\right)$, we find from Eq. (11.45) that the principal radii of the sphere are

$$R_1 = \frac{\left[1 + (Z/r)^2\right]^{3/2}}{(1/r)\left(1 + Z^2/r^2\right)} = \sqrt{Z^2 + r^2} = a \text{ and } R_2 = r\left(1 + \frac{z^2}{r^2}\right)^{1/2} = \sqrt{r^2 + Z^2} = a.$$

Thus, for a spherical shell, both the principal radii of curvature are equal to the radius of the generating circle a.

(d) Hyperboloid of revolution (Fig. 11.9f)

The equation of the generating curve (hyperbola) is

$$\frac{r^2}{a^2} - \frac{Z^2}{b^2} = 1, \tag{e}$$

where a is one-half the length of the reference section of the hyperboloid and b is some characteristic dimension of the hyperboloid. The latter may be evaluated by substituting the base coordinates (s, S) and the top coordinates (t, T) into the equation of the hyperbola, i.e.,

$$b = \frac{aT}{\sqrt{t^2 - a^2}} = \frac{aS}{\sqrt{s^2 - a^2}}.$$

For the radii of curvature we have to use the same formulas as for the ellipsoid (i.e., Eqs (11.46)), replacing b^2 by $-b^2$. Thus, we obtain

$$R_1 = -\frac{a^2b^2}{\left(a^2\sin^2\varphi - b^2\cos^2\varphi\right)^{3/2}}, \quad R_2 = \frac{a^2}{\left(a^2\sin^2\varphi - b^2\cos^2\varphi\right)^{1/2}}. \tag{11.48}$$

The principal radii of curvature for convex shells of revolution formed by rotating curves of the second order about their axes of symmetry can also be computed from the following equations [5]:

$$R_1 = \frac{R_0}{\left(1 + \gamma \sin^2 \varphi\right)^{3/2}}, \quad R_2 = \frac{R_0}{\left(1 + \gamma \sin^2 \varphi\right)^{1/2}}, \tag{11.49}$$

where the parameter R_0 equals the value of the radii of curvature at $\varphi = 0$, i.e., at the vertex of the corresponding shell, and the parameter γ takes on the following values:

$\gamma = 0$ for a spherical shell;

$\gamma = -1$ for paraboloids;

$\gamma > -1$ for ellipsoids; and

$\gamma < -1$ for hyperboloids.

11.8.2 Cylindrical shells

A cylinder is generated by moving a straight line along a curve while maintaining it parallel to its original position. It follows from this definition that through every point of the cylinder one may pass a straight line that lies entirely on this surface. These lines are called the *generators*. All planes that are normal to the generators intersect the cylinder in identical curves, which are called *profiles*. The cylinder is named after the shape of the profile, i.e., a circular, elliptical, or parabolic cylinder. Of these shells, only the circular cylinder is a shell of revolution, whereas the others represent shells of translation (see Sec. 11.7.1(b)) since they can be generated by the translation of a straight line.

Let us consider a cylindrical shell of a general shape, as shown in Fig. 11.13.

We use the cylindrical coordinate system to describe the position of a reference point on a cylindrical shell middle surface. Thus, the curvilinear coordinates of the reference point may be taken as

$$\alpha = x, \quad \beta = \theta, \tag{11.50}$$

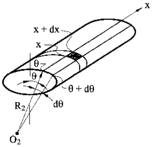

Fig. 11.13

where x is the distance measured from some reference profile to the point of interest and θ is the angle between the normal to the shell at a point and a reference normal at a chosen origin.

Consider an element of the shell, bounded by sections $x, x + \mathrm{d}x$ and $\theta, \theta + d\theta$ (Fig. 11.13). The first quadratic form of the surface will be here, as follows:

$$\mathrm{d}s^2 = \mathrm{d}x^2 + R_2^2 \mathrm{d}\theta^2, \tag{11.51}$$

where R_2 is the second principal radius of curvature, while the first principal radius is infinite, i.e., $R_1 = \infty$. Comparing the above with the relation (11.12), one can obtain the Lamé parameters for the cylindrical shell of a general shape, as follows:

$$A = 1, \quad B = R_2. \tag{11.52}$$

For a circular cylindrical shell, $R_2 = \mathrm{const} = R$, where R is the radius of the circular cylinder. So, the Lamé parameters for the circular cylindrical shell are

$$A = 1, \quad B = R = \mathrm{const}. \tag{11.53}$$

11.8.3 Conical shells

In a conical shell, the meridional angle φ is a constant and can no longer serve as a coordinate of the meridian. The location of a point on the middle surface will be defined by the radius vector $\mathbf{r}$ taken from the top of the cone (point O in Fig. 11.14) along its generator, and angle θ formed by a meridional plane passing through that point with some reference meridional plane. Let the length of the vector $\mathbf{r}$ be s and the slope of the generator to the cone base be α. The projections of $\mathbf{r}$ on the global coordinate axes, X, Y, and Z (see Fig. 11.14) are

$$X = s\cos\alpha\cos\theta, \quad Y = s\cos\alpha\sin\theta, \quad Z = s\sin\alpha. \tag{11.54}$$

The vector $\mathbf{r}$ can be resolved along the unit vectors $\mathbf{i}, \mathbf{j}$, and $\mathbf{k}$, as follows:

$$\mathbf{r} = s(\mathbf{i}\cos\alpha\cos\theta + \mathbf{j}\cos\alpha\sin\theta + \mathbf{k}\sin\alpha). \tag{11.55}$$

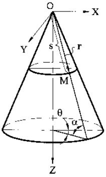

Fig. 11.14

The values s and θ will be considered as the curvilinear coordinates on the middle surface, as follows:

$$\alpha = s \quad \text{and} \quad \beta = \theta. \tag{11.56}$$

The coefficients of the first quadratic form are determined from Eqs (11.12) and (11.10), i.e.,

$$A^2 = \left(\frac{\partial \mathbf{r}}{\partial \alpha}\right)^2 \quad \text{and} \quad B^2 = \left(\frac{\partial \mathbf{r}}{\partial \beta}\right)^2.$$

Substituting for **r** from Eq. (11.55), then differentiating with respect to α and β and taking into account relations (11.56), we obtain the Lamé parameters for a conical shell in the form

$$A = 1 \quad \text{and} \quad B = s \cos \alpha. \tag{11.57}$$

11.8.4 Shallow shells

A shallow shell is defined as a shell having a relatively small raise as compared to its spans (Fig. 11.15).

A shell is said to be a shallow if at any point of its middle surface the following inequalities hold:

$$\left(\frac{\partial z}{\partial x}\right)^2 \ll 1, \quad \left(\frac{\partial z}{\partial y}\right)^2 \ll 1 \tag{11.58}$$

where $z = z(x, y)$ represents the equation of the shell middle surface. Referring to Fig. 11.15b, one sees the effect of this simplification. Consider a differential element of the middle surface bounded by the intersections with two planes parallel to the Oyz coordinate plane and separated by a distance dx, and two planes parallel to the Oxz coordinate plane separated by a distance dy. From Fig. 11.15b, it follows that

$$\mathrm{d}s_1 \cong \mathrm{d}x\left[1 + (z, x)^2\right]^{1/2} \tag{11.59a}$$

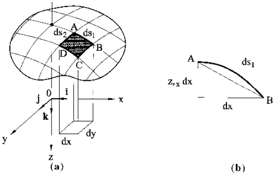

Fig. 11.15

Similarly, we can write

$$ds_2 \cong dy\left[1 + (z,y)^2\right]^{1/2}. \tag{11.59b}$$

These expressions, due to the geometric simplification (Eq. (11.58)), may be written simply as

$$ds_2 \approx dy \quad \text{and} \quad ds_1 \approx dx. \tag{11.60}$$

Practically, the above imply that the curvilinear coordinates α and β may be selected as the Cartesian coordinates x and y with the following Lamé parameters:

$$A = B = 1. \tag{11.61}$$

PROBLEMS

11.1 Verify Eqs (11.28) and (11.29).
11.2 Draw sketches of the following meridians and calculate the principal curvatures κ_1 and κ_2 in each case: (a) $Z = Ar^2$, and (b) $(r/a)^2 - (z/b)^2 = 1$.
11.3 Explain the difference between the first and second quadratic forms from the geometric point of view.
11.4 Roof shell structures often have a shape of surfaces of translation (see Sec. 11.7.1(b)). The equation of such a surface can be assigned as $Z = \varphi(X) + \psi(Y)$. Assuming that a location of a point on this surface is given by the Cartesian coordinates $\alpha = x$ and $\beta = y$, determine the coefficients of the first quadratic form for the nonshallow shell of translation.
11.5 Verify Eqs. (11.45) and (11.47).
11.6 Verify that the Gauss–Codazzi relations are satisfied for a shell of revolution with the parameter A given by equation $A = [1 + (r,_Z)^2]^{1/2}$.
11.7 Verify Eqs (11.48).
11.8 Calculate the Lamé parameters for a conical shell in terms of the coordinates Z and θ (see Fig. 11.15), i.e., for $\alpha = Z$ and $\beta = \theta$.
11.9 Prove that surfaces possessing the same Lamé parameters will have the same Gaussian curvature.

REFERENCES

1. Louis, A., *Differential Geometry*, Harper and Row, New York, 1967.
2. Stoker, J.J., *Differential Geometry*, Wiley-Interscience, New York, 1969.
3. Kreyszig, E., *Differential Geometry*, University of Toronto, Toronto, 1959.
4. Kelkar, V.S. and Sewell, R.T., *Analysis & Design of Shell Structures*, Prentice-Hall, Englewood Cliffs, New Jersey, 1987.
5. Novozhilov, V.V., *Thin Shell Theory*, P. Noordholf, Groningen, The Netherlands, 1964.

As was mentioned in Sec. 10.3, the above Kirchhoff's hypotheses together with small displacement and thinness of shell assumptions are called the Kirchhoff–Love assumptions. According to the Kirchhoff assumptions, deformations throughout the whole volume of the shell material are completely defined by deformations and changes in curvature of the middle surface. Thus, the adoption of these hypotheses reduces the three-dimensional (3D) shell problem to the two-dimensional (2D) problem of equilibrium and straining of the middle surface of a shell. So, the shell will be regarded as a 2D body, i.e., a collection of material points situated on the middle surface.

The general linear theory of thin shells includes the three sets of equations: kinematic (strain–displacement relations), constitutive, and equilibrium. These equations must be complemented with prescribed boundary conditions on the shell edges.

12.2 KINEMATICS OF SHELLS

12.2.1 Variation of the displacements across the shell thickness

Let the middle surface of the undeformed shell be associated with the curvilinear coordinates α and β, and the coordinate lines α and β coincide with the lines of curvature, as shown in Fig. 12.1. Apart from the global (fixed) Cartesian coordinate system adopted in Chapter 11, let us introduce the local (movable) Cartesian coordinate system $Oxyz$. The x and y axes coincide with the directions of tangents to the curvilinear coordinate lines α and β at a point O of the middle surface, and the z axis points along the normal to this surface at the same point. Notice that the previously introduced triad of unit vectors, $\mathbf{e}_1, \mathbf{e}_2$, and $\mathbf{e}_3$ (see Sec. 11.5) form the basis of this local coordinate system. The positive directions of the x, y, and z axes coincide with the positive directions of the unit vectors, respectively. In particular, the positive direction of the z axis is to the center of curvature of the shell (for elliptic and parabolic points of the middle surface), as shown in Fig. 12.1. Such a direction of the z axis is consistent with the previously adopted positive direction of that axis in the plate bending theory (see Sec. 2.2).

Consider a material point M on the middle surface, as shown in Fig. 12.2. As a result of a deformation, this point moves from M on the undeformed middle surface to a point M_1 on the deformed middle surface. We identify this displacement of point M by the vector $\mathbf{D}$. This vector will be a function of the coordinates α and β, i.e.,

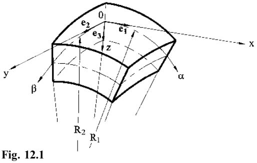

Fig. 12.1

Let us examine a variation of the strain components across the shell thickness. For this purpose, we pass within the shell an equidistant surface located at a distance z from the middle surface, where $-h/2 \le z \le h/2$. Locate a point on this surface by the same coordinates α and β that were used for the middle surface. According to Kirchhoff's assumptions, points lying on one normal to the middle surface remain on the same normal after deformation. Therefore, the above coordinates remain valid for the equidistant surface too. It can be proven (see Appendix D) that if the α- and β-coordinate lines coincide with the lines of curvature on the middle surface, then they are orthogonal, and may also serve as lines of curvature for the equidistant surface.

Figure 12.3 shows a section of the shell by a plane normal to the middle surface. Consider two pairs of neighboring points, M and N, lying along line $\alpha = \text{const.}$ on the middle surface, and their counterparts M^z and N^z on the equidistant surface, located at a distance z from the middle surface. In virtue of Kirchhoff's assumptions, adopted in the general shell theory, all these points will be located on the same normals after deformation and the distance between them in the normal direction (in the z direction) remains unchanged.

If the radius of curvature of arc MN on the middle surface is R_1, then the corresponding radius of curvature of arc M^zN^z on the equidistant surface (by inspection of Fig. 12.3) is

$$R_1^z = R_1 - z. \tag{12.6}$$

It follows from the above that R_1^z is the first principal radius of curvature of the equidistant surface. Moreover, if the length of arc MN is $\mathrm{d}s_1 = A\mathrm{d}\alpha$, then the length of the corresponding arc M^zN^z of the equidistant surface and its Lamé parameter are determined as follows:

$$\mathrm{d}s_1^z = A^z\mathrm{d}\alpha = A\left(1 - \frac{z}{R_1}\right)\mathrm{d}\alpha, \tag{12.7}$$

$$A^z = A\left(1 - \frac{z}{R_1}\right). \tag{12.8}$$

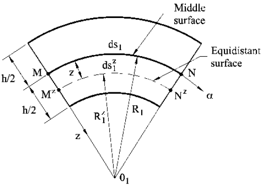

Fig. 12.3

Substituting for the strain components from Eqs (12.22) into the above, we express the stress components at any point across the thickness of the shell in terms of the middle surface strain components, changes in curvature, and twist, as follows:

$$\sigma_1^z = \frac{E}{1-\nu^2}[\varepsilon_1 + \nu\varepsilon_2 + z(\chi_1 + \nu\chi_2)], \quad \sigma_2^z = \frac{E}{1-\nu^2}[\varepsilon_2 + \nu\varepsilon_1 + z(\chi_2 + \nu\chi_1)],$$
$$\tau_{12}^z = \frac{E}{1+\nu}\left(\frac{1}{2}\gamma_{12} + z\chi_{12}\right). \tag{12.33}$$

Figure 12.4 shows a space differential element isolated from a shell by means of four sections normal to its middle surface and tangential to the lines α and $\alpha + \mathrm{d}\alpha$, β and $\beta + \mathrm{d}\beta$. The height of this element is finite and equals the shell thickness h. In this figure, the stresses acting on the volume element are indicated. The sign convention and subscript notation of the stress components are that of the theory of elasticity (see Sec. 1.4) and adapted in the treatment of thin shells, where the subscripts 1, 2, and 3 correspond to the axes α, β, and z, respectively. So, all stresses are shown positive in Fig. 12.4. For any orthogonal coordinates, the condition of equilibrium of moments on a differential element requires that

$$\tau_{12}^z = \tau_{21}^z, \quad \tau_{13}^z = \tau_{31}^z, \quad \text{and} \quad \tau_{23}^z = \tau_{32}^z. \qquad .$$

12.3.2 The stress resultants and stress couples in shells

It follows from Eq. (12.33) that the stress components are linearly distributed across the thickness of the elastic shell; therefore, it is convenient to integrate the stress distribution through the shell thickness, and then to replace the usual consideration of stresses by a consideration of statically equivalent *stress resultants and stress couples* applied to the middle surface, just as was done in the plate bending theory (see Sec. 2.3). These stress resultants and stress couples are also referred to as the *internal forces and moments*, respectively. By performing such integrations, the variations with respect to z are completely eliminated to give a 2D theory of thin shells. The elements of area of the cross sections (shaded in Fig.12.4) are

$$\mathrm{d}s_1^z = A^z \mathrm{d}\alpha \mathrm{d}z = A\left(1 - \frac{z}{R_1}\right)\mathrm{d}\alpha \mathrm{d}z; \quad \mathrm{d}s_2^z = B^z \mathrm{d}\beta \mathrm{d}z = B\left(1 - \frac{z}{R_2}\right)\mathrm{d}\beta \mathrm{d}z. \tag{12.34}$$

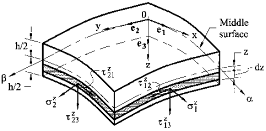

Fig. 12.4

Let us define the in-plane normal force N_1 as the resultant of the normal stresses σ_1 acting on plane face yz per unit length of the element. Thus, we have the following:

$$N_1 B\mathrm{d}\beta = \int_{-h/2}^{h/2} \sigma_1^z \mathrm{d}s_2^z = \int_{-h/2}^{h/2} \sigma_1^z B\left(1 - \frac{\mathrm{z}}{R_2}\right)\mathrm{d}\beta\mathrm{d}z,$$

from which

$$N_1 = \frac{1}{B\mathrm{d}\beta}\int_{-h/2}^{h/2} \sigma_1^z B\mathrm{d}\beta\left(1 - \frac{z}{R_2}\right)\mathrm{d}z \quad \text{or} \quad N_1 = \int_{-h/2}^{h/2} \sigma_1^z\left(1 - \frac{z}{R_2}\right)\mathrm{d}z. \tag{12.35a}$$

Similarly, we can define the in-plane shear force N_{12} and the transverse shear force Q_1, which are the resultants of the shear stress components τ_{12} and τ_{13}, respectively, and act on the same yz plane face:

$$N_{12} = \int_{-h/2}^{h/2} \tau_{12}^z\left(1 - \frac{z}{R_2}\right)\mathrm{d}z \tag{12.35b}$$

$$Q_1 = \int_{-h/2}^{h/2} \tau_{13}^z\left(1 - \frac{z}{R_2}\right)\mathrm{d}z. \tag{12.35c}$$

Expression for the remaining stress resultants per unit length are derived in a similar manner. They are given by the following:

$$N_2 = \int_{-h/2}^{h/2} \sigma_2^z\left(1 - \frac{z}{R_1}\right)\mathrm{d}z, \tag{13.35d}$$

$$N_{21} = \int_{-h/2}^{h/2} \tau_{21}^z\left(1 - \frac{z}{R_1}\right)\mathrm{d}z, \tag{12.35e}$$

$$Q_2 = \int_{-h/2}^{h/2} \tau_{23}^z\left(1 - \frac{z}{R_1}\right)\mathrm{d}z. \tag{12.35f}$$

Taking, next, the moments of the stress components σ_1^z and τ_{12}^z about the y and x axes, we will arrive to the following two new quantities:

$$M_1 = \int_{-h/2}^{h/2} \sigma_1^z z\left(1 - \frac{z}{R_2}\right)\mathrm{d}z \tag{12.36a}$$

and

$$M_{12} = \int_{-h/2}^{h/2} \tau_{12}^z z\left(1 - \frac{z}{R_2}\right)\mathrm{d}z, \tag{12.36b}$$

which are referred to, as mentioned previously, as the stress couples or the *bending* and *twisting moments*, respectively, acting on plane face yz. These moments are given to per unit length of the element of Fig. 12.4. Similarly, we can define the stress couples or the bending and twisting moments assigned on plane face xz, as follows:

$$M_2 = \int_{-h/2}^{h/2} \sigma_2^z z\left(1 - \frac{z}{R_1}\right)\mathrm{d}z, \tag{12.36c}$$

$$M_{21} = \int_{-h/2}^{h/2} \tau_{21}^z z\left(1 - \frac{z}{R_1}\right)\mathrm{d}z. \tag{12.36d}$$

The positive senses of the stress resultants and stress couples are shown in Fig. 12.5; the sign convention adopted in this figure is the same as for thin plates (see Sec. 2.3).

Notice in the above definitions of the stress resultants and stress couples that the symmetry of the stress tensor ($\tau_{12} = \tau_{21}$) does not necessarily imply that N_{12} and N_{21} are either equal or that M_{12} and M_{21} are equal for a thin shell of an arbitrary shape, except for a spherical shell.

In the general linear theory of thin shells presented above, six internal forces, $N_1, N_{12}, N_{21}, N_2, Q_1$, and Q_2, and four moments, M_1, M_2, M_{12} and M_{21}, characterize completely the state of stress of the shell, because the knowledge of these quantities enables one to determine the stress components at any point of the shell, as follows:

$$\begin{aligned}
\sigma_1^z &= \left(\frac{N_1}{h} + \frac{12M_1}{h^3}z\right)\frac{1}{1-\frac{z}{R_2}} \approx \frac{N_1}{h} + \frac{12M_1}{h^3}z; \\
\sigma_2^z &= \left(\frac{N_2}{h} + \frac{12M_2}{h^3}z\right)\frac{1}{1-\frac{z}{R_1}} \approx \frac{N_2}{h} + \frac{12M_2}{h^3}z, \\
\tau_{12}^z &= \frac{1}{2h}(N_{12}+N_{21}) + \frac{6}{h^3}(M_{12}+M_{21})z.
\end{aligned} \tag{12.37}$$

The determination of the transverse shear stresses τ_{13} and τ_{23} from their resultants Q_1 and Q_2 is not as precise, even within the framework of the present theory, as is the determination of σ_1, σ_2, and τ_{12}. In this case, it is reasoned, as in the theory of beams and thin plates, that the transverse shear stresses are parabolically distributed across the thickness of the shell. Assuming that the shear stresses are lacking on the outer and inner surfaces of the shell, we obtain the following expression for the transverse shear stresses:

$$\tau_{i3}^z = \frac{6}{5}\frac{Q_i}{h}\left[1 - \left(\frac{2z}{h}\right)^2\right], \quad i = 1, 2, \tag{12.38}$$

where, for the sake of convenience, a "form factor" of 6/5 is introduced. It represents the ratio of peak shear stress to average shear stress across the thickness of the shell.

As mentioned previously, general theory of thin shells presented was based on the Kirchhoff–Love assumptions. Now is the time to discuss these assumptions applied to the preceding derivations of the stress resultants and stress couples.

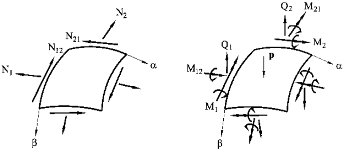

Fig. 12.5

1. We have found that, as a result of the first Kirchhoff assumption, $\gamma_{13} = \gamma_{23} = 0$ and therefore $\tau_{13} = \tau_{23} = 0$ from Hooke's law (Eqs 12.29). Nevertheless, we have defined the nonvanishing shear stress resultants Q_1 and Q_2 as integrals of τ_{13} and τ_{23} over the shell thickness. A similar situation has been observed in the plate bending theory (see Sec. 2.3), as well as in the elementary theory of beams. Here, as in the plate bending theory, the Q_1 and Q_2 resultants must be retained for purposes of equilibrium. However, they cannot be determined directly by integrating the shear stresses τ_{13} and τ_{23} over the shell thickness as was done for other stress resultants. As in the plate bending theory, the transverse shear forces Q_1 and Q_2 may be found from equilibrium conditions set up for a differential element; this is shown later.

2. We have also found that, as a result of the first and second Kirchhoff's assumptions, $\varepsilon_3 = \sigma_3 = 0$. If only σ_3 were assumed to vanish, then the following expression for the normal strain ε_3 could be obtained from Eqs (12.28) by setting $\sigma_3 = 0$. We have

$$\varepsilon_3 = -\frac{\nu}{1-\nu}(\varepsilon_1 + \varepsilon_2). \tag{12.39}$$

From this expression it would appear that the simultaneous vanishing of both the transverse normal stress and normal strain is inconsistent. These inconsistencies and deficiencies specify an approximate character of the general linear thin shell theory. However, as mentioned previously, the error introduced by Kirchhoff's assumptions into the shell theory is of the order of h/R_i in comparison with unity.

12.3.3 Equilibrium of the shell element

Consider a differential element isolated from a shell and bounded by two pairs of the normal sections passing through the α- and β-coordinate lines (Fig. 12.4) and specify its equilibrium under all external and internal forces. The external forces will comprise some surface loads applied to the upper and lower surfaces of the element. As mentioned previously, the stress components, continuously distributed across the shell thickness, are replaced by statically equivalent internal forces and moments and applied to the middle surface (Fig. 12.5). An analogous operation can be executed for the external loads by replacing them by statically equivalent forces distributed over the middle surface. Let us resolve the surface load $\mathbf{p}$ into components in the directions of $\mathbf{e_1}$, $\mathbf{e_2}$, and $\mathbf{e_3}$ are denoted by p_1, p_2, and p_3. Thus,

$$\mathbf{p} = p_1\mathbf{e}_1 + p_2\mathbf{e}_2 + p_3\mathbf{e_3}. \tag{12.40}$$

Hence, instead of considering the equilibrium of the 3D element of the shell shown in Fig. 12.4, one can study the equilibrium of the 2D element of the middle surface shown in Fig. 12.5.

Let us consider the equilibrium conditions of this element of the middle surface loaded by the external and internal forces and moments. The force and moment equilibrium for the shell element (the resultant force and resultant moment of all the external and internal forces applied to the middle surface are zero) results in the following scalar equations:

direction of the closed coordinate the conditions of periodicity must be formulated as the boundary conditions. Along the other, the open coordinate, it is necessary to set up the boundary conditions, which are to be satisfied in solving the governing differential equations of the general shell theory.

3. A *shell is open with regard to both coordinate lines* α *and* β. In this case, it is required to set up certain boundary conditions in the directions of both principal directions. Proceeding now to this general case, we confine ourselves to the simplest case where the boundaries coincide with the lines of principal curvature of the middle surface (the α- and β- coordinate lines), since this case is encountered most frequently in practice.

Let, for example, the line $\beta = \beta^*$ be a boundary of the shell. The stresses acting on the boundary can be reduced to the three internal forces N_2, N_{21}, and Q_2 and two moments M_2 and M_{21}. The deformations on the same boundary are characterized by the three displacement components u, v, and w and two slopes ϑ_1 and ϑ_2. Thus, at first glance, five boundary conditions must be prescribed on the edge line $\beta = \beta^*$. However, this is not true: due to the Kirchhoff kinematic hypothesis (the first Kirchhoff assumption), not all the above-mentioned quantities are independent. The slope of the normal to the shell boundary, ϑ_2, is connected with the displacements w and v on this boundary by the condition of the preservation of the normal. Therefore, the number of independent displacements (and hence, the corresponding generalized forces) equals four, and only the four boundary conditions can be assigned on each edge of the shell. By the way, as follows from the above, such a number of independent boundary conditions corresponds to the eighth order of the governing differential equations of the general linear theory of thin shells.

Thus, the five forces and moments assigned for the *static boundary conditions* on the shell boundary (i.e., the boundary conditions expressed in terms of the internal forces and moments) can be reduced to four quantities in accordance with Kirchhoff's postulates. This can be carried out in a similar manner to that done in the plate theory (Sec. 2.5): namely, the three boundary quantities, N_2, N_{21}, and M_{21}, may be replaced with the two boundary quantities with an acceptable accuracy.

Figure 12.6 shows two adjacent differential segments of the boundary $\beta = \beta^*$ of the middle surface, each of length $\mathrm{d}s_1$, near some point m_1. The boundary curve mm_1m_2 may be approximated by a polygon formed by two small segments of equal length. The length of each such segment with a high order of accuracy may be set equal to the length of the arc spanning, i.e., $mm_1 = m_1m_2 \approx \mathrm{d}s_1$. Let points n_1 and n_2 be halfway between the points m and m_1, m_1 and m_2, respectively. It is evident that $n_1n_2 \approx \mathrm{d}s_1$. Let $M_{21}ds_1$ and

$$\left(M_{21} + \frac{\partial M_{21}}{\partial s_1}\mathrm{d}s_1\right)\mathrm{d}s_1$$

be the resultants of the twisting moments distributed over segments mm_1 and m_1m_2, respectively. These act at the midpoints n_1 and n_2. Further, we replace each of the above resultant couples by a pair of equal and opposite forces with the moment arms $\mathrm{d}s_1$ and applied at end points of the corresponding segments. So, at end points m and m_1 the forces $(M_{21}ds_1)/ds_1 = M_{21}$, acting normal to the chord mm_1, are applied. Similarly, the forces $M_{21} + (\partial M_{21}/\partial s_1)ds_1$, acting normal to the chord m_1m_2, will be applied at end points m_1 and m_2. Thus at each point of the corners of the polygon,

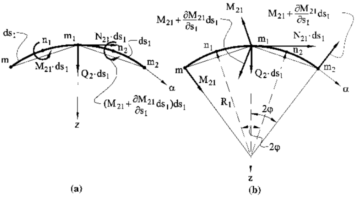

Fig. 12.6

two concentrated forces from twisting moments distributed over the adjacent segments are applied, as shown in Fig. 12.6b for corner point m_1.

Projecting both these forces, acting at a point m_1, on the direction of the normal to the middle surface (the direction of the transverse shear force Q_2) and on the direction of the tangent to the middle surface (the direction of the in-plane shear force N_{21}), we obtain:

(a) in the first case

$$+M_{21}\frac{\partial M_{21}}{\partial s_1}\mathrm{d}s_1 - M_{21} = \frac{\partial M_{21}}{\partial s_1}\mathrm{d}s_1; \tag{a}$$

(b) in the second case

$$-\left(2M_{21} + \frac{\partial M_{21}}{\partial s_1}\mathrm{d}s_1\right)\varphi, \tag{b}$$

where 2φ is the angle between the normals to the middle surface at points n_1 and n_2, i.e., $2\varphi = \mathrm{d}s_1/R_1$. Substituting this value for φ into the expression (b) and retaining only the first-order quantities, one finds $-(M_{21}/R_1)\mathrm{d}s_1$. Thus, along the shell edge $\beta = \beta^*$, the twisting moment can be replaced by the distributed normal (transverse) shear forces $\partial M_{21}/\partial s_1$ and distributed tangential (in-plane) shear forces $-M_{21}/R_1$.

As mentioned previously (see Sec. 2.5), the replacement of the twisting moment by statically equivalent forces results in a certain redistribution of the stresses over the thickness of the shell along its boundaries. By the St.Venant principle, the effect of this approximation cannot be significant; it can only be noticeable within the immediate neighborhood of the boundaries (at distances of the order of the shell thickness).

It follows from the above that the boundary conditions on the edge $\beta = \beta^*$ can be formulated in terms of the following four quantities:

12.7 TYPES OF STATE OF STRESS FOR THIN SHELLS

All equations mentioned in Sec. 12.6 are linear for both techniques, which, of course, greatly simplifies their study and solution. However, shell problems associated with calculations of the stress and strain components remain very difficult. As a rule, the governing, eight-order partial differential equations of the general shell theory have variable coefficients. Mathematical difficulties associated with integration of such a type of differential equations are evident. Even for the simplest circular cylindrical shells for which the governing equations have constant coefficients, cumbersome computations remain involved and,by far, not all problems of practical interest for such shells have been solved. Consequently, attempts of scientists and engineers engaged in the practical stress analysis of shell structures were directed towards the search for possibilities of simplifying the above governing differential equations of the general shell theory and shell problems themselves. Several approximate methods and the corresponding shell models based upon some additional assumptions and upon simplified governing equations are considered in Chapter 17.

Previously, in presenting the general linear shell theory, it was assumed that the flexural stresses are values of the same order as the stresses caused by in-plane (membrane) stresses. If one of the above-mentioned types of stresses is negligible in comparison with another one, then it is possible to introduce considerable simplifications in the general linear shell theory. Consider some possible types of state of stress for thin shells.

1. If the flexural stresses are negligible compared with the membrane stresses then such a type of state of stress is called a *membrane or momentless state of stress*. The governing equations of the membrane theory can be obtained directly from the equations of the general shell theory by neglecting the effect of the bending and twisting moments, as well as the transverse shear forces, on the state of stress and strain of thin shells. In some cases, the membrane theory describes the state of stress and strain with reasonable accuracy, since the bending and twisting moments are of negligible magnitudes: for example, hollow spherical shells subjected to inside and outside uniform pressure are in the pure membrane state of stress.

2. If, to the contrary, the membrane stresses are negligible in comparison with the flexural stresses, then such a type of state of stress is referred to as a pure *flexural or moment state of stress*. Note that the definitions of the ‘‘membrane’’ and ‘‘pure flexural’’ states of stress are not quite correct because the membrane state of stress admits an existence of small flexural stresses and, in turn, small membrane stresses may occur in a pure flexural state of stress. It was mentioned previously that shells, due to their small thickness, possess a relatively small flexural stiffness and, therefore, they are poorly adapted to resisting in bending. Even relatively small bending moments may cause considerable flexural stresses and displacements in shells. Therefore, a pure flexural type of the state of stress is dangerous and technically disadvantageous for thin shells. It should be avoided by introducing some intermediate reinforcements, by selecting the corresponding shape of the shell, by choosing the type of supports, etc. Conversely, the membrane state of stress, at which the shell is uniformly stressed across its thickness, is technically the most advantageous. So, engineers designing a shell should aim at such a state of stress.

3. If the flexural and membrane stresses are of the same order, then such a state of stress is called a *mixed state of stress, or edge effect*. The term ‘‘edge effect’’ is

13

The Membrane Theory of Shells

13.1 PRELIMINARY REMARKS

It was shown in Chapter 12 that a thin elastic shell supports an arbitrary external loading by means of stress resultants (internal forces) and stress couples (bending and twisting moments). Under appropriate loading and boundary conditions, however, the resulting bending and twisting moments are either zero, or so small that they may be neglected. Such a state of stress is referred to as the *membrane state of stress* because of the analogy to membranes that cannot support bending and twisting moments. The corresponding theory of thin shells that deals with this state of stress is called the *membrane theory of shells*. It follows from the above that the membrane theory neglects all moments, i.e.,

$$M_1 = M_2 = H = 0. \tag{13.1}$$

In turn, it follows from the corresponding moment relations

$$M_1 = D(\chi_1 + \nu\chi_2), \quad M_2 = D(\chi_2 + \nu\chi_1), \quad H = D(1-\nu)\chi_{12}, \tag{13.2}$$

that neglecting the moments will be justified either when the shell has a very small flexural stiffness, D, or when the changes in curvature and in twist of the middle surface, χ_1, χ_2, and χ_{12}, are very small. In the first case, we deal with an absolutely flexible shell, the *membrane*; in the second case, with the momentless or the membrane state of stress of a shell that has a finite flexural stiffness. Although, both these problems are described by one and the same theory, a distinction must be made between them because they resist the applied loading differently. An absolutely flexible shell (for instance, made from cloth) is not able to sustain compressive forces since any small compression forces will cause the loss of stability of its shape. Therefore, these shells may resist the applied loads only in tension.

Shells with finite flexural stiffness, in contrast to absolutely flexible shells, may resist in both the membrane states of compressive as well as tensile forces. They lose stability only when the compressive forces exceed a certain critical value. For absolutely flexible shells, since they do not possess a resistance to bending, only the membrane state of stress is possible, while for shells with finite stiffness such a state of stress is only one of the possible stress conditions. In this chapter we consider only shells with a finite flexural stiffness.

13.2 THE FUNDAMENTAL EQUATIONS OF THE MEMBRANE THEORY OF THIN SHELLS

The governing equations of the membrane theory can be obtained directly from the equations of the general theory of thin shells derived in Chapter 12. For this purpose, it is assumed that, in view of the smallness of the changes of curvature and twist, the moment terms in the equations of equilibrium for a shell element are unimportant, although in principle the shell may resist the external loads in bending. Note that neglecting the moments leads to neglecting the normal shear forces. Thus, for the membrane theory of thin shells, we can assume that

$$M_1 = M_2 = H = Q_1 = Q_2 = 0. \tag{13.3}$$

Introducing Eq. (13.3) into Eqs (12.44) and taking into account Eq. (12.43), one arrives at the following system of differential equations:

$$\begin{aligned}
&\frac{\partial}{\partial\alpha}(N_1 B) + \frac{1}{A}\frac{\partial}{\partial\beta}\left(A^2 S\right) - N_2\frac{\partial B}{\partial\alpha} + ABp_1 = 0,\\
&\frac{\partial}{\partial\beta}(N_2 A) + \frac{1}{B}\frac{\partial}{\partial\alpha}\left(B^2 S\right) - N_1\frac{\partial A}{\partial\beta} + ABp_2 = 0,\\
&N_1\frac{1}{R_1} + N_2\frac{1}{R_2} + p_3 = 0,
\end{aligned} \tag{13.4}$$

where $N_{12} = N_{21} = S$ (since $H = 0$).

In this system, the number of unknowns is equal to the number of equations, so the problem of the membrane theory of shells is statically determinate (that is true for the equilibrium of an infinitely small shell element but is not always true for the equilibrium of the entire shell). This means that if the external load components, p_1, p_2, and p_3, are known, then the membrane forces and stresses for such a shell are uniquely determined from Eqs (13.4).

Having determined the membrane forces, the shell displacements may be found. Solving the constitutive equations (12.45) for strains, and substituting them into Eqs (12.23), yields the following system of the three partial differential equations for the displacements:

$$\begin{aligned}
\varepsilon_1 &= \frac{1}{A}\frac{\partial u}{\partial\alpha} + \frac{v}{AB}\frac{\partial A}{\partial\beta} - \frac{w}{R_1} = \frac{1}{Eh}(N_1 - \nu N_2),\\
\varepsilon_2 &= \frac{1}{B}\frac{\partial v}{\partial\beta} + \frac{u}{AB}\frac{\partial B}{\partial\alpha} - \frac{w}{R_2} = \frac{1}{Eh}(N_2 - \nu N_1),\\
\gamma_{12} &= \frac{B}{A}\frac{\partial}{\partial\alpha}\left(\frac{v}{B}\right) + \frac{A}{B}\frac{\partial}{\partial\beta}\left(\frac{u}{A}\right) = \frac{2(1+\nu)}{Eh}S.
\end{aligned} \tag{13.5}$$

Now we present, without proof, the general conditions under which the membrane theory is valid. It can be shown that these conditions are necessary and sufficient for an existence of the momentless state of stress in thin shells and that they correspond to the minimum of strain energy stored by a shell during its straining. These conditions are [2]:

(a) The boundaries of a shell are free from transverse shear forces and moments. Loads applied to the shell boundaries must lie in planes that are tangent to the middle surface of the shell.
(b) The normal displacements and rotations at the shell edges are unconstrained: that is, these edges can displace freely in the direction of the normal to the middle surface.
(c) A shell must have a smoothly varying and continuous surface.
(d) The components of the surface and edge loads must be also smooth and continuous functions of the coordinates.

If these conditions are violated, fully or partially, flexural stresses occur. If designers do not succeed in eliminating these stresses completely, they must aim at localizing them and limiting their magnitude. Thus, the solutions given by the membrane theory must, in many cases, be supplemented by a solution of the equations of the bending theory in those parts of the shell where bending proves to be important. Such a combination of the bending and membrane theories is one of the important ideas on the basis of which the majority of problems of the shell theory are being solved at present. It should be also noted that even if the membrane stresses are sometimes combined with flexural stresses, the membrane theory does not lose its significance because already at a small distance from a bending zone, the state of stress may be usually considered as momentless.

13.4 THE MEMBRANE THEORY OF SHELLS OF REVOLUTION

Consider a particular case of a shell described by a surface of revolution (Fig. 11.12). The midsurface of such a shell of revolution, as mentioned in Sec. 11.8, is generated by rotating a meridian curve about an axis lying in the plane of this curve (the Z axis).

The geometry of shells of revolution is addressed in Sec. 11.8. There it is mentioned that meridians and parallel circles can be chosen as the curvilinear coordinate lines for such a shell because they are lines of curvature, and form an orthogonal mesh on its midsurface. Let us locate a point on the middle surface by the spherical coordinates θ and φ (see Sec. 11.8), where θ is the circumferential angle characterizing a position of a point along the parallel circle, whereas the angle φ is the meridional angle, defining a position of that point along the meridian. The latter represents the angle between the normal to the middle surface and the shell axis (Fig. 11.12a). As before, R_1, R_2 are the principal radii of curvature of the meridian and parallel circle, respectively, and r is the radius of the parallel circle. The Lamé parameters for shells of revolution in the above-mentioned spherical coordinate system are given by Eqs (11.39). Notice that, due to the symmetry of shells of revolution about the Z axis, these parameters are functions of φ only and do not depend upon θ. Referring to Fig. 11.12a and b, we can obtain by inspection the following relations:

(see Sec. 12.2), respectively, where the y axis points in the tangent direction along the meridian and the z axis is a normal to the middle surface at that point (Fig. 13.1). The load component p_2 (acting along the x axis) is assumed to be absent. The presence of this component implies that the shell is twisted about its axis. If $p_2 = 0$ and edge forces in the circumferential direction are also zero, then, as follows from the second Eq. (13.7), in the case of axisymmmetrical loading,

$$S = N_{12} = N_{21} = 0. \tag{13.31}$$

The nonzero membrane forces are shown in Fig. 13.1.

The first and third equations of the system (13.7) after some algebra transformations, eliminating N_2, and taking into account Eqs (13.6), may be reduced to the following equation:

$$\frac{\mathrm{d}}{\mathrm{d}\varphi}(N_1 r \sin\varphi) + rR_1(p_1 \sin\varphi + p_3 \cos\varphi) = 0. \tag{13.32}$$

Integrating this equation from φ_0 to φ, one finds

$$\begin{aligned} [N_1 r \sin\varphi]_{\varphi_0}^{\varphi} &= -\int_{\varphi_0}^{\varphi} rR_1(p_1 \sin\bar{\varphi} + p_3 \cos\bar{\varphi})\mathrm{d}\bar{\varphi} \quad \text{or} \\ N_1 r \sin\varphi &= -\int_{\varphi_0}^{\varphi} rR_1(p_1 \sin\bar{\varphi} + p_3 \cos\bar{\varphi})\mathrm{d}\bar{\varphi} + N_1^{(0)} b \sin\varphi_0, \end{aligned} \tag{13.33a}$$

where φ_0 is the angle corresponding to the shell edge (for instance, at the top) where the boundary conditions are specified; $N_1^{(0)}$ and $r_0 = b$ are the meridional force, and the radius of the parallel circle, respectively, at the shell edge $\varphi = \varphi_0$ (Fig. 13.2); and $\bar{\varphi}$ is a dummy variable.

Solving Eq. (13.33a) for N_1 and taking into account Eq. (13.6a), yields

$$N_1 = -\frac{1}{R_2 \sin^2\varphi}\int_{\varphi_0}^{\varphi} R_1 R_2 (p_1 \sin\bar{\varphi} + p_3 \cos\bar{\varphi}) \sin\bar{\varphi}\mathrm{d}\bar{\varphi} + \frac{N_1^{(0)} R_2^{(0)} \sin^2\varphi_0}{R_2 \sin^2\varphi} \tag{13.33b}$$

where $b = R_2^{(0)} \sin\varphi_0$. $R_2^{(0)}$is the principal radius of curvature at the shell edge $\varphi = \varphi_0$.

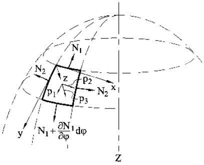
N$_1$
N$_2$
z
p$_2$
p$_1$
N$_2$
x
p$_3$
y
$N_1 + \frac{\partial N_1}{\partial\varphi} \mathrm{d}\varphi$
Z

Fig. 13.1

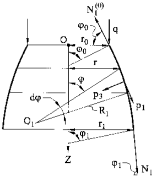

Fig. 13.2

Let a shell, in addition to the surface load components p_1 and p_3, be subjected to some line load q per unit length of the top parallel circle, $\varphi = \varphi_0$. This may be, for example, the weight of a skylight of a dome. From Fig. 13.2, $N_1^{(0)} = -q/\sin\varphi_0$; substituting into Eq. (13.33a) gives

$$N_1 r \sin\varphi = -\left[\int_{\varphi_e}^{\varphi} rR_1(p_1 \sin\bar{\varphi} + p_3 \cos\bar{\varphi})\mathrm{d}\bar{\varphi} + qb\right]. \tag{13.34}$$

This equation may be easily interpreted if we multiply both sides of Eq. (13.34) by 2π. We have

$$N_1(2\pi r)\sin\varphi = -2\pi\int_{\varphi_0}^{\varphi} rR_1(p_1 \sin\bar{\varphi} + p_3 \cos\bar{\varphi})\mathrm{d}\bar{\varphi} - 2\pi bq. \tag{13.35}$$

Referring to Fig. 13.2, one can conclude that the left-hand side of this equation is the vertical component of the resultant of meridional forces N_1over a parallel circle determined by angle φ. As seen from Fig.13.2, $2\pi r R_1 \mathrm{d}\varphi$ is the area of an elementary ring corresponding to an infinitesimal angle dφ; and $p_1 \sin\varphi$ and $p_3 \cos\varphi$ are the vertical components of the surface load. Hence, the integrand function of Eq. (13.35) represents a vertical component of the surface load corresponding to the elementary ring. Integrating over φ, we obtain the vertical component of the resultant of all surface loads acting on the shell above the parallel circle φ where $N_1$is to be determined. So, we can rewrite Eq. (13.35), as follows:

$$N_1(2\pi r)\sin\varphi = -F,$$

from which

$$N_1 = -\frac{F}{2\pi r \sin\varphi}, \tag{13.36}$$

where

$$F = 2\pi[\int_{\varphi_0}^{\varphi} rR_1(p_1 \sin\bar{\varphi} + p_3 \cos\bar{\varphi})\mathrm{d}\bar{\varphi} + qb] \tag{13.37}$$

is the vertical component of all external loading applied above the parallel circle φ of the shell where N_1 is desired. Thus, Eq. (13.35) represents the static equilibrium condition: i.e., the force summation in the direction of the shell axis (the Z axis) is zero. Note that in the case of a shell closed at its apex, $\varphi_0 = 0$ and N_1 becomes

$$N_1 = -\frac{1}{r \sin\varphi} \int_0^{\varphi} r R_1 (p_1 \sin\bar{\varphi} + p_3 \cos\bar{\varphi}) \mathrm{d}\bar{\varphi}. \tag{13.38}$$

Having determined N_1 from Eq. (13.34) or Eq. (13.36), or Eq. (13.38), we can calculate N_2 from the third Eq. (13.7), as follows:

$$N_2 = -R_2 \left(p_3 + \frac{N_1}{R_1} \right). \tag{13.39}$$

Now we can discuss the *displacements in symmetrically loaded shells of revolution*. For this particular case, $v = 0$ and $\gamma_{12} = 0$ and the system of Eqs (13.16) may be simplified to the following:

$$\begin{aligned} \frac{1}{R_1} \frac{\mathrm{d}u}{\mathrm{d}\varphi} - \frac{w}{R_1} &= \frac{1}{Eh}(N_1 - \nu N_2) = \varepsilon_1, \\ \frac{u}{R_2} \cot\varphi - \frac{w}{R_2} &= \frac{1}{Eh}(N_2 - \nu N_1) = \varepsilon_2, \end{aligned} \tag{13.40}$$

where u and w are displacements along the tangent and normal to the meridian curve (or along the y and z axes, as shown in Fig. 13.1), respectively. Knowing N_1 and N_2 for a given shell problem, we can evaluate the strain components, ε_1 and ε_2, and then, u and w from Eqs. (13.40). For this purpose, eliminating w from Eqs (13.40), one finds that

$$\frac{1}{R_2} \left(\frac{\mathrm{d}u}{\mathrm{d}\varphi} - u \cot\varphi \right) = \left(\frac{R_1}{R_2} \right) \varepsilon_1 - \varepsilon_2. \tag{13.41}$$

Multiplying both sides of the above equation by $R_2 \csc\varphi$, we have, after some mathematics,

$$\frac{\mathrm{d}}{\mathrm{d}\varphi}(u \csc\varphi) = f_1(\varphi), \tag{13.42a}$$

where

$$f_1(\varphi) = \frac{R_2}{\sin\varphi} \left(\frac{R_1}{R_2} \varepsilon_1 - \varepsilon_2 \right). \tag{13.42b}$$

The function $f_1(\varphi)$ can be found when N_1 and N_2 have been determined. Integrating Eq. (13.42a), we obtain the following expression for u:

$$u = \sin\varphi \int f_1(\varphi) \mathrm{d}\varphi + C_1 \sin\varphi, \tag{13.43}$$

where C_1 is a constant of integration. Substituting for u from Eq. (13.43) into the second Eq. (13.40), one finds the following expression for w:

$$w = \cos\varphi \int f_1(\varphi) \mathrm{d}\varphi + C_1 \cos\varphi - \varepsilon_2 R_2. \tag{13.44}$$

$$\frac{\mathrm{d}w}{\mathrm{d}\varphi} = \cos\varphi \cdot f_1(\varphi) - \sin\varphi \int f_1(\varphi)\mathrm{d}\varphi - C_1 \sin\varphi - \varepsilon_2 \frac{\mathrm{d}R_2}{\mathrm{d}\varphi} - R_2 \frac{\mathrm{d}\varepsilon_2}{\mathrm{d}\varphi}. \tag{13.47b}$$

The displacement u is given by Eq. (13.43). Adding the right-hand sides of Eqs (13.47b) and (13.43), we obtain ϑ_1, as follows:

$$\vartheta_1 = \frac{1}{R_1}\left(\cos\varphi \cdot f_1(\varphi) - \varepsilon_2 \frac{\mathrm{d}R_2}{\mathrm{d}\varphi} - R_2 \frac{\mathrm{d}\varepsilon_2}{\mathrm{d}\varphi}\right),$$

or substituting for $f_1(\varphi)$ from Eq. (13.42b) results in the following:

$$\vartheta_1 = \cot\varphi\left(\varepsilon_1 - \frac{R_2}{R_1}\varepsilon_2\right) - \frac{\varepsilon_2}{R_1}\frac{\mathrm{d}R_2}{\mathrm{d}\varphi} - \frac{R_2}{R_1}\frac{\mathrm{d}\varepsilon_2}{\mathrm{d}\varphi}. \tag{13.48a}$$

Let us present this expression in the explicit form for a special case of spherical shells only. Substituting $R_1 = R_2 = R$ into the above equation, we obtain

$$\vartheta_1 = \cot\varphi(\varepsilon_1 - \varepsilon_2) - \frac{\mathrm{d}\varepsilon_2}{\mathrm{d}\varphi}. \tag{13.48b}$$

Inserting the strains in terms of N_1 and N_2 into this equation, we obtain the following expression of ϑ_1 for a sphere:

$$Eh\vartheta_1 = \cot\varphi(1+\nu)(N_1 - N_2) - \frac{\mathrm{d}N_2}{\mathrm{d}\varphi} + \nu\frac{\mathrm{d}N_1}{\mathrm{d}\varphi}. \tag{13.48c}$$

13.6 MEMBRANE ANALYSIS OF CYLINDRICAL AND CONICAL SHELLS

Cylindrical and conical shells have straight generators and, therefore, the radius of the curvature in the meridional direction is infinite. It will be shown that the vanishing one out of the two principal curvatures leads to a great simplification in the analysis of such a type of shells. For this reason, we treat these shells as a separate category of membrane shells.

13.6.1 General cylindrical shells

We consider cylindrical shells with an arbitrary shape of the cross section (or profile): e.g., circular, elliptical, parabolic, and cylinders of open or closed types. The peculiarities of the geometry of these shells were analyzed in Sec. 11.8. Since the generators of cylindrical shells are straight, such shells have zero Gaussian curvatures and, hence, have developable surfaces (see Sec. 11.7).

Using the cylindrical coordinates x and θ to describe the position of a reference point on the cylindrical shell middle surface (Fig. 11.13), the Lamé parameters are given by the relations (11.52), i.e.,

$$A = 1, \quad B = R_2, \tag{13.49}$$

where $R_2 = R_2(\theta)$ is the second principal radius of curvature, while the first radius of curvature $R_1 = \infty$. Notice that for a circular cylindrical shell $R_2 = \text{const} = R$, where

arbitrary functions $f_1(\theta)$ and $f_2(\theta)$, which arise in integrating the equilibrium equations, are continuous together with their derivatives up to the second and third derivatives. This also imposes certain limitations on admissible types of loading and boundary conditions in order that membrane theory can be applied.

One important comment should be mentioned. It follows from Eqs (13.54) and (13.55) that the membrane forces and displacements increase without limit with an increase of the shell length. This is a natural result of the membrane analysis of a cylindrical shell in which th flexural rigidity of the circumferential cross sections of the shell is neglected and all loading is directly transmitted to the shell ends. Therefore, the area of application of the membrane theory of cylindrical shells is restricted by fairly short shells ($l/R \ll \sqrt{R/h}$) [2]. So, there is a variety of requirements that govern the applicability of the membrane theory of cylindrical shells. These requirements are concerned with the type of shell supports, type of loading, and length of the shell.

An impression may be formed that the membrane theory of cylindrical shells is practically of no use because of the limitations mentioned above. However, this is not true. In some cases, the membrane theory of cylindrical shells allows one to obtain simple and, at the same time, sufficiently accurate solutions. In particular, it is applicable to the analysis of cylindrical shells reinforced by stiffeners. In this case, the external loading applied to the closely spaced at equal distances stiffeners is distributed by the stiffener elements in such a way that the condition of slowly varying deformation in the circumferential direction is satisfied.

13.6.2 Conical shells

Figure 13.3a shows a conical shell in the form of a frustum of a cone. The meridian of the shell has zero curvature, while the radius of the second principal curve is R_2. The radius of the parallel circle is denoted by r. In this typical case, the angle φ is a constant and can no longer serve as a coordinate on the meridian. Instead, we introduce the coordinate s, the distance of a point of the middle surface, usually measured from the vertex, along the generator, i.e., $\alpha = s$. Another coordinate is the

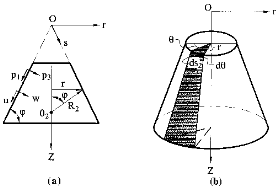

Fig. 13.3

circumferential angle θ in the horizontal plane measured on the parallel circle, i.e., $\beta = \theta$.

For such a shell, a length of the element along the meridian is ds_1 and along the parallel circle is $ds_2 = r d\theta$. It follows from Fig. 13.3a and b that

$$R_2 = s \cot\varphi, \quad r = s\cos\varphi. \tag{13.56}$$

Thus, the Lamé parameters for the given coordinate system are

$$A = 1 \quad \text{and} \quad B = r = s\cos\varphi. \tag{13.57}$$

Substituting the above into Eqs (13.4) and (13.5), we obtain the equilibrium and kinematic equations, respectively. The equilibrium equations for the conical shell are given by

$$\begin{aligned} \frac{\partial}{\partial s}(N_1 s) + \frac{1}{\cos\varphi}\frac{\partial S}{\partial\theta} - N_2 + sp_1 = 0, \\ \frac{1}{\cos\varphi}\frac{\partial N_2}{\partial\theta} + \frac{1}{s}\frac{\partial}{\partial s}\left(Ss^2\right) + sp_2 = 0, \\ \frac{1}{s}\tan\varphi N_2 + p_3 = 0. \end{aligned} \tag{13.58}$$

The kinematic equations for displacement components have the form

$$\begin{aligned} &\frac{\partial u}{\partial s} = \varepsilon_1 \\ &\frac{1}{\cos\varphi}\frac{\partial v}{\partial\theta} + u - w\tan\varphi = \varepsilon_2 s \\ &s\frac{\partial}{\partial s}\left(\frac{v}{s}\right) + \frac{1}{s\cos\varphi}\frac{\partial u}{\partial\theta} = \gamma_{12} \end{aligned} \tag{13.59}$$

We come now to determining the membrane forces and displacements for conical shells. From the last Eq. (13.58), we have

$$N_2 = -p_3 s \cdot \cot\varphi. \tag{13.60}$$

Substituting the above into the second Eq. (13.58), one finds that

$$\frac{\partial}{\partial s}\left(Ss^2\right) = -s^2\left(p_2 - \frac{1}{\sin\varphi}\frac{\partial p_3}{\partial\theta}\right).$$

Integrating this expression over s, we obtain

$$S = \frac{1}{s^2}\left[f_1(\theta) - \int_s s^2\left(p_2 - \frac{1}{\sin\varphi}\frac{\partial p_3}{\partial\theta}\right)ds\right]. \tag{13.61}$$

Integrating the above, yields

$$N_1 = -\left[\frac{1}{s}\int (p_1 + p_3 \cot\varphi) s \mathrm{d}s + \frac{C}{s}\right], \tag{13.68}$$

where C is a constant of integration.

13.7 THE MEMBRANE THEORY OF SHELLS OF AN ARBITRARY SHAPE IN CARTESIAN COORDINATES

The boundary contour of shells of an arbitrary shape does not usually coincide with the lines of curvature. As an example, one can mention shells of double curvature which are commonly used for roofs of buildings. A membrane analysis of such shells is more conveniently performed using Cartesian coordinates whose x and y axes lie in a horizontal plane with the z axis pointing in the vertical direction to the plane above. The middle surface of the shell can be assigned by the following equation in the Cartesian coordinate system:

$$z = f(x, y). \tag{13.69}$$

In this coordinate system, we consider an element $ABCD$ of the shell obtained by making sections at the locations $x, x + \mathrm{d}x$, and $y, y + \mathrm{d}y$ (Fig. 13.4).

These sections are not necessarily the lines of curvature in a general case (the exceptions are cylindrical surfaces for which the x axis is directed along generators). They are not mutually perpendicular. Hence, angle ω between sides AB and AD is not necessarily a right angle and element $ABCD$ is a skew quadrilateral with sides $\mathrm{d}s_1$ and $\mathrm{d}s_2$ in space. Its projection in the xy plane is a rectangle $\bar{A}\bar{B}\bar{C}\bar{D}$ with sides $\mathrm{d}x$ and $\mathrm{d}y$. Let φ and ϕ be the angles which sides AD and AB make with the xy plane. Correspondingly, the lengths AD and AB of the shell element are $(\mathrm{d}x/\cos\varphi)$ and $(\mathrm{d}y/\cos\phi)$, respectively. The midsurface area of the element $ABCD$ becomes $(\mathrm{d}x/\cos\varphi)(\mathrm{d}y/\cos\phi)\sin\omega$.

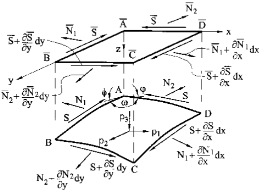
$\bar{N}_2$
$\bar{S}$
$\bar{A}$
$\bar{D}$
x
$\bar{N}_1$
$\bar{S}$
$\bar{S}+\frac{\partial \bar{S}}{\partial y}\mathrm{d}y$
$\bar{B}$
z
$\bar{C}$
$\bar{N}_1+\frac{\partial \bar{N}_1}{\partial x}\mathrm{d}x$
$\bar{S}+\frac{\partial \bar{S}}{\partial x}\mathrm{d}x$
y
$\bar{N}_2+\frac{\partial \bar{N}_2}{\partial y}\mathrm{d}y$
N_2
S
N_1
ϕ
A
φ
ω
S
p_3
D
$S+\frac{\partial S}{\partial x}\mathrm{d}x$
p_1
B
p_2
$N_1+\frac{\partial N_1}{\partial x}\mathrm{d}x$
$S+\frac{\partial S}{\partial y}\mathrm{d}y$
C
$N_2-\frac{\partial N_2}{\partial y}\mathrm{d}y$

Fig. 13.4

The curves $x = \text{const}$ and $y = \text{const}$ on the shell midsurface can be used as coordinate curves, and we denote by N_1, N_2, and S the membrane stress resultants at any point on the shell. It should be noted that the directions of these forces make up non-right angles with the corresponding sides of the element. These membrane forces are shown in Fig. 13.4. Two out of all unknown forces (N_1 and S) are parallel to the plane Oxz, and, therefore, have no components in the direction of the y axis. Two others (N_2 and S on sides AD and BC) have no components in the x direction. These considerations simplify setting up the equation of equilibrium.

Figure 13.4 also shows the surface load components, where p_1 and p_2 are parallel to the x and y axes, respectively, and p_3 acts in the z direction. These load components are defined per unit are of the shell midsurface.

We set up the equation of equilibrium in the direction of the x axis. Consider a side AB. The membrane force per unit length acting on this side is $N_1(\mathrm{d}y/\cos\phi)$ and its component in the x direction is $N_1(\mathrm{d}y/\cos\phi)\cos\varphi$. The in-plane shear force S of the same direction has a component in the x direction of the form $S(\mathrm{d}x/\cos\varphi)\cos\varphi$. By analogy, the components of the membrane forces acting on the opposite side CD can be represented, as follows:

$$\left(N_1 + \frac{\partial N_1}{\partial x}\mathrm{d}x\right)\frac{\mathrm{d}y}{\cos\left(\phi + \frac{\partial\phi}{\partial x}\mathrm{d}x\right)}\cos\left(\varphi + \frac{\partial\varphi}{\partial x}\mathrm{d}x\right),$$

$$\left(S + \frac{\partial S}{\partial y}\mathrm{d}y\right)\cos\left(\varphi + \frac{\partial\varphi}{\partial y}\mathrm{d}y\right)\frac{\mathrm{d}x}{\cos\left(\varphi + \frac{\partial\varphi}{\partial y}\mathrm{d}y\right)}.$$

Summing these forces with the corresponding signs, taking into account that the resultant force due to the loading p_1 is obtained by multiplying p_1 by the area of the element $ABCD$, and canceling out the common factor $\mathrm{d}x\mathrm{d}y$, we obtain the following after some simplifications and assuming that the angles φ and ϕ are small:

$$\frac{\partial}{\partial x}\left(N_1\frac{\cos\varphi}{\cos\phi}\right) + \frac{\partial S}{\partial y} + p_1\frac{\sin\omega}{\cos\phi\cos\varphi} = 0. \tag{13.70a}$$

Similarly, we can obtain the following equilibrium equation for the components of the membrane forces in the y direction:

$$\frac{\partial}{\partial y}\left(N_2\frac{\cos\phi}{\cos\varphi}\right) + \frac{\partial S}{\partial x} + p_2\frac{\sin\omega}{\cos\phi\cos\varphi} = 0. \tag{13.70b}$$

Let us set up an equation of equilibrium for all the membrane forces in the z direction. The component of the force N_1 in the z direction is $N_1(\mathrm{d}y/\cos\phi)\sin\varphi$ and the component of the in-plane shear force S in the same direction referred to the same side of the element $ABCD$ is $S(\mathrm{d}y/\cos\phi)\sin\varphi$. The corresponding expressions can be obtained for the two other components of the membrane forces. So, the equation of equilibrium for the membrane forces in the z direction is derived after some simplifications, as follows:

$$\frac{\partial}{\partial x}\left(N_1\frac{\sin\varphi}{\cos\phi}\right) + \frac{\partial}{\partial y}\left(N_2\frac{\sin\phi}{\cos\varphi}\right) + \frac{\partial}{\partial y}(S\tan\varphi) + \frac{\partial}{\partial x}(S\tan\phi) + p_3\frac{\sin\omega}{\cos\phi\cos\varphi} = 0. \tag{13.70c}$$

The values of the trigonometric functions entering into Eqs (13.70) can be expressed in terms of the partial derivatives of the equation of a surface given by Eq. (13.69), i.e.,

$$\tan\varphi = \frac{\mathrm{d}z}{\mathrm{d}x}, \quad \tan\phi = \frac{\mathrm{d}z}{\mathrm{d}y}; \tag{13.71a}$$

hence,

$$\cos\varphi = \frac{1}{\sqrt{1+\left(\frac{\partial z}{\partial x}\right)^2}}, \quad \sin\varphi = \frac{\partial z/\partial x}{\sqrt{1+\left(\frac{\partial z}{\partial x}\right)^2}}, \quad \text{etc.} \tag{13.71b}$$

It can be easily noted that the expressions

$$\left(N_1\frac{\mathrm{d}y}{\cos\phi}\right)\cos\varphi, \left(N_2\frac{\mathrm{d}x}{\cos\varphi}\right)\cos\phi; \quad \left(S\frac{\mathrm{d}y}{\cos\phi}\right)\cos\phi, \left(S\frac{\mathrm{d}x}{\cos\varphi}\right)\cos\varphi$$

represent projections of the membrane forces acting on sides of the shell skew quadrilateral element $ABCD$ on the coordinate plane xy or the membrane forces acting on sides of the rectangle $\bar{A}\bar{B}\bar{C}\bar{D}$, as shown in Fig. 13.4. Let us denote these projections by $\bar{N}_1\mathrm{d}y$, $\bar{N}_2\mathrm{d}x$, and $\bar{S}\mathrm{d}x$, i.e.,

$$\bar{N}_1 = N_1\frac{\cos\varphi}{\cos\phi}, \quad \bar{N}_2 = N_2\frac{\cos\phi}{\cos\varphi}, \quad \bar{S} = S. \tag{13.72}$$

Using these notations, we can rewrite equations of equilibrium, Eqs (13.70), as follows

$$\frac{\partial\bar{N}_1}{\partial x} + \frac{\partial\bar{S}}{\partial y} + \bar{p}_1 = 0, \tag{13.73a}$$

$$\frac{\partial\bar{S}}{\partial x} + \frac{\partial\bar{N}_2}{\partial y} + \bar{p}_2 = 0, \tag{13.73b}$$

$$\frac{\partial}{\partial x}\left(\bar{N}_1\tan\varphi\right) + \frac{\partial}{\partial y}\left(\bar{N}_2\tan\phi\right) + \frac{\partial}{\partial y}\left(\bar{S}\tan\varphi\right) + \frac{\partial}{\partial x}\left(\bar{S}\tan\phi\right) + \bar{p}_3 = 0. \tag{13.73c}$$

where

$$\bar{p}_1 = p_1\frac{\sin\omega}{\cos\phi\cos\varphi}, \quad \bar{p}_2 = p_2\frac{\sin\omega}{\cos\phi\cos\varphi}, \quad \bar{p}_3 = p_3\frac{\sin\omega}{\cos\phi\cos\varphi} \tag{13.74}$$

are the surface load components per unit area of the projection of the shell element on the xy plane in the x, y, and z directions, respectively.

Equation (13.73c) can be rewritten by substituting for the tangents from Eqs (13.71a), as follows:

$$\bar{N}_1\frac{\partial^2 z}{\partial x^2} + 2\bar{S}\frac{\partial^2 z}{\partial x\partial y} + \bar{N}_2\frac{\partial^2 z}{\partial y^2} = -\bar{p}_3 - \left(\frac{\partial\bar{N}_1}{\partial x} + \frac{\partial\bar{S}}{\partial y}\right)\frac{\partial z}{\partial x} - \left(\frac{\partial\bar{S}}{\partial x} + \frac{\partial\bar{N}_2}{\partial y}\right)\frac{\partial z}{\partial y}. \tag{13.75}$$

14

Application of the Membrane Theory to the Analysis of Shell Structures

We consider below an application of the membrane theory of thin shells, developed in Chapter 13, to the analysis of various shell structures. The membrane theory can be applied with various levels of accuracy to the stress analysis of two kinds of shell structures: facilities for storage of water, gas, oil, etc. (elevated water towers, silos, pressure vessels, tanks, closures, etc.) and long-span roofs of buildings or domes.

14.1 MEMBRANE ANALYSIS OF ROOF SHELL STRUCTURES

14.1.1 Axisymmetrically loaded dome roofs

(a) Spherical domes: self-weight

First, we consider a dome closed at its apex and subjected to a dead load of p per unit area of the middle surface (e.g., own weight, weight of cladding, etc.), as shown in Fig. 14.1a.

Resolving the dead load p into components along the normal, p_3, and meridional, p_1, directions, with respect to the middle surface of the dome, we obtain the following relationships:

$$p_3 = p\cos\varphi,\; p_1 = p\sin\varphi. \tag{14.1}$$

Substituting the above into Eq. (13.38), taking into account Eq. (13.6a) and noting that for a sphere $R_1 = R_2 = R$, we obtain the following expression for the meridional force:

$$N_1 = -\frac{1}{R\sin^2\varphi}\int_0^{\varphi} R^2 \sin\bar{\varphi}(p\sin^2\bar{\varphi} + p\cos^2\bar{\varphi})\mathrm{d}\bar{\varphi},$$

or

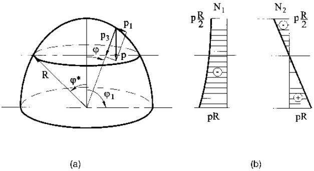

Fig. 14.1

$$N_1 = -pR\frac{1-\cos\varphi}{1-\cos^2\varphi} = -\frac{pR}{1+\cos\varphi}. \tag{14.2}$$

Then, substituting Eq. (14.2) into Eq. (13.39) gives the expression for the circumferential force, as follows:

$$N_2 = -pR\cos\varphi + \frac{pR}{1+\cos\varphi} = -pR\left(\cos\varphi - \frac{1}{1+\cos\varphi}\right). \tag{14.3}$$

At the crown of the dome where $\varphi = 0$, we have the following:

$$N_1 = N_2 = -\frac{pR}{2}.$$

The meridional force, N_1, is compressive along the meridian of the dome, increasing from the apex to the bottom of the dome. The circumferential compressive force N_2, near the crown, decreases gradually with the increase of φ and changes sign. Diagrams of the distribution of the membrane forces N_1 and N_2 are shown in Fig. 14.1b.

Denote by φ^* the coordinate of the parallel circle on which $N_2 = 0$. This parallel circle is called the *line of transition*. Below this line, the circumferential force,N_2, is tensile only under the loading shown in Fig. 14.1a. The coordinate φ^* of the line of transition may be found from Eq. (14.3), equating the term in the parenthesis to zero and putting $\varphi = \varphi^*$. We have

$$\cos\varphi^* - \frac{1}{1+\cos\varphi^*} = 0,$$

from which $\varphi^* = 51^\circ 49'$.

Spherical domes whose opening angle is less then $2\varphi^*$ are free from tensile stresses. At the base of a semi-sphere ($\varphi = \varphi_1 = 90^\circ$), $N_2 = pR$, $N_1 = -pR$.

The presence of the line of transition enables one to avoid considerable bending near the base of a dome. Let us consider this statement in detail. Resolve the membrane force $N_1^{(1)}$, acting at the base of the dome ($\varphi = \varphi_1$), into two components: the vertical V and horizontal H, as shown in Fig. 14.2a. The vertical component V

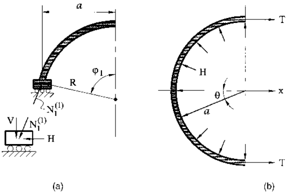

(a)

(b)

Fig. 14.2

will be transmitted to the wall on which the dome rests, while the assimilation of the horizontal component H requires a special structural element called a thrust (or supporting) ring. A half-plan of the ring is shown in Fig. 14.2b. The shell is assumed to extend to the centroid of the ring to eliminate the introduction of eccentricity.

The vertical and horizontal components of the membrane force N_1 are found to be

$$V = N_1^{(1)} \sin\varphi_1, \quad H = -N_1^{(1)} \cos\varphi_1. \tag{14.4}$$

The horizontal component, H, being applied to the thrust ring produces its tension in the circumferential direction. Let T be the circumferential tension in the ring. We can evaluate T by summing forces in the x direction on Fig. 14.2b and assuming that the radius of the ring is approximately equal to a, i.e., to the radius of the parallel circle at the shell base ($\varphi = \varphi_1$), as follows:

$$2T = \int_{-\pi/2}^{\pi/2} -N_1^{(1)} \cos\varphi_1 \cos\theta (a\,d\theta) \quad \text{or} \quad T = -N_1^{(1)} a \cos\varphi_1. \tag{14.5}$$

For the spherical shell we have $a = R\sin\varphi_1$. So that

$$T = -N_1^{(1)} R \cos\varphi_1 \sin\varphi_1. \tag{14.6}$$

For the self-weight case, we find by substituting Eq. (14.2) into Eq. (14.6) that

$$T = pR^2 \frac{\cos\varphi_1 \sin\varphi_1}{1 + \cos\varphi_1}. \tag{14.7}$$

Comparing Eq. (14.7) and the graph for N_2 in Fig. 14.1b, we can conclude that there could be a strain incompatibility at the junction between the shell edge and the thrust ring. For $\varphi_1 < 51^\circ 49'$, the circumferential force N_2 is compressive while the ring force T is tensile for all $\varphi_1 < 90^\circ$. Thus, the dome, which has been shown to be in a state of compression through the membrane stress analysis, must accommodate somewhat the circumferential expansion of the base ring accompanying the tensile force T. Clearly, this cannot be accomplished with membrane action alone, and bending must be considered to satisfy deformational continuity. It should be noted that the bending effects introduced are usually confined to a relatively small portion of the shell adjacent to the base, and membrane action will still predominate throughout most of the shell.

However, if $\varphi > 51^\circ 49'$ the circumferential force N_2 will be tensile and, hence, will coincide with the sign of the circumferential tension in the ring. So, the possibility arises of selecting the cross-sectional area of the thrust ring in such a way that the elongation of the shell edge would be equal to stretching the ring. The circumferential strains of the shell edge, $\varepsilon_2^{(\mathrm{s})}$, and the thrust ring, $\varepsilon_2^{(\mathrm{r})}$, are found to be

$$\varepsilon_2^{(\mathrm{s})} = \frac{1}{E_s h}\left(N_2^{(1)} - \nu_s N_1^{(1)}\right); \quad \varepsilon_2^{(\mathrm{r})} = \frac{\sigma_2^{(\mathrm{r})}}{E_r} = \frac{T}{E_r A_r} = -\frac{N_1^{(1)} a}{E_r A_r}\cos\varphi_1. \tag{14.8}$$

In Eqs (14.8), $N_1^{(1)}$ and $N_2^{(1)}$ are the meridional and circumferential forces at the shell base, respectively, i.e., at $\varphi = \varphi_1$; E_s and ν_s are the modulus of elasticity and Poisson's ratio, respectively, of the shell material; E_r and A_r are the modulus of elasticity and cross-sectional area of the thrust ring, respectively. The required cross-sectional area of the thrust ring can be determined from the following compatibility condition:

$$\varepsilon_2^{(\mathrm{s})} = \varepsilon_2^{(\mathrm{r})}. \tag{14.9}$$

Substituting Eqs (14.8) into Eq. (14.9) yields the required area of the cross section of the thrust ring, as follows:

$$A_r = \left|\frac{\cos\varphi_1}{\dfrac{N_2^{(1)}}{N_1^{(1)}} - \nu_s}\right| \frac{E_s}{E_r} ah, \tag{14.10}$$

where $N_1^{(1)}$ and $N_2^{(1)}$are given by Eqs (14.2) and (14.3) by substituting φ_1 for φ.

Having determined the internal forces, we can calculate the meridional, σ_1, and circumferential, σ_2, membrane stress components, as follows:

$$\sigma_1 = \frac{N_1}{h} = -\frac{p}{h}\frac{R}{1+\cos\varphi}, \quad \sigma_2 = \frac{N_2}{h} = -\frac{p}{h}R\left(\cos\varphi - \frac{1}{1+\cos\varphi}\right). \tag{14.11}$$

Let us now determine the displacements of the spherical dome supporting its own weight (Fig. 14.1a). Substituting for the membrane forces N_1 and N_2 from Eqs (14.2) and (14.3) into the right-hand sides of Eqs (13.5) gives the strains ε_1 and ε_2. Introducing the latter into Eqs (13.42b) results in the following expressions for $f_1(\varphi)$:

$$f(\varphi) = \frac{R^2 p(1+\nu)}{Eh}\left(\cos\varphi - \frac{2}{1+\cos\varphi}\right). \tag{14.12}$$

Inserting the above expression into Eq. (13.43), and evaluating the integrals, yields the following expression for u:

$$u = \frac{pR^2(1+\nu)}{Eh}\left[\sin\varphi\ln(1+\cos\varphi) - \frac{\sin\varphi}{1+\cos\varphi}\right] + C_1\sin\varphi, \tag{14.13}$$

where C_1 is a constant of integration that can be evaluated from boundary conditions on the dome base, i.e., Fig.14.2a, $u = 0|_{\varphi=\varphi_1}$. It follows from the above that

$$C_1 = \frac{pR^2(1+\nu)}{Eh}\left[\frac{1}{1+\cos\varphi_1} - \ln(1+\cos\varphi_1)\right].$$

Upon substitution of this value into Eq. (14.13), the deflection u is obtained in the form

$$u = \frac{pR^2(1+\nu)}{Eh}\sin\varphi\left[\ln\frac{1+\cos\varphi}{1+\cos\varphi_1} + \frac{\cos\varphi - \cos\varphi_1}{(1+\cos\varphi)(1+\cos\varphi_1)}\right]. \tag{14.14}$$

Then Eq. (13.44) yields w.

Up to this point, we have assumed that domes were closed at their apex. Now let us analyze the membrane forces distribution in a spherical dome under self-weight, which has a skylight at its top (Fig. 14.3).

In this case, the dome has the form of a truncated sphere with a reinforcing ring used to support the upper structure (skylight). We assume that p is the weight of the shell surface per unit area and there is a line load q per unit length at the top of the dome, due to the weight of the skylight, hood, etc. To find N_1, we substitute $R_1 = R_2 = R$, and $p_3 = p\cos\varphi$, $p_1 = p\sin\varphi$, and $r = R\sin\varphi$ into Eq. (13.34). We have the following:

$$\begin{aligned} N_1 &= -\frac{1}{R\sin^2\varphi}\left[\int_{\varphi_0}^{\varphi} R^2\sin^2\bar{\varphi}\left(p\sin^2\bar{\varphi} + p\cos^2\bar{\varphi}\right)\sin\bar{\varphi}\,\mathrm{d}\bar{\varphi} + qb\right] \\ &= pR\frac{\cos\varphi - \cos\varphi_0}{\sin^2\varphi} - q\frac{b}{R\sin^2\varphi}, \end{aligned}$$

where b is the radius of the parallel circle at the dome top. Since $b = R\sin\varphi_0$, we obtain

$$N_1 = \frac{1}{\sin^2\varphi}\left[pR(\cos\varphi - \cos\varphi_0) - q\sin\varphi_0\right]. \tag{14.15}$$

Substituting the above into Eq. (13.39), we obtain

$$N_2 = \frac{1}{\sin^2\varphi}\left[-pR\left(\cos\varphi\sin^2\varphi - \cos\varphi_0 + \cos\varphi\right) + q\sin\varphi_0\right]. \tag{14.16}$$

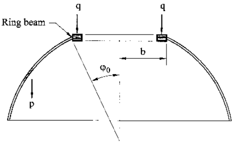

Fig. 14.3

(b) Spherical domes: live or snow loads

Live or snow loads are applied in such a way that they are uniformly distributed over the plan area of the shell surface as opposed to self-weight loading, which is uniformly distributed over the surface area. If q is the loading defined on the plan area, then referring to Fig. 14.4a, we can obtain an equivalent load p defined on the surface area from the following relationship ($\mathrm{d}s = R\mathrm{d}\varphi$):

$$pR\mathrm{d}\varphi = (qR\mathrm{d}\varphi)\cos\varphi \quad \text{or} \quad p = q\cos\varphi. \tag{14.17}$$

Thus, from Eqs (14.1), we obtain

$$p_3 = q\cos^2\varphi, \quad p_1 = q\sin\varphi\cos\varphi. \tag{14.18}$$

Substituting these values into Eq. (13.38) and again setting $R_1 = R_2 = R$ and $r = R\sin\varphi$, we have

$$N_1 = -\frac{1}{R\sin^2\varphi}\int_0^{\varphi} qR^2\left(\sin^2\bar{\varphi}\cos\bar{\varphi} + \cos^3\bar{\varphi}\right)\sin\bar{\varphi}\mathrm{d}\bar{\varphi}.$$

Evaluating this integral yields the following expression for the meridional force:

$$N_1 = -\frac{qR}{2}. \tag{14.19}$$

Substituting this into Eq. (13.39) we obtain the circumferential force:

$$N_2 = -\frac{qR}{2}\cos 2\varphi. \tag{14.20}$$

The meridional and circumferential forces distributions are shown in Fig. 14.4b. Referring to these diagrams, we can see that N_1 is compressive throughout the dome, from $\varphi = 0°$ to $\varphi = 90°$, while N_2 is a tensile force beyond $\varphi = 45°$.

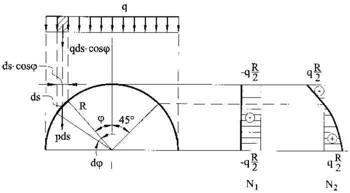

(a) (b)

Fig. 14.4

14.1.2 Conic roofs: axisymmetric loading

Consider a planetarium dome that may be approximated as an edge-supported truncated cone. We derive expressions for the circumferential and meridional forces for two conditions of loading: (a) self-weight of the shell per unit area of its middle surface (Fig. 14.5a) and (b) snow load uniformly distributed over the shell plan (Fig. 14.5b). Both types of loading are axisymmetric.

For the analysis of this dome under its self-weight, we use the equations derived in Sec. 13.6.2 for conical shells. For the axisymmetric loading, these equations are simplified – namely, $S = 0$ – and the remaining membrane forces are functions of the s coordinate only. The circumferential force N_2 is given by Eq. (13.60). We have the following:

$$N_2 = -p_3 s \cot\varphi, \tag{14.21}$$

where the coordinate s defines the distance of a point of the middle surface measured from the vertex along the generator of the shell, as shown in Fig. 14.5a.

Substituting for N_2 from Eq. (14.21) into the first Eq. (13.58) and setting $S = 0$, we obtain the following expression for the meridional force N_1:

$$N_1 = -\frac{1}{s}\left[\int (p_1 + p_3 \cot\varphi) s\,\mathrm{d}s + C\right], \tag{14.22}$$

where C is a constant of integration. Substituting for p_1 and p_3 from Eq. (14.1) into Eq. (14.22), yields the following:

$$N_1 = -\frac{p}{s}\int_{s_0}^{s} (\sin\varphi + \cos\varphi\cot\varphi)\bar{s}\,\mathrm{d}\bar{s} + \frac{C}{s}. \tag{14.23}$$

As no force acts at the top edge of the shell, $C = 0$ and we obtain

$$N_1 = -\frac{p}{s}\int_{s_0}^{s} \frac{\bar{s}}{\sin\varphi}\,\mathrm{d}\bar{s}.$$

and, finally,

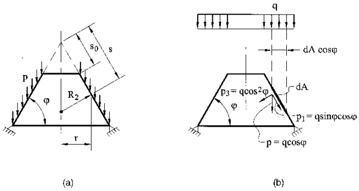

Fig. 14.5

$$N_1 = -\frac{p}{2s}\frac{s^2 - s_0^2}{\sin\varphi}. \tag{14.24}$$

The circumferential force N_2 may be determined from Eq. (14.21) by substituting $p_3 = p\cos\varphi$. We have

$$N_2 = -ps\frac{\cos^2\varphi}{\sin\varphi}. \tag{14.25}$$

To analyze the force components due to the snow load q, defined on the plan area, we use the relations (14.18) to determine the equivalent load components defined on the surface area. Substituting the above relations into Eq. (14.22) yields

$$N_1 = -\frac{1}{s}\int(q\sin\varphi\cos\varphi + q\cos^2\varphi\cot\varphi)s\mathrm{d}s + \frac{C}{s}. \tag{14.26}$$

Evaluating this integral gives the following expression for the meridional force:

$$N_1 = -\frac{qs}{2}\cot\varphi + \frac{C}{s}.$$

The condition that $N_1 = 0$ at $s = s_0$ leads to the following expression for C:

$$C = 0.5qs_0\cot\varphi.$$

Hence,

$$N_1 = -\frac{q}{2s}\left(s^2 - s_0^2\right)\cot\varphi. \tag{14.27}$$

The circumferential force N_2 may be found from Eq. (13.60) by substituting for p_3 from the first relation (14.18), as follows:

$$N_2 = -qs\frac{\cos^3\varphi}{\sin\varphi}. \tag{14.28}$$

The membrane stresses are obtained by dividing the membrane forces given by Eqs (14.27) and (14.28) by the shell thickness h.

14.1.3 Cylindrical shell roofs

Circular cylindrical shells, or ''barrel'' shells, are frequently used for roof structures. Such a roof structure represents an open cylindrical shell having two curvilinear and two straight edges, as shown in Fig. 14.6a. Cylindrical shell roofs may be supported along curvilinear edges by rigid arches, frames, or solid wall supports that are stiff against deformations in their own planes but that are nearly perfectly flexible for deformations perpendicular to their planes; such supports are called diaphragms. Along the rectilinear edges, these cylindrical shells are supported by the edge beams. The shell roof may be either dome-type convex or suspended membrane-type concave: the former is made of reinforced concrete and is used for relatively small spans, while membrane shell roofs are made of metal (e.g., steel, aluminum alloys) and can cover large span structures.

Consider a circular cylindrical barrel shell of length L under its self-weight (Fig. 14.6a). If p is the dead load per unit area of the shell surface, we can resolve it into components along the normal and circumferential directions.

We have

Thus,

$$f_1(\theta) = \frac{L}{2}F(\theta) + C. \tag{14.33}$$

For a given constant loading along x, we expect that the membrane forces N_1 and N_2 will be symmetrical, while S will be inversely symmetrical about the shell midspan, i.e., at $x = L/2$. Thus,

$$S = 0|_{x=L/2} \tag{14.32b}$$

Substituting for p_3 and p_2 from Eq. (14.29) into Eq. (14.31), we obtain

$$F(\theta) = p\sin\theta + \frac{p}{R}R\sin\theta = 2p\sin\theta, \tag{14.34}$$

and inserting the above together with Eq. (14.33) into the second Eq. of (14.30), we can write the expression for S in the following explicit form:

$$S = -2px\sin\theta + \frac{L}{2}2p\sin\theta + C = 2p\sin\theta\left(\frac{L}{2} - x\right) + C. \tag{14.35}$$

Applying the condition (14.32b), we obtain

$$C = 0.$$

Finally, all the membrane forces for the given loading may be represented in the form

$$N_1 = -\frac{px}{R}(L - x)\cos\theta; \quad N_2 = -pR\cos\theta; \quad S = 2p\left(\frac{L}{2} - x\right)\sin\theta. \tag{14.36}$$

The variation of N_1, N_2, and S over the depth of the cross section x = L/4of the semicircular barrel shell under self-weight is shown in Fig. 14.6b.

It follows from Eqs (14.36) that $N_2 = 0$ at $\theta = \pm\pi/2$. However, the shear force S does not vanish on the straight edges of the shell, as it is required there for the free edges. Figure 14.6a shows the variation of the membrane shear forces S from $x = 0$ to $x = L$ at the edge $\theta = \pi/2$. From this diagram, it is seen that these edge forces are self-equilibrating. To resist these forces, the edge members are employed. The latter are loaded by forces equal and opposite to the edge forces on the shell, i.e., S. Since the edge shell is compressed by the shear forces S, the edge member is stressed in tension only (Fig. 14.6a). Thus, the edge members are subjected to tensile axial loads $2p(L/2 - x)$ (for $\theta = \pi/2$) and they have free ends at the diaphragm supports. This tensile loading is balanced by the internal axial forces $T(x)$, which are zero at $x = 0$, L and may be found from the free-body diagram of the part of this edge member. We obtain from equilibrium the following expressions:

$$T(x) = \int_0^x 2p\left(\frac{L}{2} - x\right)\mathrm{d}x = 2p\left(\frac{L}{2}x - x^2\right).$$

This force has a maximum at $x = L/2$, which is given by

$$T_{\max} = \frac{pL^2}{4}.$$

The total compressive force on the cross section of the shell at $x = L/2$ may be obtained by substituting $x = L/2$ into the first Eq. (14.36) and integrating over the cross section. We have, at $x = L/2$,

$$R = 2\int_0^{\pi/2} N_1 R\mathrm{d}\theta = -\frac{pL^2}{2}\int_0^{\pi/2} \cos\theta\mathrm{d}\theta = -\frac{pL^2}{2}.$$

It is seen that this unbalanced compressive force on the shell cross section is balanced by the tensile forces $T_{\max}$ in the two edge beams, which must be provided. Similarly, equilibrium will be satisfied on any other section along the shell span. Thus, a semicircular barrel shell can support dead load under membrane conditions if the tension edge members are provided at their bottom edges. However, the membrane conditions are not satisfied because of the incompatibility of deformations at the shell edges. Indeed, as follows from the first Eq. (14.36), $N_1 = 0$ at $\theta = \pm\pi/2$. On the other hand, the edge member has tensile forces $T(x)$, which will cause it to extend in the axial direction. Moreover, due to its own weight, the edge member will tend to deflect vertically. These deflections will be different from the vertical deformations of the shell and edge members. The membrane theory alone cannot eliminate these incompatibilities of deformations and must be complemented by the bending theory (see Chapter 15).

When a cylindrical shell cross section has edges with an angle θ different from 90° (e.g., less than 90°), there arise further complications associated with an application of the membrane theory. In fact, in this case, N_2 (see the second Eq. of (14.36)) will now be nonzero at the longitudinal edges. Thus, the edge member has to resist both N_2 and S forces from the shell edges. This gives rise to further incompatibilities of deformation and requires an application of the bending theory of shells.

The procedure for the membrane analysis of cylindrical shells under self-weight described above is a particular case of a more general approach based on a Fourier series expansion. The governing differential equations for the membrane forces in cylindrical shells are given by Eqs (13.50). These equations have constant coefficients in x and, hence, they can be solved by representing solutions in the form of cosine and sine functions in x.

For barrel shells having simply supported edges $x = 0$ and $x = L$, which are commonly constructed as roof structures, the solutions of Eqs (13.50) can be represented as follows:

$$N_1 = \sum_{n=1}^{\infty} N_{1n} \sin\frac{n\pi x}{L}, \quad S = \sum_{n=0}^{\infty} S_n \cos\frac{n\pi x}{L}, \quad N_2 = \sum_{n=1}^{\infty} N_{2n} \sin\frac{n\pi x}{L}. \qquad (14.37)$$

It can be shown that the above solutions satisfy the simply supported boundary conditions. The load components are also expanded into Fourier series in x. This can be done by assuming odd extensions of the loads in the interval $(0, L)$ (refer to Appendix B). Introducing Eqs (14.37) and the load expansions into Eqs (13.50), solutions for membrane stress resultants can be obtained (after solving the resulting ordinary differential equations).

14.1.4 Shell roofs in the form of an elliptic or hyperbolic paraboloid covering rectangular areas

Such a type of roof is commonly used for covering public and sports buildings. Elliptic and hyperbolic paraboloids, considered in this section, fall into the category of shells of translation introduced in Sec. 11.7.

At first, assume that an *elliptic paraboloid* covers a rectangular area with the dimensions $2a \times 2b$ and that it is subjected to a uniform vertical surface load of intensity $p_3 = p$ (Fig. 14.7a). The equation of the shell middle surface in this case can be represented as

$$z = f\left(\frac{x^2}{2a^2} + \frac{x^2}{2a^2}\frac{y^2}{2b^2}\right)y^2. \tag{14.38}$$

Taking into account, we obtain

$$\frac{\partial^2 z}{\partial x^2} = \frac{f}{a^2}, \frac{\partial^2 z}{\partial y^2} = \frac{f}{b^2}, \quad \text{and} \quad \frac{\partial^2 z}{\partial x \partial y} = 0.$$

Assume, for simplicity, that $\bar{p}_3 \approx p_3 = p$, i.e., the vertical surface load per unit area of the middle surface is approximately equal to the vertical load of the horizontal projection of the middle surface. Then, substituting the above into Eq. (13.78), yields the following:

$$\frac{1}{b^2}\frac{\partial^2 \Phi}{\partial x^2} + \frac{1}{a^2}\frac{\partial^2 \Phi}{\partial y^2} = -\frac{p}{f}. \tag{14.39}$$

Assume then that the shell edges are attached to supporting arches, so that the membrane forces N_1 and N_2 are zero and the vertical load is transmitted to the supports by means of the membrane shear forces. Express these boundary conditions in terms of the function Φ. Taking into account the relations (13.77) and (13.72), we can write the boundary conditions on the shell edges as follows:

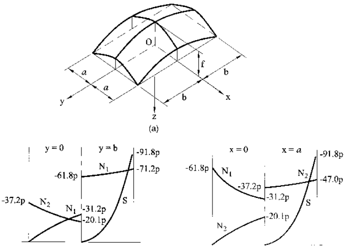

Fig. 14.7

$$
\begin{aligned}
\bar{N}_1 &= -\frac{4pa^2}{\pi f}\sum_n \frac{\sin(n\pi/2)}{n\cosh(n\pi/2)}\cos\alpha_n x\cosh\beta_n y,\\
\bar{N}_2 &= \frac{4pb^2}{\pi f}\sum_n \frac{\sin(n\pi/2)}{n\cosh(n\pi/2)}\cos\alpha_n x\cosh\beta_n y - \frac{pb^2}{f},\\
\bar{S} &= -\frac{4pab}{\pi f}\sum_n \frac{\sin(n\pi/2)}{n\cosh(n\pi/2)}\sin\alpha_n x\sinh\beta_n y.
\end{aligned}
\tag{14.45}
$$

Having determined the components of the horizontal projections of the membrane forces, we can calculate the membrane forces themselves using the relations (13.72).

Figures 14.7b and c show the membrane force diagrams for a shell with the following dimensions: $a = 25\,\mathrm{m}$, $b = 20\,\mathrm{m}$, and $f_x = f_y = 5\,\mathrm{m}$ (from Ref. [1]). It follows from these diagrams that the membrane shear forces increase very rapidly approaching infinity at the corner points. This testifies that the membrane theory alone cannot be applied near the corner points. However, the given formulas and relations describe quite accurately the stress state throughout the shell, except for comparatively small areas near the corner points. In addition, they indicate that these areas should be reinforced due to the presence of the bending and twisting moments.

A roof in the form of a *hyperbolic paraboloid,* covering the rectangular area, can be analyzed similarly. The equation of such surface is given by

$$z = f\left(\frac{x^2}{2a^2} - \frac{y^2}{2b^2}\right) \tag{14.46}$$

The governing differential equation for the function Φ will differ from Eq. (14.39) by the sign for the first term only, i.e.,

$$-\frac{1}{b^2}\frac{\partial^2\Phi}{\partial x^2} + \frac{1}{a^2}\frac{\partial^2\Phi}{\partial y^2} = -\frac{p}{f}. \tag{14.47}$$

Its solution can be represented in the form

$$\Phi = \sum_n C_n \sin\alpha_{n-1}x\cos\beta_{n-1}y - \frac{pb^2}{2f}x^2, \tag{14.48}$$

where

$$\alpha_{n-1} = \frac{\pi(n-1)}{2a}, \quad \beta_{n-1} = \frac{\pi(n-1)}{2b}; \quad n = 1, 3, 5, \ldots.$$

Here

$$C_n = -\frac{16pa^2b^2\left(1 - \cos\frac{n-1}{2}\pi\right)}{(n-1)^3\pi^3 f\cos\frac{n-1}{2}\pi}.$$

Having determined Φ, we can calculate $\bar{N}_1$, $\bar{N}_2$, and $\bar{N}_{12}$ as follows:

$$\begin{aligned}
\bar{N}_1 &= -\sum_n C_n \beta_{n-1}^2 \sin \alpha_{n-1} x \cos \beta_{n-1} y, \\
\bar{N}_2 &= -\sum_n C_n \alpha_{n-1}^2 \sin \alpha_{n-1} x \cos \beta_{n-1} y - \frac{pb^2}{f}. \\
\bar{N}_{12} &= \sum_n C_n \alpha_{n-1} \beta_{n-1} \cos \alpha_{n-1} x \sin \beta_{n-1} y
\end{aligned} \tag{14.49}$$

Roofs with hyperbolic paraboloid surfaces are commonly made as suspended shells, because in this shape the roof's state of stress is in good agreement with the momentless scheme of the analysis.

14.1.5 Asymmetrically loaded domes: wind loading

In the general case of asymmetrically loaded domes, the governing equations of the membrane theory of shells of revolution must be solved without the simplifications provided by the axisymmetric membrane theory. As an example of the application of the general membrane theory, we consider shells subjected to wind loads.

The value and distribution of the wind loading can be established by testing models of structures in wind tunnels. There are special standard relationships that allow us to determine the value and distribution of wind loading for commonly used types of structures.

It is usual to represent dynamic loading, such as wind and earthquake effects, by statically equivalent for the purposes of design. The wind load on shell structures is composed of pressure on the wind side and suction on the leeward side. Here the load component acting perpendicular to the middle surface p_3 is taken into account. The components p_1 and p_2 are due to the friction forces and are of negligible magnitude. Assuming, for the sake of simplicity, that the wind acts in the direction of the meridian plane $\theta = 0^\circ$, the components of the wind pressure are of the form [2]

$$p_1 = p_2 = 0, \;\; p_3 = p \sin\varphi \cos\theta, \tag{14.50}$$

where p represents the static wind pressure intensity. Figure 14.8 shows the distribution of the wind load given by Eq. (14.50) on a spherical dome.

The differential equation (13.23) for the wind loading, given by Eq. (14.50), has the following form (making $n = 1$):

$$\frac{1}{R_1 R_2 \sin\varphi} \frac{\mathrm{d}}{\mathrm{d}\varphi} \left(\frac{R_2^2 \sin\varphi}{R_1} \frac{\mathrm{d}U_1}{\mathrm{d}\varphi} \right) - \frac{U_1}{R_1 \sin^2\varphi} = F_1(\varphi), \tag{14.51}$$

where

$$F_1(\varphi) = -p\left[\frac{1}{R_1 R_2 \sin\varphi} \frac{\mathrm{d}}{\mathrm{d}\varphi} \left(R_2^3 \sin^3\varphi \cos\varphi \right) - R_2 \sin\varphi \right]. \tag{14.52}$$

$$N_1 = -\frac{p}{R_2^2 \sin^3 \varphi}\left[C_1 \int_{\varphi_0}^{\varphi} R_1 \sin \bar{\varphi} \mathrm{d}\bar{\varphi} + \int_{\varphi_0}^{\varphi} \Phi(\bar{\varphi}) R_1 \sin \bar{\varphi} \mathrm{d}\bar{\varphi} + C_2\right] \cos \theta, \qquad (14.58)$$

$$N_2 = -p\left\{R_2 \sin \varphi - \frac{1}{R_1 R_2 \sin^3 \varphi}\left[C_1 \int_{\varphi_0}^{\varphi} R_1 \sin \bar{\varphi} \mathrm{d}\bar{\varphi} + \int_{\varphi_0}^{\varphi} \Phi(\bar{\varphi}) R_1 \sin \bar{\varphi} \mathrm{d}\bar{\varphi} + C_2\right]\right\} \cos \theta. \qquad (14.59)$$

Knowing U_1, we can determine V_1 from the first Eq. (13.11). We have the following

$$\begin{aligned}\frac{\partial V}{\partial \theta} = -p_3 R_2^3 \sin^2 \varphi \cos \varphi - \frac{R_2^2 \sin \varphi}{R_1} \frac{\partial U}{\partial \varphi} = -p\Bigg\{ & R_2^3 \sin^3 \varphi \cos \varphi \\ & - \left[C_1\left(R_2 \sin \varphi - \cot \varphi \int_{\varphi_0}^{\varphi} R_1 \sin \bar{\varphi} \mathrm{d}\bar{\varphi}\right) + \Phi(\varphi) R_2 \sin \varphi \right. \\ & \left. - \cot \varphi \int_{\varphi_0}^{\varphi} \Phi(\bar{\varphi}) R_1 \sin \bar{\varphi} \mathrm{d}\bar{\varphi} - C_2 \cot \varphi\right]\Bigg\} \cos \theta.\end{aligned}$$

Taking into account the second relation (13.10), we obtain the following (again dropping the superscript 1 for the membrane shear force):

$$\begin{aligned}S = \frac{V}{R_2^2 \sin^2 \varphi} = -p\Bigg[& R_2 \sin \varphi - C_1\left(\frac{1}{R_2 \sin \varphi} - \frac{\cos \varphi}{R_2^2 \sin^3 \varphi} \int_{\varphi_0}^{\varphi} R_1 \sin \bar{\varphi} \mathrm{d}\bar{\varphi}\right) \\ & - \frac{\Phi(\varphi)}{R_2 \sin \varphi} + \frac{\cos \varphi}{R_2^2 \sin^3 \varphi} \int_{\varphi_0}^{\varphi} \Phi(\bar{\varphi}) R_1 \sin \bar{\varphi} \mathrm{d}\bar{\varphi} + \frac{C_2 \cos \varphi}{R_2^2 \sin^3 \varphi}\Bigg] \sin \theta.\end{aligned} \qquad (14.60)$$

The constants of integration, C_1 and C_2, are to be evaluated by assigning the membrane forces N_1 and N_2 on the upper edge of the shell, i.e., at $\varphi = \varphi_0$. Denoting these forces by $N_1^{(0)}$ and $S^{(0)}$, and letting $\varphi = \varphi_0$ in Eqs (14.58) and (14.60), we obtain the following expressions:

$$\begin{aligned}C_1 &= -\frac{1}{p}\left[N_1^{(0)}\left(R_2^{(0)}\right)^2 \sin \varphi_0 \cos \varphi_0 - S^{(0)} R_2^{(0)} \sin \varphi_0\right], \\ C_2 &= -\frac{\left[\left(R_2^{(0)}\right)^2 \sin^3 \varphi_0\right]}{p} N_1^{(0)}.\end{aligned} \qquad (14.61)$$

For domes closed at the vertex, we have $\varphi_0 = 0$ and $C_1 = C_2 = 0$.

As an example, let us determine the expressions for the membrane forces for a spherical dome of radius R (see Fig. 14.8). For this particular case, $R_1 = R_2 = R$, $\varphi_0 = 0$ and

$$
\begin{aligned}
\Phi(\varphi) &= R^2\left(\sin^2\varphi\cos\varphi - \int_0^{\varphi}\sin^3\bar{\varphi}\mathrm{d}\bar{\varphi}\right) = R^2[\sin^2\varphi\cos\varphi - (1-\cos\varphi) \\
&\quad + \frac{1}{3}(1-\cos^3\varphi)] \\
N_1 &= -\frac{pR}{\sin^3\varphi}\int_0^{\varphi}\left[\sin^3\bar{\varphi}\cos\bar{\varphi} - (1-\cos\bar{\varphi})\sin\bar{\varphi} + \frac{1}{3}(1-\cos^3\bar{\varphi})\sin\bar{\varphi}\right]\mathrm{d}\bar{\varphi}\cos\theta \\
&= -\frac{pR}{3\sin^3\varphi}\left[\sin^2\varphi(1+\sin^2\varphi) - 2(1-\cos\varphi)\right]\cos\theta, \\
S &= -\frac{pR}{3\sin^3\varphi}\left[2-\cos\varphi(2+\sin^2\varphi)\right]\sin\theta, \\
N_2 &= -\frac{pR}{3\sin^3\varphi}\left[\sin^2\varphi(2\sin^2\varphi-1) + 2(1-\cos\varphi)\right]\cos\theta.
\end{aligned}
\tag{14.62}
$$

It is seen from Eqs (14.62) that the maximum values of the membrane forces occur as follows:

- for the meridional forces, N_1, at $\varphi \approx \pi/4$ and $\theta = 0,\pi$;
- for the circumferential forces, N_2 at $\varphi = \pi/2$ and $\theta = 0,\pi$; and
- for the shear forces, S, at $\varphi = \pi/2$ and $\theta = \pi/2, 3\pi/2$.

At the top of the dome ($\varphi = 0$), all the membrane forces are zero. Figure 14.9 depicts the variations of N_1 and N_2 along the meridian $\theta = 0$ and the variation of S along the meridian $\theta = 90^\circ$.

14.2 MEMBRANE ANALYSIS OF LIQUID STORAGE FACILITIES

14.2.1 Introduction

Liquid storage facilities in the form of tanks, elevated water towers, cooling towers, etc., are widely used. They are made of steel or concrete and represent multishell structures, i.e., a combination of spherical, cylindrical, and conical shells, and

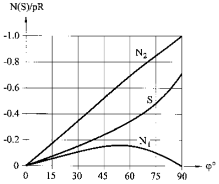

Fig. 14.9

circular plate, and circular rings located axisymmetrically. They are loaded axisymmetrically, to withstand water or gas pressure, dead or live loads, etc., or asymmetrically, for example, to withstand wind pressure. First, we consider the axisymmetric-type loading.

The walls of closed tanks designed for carrying liquids and gases are subjected to normal pressure forces p_3 (see Fig. 14.10). These forces consist of an excess pressure of gases p^* and the hydrostatic liquid pressure. The law of varying of the hydrostatic pressure over the tank depth can be expressed as

$$p_3 = -[p^* + \gamma_l(x - x^*)], \tag{14.63}$$

where γ_l is the specific weight of the liquid; x and x^* are the coordinates of parallels corresponding to the cross section of interest and the upper level of liquid, respectively. These coordinates are measured from a vertex of the tank or from its upper edge (Fig. 14.10).

Let us go from the x coordinate to the angular coordinate φ. Using the relationships

$$\frac{\mathrm{d}x}{\mathrm{d}r} = \tan\varphi, \quad \frac{\mathrm{d}r}{\mathrm{d}\varphi} = R_1\cos\varphi, \tag{14.64}$$

we find

$$\mathrm{d}x = \tan\varphi \mathrm{d}r, \quad x = \int_{\varphi_0}^{\varphi} \tan\bar{\varphi}\mathrm{d}r = \int_{\varphi_0}^{\varphi} R_1 \sin\bar{\varphi}\mathrm{d}\bar{\varphi} \tag{14.65}$$

and

$$x - x^* = \int_{\varphi_0}^{\varphi} R_1 \sin\bar{\varphi}\mathrm{d}\bar{\varphi} - \int_{\varphi_0}^{\varphi^*} R_1 \sin\bar{\varphi}\mathrm{d}\bar{\varphi} = \int_{\varphi^*}^{\varphi} R_1 \sin\bar{\varphi}\mathrm{d}\bar{\varphi}. \tag{14.66}$$

Substituting the above into Eq. (14.63), we obtain

$$p_3 = -\left[p^* + \gamma_l \int_{\varphi^*}^{\varphi} R_1 \sin\bar{\varphi}\mathrm{d}\bar{\varphi}\right], \tag{14.67}$$

where φ_0 and φ^* are the meridional angles corresponding to the coordinates $x = 0$ and $x = x^*$, respectively.

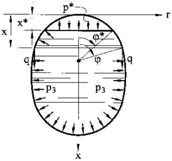

Fig. 14.10

$$N_1 = \frac{p^* R}{2} + \frac{\gamma_l R^2}{\sin^2 \varphi} \int_{\pi}^{\varphi} \cos \bar{\varphi} \sin \bar{\varphi} \mathrm{d}\bar{\varphi} \int_{\varphi^*}^{\varphi} \sin \bar{\varphi} \mathrm{d}\bar{\varphi} = \frac{p^* R}{2} + \frac{\gamma_l R^2}{6} \left(3 \cos \varphi^* + 2 \frac{1 + \cos^3 \varphi}{\sin^2 \varphi} \right) \tag{14.72}$$

It follows from Eq. (14.70) that, at the support, for $\varphi = \pi/2$, we derive

$$N_1^{'} = \frac{p^* R}{2} + \frac{\gamma_l R^2}{6} \cos^3 \varphi^*.$$

On the other hand, from Eq. (14.72), for $\varphi = \pi/2$, the meridional force is

$$N_1^{''} = \frac{p^* R}{2} + \frac{\gamma_l R^2}{6} (3 \cos \varphi^* + 2).$$

Thus, the value of the abrupt change in the meridional force at the support level in the diametrical plane is

$$\Delta N_1 = N_1^{''} - N_1^{'} = \frac{\gamma_l R^2}{6} (3 \cos \varphi^* + 2 - \cos^3 \varphi^*). \tag{14.73}$$

In particular, if the spherical tank is completely filled by a liquid only, i.e., $p^* = 0$ and $\varphi^* = 0$, then

$$\Delta N_1 = \frac{2}{3} \gamma_l R^2. \tag{14.74a}$$

Recalling that the volume of the sphere is $V = \frac{4}{3} \pi R^3$, we can rewrite Eq. (14.74a), as follows:

$$\Delta N_1 = \frac{V \gamma_l}{2 \pi R}. \tag{14.74b}$$

The above represents the meridional force, which balances the liquid weight filling the spherical tank. Thus, the meridional forces N_1 at the sphere portion $0 \leq \varphi < \pi/2$ are to be determined from Eq. (14.70) and at the portion $\pi/2 \leq \varphi \leq \pi$ from Eq. (14.72). The circumferential force N_2 is determined from Eq. (14.71) for both portions of the sphere, taking into account that N_1 for the upper and lower portions are given by Eqs (14.70) and (14.72), respectively. It is seen from the above equations that the maximum values of the meridional forces take place when the spherical storage tank is completely filled by a liquid.

Determine the limit of the second term in parentheses of Eq. (14.72) when $\varphi \to \pi$. Using the L'Hospital's rule, we obtain

$$N_1 \big|_{\varphi = \pi} = \frac{p^* R}{2} + \frac{\gamma_l R^2}{2} (1 + \cos \varphi^*). \tag{14.75}$$

With the use of Eq. (14.71), it will be easily established that

$$N_1 |_{\varphi = \pi} = N_2 |_{\varphi = \pi}.$$

The meridional and circumferential force, N_1 and N_2, diagrams for the spherical storage tank filled completely by a liquid of a specific weight γ_l are shown in Fig. 14.11.

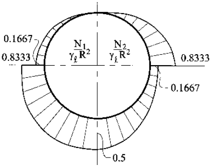

Fig. 14.11

Determination of the meridional and circumferential forces in the spherical tank caused by a *self-weight and snow loading* should present no problems. We denote the load intensity due to the self-weight and snow cover by q_1 and q_2, respectively. The latter will be assumed to be uniform at the portion from the tank vertex to the parallel that corresponds to some value $\varphi = \varphi_2$.

It follows from Eq. (14.1) and Eq. (14.10) that

$$p_1 = q \sin\varphi \quad \text{and} \quad p_3 = q\cos\varphi.$$

Substituting the above into Eq. (13.33b) and taking into account that for a closed spherical tank $R_1 = R_2 = R$ and $\varphi_0 = 0$ and $N_1^{(0)} = 0$, we obtain

$$N_{1q} = -\frac{qR}{\sin^2\varphi}\int_0^{\varphi} \sin\bar{\varphi}\,\mathrm{d}\bar{\varphi} = -\frac{qR}{\sin^2\varphi}(1-\cos\varphi). \tag{14.76}$$

Here, by q it is meant that $q = q_1 + q_2$ for $0 \le \varphi \le \varphi_2$ and q_1 for $\varphi_2 \le \varphi \le \pi/2$.

The meridional force at the lower portion of the tank is derived from Eq. (14.76). Assuming again that the reference point for angles φ is taken at the lower sphere vertex, we obtain

$$N_{1q} = -\frac{qR}{\sin^2\varphi}\int_{\pi}^{\varphi} \sin\bar{\varphi}\,\mathrm{d}\bar{\varphi} = \frac{qR}{\sin^2\varphi}(1+\cos\varphi). \tag{14.77}$$

Referring to Eqs (14.76) and (14.77) we can conclude that the meridional forces due to the self-weight are compressive over the sphere portion $0 \le \varphi \le \pi/2$, i.e., they are opposite in sign to the forces due to the internal excessive pressure. Over the sphere portion $\pi/2 \le \varphi \le \pi$, the meridional forces load the shell. It can be shown that the values of N_1 change abruptly for $\varphi = \pi/2$ and the amount of this change is equal to the weight of the sphere and snow load per unit the perimeter of the diametrical section of the sphere.

14.2.3 Cylindrical tank with bottom in the form of ellipsoid of revolution: axisymmetric loading

Assume that a cylindrical tank is filled by a liquid with a specific weight γ_l to the level x^* from the top of its cylindrical part, as shown in Fig. 14.12a. In addition, it is

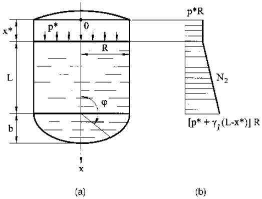

Fig. 14.12

subjected to the gas vapor pressure p^*. Hence, the total normal pressure is determined, as before, by Eq. (14.63). The origin of the coordinate x is taken at the top of the cylinder.

At first, we consider the cylindrical portion of the tank. For the cylinder, $R_1 = \infty$, $R_2 = R$ and from the third Eq. (13.7) and Eq. (14.63), it follows that

$$N_2 = R[p^* + \gamma_l(x - x^*)] \quad \text{for} \quad x \geq x^*. \tag{14.78}$$

The distribution of N_2 for the cylindrical portion of the tank is shown in Fig. 4.12b. As seen from this diagram, N_2 is constant and it equals p^*R over the cylindrical portion where the hydrostatic pressure of the liquid is absent. Then, this force varies according to the linear law of the rise of the hydrostatic pressure and reaches its maximum value at the lower edge of the cylinder. The value of the meridional force N_1 depends on the location of the tank supports. In any case, this force can be directly found from equilibrium of the portion of the cylinder intersected by a plane, perpendicular to the axis of the tank. So, if the tank is suspended at the upper edge of its cylinder, the meridional force is expressed

$$N_1 = \frac{p^*R}{2} + \frac{G_\Sigma}{2\pi R} \tag{14.79}$$

where, $G_\Sigma = G_q + G_l$; $G_q = \int_x^L q_t \mathrm{d}x$ is the self-weight of a portion of the tank located below the section of the interest; q_t is the self-weight of the tank per unit length; and G_l is the self-weight of a liquid filling the cylinder. If the tank is supported at the junction with the lower bottom, then

$$N_1 = \frac{p^*R}{2} - \frac{1}{2\pi R}\int_0^x q_t \mathrm{d}\bar{x}. \tag{14.80}$$

If q_t= const, then the meridional force is

$$N_1 = \frac{p^*R}{2} - \frac{q_t x}{2\pi R}. \tag{14.81}$$

$$N_{1\,\max} = N_{2\,\max}\big|_{\varphi=\pi/2} = \frac{R^2}{b}[p^* + \gamma_l(L+b)].$$

The meridional force, N_1, for the bottom is tensile. The circumferential force, N_2, for shallow bottoms changes its sign as it approaches the junction with the cylindrical portion of the tank, i.e., from a tensile force it becomes compressive. The meridional and circumferential force diagrams for a shallow bottom are shown in Fig. 14.13.

It should be kept in mind that at the transition from the cylindrical part of the tank to its bottom, the meridional curvature changes abruptly. The compatibility of deformations is achieved here owing to the occurrence of additional circumferential forces and bending moments. In this zone, called also ‘‘the edge effect zone,’’ the membrane shell theory can give significant errors. However, the moment state of stress will diminish quickly, as we go away from the junction. Therefore, the thickness of the wall for both the cylindrical portion of the tank and its bottom can be selected from the membrane shell theory. However, at the edge effect zone, the corresponding reinforcement of the tank is needed (e.g., this reinforcement can be provided by setting up a ring beam or sheets of larger thickness, etc.).

14.2.4 The axisymmetrically loaded Intze tank

Elevated tanks of different forms of shells of revolution serve for water storage in a city or town. These water tanks are made of steel or concrete. An economical form of these tanks that is commonly constructed is the *Intze tank,* which is shown schematically in Fig. 14.14a.

The Intze tank consists of a roof shell, cylindrical wall, conical shell, ring beam, bottom shell, and supporting structure. The tank is filled with a liquid up to the top of the cylindrical wall. We consider below the membrane analysis of the Intze tank made of concrete and shown in Fig. 14.14a. The Intze tank can be separated into the elementary shell components as mentioned above, shown in Fig. 14.14b. Each shell component will be treated as a membrane shell according to the general procedure introduced in Chapter 13.

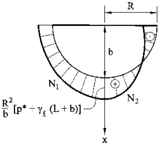

Fig. 14.13

jointly by the edge zones of the roof and the wall near the junction. A more accurate stress analysis of such a junction, including the moment shell theory, is given in the next chapter.

The water load acting on the cylindrical part of the tank causes the circumferential membrane forces only, $N_2^{(s)}$. It is equal to

$$N_2^{(s)} = \gamma_l a x, \tag{14.88a}$$

where γ_l is the water density. The maximum compressive meridional force $N_1^{(s)}$ occurs at the base of the cylinder and is

$$N_{1\max}^{(s)} = V_1 + \gamma_c h_s L, \tag{14.88b}$$

where γ_c and h_s are the concrete density and the wall thickness of the cylinder, respectively. The maximum circumferential force acts at the base of the cylinder. It is equal to

$$N_{2\max}^{(s)} = \gamma_l a L. \tag{14.88c}$$

Ring beam

At the top of the cone, the meridional compressive force $N_{1\max}^{(s)}$ is given by Eq. (14.88b). Neglecting the self-weight of the ring, this force is directly applied to the top of the cone, as shown in Fig. 14.14b. The above force can be resolved into a component along the cone, $N_1^{(c)} = N_{1\max}^{(s)}/\sin\beta$, and the horizontal component, $H_2 = N_{1\max}^{(s)}\cot\beta$. The latter component is resisted by the ring beam. The hoop tension in the ring beam is given by

$$T^{(r)} = H_2(a + d/2).$$

Conical shell

The conical shell is subjected to dead and water loads. The dead load consists of the self-weight of the conical frustum, W_c, and the total vertical load carried on top of the cone, which comes from the roof shell and the cylindrical wall, W_s. The above load components are

$$W_c = U_c h_c \gamma_c$$

where $U_c = \pi(a + r)\left[x^2 + (a - r)^2\right]^{1/2}$ $(0 \leq \times \leq l)$ is the volume of the frustum, h_c is the cone thickness, and r is the radius of the cone parallel circle of interest;

$$W_s = N_{1\max}^{(s)} 2\pi(a).$$

Then, the meridional force due to dead load and carried by the cone, $N_{1D}^{(c)}$, is given by

$$N_{1D}^{(c)} = -\frac{W_c + W_s}{2\pi r(\sin\beta)}. \tag{14.89a}$$

The circumferential force in the cone shell, $N_{2D}^{(c)}$ due to the dead load, can be obtained from the third Eq. (13.7) by letting $R_1 = \infty$ and $p_3 = \gamma_c h_c \cos\beta$.

The water load components are (using the coordinates s and β where s is measured along line OB starting from point O, as shown in Fig. 14.14b)

$$p_1 = 0, \quad p_3 = -\gamma_l[L + (S - s)\sin\beta]. \tag{14.90}$$

Substituting the above into Eq. (13.68), integrating, and using the boundary conditions for the case of water loading

$$N_{1W}^{(c)} = 0|_{s=S},$$

we obtain

$$N_{1W}^{(c)} = -\frac{\gamma_l \cot\beta}{6s}\left[2s^3 \sin\beta - 3s^2(L + S\sin\beta) + S^2(3L + S\sin\beta)\right]. \tag{14.89b}$$

The circumferential membrane force due to the water loading can be again obtained from Eq. (13.39) by letting $R_1 = \infty$ and substituting for p_3 from Eq. (14.90).

Bottom shell

The membrane forces, $N_{1D}^{(b)}$ and $N_{2D}^{(b)}$, due to dead load (the self-weight of the bottom shell) are readily obtained from Eqs (14.2) and (14.3).

Referring to Fig. 14.14b, we can find water load components, as follows:

$$p_1 = 0, \quad p_3 = \gamma_l[H_W + R(1 - \cos\varphi)],$$

where $H_W = L + f_2$ is the height of water above the top of the bottom shell. Substituting the above into Eq. (13.38), setting $R_1 = R$ and $r = R\sin\varphi$, and evaluating the integral, one obtains

$$N_{1W}^{(b)} = \frac{\gamma_l R}{6\sin^2\varphi}\left[-3H_W \sin^2\varphi + R(3\cos^2\varphi - 2\cos^3\varphi - 1)\right]. \tag{14.91}$$

The circumferential force due to water load, $N_{2W}^{(b)}$, can be obtained then from Eq. (13.39).

Finally the resultant membrane forces N_1 and N_2 from the cone and bottom shell are transmitted to the tank supports. The latter may have a variety of structures. For example, the tank may be supported on a circular ring beam (resisting the horizontal components of the cone meridional membrane force) that spans over a row of columns (resisting the vertical components of the membrane resultants). The membrane analysis of a supporting circular ring beam is quite similar to the analysis of the ring beam between conical and cylindrical shells given above.

14.2.5 Asymmetrically loaded liquid storage facilities: wind loading

In the operating conditions, liquid storage facilities (tanks, reservoirs, containers, etc.) and high-rise structures (chimneys, etc.) are subjected to unsymmetric, primarily, wind loading. In such facilities, which are not filled by liquid, as well as in high-rise structures, the wind loads can cause significant stresses and strains. If the material of these structures behaves elastically, then stresses and strains can be represented as a sum of two components. The first component corresponds to the beam state of stress of a shell with undistorted contour of its cross section. It is figured out using the well-known formulas of strength of materials [3]. The second term accounts for an additional state of stress due to the distortion of the shell cross-section contour. The ratio of these two terms depends on the geometric and rigidity parameters of a shell structure.

Wind loading is characterized by a little variation, which makes it possible to break down the general state of stress associated with a deformation of the contour of the shell cross section into pure membrane and moment (of the edge effect type) stress states. The former usually governs over the considerable part of the shell. Moreover, it determines particular solutions of the governing differential equations for the moment state of stress also. Therefore, a study of the character and value of the membrane stresses and strains due to static wind loading is of considerable interest in engineering practice. As mentioned previously, the value and law of distribution of the wind loading over the shell surface can be established by testing some models of circular cylindrical shells in wind tunnels. The experimental results obtained showed that the wind loading can be taken as a normal pressure to the shell at all points and it can be approximated by the following truncated Fourier series:

$$p_1 = p_2 = 0, \quad p_3 = p^* \sum_n p_n \cos n\theta, \tag{14.92}$$

where p^* is the maximum value of the face pressure. Wind tunnel experimental investigations showed that it is possible to be restricted by the three terms in the expansion (14.92), taking $p_0 = -0.7$, $p_1 = 0.5$, and $p_2 = 1.2$.

The distribution of the normal pressure p_3, based on the trinomial approximation mentioned above is shown in Fig. 14.15a. For not-too-high shells, one can assume the pressure to be constant along their generators. For high-level cylindrical shell structures, a variation of the wind pressure over the shell depth may be taken into account by replacing the given variable wind load with some equivalent constant load over the shell depth.

Let us consider a circular cylindrical reservoir of radius R and depth H. Assume that it is fixed at the base and is free from the shear and meridional force at the top. Then, taking the origin of the coordinate system at the shell top, we can write the above boundary conditions as follows:

$$S(\theta) = N_1(\theta) = 0\big|_{x=0}. \tag{14.93}$$

Directly from Eq. (13.52a) we obtain the expression for the membrane circumferential forces by letting $R_2 = R$:

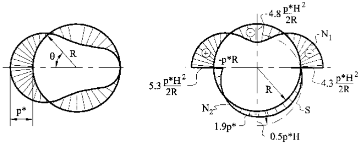

(a) (b)

Fig. 14.15

$$N_2 = -p_3 R = -p^* R \sum_n p_n \cos n\theta. \tag{14.94a}$$

Then, taking into account that $R_2 = R, p_2 = 0$, and $f_1(\theta) = 0$ (due to the boundary conditions described above), we obtain from Eq. (13.52b) the following:

$$S = -\int_0^x \frac{\mathrm{d}(-p_3 R)}{R\mathrm{d}\theta}\,\mathrm{d}\bar{x} = -p^* \cdot x \sum_n p_n n \sin n\theta \tag{14.94b}$$

From Eq. (13.52c) it follows that (letting $f_2(\theta) = 0$ and $p_1 = 0$)

$$N_1 = -\int_0^x \frac{1}{R}\frac{\partial S}{\partial \theta}\,\mathrm{d}\bar{x} = \frac{p^* x^2}{2R}\sum_n p_n n^2 \cos n\theta. \tag{14.94c}$$

In Eqs (14.94b) and (14.94c), the unknown functions $f_1(\theta)$ and $f_2(\theta)$ are equal to zero due to the prescribed boundary conditions (14.93). The diagrams of the membrane forces N_1, N_2, and S are shown in Fig. 14.15b at a section $x = H$. The circumferential force N_2 is a constant over the shell depth in the membrane theory. However, it should be noted that when we approach the supporting cross section, the bending affects the state of stress significantly. Consequently, the membrane forces N_1, N_2, and S are redistributed over the length and cross sections of the shell.

14.3 AXISYMMETRIC PRESSURE VESSELS

Pressure vessels are commonly used to resist internal pressure (pressurized liquids or gases). They are usually made of metals or composite materials. In such constructions, the stresses due to the self-weight of the vessel are negligible compared with the stresses due to the internal pressure.

Let us consider a pressure vessel in the form of a shell of revolution with an arbitrary shape of the meridian, which intersects the axis of revolution at a right angle (Fig. 14.16).

In this section, we determine the membrane forces due to the axisymmetric internal pressure, p. Thus, the applied load components are

$$p_1 = 0, p_2 = 0, \quad \text{and} \quad p_3 = -p.$$

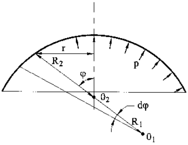

Fig. 14.16

Substituting the above into Eq. (13.38) and noting that $r = R_2 \sin\varphi$ and $\mathrm{d}r = \mathrm{d}s\cos\varphi = R_1 \mathrm{d}\varphi \cos\varphi$, we obtain the following expression for the meridional force:

$$N_1 = \frac{1}{R_2 \sin^2\varphi} \int_{r_0=0}^{r_0} p\bar{r}\mathrm{d}\bar{r} = \frac{pr^2}{2R_2 \sin^2\varphi},$$

or upon substituting $r = R_2 \sin\varphi$, we can simplify this expression, as follows:

$$N_1 = \frac{pR_2}{2}, \tag{14.95a}$$

which is valid for any shape of meridian. Now, using Eq. (13.39), we can determine N_2 as follows:

$$N_2 = pR_2\left(1 - \frac{R_2}{2R_1}\right). \tag{14.95b}$$

Let us now consider a *cylindrical pressure vessel* with *hemispherical heads* under an internal pressure p, as shown in Fig. 14.17.

For the spherical head with $R_1 = R_2 = R$, we obtain from the above

$$N_1 = N_2 = \frac{pR}{2}.$$

For the cylinder, we have $N_2 = pR$ and $N_1 = pR/2$. Determine the radial displacements of the two neighboring points A and B at the junction of the cylinder and sphere (see Fig. 14.17a). We have

$$\xi_c = R\varepsilon_2^{(\mathrm{C})} = \frac{R}{Et_{\mathrm{C}}}\left(N_2^{(\mathrm{C})} - \nu N_1^{(\mathrm{C})}\right) = \frac{pR^2}{2Et_C}(2-\nu). \tag{14.96a}$$

$$\xi_s = R\varepsilon_2^{(\mathrm{S})} = \frac{R}{Et_{\mathrm{S}}}\left(N_2^{(\mathrm{S})} - \nu N_1^{(\mathrm{S})}\right) = \frac{pR^2}{2Et_{\mathrm{S}}}(1-\nu) \tag{14.96b}$$

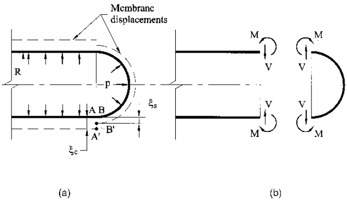

(a)

(b)

Fig. 14.17

where ξ_c and ξ_s are the radial displacements of the cylinder and sphere, respectively, at the above-mentioned neighboring points.

It follows from Eqs (14.96), that the radial displacement of the cylinder is greater than that of the sphere. Hence, in order to provide the compatibility of the radial displacements at the junction of the two shells, the shear forces, V, and bending moments, M, are to be applied at this junction, as shown in Fig. 14.17b. The situation becomes more complicated if we have a shallow spherical shell instead of a hemispherical shell as a head. In this case, the radial membrane force N_1 in the sphere, at the junction with the cylinder, has to be restricted by the cylinder as an edge load. Consequently, the displacement of the two shells is much greater and a ring beam needs to be provided at the junction to resist the radial membrane force N_1. The actual state of stress at the above junction will be discussed in detail in the next chapter.

A *toroidal shell* is also used for pressure vessels. A toroid is generated by the rotation of a closed curve about an axis passing outside. Figure 14.18a shows a shell in the shape of a toroid or doughut of circular section subjected to internal pressure p. The membrane force N_1 may be found from conditions of equilibrium of a shell segment shown in Fig. 14.18b, i.e.,

$$N_1(2\pi r)\sin\varphi = p\pi(r^2 - b^2),$$

from which

$$N_1 = \frac{p}{2}\cdot\frac{r^2 - b^2}{r\sin\varphi}.$$

Taking into account that $r = b + a\sin\varphi$, we represent N_1 in the form

$$N_1 = \frac{pa}{2}\frac{2b + a\sin\varphi}{b + a\sin\varphi}. \tag{14.97a}$$

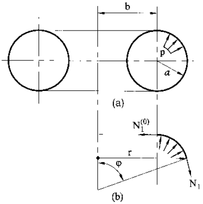

Fig. 14.18

The circumferential membrane force N_2 may be found from Eq. (13.39); substituting there $R_1 = a$, $R_2 = a + \dfrac{b}{\sin\varphi}$ and $p_3 = -p$, we have

$$N_2 = -\left(p_3 R_2 + N_1 \frac{R_2}{R_1}\right) = pR_2 - N_1 \frac{R_2}{R_1} = \frac{1}{2}pa. \tag{14.97b}$$

The radial displacement w can be determined in the usual fashion, i.e.,

$$w = r\varepsilon_2 = \frac{r}{Eh}(N_2 - \vartheta N_1).$$

However, if we try to calculate the longitudinal component of the displacement, which is parallel to the axis of the shell, u, one can show that the integral in the expression (13.43) diverges, since its integrand approaches infinity as φ goes to zero. It follows from the above that in the domain of the shell near a point $\varphi = 0$, the membrane theory does not describe the state of stress and strain of the toroidal shell, even loaded by a uniform pressure.

PROBLEMS

14.1 A hemispherical roof dome in Fig. 14.1 is subjected to its own weight. Assume that the dome is constructed of masonry having a radius of curvature $R = 40\,\mathrm{m}$. Determine the required thickness of the dome according to the maximum principal stress theory if the compressive ultimate stress $\sigma_u = 22\,\mathrm{MPa}$ and the factor of safety is 1.9.

14.2 A spherical roof dome in Fig. 14.2 is subjected to its own weight. Determine the required cross-sectional area of the thrust ring. Take $R = 35\,\mathrm{m}$, $\varphi_1 = 55^\circ$, and $h_s = 10\,\mathrm{cm}$ (thickness of the dome). Assume that the dome and the thrust ring are constructed of concrete with $\nu = 0.15$.

14.3 A planetarium dome may be approximated as an edge-supported truncated cone, as shown in Fig. 14.5b. It is subjected to a snow load with a maximum accumulation over the dome $q = 2.5\,\mathrm{kPa}$. Assume that the dome is constructed of 12 cm thick concrete having the radii of the parallel circles equal to 40 m at the base and 25 m at the top, respectively. Determine the membrane stresses in the dome.

14.4 A cooling tower may be approximated by a one-sheet hyperboloid of revolution (see Fig. 11.9f). The equation of its meridian is $r = \dfrac{a}{b}\sqrt{b^2 + z^2}$, where a and b are the parameters of the hyperbola. Determine the membrane forces, N_1 and N_2, distribution over the depth of the cooling tower under its own weight. Assume that the tower is made of concrete and $T = 22.0\,\mathrm{m}$, $S = 116.0\,\mathrm{m}$, $a = 51.5\,\mathrm{m}$, $b = 73.42\,\mathrm{m}$, and $h = 0.2\,\mathrm{m}$.
Hint: use cylindrical coordinates for the solution.

14.5 The four different dome configurations of the same height, $H = 0.5a$, are shown in Fig. P.14.1. The first dome is spherical with $R_0 = R = 1.25a$; the second dome is parabolic with $R_0 = a$; the third dome has the form of a semiellipsoid with $R_0 = 2a$ and $\gamma = 3$; and the fourth dome represents a segment of ellipsoid (the tangents of the dome meridian at its edges are not vertical) with $R_0 = 1.625a$ and $\gamma = 1.5$. All the four domes cover the same areas (of radius a) and they are made of concrete. (a) Find the meridional and circumferential forces distribution over the height of the above domes under their self-weight p in terms of a and p. (b) Determine the cross-sectional area of the thrust ring for all domes if the ring is assumed to be also made of the reinforced concrete. Take the thickness of the shell $h = a/50$ and $\nu_c = 0.15$. (c) Analyze

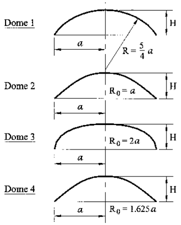

Fig. P14.1

and compare the states of stress of the four domes and on this basis select a more appropriate configuration of the dome. Justify your decision.

14.6 A circular cylindrical barrel shell of semicircular cross section is simply supported at $x = 0$ and $x = L$ (Fig. 14.6a). The shell is subjected to its self-weight p. The edge beams are employed along the rectilinear edges of the barrel shell to resist the membrane shear forces S. (a) Determine the membrane forces N_1, N_2, and S. (b) Select the required cross-sectional area of the edge beam if the shell and the above beam are made of an aluminum with $\sigma_y = 414\,\text{MPa}$, $\nu = 0.3$, and factor of safety is 2.0. Take $a = 10\,\text{m}$, $L = 30\,\text{m}$, and $h = a/100$. (c) Discuss the applicability of the membrane theory for the above barrel shell.

14.7 A horizontal circular pipe of radius a, length L, and thickness h, supporting its own weight, is made of concrete. (a) Determine the membrane forces distribution over the pipe length and over its cross section. (b) Determine the deflections $u, v,$ and w for section $x = L/2$. (c) Analyze the applicability of the membrane theory for the above shell. Take $p_1 = 0$, $p_2 = p \sin\theta$, $p_3 = p\cos\theta$, and $\nu = 0$. The boundary conditions are of the form: $N_1 = 0, v = 0|_{x=0, x=L}$.

14.8 A simply supported at ($x = 0$ and $x = L$) semicircular cylindrical shell (Fig. 14.6) is subjected to a snow load q which is uniformly distributed over its plane area. Given the radius of the shell is a, thickness is h, modulus of elasticity and Poisson's ratio are E and ν, respectively, determine the membrane stresses in the shell.

14.9 Show that the governing equation of the membrane theory for an elliptic paraboloid under the action of a symmetric normal surface loading p, Eq. (14.39), can be reduced to the following governing equation of torsion of the prismatic rod:

$$\frac{\partial^2 \Psi}{\partial \xi^2} + \frac{\partial^2 \Psi}{\partial \eta^2} = -2, \tag{P14.1}$$

where Ψ is the stress function, $\xi = x/a$, and $\eta = y/b$.

14.10 Using the results of Problem 14.9, determine the membrane forces in the shell roof approximated by an elliptic paraboloid of revolution on an equilateral triangular plan

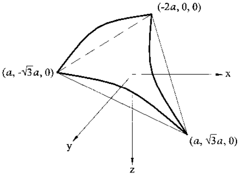

Fig. P14.2

(Fig P.14.2) due to a dead load p. Assume reasonable values for any additional properties and parameters required.
Hint: it is known from the theory of elasticity that the stress function Ψ for the torsion of the rod having a cross section in the form of an equilateral triangle is expressed in the following form:

$$\Psi = -\left[\frac{1}{6a}\left(x^3 - 3xy^2\right) - \frac{2}{3}a^2 + \frac{1}{2}(x^2 + y^2)\right]. \qquad \text{(P.14.2)}$$

14.11 An auditorium dome of span 350 ft is approximated by a spherical shell of radius 280 ft. The dome is simply supported at its ends. Determine the maximum membrane forces in the dome under the action of a wind pressure. The components of the wind pressure are given by Eqs (14.50) and $p = 15$ psf. Assume reasonable values for any additional properties required.

14.12 A circular cylindrical chimney shell of height L and radius R is subjected to a wind pressure p_3. The chimney shell is fixed at its base and free at the top. Assuming that the wind pressure is constant over the height of the chimney and in the circumferential direction is approximated by the polynomial $p_3 = p(-0.7 + 0.5\cos\theta + 1.2\cos 2\theta)$, determine the membrane forces in the shell.

14.13 A steel cylindrical pressure vessel with conical end caps is subjected to an internal pressure of $p = 1.5$ MPa, as shown in Fig. P.14.3. Using the membrane theory alone, determine the required thickness of the cylinder if the yield stress of the steel is 250 MPa. Where may additional strengthening be required?

14.14 The tank shown in Fig. P.14.4 has a cylindrical top and a conical bottom. The tank is supported by a structure (not shown) that applies only vertical forces around the parallel AB. The tank is filled to depth $H = 2.5R$ with water of weight density γ_l. Determine the expressions for the membrane forces just above and just below the parallel AB.

14.15 Redo Problem 14.14 replacing the conical bottom with a hemispherical bottom of radius R. Consider two cases: (a) the bottom convexity is directed down and (b) the bottom convexity is directed up.

14.16 The spherical tank is filled with water at a distance H from the top, as shown in Fig. P.14.5a. The tank is supported by the outlet pipe. Determine the expressions for the membrane forces if the radius of the tank is R and water density is γ_l
Hint: the volume of a spherical segment is $U = \frac{\pi l}{6}(3r_A^2 + 3r_B^2 + l^2), \quad 0 < l < 2R$.

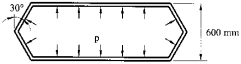

Fig. P14.3

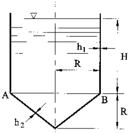

Fig. P14.4

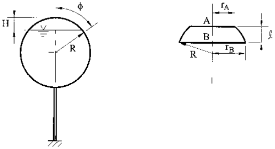

Fig. P14.5

14.17 A horizontal circular pipe of radius R, length l, and thickness h is subjected to internal gas pressure p. Determine the membrane stresses in the pipe if its ends are assumed to be built-in.

14.18 The Intze tank, shown in Fig. 14.14a, is filled with water up to the top of the cylindrical wall. The tank is made of concrete. The total load on the roof shell is taken as $p = 3.5$ kPa over its surface area. Determine (a) the membrane stresses in the roof shell, cylindrical wall, conical shell, and bottom shell; (b) the tension forces in the ring beam at the junction of the wall and cone, and in the supporting ring beam. Let $a = 7.6\,\text{m}$, $L = 7.2\,\text{m}$, $b = 4.8\,\text{m}$, $f_1 = 2.0\,\text{m}$, $f_2 = 1.3\,\text{m}$, $h_r = 95\,\text{mm}$, $h_s = 250\,\text{mm}$, and $h_b = 280\,\text{mm}$

14.19 A circular toroidal shell is subjected to internal pressure $p = 2.5\,\text{MPa}$, as shown in Fig. 14.18. The dimensions of the toroid are $a = 0.09\,\text{m}$, $b = 0.60\,\text{m}$, and $h = 1.8\,\text{mm}$. Determine the membrane stresses in the shell.

14.20 A spherical concrete dome having a span of $2a$ and height H ($H = 0.5a$) supports its own weight p. The ends of the dome have roller supports (they can freely displace in the horizontal direction). Determine (a) the horizontal displacements at the dome base and (b) the vertical displacement at its apex.

14.21 Redo Problem 14.20, except now assume that the dome is subjected to snow loading q.

REFERENCES

1. Novozhilov, V.V., *The Shell Theory* [translated from 2nd Russian edn by P.G. Lowe], Noordhoff, Groningen, The Netherlands, 1964.
2. Timoshenko, S.P. and Woinowsky-Krieger, S., *Theory of Plates and Shells*, 2nd edn, McGraw-Hill, New York, 1959.
3. Gere, J.M. and Timoshenko, S.P., *Mechanics of Materials*, 4th edn, PWS Publishing Company, Boston, 1997.

15

Moment Theory of Circular Cylindrical Shells

15.1 INTRODUCTION

The membrane theory of thin shells, discussed in previous chapters, is sufficient to analyze with a high degree of accuracy many commonly encountered loading conditions. However, at locations where the deflections are restricted, or there is a change in geometry, such as the cylindrical-to-spherical shell junction (see Sec. 14.7), the membrane theory is inadequate to maintain deflection and rotation compatibility between the shells. At these locations, discontinuity forces and moments are developed that result in bending and shear stresses in the shell. It should be noted that these bending and shear stresses are localized over a small area of the shell, and they dissipate rapidly along the shell. Many structures, such as shell roof structures, storage tanks, pressure vessels, missiles, etc., are designed according to the membrane theory and the total stress at discontinuities is determined from the membrane and moment theories. Thus, a complete analysis of various thin shell forms would require an appropriate moment theory, which is to be combined with the previously discussed membrane theory.

It should be noted that, due to the small thickness of the shell, even small bending moments cause large stresses in the shell. Therefore, it is very important to determine the bending stress–strain field correctly to insure a design reliability. The complete moment theory of thin shells is mathematically intricate. The governing differential equations of the moment theory of shells enable analytical or exact solutions only for some particular cases. Therefore, approximate shell theories were developed (see Chapter 17). The numerical methods, usually the finite element method (FEM), discussed in Chapters 6 and 18, were also applied for the moment analysis of thin shells.

We begin the moment analysis of thin shells with cylindrical shells. A cylindrical shell presents one of the most generally acceptable and optimal structural form of shells employed in engineering. A cylindrical shell, as mentioned previously, is successful in combining simplicity, compactness, and almost an ideal technological effectiveness. The latter enables one to develop items by usual rolling-up a given sheet skelps. Therefore, pattern cutting of a material and the subsequent process of manufacturing of a given structural form requires a minimum of technological effort. On the other hand, unlike the other shell forms – say, noncircular shells of revolution – the governing differential equations of the moment theory of a circular cylindrical shell of constant thickness represent a system of equations with constant coefficients, which gives us the possibility to analyzing their solutions in the general form.

15.2 CIRCULAR CYLINDRICAL SHELLS UNDER GENERAL LOADS

Here we will use the same coordinates x and θ as we did for the membrane theory of cylindrical shells (Fig. 11.13), where x is the distance of a point of interest from a datum plane normal to the generators (this plane usually coincide with one edge of the shell) and θ measures the angular distance of the point from a datum generator. In this case, the Lamé parameters are given by Eqs (11.53) and the principal radii of curvature are

$$R_1 = \infty, \quad R_2 = R. \tag{15.1}$$

The equilibrium equations of the general classical shell theory, Eqs.(12.41) and (12.42), and the relations (12.43), appear in the following form:

$$\begin{aligned} R\frac{\partial N_1}{\partial x} + \frac{\partial S}{\partial \theta} + p_1 R = 0, \\ \frac{\partial N_2}{\partial \theta} + R\frac{\partial S}{\partial x} - Q_2 - \frac{\partial H}{\partial x} + p_2 R = 0, \\ \frac{\partial Q_2}{\partial \theta} + R\frac{\partial Q_1}{\partial x} + N_2 + p_3 R = 0, \end{aligned} \tag{15.2}$$

$$\begin{aligned} \frac{\partial M_2}{\partial \theta} + R\frac{\partial H}{\partial x} - RQ_2 = 0, \\ R\frac{\partial M_1}{\partial x} + \frac{\partial H}{\partial \theta} - RQ_1 = 0. \end{aligned} \tag{15.3}$$

This system of five differential equations of equilibrium can be reduced to the following system of three equations, by eliminating the shear forces, Q_1 and Q_2, from Eqs (15.3):

$$\begin{aligned} R\frac{\partial N_1}{\partial x} + \frac{\partial S}{\partial \theta} + p_1 R = 0, \\ \frac{\partial N_2}{\partial \theta} + R\frac{\partial S}{\partial x} - \frac{1}{R}\frac{\partial M_2}{\partial \theta} - 2\frac{\partial H}{\partial x} + p_2 R = 0, \\ \frac{1}{R}\frac{\partial^2 M_2}{\partial \theta^2} + 2\frac{\partial^2 H}{\partial x \partial \theta} + R\frac{\partial^2 M_1}{\partial x^2} + N_2 + p_3 R = 0. \end{aligned} \tag{15.4}$$

Then, each solution of the equation

$$\Xi F = 0 \tag{15.18}$$

corresponds to an integral of the homogeneous equations (15.7), given by the expressions

$$u_0 = \frac{2}{1-\nu}\Xi_{13}F; \quad v_0 = \frac{2}{1-\nu}\Xi_{23}F; \quad w_0 = \frac{2}{1-\nu}\Xi_{33}F, \tag{15.19}$$

or using the explicit form of the symbols Ξ_{13}, Ξ_{23}, and Ξ_{33} from Eqs (15.9) and (15.12), we obtain

$$\begin{aligned}
u_0 &= \left\{ -\frac{\partial^3}{\partial\xi\partial\theta^2}. + \nu\frac{\partial^3}{\partial\xi^3} + a^2\left[\frac{(1+\nu)(2-\nu)}{1-\nu}.\frac{\partial^5}{\partial\xi^3\partial\theta^2} + \frac{1+\nu}{1-\nu}\frac{\partial^5}{\partial\xi\partial\theta^4} + 4\nu\frac{\partial^3}{\partial\xi^3} \right.\right. \\
&\quad \left.\left. + \frac{2\nu}{1-\nu}\frac{\partial^3}{\partial\xi\partial\theta^2} \right] \right\} F; \\
v_0 &= \left\{ (2+\nu)\frac{\partial^3}{\partial\xi^2\partial\theta} + \frac{\partial^3}{\partial\theta^3} - a^2\left[\frac{2(2-\nu)}{1-\nu}\frac{\partial^5}{\partial\xi^4\partial\theta} + \frac{4-3\nu+\nu^2}{1-\nu}\frac{\partial^5}{\partial\xi^2\partial\theta^3} + \frac{\partial^5}{\partial\theta^5} \right] \right\} F; \\
w_0 &= \left\{ \frac{\partial^4}{\partial\xi^4} + 2\frac{\partial^4}{\partial\xi^2\partial\theta^2} + \frac{\partial^4}{\partial\theta^4} + a^2\left[4\frac{\partial^4}{\partial\xi^4} + \frac{2(2-2\nu+\nu^2)}{1-\nu}\frac{\partial^4}{\partial\xi^2\partial\theta^2} + \frac{\partial^4}{\partial\theta^4} \right] \right\} F.
\end{aligned} \tag{15.20}$$

Substituting for the operators l_{ik} from the relations (15.9) into (15.12) and (15.18), we obtain the latter equation in the explicit form, as follows:

$$\begin{aligned}
&(1+4a^2)\frac{\partial^8 F}{\partial\xi^8} + 4(1+a^2)\frac{\partial^8 F}{\partial\xi^6\partial\theta^2} + \left[6 + a^2(1-\nu^2)\right]\frac{\partial^8 F}{\partial\xi^4\partial\theta^4} + 4\frac{\partial^8 F}{\partial\xi^2\partial\theta^6} + \frac{\partial^8 F}{\partial\theta^8} \\
&\qquad + (8-2\nu^2)\frac{\partial^6 F}{\partial\xi^4\partial\theta^2} + 8\frac{\partial^6 F}{\partial\xi^2\partial\theta^4} + 2\frac{\partial^6 F}{\partial\theta^6} + (1-\nu^2)\left(\frac{1}{a^2}+4\right)\frac{\partial^4 F}{\partial\xi^4} \\
&\qquad + 4\frac{\partial^4 F}{\partial\xi^2\partial\theta^2} + \frac{\partial^4 F}{\partial\theta^4} = 0.
\end{aligned} \tag{15.21}$$

Thus, the problem is reduced to funding solutions of one single eighth-order differential equation (15.21) and the function F can be considered as a potential function for the integration of the homogeneous equations (15.7). Solving Eq. (15.21), we can determine the function F and then, using the relations (15.20), find the complementary solutions, u_0, v_0, and w_0. The particular solutions for nonhomogeneous equations (15.7), u_1, v_1, and w_1, can be reduced to determining the particular integrals for the nonhomogeneous equations (15.13). In many cases, the particular solutions can be obtained from the membrane theory introduced in Chapter 13.

ordinary linear differential equation with constant coefficients. We present this equation for the function F_n:

$$d_n(F_n) \equiv (1+4a^2)\frac{\mathrm{d}^8 F_n}{\mathrm{d}\xi^8} - 4(1+a^2)n^2\frac{\mathrm{d}^6 F_n}{\mathrm{d}\xi^6} + \Bigg[6n^4 + a^2(1-\nu^2)n^4. - (8-2\nu^2)n^2$$

$$+ (1-\nu^2)\left(\frac{1}{a^2}+4\right)\Bigg]\frac{\mathrm{d}^4 F_n}{\mathrm{d}\xi^4} - 4n^2(n^2-1)^2\frac{\mathrm{d}^2 F_n}{\mathrm{d}\xi^2} + n^4(n^2-1)^2 F_n = 0. \tag{15.24}$$

Its solution can be represented in the form

$$F_n = A\mathrm{e}^{\lambda\xi} \quad (A = \text{const}).$$

Inserting the above into Eq. (15.24) and neglecting small quantities of the order of a^2 in comparison with those of order unity in its coefficients, yields the following characteristic equation for determining roots λ:

$$\lambda^8 - 4n^2\lambda^6 + 6n^4\lambda^4 - (8-2\nu^2)n^2\lambda^4 + (1-\nu^2)a^{-2}\lambda^4 - 4n^2(n^2-1)^2\lambda^2 + n^4(n^2-1)^2 = 0. \tag{15.25}$$

The detailed investigation of the roots of this equation and the corresponding analysis of the state of stress and strain of closed cylindrical shells has been carried out by Gol'denveizer [1]. In particular, it was shown in the above reference that if $n \ll a^{-1/2} = \sqrt{12}R/h$, the roots of the characteristic equation are broken down into small ($|\lambda| \approx a^{1/2}n^2$) and large ($|\lambda| \approx a^{-1/2}$) roots. The above inequality holds for closed cylindrical shells having a large and an intermediate relative reduced lengths, L/R. The small roots correspond to the basic state of stress for the shell, described by the simplified equations of the semi-membrane theory of shells (Sec. 17.2). By the way, if the relative length is not too large, so that $L/R < \frac{0.8}{n^2}\sqrt{\frac{R}{h}}$, the membrane theory can also be applied to describe a slowly varying state of stress. The large roots correspond to the edge effect state of stress described by simplified equations introduced in Sec. 17.5. Both the approximate theories mentioned above are introduced and analyzed in Chapter 17.

If $n \geq a^{-1/2}$, the above division of the roots into the small and large is impossible. The above inequality holds for closed cylindrical shells having a small and very small reduced length L/R. These shells are in a complete state of stress, which cannot be uncoupled into the previously introduced elementary stress states. However, for an analysis of these shells under general loading, the Donnell–Mushtari–Vlasov approximate theory, introduced in Sec. 17.3, can be applied. According to that theory, the characteristic equation (15.25) may be simplified significantly. It has eight mutually complex conjugate roots of the form

$$\lambda_{1-4} = \pm p_1 \pm iq_1; \quad \lambda_{5-8} = \pm p_2 \pm iq_2,$$

where $p_1, q_1, p_2,$ and q_2 are real positive numbers. To eliminate the complex quantities, the arbitrary constants are replaced according to the following expressions:

$$\begin{aligned}&A_1=\frac{1}{2i}(C_1+iC_2);\quad A_2=-\frac{1}{2i}(C_1-iC_2);\quad A_3=\frac{1}{2i}(-C_3+iC_4);\\&A_4=\frac{1}{2i}(C_3+iC_4);\\&A_5=\frac{1}{2i}(C_5+iC_6);\quad A_6=-\frac{1}{2i}(C_5-iC_6);\quad A_7=\frac{1}{2i}(-C_7+iC_8);\\&A_8=\frac{1}{2i}(C_7+iC_8).\end{aligned}\tag{15.26}$$

Then, a solution of the homogeneous equation (15.24) can be represented, as follows

$$\begin{aligned}F_n&=\mathrm{e}^{p_1\xi}(C_1\sin q_1\xi+C_2\cos q_1\xi)+\mathrm{e}^{-p_1\xi}(C_3\sin q_1\xi+C_4\cos q_1\xi)\\&\quad+\mathrm{e}^{p_2\xi}(C_5\sin q_2\xi+C_6\cos q_2\xi)+\mathrm{e}^{-p_2\xi}(C_7\sin q_2\xi+C_8\cos q_2\xi).\end{aligned}\tag{15.27}$$

Equation (15.27) involves eight constants of integration. They are evaluated from the boundary conditions on the curvilinear shell edges for the expression of the potential function, including the complementary (Eq. (15.27) and particular solutions. As mentioned previously, the latter can be obtained from the membrane shell theory. The boundary conditions (four on each curvilinear shell edge) are formulated in terms of the three displacements u, v, w, slope ϑ_2, internal forces N_1, T_1, V_1, and moment M_1. Having determined these constants, we can then calculate the potential function, the displacements and, finally, using Eqs (15.6), the stress resultants and stress couples for a closed cylindrical shell under general loads. The problem of an analysis of the shell is completed if an axisymmetric and beam states of stress, corresponding to the harmonics $n=0$ and $n=1$ (previously eliminated from the consideration) are added.

15.2.2 Analysis of open cylindrical shells

Open circular cylindrical shells are commonly used in civil engineering for roof structures. The curvilinear edges of these shells rest upon some supporting elements in the form of solid diaphragms, tied arches, elevated gridwork, arched truss, etc. These supports are rigid for deformations in their own planes but are flexible for deformations outside their planes (Fig. 15.1).

Such cylindrical shells are sometimes referred to as barrel shells (see also Sec. 14.1.3). If the length of such a barrel shell (along its meridian) is L, the above boundary conditions are of the form

$$w=0;\quad v=0;\quad N_1=0;\quad \text{and}\quad M_1=0\big|_{\xi=0.\xi=L/R},\tag{15.28a}$$

or in terms of the displacement components,

$$w=0;\quad v=0;\quad \frac{\partial u}{\partial\xi}=0;\quad \text{and}\quad \frac{\partial^2 w}{\partial\xi^2}=0\bigg|_{\xi=0,\xi=L/R}.\tag{15.28b}$$

Then, using the first and second of Eqs (15.39), we can express N_2 in terms of N_1 and w:

$$N_2 = -\frac{Eh}{R} w + \nu N_1. \tag{15.42}$$

Substituting Eq. (15.42) and Eq. (15.39) into Eq. (15.41), and assuming that $h = \text{const}$, we obtain the following equation:

$$D \frac{\mathrm{d}^4 w}{\mathrm{d}x^4} + \frac{Eh}{R^2} w = p_3 + \frac{\nu}{R} N_1. \tag{15.43}$$

A more convenient form of this equation is shown below:

$$\frac{\mathrm{d}^4 w}{\mathrm{d}x^4} + 4\beta^4 w = \frac{1}{D}\left(p_3 + \frac{\nu}{R} N_1\right), \tag{15.44}$$

where,

$$\beta^4 = \frac{Eh}{4R^2 D} = \frac{3(1-\nu^2)}{R^2 h^2} \tag{15.45}$$

β is a geometric parameter of the dimension $[\text{length}]^{-1}$. Equation (15.44) or Eq. (15.43) represent the *governing differential equation of an axsymmetrically loaded circular cylindrical shell*.

It can be easily shown that Eq. (15.44) coincides with the governing differential equation of bending of a strip-beam cut off from the shell by two neighboring longitudinal sections θ and $\theta + \mathrm{d}\theta$ and resting on an elastic Winkler foundation [5] (shaded in Fig. 15.2). The elastic foundation for the strip-beam is the support part of the shell (not shaded in Fig. 15.2), resisting its deflections at the expense of the circumferential membrane forces N_2. These forces produce a projection in the normal direction that equals $N_2 \mathrm{d}\theta$, which can be interpreted as the reactive forces of the foundation.

The shear force Q_1 is given by

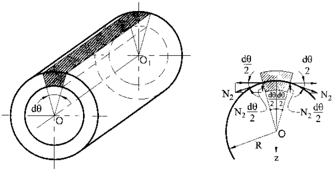

(a)

(b)

Fig. 15.2

$$w_p = 4\beta \int_0^x K[\beta(x-\xi)]\Phi(\xi)d\xi, \tag{15.51}$$

where

$$K(\beta x) = \frac{1}{4}(\cosh \beta x \sin \beta x - \sinh \beta x \cos \beta x) \quad \text{and} \quad \Phi(x) = \frac{p_3 R^2}{Eh} + \nu \frac{N_1 R}{Eh}.$$

The particular, w_p, and the complementary solutions of Eq. (15.44) can be interpreted as follows. The particular solution is the solution obtained by assuming the membrane action for the shell. This solution may not satisfy the prescribed boundary conditions of the shell. The complementary solution expresses the correction to the particular one, i.e., membrane solution, so that the prescribed boundary conditions can be satisfied for the sum of w_p and w_h.

The constants of integration, A_i, are evaluated from the boundary conditions assigned on the edges of a shell. Two boundary conditions are usually prescribed on any edge. Let us consider some typical boundary conditions for the closed cylindrical shell shown in Fig. 15.3.

(a) *The shell edge is built-in*.
In this case the boundary conditions are (Fig. 15.3a)

$$w = 0, \quad \frac{dw}{dx} = 0. \tag{15.52a}$$

(b) *The shell edge is simply supported*.
In this case the boundary conditions are (Fig. 15.3b)

$$w = 0, \quad \frac{d^2w}{dx^2} = 0 \quad (\text{since } M_1 = 0), \tag{15.52b}$$

(c) *The shell edge is free*.
The boundary conditions are, for this case (Fig. 15.3c),

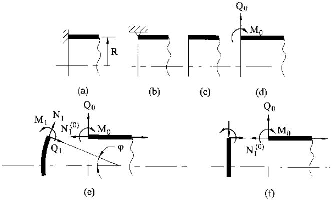

Fig. 15.3

$$\frac{d^2w}{dx^2} = 0 \quad (\text{since } M_1 = 0), \frac{d^3w}{dx^3} = 0 \quad (\text{since } Q_1 = 0). \tag{15.52c}$$

(d) *The shell edge is loaded by a given force* Q_0 *and moment* M_0 (Fig. 15.3d)
The boundary conditions for this case are of the following form:

$$-D\frac{d^2w}{dx^2} = M_0, -D\frac{d^3w}{dx^3} = Q_0. \tag{15.52d}$$

In the case of joining a cylindrical shell with a shell of another geometry (Fig. 15.3e), it is necessary to satisfy the following four boundary conditions (two conditions are required for each edge of the joining shells): equality of the deflections w or circumferential strains ε_2; equality of slopes dw/dx; equality of moments M_1; and equality of thrusts, i.e.,

$$(-N_1 \cos\varphi + Q_1 \sin\varphi)_h = (Q_0)_c, \tag{15.52e}$$

where the subscripts h and c refer to the head shell and cylindrical shell, respectively.

If a cylindrical shell is joined with the flat bottom (Fig. 15.3f), then the boundary conditions are somewhat simplified because the first condition of joining, due to the assumption of nonstretching the middle surface of the plate, has a form $w_0 = 0$, the fourth condition, (15.52e), is not needed.

15.3.1 Analysis of long cylindrical shells

To evaluate the constants of integration it is necessary to solve a system of four linear algebraic equations for four unknowns A_i $(i = 1, 2, 3, 4)$. However, for some practically important cases this procedure may be simplified. Consider a long thin cylindrical shell. Take the origin of the x axis at one of the shell edges. It is seen from Eq. (15.49) that the first two terms, which are multiplied by $e^{-\beta x}$ will diminish quickly as we go away from the edge $x = 0$. Hence, for a long cylinder, these first two terms have a negligible effect at the edge $x = L$ (where L is the length of the shell). The second two terms involving $e^{\beta x}$, in contrast, increase quickly. Taking into account that the deflections w for large values of x should be finite and small quantities, one can conclude that the constants A_3 and A_4 should be very small for the above-mentioned long shell. Thus, in the field located near the origin of the coordinates, the second two terms may be neglected, i.e., it is possible to set $A_3 = A_4 = 0$. Then, the solution becomes the following:

$$w = e^{-\beta x}(A_1 \sin\beta x + A_2 \cos\beta x) + w_p, \tag{15.53}$$

where A_1 and A_2 are constants of integration, to be determined from the boundary conditions at $x = 0$. The function w in the form of Eq. (15.53) is applicable for the shell field near its edge $x = 0$. For the field located near the opposite edge of the shell, $x = L$, the second two terms in Eq. (15.49) cannot be dropped because the factor $e^{\beta x}$ takes very large values. However, one can take a new origin of the coordinate system, locating it at the second edge of the shell and pointing the x axis out to the opposite side. Then, we can again employ the expression (15.53) and, evaluating new constants of integration A_1 and A_2, obtain the function w for the field located near the second edge of the shell.

Let us define more precisely the conditions under which a shell can be regarded as long. Assume that the permissible error of the shell stress analysis is, say, 5%. It can be easily shown that this requirement will be achieved if the following inequalities hold in this case (for $\nu = 0.3$):

$$\beta L \geq 3 \quad \text{or} \tag{15.54}$$

$$L \geq \frac{3}{\beta} = \frac{3}{\sqrt[4]{3(1-\nu^2)}}\sqrt{Rh} \approx 2.3\sqrt{Rh}, \quad \text{i.e.,} \quad L \geq 2.3\sqrt{Rh}. \tag{15.55}$$

Shells satisfying the above inequality will be referred to as *long,* or *semi-infinite shells,* and the error of approximate solutions, by using Eq. (15.53), will not be more than 5%.

Consider a long shell loaded by a uniform internal pressure $p_3 = -p = \text{const}$, an axial force $N_1^{(0)}$, and p_1, as well as the edge loads M_0 and Q_0, as shown in Fig. 15.4.

The boundary conditions for the shell edge $x = 0$ are of the form

$$-D\frac{d^2w}{dx^2} = M_0\bigg|_{x=0}; \quad -D\frac{d^3w}{dx^3} = Q_0\bigg|_{x=0}. \tag{15.56}$$

The general solution for the semi-infinite shell is taken in the form of Eq. (15.53). Substituting this solution into the conditions (15.56) yields the following values of the constants of integration:

$$A_1 = \frac{M_0}{2\beta^2 D}, \quad A_2 = -\frac{1}{2\beta^3 D}(Q_0 + \beta M_0).$$

Substituting the above constants into Eq. (15.53) yields the following equation for the deflections:

$$w = \frac{M_0}{2D\beta^2}e^{-\beta x}(\sin\beta x - \cos\beta x) - \frac{Q_0}{2D\beta^3}e^{-\beta x}\cos\beta x + w_p. \tag{15.57a}$$

Inserting the above into Eqs (15.39), (15.40), and (15.46), and letting $p_3 = -p$, we obtain

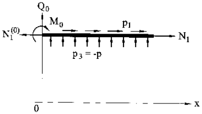

Fig. 15.4

$$\vartheta = \frac{\mathrm{d}w}{\mathrm{d}x} = \frac{M_0}{D\beta}\mathrm{e}^{-\beta x}\cos\beta x + \frac{Q_0}{2D\beta^2}\mathrm{e}^{-\beta x}(\cos\beta x + \sin\beta x) + \frac{\mathrm{d}w_p}{\mathrm{d}x}, \tag{15.57b}$$

$$M_1 = -D\frac{\mathrm{d}^2 w}{\mathrm{d}x^2} = M_0\mathrm{e}^{-\beta x}(\cos\beta x + \sin\beta x) + \frac{Q_0}{\beta}\mathrm{e}^{-\beta x}\sin\beta x - D\frac{\mathrm{d}^2 w_p}{\mathrm{d}x^2}, \tag{15.57c}$$

$$M_1 = -D\frac{\mathrm{d}^2 w}{\mathrm{d}x^2} = M_0\mathrm{e}^{-\beta x}(\cos\beta x + \sin\beta x) + \frac{Q_0}{\beta}\mathrm{e}^{-\beta x}\sin\beta x - D\frac{\mathrm{d}^2 w_p}{\mathrm{d}x^2}, \tag{15.57d}$$

$$Q_1 = -D\frac{\mathrm{d}^3 w}{\mathrm{d}x^3} = -2M_0\beta\mathrm{e}^{-\beta x}\sin\beta x + Q_0\mathrm{e}^{-\beta x}(\cos\beta x - \sin\beta x) - D\frac{\mathrm{d}^3 w_\mathrm{p}}{\mathrm{d}x^3}, \tag{15.57e}$$

$$N_2 = -\frac{Ehw}{R} + \nu N_1 = 2R\cdot\mathrm{e}^{-\beta x}\beta^2\left[M_0(\cos\beta x - \sin\beta x) + \frac{Q_0}{\beta}\cos\beta x\right] + p_0 R. \tag{15.57f}$$

The normal stress components are given by

$$\sigma_1 = \frac{N_1}{h} + \frac{12M_1}{h^3}z, \quad \sigma_2 = \frac{N_2}{h} + \frac{12M_2}{h^3}z. \tag{15.58}$$

Example 15.1

A long cylindrical shell is subjected to end moment m, as shown in Fig. 15.5a. Derive and plot the values of w and M_1 along the βx axis.

Solution

From Eqs (15.57), setting $M_0 = -m$, we have the following:

$$w = -\frac{m}{2D\beta^2}\mathrm{e}^{-\beta x}(\sin\beta x - \cos\beta x); \quad M_1 = -m\mathrm{e}^{-\beta x}(\cos\beta x + \sin\beta x).$$

On the loaded edge of the shell, $x = 0$, we obtain the following:

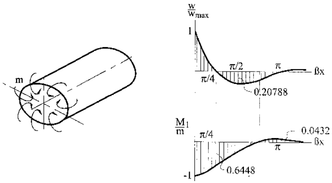

(a) (b)

Fig. 15.5

$$w|_{x=0} = w_{\max} = \frac{m}{2D\beta^2}; \quad M_1\big|_{x=0} = M_{1\,\max} = -m.$$

Figure 15.5b shows the plots of the deflections and moments in a dimensionless form over the shell length. It is seen that all these values practically diminish at a distance $x = 2.3\sqrt{Rh}$ from the loaded edge of the shell. Such a sharp decrease of the moment state components, as we move away from the loaded shell edge, is called the *edge effect*. It will be discussed in more detail later, in Sec. 17.5.

Example 15.2

Determine the stresses and deformations in a long thin-walled cylinder with a rigid end, as shown in Fig. 15.6a. The cylinder is subjected to an internal pressure of intensity p. Assume that $R = 1.2\,\text{m}$, $h = 0.01\,\text{m}$, $p_3 = -p = \text{const}$, and $\nu = 0.3$.

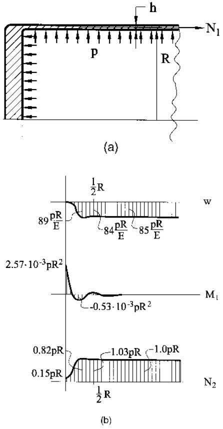
h
N1
p
R
(a)
½R
w
89 pR/E
84 pR/E
85 pR/E
2.57·10⁻³pR²
M1
-0.53·10⁻³pR²
0.82pR
0.15pR
1.03pR
1.0pR
N2
½R
(b)

Fig. 15.6

Solution

Since the end is absolutely rigid, the shell edge may be assumed to be built-in with the end, and the boundary conditions are given by Eqs (15.52a). Making $p_1 = 0$, we can find the meridional force at the edge $x = 0$ from the equilibrium of part of the shell cut off along the circle $x = \text{const}$. We have the following:

$$N_1^{(0)}(2\pi R) = p(\pi R^2), \text{ from which } N_1^{(0)} = \frac{pR}{2}.$$

Thus $N_1 = N_1^{(0)} = pR/2 = \text{const}$ and the particular solution (Eq. (15.50)) is of the form

$$w_{\mathrm{p}} = -\frac{pR^2}{Eh}(1 - \nu/2).$$

The geometric parameter is

$$\beta = \sqrt[4]{\frac{3(1-\nu^2)}{R^2h^2}} = 11.73(1/\mathrm{m}).$$

Substituting for w and $\vartheta = \mathrm{d}w/\mathrm{d}x$ from Eqs (15.57a) and (15.57b) into the boundary conditions (15.52a), we obtain the two following equations:

$$-\frac{M_0}{2D\beta^2} - \frac{Q_0}{2D\beta^3} - p\frac{R^2}{Eh}\left(1 - \frac{\nu}{2}\right) = 0; \quad \frac{M_0}{\beta D} + \frac{Q_0}{2\beta^2 D} = 0.$$

Solving these equations for M_0 and Q_0 gives

$$M_0 = \frac{p}{2\beta^2}\left(1 - \frac{\nu}{2}\right), \quad Q_0 = -\frac{p}{\beta}\left(1 - \frac{\nu}{2}\right).$$

Then, using Eqs (15.57), we can determine the following deflections, internal forces, and moments:

$$w = \frac{pR^2}{Eh}\left(1 - \frac{\nu}{2}\right)\left[\mathrm{e}^{-\beta x}(\sin\beta x + \cos\beta x) - 1\right],$$

$$N_2 = pR\left[1 - \left(1 - \frac{\nu}{2}\right)\mathrm{e}^{-\beta x}(\cos\beta x + \sin\beta x)\right],$$

$$M_1 = \frac{p}{2\beta^2}\left(1 - \frac{\nu}{2}\right)\mathrm{e}^{-\beta x}(\cos\beta x - \sin\beta x), \; M_2 = \nu M_1.$$

Figure 15.6b shows the diagrams of w, M_1, and N_2 along the shell length. The maximum bending moments occur at the junction of the shell and the head (at $x = 0$) and they are, as follows:

$$M_{1\max} = \frac{p}{2\beta^2}\left(1 - \frac{\nu}{2}\right) = 3.08 \times 10^{-3} p \ (\mathrm{Nm/m}),$$

$$M_{2\max} = \nu M_{1\max} = 0.924 \times 10^{-3} p \ (\mathrm{Nm/m}).$$

The tensile membrane forces at $x = 0$ are

$$N_1 = \frac{pR}{2} = 0.6p, \quad N_2 = pR(1 - (1 - \nu/2)) = 0.18p \ (\mathrm{N/m}).$$

The maximum normal stresses at outside points of the shell section located at the junction of the shell and head ($x = 0$) are the following:

$$\sigma_1 = \frac{6M_1}{h^2} + \frac{N_1}{h} = 184.8p + 60p = 244.8p \ (\mathrm{N/m^2}),$$

$$\sigma_2 = \frac{6M_2}{h^2} + \frac{N_2}{h} = 55.4p + 18p = 73.4p \ (\mathrm{N/m^2}).$$

At sections of the cylinder remote from the end, the bending moments vanish and the tensile membrane forces take the following values:

$$N_1 = \frac{pR}{2} = 0.6p, \quad N_2 = pR = 1.2p \ (\mathrm{N/m}).$$

The zone of the bending stresses is very small and at a distance of $R/16$ from the head, the bending stresses vanish.

Example 15.3

Determine the normal stresses in the cylinder of Example 15.2, (Fig. 15.6a), assuming that the flat end has a thickness comparable with the thickness of cylinder wall. Given: h (thickness of the cylinder wall) $= 0.01\,\mathrm{m}$, h_1 (thickness of the head) $= 0.04\,\mathrm{m}$, $R = 1.2\,\mathrm{m}$, $\nu = 0.3$, $E = 200\,\mathrm{GPa}$, and $p = \mathrm{const}$.

Solution

Separate mentally the cylinder and end into two independent components by taking a section at the point of intersection of the middle surfaces of the cylinder and end. This point may be regarded as a junction. Since the deformations of the independent components (cylinder and end) do not match each other at the junction, we have to apply unknown forces and couples, Q_0, M_0, and $N_1^{(0)}$, as shown in Fig. 15.7. These unknown forces and couples are to be determined from the compatibility conditions at the junction of the cylinder and end. We make the following reasonable assumption that stretching of the flat end may be neglected, i.e., the end is infinitely rigid for any in-plane deformations. Then, the compatibility conditions can be formulated as follows:

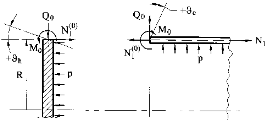

Fig. 15.7

$$w_c = 0\big|_{x=0}\ (a) \quad \text{and} \quad \vartheta_c\big|_{x=0} = \vartheta_h\big|_{r=R}\ (b), \tag{15.59}$$

i.e., the deflection of the cylinder at the junction is zero and the relative rotation of the wall of cylinder, ϑ_c, and flat end, ϑ_h, at the junction is also zero. The positive directions of the rotations are shown in Fig. 15.7. We have two equations and three unknowns. However, the meridional membrane force can be directly determined from the equilibrium conditions of the head, i.e.,

$$p(\pi R^2) = N_1(2\pi R), \quad \text{from which } N_1 = \frac{pR}{2}. \tag{a}$$

Deflections and slopes of the edge of the cylinder may be determined from Eqs (15.57) and (15.50) with regard to Eq. (a), as follows:

$$w_c\big|_{x=0} = -\left[\frac{M_0}{2D\beta^2} + \frac{Q_0}{2D\beta^3} + \frac{pR^2}{Eh}\left(1 - \frac{\nu}{2}\right)\right], \quad \vartheta_c\big|_{x=0} = \frac{M_0}{D\beta} + \frac{Q_0}{2D\beta^2}. \tag{b}$$

The angle of rotation of a normal of the end edge, ϑ_h, due to p and M_0 can be obtained by differentiating Eqs (4.26) and (4.38) with respect to r. Letting $p_0 = -p$ and $a = R$ in Eq. (4.26) and $b = 0$, $m_2 = 0$, and $m_1 = M_0$ in Eq. (4.39), yields, after differentiation the following expression for ϑ_h,

$$\vartheta_h\big|_{r=R} = \vartheta_h(p)\big|_{r=R} + \vartheta_h(M_0)\big|_{r=R} = \frac{pR^3}{8D_1(1+\nu)} - \frac{M_0 R}{D_1(1+\nu)}. \tag{c}$$

In writing this equation, it has been taken into account that the angles of rotation of normals to the end middle surface produced by p and M_0 have different signs (see Fig. 15.7) at the junction.

Substituting for w_c, ϑ_c, and ϑ_h from Eqs (b) and (c) into Eq. (15.59) yields the following equations for the unknowns M_0 and Q_0:

$$\frac{M_0}{2D\beta^2} + \frac{Q_0}{2D\beta^3} + \frac{pR^2}{Eh}\left(1 - \frac{\nu}{2}\right) = 0; \quad \frac{M_0}{D\beta} + \frac{Q_0}{2D\beta^2} = -\frac{M_0 R}{D_1(1+\nu)} + \frac{pR^3}{8D_1(1+\nu)} \tag{d}$$

where

$$\beta = 11.734\ (1/\text{m})\ (\text{see Example 15.2}),$$

$$D = \frac{Eh^3}{12(1-\nu^2)} = 18.315 \times 10^3 (\text{Nm}), \text{ and}$$

$$D_1 = \frac{Eh_1^3}{12(1-\nu^2)} = 1172 \times 10^3 (\text{Nm}).$$

Using the above numerical data, and solving Eqs (d) for M_0 and Q_0, yields the following:

$$M_0 = 0.04783p\ (\text{Nm/m}), \quad Q_0 = -0.5972 \times 10^{-2} p\ (\text{N/m}).$$

Note that for an absolutely rigid end, the bending moment at the junction was

$$M_1 = 0.00308p \ (\mathrm{Nm/m}).$$

Thus, because of the compliance of the flat end, the bending moment at the cylinder edge increases more than 10 times. This can be explained by the fact that the end is deflected as if it turns the edge of the cylinder inside out. The bending moment diagrams are shown in Fig. 15.8.

The maximum stresses at the center of the head are

$$\sigma_r = \sigma_t = \frac{6M_1}{h_1^2} = \frac{0.252p(6)}{4^2(10^{-4})} = 945p \ (\mathrm{N/m^2}).$$

The maximum stresses in the cylinder occur in the neighborhood of the edge. They are

$$\sigma_1 = \frac{pR}{2h} + \frac{6M_1}{h^2} = 2930p \ \mathrm{N/m^2}); \quad \sigma_2 = \nu\left(\frac{pR}{2h} + \frac{6M_1}{h^2}\right) = 879p \ (\mathrm{N/m^2}).$$

The tensile stresses in the cylinder away from the edge are

$$\sigma_1 = \frac{pR}{2h} = 60p, \quad \sigma_2 = \frac{pR}{h} = 120p \ (\mathrm{N/m^2}).$$

Example 15.4

A long thin-walled cylindrical shell is subjected to a circumferential line load P (force/length), as shown in Fig. 15.9. Determine the expressions for the deflections, internal forces, and bending moments.

Solution

Consider a free-body diagram of the small ring cut from the shell and enclosing the line load P, as shown in Fig. 15.10. For the right half of the cylinder, the following boundary conditions may be formulated from the symmetry of the loading:

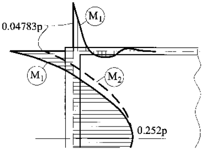

Fig. 15.8

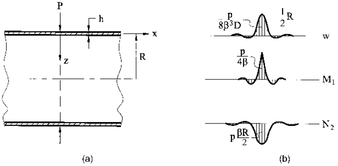
P
h
x
z
R
(a)
p
8β³D
l
2
R
w
p
4β
M₁
N₂
p βR
2
(b)

Fig. 15.9

$$\frac{\mathrm{d}w}{\mathrm{d}x} = 0\bigg|_{x=0}, \tag{15.60a}$$

$$Q_0 = -\frac{P}{2}\bigg|_{x=0} \quad \text{(see Fig. 15.10).} \tag{15.60b}$$

Substituting for $\mathrm{d}w/\mathrm{d}x$ from Eq. (15.57b) into Eq. (15.60a) yields

$$\frac{M_0}{\beta D} + \frac{Q_0}{2\beta^2 D} = 0,$$

or taking into account Eq. (15.60b), we obtain from the above $M_0 = \frac{P}{4\beta}$.

Inserting the above into Eqs (15.57), we obtain the following expressions for the deflections, internal forces, and bending moments:

$$w = \frac{P}{8\beta^3 D}\mathrm{e}^{-\beta x}(\sin\beta x + \cos\beta x), \tag{15.61a}$$

$$M_1 = \frac{P}{4\beta}\mathrm{e}^{-\beta x}(\cos\beta x - \sin\beta x),\ M_2 = \nu M_1, \tag{15.61b}$$

$$N_2 = -\frac{EhP}{8\beta^3 RD}\mathrm{e}^{-\beta x}(\sin\beta x + \cos\beta x),\ N_1 = 0. \tag{15.61c}$$

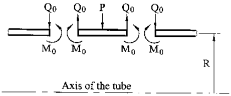
Q₀
Q₀
P
Q₀
Q₀
M₀
M₀
M₀
M₀
R
Axis of the tube

Fig. 15.10

The deflection, bending moment, and circumferential force diagrams are shown in Fig. 15.9b.

Expressions (15.61) may be used as Green's functions for determining the deflections, internal forces, and bending moments in long cylindrical shells subjected to radial loading uniformly distributed around the circumference of a shell, but arbitrarily distributed along the x axis (along the shell meridian), as shown in Fig. 15.11. For the use of w in the form of Eq. (15.61a) as Green's function, we rewrite it as follows:

$$w(x) = \frac{P}{8\beta^3 D} \cdot F(\beta x), \tag{15.62a}$$

where

$$F(\beta x) = \mathrm{e}^{-\beta x}(\sin \beta x + \cos \beta x). \tag{15.62b}$$

First, we assume that a point of observation A (point where the deflection is to be determined) is located outside the loaded region $p(\xi)$, as shown in Fig. 15.11a. Take the origin of the Cartesian coordinate system at a point A. The elementary deflection at point A caused by an elementary radial line load $p(\xi)\mathrm{d}\xi$ applied at a distance ξ from the origin is given by Eq. (15.62a), replacing P with $p\mathrm{d}\xi$, and x with ξ:

$$\mathrm{d}w_A = p(\xi)\mathrm{d}x \frac{F(\beta\xi)}{8\beta^3 D}.$$

The deflection at point A produced by the entire load is derived as follows:

$$w_A = \frac{1}{8\beta^3 D} \int_a^{a+L} p(\xi) F(\beta\xi) \mathrm{d}\xi, \tag{15.63}$$

which can be calculated once $p(\xi)$ is specified. Consider a particular case, $p = \text{const}$. Inserting Eq. (15.62b) into the above and letting $p = \text{const}$, we obtain the following after integration:

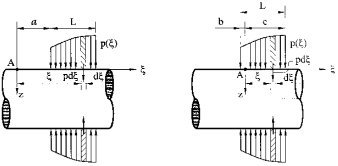

(a) (b)

Fig. 15.11

$$w_A = \frac{pR^2}{2Eh} \mathrm{e}^{-\beta a}\left[\cos \beta a - \mathrm{e}^{-\beta L} \cos \beta(a+L)\right]. \tag{15.64}$$

Secondly, locate the point of observation, A, within the loaded region, as shown in Fig. 15.11b. Let us take the origin of the Cartesian coordinates again at point A. An elementary deflection at that point owing to load $p\mathrm{d}\xi$ is given by Eq. (15.62). Thus, the resulting deflection at point A produced by the entire load can be again obtained by integration of Eq. (15.62). We have

$$w_A = \frac{1}{8\beta^3 D}\left[\int_0^b p(\xi)F(\beta\xi)\mathrm{d}\xi + \int_0^c p(\xi)F(\beta\xi)\mathrm{d}\xi\right]. \tag{15.65}$$

If $p = \text{const}$, then inserting Eq. (15.62b) into the above and putting $p = \text{const}$, we obtain the following after integration:

$$w_A = \frac{pR^2}{2Eh}\left[2 - \mathrm{e}^{-\beta b} \cos \beta b - \mathrm{e}^{-\beta c} \cos \beta c\right]. \tag{15.66}$$

Note that if the distance a is large and L is finite, then, as follows from Eq. (15.64), $w_A \approx 0$. This agrees well with the physical meaning. If b and c are large in Eq. (15.66), then the deflection will be approximately equal to pR^2/Eh, which represents the deflection of a long cylindrical shell subjected to an axisymmetrical uniform load of intensity $p = \text{const}$.

Example 15.5

A stiffening ring is placed around a long cylinder at a distance remote from the ends, as shown in Fig. 15.12a. The cylinder is subjected to an internal pressure of intensity p. The radius of the shell middle surface is R and the wall thickness is h. The ring dimensions are h_i (thickness of the ring) and b_i (the width of the ring). Determine the stresses at the ring attachment. Assume that the ring does not resist rotation, the dimensions of the ring cross section are small compared with the shell radius, and the shell and ring are made of one and the same material.

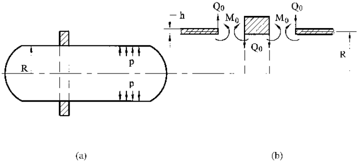

(a)

(b)

Fig. 15.12

Solution

Figure 15.12b shows the free-body diagram of the ring and adjacent parts of the cylinder walls. The contact forces and moments between the cylinder and ring are the shear force Q_0 and the bending moment M_0. Compatibility of the deflections for the shell, w_s, and for the ring, w_r, require that

$$w_s = w_r. \tag{a}$$

From symmetry, the angle of rotation of the shell, ϑ_s, due to the pressure and contact forces, Q_0, and moments, M_0, must be zero. So, the second compatibility equation is the following:

$$\vartheta_s = 0. \tag{b}$$

The deflection of the ring due to $2Q_0$ is

$$w_r = \frac{(2Q_0 R)R}{A_i E}, \tag{c}$$

where $A_i = b_i \cdot h_i$ is the cross-sectional area of the ring. The deflection of the shell due to the pressure and contact forces and moments is determined by Eq. (15.57a), as follows:

$$w_s = -\left[\frac{M_0}{2D\beta^2} + \frac{Q_0}{2D\beta^3} + \frac{pR^2}{Eh}\left(1 - \frac{\nu}{2}\right)\right]. \tag{d}$$

The signs for w_r and w_s due to the internal pressure and contact forces and moments are in an agreement with the general sign convention adopted in this book for the deflections w in thin shells. The angle of rotation of the shell due to the pressure and contact forces and moments at the ring attachment is determined by Eq. (15.57b) as follows:

$$\vartheta_s = \frac{\mathrm{d}w_s}{\mathrm{d}x} = \frac{M_0}{\beta D} + \frac{Q_0}{2\beta^2 D} \tag{e}$$

(it can be easily shown by inspection that M_0 and Q_0 produce rotation of the same signs).

Substituting for w_s and ϑ_s from Eqs (d) and (e) into Eqs (a) and (b), results in the following equations:

$$\begin{aligned} &\frac{2Q_0 R^2}{A_i E} = -\left[\frac{M_0}{2D\beta^2} + \frac{Q_0}{2D\beta^3} + \frac{pR^2}{Eh}\left(1 - \frac{\nu}{2}\right)\right], \\ &\frac{M_0}{\beta D} + \frac{Q_0}{2\beta^2 D} \end{aligned} \tag{f}$$

Solving this system of equations for M_0 and Q_0 gives the following:

$$M_0 = \frac{p}{2h\beta}\frac{1 - \nu/2}{(2/A_i + \beta/h)}, \quad Q_0 = -\frac{p}{h}\frac{1 - \nu/2}{(2/A_i + \beta/h)}. \tag{15.67}$$

Differentiating the above and using relations (15.75) leads to the following expressions for ϑ, M_1, and Q_1

$$\vartheta = -4\beta(w_0 - w_{\mathrm{p}0})V_4(\beta x) + (\vartheta_0 - w'_{\mathrm{p}0})V_1(\beta x) - \frac{1}{\beta}\left(\frac{M_{10}}{D} + w''_{\mathrm{p}0}\right)V_2(\beta x)$$

$$- \frac{1}{\beta^2}\left(\frac{Q_{10}}{D} + w'''_{\mathrm{p}0}\right)V_3(\beta x) + w'_{\mathrm{p}}, \tag{15.79}$$

$$M_1 = 4D\beta^2(w_0 - w_{\mathrm{p}0})V_3(\beta x) + 4D\beta(\vartheta_0 - w'_{\mathrm{p}0})V_4(\beta x) + (M_{10} + Dw''_{\mathrm{p}0})V_1(\beta x)$$

$$+ \frac{1}{\beta}(Q_{10} + Dw'''_{\mathrm{p}0})V_2(\beta x) - Dw''_{\mathrm{p}}, \tag{15.80}$$

$$Q_1 = 4D\beta^3(w_0 - w_{\mathrm{p}0})V_2(\beta x) + 4D\beta^2(\vartheta_0 - w'_{\mathrm{p}0})V_3(\beta x) - 4\beta(M_{10} + Dw''_{\mathrm{p}0})V_4(\beta x)$$

$$+ (Q_{10} + Dw'''_{\mathrm{p}0})V_1(\beta x) - Dw'''_{\mathrm{p}}. \tag{15.81}$$

The particular solution is determined by Eq. (15.50). If $p_3 = \mathrm{const}$ and $N_1 = \mathrm{const}$, then $w'_p = w_p{}'' = w'''_p = 0$.

Since two out of the four initial parameters are usually known from the boundary conditions on the shell edge $x = 0$, then the problem of evaluating the constants of integration is reduced to a solution of a system of algebraic equations for two unknowns. The latter is set up from the boundary conditions at the shell edge $x = L$ (where L is the shell length).

Example 15.6

Determine the equation of the deflected surface of a short cylindrical shell of radius R loaded by uniformly distributed moments m along the edge $x = L$, as shown in Fig. 15.13.

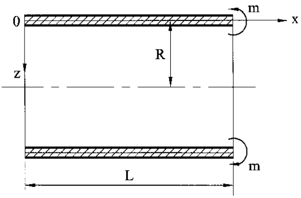

Fig. 15.13

Solution

Since for the edge $x = 0$, $M_1 = 0$, $Q_1 = 0$, and no transverse load is applied to the shell, then the deflection surface of the shell is of the form

$$w = w_0 V_1(\beta x) + \frac{1}{\beta}\vartheta_0 V_2(\beta x). \tag{a}$$

The initial parameters, w_0 and ϑ_0, may be evaluated from the boundary conditions on the edge $x = L$. The boundary conditions are

$$M_1 = m\big|_{x=L}, \quad Q_1 = 0\big|_{x=L}. \tag{b}$$

Inserting the expressions for the bending moment and shear force, Eqs (15.80) and (15.81), into the above, yields the following equations:

$$\begin{aligned} 4D\beta^2 w_0 V_3(\beta L) + 4D\beta\vartheta_0 V_4(\beta L) &= m, \\ 4D\beta^3 w_0 V_2(\beta L) + 4D\beta^2\vartheta_0 V_3(\beta L) &= 0. \end{aligned} \tag{c}$$

Solving these equations for w_0 and ϑ_0 gives

$$w_0 = -\frac{mV_3(\lambda)}{4D\beta^2[V_4(\lambda)V_2(\lambda) - V_3^2(\lambda)]}, \quad \vartheta_0 = \frac{mV_2(\lambda)}{4D\beta[V_4(\lambda)V_2(\lambda) - V_3^2(\lambda)]},$$

where $\lambda = \beta L$. Substituting the above into Eq. (15.78) gives the deflection surface of the short cylindrical shell loaded by a uniformly distributed moment m applied along the edge $x = L$:

$$w(x) = \frac{m}{4D\beta^2[V_4(\lambda)V_2(\lambda) - V_3^2(\lambda)}[-V_3(\lambda)V_1(\beta x) + V_2(\lambda)V_2(\beta x)]. \tag{15.82}$$

In a general case of loading, a cylindrical shell may be subjected to circumferential axisymmetric line loads P and moments m, respectively, as well as to uniform pressure p distributed over some shell length, as shown in Fig. 15.14. This shell can be divided into several segments (I, II, III, etc.) between sections where the loading conditions change. For each such segment, the function w will be different. To avoid the determination of a large number of constants of integration, it is convenient to set up a *general-purpose equation* of the middle surface of the shell which is continuous function of x throughout a shell in spite of the discontinuity of the loading diagram.

In setting up the general-purpose equation of the deflection surface of the shell, it should be taken into account that the function w and its first derivative should be continuous everywhere. The second derivative changes abruptly at sections where the radial moments m are applied, the third derivative may have a jump at sections where the radial forces P are applied, etc.

Dropping intermediate mathematics, we present below the general-purpose equation of the deflections for a cylindrical shell subjected to discontinuous loads, as shown in Fig.15.14:

$$
\begin{aligned}
w(x) = {} & (w_0 - w_{\mathrm{p}0})V_1(\beta x) + \frac{1}{\beta}(\vartheta_0 - w'_{\mathrm{p}0})V_2(\beta x) - \frac{1}{\beta^2}\left(\frac{M_{10}}{D} + w''_{\mathrm{p}0}\right)V_3(\beta x) \\
& - \frac{1}{\beta^2}\left(\frac{Q_{10}}{D} + w'''_{\mathrm{p}0}\right)V_4(\beta x) + w_{\mathrm{p}1}\Big|_{\mathrm{I}} - \frac{P}{D\beta^3}V_4[\beta(x - l_P)]\Big|_{\mathrm{II}} \\
& - \frac{m}{D\beta^2}V_3[\beta(x - l_m)]\Big|_{\mathrm{III}} + \left(-p + \frac{\nu N_1}{R}\right)\frac{R^2}{Eh}\left\{1 - V_1[\beta(x - l_N)]\right\}\Big|_{\mathrm{IV}},
\end{aligned}
\tag{15.83}
$$

where $w_{\mathrm{p}1}$ is a particular solution for the first segment; l_P, l_m, and l_N are the coordinates of an application of the applied line forces P, moments m, and meridional forces N_1, respectively. In a general case, a number of terms in Eq. (15.83) depend on a number of discontinuous loads applied to the shell. The signs of the terms adopted in this equation correspond to directions of loads indicated in Fig. 15.14 and to the sign convention for deflections used in this book. The initial parameters w_0, ϑ_0, M_{10}, and Q_{10} are determined, as usual, from the boundary conditions. Two of them are known for $x = 0$, the remaining two parameters are evaluated from the boundary conditions at the shell edge $x = L$.

Example 15.7

A short cylinder is loaded by two moments m uniformly distributed along circular sections $x = 2.5\,\mathrm{in.}$ and $x = 7.5\,\mathrm{in.}$, respectively, as shown in Fig. 15.15. Assuming that $R = 20\,\mathrm{in.}$, $h = 1\,\mathrm{in.}$, $\nu = 0.3$, and $L = 10\,\mathrm{in.}$, determine the equation of the deflected midsurface of the cylinder.

Solution

For the given data,

$$
\beta = \sqrt[4]{\frac{3(1-\nu^2)}{h^2R^2}} = \sqrt[4]{\frac{3(1-0.3^2)}{(1)^2(20)^2}} = 0.28741/\mathrm{in.}
$$

Taking the origin of the coordinate system at the left edge of the shell, we can write the general-purpose equation (Eq. (15.83)) for the problem under consideration:

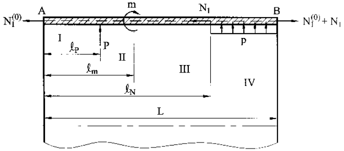

Fig. 15.14

where $D_0 = \text{const}$ is the flexural stiffness of the shell at some reference section, say, at $\xi = 0$; $D = D(x)$ is the flexural stiffness at a section of interest.

Applying the above-introduced dimensionless variables and parameters (Eqs (15.87)), one can represent Eqs (15.86) in the form

$$
\begin{aligned}
&\frac{1}{d\xi} = X_2, \quad \frac{\mathrm{d}X_2}{\mathrm{d}\xi} = -\frac{D_1}{D} X_3, \quad \frac{\mathrm{d}X_3}{\mathrm{d}\xi} = X_4, \\
&\frac{\mathrm{d}X_4}{\mathrm{d}\xi} = \frac{EhR^2}{D_0} X_1 - \frac{R^3}{D_0}\left(p_3 + \nu \frac{N_1}{R}\right).
\end{aligned} \tag{15.88}
$$

This system of first-order ordinary differential equations is equivalent to the fourth-order single differential equation (15.84). In turn, the former system may be written in the following matrix form:

$$
\frac{d\mathbf{X}}{d\xi} = \mathbf{A}(\xi)\mathbf{X} + \mathbf{f}, \tag{15.89}
$$

where

$$
\mathbf{X} = \begin{bmatrix} X_1 \\ X_2 \\ X_3 \\ X_4 \end{bmatrix} \tag{15.90}
$$

is the column vector that characterizes the parameters of the state of stress and strain at a section of interest and

$$
\mathbf{A} = \begin{bmatrix} 0 & 1 & 0 & 0 \\ 0 & 0 & -D_0/D & 0 \\ 0 & 0 & 0 & 1 \\ \frac{EhR^2}{D_0} & 0 & 0 & 0 \end{bmatrix}, \quad \mathbf{f} = \begin{bmatrix} 0 \\ 0 \\ 0 \\ -\frac{R^3}{D_0}\left(p_3 + \nu \frac{N_1}{R}\right) \end{bmatrix} \tag{15.91}
$$

are the square matrix (4×4) and the column vector of the right-hand sides, respectively. The system of differential equations (15.89) may be efficiently solved numerically using, for example, the sweep method [9] or Godunov's method of discrete orthogonalization [10].

Example 15.8

Consider a circular cylindrical shell of variable thickness under the action of pressure p. Two cases of variation of the shell thickness are analyzed: (a) $h_1 = h_0\left(-\frac{1}{c^2}x^2 + \frac{4}{3}\right)$ and (b) $h_2 = h_0 = \text{const}$, as shown in Fig. 15.16a and b, respec-

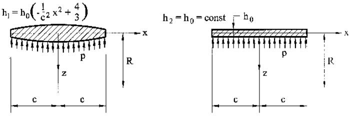
$h_1 = h_0\left(-\frac{1}{c^2}x^2 + \frac{4}{3}\right)$
x
p
z
R
c
c
$h_2 = h_0 = \text{const}$
h_0
x
p
z
R
c
c

(a) (b)

Fig. 15.16

tively. As this takes place, the area of an axial cross section for all the three shells is identical in the interval $-c \le x \le c$, i.e., the above shells are of the same weight. The parallel edges of the shells are simply supported. Assuming that $h_0 = 0.5$, $c = 20$, $R = 15$, and $\nu = 0.3$, determine the deflections, internal forces, and moments in the shell.

Solution

Since the shells and loading are symmetrical about $x = 0$, all the above problems are solved for the interval $0 \le x \le c$. Boundary conditions of the simply supported type for the shell edge $x = c$ and the symmetry conditions for the section $x = 0$ are prescribed. The numerical values of the components of the state of stress and strain are given in Table 15.1 for $h = h_1$. Analogous results are given in Table 15.2 for $h = h_2$. The system of ordinary differential equations (15.89) was solved by Godunov's method of discrete orthogonalization. From these tables it is seen how the thickness redistribution of the shell influences the state of stress and strain under the condition of the conservation of the shell weight. It makes it possible to select the most efficient parameters of shell structures.

Table 15.1

x	$(M_1/p) \times 10$	$(N_1/p) \times 10^{-1}$	Q_1/p	$(w/\frac{p}{E}) \times 10^{-3}$
0	-0.31633	0.40996	0	0.30976
2	-0.32035	0.40996	-0.39650×10^{-3}	0.31210
4	-0.33230	0.40996	-0.82848×10^{-3}	0.31931
6	-0.35740	0.40996	-1.18812×10^{-2}	0.33193
8	-0.42139	0.40996	-0.50151×10^{-2}	0.35117
10	-0.58015	0.40996	-0.11284×10^{-1}	0.37985
12	-0.86017	0.40996	-0.14980×10^{-1}	0.42531
14	-0.99610	0.40996	-0.97754×10^{-2}	0.50433
16	0.1056×10^{-1}	0.40996	0.10333	0.63605
18	0.29781	0.40996	0.14807	0.71609
20	0	0.40996	-0.73044	0

Table 15.2

x	M_1/p	N_1/p	Q_1/p	$(w/\frac{p}{E}) \times 10^{-3}$
0	0.13028×10^{-4}	0.42808×10	0	0.41154
2	0.31492×10^{-3}	0.42808×10	0.29494×10^{-3}	0.41153
4	0.10442×10^{-2}	0.42808×10	0.33756×10^{-3}	0.41140
6	0.82148×10^{-3}	0.42808×10	-0.91417×10^{-3}	0.41095
8	-0.44991×10^{-2}	0.42808×10	-0.48864×10^{-2}	0.41030
10	-0.18990×10^{-1}	0.42808×10	-0.97479×10^{-2}	0.41154
12	-0.27954×10^{-1}	0.42808×10	0.55193×10^{-2}	0.41935
14	0.39696×10^{-1}	0.42808×10	0.73855×10^{-1}	0.43480
16	0.30266	0.42808×10	0.18704	0.43047
18	0.65488	0.42808×10	0.82290×10^{-1}	0.31639
20	0	0.42808×10	-0.97407	0

This example has been taken from Ref. [10]

PROBLEMS

15.1 Indicate cases when the membrane theory alone cannot describe adequately the state of stress of cylindrical shells under applied transverse loading.

15.2 Verify Eqs (15.21) and (15.24).

15.3 What are the conditions at which a complete state of stress in open and closed cylindrical shells can be broken down into elementary states of stress? Characterize these elementary stress states.

15.4 A long steel pipe is subjected to the edge line load Q_0 that is applied uniformly around the circumference $x = 0$. The radius and thickness of the pipe are $R = 0.5\,\mathrm{m}$ and $h = 5\,\mathrm{mm}$, respectively. (a) Derive and plot the values of w and M vs. βx. (b) Determine the distance x at which the deflections and moments are 5% of their absolute maximum values. Take $E = 200\,\mathrm{GPa}$, and $\nu = 0.3$.

15.5 A very long cylinder of radius R and of thickness h is subjected to uniform loading p_0 over L of its length (Fig. 15.11) (a) Determine the ratio of maximum bending stress to maximum magnitude of membrane stress. (b) Calculate the deflections and bending moments at a point A for two cases of location of that point, as shown in Figs 15.11a and b. Take $R = 1.5\,\mathrm{m}$, $h = 6\,\mathrm{mm}$, $p_0 = 5\,\mathrm{kPa}$, $E = 200\,\mathrm{GPa}$, and $\nu = 0.3$.

15.6 Verify Eqs (15.57).

15.7 The infinite circular cylinder of radius R is subjected to a uniformly distributed around a circumference moment m, as shown in Fig. P.15.1. Assuming that the moment is applied near the center of the cylinder, find the expressions for w, ϑ, M_1, and Q_1 as functions of m and x.

15.8 A stiffening ring is placed around a long steel cylindrical shell at a distance remote from the ends, as shown in Fig. 15.12a. The cylinder is loaded by an internal pressure p_0. Determine stress at the ring attachment if: (a) the ring is assumed to be infinitely rigid and (b) the ring is assumed to be 100 mm wide and 10 mm thick. Take the radius of the cylinder as 1.25 m and its thickness as 6 mm, $p_0 = 10\,\mathrm{kPa}$, $E = 200\,\mathrm{GPa}$, and $\nu = 0.3$.

15.9 Determine stresses in a cylindrical component reinforced by a ring and subjected to internal pressure $p = 4$ MPa (Fig. P.15.2). All dimensions in Fig. P.15.2 are given in mm. Take $E = 200\,\mathrm{GPa}$, and $\nu = 0.3$.

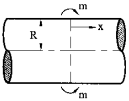

Fig. P15.1

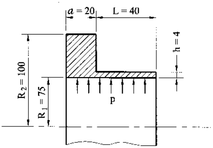

Fig. P15.2

15.10 A long cylindrical shell is reinforced by two equal stiffening rings at a distance 5 cm from one another. Both stiffening rings are placed far from the shell ends. The shell is loaded by an internal pressure p_0. Determine the deflections and stresses at the ring attachments if each ring has a rectangular cross section 2.5 cm wide and 0.5 cm thick. The parameters of the shell are $R = 1.5\,\text{m}$. $h = 5\,\text{mm}$. Take $p_0 = 500\,\text{kPa}$, $E = 200\,\text{GPa}$, and $\nu = 0.3$.

15.11 A long cylindrical pipe of diameter $D = 1.0$ m and of wall thickness $h = 6$ mm is subjected to load P, uniformly distributed along a circular cross section (Fig. 15.9). Determine the value of P required according to the Tresca criterion. Use $\sigma_{ys} = 220$ MPa, $E = 200\,\text{GPa}$, and $\nu = 0.3$.

15.12 Consider a semi-infinite cylindrical shell of radius R and thickness h loaded by an internal pressure $p_0 = \text{const}$. Compare the maximum values of bending stresses, σ_1, for two types of boundary conditions, prescribed on the shell edge $x = 0$: built-in and simply supported edges. Indicate in the solution the locations of these maximum stresses.

15.13 A stepped water tower, shown in Fig. P.15.3, is filled to capacity with a liquid of specific weight γ. Determine the values of the discontinuity moments and shear forces along the joint and at the base of the tower. Assume that the water tower is built-in at its base. The self-weight of the tower can be neglected. Take $H = 4.0\,\text{m}$, $R = 1\,\text{m}$, $H_1 = 1.0\,\text{m}$, $h_1 = 25\,\text{mm}$, $h_2 = 15\,\text{mm}$, $E = 30\,\text{GPa}$, $\gamma = 9800\,\text{N/m}^3$, and $\nu = 0.15$.

15.14 Solve a problem of Example 15.7 (see Fig. 15.15) replacing the two moments applied to the short shell by two equal line forces P distributed along circular sections of a shell $x = 2.5\,\text{in.}$ and $x = 7.5\,\text{in.}$

15.15 Verify the general-purpose equation of the middle surface deflections, Eq. (15.83).

16

The Moment Theory of Shells of Revolution

16.1 INTRODUCTION

As mentioned**,** shells of revolution belong to a highly general class of shells frequently used in engineering. One representative of this class, cylindrical shells, was considered in Chapter 15, and we will not dwell on these shells. The shell types analyzed in this chapter are subclasses of shells of revolution having non-zero Gaussian curvature. As mentioned in Sec. 11.7, such shells have non-developable surfaces. Hence, they are stronger, stiffer, and more stable than shells with zero Gaussian curvature. These shells are frequently used to cover the roofs of sport halls and large liquid storage tanks. The containment shield structures of nuclear power plants also have dome-like roofs. Various pressure vessels are either completely composed of a single rotational shell or have shells of revolution at their end caps. Conical shells with zero Gaussian curvature are also representative of this class of shells: they are used to cover liquid storage tanks and the nose cones of missiles and rockets.

In the membrane analysis of shells of revolution considered in Chapters 13 and 14, we saw that the membrane theory alone cannot accommodate all the loads, support conditions, and geometries in actual shells. Thus, in a general case, shells of revolution experience both stretching and bending to resist an applied loading, which distinguishes significantly the bending of shells from the elementary behavior of plates (see also Sec. 10.4).

However, the character of bending deformation may be different. If a shell of revolution is subjected to a concentrated force (Fig. 16.1a), bending exerts a crucial effect on its strength, because, in this case, the bending deformation increases with a growth of the forces until the load-carrying capacity of the shell structure is exhausted. In places of junction of a shell with its supports (Fig. 16.1b) or other structural members (shell of another geometry, ring beam, etc.), or in places of jump change in

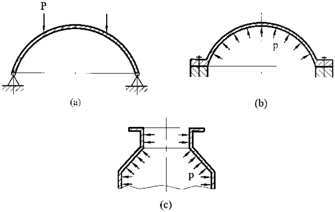

Fig. 16.1

the radii of curvature (Fig. 16.1c), the bending has another character; here, bending propagates only if it is needed to eliminate the discrepancies between the membrane displacements or to satisfy the conditions of statics. If a shell material is ductile, the bending deformations of the latter type are usually decreased and do not practically influence the load-carrying capacity of shell structures. If the material of the shell is brittle, the bending deformations remain proportional to the applied loads until failure and can result in a significant decrease in the strength of the shell structure

In this chapter we consider the bending theory of shells of revolution. It should be noted that the solutions of the governing differential equations involve many difficulties for a general shell of revolution, and therefore, we solve these equations for some particular shell geometries and load configurations that are frequently used in engineering practice.

16.2 GOVERNING EQUATIONS

We present below the governing differential equations of the moment theory of shells of revolution of an arbitrary shape. As curvilinear coordinates α and β of a point on the shell middle surface, it is convenient to take the spherical coordinates, introduced in Sec. 11.8, and used in the membrane theory of shells of revolution in Chapters 13 and 14. Thus, we take $\alpha = \varphi$ and $\beta = \theta$. As before, the angle φ defines the location of a point along the meridian, whereas θ characterizes the location of a point along the parallel circle (see Fig. 11.12). Let R_1 and R_2 be the principal radii of curvature of the meridian and parallel circle, respectively. Obviously, R_1 and R_2 will be functions of φ only, i.e., $R_1 = R_1(\varphi)$ and $R_2 = R_2(\varphi)$. The Lamé parameters in this case are determined by the following formulas (see Sec. 11.8):

$$A = R_1(\varphi), \quad B = R_2(\varphi)\sin\varphi, \quad r = R_2 \sin\varphi. \tag{16.1}$$

The Codazzi and Gauss conditions are given by Eqs (11.41).

Let us consider the kinematic relations of the moment theory of shells of revolution. Displacement components of the middle surface along the given coordi-

$$
\begin{aligned}
&L(U)+\nu U=EhR_1\vartheta_1+\Phi(\varphi),\\
&L(\vartheta_1)-\nu\vartheta_1=-\frac{R_1}{D}U.
\end{aligned}
\tag{16.30}
$$

where

$$
L(..)=\frac{R_2}{R_1}\frac{\mathrm{d}^2(..)}{\mathrm{d}\varphi^2}+\left[\frac{\mathrm{d}}{\mathrm{d}\varphi}\left(\frac{R_2}{R_1}\right)+\frac{R_2}{R_1}\cot\varphi\right]\frac{\mathrm{d}(..)}{\mathrm{d}\varphi}-\cot^2\varphi(..)\left(\frac{R_1}{R_2}\right)
\tag{16.31}
$$

Equations (16.30) are the governing differential equations of the axisymmetric bending of shells of revolution of constant thickness. A particular solution of the system of ordinary differential equations (16.30) can be found from the membrane theory of axisymmetrically loaded shells of revolution (see Sec. 13.5).

Setting

$$
U=\frac{1}{R_1}(L(\psi)-\nu\psi),\quad \vartheta_1=-\frac{1}{D}\psi,
\tag{16.32}
$$

where ψ is some function of forces and displacements. We identically satisfy the second Eq. (16.30). Inserting Eqs (16.32) into the first Eq. (16.30), we obtain

$$
L\left[\frac{1}{R_1}L(\psi)\right]-\nu L\left(\frac{\psi}{R_1}\right)+\frac{\nu}{R_1}L(\psi)+\left(\frac{EhR_1}{D}-\frac{\nu^2}{R_1}\right)\psi=\Phi(\varphi).
\tag{16.33}
$$

If the radius of the shell curvature $R_1=\text{const}$ (sphere, cone, toroid), then Eq. (16.33) takes the following form:

$$
LL(\psi)+\mu^2\psi=R_1\Phi(\varphi),
\tag{16.34}
$$

where

$$
\mu^2=\frac{EhR_1^2}{D}-\nu^2\approx b^2
\tag{16.35}
$$

and $b^2=12(1-\nu^2)R_1^2/h^2$ is the basic characteristic of a shell. Equation (16.34) can be represented in the form

$$
[L+i\mu][L(\psi)-i\mu\psi]=R_1\Phi(\varphi),
\tag{16.36}
$$

and its general solution can be obtained in a complex form.

It is convenient to express the boundary conditions of the shell of revolution via the horizontal, ξ, and vertical, η, displacements of a point of the middle surface, as shown in Fig. 16.2. The formulas that relate the displacement components u and v to the displacements ξ and η can be directly obtained from Fig, 16.2, i.e.,

$$
\xi=w\sin\varphi-u\cos\varphi,\ \eta=w\cos\varphi+u\sin\varphi.
\tag{16.37}
$$

Let us consider some typical boundary conditions for the shells of revolution shown in Fig. 16.3.

(a) *The edge of a shell is built-in* (Fig. 16.3a)
The boundary conditions are of the form

$$
\vartheta_1=\xi=0|_{\varphi=\varphi_e}.
\tag{16.38a}
$$

$$\varepsilon_2 = 0|_{\varphi=\varphi_e} \quad \text{or} \quad N_2 - \nu N_1 = 0|_{\varphi=\varphi_e} \tag{16.38b}$$

(b) *The edge of a shell is pinned* (Fig. 16.3b)
In this case

$$\begin{aligned} &\xi = 0|_{\varphi=\varphi_e} \quad \text{or} \quad \varepsilon_2 = 0, \quad N_2 - \nu N_1 = 0|_{\varphi=\varphi_e} \quad \text{and} \\ &M_1 = 0|_{\varphi=\varphi_e} \quad \text{or} \quad \frac{1}{R_1}\frac{\mathrm{d}\vartheta_1}{\mathrm{d}\varphi} + \nu\frac{\cot\varphi}{R_2}\vartheta_1 = 0|_{\varphi=\varphi_e}. \end{aligned} \tag{16.38c}$$

(c) *The edge of a shell is simply supported* (Fig. 16.3c)
In this case the boundary conditions are of the form

$$\begin{aligned} &M_1 = 0\Big|_{\varphi=\varphi_e} \quad \text{or} \quad \frac{1}{R_1}\frac{\mathrm{d}\vartheta}{\mathrm{d}\varphi} + \nu\frac{\cot\varphi}{R_2}\vartheta_1 = \Big|_{\varphi=\varphi_e} \quad \text{and} \\ &N_1\cos\varphi_e + Q_1\sin\varphi_e = 0\Big|_{\varphi=\varphi_e}. \end{aligned} \tag{16.38d}$$

(d) *The edge of a shell is free* (Fig. 16.3d)
Here the boundary conditions are

$$\begin{aligned} &M_1 = 0|_{\varphi=\varphi_e} \quad \text{or} \quad \frac{1}{R_1}\frac{\mathrm{d}\vartheta_1}{\mathrm{d}\varphi} + \nu\frac{\cot\varphi}{R_2}\vartheta_1 = 0|_{\varphi=\varphi_e} \\ &Q_1 = 0|_{\varphi=\varphi_e} \quad \text{or} \quad U = 0|_{\varphi=\varphi_e}. \end{aligned} \tag{16.38e}$$

(e) *The edge of a shell is loaded by edge forces* N_e, Q_e, *and* M_e (Fig. 16.3e)
In this case the boundary conditions are

$$\begin{aligned} &M_1 = M_e\big|_{\varphi=\varphi_e} \quad \text{or} \quad \frac{1}{R_1}\frac{\mathrm{d}\vartheta_1}{\mathrm{d}\varphi} + \nu\frac{\cot\varphi}{R_2}\vartheta_1 = M_e\big|_{\varphi=\varphi_e} \\ &Q_1 = Q_e\big|_{\varphi=\varphi_e} \quad \text{or} \quad U = Q_e R_2\big|_{\varphi=\varphi_e}. \end{aligned} \tag{16.38f}$$

(f) *A shell is built-in from both sides* (Fig. 16.3f)
Since such a shell is statically indeterminate, we must impose the following five conditions:

$$\begin{aligned} &\vartheta_1 = 0|_{\varphi=\varphi_{e_1}}, \quad \varepsilon_2 = 0|_{\varphi=\varphi_{e_1}}; \quad \vartheta_1 = 0|_{\varphi=\varphi_{e_2}}, \quad \varepsilon_2 = 0|_{\varphi=\varphi_{e_2}}, \\ &\eta_{A/B} = 0 \quad \text{or} \quad \int_{\varphi=\varphi_{e_1}}^{\varphi=\varphi_{e_2}} (\varepsilon_1\sin\varphi + \vartheta_1\cos\varphi)R_1\mathrm{d}\varphi = 0. \end{aligned} \tag{16.38g}$$

(g) *Two joined shells* (Fig. 16.3g)
It is necessary for this case to satisfy the four boundary conditions, namely,

$$\begin{aligned} &\xi_e^{(1)} = \xi_e^{(2)} \quad \text{or} \quad \varepsilon_{2\mathrm{e}}^{(1)} = \varepsilon_{2e}^{(2)}, \\ &\vartheta_{1e}^{(1)} = \vartheta_{1e}^{(2)}, \quad M_{1e}^{(1)} = M_{1e}^{(2)}, \\ &N_{1e}^{(1)}\cos\varphi_{e_1} + Q_{1e}^{(1)}\sin\varphi_{e_1} = N_{1e}^{(2)}\cos\varphi_{e_2} - Q_1^{(2)}\sin\varphi_{e_2}. \end{aligned} \tag{16.38h}$$

The last condition expresses the equality of the radial forces (thrusts).
(h) If a shell is closed at its vertex, for $\varphi = 0$, then the following conditions must be satisfied:

$$\vartheta_1 = 0|_{\varphi=0} \quad \text{and} \quad Q_1 = 0|_{\varphi=0}. \tag{16.39}$$

16.4 APPROXIMATE METHOD FOR SOLUTION OF THE GOVERNING EQUATIONS (16.30)

The solution of the governing differential equations (16.30) is quite complicated. In the present section, we introduce one approximate method for the bending analysis of shells of revolution under axisymmetric edge loads.

Figure 16.4 shows two shells of revolution subjected to distributed over the edge loads N_{1e}, M_e and Q_e. The first shell (Fig. 16.4a) is a shallow one. In axisymmetric bending of such a shell, the radial displacements and the corresponding circumferential tensile deformations are small near the loaded edge. Therefore, deformations caused by the bending moments diminish slowly and their influence may extend over, practically, the entire shell.

In the second case, shown in Fig. 16.4b, the slope of the normal, ϑ_1, is large. Here, considerable circumferential tension occurs near the loaded edge as the shell bends axisymmetrically. As a consequence, the bending deformations diminish rapidly and they practically vanish at a small distance from the edge.

The effect of the circumferential tension in an axisymmetric bending of a shell with large angle of rise is similar to that of an elastic foundation. A similar effect of rapid decrease of the bending deformations near the loaded edge was observed in the axisymmetrically loaded cylindrical shells in Sec. 15.5. Based on this analogy, a very efficient approximate method may be developed for shells of revolution with large angle of a rise and subjected to edge loading. This method uses the following assumptions:

(a) *All functions characterizing the stress and strain components in a shell near its edge, as well as their first derivatives, are small compared with their higher derivatives.*
This assumption is based on that fact that all the considered functions will contain multipliers of the type $\mathrm{e}^{-\alpha\varphi}$, where φ is the angle measured from the shell edge of interest and α is some parameter. In differentiating these functions, the parameter αappears every time in the form of the multiplier. Since these functions are rapidly decaying, the value of the parameter α is large. Therefore, values of the first derivative are sufficiently greater than the values of the functions themselves, and values of the second derivatives are greater than the first derivatives, etc., i.e.,

$$\frac{\mathrm{d}^n U_n}{\mathrm{d}\varphi^n} \gg \frac{\mathrm{d}^{(n-1)} U_n}{\mathrm{d}\varphi^{n-1}} \quad \text{and} \quad \frac{\mathrm{d}^n \vartheta_1}{\mathrm{d}\varphi^n} \gg \frac{\mathrm{d}^{(n-1)} \vartheta_1}{\mathrm{d}\varphi^{n-1}}.$$

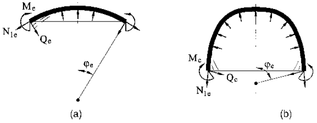

Fig. 16.4

On this basis, terms containing the functions themselves and their first derivatives on the left-hand side of Eqs (16.30) are dropped. The function $\Phi(\varphi)$ on the right-hand side of Eqs (16.30) is zero for loads applied to the edge of the shell. As a result, the governing differential equations (16.30) take the form

$$\frac{R_2}{R_1}\frac{\mathrm{d}^2 U}{\mathrm{d}\varphi^2} = EhR_1\vartheta_1, \tag{16.40a}$$

$$\frac{R_2}{R_1}\frac{\mathrm{d}^2 \vartheta_1}{\mathrm{d}\varphi^2} = -\frac{R_1}{D}U. \tag{16.40b}$$

(b) *The radii of curvature,* R_1 *and* R_2*, are assumed to be constant near the shell edge*. This is true for spherical shells only. For shells of other shapes this assumption is carried out the more precisely the closer the shape of a shell approaches a spherical one.

The approximate method for the bending analysis of axisymmetrically loaded spherical shells of revolution based on the above-mentioned assumptions was first introduced by H. Reissner [6] and Geckeler [7]; it was then generalized to shells of revolution of an arbitrary shape of a meridian by Meissner [5,8]. Equations (16.40) can be reduced to a single differential equation with one unknown. Differentiating Eq. (16.40a) twice with regard to the second assumption, and inserting $\mathrm{d}^2\vartheta_1/\mathrm{d}\varphi^2$ into Eq. (16.40b), we obtain the following fourth-order governing differential equation:

$$\frac{\mathrm{d}^4 U}{\mathrm{d}\varphi^4} + 4\alpha^4 U = 0, \tag{16.41}$$

where

$$\alpha = R_1\sqrt[4]{\frac{3(1-\nu^2)}{R_2^2 h^2}}. \tag{16.42}$$

Note that it is impossible to neglect the function U compared with its fourth derivative in Eq. (16.41) because the multiplier $4\alpha^4$ is sufficiently large.

Equation (16.41) is referred to as the *edge effect differential equation* because its solution is expressed in terms of rapidly damped functions. The edge effect governing equation and the corresponding numerical procedure for the general theory of thin shells is discussed in more detail in Sec. 17.5. Equation (16.41) is analogous to that of an axisymmetric deformation of a circular cylindrical shell (see Eq. (15.44)). Hence, we can apply the edge effect technique developed in Sec. 15.3 to axisymmetric bending analysis of shells of revolution. The general solution of Eq. (16.41) for U can be written in the form

$$U = \mathrm{e}^{-\alpha\varphi}(B_1\sin\alpha\varphi + B_2\cos\alpha\varphi) + \mathrm{e}^{\alpha\varphi}(B_3\sin\alpha\varphi + B_4\cos\alpha\varphi). \tag{16.43}$$

It is convenient to introduce a new independent variable ω, representing also the angular coordinate and counting off from the shell edge, as shown in Fig. 16.5.

If the lower shell edge is of interest (Fig. 16.5a), then

$$\omega = \varphi_e - \varphi. \tag{16.44a}$$

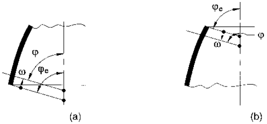

Fig. 16.5

If the upper shell edge is of interest (Fig. 16.5b), then the angle ω is counted off oppositely and

$$\omega = \varphi - \varphi_e. \tag{16.44b}$$

Since, in both the above-mentioned cases,

$$\frac{\mathrm{d}^4 U}{\mathrm{d}\varphi^4} = \frac{\mathrm{d}^4 U}{d\omega^4},$$

in the transition to a new variable, the differential equation remains unchanged, i.e.,

$$\frac{\mathrm{d}^4 U}{\mathrm{d}\omega^4} + 4\alpha^4 U = 0. \tag{16.45}$$

The solution of this equation can be written in the form

$$U = \mathrm{e}^{-\alpha\omega}(C_1 \sin\alpha\omega + C_2 \cos\alpha\omega) + \mathrm{e}^{\alpha\omega}(C_3 \sin\alpha\omega + C_4 \cos\alpha\omega), \tag{16.46}$$

where $C_1, \ldots, C_4$ are constants to be determined from the boundary conditions. Since the function U has to die down as the angle ω increases, the second term in Eq. (16.46), involving the multiplier $\mathrm{e}^{\alpha\omega}$, must vanish as we move away from the loaded edge of the shell. Therefore, the constants C_3 and C_4 should be equal to zero and the above solution takes the form

$$U = \mathrm{e}^{-\alpha\omega}(C_1 \sin\alpha\omega + C_2 \cos\alpha\omega). \tag{16.47}$$

This solution describes the moment state of stress and strain near a loaded edge (either bottom or top). However, in differentiating Eq. (16.47), it should be taken into account that on the top edge of the shell angle ω is counted off in the side of an increase of angle φ; therefore, $\mathrm{d}U/\mathrm{d}\varphi = \mathrm{d}U/d\omega$. On the bottom edge, reference directions of angles φ and ω are opposite, therefore, $\mathrm{d}U/\mathrm{d}\varphi = -\mathrm{d}U/\mathrm{d}\omega$. Let us determine the derivatives of the function U with respect to φ, as follows:

$$\frac{\mathrm{d}U}{\mathrm{d}\varphi} = \pm\alpha\mathrm{e}^{-\alpha\omega}[C_1(\cos\alpha\omega - \sin\alpha\omega) - C_2(\cos\alpha\omega + \sin\alpha\omega)],$$

$$\frac{\mathrm{d}^2 U}{\mathrm{d}\varphi^2} = 2\alpha^2\mathrm{e}^{-\alpha\omega}[-C_1 \cos\alpha\omega + C_2 \sin\alpha\omega],$$

$$\frac{\mathrm{d}^3 U}{\mathrm{d}\varphi^3} = \pm 2\alpha^3\mathrm{e}^{-\alpha\omega}[C_1(\cos\alpha\omega + \sin\alpha\omega) + C_2(\cos\alpha\omega - \sin\alpha\omega)].$$

$$\vartheta_{1e} = \pm \frac{M_e}{\alpha D} R_1 + \frac{Q_e R_1^2}{2\alpha^2 D},$$
$$N_{1e} = -Q_e \cot \varphi_e, \; N_{2e} = M_e \frac{2R_2\alpha^2}{R_1^2} \pm Q_e \frac{2R_2\alpha}{R_1},$$
$$\varepsilon_{2e} = \frac{1}{Eh}\left[M_e \frac{2R_2\alpha^2}{R_1^2} \pm Q_e \frac{2R_2\alpha}{R_1} + \nu Q_e \cot \varphi_e \right], \quad \xi_e = \varepsilon_{2e} r_e = \varepsilon_{2e} R_{2e} \sin \varphi_e. \tag{16.51}$$

The upper signs in all the above equations refer to the top edge of the shell, whereas the lower signs refer to the bottom edge. If a shell of revolution is loaded by the horizontal force (thrust) H_e per unit length applied to the shell edge $\varphi = \varphi_e$, then the internal forces and deformations can also be determined from Eqs (16.50) and (16.51) by substituting for Q_e from the following equation:

$$Q_e = \pm H_e \sin \varphi_e. \tag{16.52}$$

If an arbitrary surface load is applied to the shell of revolution, then the solutions (16.48) must be complemented by a particular solution of the nonhomogeneous equations. This particular solution in most cases is determined from the membrane theory of shells introduced in Chapter 13 .

The accuracy of the introduced approximate Geckeler's analysis was analyzed in Refs [5–9]. It has been established that for thin shells with fairly big angle of rise, these formulas give satisfactory accurate results. The error of approximate formulas of the edge effect theory has an order of $\sqrt{h \cot^2 \varphi / R}$. Practically, this method can be used if the angle of the shell edge $\varphi_e > 35^\circ$.

In the next section we apply the approximate solution procedure discussed above to the analysis of some specific geometric forms of shells of revolution used in practical application. We assume that for the geometry of the shells under consideration all requirements about accuracy of applicability of the approximate method introduced above are satisfied.

16.5 AXISYMMETRIC SPHERICAL SHELLS, ANALYSIS OF THE STATE OF STRESS AT THE SPHERICAL-TO-CYLINDRICAL JUNCTION

For spherical shells, $R_1 = R_2 = R$, and the governing equations of axisymmetric bending of shells of revolution, Eqs (16.40) are simplified. The solution procedure based on the approximate method introduced in Sec. 16.4, as applied to the bending analysis of axisymmetrically loaded spherical shells, is illustrated below by the following examples.

Example 16.1

Calculate stresses in the hemispherical shell stiffened on its edge by a flange and loaded by an internal pressure p which is balanced by a force P, as shown in Fig. 16.6a. Given $R = 50\,\text{cm}$, $h = 0.3\,\text{cm}$, $r_1 = 49.85\,\text{cm}$, $r_2 = 53\,\text{cm}$, $r_3 = 51.6\,\text{cm}$, $b = 3.15\,\text{cm}$, $h_1 = 0.8\,\text{cm}$, $\nu = 0.3$, and $E = 20\,\text{GPa}$.

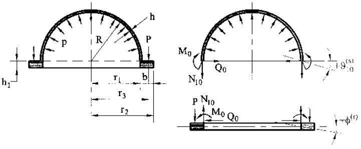

(a) (b)

Fig. 16.6

Solution

Detach the spherical shell from the flange and apply to them the interface forces and moments M_0, Q_0, and N_{10}, as shown in Fig. 16.6b. The meridional force can be determined from the equilibrium condition, i.e.,

$$N_{10} = \frac{p(\pi r_1^2)}{2\pi R} = 24.8p(\mathrm{N/cm}).$$

The bending moment M_0 and shear force Q_0 must be found from the compatibility of deformations conditions at the junction of the shell and flange.

Deformations of the flange may be calculated from the corresponding formulas of the theory of axisymmetrical deformations of rings [11,12]. Geometrical properties of the ring cross section are

$$I_1 = \int_A \frac{\mathrm{d}A}{r} = h_1 \ln\frac{r_2}{r_1} = 0.049\,\mathrm{cm}, \quad I_3 = \int_A \frac{z^2}{r}\mathrm{d}A = \frac{h_1^3}{12}\ln\frac{r_2}{r_1} = 2.614 \times 10^{-3}\mathrm{cm}^2.$$

Determine the internal bending moment $M^{(r)}$ and the membrane normal force $N^{(r)}$ at a cross section of the ring. We have

$$N^{(r)} = ph_1 r_1 + Q_0 R = 39.9p + 50Q_0,$$

$$M^{(r)} = pr_3^2 - N_{10}R^2 + M_0 R + Q_0 R\frac{h_1}{2} = 1.99 \times 10^3 p + 50M_0 + 20Q_0.$$

The angle of rotation of the ring section is

$$\phi^{(r)} = \frac{M^{(r)}}{EI_3} = \frac{1}{E}\left[0.7605 \times 10^6 p + 19.13 \times 10^3 M_0 + 7.65 \times 10^3 Q_0\right](\mathrm{rad}). \tag{a}$$

The radial displacement of the ring, $\xi^{(r)}$, at a point of the junction with the shell is

$$\xi^{(r)} = \frac{N^{(r)}}{EI_1} + \frac{\phi^{(r)}h_1}{2} = \frac{1}{E}\left[0.305 \times 10^6 p + 7.65 \times 10^3 M_0 + 4.08 \times 10^3 Q_0\right](\mathrm{cm}). \tag{b}$$

Solving these equations, yields

$$M_0 = -33.8p(\mathrm{N \cdot cm/cm}), \quad Q_0 = -10.7p(\mathrm{N/cm}).$$

The maximum stresses occur at an outside point of the shell at $\varphi = 90^\circ$. They are

$$\sigma_{1\max} = \frac{N_1}{h} - \frac{6M_1}{h^2}; \quad \sigma_{2\max} = \frac{N_2}{h} - \frac{6M_2}{h^2}, \tag{g}$$

where

$$N_1 = N_{10} = 24.8p(\mathrm{N/cm}), \quad M_1 = M_0 = -33.8p(\mathrm{N \cdot cm/cm});$$

$$N_2 = N_{20} + N_{2p}(\mathrm{N/cm}), \quad M_2 = \nu M_1 = -10.1p(\mathrm{N \cdot cm/cm}),$$

and N_{20} is given by Eq. (16.49), i.e.,

$$N_{20} = M_0 \frac{2\alpha^2}{R} - Q_0(2\alpha) = -17.32p \ (\mathrm{N/cm}).$$

Finally, N_2 can be determined as follows:

$$N_2 = N_{2\mathrm{p}} + N_{20} = 24.8p - 17.32p = 7.48p \ (\mathrm{N/cm}).$$

Substituting all the above data into Eqs (g) yields the following values of the maximum stresses:

$$\sigma_{1\max} = \frac{24.8p}{0.3} + \frac{6(33.8p)}{(0.3)^2} = 2336p(\mathrm{N/cm^2});$$

$$\sigma_{2\max} = \frac{7.48p}{0.3} + \frac{6(10.1p)}{(0.3)^2} = 698.2(\mathrm{N/cm^2}).$$

These values of the normal stresses coincide with the numerical data obtained in Ref. [12], where the same problem had been solved using the exact governing equations (16.30). The above-mentioned coincidence for this case can be explained by the fact that the meridional angle at the shell edge, φ_e, is equal to 90° and the radii of curvature had constant values throughout the shell.

Example 16.2

Consider a cylindrical vessel, made of steel, with a hemispherical head, as shown in Fig. 16.7a, under an internal pressure p. Determine the internal forces, moments, and stresses at the junction of the cylindrical and spherical shells. Given the radii of the cylinder and sphere are assumed to be the same and equal $R = 1.5$ m, the thickness of the cylinder and shell is $h = 0.01$ m, $E = 200$ GPa, and $\nu = 0.3$.

Solution

First, consider the *membrane state* of stress of the cylinder and head separately (Fig. 16.7b). *In the spherical shell* (*at the junction*):

$$N_{1\mathrm{p}}^{(\mathrm{s})} = N_{2\mathrm{p}}^{(\mathrm{s})} = \frac{pR}{2}, \quad \xi_{\mathrm{p}}^{(\mathrm{s})} = -\frac{pR^2}{2Eh}(1-\nu).$$

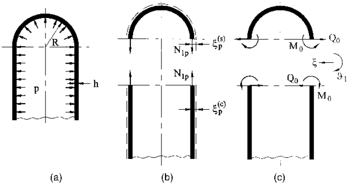

Fig. 16.7

In the cylindrical shell (at the junction):

$$N_{1\mathrm{p}}^{(\mathrm{c})} = \frac{pR}{2}, \quad N_{2\mathrm{p}}^{(\mathrm{c})} = pR, \quad \xi_{\mathrm{p}}^{(\mathrm{c})} = -\frac{R}{Eh}\left(N_{2\mathrm{p}}^{(\mathrm{c})} - \nu N_{1\mathrm{p}}^{(\mathrm{c})}\right) = -\frac{pR^2}{Eh}(2-\nu).$$

In the above equations $\xi_{\mathrm{p}}^{(\mathrm{s})}$ and $\xi_{\mathrm{p}}^{(\mathrm{c})}$ refer to the membrane radial (horizontal) displacements at the juncture of the hemisphere and cylinder, respectively. Since at the junction of two shells $N_{1\mathrm{p}}^{(\mathrm{s})} = N_{1\mathrm{p}}^{(\mathrm{c})}$, then the membrane state of stress satisfies the static conditions of joint operation of the two shells. However, conditions of deformations' compatibility are not satisfied because the radial displacements of the cylindrical shell at the juncture are greater than the corresponding radial displacements of the spherical shell. Therefore, at the junction of the two shells, the interface force Q_0 and moment M_0 occur (Fig. 16.7c). These interface force and moment cause the *moment stress of the edge effect type* in the vicinity of the joint (see also Sec. 17.5). The values of the interface force and moment may be found from the conditions of compatibility of deformations at the junction of the spherical and cylindrical shells. Equating the total (i.e., caused by both the membrane state and edge effect) radial displacements and the angles of rotation at the juncture of the shells (the positive directions for displacements and angles of rotation are shown on the right part of Fig. 16.6c), we obtain the following:

$$\begin{aligned} &-\xi_{\mathrm{p}}^{(\mathrm{s})} - Q_0\xi_Q^{(\mathrm{s})} - M_0\xi_M^{(\mathrm{s})} = -\xi_{\mathrm{p}}^{(\mathrm{c})} + Q_0\xi_Q^{(\mathrm{c})} - M_0\xi_M^{(\mathrm{c})} \\ &-M_0\vartheta_{1M}^{(\mathrm{s})} - Q_0\vartheta_{1Q}^{(\mathrm{s})} = M_0\vartheta_{1M}^{(\mathrm{c})} - Q_0\vartheta_{1Q}^{(\mathrm{c})}, \end{aligned} \tag{a}$$

where ξ_Q, ξ_M and $\vartheta_{1Q}, \vartheta_{1M}$ refer to the radial displacements and slopes at the juncture caused by the unit interface shear force, $Q_0 = 1$, and unit bending moment, $M_0 = 1$; superscripts s and c stand for the hemisphere and cylinder, respectively. The deformation components at the junction for both cylindrical and spherical shells may be determined from Eqs (16.51) by setting $\varphi_e = \pi/2$ and making $R_1 = \infty$, $R_2 = R$ and $\alpha = \beta R$ for the cylindrical shell and letting $R_1 = R_2 = R$ and $\varphi = \pi/2$ for the spherical shell. Consequently, we obtain

$$\xi_Q^{(s)} = \xi_Q^{(c)} = \frac{1}{2D\beta^3},\ \xi_M^{(s)} = \xi_M^{(c)} = \frac{1}{2D\beta^2},\ \vartheta_{1\mathrm{M}}^{(s)} = \vartheta_{1M}^{(c)} = \frac{1}{D\beta},\ \vartheta_{1Q}^{(s)} = \vartheta_{1Q}^{(s)} = \frac{1}{2D\beta^2},$$

where

$$\beta = \frac{\alpha}{R} = \frac{\sqrt[4]{3(1-\nu^2)}}{\sqrt{Rh}} = 10.4931\ (1/\mathrm{m}).$$

Then, it follows from the compatibility equations (a) that

$$M_0 = 0, Q_0 = \frac{\xi_{\mathrm{p}}^{(c)} - \xi_{\mathrm{p}}^{(s)}}{\xi_Q^{(s)} + \xi_Q^{(c)}} = \frac{pR^2(D\beta^3)}{2Eh} = \frac{p\sqrt{Rh}}{8\sqrt[4]{3(1-\nu^2)}} = 0.01191p\ (\mathrm{N}\cdot\ \mathrm{m/m}).$$

Using Eqs (16.48) and (15.57), we can obtain the displacements and stress resultants and couples caused by the edge loads and the given internal pressure in both the cylindrical and spherical shells.

Figure 16.8a and b shows the bending moment M_1 and circumferential force N_{2m} diagrams, where N_{2M} is due to the edge loads only.

The maximum values of M_1 and N_{2M} at the junction of the two shells are found to be

$$M_{1\,\max} = \frac{pR^2}{2Eh} D\beta^2 \mathrm{e}^{-\pi/4} \frac{\sqrt{2}}{2} = 3.6 \times 10^{-4} p\ (\mathrm{N}\cdot\mathrm{m/m});$$

$$\left|N_{2M}\right| = Q_0 2\alpha = 0.375p\ (\mathrm{N/m}).$$

Note that N_{2M} has different signs for the cylindrical and spherical shells at the juncture (see Fig. 16.8b).

The normal stresses due to the bending edge effect are

$$\sigma_{1M} = \frac{6M_{1\,\max}}{h^2} = 0.146\frac{pR}{h} = 21.9p, \sigma_{2M} = 0.1\sigma_{1M} = 2.19p.$$

The circumferential force N_{2M} eliminates a discontinuity in the forces of the membrane state. It can be easily shown that the total membrane force $N_2 = N_{2p} + N_{2M}$ is identical for both shells at the junction and equal $N_2 = 1.125p$. Thus, the total circumferential force N_2 varies continuously in the compound shell, as shown in Fig. 16.8c.

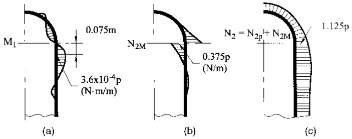

Fig. 16.8

It is seen that the stresses due to the edge effect have a magnitude of the same order (pR/h) as the membrane stresses in the shells under consideration. This is typical for shells at which the edge effect occurs, because the compatibility of deformations is not satisfied by the membrane state only.

Example 16.3

A compound steel shell consists of a cylinder (radius R and wall thickness h) and of a head in the form of a spherical segment (radius $R_s = 2R$ and thickness h), as shown in Fig. 16.9a. This compound shell is subjected to an internal pressure p. Determine the internal forces and moments in the compound shell if $R = 1.5\,\mathrm{m}$, $h = 0.02\,\mathrm{m}$, $\nu = 0.3$, $E = 200\,\mathrm{GPa}$, and $\varphi_1 = 30^\circ$.

Solution

First, consider the membrane state of the head and cylinder separately, as shown in Fig. 16.9b. From the membrane shell theory, it follows that

$$N_{1\mathrm{p}}^{(\mathrm{s})} = N_{2\mathrm{p}}^{(\mathrm{s})} = \frac{pR_s}{2} = pR; \quad N_{1\mathrm{p}}^{(\mathrm{c})} = \frac{pR}{2},\, N_{2\mathrm{p}}^{(\mathrm{c})} = pR \tag{a}$$

where, again, the subscript p refers to the membrane solution and superscripts s and c stand for the sphere and cylinder, respectively. It is seen from Fig. 16.9b that, apart from the latter example, the membrane state alone does not satisfy the conditions of static equilibrium in the head and cylinder. Therefore, the *edge effect* occurs at the junction of the compound shell to satisfy both the statics and compatibility of deformations conditions.

Consider the edge effect procedure being applied to the given compound shell. The membrane force $N_{1\mathrm{p}}^{(\mathrm{s})}$ at the edge of the head has a horizontal component, which is equal to

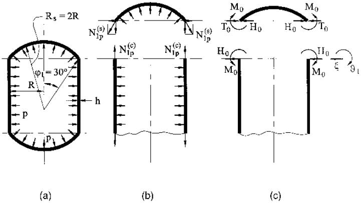

Fig. 16.9

$$T_0 = N_{1\mathrm{p}}^{(\mathrm{s})} \cos\varphi_1 = pR\frac{\sqrt{3}}{2}. \tag{b}$$

To ensure that the shell loading by the membrane scheme (Fig. 16.9b), together with the edge effect, would be equivalent to the given loading applied to the compound shell, it is necessary to include the thrust that is equal and oppositely directed to T_0 among the edge effect forces, as shown in Fig. 16.8c. Thus, in applying the edge effect solution procedure, we should assume that the cylindrical shell is loaded by the edge moment M_0 and shear force H_0, whereas the spherical shell is loaded by the edge moment M_0 and thrust $(H_0 - T_0)$, as shown in Fig. 16.9c. The unknown quantities M_0 and H_0 are evaluated from the compatibility of deformations' conditions, i.e., the radial (horizontal) displacements and angles of rotation of normals should be identical at the juncture of both shells. Equating the edge radial displacements of the sphere and cylinder at the juncture, we obtain

$$\xi^{(\mathrm{s})} = \xi^{(\mathrm{c})} \tag{c}$$

where,

$$\begin{aligned} \xi^{(\mathrm{s})} &= -\frac{R}{Eh}\left(N_{2\mathrm{p}}^{(\mathrm{s})} - \nu N_{1\mathrm{p}}^{(\mathrm{s})}\right) + (T_0 - H_0)\xi_H^{(\mathrm{s})} - M_0 \xi_M^{(\mathrm{s})} \\ \xi^{(\mathrm{c})} &= -\frac{R}{Eh}\Big(N_{2\mathrm{p}}^{(\mathrm{c})} - \nu N_{1\mathrm{p}}^{(\mathrm{c})}) + H_0 \xi_H^{(\mathrm{c})} - M_0 \xi_M^{(\mathrm{c})}. \end{aligned} \tag{d}$$

In Eqs (c) and (d), the first terms on the right-hand sides correspond to the membrane solution.

The conditions of compatibility for the slopes (the positive direction of the slopes is shown in Fig. 16.9c to the right) has the form

$$(T_0 - H_0)\vartheta_{1H}^{(\mathrm{s})} - M_0 \vartheta_{1M}^{(\mathrm{s})} = -H_0 \vartheta_{1H}^{(\mathrm{c})} + M_0 \vartheta_{1M}^{(\mathrm{c})}. \tag{e}$$

In Eqs. (d) and (e), the subscripts H and M indicate the cause of the corresponding displacements. The coefficients $\xi_H^{(\mathrm{s})}$, $\xi_M^{(\mathrm{s})}$, $\vartheta_{1H}^{(\mathrm{s})}$, $\vartheta_M^{(\mathrm{s})}$ and $\xi_{\mathrm{H}}^{(\mathrm{c})}$, $\xi_M^{(\mathrm{c})}$, $\vartheta_{1H}^{(\mathrm{c})}$, $\vartheta_{1M}^{(\mathrm{c})}$ can be calculated from Eqs (16.51) by setting $R_1 = R_2 = R_s = 2R$, $\varphi_e = \varphi_1$, and replacing Q_0 with $H_0 \sin\varphi_1$ or $T_0 \sin\varphi_1$) according to Eq. (16.50) for the spherical shell, and by setting $R_1 = \infty$, $R_2 = R$, and $\varphi_e = \varphi_1$ for the cylindrical shell. As a result, we obtain

$$\begin{aligned} &\xi_H^{(\mathrm{s})} = \frac{\sin^2\varphi_1}{2D\beta_s^3}, \quad \xi_M^{(\mathrm{s})} = \frac{\sin\varphi_1}{2D\beta_s^2}; \quad \vartheta_{1M}^{(\mathrm{s})} = \frac{1}{D\beta_s}; \quad \vartheta_{1H}^{(\mathrm{s})} = \xi_M^{(\mathrm{s})}, \\ &\xi_H^{(\mathrm{c})} = \frac{1}{2D\beta_c^3}, \quad \xi_M^{(\mathrm{c})} = \frac{1}{2D\beta_c^2}, \quad \vartheta_M^{(\mathrm{c})} = \frac{1}{D\beta_c}, \quad \vartheta_{1H}^{(\mathrm{c})} = \xi_M^{(\mathrm{c})}, \\ &\beta_s = \frac{\sqrt[4]{3(1-\nu^2)}}{\sqrt{2Rh}}, \quad \beta_c = \frac{\sqrt[4]{3(1-\nu^2)}}{\sqrt{Rh}}. \end{aligned} \tag{f}$$

Substituting the numerical data into the relations (a), (b), (d), and (f), one obtains the following:

$$D = \frac{Eh^3}{12(1-\nu^2)} = 146.52 \times 10^3 (\mathrm{Nm});\ \ \beta_c = 7.4213(1/\mathrm{m});\ \ \beta_s = 5.2477(1/\mathrm{m});$$

$$N_{1\mathrm{p}}^{(\mathrm{s})} = N_{2\mathrm{p}}^{(\mathrm{s})} = 1.5p\ (\mathrm{N/m});\ \ N_{1\mathrm{p}}^{(\mathrm{c})} = 0.75p\ (\mathrm{N/m});\ \ N_{2\mathrm{p}}^{(\mathrm{c})} = 1.5p;\ \ T_0 = 1.3p\ (\mathrm{N/m});$$

$$\xi_H^{(\mathrm{s})} = 0.005903 \times 10^{-6} (\mathrm{m}^2/\mathrm{N});\ \ \xi_M^{(\mathrm{s})} = 0.06196 \times 10^{-6} (\mathrm{m/N});$$

$$\vartheta_M^{(s)} = 1.301 \times 10^{-6} (1/\mathrm{N});$$

$$\xi_H^{(\mathrm{c})} = 0.008362 \times 10^{-6} (\mathrm{m}^2/\mathrm{N});\quad \xi_M^{(\mathrm{c})} = 0.06196 \times 10^{-6} (\mathrm{m/N});$$

$$\vartheta_M^{(\mathrm{c})} = 0.9196 \times 10^{-6} (1/\mathrm{N}).$$

Substituting the above into the compatibility equations (c) and (e) and taking into account the relations (d), we can calculate H_0 and M_0. We have

$$H_0 = 0.5401p\ (\mathrm{N/m});\quad M_0 = 0.03627p\quad (\mathrm{N \cdot m/m}).$$

Using Eqs (16.48) for a spherical shell and Eqs (15.57) for the cylindrical shell, we can determine the membrane forces N_2, N_1 and bending moments M_1, M_2 in the spherical and cylindrical parts of the given compound shell. The equations for the membrane forces and bending moments are of the following form:

– *for the cylindrical shell*

$$\begin{aligned} &N_2^{(\mathrm{c})} = 1.5p\big[1 - 4.0075\mathrm{e}^{-\beta_c x}(\cos\beta_c x + \sin\beta_c x)\big];\quad N_1^{(\mathrm{c})} = 0.75p;\\ &M_1^{(\mathrm{c})} = 0.03627p\mathrm{e}^{-\beta_c x}(\cos\beta_c x - \sin\beta_c x), \end{aligned} \tag{g}$$

where the coordinate x is counted off from the juncture of the spherical and cylindrical shells.

–*for the spherical shell*

$$\begin{aligned} &N_2^{(\mathrm{s})} = 1.5p[1 - 4.0075\mathrm{e}^{-\alpha\omega}(\cos\alpha\omega + \sin\alpha\omega)];\\ &N_1^{(\mathrm{s})} = 1.5p[1 - 0.44\mathrm{e}^{-\alpha\omega}\cos\alpha\omega];\\ &M_1^{(\mathrm{s})} = 0.03627p\mathrm{e}^{-\alpha\omega}(\cos\alpha\omega - \sin\alpha\omega), \end{aligned} \tag{h}$$

where $\alpha = R_s\beta_s$ and $\omega = \varphi_1 - \varphi = 30^\circ - \varphi$.

The diagrams of the membrane force N_2 and bending moment M_1 are shown in Fig. 16.10.

The maximum normal stresses occur in the cylindrical shell at points in its inner surface at the junction with the sphere segment. The total meridional stress is tensile at the above points and is equals to

$$\sigma_1 = \frac{N_1}{h} + \frac{6M_1}{h^2} = 37.5p + 544p = 581.5p. \tag{i}$$

The circumferential stress at the same points is compressive and is given by

$$\sigma_2 = \frac{N_2}{h} + \nu\frac{6M_1}{h^2} = -61.8p. \tag{j}$$

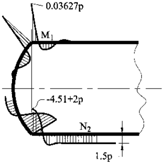

Fig. 16.10

It can be shown that in the given compound shell the edge effect normal stress is larger by an order of magnitude $\sqrt{(R/h)}$ than the corresponding membrane stress. Therefore, the compound shell, like that analyzed in this example, is inefficient.

However, it is possible to essentially decrease the stresses at the junction of compound shell structures. Figure 16.11a shows two shells, cylindrical and spherical, joined by a ring. The latter is supposed to support the thrust T_0 (Fig. (16.11a)). In the analysis of such shell structures, one can assume that the bending stiffness of the ring in the direction perpendicular to its plane is negligible. Thus, the ring resists only the radial load in its own plane. The free-body diagrams of the shells and ring are shown in Fig. 16.11b.

Let us determine the stress components at the junction of the two shells, shown in Fig. 16.11. The geometrical and mechanical parameters of the shells are taken from Example 16.3.

The values of the unknown interface forces, H_1 and H_2, as well the moment M_0, are evaluated from the conditions of deformations, compatibility of the shell parts and ring. Let the shell and ring be made of the same material. Assume that the

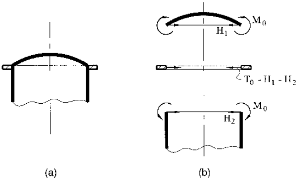

Fig. 16.11

Comparing this bending stress due to the edge effect with the corresponding stress from the previous example, we can conclude that the setup of the ring allows one to decrease the edge effect maximum stress by more than two times, although the above stress remains quite considerable.

16.6 AXISYMMETRICALLY LOADED CONICAL SHELLS

For a conical shell, a distance s measured from the vertex of the cone along the straight meridian may be conveniently taken as a meridional coordinate of a point on the middle surface (see Sec. 13.6.2). Replacing the variable φ with a new variable s, we use the following obvious relationships

$$\mathrm{d}s = R_1 \mathrm{d}\varphi, \frac{\mathrm{d}(\ldots)}{\mathrm{d}\varphi} = R_1 \frac{\mathrm{d}(\ldots)}{\mathrm{d}s} \tag{16.53a}$$

For conical shells R_1 is a constant at infinity and does not vary with s, so that $\mathrm{d}R_1/\mathrm{d}s = 0$; hence,

$$\frac{\mathrm{d}^2(\ldots)}{\mathrm{d}\varphi^2} = R_1^2 \frac{\mathrm{d}^2(\ldots)}{\mathrm{d}s^2} \quad \text{and} \quad R_2 = s\cot\varphi, \frac{\mathrm{d}R_2}{\mathrm{d}s} = \cot\varphi. \tag{16.53b}$$

where φ is the constant value for all points on the straight meridian (Fig. 13.3).

In this section, we are concerned with the bending theory of a conical shell subjected to axisymmetrically applied edge loads. Therefore, we seek only solutions of the homogeneous bending theory equations (the edge effect solutions), because the membrane solution may be used as a particular integral of the general theory equations for conical shells. Using the relationships (16.53), we can rewrite the governing equation (16.28) in terms of the variable s, setting $R_1 = \infty$ for conical shells and $\Phi(\varphi) = 0$, as follows:

$$\begin{aligned} &\frac{\mathrm{d}^2\vartheta_1}{\mathrm{d}s^2} + \frac{1}{s}\frac{\mathrm{d}\vartheta_1}{\mathrm{d}s} - \frac{1}{s^2}\vartheta_1 = -\frac{1}{DR_2}U, \\ &\frac{\mathrm{d}^2U}{\mathrm{d}s^2} + \frac{1}{s}\frac{\mathrm{d}U}{\mathrm{d}s} - \frac{1}{s^2}U = \frac{Eh}{R_2}\vartheta_1, \end{aligned} \tag{16.54a}$$

or in the following operator form

$$\begin{aligned} &L_1(\vartheta_1) + \frac{1}{D}U = 0 \\ &L_1(U) - Eh\vartheta_1 = 0 \end{aligned} \tag{16.54b}$$

where the operator $L_1(..)$ is given by

$$L_1(\ldots) \equiv \cot\varphi\left[s\frac{\mathrm{d}^2(\ldots)}{\mathrm{d}s^2} + \frac{\mathrm{d}(\ldots)}{\mathrm{d}s} - \frac{1}{s}(\ldots)\right].$$

The solution of the governing differential equations (16.54b) can be expressed in terms of the Bessel functions or their modifications [13]. However, this rigorous approach is not suited to practical engineering calculations, as it is too lengthy even when tables of the Bessel functions are available. The problem of straining the conical shells may be solved by using the numerical methods introduced in Chapter 6 or by the finite element method technique [3,4].

$$
\begin{aligned}
U &= \mp M_e 2\beta R_2 \mathrm{e}^{-\beta x} \sin \beta x + Q_e R_2 \mathrm{e}^{-\beta x}(\cos \beta x - \sin \beta x), \\
N_1 &= \cot \varphi\left[\pm M_e 2\beta \mathrm{e}^{-\beta x} \sin \beta x - Q_e \mathrm{e}^{-\beta x}(\cos \beta x - \sin \beta x)\right], \\
N_2 &= 2\beta R_2\left[M_e \beta \mathrm{e}^{-\beta x}(\cos \beta x - \sin \beta x) \pm Q_e \mathrm{e}^{-\beta x} \cos \beta x\right], \\
M_1 &= M_e \mathrm{e}^{-\beta x}(\cos \beta x + \sin \beta x) \pm Q_e \frac{1}{\beta} \mathrm{e}^{-\beta x} \sin \beta x,\ M_2 = \nu M_1, \\
\vartheta_1 &= \pm M_e \frac{1}{\beta D} \mathrm{e}^{-\beta x} \cos \beta x + Q_e \frac{1}{2\beta^2 D} \mathrm{e}^{-\beta x}(\cos \beta x + \sin \beta x), \\
\xi &= \varepsilon_2 r = R_2 \sin \varphi \frac{1}{Eh}(N_2 - \nu N_1).
\end{aligned}
\tag{16.59}
$$

The positive directions of the edge force Q_e and moment M_e are shown in Fig. 16.12. The upper sign in Eqs (16.59) refers to the top edge (at $\varphi = \varphi_{e1}$) and the lower sign refers to the bottom edge (at $\varphi = \varphi_{e2}$) of the shell.

Example 16.4

Determine the internal forces in a conical shell subjected to the edge loads m and H, as shown in Fig. 16.13. Given $h = 0.5$ in, $\varphi = 60^\circ$, $s_1 = 10$ in., $s_2 = 30$ in., $R_2 = s_2 \cot \varphi = 17.3$ in., and $\nu = 0.3$.

Solution

The parameter β for the bottom edge is obtained from Eq. (16.57):

$$\beta = \sqrt[4]{\frac{3(1-\nu^2)}{R_2^2 h^2}} = 0.4371 \quad (1/\text{in.}).$$

The edge loads on the bottom edge are

$$M_e = m, \quad Q_e = H \sin 60^\circ = 0.866H.$$

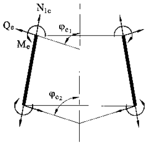

Fig. 16.12

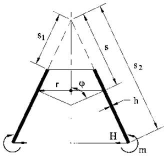

Fig. 16.13

Using Eqs (16.59) and setting $x = 0$, we can calculate the angle of rotation of the normal to the meridian, ϑ_1, and the internal forces at the bottom edge. We have

$$\vartheta_1 = -\frac{m}{\beta D} + \frac{Q_e}{2\beta^2 D} = -2.29\frac{m}{D} + 2.28\frac{H}{D},$$

$$N_1 = -Q_e \cot\varphi = -0.5H,$$

$$N_2 = 2\beta R_2(m\beta - Q_e) = 6.58m - 13.1H.$$

Comparing these numerical data with those obtained by using the exact edge effect procedure based on the use of the Bessel functions [12], we can conclude that the error of this approximate analysis does not exceed 1% for the given case.

16.7 AXISYMMETRIC DEFORMATION OF TOROIDAL SHELLS

Structural components having a form of toroidal shells are commonly used in mechanical engineering. Housings of pumps, hydraulic clutches, tanks, bellows, etc., are examples of such shape of a shell. The shape of a toroidal shell is characterized by the radii R and a and by the following parameters (Fig.16.14):

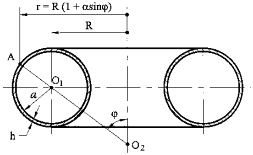

Fig. 16.14

$$\alpha = \frac{a}{R}, \quad \beta = \frac{a}{h}. \tag{16.60}$$

For a toroidal shell, the principal radii of curvature are (Fig. 16.13)

$$O_1A = R_1 = a = \text{const}, \quad O_2A = R_2 = R\frac{1 + \alpha \sin\varphi}{\sin\varphi}, \tag{16.61}$$

where φ is the angular coordinate varying in the range $-180^\circ < \varphi < 180^\circ$. Toroidal shells, except for shallow part near $\varphi = 0$, can be successfully analyzed by the methods of the theory of edge effect (see Sec. 16.4).

For shells including the shallow part near $\varphi = 0$, the problem becomes more complicated. Considerable difficulties are associated with determining a particular solution of the nonhomogeneous governing differential equations, because the membrane solution near $\varphi = 0$ becomes invalid. Thus, toroidal shells must be analyzed by using the governing equations of the general moment theory of axisymmetric shells of revolution. Substituting for the principal radii of curvature from the relations (16.61) into Eqs (16.30), we obtain the following governing differential equations of the axisymmetric deformation of toroidal shells:

$$\begin{aligned} &L_2(U) + \nu L_2(U) = Eha\vartheta_1(\varphi) + \Phi^*(\varphi),\\ &L_2(\vartheta_1) - \nu\vartheta_1 = -\frac{a}{D}U, \end{aligned} \tag{16.62}$$

where

$$\begin{aligned} L_2(\ldots) &= \frac{1 + \alpha\sin\varphi}{\sin\varphi}\frac{\mathrm{d}^2(\ldots)}{\mathrm{d}\varphi^2} + \cot\varphi\frac{\mathrm{d}(\ldots)}{\mathrm{d}\varphi} - \frac{\alpha\cot\varphi\cos\varphi}{1 + \alpha\sin\varphi}(\ldots),\\ \Phi^*(\varphi) &= a^2\frac{\mathrm{d}}{\mathrm{d}\varphi}\left[p_3\frac{(1 + \alpha\sin\varphi)^2}{\alpha^2\sin^2\varphi}\right] + p_1a^2\frac{(1 + \alpha\sin\varphi)}{\alpha\sin\varphi}\left(\frac{1 + \alpha\sin\varphi}{\alpha\sin\varphi} + \nu\right)\\ &\quad + F(\varphi)\frac{\cos\varphi(2 + 3\alpha\sin\varphi)}{\alpha\sin^4\varphi(1 + \alpha\sin\varphi)}. \end{aligned} \tag{16.63}$$

The solution of Eqs (16.62) can be obtained by numerical methods introduced in Chapter 6 – in particular, by the finite element method.

PROBLEMS

16.1 Derive Eqs (16.5).

16.2 Derive Eqs (16.9).

16.3 Show that the vertical displacement of a point in the middle surface of shell of revolution, η (see Fig. 16.1) are governed by the following equation

$$\eta = \int_{\varphi_0}^{\varphi}(\varepsilon_1\sin\bar{\varphi} + \vartheta_1\cos\bar{\varphi})R_1\,\mathrm{d}\bar{\varphi}.$$

16.4 Verify Eqs (16.50).

16.5 Consider a spherical dome supporting its own weight and described in Sec. 14.1.1. Assume that the supports are as shown in Fig. 14.2a. (a) Determine the bending stresses and (b) compare the bending and membrane stresses. Assume reasonable values for any additional properties and parameters required.

16.6 A dome in the form of a spherical segment is clamped around its base and is loaded by an external pressure $p = 1.5$ MPa. Determine the force and moment applied to the base of the shell by support. Take φ_1 (the meridional angle at the shell base) = 55°, $E =$ 200 GPa, $\nu = 0.3$, $h = 20$ mm, and $R = 1500$ mm.

16.7 A cylindrical tank is capped by a hemispherical shell, as shown in Fig. 16.6. The tank is loaded by an internal pressure $p = 1.4$ MPa. Determine the discontinuity stresses at the junction. Take the allowable membrane stress $\sigma_{\text{all}} = 120$ Mpa, $E = 200$ GPa $\nu = 0.3$, $R = 1000$ mm, $h_c = h_s = 12$ mm, where h_c and h_s are the thicknesses of the cylindrical tank and hemispherical shell, respectively.

16.8 A hemispherical cap of radius R and thickness h is loaded by uniformly applied to the free edge of the cap moments M_0. Determine the length L, measured along the meridian from the loaded edge of the cap, where the internal moment M_1 diminishes to 1% of moment M_0. How does this length compare with that in Example 15.1 for a cylindrical shell?

16.9 Redo Problem 16.8 replacing the moments M_0 with uniformly applied horizontal forces Q_0 to the free edge of the cap.

16.10 What is the maximum stress at the junction of the flat circular plate and (a) hemispherical shell (Fig. P.16.1a) and (b) conical shell with $\alpha = 37°$ (Fig. P.16.1b)? Both shells are subject to an internal pressure of $p = 1.5$ MPa. Let $E = 200$ GPa, and $\nu = 0.27$.

16.11 A conical frustum has a free edge at its top and it is built-in at the base. The shell is subject to internal pressure p. Determine the internal forces and bending moments in the shell. Let the radii of the parallel circles at the shell top and its base be 5.5 m and 8.5 m, respectively, $h = 60$ mm, $E = 200$ GPa, and $\nu = 0.3$. Employ the approximate method of Sec. 16.4 to determine the bending stress resultants and couples.

16.12 Calculate the displacements of the edge of the hemispherical shell shown in Fig. 16.5a. For your calculations use the numerical data in Example 16.1.

16.13 Compare the values of the normal stresses in the spherical shell segment for four variants of boundary conditions at its base: (a) the shell is loaded by a normal meridional force N_e applied to its free edge; (b) the shell is built-in; (c) the shell has roller supports at its free edge; and (d) the shell is simply supported. The shell is subjected to an external normal pressure p. Let $R = 30h$ and $\varphi_1 = 35°$(meridional angle at the shell base) for all the above-mentioned shells. Employ the approximate method of Sec. 16.4 for the solution.

16.14 Consider the Intze-type water tank of Problem 14.18 (Fig. 14.14a). (a) Find the bending stress resultants and couples in the wall and the roof and plot their diagrams. (b) Assume that there is no ring beam at B. Find the final value of N_2 in the cone at B using the moment theory. Neglect the effects of discontinuities at C on the stresses

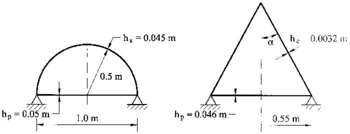

Fig. P16.1

at B. In your calculations assume that the modulus of elasticity of the wall and the roof are the same and Poisson's ratios are zero. Use the numerical data in Problem 14.18 for the solution.

16.15 Find the bending field in the intersection of the cylindrical wall and its conical end caps in the cylindrical pressure vessel shown in Fig. P.14.4. Take $H = 2R = 2\,\text{m}$, $h_1 = 10$ mm, $h_2 = 12\,\text{mm}$, $E = 200$ GPa, $\nu = 0.3$.

16.16 Consider the water tank shown in Fig. P.14.3. Perform a complete analysis of this tank. Let $R = 500\,\text{mm}$, $H = 2R$, and $h_1 = h_2 = 5\,\text{mm}$. Assume reasonable values for any additional properties required.

16.17 Consider a conical shell with a central angle α, the base radius a, and thickness h. The lower edge of this cone is fixed against rotation and translation. The shell is subjected to its own weight with intensity p. Perform a complete analysis of this shell.

16.18 Verify Eqs 16.62.

REFERENCES

1. Collatz, L., The *Numerical Treatment of Differential Equations*, 3rd edn, Springer-Verlag, Berlin, 1966.
2. Godunov, S.K., *Ordinary Differential Equations with Constant Coefficients* (translated from Russian), Providence, R.I. American Mathematical Society, 1997.
3. Zienkiewicz, O.C., *The Finite Element Method*, McGraw-Hill, New York, 1977.
4. Ashwell, D.G. and Gallagher, R.H. (eds) *Finite Elements for Thin Shells and Curved Members*, Wiley, London, 1976.
5. Meissner, E., Das elastizitatsproblem für dünne schalen von ringflächen, kugel-, and kegelform, *Physik Zeit*., vol. 14, pp. 343–349 (1913).
6. Reissner, H., *Spannungen in Kugelschalen* , Müller, Breslau-Festscher, 1912.
7. Geckeler, J., *Über die Festigkeit Achsensymmetrischer Schalen*, Forschg.-Arb. Ingwes, p. 276, Berlin, 1926.
8. Meissner, E., Über elastizität und festigkeit dünner schalen, *Viertelschr d Natur, Ges*, Bd. 60, Zürich, 1915.
9. Novozhilov, V.V., *The Theory of Thin Elastic Shells,* P. Noordhoff Ltd, Groningen, the Netherlands, 1964.
10. Timoshenko, S.P. and Goodier, J.N., *Theory of Elasticity*, 3rd edn, McGraw-Hill, New York, 1970.
11. Feodosyev, V., *Strength of Materials*, Izdatelstvo Mir, Moscow, 1968.
12. Boyarshinov, S.V., *The Fundamentals of Structural Mechanics of Machines*, Izdatelstvo Mashinostroenie, Moscow, 1973 (in Russian).
13. Watson, G.N., *Theory of Bessel Functions*, 2nd edn, Cambridge University Press, Cambridge, 1944.
14. Biderman, V.L., *Mechanics of Thin-Walled Structures*, Izdatelstvo Mashinostroenie, Moscow, 1977 (in Russian).

17.2.1 The governing differential equations of the semi-membrane theory

It was mentioned previously that the membrane theory is inapplicable for the stress analysis of long cylindrical shells. Another deficiency of the membrane theory is the impossibility of satisfying the prescribed boundary conditions on the longitudinal edges of an open cylindrical shell. Vlasov [1] proposed an approximate approach, the so-called *semi-membrane theory of cylindrical shells*, which is free of those drawbacks. Moreover, this theory is significantly simpler than the general theory of cylindrical shells. As a result, Vlasov's theory has been widely adapted in engineering practice for the analysis of cylindrical shell structures.

The semi-membrane theory is based on the following assumptions (along with the general Kirchhoff–Love hypotheses):

1. *The bending, M_1, and twisting, H, moments at sections normal to the shell generator are insignificant and may be neglected.* This means that the normal stresses are assumed to be uniformly distributed across the shell thickness at a section, perpendicular to the longitudinal axis of the shell.
2. *The circumferential strain ε_2 and shear strain γ_{12} in the middle surface are neglected.*
3. *Poisson's ratio is zero, i.e., $\nu = 0$.*

Introducing these assumptions implies that a real shell is replaced by the model depicted in Fig. 17.1a. According to this model, a shell consists of innumerable sets of transverse elementary curvilinear strips connected by hinged bonds. Each such strip works in bending in the plane of the shell cross section. Forces are transmitted from strip to strip by means of rods. The latter can transmit only in-plane normal and shear forces, N_1 and S, respectively. Non-zero stress resultants and couples are shown in Fig. 17.1b.

The assumptions introduced above are justified by some physical considerations. Gol'denveizer [5] and Novozhilov [2] showed that these assumptions are mathematically equivalent to the inequality

$$\left|\frac{\partial^2 f}{\partial x^2}\right| \ll \left|\frac{\partial^2 f}{\partial \theta^2}\right|, \tag{17.1}$$

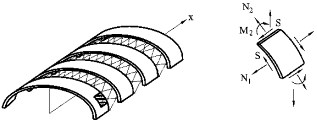

(a) (b)

Fig. 17.1

The constants of integration are evaluated from boundary conditions prescribed on the edges of a shell for the total solution (Eq. (17.23)).

For a very long shell that satisfies the following condition

$$\beta_k L \geq 3 \quad \text{or} \quad L \geq 2.5R\sqrt{\frac{R}{h}} \quad (k \geq 2) \tag{17.25}$$

it is advantageous to represent the total solution in the following form, analogous to the expression (15.53):

$$V_k = C_{1k} e^{-\beta_k x} \sin \beta_k x + C_{2k} e^{-\beta_k x} \cos \beta_k x + V_{kp}. \tag{17.26}$$

The constants C_{1k} and C_{2k} are evaluated from boundary conditions prescribed at the shell edge $x = 0$.

Example 17.1

A simply supported thin-walled cylindrical tube with flat ends is filled by water up to the level H, as shown in Fig. 17.2. Determine the deformations and stresses due to the water pressure. Given $L = 40\,\text{m}$, $2R = 3.2\,\text{m}$, and $H = 0.516\,\text{m}$.

Solution

The water pressure on the cylindrical wall of the tube and on its ends is given by the following:

$$\text{for} -\theta_0 \leq \theta \leq \theta_0 \quad p_3 = -\gamma_l R(\cos\theta - \cos\theta_0), \tag{a}$$

$$\text{for } \theta_0 \leq \theta \leq (2\pi - \theta_0) \quad p_3 = 0, \tag{b}$$

where γ_l is the specific weight of water. The negative sign in Eq. (a) is taken because p_3 is assumed to be positive in the inward direction.

The pressure on the bottoms and on the cylindrical surface may be considered independent from one another. Since the ends have a significant stiffness against deformations in their own planes that excludes the possibility of distortion of the shape of the circumference near the tube edge, the pressure on the bottom will cause an eccentric tension of the tube.

Determine the deformation of the tube caused by the water pressure on the cylindrical surface of the tube. Let us expend the pressure into the following series in θ:

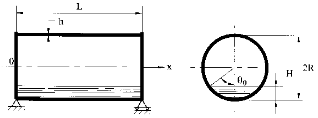

(a) (b)

Fig. 17.2

$$v = 0|_{x=0,L} \quad \text{and} \quad N_1 = 0\big|_{x=0,L}. \tag{i}$$

(It is assumed that the shell ends offer no resistance to the displacements that are perpendicular to the end planes. The water pressure is of no concern here; it may be taken into account separately.) Using Eqs (17.8a) and (17.19), we can rewrite the boundary conditions (k) in terms of the function V_k as follows:

$$V = 0_k\big|_{x=0,L} \quad \text{and} \quad \left(\frac{\mathrm{d}^2 V_k}{\mathrm{d}x^2}\right) = 0\Bigg|_{x=0,L}. \tag{j}$$

Due to the symmetry of the boundary conditions, the general solution of the differential equation (h) can be conveniently represented in the form of the following trigonometric series:

$$V_k = \sum_{m=1,3,5,\ldots}^{\infty} A_{km} \sin\frac{m\pi x}{L}. \tag{k}$$

It can be easily shown that V_k in the form of the series (k) satisfies all the boundary conditions (i). Inserting the series (m) into the differential equation (h) results in the equality

$$\sum_{m=1,3,5,\ldots}^{\infty} A_{km}\left(\frac{m\pi}{L}\right)^4 \sin\frac{m\pi x}{L} + 4\beta_k^4 \sum_{m=1,3,5,\ldots}^{\infty} A_{km} \sin\frac{m\pi x}{L} = -\frac{2k^3 \gamma_l f_k}{\pi E h R}. \tag{l}$$

To determine the coefficients A_{km}, we multiply both sides of the above equation by $\sin m\pi x/L$ and integrate from 0 to L. As a result, we obtain

$$A_{km} = -\frac{8k^3 \gamma_l f_k L^4}{m\pi^2 REh(m^4\pi^4 + 4\beta_k^4 L^4)}. \tag{m}$$

Inserting the above into Eqs (k) and (17.19), yields the following trigonometric series for v:

$$v = -\sum_{k=1,2,\ldots}^{\infty} \sum_{m=1,3,5,\ldots}^{\infty} \frac{8k^3 \gamma_l f_k L^4}{m\pi^2 REh(m^4\pi^4 + 4\beta_k^4 L^4)} \sin\frac{m\pi x}{L} \sin k\theta. \tag{n}$$

These series converge very rapidly. Knowing v, we can calculate the remaining displacement components u and w (see Eqs (17.6)) and the stress resultants and couples (see Eqs (17.7)–(17.11)). For $k = 1$, the parameter $\beta_k = 0$ and the corresponding solution will coincide with the elementary solution of the bending theory of a beam.

Let us present the solution of the same problem assuming that the tube is supported by a rigid collar at its midspan, as shown in Fig. 17.3. It is assumed that the collar prevents completely a distortion of the circular cross section of the tube.

In this case, the shell has two segments. Taking the origin of the coordinate system at a middle point of the shell length, one can write the following boundary conditions for function V_k $(k \geq 2)$:

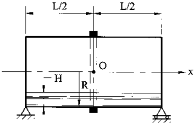

Fig. 17.3

$$\begin{aligned} &u = 0, \quad v = 0, \quad V_k = 0, \quad \frac{\mathrm{d}V_k}{\mathrm{d}x} = 0 \Big|_{x=0} \quad \text{and} \\ &v = 0, \quad N_1 = 0, \quad V_k = 0, \quad \frac{\mathrm{d}^2 V_k}{\mathrm{d}x^2} = 0 \Big|_{x=L/2} . \end{aligned} \tag{o}$$

Since these boundary conditions are asymmetric, the solution should be sought in the form of Eq. (17.23), (17.24) i.e., as the sum of V_{kc} and $V_{k\mathrm{p}}$. Evaluating the constants of integration A_{ik} ($i = 1, 2, 3, 4$) in the above solution from the boundary conditions (o), we can determine the circumferential displacement v from Eq. (17.19) and then can calculate all the displacement and stress components. Figure 17.4 depicts the diagrams of the meridional normal stresses $\sigma_1$over the middle cross section of the tube:

(a) according to the elementary beam bending theory (Fig. 17.4a);
(b) based on Vlasov's theory, in the absence of the reinforcing collar (Fig. 17.4b); and
(c) based on Vlasov's theory but with the rigid collar at the tube midspan (Fig. 17.4c).

Figure 17.5 shows the diagrams of the meridional normal stresses σ_1 in the lower stretched fiber along the tube length for the above-mentioned three cases.

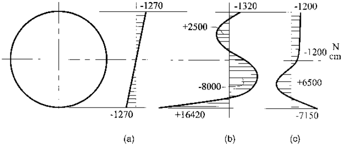

Fig. 17.4

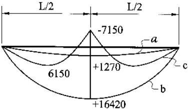

Fig. 17.5

The last two solutions (for Cases b and c) were obtained by retaining four terms in the expansion (m).

Comparing the bending stress diagrams depicted in Figs 17.4 and 17.5, one concludes that:

(a) Stresses in the shell for the given loading differ significantly from those calculated by the elementary beam bending theory.
(b) The bending stresses are noticeably reduced if a rigid collar, preventing a distortion of the tube cross section, is present. The character of the stress distribution is also changed.

This example was taken from Ref. [6].

If a large number of rigid collars were placed over the shell length in such a way that all its cross sections remained circular and undistorted, the deformations and stresses would not be different from those calculated by the beam bending theory. Based on the above, one can conclude that the most efficient way of decreasing stresses in shell structures is to attach rigid collars to the shells. If a shell is loaded by a concentrated force, normal to the shell middle surface, then it is sufficient to set up only one rigid collar at a place of the force application. In this case, the shell will deform as a beam, i.e., without distortion of its cross section.

In conclusion, let us discuss some issues regarding accuracy and area of application of the semi-membrane theory. It was indicated earlier (see Chapter 13) that the accuracy of solutions given by the membrane theory depends on the smoothness of a shell geometry, the smoothness of an applied loading, and on the formulation of boundary conditions. However, for a cylindrical shell, in addition to these requirements, one more requirement is added – namely, a shell length (see Sec. 13.6). It was shown in that section that the accuracy of the membrane solution decreases with an increase in the shell length, even if the other requirements of the existence of the membrane state of stress are satisfied. From a physical point of view, this means that for a long cylindrical shell the boundary conditions have little effect on the stresses and deformations in its middle part and these boundary conditions cannot prevent the appearance of significant bending stresses in this part of the shell (if an external loading is capable of causing the bending stresses).

Thus, the semi-membrane theory holds an intermediate place between the membrane theory and the general theory of thin shells (see Chapter 12). It can be applied to relatively long open and closed cylindrical shells with an arbitrary shape of the cross section if the variation of the displacement and stress components in the direction of the shell generator is smoother than their variation in the circumferential

It can be shown that the first two equations of the above system are automatically satisfied if we substitute for χ_1, χ_2, and χ_{12} from the kinematic relations (17.29). The third equation of the system (17.35), after substituting for $\varepsilon_1, \varepsilon_2$, and γ_{12} from Eqs (12.45) together with Eqs (17.31), and for χ_1, χ_2, and χ_{12} from Eqs (17.29), and after some transformations with the use of the Codazzi–Gauss relations, takes the form

$$\nabla^2\nabla^2\Phi + Eh\nabla_k^2 w = 0. \tag{17.33b}$$

Thus, the *system of the governing differential equations of the approximate DMV theory* of thin shells have the following form:

$$\begin{aligned} -\nabla_k^2\Phi + D\nabla^2\nabla^2 w &= p_3, \\ \nabla^2\nabla^2\Phi + Eh\nabla_k^2 w &= 0. \end{aligned} \tag{17.36}$$

The first equation of the above system is the equilibrium equation, whereas the second one represents the compatibility equation. For a flat plate, $\kappa_1 = 0$ and $\kappa_2 = 0$, and therefore, $\nabla_k^2(\ldots) = 0$. Hence, for flat plates, the first and second Eqs (17.36) are uncoupled. The second equation, $\nabla^2\nabla^2\Phi = 0$, determines the Airy stress function of the plane stress problem, and the second one, $D\nabla^2\nabla^2 w = p_3$, describes the plate bending problem, as discussed in Part I of the book. The operator ∇_k^2, depending upon the shell curvatures, characterizes in Eqs (17.36) the coupled effect between the bending and membrane stress resultants.

In conclusion, let us briefly discuss a practical application of the DMV theory of thin shells. As mentioned previously, it can be applied to closed or open shells of any geometry if the state of stress is rapidly varying, at least, in one direction. It should be noted that solutions of the membrane shell problem and problem of pure bending are given by slowly varying functions. Therefore, the DMV theory can give a serious error in the stress analysis of such shell problems only if a shell area under consideration is not small compared with the radius $|R|_{\min}$. The DMV theory can be applied successfully to the analysis of thin shells whose state of stress is described by rapidly varying functions as, for instance, in the edge effect state of stress, discussed in detail in Sec. 17.5 for thin shells of any geometry. The DMV theory can also be correctly applied to the stress analysis of the shallow shells introduced in the next section. Lur'e [8] showed that the analysis of not too long $\left(\frac{L}{R} \le 0.75\sqrt{\frac{R}{h}}\right)$ cylindrical shells, based on the DMV theory, gives sufficiently accurate results even for slowly varying loads.

17.4 THEORY OF SHALLOW SHELLS

Shallow shells are frequently used for roof structures of industrial and public buildings. They are also used in mechanical and aerospace engineering applications. The theory of shallow shells can be also used to analyze shells that become locally shallow when the original shell is divided into finite segments or elements (see, for instance, Chapter 19).

Shallow shells were introduced in Sec. 11.8.4. Let us define a shallow shell in a more rigorous manner. Take the Cartesian coordinates x and y of the projections of points of the shell's middle surface on the coordinate plane Oxy as curvilinear

(d) No displacements of the shell edge are allowed in the y direction, i.e.,

$$v = 0. \tag{17.47b}$$

In solving real design problems, various combinations of these boundary conditions can be met. For example, for a clamped shell edge that is parallel to the y axis, the boundary conditions are given by

$$u = v = w = \frac{\partial w}{\partial x} = 0. \tag{17.48}$$

If a shell edge rests on a diaphragm that is absolutely rigid in its own plane and flexible out of the plane, the boundary conditions have the form

$$\frac{\partial^2 \Phi}{\partial y^2} = 0, \quad v = w = \frac{\partial^2 w}{\partial x^2} = 0. \tag{17.49a}$$

If a shell edge can displace freely along this diaphragm, then we have

$$\frac{\partial^2 \Phi}{\partial y^2} = \frac{\partial^2 \Phi}{\partial x \partial y} = 0, \quad w = \frac{\partial^2 w}{\partial x^2} = 0. \tag{17.49b}$$

Similarly, the boundary conditions can be presented for the shell edge $y = \text{const}$.

For the analysis of shallow shells it is necessary to solve the system of equations (17.36), satisfying the above boundary conditions for the functions w and Φ. For a solution of these equations, some analytical and numerical methods, introduced in Chapter 6, may be applied. One of the most adapted analytical methods for solving this system of linear differential equations for a shallow shell with constant curvatures whose edges form a rectangular plane is the Fourier method of double series, which is similar to the Navier method discussed in Sec. 3.3 for bending of rectangular plates. Variational methods are frequently used for analyses of shallow shells. In order to apply the variational methods introduced in Chapter 6, let us set up the expression for the strain energy of shallow shells. Substituting for N_1, N_2, and S from Eqs (17.45a) and for M_1, M_2, and H from Eqs (17.45b) into Eq. (12.52) and setting $A = B = 1$, we obtain the following expression for the strain energy of shallow shells:

$$\begin{aligned} U = {} & \frac{1}{2Eh} \int\!\!\int_A \left\{ \left(\frac{\partial^2 \Phi}{\partial x^2} + \frac{\partial^2 \Phi}{\partial y^2} \right)^2 - 2(1+\nu) \left[\frac{\partial^2 \Phi}{\partial x^2} \frac{\partial^2 \Phi}{\partial y^2} - \left(\frac{\partial^2 \Phi}{\partial x \partial y} \right)^2 \right] \right\} \mathrm{d}A \\ & + \int\!\!\int_A \frac{D}{2} \left\{ \left(\frac{\partial^2 w}{\partial x^2} + \frac{\partial^2 w}{\partial y^2} \right)^2 - 2(1-\nu) \left[\frac{\partial^2 w}{\partial x^2} \frac{\partial^2 w}{\partial y 2} - \left(\frac{\partial^2 w}{\partial x \partial y} \right)^2 \right] \right\} \mathrm{d}A, \end{aligned} \tag{17.50}$$

where A is the area of the middle surface of the shallow shell.

Writing the corresponding expressions for work done by external loads, W_e, and the total potential energy, Π, we can apply the Ritz method (see Sec. 6.6) for solving various problems of shallow shell analysis.

Example 17.2

A shallow, rectangular in a plane, shell of sides a and b, is subjected to a normal uniform surface load $p_0 = \text{const}$ directed downward. The middle surface of the shell has the form of an elliptic paraboloid:

$$z = f\left[\frac{f_1}{f}\left(2\frac{x}{a} - 1\right)^2 + \frac{f_2}{f}\left(2\frac{y}{b} - 1\right)^2 - 1\right], \tag{a}$$

where $f = f_1 + f_2$ is the rise of the shell (Fig. 17.6). The shell rests on the diaphragms along its edges. These diaphragms are absolutely rigid in their planes and flexible out of the planes. Determine the deflections, internal forces, and moments.

Solution

Determine the principal curvatures of the shell. It follows from Eqs (17.41) that we have

$$\kappa_1 = 8\frac{f_1}{a^2}, \kappa_2 = 8\frac{f_2}{b^2}, \quad \kappa_{12} = 0. \tag{a}$$

Substituting the above into the expressions (17.44), we can write the system of equations (17.36), as follows (making $p_3 = p_0$):

$$\begin{aligned} &D\nabla^2\nabla^2 w - 8\frac{f_1}{a^2}\frac{\partial^2\Phi}{\partial y^2} - 8\frac{f_2}{b^2}\frac{\partial^2\Phi}{\partial x^2} = p_0, \\ &\frac{1}{Eh}\nabla^2\nabla^2\Phi + 8\frac{f_1}{a^2}\frac{\partial^2 w}{\partial y^2} + 8\frac{f_2}{b^2}\frac{\partial^2 w}{\partial x^2} = 0. \end{aligned} \tag{b}$$

The boundary conditions on the shell edges have a form of Eqs (17.49a). Taking into account the expressions (17.45), these boundary conditions can be represented, as follows:

$$w = 0\big|_{x=0,a}; \quad \frac{\partial^2 w}{\partial x^2} = 0\Bigg|_{x=0,a}; \quad \frac{\partial^2\Phi}{\partial y^2} = 0\Bigg|_{x=0,a}; \quad v = 0|_{x=0.a}; \tag{c}$$

$$w = 0\big|_{y=0,b}; \quad \frac{\partial^2 w}{\partial y^2} = 0\Bigg|_{y=0,b}; \quad \frac{\partial^2\Phi}{\partial x^2} = 0\Bigg|_{y=0,b}; \quad u = 0|_{y=0,b}. \tag{d}$$

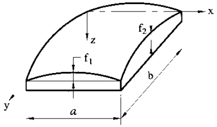

Fig. 17.6

Solving this system for unknown functions φ_{mn} and w_{mn}, gives

$$w_{mn} = \left[\frac{\pi^4 n^4 h^4}{12(1-\nu^2)b^4} A_{mn} + \frac{64 f^2 h^2}{A_{mn} a^4}\left(\frac{f_1}{f} + \frac{m^2}{n^2}\frac{f_2}{f}\right)^2\right]^{-1} \frac{p_{mn} h}{E},$$
$$\varphi_{mn} = \frac{8Eb^2 fh}{\pi^2 A_{mn} a^2 n^2}\left(\frac{f_1}{f} + \frac{m^2 f_2}{n^2 f}\right) w_{mn}, \tag{i}$$

where

$$A_{mn} = \left(\frac{m^2 b^2}{n^2 a^2} + 1\right)^2; \quad m, n = 1, 3, 5, \ldots. \tag{j}$$

Having determined the functions w and Φ, the internal forces and moments may be found from Eqs (17.45). We have the following:

$$M_1 = D \sum_{m=1,3,\ldots}^{\infty} \sum_{n=1,3,\ldots}^{\infty} w_{mn}\left(\frac{m^2\pi^2}{a^2} + \nu\frac{n^2\pi^2}{b^2}\right) \sin\frac{m\pi x}{a} \sin\frac{n\pi y}{b},$$
$$M_2 = D \sum_{m=1,3,\ldots}^{\infty} \sum_{n=1,3,\ldots}^{\infty} w_{mn}\left(\frac{n^2\pi^2}{b^2} + \nu\frac{m^2\pi^2}{a^2}\right) \sin\frac{m\pi x}{a} \sin\frac{n\pi y}{b},$$
$$H = -D(1-\nu) \sum_{m=1,3,\ldots}^{\infty} \sum_{n=1,3,\ldots}^{\infty} w_{mn}\frac{mn\pi^2}{ab} \cos\frac{m\pi x}{a} \cos\frac{n\pi y}{b},$$
$$N_1 = -\sum_{m=1,3,\ldots}^{\infty} \sum_{n=1,3,\ldots}^{\infty} \varphi_{mn}\frac{n^2\pi^2}{b^2} \sin\frac{m\pi x}{a} \sin\frac{n\pi y}{b},$$
$$N_2 = -\sum_{m=1,3,\ldots}^{\infty} \sum_{n=1,3,\ldots}^{\infty} \varphi_{mn}\frac{m^2\pi^2}{a^2} \sin\frac{m\pi x}{a} \sin\frac{n\pi y}{b},$$
$$S = -\sum_{m=1,3,\ldots}^{\infty} \sum_{n=1,3,\ldots}^{\infty} \varphi_{mn}\frac{mn\pi^2}{ab} \cos\frac{m\pi x}{a} \cos\frac{n\pi y}{b}. \tag{k}$$

Setting in the relations (i) $f_1 = f_2 = 0$, we obtain the expressions for w_{mn}, which are valid for a rectangular simply supported plate, i.e.,

$$w_{mn} = \frac{p_{mn}}{D}\left(\frac{m^2\pi^2}{a^2} + \frac{n^2\pi^2}{b^2}\right)^2. \tag{l}$$

Some numerical values of the deflections, internal forces and moments were calculated with the use of Eqs (k) for the given shallow shell. The values of dimensionless coefficients $\bar{w}$, $\bar{\boldsymbol{M}}$, $\bar{\boldsymbol{N}}$ are given in Table 17.1 at the central point of the square shallow shell ($a = b$) for various dimensionless parameters $\lambda = f/h$ (λ characterizes the shallowness of a shell). The values of the deflections, internal forces, and moments are determined from the following relations:

$$w = \bar{w}\frac{p_0 a^4}{D10^4}; \quad N_1 = N_2 = -\bar{\boldsymbol{N}}\frac{p_0 a^2}{h10^2}; \quad M_1 = M_2 = \bar{\boldsymbol{M}}\frac{p_0 a^2}{10^2}. \tag{m}$$

Table 17.1

Parameter λ	Values of the dimensionless coefficients at the central point of the shell				
	Shallow shell			Plate ($\lambda = 0$)	
	$\bar{w}$	$\bar{N}$	$\bar{M}$	$\bar{w}$	$\bar{M}$
0.5	36.2101	4.2401	3.7985	39.4215	4.250
1.0	27.2112	6.3618	2.7911	39.4215	4.250
1.5	19.200	6.7200	1.9396	39.4215	4.250
2.0	13.4115	6.2501	1.1988	39.4215	4.250
3.0	7.0851	4.9501	0.5066	39.4215	4.250
4.0	4.1200	3.8102	0.2106	39.4215	4.250
5.0	2.6100	3.0115	0.07086	39.4215	4.250
6.0	1.7511	2.4510	0.01398	39.4215	4.250
10.0	0.5601	1.3102	−0.02180	39.4215	4.250
20.0	0.1364	0.6201	−0.00021	39.4215	4.250

The given numerical data for the shallow shell are compared in the table with the values of the deflections and bending moments in a rectangular simply supported plate having the same linear dimensions (a and b) as the shallow shell and subjected to the same load p_0. It follows from Table 17.1 that with an increase in the parameter λ, the load-carrying mechanism of the shallow shell changes: its stiffness increases and bending moments are diminished, i.e., for large values of λ the shallow shell supports a given normal surface load p_3 practically due to the membrane action only. Of course, this qualitative conclusion is valid not only for the considered shell but also for all of the classes of shallow shells. Comparison of the ordinates of bending moments (and deflections) in shallow shells and flat plates shows that the above-mentioned values are significantly greater (by one order) in flat plates than in shallow shells for certain values of the parameter $\lambda = f/h$ ($f = f_1 + f_2$).

To analyze the load-carrying mechanism of shallow shells subjected to a normal surface load, Fig. 17.7 illustrates some numerical results of the analysis of the shallow shell with the following geometrical and mechanical characteristics: $a = b = 10\,\mathrm{m}$, $h = 0.1\,\mathrm{m}$, $f_1 = f_2 = 0.5\ \mathrm{m}$, $E = 40\,\mathrm{GPa}$, $\nu = 0.17$, and $p_3 = p_0 = \mathrm{const}$. For this shell $D = \frac{Eh^3}{12(1-\nu^2)} = 3.4326 \times 10^6\ \mathrm{N \cdot m}$.

Figure 17.7 shows the diagrams of the deflection, w, membrane force, N_1, and bending moment, M_1, along the central section ($x = a/2$) of the shell. It should be noted that the location of the maximum deflection in the shallow shell shifts from the center (as it was in a flat plate) towards the supports. The bending moment distributions in the shell, both qualitatively and quantitatively, differ from those in flat plates. The numerical results in Fig. 17.7 and in Table 17.1 were obtained by retaining the six terms in the series (e), and eight and 10 terms in the series (k) for the deflections, membrane forces, and bending moments, respectively. In conclusion, let us make some comments.

1. When a shallow shell rise, f, increases, the shell geometry will differ noticeably from plane geometry, i.e., the first basic assumption of the shallow shell theory

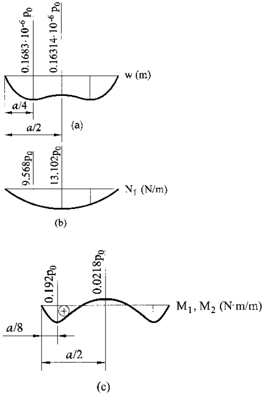

Fig. 17.7

will become more and more rough. The second basic assumption (the basic assumption of the DMV theory) remains still to be justified up to some value of $f = f^*$. The latter is determined by peculiarities of the shell geometry and loading. Therefore, for $f > f^*$ there is a good reason to analyze such shells by applying the more general DMV theory.

2. As mentioned previously, a shallow shell is an open shell that differs little from a plane. However, in some exceptional cases, non-shallow shells and closed shells can also be analyzed by the shallow shell theory. Such a case may be when a non–shallow shell is divided into parts some of which can be approximated by shallow shells. The most important such cases are (a) a non-shallow shell reinforced by equally spaced stiffeners for which any shell part between the stiffeners can be treated as a shallow shell and (b) buckling of shells of any geometry when this buckling is accompanied by a large number of bulgings whose dimensions are small compared with the minimum radius of the shell curvature (see Chapter 19).

17.5 THE THEORY OF EDGE EFFECT

In this section we introduce one more approximate theory of thin shells. As mentioned in Sec. 17.3, a thin shell can be found in the basic state of stress that is characterized by slowly varying deformations and stresses. The membrane (see Chapters 13 and 14) and pure bending stress states fall into the category of the basic state of stress. The pure bending state rarely occurs. It is possible for nonrigid shells only whose constraints allow such a type of bending. In some cases, the state of stress in thin shells can be separated into the following two components: the basic (mainly, membrane) for the entire shell and the mixed, mostly, a moment state, called *edge effect*, localizing near shell boundaries or near other sites at which the membrane theory does not apply. The latter state of stress can be superimposed on the basic state that essentially simplifies the obtaining of the general state of stress in a shell. It was indicated in Chapters 13–16 that the membrane solution alone for some shell geometries, loadings, and supports cannot satisfy the prescribed boundary conditions at the shell edges, the known conditions of continuity, equilibrium and/or kinematic constraints at the edge effect zones. Gol'denveizer termed the sources of edge effects ''*lines of distortion*.'' To facilitate their identification, Gol'denveizer listed these as [5]:

(a) the physical edges of a shell;
(b) lines along which discontinuities of the components of external loads or of certain their derivatives occur;
(c) lines along which the middle surface of a shell has a break or the curvature of the middle surface changes abruptly; and
(d) lines along which the rigidity of a shell or its thickness undergoes sudden changes.

The edge effect can be defined as such a state of stress and strain at which stresses and displacements vary slightly along the lines of distortion, but decay rapidly in the normal direction to those lines.

The edge effect concept was demonstrated in Chapters 15 and 16 for axisymmetrically loaded circular cylindrical shells and shells of revolution, respectively. This section is concerned with constructing the general theory of the edge effect for shells of any geometry subjected to asymmetric loading.

In deriving the governing differential equations of the theory of edge effect, we make the following assumptions:

1. The lines of distortion coincide with one of the lines of curvature (for definiteness sake, with the β-coordinate line).

   Let us introduce the so-called *asymptotic line* as a line along which the normal curvature of the surface, $1/R_i$, is zero. For example, a generator of a cylindrical surface can be considered as an asymptotic line. In the theory of edge effect, it is assumed that the lines of distortion at any point of the middle surface do not touch the asymptotic line. In this case, the edge effect always takes place and it is called *simple edge effect*. If the distortion line touches an asymptotic line, then such an edge effect is referred to as a *complex* one. In this section we analyze only the simple edge effect.
2. The normal component of displacement, w, in zones of the edge effect is significantly greater than the in-plane components, u and v.

3. Functions f that characterize the state of stress and strain (displacements, internal forces, and moments) vary significantly more rapidly in the direction of the α-coordinate line than in the direction of the β-coordinate line, i.e.,

$$\left|\frac{\partial f}{A\partial\alpha}\right| \gg \left|\frac{\partial f}{B\partial\beta}\right|. \tag{17.51}$$

(4) The Lamé parameters, A and B, as well as the radii of curvature, have a small variation in the direction of the α-coordinate line, i.e.,

$$\begin{aligned} &\frac{\partial A}{\partial\alpha} \ll A; \quad \frac{\partial B}{\partial\alpha} \ll B, \\ &\frac{\partial R_1}{\partial\alpha} \ll R_1; \quad \frac{\partial R_2}{\partial\alpha} \ll R_2. \end{aligned} \tag{17.52}$$

A rapid decay of the edge effect state of stress, as we move away along the normal to the line of distortion is a very important characteristic of a shell. It is caused by the shell thinness and by the curvilinearity of its surface. Let us explain this phenomenon in more detail in the following simple example.

Figure 17.8 shows a flat cantilever plate and an open circular cylindrical shell loaded by uniformly distributed bending moments, $m = \text{const}$, applied to the free edges of the plate and shell.

It is evident, that the cantilever plate will resist the external moment load by means of bending only (producing the bending and twisting moments, and shear forces); no membrane forces occur in its middle surface (Fig. 17.8a). The cantilever shell will support the applied distributed moments m not only by means of the bending but also by straining the middle surface. The latter is accompanied by an appearance of the circumferential membrane forces N_2 in the longitudinal sections of the shell $\varphi = \text{const}$, i.e., in the sections perpendicular to the edge $x = a$ (Fig. 17.8b). The larger the shell curvature $1/R$, the stiffer is the shell in its middle surface and the greater is the role of the membrane forces N_2 in resisting the applied bending load. The availability of the circumferential forces N_2 will cause the internal bending moment to decrease rapidly as we move away from the loaded edge in the normal direction to the edge. This phenomenon is quite understandable if we recall the

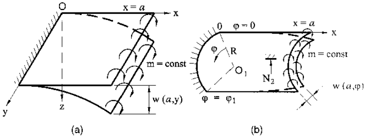

Fig. 17.8

analogy between a shell and a flat plate resting on an elastic Winkler-type foundation. The normal projections of the circumferential forces N_2 are interpreted as the reactions of the Winkler-type foundation (see Fig. 15.2 and the corresponding explanations in Sec. 15.3). Thus, the cylindrical shell shown in Fig. 17.8b acts as a flat cantilever plate resting on some elastic foundation. It is well known that stresses and displacements in such a flat cantilever plate, loaded by the distributed moments m applied along its free edge, decay rapidly as we move away from this loaded edge due to the distributed character of the elastic foundation.

For a more complete insight into the physical nature of the edge effect phenomenon, it is instructive to turn our attention to the general principles of mechanics: in particular, to the principle of minimum potential energy (see Sec. 2.6.2). It is easy to verify that the potential energy caused by bending moments is considerably larger than the potential energy due to the membrane forces. Hence, if we move away from a loaded zone that causes bending (for example, from a fixed shell edge) then, based on the principle of minimum potential energy, the process of the moment and shear force damping should begin. This a reason for the occurrence of rapidly decaying state of stress-edge effects.

Another situation occurs near the straight edges and other lines of disturbance of the state of stress and strain of a shell (the asymptotic lines). Assume, for example, that the edge $\varphi = 0$ is fixed and the other edges are free to displace. If the external moment m is applied to the edge $\varphi = \varphi_1$ then the circumferential forces N_2 are not needed for equilibrium. Therefore, the bending moments decrease slightly as we move away from the line of disturbance (in this case $\varphi = \varphi_1$) and a given state of stress cannot be separated into the membrane type and edge effect. Thus, near straight edges of open cylindrical shells, the simple edge effect concept cannot be applicable. The possibilities of simplifying the governing differential equations are more restricted here than in the case of the simple edge effect.

Now we derive the governing differential equation of the simple edge effect assuming the β-coordinate line is the distortion line. Due to the adopted assumptions (see assumptions 3 and 4), the Laplace operator, $\nabla^2 f$, and the operator $\nabla_k^2 f$ can be simplified to the form

$$\nabla^2 f \approx \frac{\partial}{A\partial\alpha}\left(\frac{\partial f}{A\partial\alpha}\right); \quad \nabla_k^2 f \approx \frac{1}{R_2}\frac{\partial}{A\partial\alpha}\left(\frac{\partial f}{A\partial\alpha}\right). \tag{17.53}$$

Since all functions describing the state of stress and strain in the zone of the simple edge effect represent some rapidly varying functions, we can use the differential equations of the DMV theory introduced in Sec. 17.3. These equations will be homogeneous for the edge effect problems. Taking into account the relations (17.53), the differential equations (17.36) for the edge effect analysis can be written in the following form:

$$\begin{aligned} &D\frac{\partial}{A\partial\alpha}\frac{\partial}{A\partial\alpha}\frac{\partial}{A\partial\alpha}\frac{\partial w}{A\partial\alpha} - \frac{1}{R_2}\frac{\partial}{A\partial\alpha}\frac{\partial\Phi}{A\partial\alpha} = 0,\\ &\frac{1}{Eh}\frac{\partial}{A\partial\alpha}\frac{\partial}{A\partial\alpha}\frac{\partial}{A\partial\alpha}\frac{\partial\Phi}{A\partial\alpha} + \frac{1}{R_2}\frac{\partial}{A\partial\alpha}\frac{\partial w}{A\partial\alpha} = 0. \end{aligned} \tag{17.54}$$

As mentioned previously, only the rapidly varying functions are of interest in the theory of the edge effect. Therefore, in integrating Eqs (17.54), arbitrary functions that depend linearly upon α should be dropped (these functions characterize the

The transverse shear forces may be found from the corresponding equilibrium equations of the DMV theory, i.e.,

$$Q_1 = -D\frac{\partial}{A\partial\alpha}(\nabla^2 w); \quad Q_2 = -D\frac{\partial}{B\partial\beta}(\nabla^2 w).$$

Using the relations (17.53), the above relations appear, as follows:

$$Q_1 = -D\frac{\partial^3 w}{\partial s_1^3}; \quad Q_2 \approx 0. \tag{17.62}$$

The above relations and equations of the general edge effect theory were introduced for the case when the distortion line coincides with the β-coordinate line. Similarly, the corresponding equations can be presented for the α-coordinate line as a distortion line and, generally, for the case when the shell edge does not coincide with the line of curvature [5].

In conclusion, one notes the following:

1. The edge effect theory introduced above cannot be applied to the case when the shell boundary or another distortion line coincides with the asymptotic line.
2. If a considered state of stress and strain varies rapidly not only in the direction of the normal to the shell boundary but also along the boundary itself, the stress analysis of such a shell can be carried out by the DMV theory introduced in Sec. 17.3.
3. The governing differential equation of the edge effect, Eq. (17.56), is only approximate. The exact solution of the shell problems by the edge effect theory requires an integration of the system of the partial differential equations of the general theory of thin shells and therefore has no advantages from separation of a given state of stress into the membrane state and edge effect. Thus, the latter is taken into account only approximately.
4. The solution (17.57) makes it possible to satisfy the two boundary conditions on the corresponding shell edge. It is evident that these boundary conditions must be formulated for the sum of the membrane solution and the solution given by Eq. (17.56).

PROBLEMS

17.1 Verify Eqs (17.12) and (17.16).

17.2 Specify the area of application of the semi-membrane theory to the analysis of open and closed cylindrical shells.

17.3 A simply supported, at $x = 0$ and $x = L$, cylindrical tube is filled by water up to the level H (Fig. 17.2). The tube is reinforced by two equally spaced, rigid along the tube length, collars in such a way that they prevent a distortion of the tube cross sections. Applying the semi-membrane theory, determine the axial normal stress, σ_1, distribution over the shell cross section where the collar is attached to the tube. Let $L = 30\,\text{m}$, $R = 5.5\,\text{m}$, $h = 5.0\,\text{cm}$, $H = 1.2\,\text{m}$, $E = 210\,\text{GPa}$, and $\nu = 0.3$.

17.4 A simply supported, at $x = 0$ and $x = L$, closed circular cylindrical shell is subjected to a uniform vertical line load q, as shown in Fig. P.17.1. Determine the axial normal stress, σ_1, distribution in the lower stretched fiber along the shell length. Compare this

$= 1$, $n = 3$; $m = 3$, $n = 1$; $m = 3$, $n = 3$) in the expansions (e) and (f) in Example 17.1. Let $a = 2.0\,\text{m}$, $h = 20\,\text{mm}$, $f_1 = f_2 = 250\,\text{mm}$, $p = 2\,\text{kPa}$, $G = 30\,\text{GPa}$, and $\nu = 0$.

17.16 A shallow shell of double curvature, shown in Fig. 17.6, is supported by diaphragms at its edges (the boundary conditions are given by Eqs (c) and (d) in Example 17.1). The shell is subjected to a uniformly distributed load of intensity p. Determine the deflections, in-plane forces, and bending moments in the shell. Take four terms in the expansions (e) and (f) (see problem 17.15). Take $a = 10\,\text{m}$, $b = 12\,\text{m}$, $\kappa_1 = 0.04/l$, m, $\kappa_2 = 0.02781/\text{m}$, $h = 30\,\text{mm}$, $E = 22\,\text{GPa}$, and $\upsilon = 0$.

17.17 Show that if deflection w is a rapidly varying function, at least in one of the coordinate directions, then the following estimate takes place:

$$\frac{|\nabla^2 w|}{\left|\frac{w}{R_1 R_2}\right|} \sim C^2$$

where $C \gg 1$.

17.18 Based on the results of Problem 17.7, derive Eqs (17.62).

17.19 Specify the area of application of the edge effect theory for open and closed cylindrical shells loaded asymmetrically.

REFERENCES

1. Vlasov, V.Z., *General Theory of Shells and its Applications in Engineering*, NASA Technical Translation TTF-99, Washington DC, 1964.
2. Novozhilov, V.V., *Thin Shell Theory* (translated from 2nd Russian edn. by P.G. Lowe), Noordhoff, Groningen, The Netherlands, 1964.
3. Donnell, L.H., *Stability of Thin Walled Tubes under Torsion*, NACA, Report No. 479, Washington, DC, 1933.
4. Mushtari, Kh.M., Certain generalizations of the theory of thin shells, *Izv Fiz Mat ob-va pri Kaz Un-te*, vol. 11, No. 8 (1938) (in Russian).
5. Gol'denveizer, A.L, *Theory of Elastic Shells* (translated from Russian by G. Herrmann), Pergamon Press, New York, 1961.
6. Boyarshinov, S.V., *The Fundamentals of Structural Mechanics of Machines*, Mashinostroenie, Moscow, 1973 (in Russian).
7. Biderman, V. L., *Mechanics of Thin-Walled Structures*, Izdatel'stvo ''Mashinostroenie'', Moscow, 1977 (in Russian).
8. Lur'e, A.L., General theory of elastic shells, *Prikl Mat Mekh*, vol. 4, No. 1, pp. 7–34 (1940) (in Russian).

Substituting Eqs (18.2) into Eqs (12.35) and (12.36) with the use of the relations (12.22), and integrating over z from $-h/2$ to $h/2$, one obtains

$$N_1 = B(\varepsilon_1 + \nu\varepsilon_2) - \frac{N_T}{1-\nu}; \; N_2 = B(\varepsilon_2 + \nu\varepsilon_1) - \frac{N_T}{1-\nu};$$

$$N_{12} = N_{21} = S = B\frac{1-\nu}{2}\gamma_{12}; \tag{18.3}$$

$$M_1 = D(\kappa_1 + \nu\kappa_2) - \frac{M_T}{1-\nu}; \quad M_2 = D(\kappa_2 + \nu\kappa_1) - \frac{M_T}{1-\nu};$$

$$M_{12} = M_{21} = H = D(1-\nu)\kappa_{12}, \tag{18.4}$$

where

$$B = Eh/(1-\nu^2) \tag{18.5}$$

is the shell stiffness in tension and N_T and M_T are the thermal stress resultants, as given by Eqs (7.8). The equations of static equilibrium, Eqs (12.41) and (12.42), and kinematic equations, Eqs (12.23) and (12.24), of the general shell theory remain unchanged. Thus, a set of thermoelastic governing differential equations within the framework of the Kirchhoff–Love postulates consists of Eqs (12.23), (12.24), (12.41), (12.42), and (18.3)–(18.5). As mentioned in Chapter 12, these equations in some cases must be complemented with the equations of compatibility. The solutions of the above equations must satisfy the prescribed boundary conditions on shell edges.

As for thin plates, the thermal stresses in a shell can occur in the following cases: in a nonuniform heating; if thermal deformations are restricted by imposed constraints; in heating of multilayered shells composed of heterogeneous materials, etc. However, not any nonuniform heating causes the thermal stresses. For instance, if the temperature varies linearly over the length of a cylindrical shell and is constant over its circumference and thickness, then the shell's middle surface becomes a conical surface, but no stresses occur.

The isothermal analogy, introduced in Sec. 7.1 for the thermoelastic plate bending problems, can be applied also for solving the thermoelastic governing shell equations together with appropriate boundary conditions. According to this analogy, the thermoelastic terms entering on the right-hand side of the governing equations may be treated as some fictitious and known surface loading. In the next sections, the thermoelastic shell equations will be applied for stress analysis of some particular shell forms and loadings.

18.1.2 Circular cylindrical shells under axisymmetric nonuniform heating

Assume that the heating of a circular cylindrical shell is axisymmetric and varies linearly across its thickness according to the following law:

$$T = T_0 + \Delta T\frac{z}{h}, \tag{18.6}$$

where $T_0 = (T_1 + T_2)/2$ is an average temperature of the shell wall; $\Delta T = T_1 - T_2$ is a temperature change; and T_1 and T_2 are the temperatures of the lower and upper surfaces of the shell, respectively.

The technique of integrating Eq. (18.11) is not different from that discussed in Sec. 15.3.

As mentioned previously, the thermal terms on the right-hand side of Eq. (18.11) can be interpreted as some fictitious surface load, q_T. So, we can rewrite Eq. (18.11), as follows:

$$\frac{\mathrm{d}^4 w}{\mathrm{d}x^4} + 4\beta^4 w = \frac{1}{D}\left(p_3 - q_T + \frac{\nu N_1}{R}\right), \tag{18.13}$$

where

$$q_T = \frac{D(1+\nu)\alpha}{h}\frac{\mathrm{d}^2(\Delta T)}{\mathrm{d}x^2} + \frac{Eh}{R}\alpha T_0. \tag{18.14}$$

Using the principle of superposition, the given thermoelastic problem for a circular cylindrical shell can be broken down into two independent problems. The first problem involves only thermal effects produced by q_T. In this case, only the particular solution is of interest (all constants of integration are assumed to be zero). The second problem deals with external forces, p_3 and N_1. Its solution was presented in Sec. 15.3. The constants of integration are evaluated in such a way that the sum of the solutions of these two problems satisfies the prescribed boundary conditions.

Example 18.1

An infinitely long circular cylindrical shell is heated according to Eq. (18.6). The temperature is a constant along the shell length. Determine the thermal stresses.

Solution

A given thermal field can be represented as a superposition of a uniform heating $T_0 = (T_1 + T_2)/2$, which produces no stresses, and of the thermal change $\Delta T = T_1 - T_2$ (Fig. 18.1).

Let us consider the state of stress corresponding to the thermal jump mentioned above. Since the temperature does not vary along the shell length, then all values are constant over the length, and, hence, a general solution of the thermal homogeneous equation is nonexistent. The particular solution (Eq. (18.12)) for $p_3 = 0$, $N_1 = 0$, and $T_0 = 0$ is also zero. Thus, the deflections of points of the middle surface w and the circumferential force N_2, according to Eq. (18.8b), are also equal

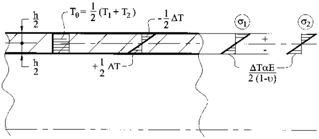

Fig. 18.1

to zero. However, the bending moments in this case are not equal to zero; it follows from Eqs. (18.9) that they are

$$M_1 = M_2 = -(1+\nu)\frac{\alpha D}{h}\Delta T. \tag{18.15}$$

A special feature of this thermal problem is that, in spite of the presence of the bending moments, the curvature of the middle surface does not change. It can be explained as follows: change in curvature caused by a nonuniform heating is compensated by a curvature change produced by the bending moments given by Eq. (18.15). The values of the bending stresses at the upper and lower points of the shell surfaces are found to be the following:

$$\sigma_{1\,\max} = \mp\frac{6M_1}{h^2} = \pm\frac{\alpha E}{2(1-\nu)}\Delta T; \quad \sigma_{2\,\max} = \mp\frac{6M_2}{h^2} = \pm\frac{\alpha E}{2(1-\nu)}\Delta T.$$

The bending stress diagrams across the shell thickness are shown in Fig. 18.1. They also illustrate the above statement about the lack of a change in curvature for the given thermal field.

Example 18.2

A cylindrical stepped shell is shown in Fig. 18.2a. The shell is heated over its lower surface up to the temperature $T_1 = 120^\circ$C and over the upper surface to the temperature $T_2 = 50^\circ$C. The temperatures are constant over the shell length. Given $R = 0.5\,\mathrm{m}$, $h_1 = 2\times 10^{-2}\,\mathrm{m}$, $h_2 = 1\times 10^{-2}\,\mathrm{m}$, the shell material is a structural steel with $\nu = 0.3$, $E = 200\,\mathrm{GPa}$, and $\alpha = 12\times 10^{-6}/^\circ C$. Determine the thermal stresses. Assume that the shell is sufficiently long.

Solution

The given thermal field can again be broken down into a uniform heating $T_0 = (T_1 + T_2)/2 = 85^\circ$C and temperature jump $\Delta T = T_1 - T_2 = 70^\circ$C. Since the uniform heating produces no thermal stresses, it will not be taken into further account. Assume that the given shell is cut into two parts: the first of constant thickness h_1 and the second of constant thickness h_2. If they were really separated then they would be subjected to the thermal jump ΔT and, consequently, were additionally loaded by

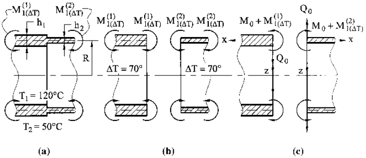

Fig. 18.2

the bending moments at shell edges, as shown in Fig. 18.2b. These moments can be calculated from Eqs. (18.15):

– for the first part of the shell ($h = h_1$),

$$M^{(1)}_{1(\Delta T)} = -\alpha \Delta T(1+\nu)\frac{D_1}{h_1} = -\frac{\alpha \Delta T E h_1^2}{12(1-\nu)} = -8000\ \mathrm{N \cdot m/m};$$

– for the second part of the shell ($h = h_2$),

$$M^{(2)}_{1(\Delta T)} = -\alpha \Delta T(1+\nu)\frac{D_2}{h_2} = -\frac{\alpha \Delta T E h_2^2}{12(1-\nu)} = -2000\ \mathrm{N \cdot m/m}.$$

At a state shown in Fig. 18.2c, the shell is loaded by the interface moments, M_0 and shear forces, Q_0 at the junction of the two shell parts only, where M_0 and Q_0 are the interface bending moment and shear force that actually act at the junction of the stepped shell and $M^{(1)}_{1(\Delta T)}$ and $M^{(2)}_{1(\Delta T)}$ have been added to compensate the moments applied to the shell in the state shown in Fig. 18.2b. To determine the interface moment M_0 and shear force Q_0, it is sufficient to consider only the state shown in Fig. 18.2c and set up the conditions of compatibility for deformations at the junction of the two shell parts. The latter are of the following form:

$$w^{(1)} = w^{(2)}; \quad \vartheta^{(1)}_1 = -\vartheta^{(2)}_1; \tag{a}$$

i.e., the deflections and slopes of the normals for the two shell parts at the junction should be the same. The negative sign in Eq. (a) is taken because the direction of the x axis for the first and second parts of the shell is opposite. The deflections, $w^{(1)}$ and $w^{(2)}$, and slopes, $\vartheta^{(1)}_1$ and $\vartheta^{(2)}_1$, may be determined from Eqs (15.57). For the first (left) shell part, setting $x = 0$ and $w_{\mathrm{p}} = 0$, we obtain

$$w^{(1)} = -\frac{M_0 + M^{(1)}_{1(\Delta T)}}{2D_1\beta_1^2} + \frac{Q_0}{2D_1\beta_1^3}; \quad \vartheta^{(1)}_1 = \frac{M_0 + M^{(1)}_{1(\Delta T)}}{D_1\beta_1} - \frac{Q_0}{2D_1\beta_1^2}. \tag{b}$$

Similarly, for the second shell part, again setting $x = 0$ and $w_{\mathrm{p}} = 0$, we have the following:

$$w^{(2)} = -\frac{M_0 + M^{(2)}_{1(\Delta T)}}{2D_2\beta_2^2} - \frac{Q_0}{2D_2\beta_2^3}; \quad \vartheta^{(2)}_1 = \frac{M_0 + M^{(2)}_{1(\Delta T)}}{D_2\beta_2} + \frac{Q_0}{2D_2\beta_2^2}. \tag{c}$$

Computing the geometric properties of the stepped shell, we have

$$D_1 = \frac{Eh_1^3}{12(1-\nu^2)} = 146.8\,\mathrm{kN \cdot m}; \quad D_2 = \frac{Eh_2^3}{12(1-\nu^2)} = 18.33\,\mathrm{kN \cdot m}$$

$$\text{or} \quad D_2 = \frac{D_1}{8};$$

$$\beta_1 = \sqrt[4]{\frac{3(1-\nu^2}{R^2h_1^2}} = 12.85\ \frac{1}{\mathrm{m}}; \quad \beta_2 = \sqrt[4]{\frac{3(1-\nu^2)}{R^2h_2^2}} = 18.13\ \frac{1}{\mathrm{m}} = \beta_1\sqrt{2};$$

$$M^{(1)}_{1(\Delta T)} = 8000\mathrm{N \cdot m/m}; \quad M^{(2)}_{1(\Delta T)} = 2000\mathrm{N \cdot m/m} = \frac{1}{4}M^{(1)}_{1(\Delta T)}.$$

Substituting Eqs (b) and (c) into the compatibility equations (a), we obtain the following system of two equations:

$$3M_0 + 0.298Q_0 = 0 \quad \text{and} \quad 10^{-3}(3.539M_0 + 0.0623Q_0) = -10.258.$$

Solving these equations for M_0 and Q_0, yields

$$M_0 = -3523\ \mathrm{N \cdot m/m}; \quad Q_0 = 35480\ \mathrm{N/m}.$$

Having determined M_0 and Q_0, we can calculate the deflections, internal forces, and bending moments from Eqs (15.57). Summing them with the corresponding values of the state shown in Fig. 18.2b, we obtain the final expressions of the thermoelastic deflections and stress resultants and couples for the given problem (Fig. 18.2a). The most stressed point is located at the outside surface of the thinner part of the shell, near the stepped transition. The internal forces, bending moments, and normal stresses in this place are

$$M_1 = -3523\ \mathrm{N \cdot m/m}; \quad M_2 = -2460\ \mathrm{N \cdot m/m}; \quad N_1 = 0;$$

$$N_2 = 142656\ \mathrm{N/m}; \quad w = 0.413 \times 10^{-3}\ \mathrm{m} = 0.413\,\mathrm{mm};$$

$$\sigma_1 = \frac{6M_1}{h_2^2} = 211.4\,\mathrm{MPa}; \quad \sigma_2 = \frac{N_2}{h_2} + \frac{6M_2}{h_2^2} = 161.9\,\mathrm{MPa}.$$

As we move away from the stepped transition, the bending moments, $M_{1(\Delta T)}$ and $M_{2(\Delta T)}$, occur in the shell wall. These moments induce the normal stresses, which are found to be

$$\sigma_1 = \sigma_2 = 120\,\mathrm{MPa}.$$

18.1.3 Thermoelastic stress analysis of shallow shells

The general assumptions and governing equations of the shallow shell theory were developed in Sec. 17.4. As mentioned in Sec. 18.1, the equilibrium and kinematic equations of the shell theory remain unchanged, whereas the constitutive relations should be changed in the thermoelastic stress analysis.

Solving the first two equations (18.3) for the strain components ε_1 and ε_2 yields the following:

$$\varepsilon_1 = \frac{1}{Eh}(N_1 - \nu N_2 + N_T); \quad \varepsilon_2 = \frac{1}{Eh}(N_2 - \nu N_1 + N_T). \tag{18.16}$$

Now repeating the procedure of deriving the governing differential equations of the shallow shell described in Secs 17.3 and 17.4, with the use of the constitutive equations (18.3), (18.4), and (18.16), yields the following equations:

$$\begin{aligned} &D\nabla^2\nabla^2 w - \nabla_k^2\Phi = p_3 - \frac{1}{1-\nu}\nabla^2 M_T, \\ &\frac{1}{Eh}\nabla^2\nabla^2\Phi + \nabla_k^2 w = -\frac{1}{Eh}\nabla^2 N_T, \end{aligned} \tag{18.17}$$

where the stress function Φ and operator ∇_k^2 were introduced in Sec. 17.4, and the quantities N_T and M_T are given by Eqs (7.8). This system of equations represents the *thermoelastic governing differential equations of the shallow shell*. Hence, if the values of N_T and M_T remain constant or vary linearly along the coordinate lines x and y, then the governing differential equations of the thermoelastic shallow shell stress analysis remain of the same type as for a non-thermally affected shell. However, a thermal

According to the general rules of differentiating, the following equalities hold:

$$\frac{\partial^2}{\partial y^2}\left[\frac{1}{2}\left(\frac{\partial w}{\partial x}\right)^2\right]=\left(\frac{\partial^2 w}{\partial x\partial y}\right)^2+\frac{\partial w}{\partial x}\frac{\partial^3 w}{\partial x\partial y^2};\ \frac{\partial^2}{\partial x^2}\left[\frac{1}{2}\left(\frac{\partial w}{\partial y}\right)^2\right]=\left(\frac{\partial^2 w}{\partial x\partial y}\right)^2+\frac{\partial w}{\partial y}\frac{\partial^3 w}{\partial x^2\partial y};$$

$$\frac{\partial^2}{\partial x\partial y}\left(\frac{\partial w}{\partial x}\frac{\partial w}{\partial y}\right)=\frac{\partial^3 w}{\partial x^2\partial y}\frac{\partial w}{\partial y}+\left(\frac{\partial^2 w}{\partial x\partial y}\right)^2+\frac{\partial^2 w}{\partial x^2}\frac{\partial^2 w}{\partial y^2}+\frac{\partial w}{\partial x}\frac{\partial^3 w}{\partial x\partial y^2}.$$

Inserting these equalities in the above equation yields the following:

$$\begin{aligned}&\frac{\partial^2}{\partial y^2}(N_1-\nu N_2)+\frac{\partial^2}{\partial x^2}(N_2-\nu N_1)-2(1+\nu)\frac{\partial^2 S}{\partial x\partial y}\\&\quad= Eh\left[\left(\frac{\partial^2 w}{\partial x\partial y}\right)^2-\frac{\partial^2 w}{\partial x^2}\frac{\partial^2 w}{\partial y^2}-\frac{1}{R_1}\frac{\partial^2 w}{\partial y^2}-\frac{1}{R_2}\frac{\partial^2 w}{\partial x^2}\right].\end{aligned}\tag{18.23}$$

Equation (18.23) represents the *equation of compatibility of deformations* of the nonlinear shallow shell theory in terms of the membrane forces and deflections.

Let us introduce the stress function Φ according to the relations (17.45a). Substituting for Φ from the above relations into Eqs (18.23), results in

$$\nabla^2\nabla^2\Phi=Eh\left[\left(\frac{\partial^2 w}{\partial x\partial y}\right)^2-\frac{\partial^2 w}{\partial x^2}\frac{\partial^2 w}{\partial y^2}-\nabla_k^2 w\right],\tag{18.24}$$

where the operators ∇^2 and ∇_k^2 are given by Eqs (17.44).

Now we are coming to constructing the equations of equilibrium for a shallow shell element subjected to a transverse surface load p_3. The positive directions of the internal forces and moments acting on the element are shown in Fig. 12.5. The derivation of the equations of equilibrium in the nonlinear theory of shallow shells has some peculiarities. The force summations in the x and y directions, as well as the moment summations about the above axes, are set up as for the linear shell theory. This involves neglecting the changes in transition of the shell element from its initial (undeformed) to the deflected state, and the initial curvatures of the above element are also neglected. However, the force summation into the z direction is set up by taking into account both the initial curvatures of the element and its consequent distortion acquired as a result of shell straining under action of applied loads. It can be shown that the above equation of equilibrium will have the form of the third Eq. (12.41), derived for the linear shell theory, but complemented by the same terms as for the corresponding equilibrium equation of the nonlinear theory of flat plates (see Eq. (3.91). The system of simplifications adopted in the nonlinear shallow shell theory results in the following equations of equilibrium:

$$\begin{aligned}&\frac{\partial N_1}{\partial x}+\frac{\partial S}{\partial y}=0;\\&\frac{\partial N_2}{\partial y}+\frac{\partial S}{\partial x}=0;\end{aligned}\tag{18.25}$$

In conclusion, let us formulate some qualitative considerations about the mechanical behavior of a geometrically nonlinear shell under applied loading. For simplicity, consider a flexible spherical shallow shell. Such a shell is governed by Eqs (18.31), if we let $R_1 = R_2 = R$. We obtain the following system of equations:

$$\begin{aligned} &\frac{1}{Eh}\nabla^2\nabla^2\Phi + \left[\frac{1}{2}L(w, w) + \frac{1}{R}\nabla^2 w\right] = 0, \\ &D\nabla^2\nabla^2 w - \left[\frac{1}{R}\nabla^2\Phi + L(\Phi, w)\right] = p_3. \end{aligned} \tag{a}$$

Assume that the stress function Φ is assigned in the first approximation, as follows:

$$\Phi = A(p_3)\cdot w, \tag{b}$$

where $A(p_3)$ is a function of loading only. Substituting for Φ from Eq. (b) into Eq. (a), one obtains

$$\begin{aligned} &\frac{A}{Eh}\nabla^2\nabla^2 w + \frac{1}{R}\nabla^2 w + \frac{1}{2}L(w, w) = 0, \\ &D\nabla^2\nabla^2 w - \frac{A}{R}\nabla^2 w - AL(w, w) = p_3. \end{aligned}$$

Eliminating the nonlinear term $L(w, w)$ from the above equations, we obtain the following equation:

$$D^*\nabla^2\nabla^2 w + \frac{1}{R}\nabla^2 w = p_3^*, \tag{c}$$

where

$$D^*(p_3) = \frac{2A}{Eh} + \frac{D}{A}, \quad p_3^* = \frac{p_3}{A}. \tag{d}$$

The quantity $D^*(p_3)$ is made up of the extensional stiffness Eh and the flexural stiffness D. Therefore, it can be called the composite stiffness of the shell. Obviously, the latter depends on the loading p_3.

For a flexible plate, $R = \infty$, and Eq. (c) becomes

$$D^*\nabla^2\nabla^2 w = p_3^*. \tag{e}$$

Equations (c) and (e) are linear equations. Thus, a geometrically nonlinear shell or plate can be considered as a linear system whose flexural and extensional stiffnesses are replaced with some variable composite stiffness, D, given by the first Eq (d) and depending on the applied loading. The above consideration can be used for an approximate shell or plate analysis.

Example 18.3

Analyze the state of stress and strain in a cylindrical shallow shell of radius R having a rectangular configuration in a plan (see Fig. 18.3a). Assume that the shell is lengthened in the y direction ($b \gg a$) and is subjected to a uniform transverse surface load of intensity p. The straight edges of the shell are hinged and the displacement along the x axis is eliminated.

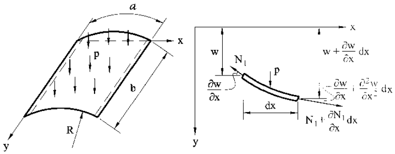

(a) (b)

Fig. 18.3

Solution

Let us confine our study to the analysis of the middle part of the shell that is sufficiently remote from the short curvilinear edges. A curved surface of this part of the shell can be considered as a cylindrical surface. Just as has been done for the cylindrical bending of flat plates (see Sec. 3.2.1), the bending of the given part of the shell will be identical to the bending of a unit curvilinear, simply supported at $x = 0$ and $x = a$, shallow strip, isolated from the shell. For such a strip, $w = w(x)$. Since the deformations in the y direction of such a strip are restrained because of an interaction of neighboring strips, then it can be assumed that the relative deformation in the y direction is zero, i.e., $\varepsilon_2 = 0$. It can also be shown that the membrane force $N_1 =$ const over the shell width. The latter can be checked by considering the equilibrium of a shell element detached from the transverse shell strip, which is subjected to the membrane forces and given loading p, as shown in Fig. 18.3b. For a shallow shell and assumptions adopted in the nonlinear theory, the tangent to the curved axis of the shell strip can be neglected, i.e., it is possible to assume that N_1 is a constant over the shell width.

Thus, the equation of equilibrium (18.29) of the nonlinear shallow shell theory acquires, in this particular case, the following form (taking into account that $N_1 = \partial^2\Phi/\partial y^2$):

$$D\frac{\mathrm{d}^4 w}{\mathrm{d}x^4} - N_1\frac{\mathrm{d}^2 w}{\mathrm{d}x^2} - \frac{N_1}{R} = p. \tag{18.32}$$

The solution of this equation is sought in the form of the following series:

$$w(x) = \sum_{m=1}^{\infty} f_m \sin\frac{m\pi x}{a}. \tag{18.33}$$

It is evident that $w(x)$ in the form of Eq. (18.33) satisfies the prescribed boundary conditions for the deflections.

We solve the above problem in the first approximation, retaining the first term in the expansion (18.33) only. We apply the Galerkin method (see Sec. 6.5) for the solution of Eq. (18.32). Let us introduce

$$\frac{\pi^5}{16}\frac{f_1^3}{h^3} - \frac{3\pi^2}{4}\frac{f_1^2}{Rh^3} + \left(\frac{\pi^5}{48} + \frac{2a^4}{4R^2h^2}\right)\frac{f_1}{h} = (1-\nu^2)\frac{pa^4}{Eh^4}. \tag{18.40}$$

The relationship between the dimensionless parameters $p^* = (1-\nu^2)pa^4/Eh^4$ and f_1/h is illustrated in Fig. 18.4 (taken from Ref. [7]). The curves of this figure are given for various values of $k^* = a^2/Rh$. Figure 18.4 shows the four different plots; the straight line 1 indicates the relationship p^* of f_1/h due to the linear theory of shallow shells, whereas the three other curves describe the relationship in the large-deflection theory for various values of the parameter k^*.

It is seen that for a relatively small parameter k^*, the relationship p^* of f_1/h is single-valued (curve 2 refers to a flexible flat plate with $k^* = 0$; and curve 3 stands for $k^* = 4.475$). However, for larger values of this parameter (curve 4 stands for $k^* = 40$) the above relationship is not uniquely defined, i.e., the three real roots of Eq. (18.40) correspond to one and the same value of p^*. This is a consequence of some peculiarities of straining the large-deflection shallow shell in the process of increasing the applied loading. As long as the parameter p^* increases from zero to the value of 1025 (the ordinate of point A on the curve), the deflection amplitude grows continuously up to the value $\sim 2.2h$, as is indicated by the branch OA of the curve. However, as soon as the load parameter p^* becomes larger than a certain value (about 1025), the given cylindrical shallow shell undergoes the so-called snap through, i.e., the deflection changes its value by jumping from approximately $2.2h$ (the abscissa of point A on the curve) to approximately $11.1h$ (the abscissa of point D on the curve). Upon unloading after this snap through, the shell does not return to its initial configuration of equilibrium. The permanent deflection measured by the abscissa of point E remains in the shell. To return the panel to its initial configuration it is necessary to apply to it a load of another sign whose dimensional parameter $p^* = -959.7$ (the ordinate of point B on the curve 4). At this load, an inverse snap through of the panel occurs. This snap through corresponds to the transition from point B to point F on curve 4.

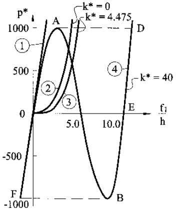

Fig. 18.4

It is clear that the linear relationship between p^* and f_1/h presented by the straight line 1 leads to incorrect quantitative and qualitative results of the stress and strain analysis of the given shell.

18.3 ORTHOTROPIC AND STIFFENED SHELLS

18.3.1 Introduction

In the previous chapters of Part II, only homogeneous and isotropic shells were considered. This permitted the study of the effects of different types of a shell geometry, edge constraints, loading, etc., upon stress and strain components using various shell theories. In this section, the complicated effects associated with material anisotropy and geometric nonhomogeneity, e.g., shell reinforcement, are considered. Obviously, each such effect causes complications in the governing differential equations of the general shell theory. We present below the general equations and relations for orthotropic and stiffened (structurally orthotropic) shells in the framework of the linear (classical) shell theory. It should be noted that the governing differential equations of the theory of orthotropic and stiffened shells may be derived in much the same way as was done for the theory of isotropic and homogeneous shells in Chapter 12. In fact, as mentioned in Sec. 12.5, the general linear theory of thin isotropic shells consists of the three sets of equations: the strain–displacement relations, Eqs (12.22)–(12.24); equations of equilibrium (or motion for dynamic problems), Eqs (12.41) and (12.42); and the constitutive equations (12.32) or (12.45) and (12.46). These three sets of equations are to be completed by appropriate boundary conditions. The first two sets of equations, without changes, are carried over into the theory of the orthotropic shells, whereas the constitutive equations (12.32) or (12.45) and (12.46), used for isotropic shells, are not valid for the above orthotropic shells and must be modified. First, we consider the stress–strain relations for orthotropic shells and then generalize them for stiffened shells.

18.3.2 Orthotropic shells

A material is orthotropic if its mechanical characteristics are specified along two mutually orthogonal directions (for a two-dimensional space). Such a material has different values for E, G, and ν for each direction (see Sec. 7.2). For instance, shells made of delta wood, plywood, fiberglass, metallic composites, and other composite materials fall into the category of orthotropic shells. We assume that the orthotropic material of the shell is so arranged that at each point of the shell its mutually orthogonal directions of elastic symmetry coincide with the principal lines of curvature on the shell's middle surface. For such orthotropic material of a shell, the stress components are related to strain components at any point located at a distance z from the middle surface, as follows:

$$\sigma_1^z = \frac{E_1}{1-\nu_1\nu_2}(\varepsilon_1^z + \nu_2\varepsilon_2^z); \quad \varepsilon_2^z = \frac{E_2}{1-\nu_1\nu_2}(\varepsilon_2^z + \nu_1\varepsilon_1^z); \quad \tau_{12}^z = G\gamma_{12}^z, \tag{18.41}$$

where E_1 and E_2 are the moduli of elasticity in the directions of the α- and β-coordinate axes, respectively; ν_1 and ν_2 are the Poisson's ratios corresponding to the above axes; and G is the shear modulus. It should be noted that the moduli of

Basically, two approaches are possible for the analysis of stiffened shells. If the distance between the stiffeners is too large, then the shell structure must be presented as a combination of shell and stiffener elements, each having its own governing equations and coupled to one another by equations of continuity. However, if the stiffening elements are relatively closely spaced, then a shell structure can be considered as orthotropic, the *structurally orthotropic shell* (see Sec. 7.2). In the latter case, the rigidities of the stiffeners can be "smeared" along the shell middle surface to yield an equivalent homogeneous orthotropic shell. Only the second approach is considered in this book.

Consider a thin shell, reinforced by closely spaced stiffeners, in two mutually perpendicular directions, attached to the inside of the shell skin, as illustrated in Fig. 18.5. Assume that the depth of the stiffeners is small compared with the principal radii of curvature of the shell middle surface and that the stiffeners, unlike the shell skin, undergo a uniaxial state of stress. For the sake of simplicity, assume that the stiffeners and skin are made of the same isotropic material. As mentioned previously, such a gird-stiffened shell is replaced by a structurally orthotropic unstiffened (homogeneous) shell. Let us set up the constitutive equations for the above shell by modifying the expressions (12.45) and (12.46). For the shell wall construction that is not symmetrical relative to the shell middle surface (see Fig. 18.5b), there is coupling between extensional forces and curvature change and between bending moments and extensional strain. Taking into account the above considerations and neglecting the terms of order z/R_i with respect to unity in Eqs (12.35) and substituting for the stress components from Eqs. (12.33), one can write the above expressions for the stress resultants for the structurally orthotropic shells. The membrane force N_1 is given by

$$N_1 d_\beta = d_\beta \int_{-h/2}^{h/2} \sigma_1^z dz + \int_{A_\alpha} \sigma_1^z dA_\alpha = d_\beta \frac{Eh}{1-\nu^2}(\varepsilon_1 + \nu\varepsilon_2) + \varepsilon_1 E A_\alpha + \chi_1 E F_\alpha. \tag{18.46}$$

Dividing both sides of the above equation by d_α, one obtains the following expression for N_1:

$$N_1 = \varepsilon_1 B_{11} + \varepsilon_2 B_{12} + \chi_1 K_{11}. \tag{18.47a}$$

In a similar manner, the expressions for the membrane force N_2 and S are given by

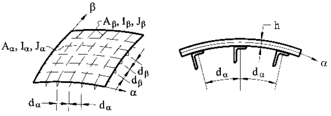

(a) (b)

Fig. 18.5

substitutes for χ_1, χ_2, and χ_3 from the kinematic relations (17.29). Substituting for the in-plane strain components from Eqs (18.60) into the third compatibility equation (18.59) yields

$$\frac{1}{B_s}\left[B_{22}\frac{\partial^2 N_1}{\partial y^2} - B_{12}\frac{\partial^2 N_2}{\partial y^2} - K_{11}B_{22}\frac{\partial^2 \kappa_1}{\partial y^2} + K_{22}B_{12}\frac{\partial^2 \kappa_2}{\partial y^2} + B_{11}\frac{\partial^2 N_2}{\partial x^2} - B_{12}\frac{\partial^2 N_1}{\partial x^2}\right.$$
$$\left. + K_{11}B_{12}\frac{\partial^2 \chi_1}{\partial x^2} - K_{22}B_{11}\frac{\partial^2 \chi_2}{\partial x^2}\right] - \frac{1}{B_{33}}\frac{\partial^2 S}{\partial x \partial y} = \nabla_k^2 w \tag{18.65}$$

or, using the strain–displacement relations (17.43) and Eqs (17.45), we obtain

$$\nabla_{2s}^4 \Phi - L_K w = 0, \tag{18.66}$$

where

$$\nabla_{2s}^4(\ldots) \equiv \frac{B_{11}}{B_s}\frac{\partial^4}{\partial x^4}(\ldots) + 2\left(\frac{1}{2B_{33}} - \frac{B_{12}}{B_s}\right)\frac{\partial^4}{\partial x^2 \partial y^2} + \frac{B_{22}}{B_s}\frac{\partial^4}{\partial y^4}(\ldots). \tag{18.67}$$

Equations (18.63) and (18.66) form the *system of governing differential equations for the shallow structurally orthotropic shells.*

It can be shown that for shallow unstiffened and isotropic shells, the operators (18.64) and (18.67) become

$$L_K(\ldots) = -\nabla_k^2(\ldots); \quad \nabla_{1s}^4(\ldots) = D\nabla^4(\ldots); \quad \nabla_{2s}^4(\ldots) = \frac{1}{Eh}\nabla^4(\ldots), \tag{18.68}$$

where $\nabla^4(\ldots)$ is the biharmonic operator given by Eq. (2.26). Equations (18.63) and (18.66) will be reduced to the system of equations (17.36) introduced in Secs 17.3 and 17.4.

18.4 MULTILAYERED SHELLS

Consider a thin multilayered shell of revolution of a constant thickness, composed of n isotropic and orthotropic layers of variable thickness, whose mechanical parameters vary along the meridian only (see Fig. 18.6). Many of structures made of composite materials can be presented as multilayered orthotropic shells of revolution.

It is supposed that the above layers deform without slipping and separation. The stress components on planes, that are tangent to the contact surface, have no discontinuities and the material of the shell layers obeys Hooke's law.

The coordinate surface does not necessarily coincide with the contact surface of two adjacent layers. If a shell is composed of layers of identical thickness, then the coordinate surface is chosen to be parallel to the contact surfaces. It is also assumed that the deformations are small, the Kirchhoff–Love hypotheses are valid for the entire shell packet, and the mechanical parameters of each layer are not too different from one another, i.e., the shell is not significantly nonhomogeneous across its thickness. The axes of orthotropy in all layers of the shell packet are assumed to be parallel to the coordinate lines. Let the coordinate surface of the multilayered shell, chosen from some considerations, be referred to the curvilinear orthogonal coordinate system $\alpha = s$ and $\beta = \theta$, where s is the length of the meridian arc, measured

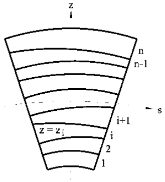

Fig. 18.6

from some reference shell cross section and θ is the circumferential angle measured from some reference meridian. For this coordinate system, the Lamé parameters are

$$A = 1 \quad \text{and} \quad B = r, \tag{18.69}$$

where r is the radius of the parallel circle.

There exists an obvious relationship between the spherical coordinates adopted in Sec. 11.8 and the coordinates mentioned above, i.e.,

$$\cos\theta \mathrm{d}s = \mathrm{d}r. \tag{18.70}$$

The entire shell is referred to the coordinate system z, θ, s. Then, the equations $z_i = z_i(s, \theta)$ $(i = 1, 2, \ldots, n-1)$ assign the contact surfaces for the i and $i+1$ layers, and bounding (lower and upper) surfaces are given by the equations $z_0 = z_0(s, \theta)$ and $z_n = z_n(s, \theta)$ (Fig. 18.6). Due to the above-mentioned assumptions adopted in the multilayered shell theory, it is possible to replace the usual consideration of stresses over the entire shell packet by a consideration of statically equivalent stress resultants and stress couples, just as has been done for isotropic shells in Sec. 12.3.2. So, by analogy with Eqs (12.35) and (12.36), we obtain the following expressions for the internal forces and moments:

$$\begin{aligned}
N_1 &= \sum_{i=1}^{n} \int_{z_{i-1}}^{z_i} \sigma_1^i \left(1 - \frac{z}{R_2}\right) \mathrm{d}z; \quad N_2 = \sum_{i=1}^{n} \int_{z_{i-1}}^{z_i} \sigma_2^i \left(1 - \frac{z}{R_1}\right) \mathrm{d}z; \\
N_{12} &= \sum_{i=1}^{n} \int_{z_{i-1}}^{z_i} \tau_{12}^i \left(1 - \frac{z}{R_1}\right) \mathrm{d}z; \quad N_{21} = \sum_{i=1}^{n} \int_{z_{i-1}}^{z_i} \tau_{21}^i \left(1 - \frac{z}{R_2}\right) \mathrm{d}z; \\
Q_1 &= \sum_{i=1}^{i=n} \int_{z_{i-1}}^{z_i} \tau_{1z}^i \left(1 - \frac{z}{R_2}\right) \mathrm{d}z; \quad Q_2 = \sum_{i=1}^{n} \int_{z_{i-1}}^{z_i} \tau_{2z}^i \left(1 - \frac{z}{R_1}\right) \mathrm{d}z; \\
M_1 &= \sum_{i=1}^{n} \int_{z_{i-1}}^{z_i} \sigma_1^i \left(1 - \frac{z}{R_2}\right) z \mathrm{d}z; \quad M_2 = \sum_{i=1}^{n} \int_{z_{i-1}}^{z_i} \sigma_2^i \left(1 - \frac{z}{R_1}\right) z \mathrm{d}z; \\
M_{12} &= \sum_{i=1}^{n} \int_{z_{i-1}}^{z_i} \tau_{12}^i \left(1 - \frac{z}{R_1}\right) z \mathrm{d}z; \quad M_{21} = \sum_{i=1}^{n} \int_{z_{i-1}}^{z_i} \tau_{21}^i \left(1 - \frac{z}{R_2}\right) z \mathrm{d}z.
\end{aligned} \tag{18.71}$$

The equations of equilibrium, kinematic relations, and constitutive equations (18.73) can be reduced to the eight-order system of 12 governing differential equations involving 12 unknown functions of the displacements, internal forces, and moments for the multilayered orthotropic shells of revolution. The higher order of this system and large number of equations and unknown functions present major problems for its solving. So, only numerical and approximate methods discussed in Chapter 6 can be employed for the analysis of the state of stress and strain of multilayered orthotropic shells.

18.5 SANDWICH SHELLS

Sandwich shells are commonly used in aircraft construction, shipbuilding, industrial building, etc., because they are quite efficient constructions: high strength is successfully combined with low weight. In this section we present a small-deflection elastic theory of orthotropic sandwich shallow shells that takes into account deformations due to the transverse shear. This theory represents a natural extension of the small-deflection theory of orthotropic sandwich plates introduced in Sec. 7.6.

The sandwich shell construction is quite similar to the sandwich plate introduced in Sec. 7.6 (see Fig. 7.8). The load-carrying flexural mechanism of a sandwich shell is also analogous to that of a sandwich plate. Assume that all the sandwich construction notations introduced in the plate sandwich theory in Sec. 7.6 are also adopted in the shell sandwich.

The basic theory of orthotropic sandwich cylindrical shells was developed by Stein and Mayers [9]. We present this theory as applied to shallow sandwich shells. It is assumed that a sandwich shell – just as discussed previously for a sandwich plate – behaves elastically as a homogeneous orthotropic shell with some mechanical properties, which characterize its mechanical behavior and peculiarities of its load-carrying mechanism under applied loads. The seven physical constants that characterize the flexural mechanism of flat plates have been presented in Sec. 7.6 (the subscripts x and y adopted in the sandwich plate theory are replaced by the subscripts 1 and 2 for the sandwich shell). These constants were the flexural stiffnesses D_1 and D_2, the flexural Poisson's ratios ν_1 and ν_2, the twisting stiffness D_{12}, and the shear stiffnesses D_{Q_1} and D_{Q_2}. Four of constants are related to each other by the following equality (see Sec. 7.6):

$$\nu_1 D_2 = \nu_2 D_1.$$

As mentioned previously, the behavior of a shell under applied loading differs essentially from the behavior of a flat plate. The applied loading is resisted predominantly by the in-plane stressing of the shell (see Chapter 10). Thus, the seven physical constants characterizing the flexural mechanism must be complemented by some physical constants that represent the membrane actions of a sandwich shell. The five additional constants appearing in the sandwich shell theory were introduced in Ref. [9] and are the extensional stiffnesses, Λ_1 and Λ_2, the extensional Poisson's ratios, ν_1' and ν_2', and the in-plane shear stiffness Λ_{12}. They can be introduced as follows:

$$\Lambda_1 = \frac{N_1}{\varepsilon_1}; \quad \Lambda_2 = \frac{N_2}{\varepsilon_2}; \quad \nu_1' = -\frac{\varepsilon_2}{\varepsilon_1}; \quad \nu_2' = -\frac{\varepsilon_1}{\varepsilon_2}; \quad \Lambda_{12} = \frac{N_{12}}{\gamma_{12}} = \frac{N_{21}}{\gamma_{21}} = \frac{S}{\gamma_{12}}. \tag{18.77}$$

displacements u, v, and w – are obtained. Because of the awkwardness of these five differential equations for the orthotropic sandwich shallow shell, they are not given here. The interested reader is referred to Refs [9–11], where these equations are presented.

For a special case of an isotropic sandwich shallow shell with non-direct-stress-carrying core, the physical constants are simplified to the following form:

$$\begin{aligned} &D_{Q_1} = D_{Q_2} = D_Q = \frac{d^2}{c} G_c; \quad \nu_1 = \nu_2 = \nu_1' = \nu_2' = \nu, \\ &D_1^* = D_2^* = D_s = \frac{E_f t d^2}{2(1-\nu_f^2)}; \quad D_{12} = D_s(1-\nu), \\ &\Lambda_1 = \Lambda_2 = 2E_f t; \quad \Lambda_{12} = \frac{E_f t}{1+\nu}; \quad d = c+t, \end{aligned} \tag{18.82}$$

where all the above notations are explained in Sec.7.6. For this special case, the system of the five governing differential equations for an orthotropic sandwich shallow shell can be reduced to a single eight-order differential equation in w. Dropping the intermediate and lengthy mathematical manipulations associated with deriving this equation, we present below only the final result:

$$D_s \nabla^4 \nabla^4 w + \left(1 - \frac{D_s}{D_Q} \nabla^2\right) \left[2E_f t \left(\frac{1}{R_2} \frac{\partial^2}{\partial x^2} + \frac{1}{R_1} \frac{\partial^2}{\partial y^2} \right)^2 w - \nabla^4 p_3 \right] = 0, \tag{18.83}$$

where

$$\nabla^4(\ldots) \equiv \frac{\partial^4(\ldots)}{\partial x^4} + 2\frac{\partial^4(\ldots)}{\partial x^2 \partial y^2} + \frac{\partial^4(\ldots)}{\partial y^4}$$

is a biharmonic operator.

It can be easily shown that if $R_1 \to \infty$ and $R_2 \to \infty$, this equation is equivalent to Eq. (7.135) derived in Sec. 7.5.1 for isotropic sandwich flat plates. Note that in the limiting case when the shear modulus approaches infinity, Eq. (18.83) is reduced to the governing differential equation of the homogeneous isotropic shallow shell theory with the flexural stiffness D_f, i.e., with the stiffness of a composite section composed from two facings separated by a distance which is equal to the depth of the core.

18.6 THE FINITE ELEMENT REPRESENTATIONS OF SHELLS

18.6.1 Introduction

We have seen in previous chapters of Part II that the shell problems associated with determining displacements, internal forces, and moments are described by high-order partial differential equations with variable coefficients. Only in very special cases of shell geometry, boundary conditions, and loadings is it possible to obtain reasonably accurate closed-form solutions and to develop relatively general analytical expressions for deformations and stresses (see Chapters 14–17). Such closed-form expressions, obtained in terms of arbitrary parameters defining a shell geometry, boundary conditions, and loading, are of considerable interest for a designer. In fact, the analytical solutions permit any desired parametric studies to be conducted, rapid calculation of actual stresses and deformations in shell structures, and they provide a basis for error estimates of numerical solutions obtained by approximate methods.

However, available analytical solutions of shell structural problems are, nevertheless, limited in scope and, in general, do not apply to arbitrary shapes, loading, irregular stiffening, cutouts, support conditions, and many other aspects of practical design. Therefore, not surprisingly, the development of numerical formulations over the past 50 years, notably the finite element method (FEM), has enabled one to analyze thin shell structures. As mentioned in Sec. 6.7, the FEM is a general numerical procedure that can be used to tackle any problem of structural stress analysis, including shell problems, to any desired degree of accuracy. However, initially, one needs to understand the response of the basic individual elements making up a shell structure, and then to assemble such elements by enforcing compatibility of deformations between elements at their common nodes, and equilibrium of forces and moments at all nodes, as well as constraint conditions at the boundary nodes of the structure. Then, the overall response of the complete shell structure can be predicted.

The general procedure of an application of the FEM to thin shell structures is quite similar to that discussed in Sec. 6.7 for plate bending problems. We discuss in this section some issues regarding the peculiarities of the FEM representation and formulation for thin shell structural analysis.

There are three distinct approaches to the finite element representation of thin shell structures [12]:

(a) in ''faceted'' form with flat elements;
(b) via curved elements formulated on the basis of thin shell theory; and
(c) by means of the three-dimensional (solid) elements.

This section is concerned with the flat and curved shell elements only. Various applications of the solid finite elements to the stress analysis are given in Refs [12,13,14, etc.]. We consider below several applications of the FEM to some shell geometries.

18.6.2 The finite element solutions of axisymmetrically loaded shells of revolution

The axisymmetric bending of shells of revolution was studied in Sec. 16.3. It was shown in the above section that the state of stress and strain of such shells is governed by the ordinary differential equations: i.e., the displacements, internal forces, moments, and stresses are functions of one variable (meridional coordinate) only. Let us take the length of the meridian arc, s, measured from some reference point of the shell, as the meridional coordinate of a point in the middle surface.

If we apply the FEM to the bending analysis of axisymmetrically loaded shells of revolution, then the finite element should be one dimensional. Such an element may be represented in the form of a frustum: i.e., as a ring, generated by the straight line segment between two parallel circles or ''nodes'', say, i and j, as shown in Fig. 18.7. The thickness may vary from element to element. To increase the accuracy of a solution, finite elements with curved generators are employed in some cases.

The displacement vector of a point in the midsurface is specified by two components u and w in the meridional and normal directions, respectively (see Sec. 16.3).

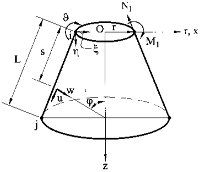

Fig. 18.7

Using the relationships $r = R_2 \sin\varphi$ and $\mathrm{d}s = R_1 \mathrm{d}\varphi$, we can rewrite the strain–displacement equations (16.11) in terms of variable s, as follows:

$$\begin{aligned}
&\varepsilon_1 = \frac{\mathrm{d}u}{\mathrm{d}s} - \frac{w}{R_1}, \quad \varepsilon_2 = \frac{1}{r}(u\cos\varphi - w\sin\varphi),\\
&\chi_1 = -\frac{\mathrm{d}\vartheta_1}{\mathrm{d}s}, \quad \chi_2 = -\frac{\cos\varphi}{r}\vartheta_1,\\
&\vartheta_1 = \frac{u}{R_1} + \frac{\mathrm{d}w}{\mathrm{d}s}
\end{aligned} \tag{18.84}$$

(for simplicity from hereon the subscript 1 in the notation for the angle of rotation ϑ is omitted).

The Codazzi–Gauss condition for shells of revolution is

$$\frac{\mathrm{d}r}{\mathrm{d}s} = \cos\varphi. \tag{18.85}$$

Introduce the displacement $\{f\}$ and strain $\{\varepsilon\}$ vectors, respectively, as follows:

$$\{f\}^T = [u, w], \tag{18.86a}$$

$$\{\varepsilon\}^T = [\varepsilon_1, \varepsilon_2, \chi_1, \chi_2]. \tag{18.86b}$$

Using the above notations, we can rewrite the kinematic relationships (18.84) for the finite element shown in Fig. 18.7 in the following matrix form:

$$\{\varepsilon\} = [R]\{f\}, \tag{18.87}$$

where

$$[R] = \begin{bmatrix}
\dfrac{\mathrm{d}}{\mathrm{d}s} & -\dfrac{1}{R_1}\\
\dfrac{\cos\varphi}{r} & -\dfrac{\sin\varphi}{r}\\
-\dfrac{\mathrm{d}}{\mathrm{d}s}\left(\dfrac{1}{r_1}\right) & -\dfrac{\mathrm{d}^2}{\mathrm{d}s^2}\\
-\dfrac{\cos\varphi}{rR_1} & -\dfrac{\cos\varphi}{r}\dfrac{\mathrm{d}}{\mathrm{d}s}
\end{bmatrix} \tag{18.88}$$

The stress resultant and couples–strain relations, Eqs. (16.13), can also be presented in the matrix form, as follows:

$$\{\sigma\} = [D]\{\varepsilon\}, \tag{18.89}$$

where

$$\{\sigma\}^T = [N_1, N_2, M_1, M_2] \tag{18.90}$$

is the stress resultants and couples vector and

$$[D] = \frac{Eh}{1-\nu^2}\begin{bmatrix} 1 & \nu & 0 & 0 \\ \nu & 1 & 0 & 0 \\ 0 & 0 & h^2/12 & \nu h^2/12 \\ 0 & 0 & \nu h^2/12 & h^2/12 \end{bmatrix} \tag{18.91}$$

is the elasticity matrix.

The strain energy, stored by an axisymmetrically loaded shell of revolution in bending, can be obtained from Eq. (12.53) by letting $S = H = 0$ and replacing $AB\mathrm{d}\alpha\mathrm{d}\beta$ with $\mathrm{d}A$. We have

$$U = \frac{1}{2}\int\int_A (N_1\varepsilon_1 + N_2\varepsilon_2 + M_1\chi_1 + M_2\chi_2)\mathrm{d}A. \tag{18.92}$$

Using the vector notations introduced above for the strains and stress resultants and couples, and noting that the area of the element $\mathrm{d}A = r\mathrm{d}s\mathrm{d}\theta$ and integrating (18.92) over θ from 0 to 2π, we can represent Eq. (18.92) for the one-dimensional finite element in Fig. 18.7, as follows:

$$U = 2\pi\int_{s_0}^{s_1} \{\varepsilon\}^T\{T\}r\mathrm{d}s, \tag{18.93}$$

where s_0 and s_1 are the end points of the s arc.

The vector of external forces can be represented in the form

$$\{P\}^T = [p_x, p_z], \tag{18.94}$$

where p_x and p_z are the horizontal (or radial) and vertical (or axial) components of an applied loading, respectively. If a shell is subjected to an external normal pressure q, then

$$p_z = q\cos\varphi, \; p_x = q\sin\varphi. \tag{18.95}$$

The work done by external loads applied along the displacements given by the vector $\{f\}$ can be represented as follows:

$$W_e = 2\pi\int_{s_0}^{s_1} \{f\}^T\{P\}r\mathrm{d}s. \tag{18.96}$$

Next, let us introduce the two nodal displacement vectors that characterize the degrees of freedom of the finite element in the form of a frustum with a straight generator (see Fig. 18.7) and designated by e, as follows:

$$\{g\}_e = \begin{Bmatrix} \{g_i\} \\ \\ \{g_j\} \end{Bmatrix}, \quad \{g_i\}^T = [u_i, w_i, \vartheta_i], \quad (i \to j), \tag{18.97}$$

$$\{\delta\}_e = \begin{Bmatrix} \{\delta_i\{ \\ \\ \{\delta_j\} \end{Bmatrix}, \quad \{\delta_i\}^T = [\xi_i, \eta_i, \vartheta_i], \quad (i \to j), \tag{18.98}$$

where $\vartheta_i = (\mathrm{d}w/\mathrm{d}s)_i$ and $\xi_{i(j)}$ and $\eta_{i(j)}$ are the horizontal (or radial) and vertical (or axial) displacements at the nodal point $i(j)$. The nodal displacement vectors introduced above are related to one another, as follows (see Eq. (16.37)):

$$\{g_i\} = [\lambda]\{\delta_i\}, \quad (i \to j) \tag{18.99}$$

where

$$[\lambda] = \begin{bmatrix} -\cos\varphi & \sin\varphi & 0 \\ \sin\varphi & \cos\varphi & 0 \\ 0 & 0 & 1 \end{bmatrix}. \tag{18.100}$$

Let us approximate the displacement field across the given finite element by the following polynomials:

$$\begin{aligned} u &= \alpha_1 + \alpha_2 s, \\ w &= \alpha_3 + \alpha_4 s + \alpha_5 s^2 + \alpha_6 s^3. \end{aligned} \tag{18.101}$$

To determine the values of the coefficients α_k $(k = 1, 2, \ldots, 6)$, the coordinate s of the nodal points is substituted in the displacement functions (18.101). This will generate six equations in which the only unknowns are the above coefficients. By so doing, we can solve for α_k in terms of the nodal displacements $u_i, w_i, \ldots, \vartheta_j$ and finally obtain the following:

$$\{f\} = [\hat{N}]\{g\}_e \tag{18.102}$$

where {f} is given by Eq. (18.86a)
and

$$[\hat{N}] = \begin{bmatrix} 1-l & 0 & 0 & l & 0 & 0 \\ 0 & 1 - 3l^2 + 2l^3 & L(l - 2l + l^2) & 0 & 3l^2 - 2l^3 & L(-l + l^2) \end{bmatrix}; \tag{18.103}$$

here $l = s/L$, where L is the length of the frustum meridian for the given finite element (see Fig. 18.7).

Substituting for the vector $\{g\}$from Eq. (18.99) into Eq. (18.102), yields

$$\{f\} = [\hat{N}]\begin{bmatrix} [\lambda] & 0 \\ 0 & [\lambda] \end{bmatrix}\{\delta\}_e = \big[[\hat{N}_i][\lambda], [\hat{N}_j][\lambda]\big]\{\delta\}_e = [N]\{\delta\}_e. \tag{18.104}$$

Equation (18.87) then leads to

$$\{\varepsilon\} = [R][N]\{\delta\}_e = [B]\{\delta\}_e, \tag{18.105}$$

where

$$[B] = \big[[B_i][\lambda], [B_j][\lambda]\big] \tag{18.106}$$

As mentioned previously, a midsurface of a shallow shell can be approximated by flat or by curved finite elements when applying the FEM technique. We consider below both two approximations of the shell geometry.

1. A curved finite element in the form of a shallow shell of double curvature

Let us consider a finite element in the form of a shallow shell of double curvature having a rectangular projection on the Oxy coordinate plane, as shown in Fig. 18.8. At each nodal (corner) point of this finite element, designated by 1, 2, 3, and 4, we consider the possible three displacement components u, v, and w in the directions of the coordinate axes x, y, and z, respectively; two angles of rotations, $\alpha \equiv \vartheta_1$ and $\beta \equiv \vartheta_2$, about the y and x axes, respectively; and the value ω modeling a twist at a nodal point of interest. Thus, the curved finite element of the shallow shell shown in Fig. 18.8, has 24 degrees of freedom.

To approximate the displacement fields in the above finite element, we make the following assumptions:

(a) The displacements $u(x, y)$ and $v(x, y)$ depend only on the in-plane displacements of the nodal points and they are distributed linearly across the finite element area. So, for example, all points of the finite element will receive only the horizontal (in the coordinate plane Oxy) displacements due to a unit displacement of the nodal point 4 along the x axis (i.e., $u_4 = 1$). The above horizontal displacements will be distributed along line 2–4, according to the relationship y/b, along line 3–4, according to x/a, and over the entire area of the finite element, according to the relationship $u(x, y) = \frac{x}{a}, \frac{y}{b}$.

(b) The deflections $w(x, y)$ do not depend on the in-plane (horizontal) displacements of the nodal points, and they can be approximated by a polynomial with 16 degrees of freedom.

These assumptions provide a way of presenting an approximation of displacements in the explicit form that avoids a very cumbersome operation of inverting the matrix $[C]$ (see Sec. 6.7.2).

The approximation of the displacements across the finite element can be given in the following compact form:

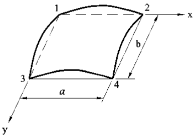

Fig. 18.8

and completeness of approximating functions. Therefore, the problem of the development of finite elements for shallow shells of double curvature is very complicated.

From a physical point of view, it is advantageous to employ flat finite elements for the analysis of shallow shells of double curvature. In this case, a shell element can be obtained as a simple combination of the corresponding elements for plane stress and for plate bending by satisfying all the necessary requirements. Geometric features of the shell are taken into account by the geometry of an inscribed polyhedron. Since the approximation accuracy of the shell surface is increased with a finer element mesh, it is possible to state that the FEM convergence will be achieved in this case.

When assigning an assemblage of flat finite elements for a shallow shell, one must inscribe the elements into the shell geometry. Therefore, one can use rectangular elements for developable surfaces on a plane (e.g., cylindrical surfaces) and triangular elements for undevelopable surfaces (e.g., spherical shells). The stiffness matrix of a rectangular (or triangular) flat shell finite element can be obtained as a simple superposition of the stiffness matrices of that element for plane stress and for plate bending. The stiffness matrix for a flat plate bending finite element was introduced in Sec. 6.7.

Consider the derivation of the stiffness matrix for the rectangular plane stress finite element 1–2–3–4 shown in Fig. 18.8 (the projection of a shallow shell curved element on the Oxy coordinate plane). Assume that the in-plane displacement pattern is defined by the following polynomials:

$$\begin{aligned} u(x,y) &= \alpha_1 + \alpha_2 x + \alpha_3 y + \alpha_4 xy, \\ v(x,y) &= \alpha_5 + \alpha_6 x + \alpha_7 y + \alpha_8 xy. \end{aligned} \tag{18.118}$$

Thus, the generalized displacements of a node of the flat rectangular finite element in a matrix form are the following

$$\begin{Bmatrix} u \\ v \end{Bmatrix} = \begin{bmatrix} 1 & x & y & xy & 0 & 0 & 0 & 0 \\ 0 & 0 & 0 & 0 & 1 & x & y & xy \end{bmatrix} \begin{Bmatrix} \alpha_1 \\ \alpha_2 \\ \dots \\ \alpha_8 \end{Bmatrix} = [N]\{\alpha\}. \tag{18.119}$$

Let us introduce the nodal displacement vector of the above-mentioned element, as follows:

$$\{\delta\}_e^T = [u_1, v_1, u_2, v_2, \dots, u_4, v_4]. \tag{18.120}$$

It is seen that the displacement functions (18.118) contain the same number of unknown parameters α_k ($k = 1, 2, \dots, 8$) as the number of the nodal displacements u_i and $v_i (i = 1, \dots, 4)$ and yield the linear displacements along the element sides. If we express the above coefficients α_k via nodal displacements, i.e., via the components of the element displacement vector $\{\delta\}_e$, we obtain

$$\{\delta\}_e = [C]\{\alpha\}, \tag{18.121}$$

where $[C]$ is an 8×8 matrix whose terms depend on the x and y coordinates of the nodal points of the given finite element. From Eq. (18.121), the vector $\{\alpha\}$ can be expressed as a function of the finite element nodal displacement vector, as follows:

$$\{\alpha\} = [C]^{-1}\{\delta\}_e. \tag{18.122}$$

Since the displacement functions are now expressed in terms of the nodal displacements in the explicit form, we can follow the same procedure as described in Sec. 6.7 for evaluating the components of the stiffness matrix of the plane stress finite element.

Here, only the general information about the FEM analysis and its application to shell structures has been presented. It should be noted that many books have appeared during the last four decades and they contain extensive discussions of FEM approaches and the related numerical procedures, for example [Refs 12–17].

18.7 APPROXIMATE AND NUMERICAL METHODS FOR SOLUTION OF NONLINEAR EQUATIONS

Analysis of flexible plates and shells is reduced to a solution of nonlinear differential equations for the stress function and deflection, Eqs (7.87) and (18.31), respectively. The solution of these equations via the classical analytical route can be obtained in exceptional cases only. Therefore, approximate and numerical methods acquire a great importance for the nonlinear plate and shell analysis. These methods, based on some iterative procedures, are usually combined with other well-known variational and numerical methods, introduced in Chapter 6 and Sec. 18.6, to obtain the solution of Eqs (7.87) and (18.31) with a reasonable accuracy.

We introduce below some approximate methods specially adapted to the analysis of flexible plates and shells under external loads.

18.7.1 The method of successive approximations

Let us use the flexible plate problem to illustrate the method of successive approximations. We rewrite Eqs (7.87), as follows

$$\begin{aligned} \frac{1}{Eh}\nabla^2\nabla^2\Phi &= -\frac{1}{2}L(w, w), \\ D\nabla^2\nabla^2 w &= L(\Phi, w) + p, \end{aligned} \tag{18.123}$$

where the operator $L(\ldots)$ is given by Eq. (18.30).

In the first approximation, the above system of equations is taken in the form

$$\begin{aligned} \nabla^2\nabla^2\Phi_1 &= 0, \\ D\nabla^2\nabla^2 w_1 &= p. \end{aligned} \tag{18.124a}$$

In the second approximation, the functions Φ_1 and w_1 are substituted into the right-hand sides of Eqs (18.122). We obtain

$$\begin{aligned} \frac{1}{Eh}\nabla^2\nabla^2\Phi_2 &= -\frac{1}{2}L(w_1, w_1), \\ D\nabla^2\nabla^2 w_{21} &= L(\Phi_1, w_1) + p, \end{aligned} \tag{18.124b}$$

and equations of the $(n+1)$th approximation will have the form

$$\begin{aligned} \frac{1}{Eh}\nabla^2\nabla^2\Phi_{n+1} &= -\frac{1}{2}L(w_n, w_n), \\ D\nabla^2\nabla^2 w_{n+1} &= L(w_n, \Phi_n) + p, \end{aligned} \tag{18.124c}$$

18.2 A long thin-walled aluminum tube has free ends and is subjected to uniform temperatures $T_1 = 150^\circ\mathrm{C}$ and $T_2 = 350^\circ\mathrm{C}$ at the inner and outer surfaces, respectively. Let the mean radius of the tube be 0.8 m and its thickness $h = 10\,\mathrm{mm}$. Calculate the maximum thermal stresses in the tube if $E_a = 70\,\mathrm{GPa}$, $\alpha_a = 23 \times 10^{-6}/^\circ\mathrm{C}$, and $\nu_a = 0.3$.

18.3 Compute the discontinuity stresses at the junction of the cylindrical shell and hemispherical head, as shown in Fig. 16.6, for the uniform temperature change $\Delta T = 120^\circ\mathrm{C}$. Use the geometric and mechanical parameters of the compound shell structure given in Example 16.2 and $\alpha_s = 25 \times 10^{-6}/^\circ\mathrm{C}$. Apply the approximate method of Sec. 16.4 for the problem solution.

18.4 Compute the stresses in the hemispherical shell stiffened on its edge by a flange, as shown in Fig. 16.5. Assume that the shell and flange are made of steel with $E_s = 210\,\mathrm{GPa}$, $\nu_s = 0.3$, and $\alpha_s = 25 \times 10^{-6}/^\circ\mathrm{C}$. Take the geometric parameters of the shell and flange from Example 16.1. Apply the approximate method of Sec. 16.4 for the problem solution.

18.5 Derive Eqs (18.17).

18.6 Verify Eqs (18.24) and (18.29).

18.7 Derive Eq. (18.54).

18.8 A closed, circular cylindrical shell of length L and radius R is stiffened by equally spaced collars, at a distance $L/10$, located inside the shell. The shell is simply supported at $x = 0$ and $x = L$ and is subjected to a uniform internal pressure p. Calculate the normal stresses in the stiffened shell in terms of p if the shell and collars are made of steel with $E_s = 210\,\mathrm{GPa}$ and $\nu_s = 0.3$. Assume also that the collars have a form of the equal angle section $25 \times 25 \times 5$ mm and $R = 0.8\,\mathrm{m}$, $L = 4\,\mathrm{m}$, and $h = 1\,\mathrm{mm}$. In your calculations, consider the stiffened shell as a structurally orthotropic homogeneous shell.

18.9 Verify Eqs (18.63) and (18.66).

18.10 Derive Eqs (18.82).

18.11 Consider two extreme cases for a sandwich shallow shell given by Eqs (18.82): (a) let $R_1 \to \infty$ and $R_2 \to \infty$ and (b) let $G_c \to \infty$. Transform the above governing equation for these two cases and explain their physical sense.

18.12 Based on the representations (18.106) and (18.107), write the matrices $[B_i]$ and $\left[B_j\right]$ in the explicit form.

18.13 Write a computer code for calculating the components of the stiffness matrix for the finite element in the form of a frustum (Fig. 18.7) for an axisymmetrically loaded shell of revolution. Use the relations introduced in Sec. 18.6.2. Assume reasonable values for any shell properties required.

18.14 Using the Newton method, find a solution of the equation

$$4x^3 - 2x^2 - 4x - 3 = 0.$$

18.15 Find a solution of the differential equation for the bending moments in a simply supported beam with a variable cross section:

$$\frac{\mathrm{d}^2 y}{\mathrm{d}x^2} + (1 + x^2)y = 0,$$

$$y = 0\big|_{x=-1} \quad \text{and} \quad y = 0\big|_{x=1}$$

Use the method of successive approximations.

REFERENCES

1. Carslaw, H.S. and Jaeger, J.C., *Conduction of Heat in Solids*, 2nd edn, Oxford University Press, London, 1959.

19

Buckling of Shells

19.1 INTRODUCTION

An efficiency of the membrane stress state, based on the strength conditions only, enables one to employ a very small shell thickness, as discussed in the preceding chapters of Part II. However, a possibility of the shell buckling impedes that, causing us either to increase the shell thickness or to reinforce the shell by stiffeners. It should be noted that the shell buckling is always disastrous, unlike, for example, a column or plate buckling. Therefore, the problem of the stability in designing shell structures is extremely vital. This problem is made worse because of some specific difficulties associated with determining correctly the critical values of loads applied to thin shells. Note that these difficulties are much greater than in the buckling analysis of columns, frames, and flat plates. They are associated with a complicated mathematical description of the deformed state of shells, and with a diversity of situations at which a shell can buckle.

General postulations, definitions, and fundamentals of the structural stability theory, introduced in Chapter 8 for the plate buckling problems, can be applied also to the shell buckling analysis. In this chapter, we present a systematic but simplified analysis of shell buckling, and obtain some useful relationships between the critical values of applied loads and shell parameters. We limit ourselves to the consideration of thin shells for which elastic buckling without plastic deformation is possible.

19.2 BASIC CONCEPTS OF THIN SHELLS STABILITY

Let us compare qualitatively the buckling behavior of columns, flat plates, and shells. For the sake of simplicity, we treat a column, plate, and shell as one degree of freedom systems and consider typical diagrams of the relationship between the applied load p and some deflection parameter f in the buckling problems. We assume that the deflections are small compared with the overall dimensions of the structural member, but of the same order of magnitude as the depth of the column cross section, or the wall thickness of the plate or shell.

The representative "load–deflection" diagram for columns and plates of perfect geometric form and loaded by in-plane compressive forces p is shown in Fig. 19.1a. Each position plotted in this figure represents an equilibrium configuration of the member – stable, neutral, or unstable – depending upon whether the slope of the path at that point is positive, zero, or negative, respectively. Points not lying on this diagram, of course, correspond to nonequilibrium configurations. The equilibrium path consists of the three branches: (a) branch OA refers to an initial, unbuckled configuration of equilibrium that is assumed to be momentless; (b) two "rising" branches CA and AD refer to buckled configurations of equilibrium. Note that the curve CAD is symmetrical about the p axis. For the equilibrium path, shown in Fig. 19.1a, at the transition point A, a bifurcation of equilibrium is said to occur, since there are at least two possible states of equilibrium, $f = 0$ and $f \to \infty$. Such a

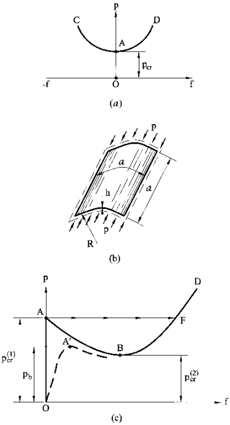

(a)

(b)

(c)

Fig. 19.1

transition point A, as mentioned in Sec. 8.2, is referred to as a *bifurcation point*, and the load at that point is called the *critical load*, p_{cr}. As shownin Fig. 19.1a, there are new and stable, buckled configurations of equilibrium in the immediate vicinity of the bifurcation point. Therefore, with the slight and smooth increase in the applied load above p_{cr}, the initial configuration of equilibrium of the structural member (column or plate) ceases to be stable, and smoothly, without any jumps, it goes over to an adjacent buckled, stable configuration of equilibrium. It follows from the above that the critical values of an applied load can be determined with the use of linear differential equations of the structural stability theory, introduced in Sec. 8.2. A geometrically nonlinear theory can be used only for describing the postbuckling behavior of the member.

Lets turn our attention to the analysis of a shell buckling process. The representative paths of equilibrium for a simply supported shallow cylindrical shell under a uniform axial loading p (Fig. 19.1b) are shown in Fig. 19.1c. The solid curve $OABD$ refers to the shell whose initial configuration is assumed to be perfect, i.e., without any geometric and other imperfections. The load p is applied statically such that the initial configuration of equilibrium of the shell is in the membrane state of stress, and thus, $f = 0$. The equilibrium path $OABD$ consists of the ''rising'' branches OA and BD, corresponding to stable equilibrium states, and the ''descending'' branch AB that corresponds to an unstable equilibrium configuration.

Point A on the curve $OABD$ can also be interpreted as a bifurcation point. However, unlike the equilibrium path, shown in Fig. 19.1a, for columns and flat plates, there are no new stable buckled configurations in the immediate vicinity of the bifurcation point A. The stable, buckled configurations of equilibrium are off from the initial ones at some finite distances (on the branch BD). Therefore, a transition from the initial configuration of equilibrium (branch OA) to a new, buckled and stable configuration of equilibrium (branch BD) occurs by a jump, i.e., the shell ''jumps'' from a stable state at A through the statically unstable state, given by the branch AB, to the stable state at F on the branch BD, as shown in Fig. 19.1c. This sudden transition from the initial configuration of equilibrium to the next, stable and buckled configuration of equilibrium, with the corresponding jump in f, is termed as *snap-through buckling*. As a result, the shell buckling analysis, in a general case, must be based on the geometrically nonlinear shell theory.

The curve $OABD$ has been analyzed above for the buckling model of some perfect shell. However, a real shell typically has some geometric and other imperfections due to manufacturing. Such irregularities of the shell geometric form are equivalent to prebuckling deformations imposed on the original shell configuration. Note, that experiments performed on columns and flat plates under in-plane compressive forces showed that they are relatively insensitive to slight geometric imperfections. This is not the case in a shell buckling process. Buckling experiments carried out on shells showed that some shells are very sensitive to geometric and loading imperfections. For instance, for the shallow cylindrical shell under consideration (Fig. 19.1b), such an elevated sensitivity to slight imperfections can be explained by the closeness of the unstable branch AB to the initial shell configuration of equilibrium given by straight line OA.

The path of shell instability for the given real shell with geometric and other imperfections is given by the dashed curve shown in Fig. 19.1c. It is seen that, due to the above-mentioned irregularities, the real shell begins to deviate from its

the initial configuration of equilibrium is assumed to be momentless, the changes in curvature and twist may occur as a result of buckling only. Therefore, the index 1 for these components will be omitted from here on.

The general procedure of the energy method in the shell buckling analysis for determining the critical values of applied loading is analogous to that discussed in Sec. 8.4 for the plate bending problems.

19.3 LINEAR BUCKLING ANALYSIS OF CIRCULAR CYLINDRICAL SHELLS

19.3.1 General

Buckling of cylindrical shells can occur in those cases when they are subjected to the action of axial compression, transverse pressure, torsion, etc. These loads can be applied either separately or in various combinations. We present below the simplified linear buckling analysis of circular cylindrical shells based on the Donnel–Mushtari–Vlasov (DMV) theory, which is assumed to be applicable with reasonable accuracy to this analysis. It has been shown (see, for instance Ref. [1]) that the simplified linear equations of the DMV theory can be applicable to the local instability shell problems if the dimensions of bulging, formed in buckling, are small compared with the shell typical dimensions, at least in one direction.

19.3.2 Critical load for an axially compressed cylinder

Consider the stability problem of a closed cylindrical shell of radius R and of length L, simply supported on its edges and subjected to uniform compressive forces q_1. This case of loading is of a great practical importance. For example, an aircraft fuselage is subjected to compressive forces transmitted from the engine at the acceleration path. Some other problems including the buckling of shells in bending, can also be reduced to application of results obtained from the case of axially symmetrical compression. Along with that, the circular cylindrical shell compressed along its generator can serve as some standard for comparing the theoretical and experimental data to check various approaches in shell stability analysis.

The boundary conditions for the deflections, w, in buckling of the shell under consideration are of the following form:

$$w = 0|_{x=0,L}; \quad \frac{\partial^2 w}{\partial x^2} = 0\bigg|_{x=0,L}. \tag{19.15}$$

The x and y coordinates can be chosen as coordinates that determine the location of a point on the middle surface. They define the position of a point along the shell generator and over the arc of its cross section, respectively, as shown in Fig. 19.2.

As a first variant of the solution of this buckling problem, let us assume that the *deflected surface of the shell after buckling is axisymmetric*, i.e., the shell cross section remains circular, as shown in Fig. 19.2. Assuming that the initial, prebuckled configuration of equilibrium of the cylindrical shell is momentless, take the equation for deflections w in buckling in the form

$$w = -f \sin\frac{m\pi x}{L}. \tag{19.16}$$

Thus, the expressions (19.43) and (19.46) can be applied to cylinders for which $Z \geq 2.85$ or whose length $L > 1.69\sqrt{Rh}/\sqrt[4]{1-\nu^2}$. Such cylinders are classified as *moderate-length cylinders*. For *short cylinders*, for Z less than 2.85, the values of $\beta = 0$ and $m = 1$ are to be substituted into Eq. (19.41). For a short and simply supported cylinder, we obtain

$$K_1 = 1 + \frac{12Z^2}{\pi^4}. \tag{19.49}$$

The critical stress for cylinders with $Z < 2.85$ is thus given by

$$\sigma_{1,\mathrm{cr}} = \frac{K_1 \pi^2 D}{hL^2}, \tag{19.50}$$

where K_1 is defined by Eq. (19.49). Expression (19.50) indicates that the critical stress of a short cylinder approaches that of a wide laterally unsupported plate as Z approaches zero or as a simply supported column.

In the foregoing analysis, it was assumed that failure would occur as a result of local surface buckling. This assumption is valid only as long as the cylinder is not extremely slender. Long narrow cylinders may become unstable as a result of Euler's column buckling (general or global instability) before the local instability stress is reached, and must therefore be checked for both modes of failure. It has thus been shown that the buckling mode of an axially loaded cylinder depends on the ratio of its length to its radius. The local instability occurs for short and moderate-length cylinders, whereas a long cylinder buckles as a column. There is a big difference between local and general bucklings of short and long cylinders. The buckling of a very long cylinder (Euler's buckling mode) does not involve surface distortion of the circular cross section at all. Instead, the member simply behaves like Euler's column. The local instability largely involves a surface distortion for short cylinders. Intermediate-length cylinders are to be found between these two extremes and represent the majority of actual cylinders. Cylinders of this type buckle by developing surface distortions in both the longitudinal and circumferential directions, and their critical stress is given by Eq. (19.46).

19.3.3 Buckling of cylindrical shells under external pressure

Consider the case when a shell is subjected to uniform external pressure of intensity p (Fig. 19.3). Such a type of loading is typical for submarine hulls and shell aircraft engine housings. Also tanks in chemical plants often experience an excessive external pressure.

The external uniform pressure causes the membrane longitudinal stress σ_1 and circumferential stress σ_2, as well as the bending stresses in a cylindrical shell. In analyzing the shell buckling, the circumferential compressive stresses are of great importance. If a shell is sufficiently long, then the critical values of the external pressure p only slightly affect the boundary conditions prescribed on the shell edges. This means that a distortion of the circular cross section will be identical throughout the length of the shell. Hence, the buckling analysis of long cylindrical shells can be replaced (for the sake of simplicity) by the analysis of the stability of a ring of unit length with the same radius and thickness as for the given shell. Such a

where

$$\hat{q}_1 = \frac{q_1 R}{Eh}, \quad \hat{p} = \frac{p}{E}\left(\frac{R}{h}\right)^2, \quad \mu = \frac{m\pi R}{nL}, \quad \eta = \frac{n^2 h}{R}. \tag{19.64}$$

It is seen that the critical combinations of values $\hat{q}_1$ and $\hat{p}$ are related to one another by a linear relationship. The plot of $\hat{q}_1$ vs $\hat{p}$ represents some polygon *ACDB*, as shown in Fig. 19.4. This figure is taken from Ref. [4].

Note that points *A* and *B* in this figure correspond to the upper critical values of axial compressive load, $\hat{q}_{1\text{cr}}$, and external pressure, $\hat{p}_{\text{cr}}$, respectively, applied separately from one another. If we join these points by a straight line, we obtain some intermediate values of $\hat{q}_1$ and $\hat{p}$ corresponding to the following equation:

$$\frac{\hat{q}_1}{\hat{q}_{1\text{cr}}} + \frac{\hat{p}}{\hat{p}_{\text{cr}}} = 1$$

or

$$\frac{q_1}{q_{1\text{cr}}} + \frac{p}{p_{\text{cr}}} = 1 \tag{19.65}$$

(the superscript 1 that refers to the upper critical loads is omitted in the above and further equations, because in the linear buckling analysis only such a critical load can be obtained).

It is easily seen that Eq. (19.65) determines the critical combination of the axial loads and external pressure conservatively with respect to the polygon. Therefore, this equation can be used as a first approximation in a practical design.

Theoretical investigations and experiments showed that an axial compression decreases the value of the external critical pressure, compared with the case when this compression is absent. An axial tension increases the value of the external critical pressure. In turn, an internal pressure increases the value of the axial compressive critical force.

Also it should be noted that in the shell buckling problems introduced above, the solutions were obtained by assigning the boundary conditions for the deflections of the type of Eqs (19.15) on the shell edges, ignoring the in-plane displacements prescribed also on these edges. The investigations associated with the effect of the in-

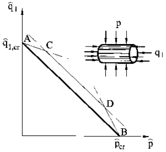

Fig. 19.4

applied loads. Let us rewrite the strain–displacement relations (18.19) to include the effects of the initial imperfections. If in the derivation of these expressions given in Sec. 18.2.2 the lateral deflection w is replaced by $w + w_{\mathrm{i}}$, then Eqs (18.19) take the form

$$\begin{aligned} \varepsilon_1 &= \frac{\partial u}{\partial x} - \kappa_1 (w + w_i) + \frac{1}{2}\left(\frac{\partial w}{\partial x}\right)^2 + \frac{\partial w}{\partial x}\frac{\partial w_{\mathrm{i}}}{\partial x}; \\ \varepsilon_2 &= \frac{\partial v}{\partial y} - \kappa_2 (w + w_i) + \frac{1}{2}\left(\frac{\partial w}{\partial y}\right)^2 + \frac{\partial w}{\partial y}\frac{\partial w_{\mathrm{i}}}{\partial y}; \\ \gamma_{xy} &= \frac{\partial u}{\partial y} + \frac{\partial v}{\partial x} + \frac{\partial w}{\partial x}\frac{\partial w}{\partial y} + \frac{\partial w_i}{\partial x}\frac{\partial w}{\partial y} + \frac{\partial w}{\partial x}\frac{\partial w_{\mathrm{i}}}{\partial y}. \end{aligned} \tag{19.71}$$

Following the procedure for the derivation of the differential equations of the large-deflection theory, given in Sec. 18.2, we obtain the following

$$\begin{aligned} \frac{D}{h}\nabla^2\nabla^2 w - L(w + w_{\mathrm{i}}; \phi) - \nabla_k^2 \phi &= \frac{p_3}{h}, \\ \frac{1}{E}\nabla^2\nabla^2 \phi &= -\frac{1}{2} L(w + 2w_{\mathrm{i}}; w) - \nabla_k^2 w \end{aligned} \tag{19.72}$$

where $\phi = \Phi / h$ and the operator $L(U, V)$ is given by Eqs. (18.30). The above equations are the *nonlinear governing equations of an initially imperfect shallow shells*.

We analyze below the postbuckling behavior of a shallow square cylindrical panel of side a, subjected to uniform compressive forces q_1 applied along the curvilinear edges of the panel, as shown in Fig. 19.5. The radius of curvature of the panel is R, and its thickness is h. The postbuckling behavior of such a panel is very similar to that of the entire cylinder, however, the calculation of the critical values of the compressive loads for this panel is less lengthy and less complicated than for the entire cylinder. The analysis presented here follows the general outline of that given by Volmir [4].

As far as the boundary conditions are concerned, it is assumed that (1) the edges are simply supported, (2) the shear force S vanishes along each edge, (3) the edges $y = 0$ and $y = a$ are free to move in the y direction, and (4) the panel retains its rectangular shape (in a plane) during buckling. These conditions are satisfied if we let

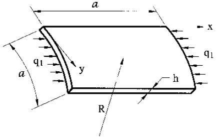

Fig. 19.5

$$\hat{q}_{1,\mathrm{cr}}^{(1)} = \frac{\pi^2}{3(1-\nu^2)} + \frac{k^2}{\pi^2}. \tag{19.89}$$

Thus, we can represent the nonlinear load–deflection relationship for the given perfect cylindrical panel as

$$\hat{q}_1 = \hat{q}_1^{(1)} + \frac{\pi^2}{8}\delta^2 - \frac{10}{3\pi^2}\mathrm{k}\delta. \tag{19.90}$$

Inserting Eq. (19.89) into Eq. (19.88) leads to the following:

$$\hat{q}_{1,\mathrm{cr}}^{(2)} = \hat{q}_{1,\mathrm{cr}}^{(1)} - \frac{200}{9\pi^6}k^2. \tag{19.91}$$

Let us turn to Eq. (19.83). As mentioned in Sec.19.2, there is a good reason to believe that the initial imperfections of a shell geometry have a great effect on the scatter of experimental data of the critical loads and on the discrepancies between the theoretical and experimental results. Figure 19.6 (taken from Ref. [11]) shows the load–deflection relationships for a flat plate with $k = 0$ (Fig. 19.6a) and for a cylindrical panel with $k = 24$ (Fig. 19.6b).

The curves in each figure depict the variation of the load parameter $\hat{q}_1$ with the total lateral deflection parameter $\delta + \delta_{\mathrm{i}}$. The curves for several different values of the initial imperfection δ_{i} are presented. It follows from Fig. 19.6a, that small initial deformations practically do not affect the buckling behavior of flat plates and the behavior of the flat plate is similar to that of a column. In fact, as in the case of the perfect plate ($\delta_{\mathrm{i}} = 0$), the critical load does not represent the maximum carrying capacity of the imperfect plate. Instead, as the deflection continues to grow, the imperfect plate is able to resist increasing loads. Furthermore, as the deflections increase, the curves of the initially imperfect plates approach that of the perfect plate.

The cylindrical panels demonstrate another behavior. A strong dependence of the maximum axial compressive load on the magnitude of the initial imperfection is seen from Fig. 19.6b. As long as the axial load is small, bending increases very gradually with an increase in the load. Then, suddenly, at a certain load whose magnitude appears to depend on the magnitude of the initial imperfection, the bending deflections begin to grow rapidly and the load drops. The important conclusion that can be drawn from this figure is that the maximum load, i.e., the buckling load, $q_{1\mathrm{b}}$ as introduced in Sec. 19.2, the initially imperfect panel can support, is considerably less that the upper critical load given by the linear stability theory. Even for very small imperfections, such as $\delta_{\mathrm{i}} = 0.05$, the maximum buckling load is only 75% of the upper critical load. Thus, small initial imperfections have a very significant effect on the buckling characteristics of cylindrical panels. The failure of the moderate-length cylinders in axial compression should be influenced profoundly by the magnitude of initial imperfections in the cylinder.

It should be noted that the general conclusions made above on the effect of the initial imperfections on the buckling characteristics of axially compressed panels are valid also for closed axially compressed cylinders. However, they are not typical for the buckling behavior of cylindrical shells under other loads.

Let us discuss briefly some important theoretical results available on the postbuckling behavior of cylinders subject to external pressure whose linear buckling analysis was presented in Sec. 19.3.3. It was shown [4,8] that the effect of nonlinear-

pressure p. Assume that the material of the shell is so arranged that at each point of the shell its mutual orthogonal directions of elastic symmetry coincide with the principal lines of curvature of the shell midsurface.

The differential equation of stability for orthotropic cylindrical shells under external pressure can be derived in much the same way as for isotropic shells (see Sec. 19.3.3). The solution of this equation can also be sought in the form of Eq. (19.34). Omitting the lengthy and cumbersome mathematics, we present below the following final expression for the critical value of external pressure, p_{cr}:

$$p_{\mathrm{cr}} = \min\left\{\left[\frac{D_n}{R^3} + h\beta_n \frac{\alpha^2}{Rt_n}\right]\frac{1}{\gamma_n}\right\}, \tag{19.92}$$

where,

$$\begin{aligned}
D_n &= D_1\alpha^4 + 2D_3\alpha^2(n^2-1) + D_2(n^2-1)^2 + (D_3 - \nu_1 D_2)\alpha^2,\\
\beta_n &= \alpha^2 + (\alpha^2 - \nu_2 n^2)\left[D_3\alpha^2 + D_2(n^2-1)\right]\frac{1}{E_2R^2h},\\
t_n &= \alpha^4\delta_2 + 2\delta_3\alpha^2 n^2 + \delta_1 n^4,\ \gamma_n = 0.5\alpha^2 + n^2 - 1,\\
\delta_1 &= \frac{1}{E_1},\quad \delta_2 = \frac{1}{E_2},\quad \delta_3 = \frac{1}{2G} - \frac{\nu_1}{E_1},\quad \alpha = \frac{\pi R}{L}.
\end{aligned} \tag{19.93}$$

The rigidities D_1, D_2, and D_G are given by Eqs (18.45b) and $D_3 = D_1\nu_2 + D_G$. It follows from Eq. (19.92), that the critical value of pressure, p_{cr}, is obtained by selecting the number of half-waves in the circumferential direction, n, so that it makes Eq. (19.92) a minimum.

19.5.2 Stability of stiffened cylindrical shells

As mentioned previously, cylinders are frequently manufactured with longitudinal (stringers) and circumferential (ribs or collars) stiffeners. An aircraft fuselage and a submarine hull are examples of stiffened shells. As a rule, stiffened shells are more efficient than unstiffened shells. In addition, they are less sensitive to initial imperfections. Therefore, the critical values of applied loads for such shells are closer to the theoretically determined values of the upper critical loads predicted by the linear stability theory.

The buckling analysis of stiffened shells, just as the corresponding analysis of stiffened plates, requires several steps. The first step in this analysis is to assess the overall or primary buckling response of the stiffened shell. The second step is to determine the local skin buckling response for skin segments located between stiffeners. The third step is to determine whether stiffener buckling has occurred at the given buckling load level. Our main concern in this book is with the primary buckling analysis of stiffened shells.

The primary buckling analysis of thin shells reinforced by closely spaced orthogonal stiffeners can be addressed conveniently with the use of the orthotropic shell theory, introduced in Sec. 18.3. In this case, the rigidities of the stiffeners are smearing along the shell middle surface, and a gird-stiffened shell is replaced by a structurally orthotropic unstiffened shell. We locate a point on the shell midsurface by the x and y coordinates (see Fig. 19.2). Following the simplified DMV theory of thin

The Galerkin method equations (see Sec. 6.5) are the following:

$$\int_0^a \int_0^b X \sin\frac{\pi x}{a} \sin\frac{\pi y}{b} \mathrm{d}x\mathrm{d}y = 0; \qquad \int_0^a \int_0^b Y \sin\frac{\pi x}{a} \sin\frac{\pi y}{b} \mathrm{d}x\mathrm{d}y = 0. \tag{19.118}$$

Substituting expressions (19.116) together with the approximations (19.117) into the above and integrating, one obtains

$$\begin{aligned} &\frac{D}{h} B_1 \frac{\pi^6}{16}\left(\frac{1}{a^2}+\frac{1}{b^2}\right)^2 - A_1 B_1 \frac{2}{3}\frac{\pi^4}{a^2 b^2} + A\frac{\pi^4}{16}\left(\frac{k_1}{b^2}+\frac{k_2}{a^2}\right) - \frac{p}{h} = 0, \\ &\frac{A_1}{E} + \frac{16 B_1^2}{3\pi^2\left(\frac{b}{a}+\frac{a}{b}\right)^2} - \left(\frac{k_1}{b^2}+\frac{k_2}{a^2}\right)\frac{B_1}{\pi^2}\frac{1}{\left(\frac{1}{a^2}+\frac{1}{b^2}\right)^2} = 0. \end{aligned} \tag{19.119}$$

Introduce the following dimensionless parameters:

$$k_1^* = \frac{k_1 a^2}{h}; \quad k_2^* = \frac{k_2 b^2}{h}; \quad k^* = k_1^* + k_2^*; \quad \lambda = \frac{a}{b}; \quad \zeta = \frac{B_1}{h}; \quad \hat{p} = \frac{p}{E}\left(\frac{ab}{h^2}\right)^2. \tag{19.120}$$

Using the above-introduced parameters, we can represent a solution of Eqs (19.119), in the following load–deflection relationship:

$$\hat{p} = \frac{32\pi^2}{9}\frac{\zeta^3}{\left(1+\frac{1}{\lambda}\right)^2} - \frac{k^*\pi^2\zeta^2}{\left(1+\frac{1}{\lambda}\right)^2} + \left[\frac{(k^*)^2\pi^2}{16\left(1+\frac{1}{\lambda}\right)^2} + \frac{\pi^6\left(\frac{1}{\lambda}+\lambda\right)^2}{192(1-\nu^2)}\right]\zeta. \tag{19.121}$$

For a square shallow shell panel and $\nu = 0.3$, the above equation simplifies to the form

$$\hat{p} = 8.77\zeta^3 - 2.46k^*\zeta^2 + [0.154(k^*)^2 + 22]\zeta. \tag{19.122}$$

For a cylindrical shallow shell panel, $\kappa_1 = 0$ and $\kappa_2 = 1/R$, then $k^* = b^2/Rh$.

Figure 19.7 illustrates the diagrams of $\hat{p}$ vs .ζ for various values of k^* and for $\lambda = 1$. These diagrams are shown by dashed lines. The numerical data presented in the Fig. 19.7 are taken from Ref. [4]. It is seen that for small values of k^* the value of $\hat{p}$ increases continuously, just as for flat plates; for large values of k^*, the diagram $\hat{p}(\zeta)$ has a descending branch. To find the value of k^* at which jumping occurs from one stable configuration of equilibrium to another, it is necessary to analyze $\mathrm{d}\hat{p}/\mathrm{d}\zeta$. Equating it to zero, one finds the values of ζ corresponding to the upper and lower values of the critical pressure previously introduced in Sec. 19.2. We have the following:

$$\zeta = \frac{3}{32}k^* \mp \frac{1}{32}\sqrt{3(k^*)^2 - \frac{\pi^4\left(1+\frac{1}{\lambda}\right)^4}{2(1-\nu^2)}}. \tag{19.123}$$

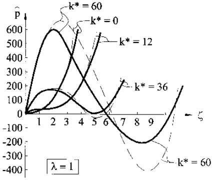

Fig. 19.7

The boundary of the domain of this jump corresponds to the case when the diagram $\hat{p}(\zeta)$ has a point of inflection with a horizontal tangent. In so doing, the expression under the radical sign must vanish. Thus, a limiting value of k^* will be of the form

$$\mathrm{k}^* = \frac{\pi^2\left(1+\frac{1}{\lambda}\right)^2}{\sqrt{6(1-\nu^2)}} \quad \text{for} \quad \zeta = \frac{3}{32}k^*. \tag{19.124}$$

If we retain four terms in series (19.177), the refined solutions will be obtained. They are shown by solid lines in Fig.19.7. It is seen from this figure that the distinctions of the refined diagrams from the first-approximation diagrams become perceptible only for "elevating" shells, starting with $k^* = 36$, and the refined diagrams give slightly lower upper critical values of pressure. However, the refined diagrams illustrate the changes in the lower critical loads: in some cases, the loads change sign.

19.8 BUCKLING OF CONICAL SHELLS

Thin conical shells find wide applications in the structures of jet engines, aircrafts, liquid storages, reservoirs, etc. Buckling analysis of conical shells is more complicated than the corresponding analysis of cylindrical shells, because of the complexity of the stability governing equations.

We consider below some final results of the linear buckling analysis of intermediate-length conical shells subjected to uniform external pressure p, as shown in Fig. 19.8. Assume that the shell ends cannot displace at their ends in the direction normal to the shell midsurface. The criterion of the "intermediate-length cylindrical shell" was introduced in Sec. 19.3. This criterion can be employed for conical shells, too, by replacing R with the mean radius of the parallel circle $r_{\mathrm{m}} = (r_1 + r_2)/2$, and by setting L equal to the length of the longitudinal axis of the shell (Fig. 19.8). For the above-mentioned shells, $n^2 > \lambda^2$, where n is the number of half-waves in the circumferential direction of the shell and $\lambda = \pi r_{\mathrm{m}}/L$. Then, the approximate relation for determining the critical value of the external pressure in a conical shell is

predicted by the linear stability theory. Some empirical equations were developed for determining the critical stresses and loads for stiffened shells of various configuration under axial compression, external pressure, torsion, shear, as well as various loading combinations [12,14,19,21]. For example, for the spherical shell with closely and equally spaced stiffeners in two mutually orthogonal directions under external pressure, the buckling value of the above pressure is given by [21]

$$p_{\mathrm{cr}} = 0.366E\left(\frac{h_{\mathrm{m}}}{R}\right)^2\left(\frac{h_{\mathrm{b}}}{h_{\mathrm{m}}}\right)^{3/2}, \tag{19.152}$$

where $h_{\mathrm{m}} = h + A/s$ is the effective membrane thickness and $h_{\mathrm{b}} = (12I/s)^{1/3}$is the effective bending thickness; A and I are the area and moment of inertia of the stiffener, s is the spacing between stiffeners.

Local buckling of the spherical shells between the stiffeners must also beconsidered for large-diameter shells. One such equation is given by

$$p_{\mathrm{cr}} = 7.42\frac{Eh^3}{Rs^2}. \tag{19.153}$$

Only a small selection of the recommended design relations for determining the critical loads in thin shells has been introduced above. The interested reader is referred to Refs [4,12,13,14,19–24].

In conclusion, note that in practice one must tend to designing the shell structures whose stability would not depend on occasional and not easily controlled factors. The basic avenues of designing such shell structures is the use of stiffened shells, sandwich shells, corrugated shells, etc. In some, the most important cases, sharpened shells are applied.

PROBLEMS

19.1 It follows from Fig. 19.1a that the path of equilibrium for a flat plate is symmetric about the vertical, p axis, whereas the corresponding path for a shallow shell is nonsymmetrical. Explain the above difference in the buckling behavior of plates and shells.

19.2 Provide a detailed deviation of Eqs (19.3).

19.3 Derive Eqs (19.4) from (19.3) by neglecting all the terms containing prebuckled rotations.

19.4 Derive Eqs (19.9) from Eqs (19.7).

19.5 A water tower support constructed of a long steel piping of 1.0 m diameter is to carry an axial compression load of 520 kN. Assuming that the supports ends are pin-connected, determine the required thickness of the shell that will prevent this tower support from buckling. Use $L = 2.0\,\mathrm{m}$, $E = 200\,\mathrm{GPa}$, $\nu = 0.3$, and a factor of safety (FS) of 3.5.

19.6 Verify Eq. (19.22)

19.7 A thin steel pipe is subjected to a vacuum pressure of 150 psi. Assuming that the pipe edges are simply supported, determine the required thickness of the pipe, preventing the pipe from buckling. Given $E = 29{,}000$ psi, $\nu = 0.3$, $L = 10$ ft, $R = 2.5$ ft, and the factor of safety (FS) is 3.0.

19.8 Determine the critical stress in a simply supported circular cylindrical panel subjected to a uniformly distributed compressive forces q_1, as shown in Fig. P.19.1. Assume that the shell edges are simply supported.
Hint: take the deflection w in the form

20

Vibrations of Shells

20.1 INTRODUCTION

The dynamic effects of time-dependent loads on shell structures are quite similar to those discussed in Chapter 9 for plates. Thus, the objectives of the vibration analysis of shells, as well the general approach for deriving the shell equations of motion, remain analogous to the plate vibration analysis introduced in Sec. 9.1.

Assume that the state of stress within a shell during vibrations has a character determined by the equations of equilibrium, and the shell middle surface deforms according to the same law during vibrations as in the static equilibrium state. Based on the above, the equations of motion of the vibrating shell can be obtained by applying the D'Alambert principle, just as it was done for vibrating plates – i.e., by adding the inertia forces to given external loads, assigned by components p_1, p_2, and p_3, namely (damping forces are not considered here):

$$p_1 \rightarrow p_1 - \rho h \frac{\partial^2 u}{\partial t^2}; \quad p_2 \rightarrow p_2 - \rho h \frac{\partial^2 v}{\partial t^2}; \quad p_3 \rightarrow p_3 - \rho h \frac{\partial^2 w}{\partial t^2}, \tag{20.1}$$

where p_1, p_2, p_3, and u, v, w are functions of the Cartesian coordinates of the middle surface and time, ρ is the mass density of the material, and h is the shell thickness. As for vibrating plates, we distinguish between *free vibrations* of shells, which occur in the absence of applied loads but are initiated by some initial conditions imposed on the shell, and *forced vibrations* of shells, which result from the application of time-dependent loads. We consider in this chapter both types of vibrations.

20.2 FREE VIBRATIONS OF CYLINDRICAL SHELLS

20.2.1 General

As mentioned in Sec. 9.1, free vibrations deal with some natural characteristics of shells. These natural vibrations occur at discrete frequencies, depending only on the geometry and material of the shell. A knowledge of the free-vibration characteristics of thin elastic shells is important both for our general understanding of the fundamentals of the shell behavior and for industrial applications of shell structures. In connection with the latter, the natural frequencies of shell structures must be known to avoid the destructive effect of resonance with adjacent rotating or oscillating equipment (such as jet and reciprocating aircraft engines, electrical machinery, marine turbines and propulsors, etc.).

Since the free vibrations occur in the absence of all external forces ($p_1 = p_2 = p_3 = 0$), we address the free-vibration analysis of shells with the solution of homogeneous partial differential equations with homogeneous boundary conditions. Let us derive the equations of the free vibrations of thin elastic cylindrical and shallow shells.

20.2.2 Axisymmetric free flexural vibrations of cylindrical shells

Consider the free flexural vibrations of a circular cylindrical shell when the radial w and longitudinal u displacements do not depend on the angular coordinate θ, and the circumferential displacement v is zero. Any cross section of such a shell will be a circular ring, and several half-waves can be placed throughout the shell length, as shown in Fig. 20.1.

The equation of axisymmetrical free vibrations can be obtained from the governing differential equation of the axisymmetrically loaded circular cylindrical shell, Eq. (15.44). One replaces, due to Eq. (20.1), the normal component of the external loading p_3 by the normal component of the inertia forces, and neglects the longitudinal component of the above forces. Thus, the differential equation of the axisymmetrically vibrating circular cylindrical shell is found to be

$$\frac{\partial^4 w}{\partial x^4} + 4\beta^4 w = -\frac{\rho h}{D}\frac{\partial^2 w}{\partial t^2}, \tag{20.2}$$

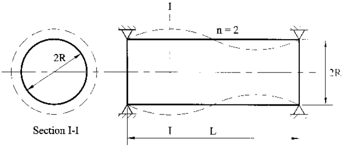

Fig. 20.1

Since the number of m may be an integer only, then, after determining m from Eq. (20.17), it should be taken to be equal to the nearest integer. The smallest natural frequency corresponds to this integer. The second derivative of Ω with respect to m will be positive; therefore, Eq. (20.17) defines a minimum.

Example 20.1

For a simply supported closed cylindrical shell of radius $R = 17$ cm and of length $L = 54$ cm, find the number of half-waves in the circumferential direction and the minimum natural frequency. Use the following geometric and mechanical parameters of the shell: $h = 0.08\,\text{cm}$, $\nu = 0.3$, $E = 200\,\text{GPa}$, and $\nu = 0.3$.

Solution

For the given geometric and mechanical shell parameters, we can find that $a^2 = 0.18 \times 10^{-5}$, $\lambda = 1$, and $T_1 = 0.9$. Substituting the above data into Eq. (20.17), gives $m = 5.1$. Hence, the minimum natural frequency of predominantly transverse vibrations, $\omega_{\min}$, takes place for five half-waves or for 10 nodal points placed over the circumference of the shell cross section. The value of ω is found from Eq. (20.15) for $m^* = 5$. The relationship between the frequency and m is shown in Fig. 20.2.

Figure 20.3 illustrates the relationship of the frequency for any fixed value of m from the shell length, L. It is seen that the frequency decreases as the length of the shell increases. However, starting from some length L^*, the frequency becomes a constant and practically coincides with the frequency determined for a shell having free edges or for a shell of an infinite length when the shell experiences only bending without stretching of the middle surface.

If a shell is not too short ($L > R$), then the natural frequency is virtually independent of the boundary conditions and it is possible to determine this frequency for a shell with any, say simply supported, boundary conditions.

The strain energy of a shell of any geometry is given by Eq. (12.51). The kinetic energy of a vibrating shell is of the following form:

$$K = \frac{\rho h}{2} \int\int_A \left[\left(\frac{\partial u}{\partial t} \right)^2 + \left(\frac{\partial v}{\partial t} \right)^2 + \left(\frac{\partial w}{\partial t} \right)^2 \right] AB\, \mathrm{d}\alpha\, \mathrm{d}\beta. \tag{20.18}$$

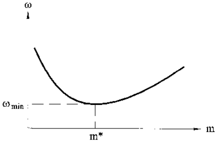

Fig. 20.2

$$\begin{gathered}
-\frac{\partial^2 \Phi}{\partial \xi^2} R + D\nabla^2\nabla^2 w + \rho h R^4 \frac{\partial^2 w}{\partial t^2} = 0, \\
\nabla^2\nabla^2\Phi + REh\frac{\partial^2 w}{\partial \xi^2} = 0.
\end{gathered} \tag{20.21}$$

The above is a set of the *governing differential equations of the undamped, free linear, transverse vibrations of circular cylindrical shells*. The details of determining the natural frequencies of cylindrical shells is explained in the illustrative problem that follows.

Example 20.2

Determine the natural frequency of free vibrations of the circular cylindrical, simply supported shell shown in Fig. 20.4. Calculate the fundamental natural frequency for the shell made of reinforced concrete and having the following geometric and mechanical parameters: $L = 55\,\text{m}$, $l = 21\,\text{m}$, $f = 4.0\,\text{m}$, $R = 15.0\,\text{m}$, $h = 0.1\,\text{m}$, $\theta_0 = 1.6\,\text{rad}$, $E = 6\,\text{GPa}$, $\rho = 1.6 \times 10^3\,\text{kg/m}^3$, and $\nu = 0$.

Solution

The simply supported boundary conditions in the adapted coordinate system are of the form

$$\begin{aligned}
&w = v = M_1 = N_1 = 0\big|_{\xi=0,\xi=L/R}, \\
&w = u = M_2 = N_2 = 0\big|_{\theta=0.\theta=\theta_0}.
\end{aligned}$$

A solution of Eqs (20.15) is sought in the form of the following series:

$$\begin{aligned}
\Phi &= \sum_{m=1}^{\infty}\sum_{n=1}^{\infty} A_{mn} \sin\lambda_n\xi \sin\mu_m\theta \cdot \sin\,\omega t, \\
w &= \sum_{m=1}^{\infty}\sum_{n=1}^{\infty} B_{mn} \sin\lambda_n\xi \sin\mu_m\theta \cdot \sin\omega t,
\end{aligned} \tag{a}$$

where

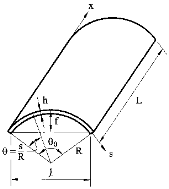

Fig. 20.4

face loads p_1, p_2, and p_3 with the inertia forces according to Eqs (20.1). The governing equations of free vibrations in displacements obtained represent the partial differential equations with variable coefficients. Their solution represents a very complicated mathematical problem.

Conducted analyses and tests showed that for small angles of conicity 2α (about 30°–40°) (see Fig. 19.8), the frequency of axisymmetric, free radial vibrations can be approximately calculated by Eqs (20.4) and (20.7) by replacing R in these equations with $r_m = (r_1 + r_2)/2$ and setting the length of the longitudinal axis of the conical shell equal to L (cylindrical shell length). It should be noted that conical shells with these angles of conicity are met in nozzle structures of jet engines. The vibration shell analyses showed that the error introduced by the above approximate procedure was not more than 5–10%. For larger angles of conicity, refined solutions, based on the governing differential equations of free vibrations mentioned above, should be employed.

The dependence of the frequency of free radial vibrations on the number of waves along the shell cross section has a minimum, just as for a cylindrical shell (see Fig. 20.2). The above minimum is explained by relations between the strain energy due to elongation and the strain energy due to bending in various undulations.

A conical shell can have longitudinal and torsional vibrations but they are of less importance than the bending and normal axisymmetric vibrations.

20.4 FREE VIBRATIONS OF SHALLOW SHELLS

The governing differential equations of free vibrations of shallow shells can be obtained from Eqs (17.36) by using the relations (20.1), setting $p_1 = p_2 = p_3 = 0$, and assuming that stiffness of the shell in the middle surface is much greater than its stiffness in the direction normal to the middle surface. Therefore, putting $\alpha = x$ and $\beta = y$ and neglecting the in-plane inertia forces, we obtain the following *differential equations of free vibrations of shallow shells*:

$$\begin{aligned} D\nabla^2\nabla^2 w - \nabla_k^2\Phi + \rho h\frac{\partial^2 w}{\partial t^2} &= 0, \\ \nabla^2\nabla^2\Phi + Eh\nabla_k^2 w &= 0, \end{aligned} \tag{20.22}$$

where the operators ∇^2 and ∇_k^2 are given by Eqs (17.44), respectively.

To determine the natural frequencies of shallow shells having arbitrary boundary conditions, the approximate and numerical methods introduced in Chapter 6 may be used. Let us consider an application of some methods to the free-vibration problems of a shallow shell given by Eqs (20.22). Assume that the projection of the shell into the Oxy coordinate plane is a rectangle with sides a and b.

1. Galerkin method

The stress function Φ and deflection w are sought in the form of the following series:

$$\begin{aligned} \Phi &= \sum_m \sum_n A_{mn}\Phi_{mn}(x, y)\sin\omega t, \\ w &= \sum_m \sum_n B_{mn}W_{mn}(x, y)\sin\omega t. \end{aligned} \tag{20.23}$$

This chapter contains only some general information about the dynamic response of thin shells. The interested reader is referred to Refs [2–5] for additional reading.

PROBLEMS

20.1 Determine the fundamental natural frequency of the axisymmetric radial free vibrations of a circular cylindrical shell of length L and radius R for the two types of boundary conditions at the shell ends $x = 0$ and $x = L$: (a) the fixed edges and (b) the simply supported edges. Let $R = 0.5\,\mathrm{m}$, $h = 8\,\mathrm{mm}$, $L = 4R$. The shell is made of steel.

20.2 Investigate the variation of frequency of free radial vibrations of a simply supported open circular cylindrical shell (see Fig. 20.4) from its length L. Take the geometric parameters of the shell in the transverse direction from Example 20.2. Let the shell length $L = 6.0, 10.0, \ldots, 54\,\mathrm{m}$ with the step of 4.0 m.
Hint: Use Eq. (b) in Example 20.2 for your calculations and take $n = 1$; $m = 1, 2.3, 4, 5$.

20.3 Consider a shallow cylindrical shell having a square plan with sides $a \times a$. Investigate an influence of the shell shallowness f/a on the frequencies of free vibrations. Take in your calculations $n = 1$; $m = 1, 2$ in the series expansions. Use the following geometric and mechanical parameters of the shell: $a = 16\,\mathrm{m}$, $h = 6\,\mathrm{cm}$, $E = 15\,\mathrm{GPa}$, $\nu = 0.15$, and $\rho = 2400\,\mathrm{kg/m^3}$. Confine your analysis to the following range: $1/20 \leq f/a \leq 1/8$.

20.4 Calculate the lowest frequency of free vibrations of a spherical shallow shell on a square plan. Assume that the shell is simply supported on its edges. Let $a = 10\,\mathrm{m}$, $f = 0.3\,\mathrm{m}$, $E = 210\,\mathrm{GPa}$, $\rho = 2300\,\mathrm{kg/m^3}$, $\nu = 0.3$, $h = 0.1\,\mathrm{m}$, and $R = 85\,\mathrm{m}$.

20.5 Calculate the lowest frequency of free vibrations of a shallow shell of double curvature on a rectangular plane (Fig. 17.6). The shell is simply supported on its ends. Let $a = 20\,\mathrm{m}$, $b = 20\,\mathrm{m}$, $h = 10\,\mathrm{cm}$, $f = 4\,\mathrm{m}$, $R_1 = 25\,\mathrm{m}$, $R_2 = 42\,\mathrm{m}$, $E = 22\,\mathrm{GPa}$, and $\nu = 0.15$.

20.6 Determine the amplitude of forced vibrations of a cylindrical shell loaded by a concentrated harmonic force $P \sin \Omega t$ applied at a point with the coordinates α_1 and β_1. Assume reasonable values for any additional properties and parameters required.
Hint: Replace the given concentrated force by a uniform load q distributed over a small portion of a cylindrical surface with sides ξ and η, so that $q = P/4R^2\xi\eta$.

20.7 Calculate the amplitude of the forced vibrations of a spherical shallow shell subjected to a uniformly distributed load $p = p_0 \sin \Omega t$. Take as the dimensions of the shell the frequencies of free vibrations from Problem 20.5. Use $p_0 = 0.8\,\mathrm{kN/m^2}$ and $\Omega = 60\,s^{-1}$.

REFERENCES

1. Vlasov,V.Z., *General Theory of Shells and Its Application in Engineering* (English trans), NASA TT F-99, Washington, DC, April 1964.
2. Kraus, H., *Thin Elastic Shells*, John Wiley and Sons, New York, 1967.
3. Flügge, W., *Statik and Dynamik der Schalen*, Springer-Verlag, Berlin, 1962.
4. Nowacki, W., *Dynamics of Elastic Systems*, John Wiley and Sons, New York, 1963.
5. Leissa, A.W., *Vibration of Shells*, NASA SP-288, Washington, DC, 1973.